frontiers | Research Topics

Peripheral blood-based biomarkers for immune monitoring of cancer and cancer therapy

Edited by
José Manuel Pinto Silva Casanova, Paulo Rodrigues-Santos and Raquel Tarazona

Published in
Frontiers in Immunology
Frontiers in Oncology

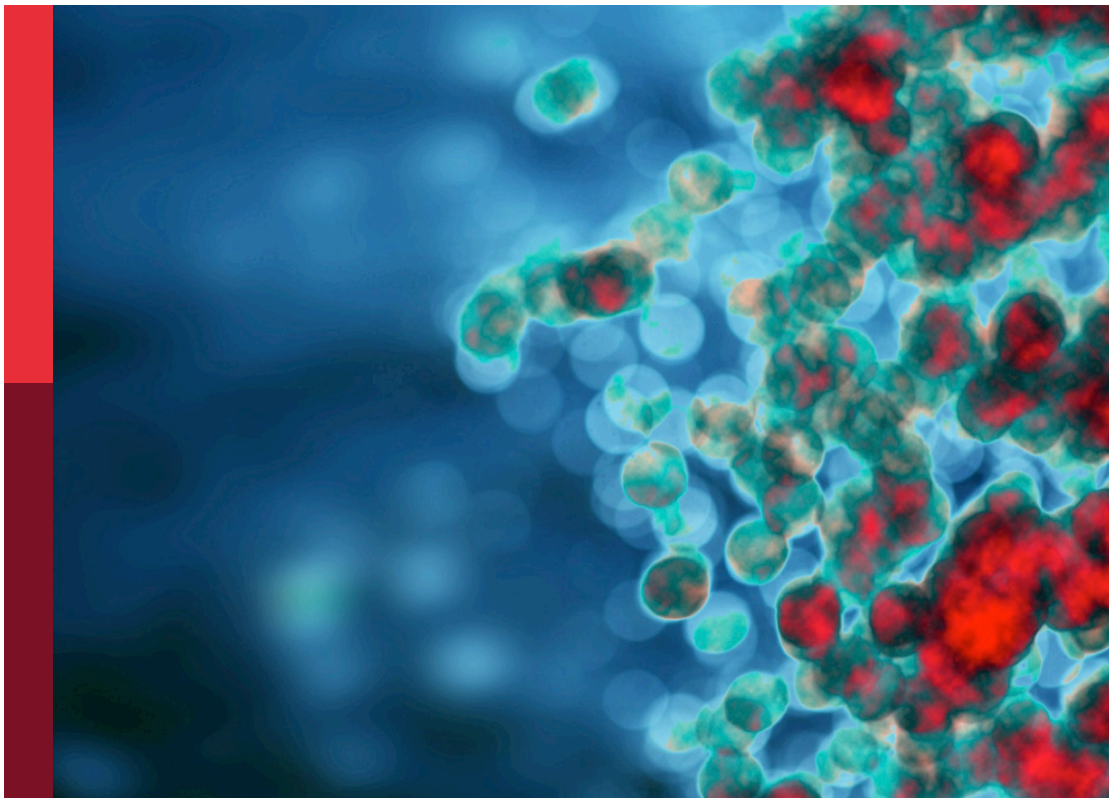

ISSN 1664-8714
ISBN 978-2-8325-6407-3
DOI 10.3389/978-2-8325-6407-3

About Frontiers

Frontiers is more than just an open access publisher of scholarly articles: it is a pioneering approach to the world of academia, radically improving the way scholarly research is managed. The grand vision of Frontiers is a world where all people have an equal opportunity to seek, share and generate knowledge. Frontiers provides immediate and permanent online open access to all its publications, but this alone is not enough to realize our grand goals.

Frontiers journal series

The Frontiers journal series is a multi-tier and interdisciplinary set of open-access, online journals, promising a paradigm shift from the current review, selection and dissemination processes in academic publishing. All Frontiers journals are driven by researchers for researchers; therefore, they constitute a service to the scholarly community. At the same time, the *Frontiers journal series* operates on a revolutionary invention, the tiered publishing system, initially addressing specific communities of scholars, and gradually climbing up to broader public understanding, thus serving the interests of the lay society, too.

Dedication to quality

Each Frontiers article is a landmark of the highest quality, thanks to genuinely collaborative interactions between authors and review editors, who include some of the world's best academicians. Research must be certified by peers before entering a stream of knowledge that may eventually reach the public - and shape society; therefore, Frontiers only applies the most rigorous and unbiased reviews. Frontiers revolutionizes research publishing by freely delivering the most outstanding research, evaluated with no bias from both the academic and social point of view. By applying the most advanced information technologies, Frontiers is catapulting scholarly publishing into a new generation.

What are Frontiers Research Topics?

Frontiers Research Topics are very popular trademarks of the *Frontiers journals series*: they are collections of at least ten articles, all centered on a particular subject. With their unique mix of varied contributions from Original Research to Review Articles, Frontiers Research Topics unify the most influential researchers, the latest key findings and historical advances in a hot research area.

Find out more on how to host your own Frontiers Research Topic or contribute to one as an author by contacting the Frontiers editorial office: frontiersin.org/about/contact

Peripheral blood-based biomarkers for immune monitoring of cancer and cancer therapy

Topic editors

José Manuel Pinto Silva Casanova — University of Coimbra, Portugal

Paulo Rodrigues-Santos — University of Coimbra, Portugal

Raquel Tarazona — University of Extremadura, Spain

Citation

Casanova, J. M. P. S., Rodrigues-Santos, P., Tarazona, R., eds. (2025). *Peripheral blood-based biomarkers for immune monitoring of cancer and cancer therapy*. Lausanne: Frontiers Media SA. doi: 10.3389/978-2-8325-6407-3

Table of contents

frontiers | Frontiers in Immunology

TYPE Original Research
PUBLISHED 11 December 2023
DOI 10.3389/fimmu.2023.1325462

OPEN ACCESS

EDITED BY
Raquel Tarazona,
University of Extremadura, Spain

REVIEWED BY
Muhammad Khan,
Guangzhou Medical University Cancer Hospital, China
Sumbal Arooj,
University of Sialkot, Pakistan

*CORRESPONDENCE
Hidetoshi Hayashi
hidet31@med.kindai.ac.jp

RECEIVED 21 October 2023
ACCEPTED 28 November 2023
PUBLISHED 11 December 2023

CITATION
Kurosaki T, Chamoto K, Suzuki S, Kanemura H, Mitani S, Tanaka K, Kawakami H, Kishimoto Y, Haku Y, Ito K, Sato T, Suminaka C, Yamaki M, Chiba Y, Yaguchi T, Omori K, Kobayashi T, Nakagawa K, Honjo T and Hayashi H (2023) The combination of soluble forms of PD-1 and PD-L1 as a predictive marker of PD-1 blockade in patients with advanced cancers: a multicenter retrospective study. *Front. Immunol.* 14:1325462. doi: 10.3389/fimmu.2023.1325462

The combination of soluble forms of PD-1 and PD-L1 as a predictive marker of PD-1 blockade in patients with advanced cancers: a multicenter retrospective study

Takashi Kurosaki[1], Kenji Chamoto[2,3], Shinichiro Suzuki[1], Hiroaki Kanemura[1], Seiichiro Mitani[1], Kaoru Tanaka[1], Hisato Kawakami[1], Yo Kishimoto[4], Yasuharu Haku[4], Katsuhiro Ito[5], Toshiyuki Sato[6], Chihiro Suminaka[6], Mami Yamaki[7], Yasutaka Chiba[8], Tomonori Yaguchi[2,3], Koichi Omori[4], Takashi Kobayashi[5], Kazuhiko Nakagawa[1], Tasuku Honjo[2] and Hidetoshi Hayashi[1]*

[1]Department of Medical Oncology, Kindai University Faculty of Medicine, Osaka-Sayama, Japan, [2]Department of Immunology and Genomic Medicine, Center for Cancer Immunotherapy and Immunobiology, Kyoto University Graduate School of Medicine, Kyoto, Japan, [3]Department of Immuno-Oncology PDT, Kyoto University Graduate School of Medicine, Kyoto, Japan, [4]Department of Otolaryngology–Head and Neck Surgery, Graduate School of Medicine, Kyoto University, Kyoto, Japan, [5]Department of Urology, Kyoto University Graduate School of Medicine, Kyoto, Japan, [6]Central Research Laboratories, Sysmex Corporation, Kobe, Japan, [7]Business Strategy Development, Sysmex Corporation, Kobe, Japan, [8]Clinical Research Center, Kindai University Hospital, Osaka-Sayama, Japan

Introduction: The clinical relevance of soluble forms of programmed cell death-1 (sPD-1) and programmed cell death-ligand 1 (sPD-L1) remains unclear. We here investigated the relation between the efficacy of PD-1 blockade and pretreatment plasma levels of sPD-1 and sPD-L1 across a broad range of cancer types.

Methods: We retrospectively analyzed clinical data from 171 patients with advanced solid tumors who received nivolumab or pembrolizumab monotherapy regardless of treatment line. The concentrations of sPD-1 and sPD-L1 were measured with a fully automated immunoassay (HISCL system).

Results: The study subjects comprised patients with head and neck cancer (n = 50), urothelial cancer (n = 42), renal cell cancer (n = 37), gastric cancer (n = 20), esophageal cancer (n = 10), malignant pleural mesothelioma (n = 6), or microsatellite instability-high tumors (n = 6). High or low levels of sPD-1 or sPD-L1 were not significantly associated with progression-free survival (PFS) or overall survival (OS) for PD-1 blockade in the entire study population. Comparison of treatment outcomes according to combinations of high or low sPD-1 and sPD-L1 levels, however, revealed that patients with low sPD-1 and high sPD-L1 concentrations had a significantly poorer PFS (HR of 1.79 [95% CI,

1.13–2.83], p = 0.01) and a tendency toward poorer OS (HR of 1.70 [95% CI, 0.99–2.91], p = 0.05) compared with all other patients.

Conclusion: Our findings suggest that the combination of low sPD-1 and high sPD-L1 levels is a potential negative biomarker for PD-1 blockade therapy.

KEYWORDS

immune checkpoint inhibitor, nivolumab, pembrolizumab, soluble PD-1, soluble PD-L1

1 Introduction

Despite the substantial improvements in cancer treatment in recent decades, advanced solid tumors diagnosed at unresectable or recurrent stages still have a poor prognosis and remain the leading cause of death worldwide (1). The development of new systemic therapies that are effective across cancer types is therefore a pressing need.

Immune checkpoint inhibitors (ICIs) are new therapeutic agents that target co-inhibitory molecules expressed on T lymphocytes and which enhance antitumor immunity (2). In particular, antibodies to programmed cell death–1 (PD-1) that block the function of this negative regulatory molecule on T cells are the most widely administered type of ICI and have revolutionized the treatment of advanced malignancies (3). However, the survival outcome for treatment with PD-1 antibodies remains unsatisfactory overall, and the greatest benefit of such treatment is restricted to just a few cancer types. Tumor-agnostic biomarkers that predict the efficacy of PD-1 blockade therapy are therefore needed for optimal patient selection.

One promising such biomarker, programmed cell death–ligand 1 (PD-L1) expression on tumor or immune cells, has been widely investigated. Whereas an association between PD-L1 expression and clinical response has been detected for specific tumor types such as non–small cell lung cancer (NSCLC), results from several prospective trials suggest that PD-L1 expression may not be a robust predictor of the response to PD-1 antibodies in all cancer types (3–6). Possible explanations for this lack of robustness include intratumoral heterogeneity and the dynamic nature of the tumor microenvironment (TME) (7). Compared with biopsy specimens that represent just a fraction of the entire TME, peripheral blood samples are thought to reflect more of the TME and therefore might be a better option for biomarker detection. Blood testing also has the advantages of being minimally invasive and providing dynamic assessments in real time.

In addition to their expression at the cell surface, the receptors and ligands that function as immune checkpoint molecules are present as soluble forms in the circulation (8, 9). Regarding PD-L1, it was reported that the correlation between the serum levels of soluble form and the tumor PD-L1 expression was weak in patients with NSCLC (10), thus soluble forms of immune checkpoint molecules have potential to be a biomarker independent of those of membranous expression. The levels of such soluble forms of PD-1 (sPD-1) and PD-L1 (sPD-L1) have been found to be related to the progression and prognosis of PD-1 blockade therapy, but only a limited number of such studies has focused on advanced solid tumors other than NSCLC and melanoma (11). The aim of the present study was to investigate the possible relation between the efficacy of PD-1 blockade therapy and pretreatment plasma levels of sPD-1 and sPD-L1 across a broad range of advanced cancers that had limited clinical focus.

2 Materials and methods

2.1 Patients

Patients were enrolled in this study if (1) they had a solid tumor at an advanced stage other than NSCLC or melanoma and were not eligible for curative treatment, (2) they had been treated with PD-1 antibody monotherapy regardless of treatment line, and (3) a blood sample collected before the start of PD-1 blockade therapy and clinicopathologic data were available. Patients were retrospectively identified from those attending Kindai University Hospital or Kyoto University Hospital. The study was conducted according to the Declaration of Helsinki, and the protocols were approved by the Institutional Review Board of each participating hospital.

2.2 Data collection

Clinicopathologic data—including sex, age, ECOG performance status, histological subtype, and white blood cell differential for a peripheral blood smear collected at the time of the first PD-1 antibody administration—were obtained from medical records. The neutrophil/lymphocyte ratio (NLR), which has been implicated as a predictive biomarker of ICI treatment outcome (12–14), was calculated for before PD-1 blockade therapy, with a value of 5 being specified as the cutoff between a high and low NLR as in previous studies (12–14). Treatment history and the therapeutic effect of the PD-1 antibody were also retrieved. Tumor response was assessed according to RECIST version 1.1 (15). Overall response rate was defined as the proportion of patients with a complete or partial response as the best overall response, which was assessed regardless of the presence of measurable disease. Progression-free survival (PFS) was measured from the time of treatment initiation to clinical or radiographic progression or death

from any cause. Overall survival (OS) was measured from the time of treatment initiation to death from any cause. Patients without documented clinical or radiographic disease progression or who were still alive were censored at the last follow-up.

2.3 Measurement of sPD-1 and sPD-L1 levels

ELISAs have been adopted for the measurement of sPD-1 and sPD-L1 concentrations in many previous studies but have limited precision and reproducibility because of the manual procedures involved (16, 17). To overcome these limitations, we used a fully automated immunoassay system based on chemiluminescent magnetic technology (HISCL system), which is rapid, sensitive, and reproducible and is able to measure sPD-1 and sPD-L1 levels accurately (11, 17). Plasma samples obtained before PD-1 antibody treatment were considered appropriate for this study; if plasma samples were not available, serum samples were permitted. The high concordance between plasma and serum concentrations was confirmed by Sysmex Corporation, the device provider and a study collaborator, with the use of commercially available paired samples (Figure S1).

2.4 Statistical analysis

Cutoff values for sPD-1 and sPD-L1 concentrations were defined as the median for each cancer type, so that survival analysis according to the soluble markers would not be affected by the potential difference in distributions of sPD-1 and sPD-L1 concentrations among cancer types. The outcome of PD-1 blockade therapy was compared between patients with high or low circulating levels of sPD-1 or sPD-L1. Pairwise comparisons of sPD-1 and sPD-L1 levels were also performed. PFS and OS curves were constructed by the Kaplan-Meier method. Between-group differences in survival analyses were assessed with the log-rank test. The hazard ratio (HR) and its 95% confidence interval (CI) were determined with the use of a Cox proportional hazard regression model. Adjustment for possible confounding factors was performed with a multivariable regression model including explanatory variables with a p value of <0.1 in univariable analysis. A two-sided p value of <0.05 was considered statistically significant. All statistical analysis was performed with Stata BE version 17.0 (StataCorp) or GraphPad Prism 9.0 software.

3 Results

3.1 Characteristics of the study population

A total of 171 patients with solid tumors were enrolled in the study, with their clinical and pathological features being summarized in Table 1. The most common cancer type was head and neck cancer (n = 50, 29.2%), followed by urothelial cancer (n = 42, 24.6%), renal cell cancer (n = 37, 21.6%), gastric cancer (n = 20, 11.7%), esophageal cancer (n = 10, 5.8%), malignant pleural mesothelioma (n = 6, 3.5%), and microsatellite instability (MSI)–high solid tumors (n = 6, 3.5%). The major histological subtypes included squamous cell carcinoma (n = 54, 31.6%), urothelial carcinoma (n = 42, 24.6%), clear cell carcinoma (n = 37, 21.6%), adenocarcinoma (n = 26, 15.2%), and others (n = 12, 7.0%). Of the 171 patients, 121 (70.8%) individuals were treated with nivolumab monotherapy and 50 (29.2%) with pembrolizumab monotherapy. Almost all patients (n = 169, 98.8%) received systemic therapy before PD-1 blockade therapy.

TABLE 1 Patient characteristics.

Characteristic	No. of patients	%
[Median age (range), years	70 (27–89)]	
Sex		
Male	123	71.9
Female	48	28.1
Cancer type		
Head and neck cancer	50	29.2
Urothelial cancer	42	24.6
Renal cell cancer	37	21.6
Gastric cancer	20	11.7
Esophageal cancer	10	5.8
Malignant pleural mesothelioma	6	3.5
MSI-high solid tumors[a]	6	3.5
Histological subtype		
Squamous cell carcinoma	54	31.6
Urothelial carcinoma	42	24.6
Clear cell carcinoma	37	21.6
Adenocarcinoma	26	15.2
Epithelioid mesothelioma	3	1.8
Sarcomatoid mesothelioma	3	1.8
Adenoid cystic carcinoma	1	0.6
Neuroendocrine carcinoma	1	0.6
Salivary duct carcinoma	1	0.6
Not otherwise specified	3	1.8
ECOG performance status		
0	46	26.9
1	100	58.5
2	17	9.9
3	7	4.1
4	1	0.6
Number of prior systemic therapies		
0	2	1.2
1	112	65.5
≥2	57	33.3
ICI regimen		
Nivolumab	121	70.8
Pembrolizumab	50	29.2

MSI, microsatellite instability; ICI, immune checkpoint inhibitor.
[a]MSI-high solid tumors included colorectal cancer (n = 4), cancer of unknown primary (n = 1), and bile duct cancer (n = 1).

3.2 Relation between soluble markers and baseline characteristics

For the total patient population, the median circulating sPD-1 and sPD-L1 concentrations were 169 pg/ml (interquartile range

[IQR], 112–257) and 248 pg/ml (IQR, 211–310), respectively. The distribution of sPD-1 and sPD-L1 levels for each cancer type is shown in Figure 1. The median sPD-1 and sPD-L1 concentrations were 132 pg/ml (IQR, 87–201) and 233 pg/ml (IQR, 192–283) for head and neck cancer, 170 pg/ml (IQR, 121–276) and 256 pg/ml (IQR, 200–309) for urothelial cancer, 229 pg/ml (IQR, 163–351) and 263 pg/ml (IQR, 205–326) for renal cell cancer, 170 pg/ml (IQR, 135–238) and 291 pg/ml (IQR, 239–333) for gastric cancer, 161 pg/ml (IQR, 106–183) and 230 pg/ml (IQR, 206–319) for esophageal cancer, 148 pg/ml (IQR, 112–171) and 247 pg/ml (IQR, 246–273) for malignant pleural mesothelioma, and 247 pg/ml (IQR, 196–434) and 261 pg/ml (IQR, 241–358) for MSI-high solid tumors, respectively. The relation between clinical features of the patients and sPD-1 and sPD-L1 levels is summarized in Table 2. The median sPD-1 level was significantly higher in elderly patients, whereas the median sPD-L1 level was significantly higher in patients who were elderly and male and had a poor ECOG performance status (≥2).

3.3 Relation between soluble markers and treatment efficacy

Among the 171 patients, there were 96 deaths and 138 disease progression events after the onset of PD-1 blockade therapy with a median follow-up time of 11.4 months. Kaplan-Meier curves for PFS and OS were constructed according to circulating sPD-1 and sPD-L1 levels in order to evaluate their independent predictive values (Figure 2). Patients with high sPD-1 (sPD-1^{high}) levels had a numerically longer PFS relative to those with low sPD-1 (sPD-1^{low}) levels (median of 4.5 vs. 3.0 months; HR of 0.76, with a 95% CI of 0.54–1.07; p = 0.11), although the difference was not statistically significant (Figure 2A). The circulating concentration of sPD-1 was also not significantly associated with OS (Figure 2B). In addition, no significant association was apparent between sPD-L1 levels and either PFS (Figure 2C) or OS (Figure 2D), although OS tended to be shorter in patients with sPD-L1^{high} concentrations relative to those with sPD-L1^{low} concentrations (median of 12.7 vs. 16.4 months, HR of 1.32 [95% CI, 0.88–1.97], p = 0.18). Subgroup analysis according to each of the three most common cancer types was shown in Figures S2, S3.

We next hypothesized that the accuracy of survival prediction might be increased by combining sPD-1 and sPD-L1 levels. Indeed, we found that patients with both sPD-1^{low} and sPD-L1^{high} concentrations tended to have a shorter PFS and OS compared with each of the other three groups of patients based on paired sPD-1 and sPD-L1 levels (Figure S4). The patients with sPD-1^{low}/sPD-L1^{high} levels had a significantly shorter PFS (median of 2.3 vs. 4.3 months, HR of 1.79 [95% CI, 1.13–2.83], p = 0.01) and a numerically shorter OS (median of 6.3 vs. 16.9 months, HR of 1.70 [95% CI, 0.99–2.91], p = 0.05) compared with the other groups of patients combined (Figure 3). We then performed multivariable analysis to eliminate bias from possible confounding factors. We adopted NLR and cancer type (renal cell cancer or not, and gastric cancer or not) as explanatory variables for PFS, and sex, ECOG performance status, NLR, and cancer type (urothelial cancer or not, renal cell cancer or not, gastric cancer or not, and MSI-high cancer or not) as those for OS, on the basis of univariable analysis (Table 3). The sPD-1^{low}/sPD-L1^{high} combination was significantly associated with not only PFS (HR of 1.62 [95% CI, 1.03–2.58], p = 0.04) but also OS (HR of 1.86 [95% CI, 1.06–3.26], p = 0.03) (Table 4). Patients with sPD-1^{low}/sPD-L1^{high} levels also had a numerically lower overall response rate compared with the other patients (16.7% vs. 34.7%, p = 0.08 [Chi-squared test]).

Finally, we conducted subgroup analysis for PFS and OS according to cancer type. The comparisons between sPD-1^{low}/sPD-L1^{high} patients and the other patients for each of the three most common cancer types in the study population are shown in Figure 4. The sPD-1^{low}/sPD-L1^{high} combination was significantly associated with a shorter PFS and OS among patients with urothelial cancer (Figure 4B, E), whereas it was not significantly associated with PFS or OS for those with head and neck cancer (Figure 4A, D) or renal cell cancer (Figure 4C, F).

4 Discussion

As far as we are aware, the present study is the first to comprehensively assess pretreatment sPD-1 and sPD-L1 levels across a broad range of advanced cancer types for patients treated with a PD-1 antibody. A notable feature of our study is the use of

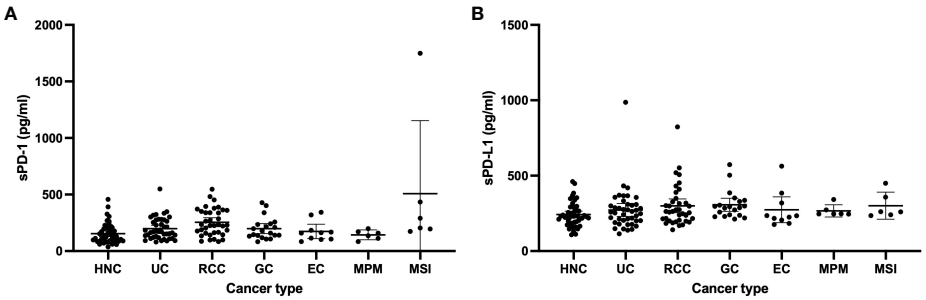

FIGURE 1
Levels of sPD-1 **(A)** and sPD-L1 **(B)** in patients with head and neck cancer (HNC, n = 50), urothelial cancer (UC, n = 42), renal cell cancer (RCC, n = 37) gastric cancer (GC, n = 20), esophageal cancer (EC, n = 10), malignant pleural mesothelioma (MPM, n = 6), or microsatellite instability (MSI)–high cancer (n = 6).

10.3389/fimmu.2023.1325462

TABLE 2 Circulating sPD-1 and sPD-L1 levels of study patients according to baseline characteristics.

Characteristic	sPD-1		sPD-L1	
	Median [IQR], pg/ml	*p*	Median [IQR], pg/ml	*p*
Age (years)				
≥70	185 [142–276]	<0.01	260 [230–318]	0.02
<70	148 [93–228]		234 [184–298]	
Sex				
Female	166 [119–264]	0.78	235 [190–279]	0.02
Male	169 [112–257]		258 [218–319]	
ECOG performance status				
≥2	203 [148–284]	0.11	302 [261–369]	0.02
0 or 1	163 [111–246]		241 [204–300]	
No. of previous regimens				
≥2	188 [136–320]	0.07	256 [220–329]	0.33
0 or 1	164 [109–235]		247 [204–302]	

sPD-1, soluble programmed cell death–1; sPD-L1, soluble programmed cell death–ligand 1; IQR, interquartile range.
The p values were determined with the Wilcoxon ranked sum test.

the HISCL system, a fully automated immunoassay with a high sensitivity and reproducibility, for measurement of the soluble markers (11, 17). We found that the combination of low sPD-1 and high sPD-L1 concentrations was associated with a shorter PFS and OS for patients with advanced solid tumors treated with nivolumab or pembrolizumab monotherapy.

Soluble PD-L1 in the circulation is thought to be produced as a result of alternative mRNA splicing or proteolytic cleavage of PD-L1 at the cell surface in tumor cells or mature dendric cells (18–20). Previous studies have found that high sPD-L1 levels at baseline were associated with a poor PFS and OS in patients treated with ICIs (10, 21–23). One possible explanation for this negative relation between sPD-L1 levels and ICI efficacy is that sPD-L1 binds to PD-1 on the surface of T lymphocytes and thereby disrupts their activation and induces apoptosis (11, 24, 25). It has also been proposed that sPD-L1 might act competitively with PD-1 antibodies and thereby attenuate their pharmacological action (26). In the present study, patients with sPD-L1^{high} levels tended to have a shorter OS, consistent with previous results. However, we considered that sPD-L1 alone was not sufficient for robust prediction of the outcome of PD-1 blockade therapy, given that we did not detect a difference in PFS between sPD-L1^{high} and sPD-L1^{low} patients.

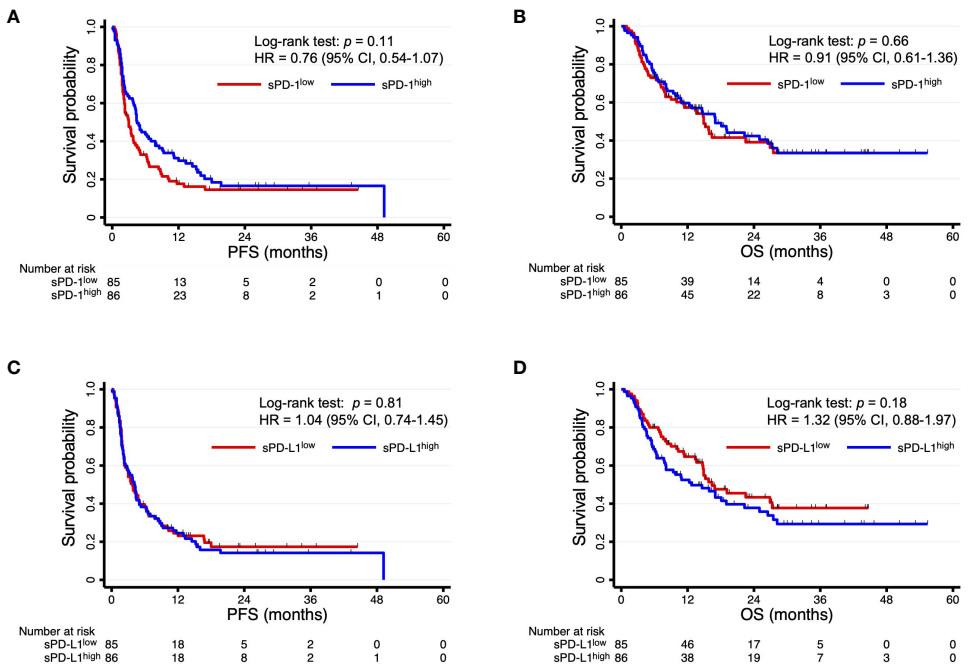

FIGURE 2
Kaplan-Meier curves of PFS **(A, C)** and OS **(B, D)** for patients with sPD-1^{high} or sPD-1^{low} levels **(A, B)** or with sPD-L1^{high} or sPD-L1^{low} levels **(C, D)**.

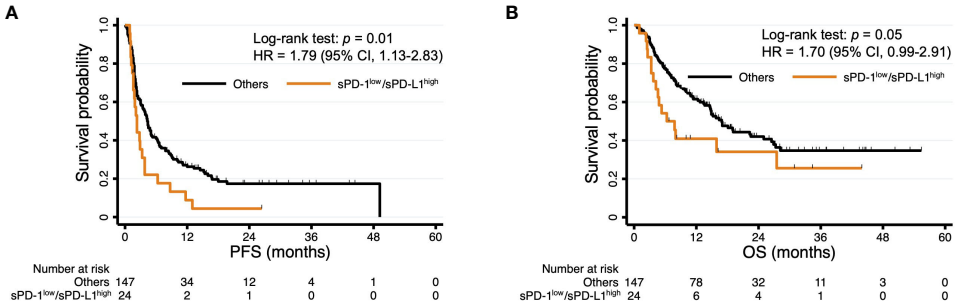

FIGURE 3
Kaplan-Meier curves of PFS **(A)** and OS **(B)** for patients with sPD-1^{low}/sPD-L1^{high} levels and all other patients. The curves for sPD-1^{low}/sPD-L1^{high} are the same as those in Figure S2.

Soluble PD-1 is thought to be generated primarily by alternative splicing of the *PDCD1* gene (27). Although the role of sPD-1 has not been fully elucidated, several preclinical studies have suggested that it promotes the activation of T lymphocytes and enhances the antitumor immune response (11, 28, 29), possibly through suppression of the interaction between PD-1 at the cell surface and its ligands. Clinical studies that have examined the association between sPD-1 levels and survival outcome of immune checkpoint blockade have reported inconsistent findings. A retrospective study of metastatic NSCLC patients treated with nivolumab found that high baseline sPD-1 levels were associated with a shorter PFS in univariable analysis (30). Another study reported that pretreatment sPD-1 levels were not related to either PFS or OS for advanced NSCLC patients treated with ICIs either alone or together with cytotoxic chemotherapy (31). In a study of patients with advanced melanoma, an increase in the sPD-1 concentration after the onset of treatment was a strong individual predictor of a better PFS for nivolumab plus ipilimumab, an antibody to cytotoxic T lymphocyte–associated protein–4 (CTLA-4), implicating sPD-1 in the activation of CD8$^+$ T lymphocytes and the antitumor immune response (32). High sPD-1 levels might be a negative predictor for PD-1 blockade therapy if sPD-1 acts as a decoy for PD-1 antibodies and thereby attenuates their action in the TME. However, elevated sPD-1 levels might also be considered a favorable factor for ICI treatment if sPD-1 inhibits the interaction between PD-1 and PD-L1 (11, 28–30). Further preclinical investigation is warranted to determine the influence of sPD-1 in the TME and its interaction with ICIs. We here found that sPD-L1^{high} levels were significantly associated with a poor PFS only in sPD-1^{low} patients, suggesting that a favorable effect of sPD-1^{high} levels on antitumor immunity

TABLE 3 Univariable analysis of progression-free survival (PFS) and overall survival (OS).

Characteristic	PFS			OS		
	HR	95% CI	*p*	HR	95% CI	*p*
Age						
≥70 years (vs. <70)	1.04	0.74–1.45	0.84	0.96	0.64–1.44	0.85
Sex						
Female (vs. male)	0.93	0.63–1.36	0.70	0.63	0.38–1.03	0.06
Cancer type (vs. others)						
Head and neck cancer	0.94	0.65–1.38	0.76	1.05	0.68–1.62	0.83
Urothelial cancer	1.02	0.69–1.50	0.93	1.93	1.25–2.98	<0.01
Renal cell cancer	0.6	0.39–0.91	0.01	0.27	0.14–0.50	<0.01
Gastric cancer	3.7	2.23–6.12	<0.01	3.01	1.76–5.15	<0.01
Esophageal cancer	1.47	0.77–2.81	0.23	0.95	0.39–2.35	0.92
Malignant pleural mesothelioma	1.68	0.74–3.84	0.21	1.13	0.36–3.58	0.83
MSI-high solid tumors	0.4	0.13–1.27	0.12	0.21	0.03–1.51	0.09
ECOG performance status						
≥2 (vs. 0 or 1)	1.32	0.83–2.11	0.23	2.33	1.39–3.90	<0.01
No. of previous regimens						
≥2 (vs. 0 or 1)	1.22	0.86–1.74	0.26	0.99	0.65–1.52	0.97
Neutrophil/lymphocyte ratio						
≥5 (vs. <5)	1.45	1.09–1.93	0.03	1.88	1.40–2.52	<0.01
Soluble markers						
sPD-1^{low}/sPD-L1^{high} (vs. others)	1.79	1.13–2.83	0.01	1.70	0.99–2.91	0.05

HR, hazard ratio; CI, confidence interval; MSI, microsatellite instability; sPD-1, soluble programmed cell death–1; sPD-L1, soluble programmed cell death–ligand 1.

10.3389/fimmu.2023.1325462

TABLE 4 Multivariable analysis of progression-free survival (PFS) and overall survival (OS).

Characteristic	PFS			OS		
	HR	95% CI	*p*	HR	95% CI	*p*
Sex Female (vs. male)				1.07	0.64–1.80	0.79
Cancer type (vs. others) Urothelial cancer Renal cell cancer Gastric cancer MSI-high solid tumors	 0.67 3.63	 0.44–1.03 2.14–6.16	 0.07 <0.01	 1.37 0.28 3.06 0.23	 0.80–2.35 0.14–0.57 1.65–5.66 0.03–1.71	 0.25 <0.01 <0.01 0.15
ECOG performance status ≥2 (vs. 0 or 1)				2.17	1.22–3.86	<0.01
Neutrophil/lymphocyte ratio ≥5 (vs. <5)	1.59	1.20–2.10	<0.01	1.93	1.42–2.62	<0.01
Soluble markers sPD-1^{low}/sPD-L1^{high} (vs. others)	1.62	1.03–2.58	0.04	1.86	1.06–3.26	0.03

HR, hazard ratio; CI, confidence interval; MSI, microsatellite instability; sPD-1, soluble programmed cell death–1; sPD-L1, soluble programmed cell death–ligand 1.

might attenuate a negative impact of sPD-L1^{high} levels on CD8^{+} T lymphocyte activation. A recent study showed that a low sPD-1/sPD-L1 ratio at baseline was associated with a shorter OS in comparison with a high sPD-1/sPD-L1 ratio in patients with advanced melanoma treated with nivolumab or pembrolizumab (33), consistent with our present results.

We found that the sPD-1^{low}/sPD-L1^{high} combination was independently associated with shorter OS as well as shorter PFS after adjustment for confounding factors in our multivariable model. In the uni- and multivariable analyses, we treated cancer types as explanatory variables, given that our study targeted a variety of advanced solid tumors. Our findings thus suggest that the sPD-1^{low}/sPD-L1^{high} combination is a promising candidate for a biomarker associated with poor efficacy of PD-1 blockade therapy across cancer types.

There are several limitations to our retrospective study. First, it lacked a validation cohort to confirm the adequacy of the selected cutoff values for sPD-1 and sPD-L1 levels. Second, it lacked a control patient group treated with chemotherapeutic or molecularly targeted agents with different mechanisms of action from ICIs, making it difficult to determine whether our observations are specific to PD-1 antibodies. The study subjects also did not receive ICI treatment other than PD-1 antibody monotherapy. Given that combinations of PD-1 or PD-L1 antibodies with a CTLA-4 antibody, or of chemotherapy with immunotherapy, have recently become important treatment options for several advanced malignancies, additional investigation is warranted to assess the relation between sPD-1^{low}/sPD-L1^{high} levels and the efficacy of these combination therapies in the front line. Third, the aim of this study was to explore the overall trends of sPD-1 and

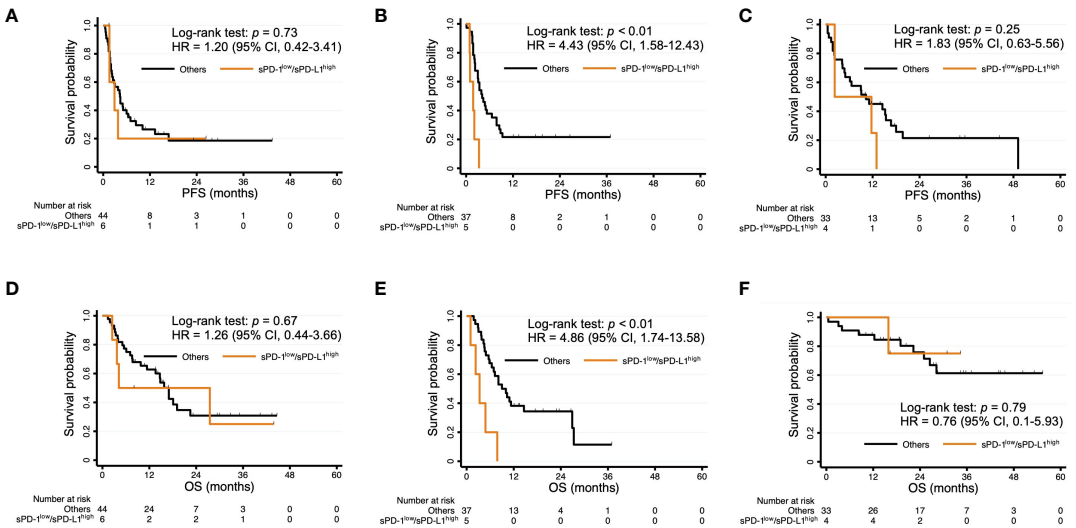

FIGURE 4
Kaplan-Meier curves of PFS **(A–C)** and OS **(D–F)** for patients with sPD-1^{low}/sPD-L1^{high} levels and the other patients among individuals with head and neck cancer **(A, D)**, urothelial cancer **(B, E)**, or renal cell cancer **(C, F)**.

sPD-L1 across a broad range of cancer types, and the sample size was insufficient to permit a detailed analysis on the specific cancer types under consideration.

In conclusion, our findings suggest that the combination of low sPD-1 and high sPD-L1 levels at baseline is a potential negative biomarker of PFS and OS for PD-1 antibody monotherapy in a variety of cancer types. Prospective evaluation will be needed to validate and confirm our observations.

Data availability statement

The raw data supporting the conclusions of this article will be made available by the authors, without undue reservation.

Ethics statement

The studies involving humans were approved by Human Genome/Gene Analysis Research Ethics Committee of Kindai University Faculty of Medicine. The studies were conducted in accordance with the local legislation and institutional requirements. The participants provided their written informed consent to participate in this study.

Author contributions

TKu: Writing – original draft, Writing – review & editing, Conceptualization, Data curation, Formal Analysis, Investigation, Methodology, Project administration, Resources, Software. KC: Conceptualization, Data curation, Formal Analysis, Investigation, Methodology, Writing – original draft, Writing – review & editing. SS: Data curation, Resources, Writing – review & editing. HKan: Data curation, Resources, Writing – review & editing. SM: Data curation, Resources, Writing – review & editing. KT: Data curation, Resources, Writing – review & editing. HKaw: Data curation, Resources, Writing – review & editing. YK: Data curation, Resources, Writing – review & editing. YH: Data curation, Resources, Writing – review & editing. KI: Data curation, Resources, Writing – review & editing. TS: Conceptualization, Data curation, Formal Analysis, Funding acquisition, Investigation, Methodology, Project administration, Resources, Writing – original draft, Writing – review & editing. CS: Conceptualization, Data curation, Formal Analysis, Funding acquisition, Investigation, Methodology, Project administration, Resources, Writing – original draft, Writing – review & editing. MY:Conceptualization, Data curation, Formal Analysis, Funding acquisition, Investigation, Methodology, Project administration, Resources, Writing – original draft, Writing – review & editing. YC: Formal Analysis, Investigation, Methodology, Writing – original draft, Writing – review & editing. TY: Data curation, Resources, Writing – review & editing. KO: Data curation, Resources, Writing – review & editing. TKo: Data curation, Resources, Writing – review & editing. KN: Supervision, Writing – review & editing. TH: Supervision, Writing – review & editing. HH: Conceptualization, Formal Analysis, Funding acquisition, Investigation, Methodology, Project administration, Writing – original draft, Writing – review & editing.

Funding

The author(s) declare financial support was received for the research, authorship, and/or publication of this article. This study was sponsored by Sysmex Corporation.

Acknowledgments

We thank all the subjects who participated in this study.

Conflict of interest

TKu: honoraria from AstraZeneca K.K. KC: grants or contracts from Meiji Seika Pharma Co., Ltd., Meiji Holdings Co., Ltd., Shimazu Corporation, and Menarini Biomarkers Singapore.; payment or honoraria from Cosmo Bio Co., Ltd., Bristol Myers Squibb Japan, Merck KGaA, AstraZeneca K.K., CHUGAI PHARMACEUTICAL CO., LTD., Novartis Pharma K.K, Hitachi, Ltd., Corning Incorporated., Agilent Technologies Japan, Ltd., and SBI Pharmaceuticals Co., Ltd.; patents to WO2017/099034, WO2018/084204, WO2017/115816, WO2020/149026, WO2019/188354, WO2021/095599, and PCT/JP2022/006843; program committee of Japanese Cancer Association.; board member of Japanese Society for Immunology, and Japanese Society of Cancer Immunology. SS: research funds from Nippon Boehringer Ingelheim Co., Ltd. HKan: lecture fees or honoraria from Chugai Pharmaceutical Co.,Ltd., and AstraZeneca K.K.; research funds from Chugai Pharmaceutical Co.,Ltd., and Takeda Pharmaceutical Co.,Ltd. SM: payment or honoraria from Taiho Pharmaceutical Co., and Ono Pharmaceutical Co. Ltd.: participation on a Data Safety Monitoring Board or Advisory Board to Chugai Pharmaceutical Co. Ltd. KT: payment or honoraria from AstraZeneca K.K., Merck Biopharma Co., Ltd., Eisai.Inc., Bristol Myers Squibb Company, ONO Pharmaceutical Co., MSD K.K., Chugai Pharmaceutical Co., Takeda Pharmaceutical Co., Ltd., Taiho Pharmaceutical Co., Ltd., and Novartis Pharma K.K. HKaw: Consulting or advisory fees from Astellas Pharma Inc. and Daiichi-Sankyo Co. Ltd.; honoraria from Bristol-Myers Squibb Co. Ltd., Ono Pharmaceutical Co. Ltd., Eli Lilly Japan K.K., MSD K.K., Chugai Pharmaceutical Co. Ltd., Daiichi-Sankyo Co. Ltd., Merck Biopharma Co. Ltd., Takeda Pharmaceutical Co. Ltd., Yakult Pharmaceutical Industry, Taiho Pharmaceutical Co. Ltd., and Nippon Kayaku Co. Ltd.; and research funding from Bristol-Myers Squibb Co. Ltd., Taiho Pharmaceutical Co. Ltd., Kobayashi Pharmaceutical Co. Ltd., and Eisai Co. Ltd. YK: honoraria from Eisai Co., Ltd. TKo: lecture fees or honoraria from Janssen Pharmaceutical K.K., Astellas Pharma Inc., and Bayer Yakuhin, Ltd. KN: honoraria from Ono Pharmaceutical Co., Ltd., Merck Biopharma Co., Ltd., Amgen Inc., Kyowa Kirin Co., Ltd., Nippon Kayaku Co., Ltd., Takeda Pharmaceutical Co., Ltd., AstraZeneca K.K., 3H Clinical Trial Inc., Chugai Pharmaceutical

Co., Ltd., Care Net, Inc., Eli Lilly Japan K.K., Medical Review Co., Ltd., MSD K.K., Medical Mobile Communications co., Ltd, Pfizer Japan Inc., YODOSHA CO., LTD., Nippon Boehringer Ingelheim Co., Ltd., Nikkei Business Publications, Inc., Taiho Pharmaceutical Co.,Ltd., Japan Clinical Research Operations, Bayer Yakuhin, Ltd., CMIC Co., Ltd., CMIC ShiftZero K.K., Novartis Pharma K.K., Life Technologies Japan Ltd., TAIYO Pharma Co., Ltd., Neo Communication, Bristol Myers Squibb Company, Daiichi Sankyo Co., Ltd., Janssen Pharmaceutical K.K., and Incyte biosciences Japan; research funding from PAREXEL International Corp., Eisai Co., Ltd., PRA HEALTHSCIENCES, AstraZeneca K.K., EPS Corporation., Mochida Pharmaceutical Co., Ltd., Kissei Pharmaceutical Co., Ltd., Labcorp Development Japan K.K.(Covance Japan Inc.), EPS International Co.,Ltd., Japan Clinical Research Operations, Daiichi Sankyo Co., Ltd., Takeda Pharmaceutical Co.,Ltd., Taiho Pharmaceutical Co.,Ltd., GlaxoSmithKline K.K., MSD K.K., Sanofi K.K., Ono Pharmaceutical Co.,Ltd., Chugai Pharmaceutical Co.,Ltd., PPD-SNBL K.K, Nippon Boehringer Ingelheim Co.,Ltd., SymBio Pharmaceuticals Limited., Sysmex Corporation, IQVIA Services JAPAN K.K., Medical Research Support, SYNEOS HEALTH CLINICAL K.K., Eli Lilly Japan K.K., Nippon Kayaku Co.,Ltd., Amgen Inc., EP-CRSU Co., Ltd., Novartis Pharma K.K., Mebix, Inc., Otsuka Pharmaceutical Co., Ltd., Bristol-Myers Squibb K.K., SRL, Inc., Janssen Pharmaceutical K.K., Pfizer R&D Japan G.K., CMIC CO., Ltd., Bayer Yakuhin, Ltd, Shionogi & Co., Ltd., Pfizer Japan Inc, Astellas Pharma Inc., Ascent Development Services, Kobayashi Pharmaceutical Co., Ltd., and Eisai Inc.; Consulting or advisor role to Eli Lilly Japan K.K., and Ono Pharmaceutical Co., Ltd.; patent royalties from Daiichi Sankyo Co., Ltd. TH: grants or contracts from Meiji Seika Pharma Co., Ltd., Meiji Holdings Co., Ltd., Shimazu Corporation, Menarini Biomarkers Singapore; Royalties or licenses from ONO PHARMACEUTICAL CO., LTD.; patents to WO2017/099034, WO2018/084204, WO2017/115816, WO2020/149026, WO2019/188354, WO2021/095599, and PCT/JP2022/006843; honorary member of Japanese Cancer Association, Japanese Society for Immunology, Japanese Biochemical Society. HH: Grants or contracts IQVIA Services JAPAN K.K., Eisai Co., Ltd., SYNEOS HEALTH CLINICAL K.K., EP-CRSU CO., LTD., EPS Corporation., Shionogi & Co., Ltd., Nippon Kayaku Co.,Ltd., Otsuka Pharmaceutical Co., Ltd., Takeda Pharmaceutical Co.,Ltd., GlaxoSmithKline K.K., MSD K.K., Sanofi K.K., Amgen Inc., Chugai Pharmaceutical Co.,Ltd., Taiho Pharmaceutical Co.,Ltd., Nippon Boehringer Ingelheim Co., Ltd., Bristol Myers Squibb Company, SRL Medisearch Inc., Janssen Pharmaceutical K.K., PRA Health Sciences Inc., CMIC CO., Ltd., Astellas Pharma Inc., Pfizer R&D Japan G.K., Ascent Development Services, Labcorp Development Japan K.K., Eisai Inc., Kobayashi Pharmaceutical Co., Ltd., Bayer Yakuhin, Ltd, Pfizer Japan Inc.; payment or honoraria from Ono Pharmaceutical Co.,Ltd., Merck Biopharma Co., Ltd., Daiichi Sankyo Co., Ltd., 3H Clinical Trial Inc., AstraZeneca K.K., Novartis Pharma K.K., Chugai Pharmaceutical Co.,Ltd., Bristol Myers Squibb Company, Eli Lilly Japan K.K., Amgen Inc., MSD K.K., Sysmex Corporation, Pfizer Japan Inc., Takeda Pharmaceutical Co.,Ltd., Nippon Boehringer Ingelheim Co.,Ltd. TS, CS and MY are employees of and receive remuneration from Sysmex Corporation. All authors had full access to all of the data in the study and had final responsibility for the decision to submit for publication.

The remaining authors declare that the research was conducted in the absence of any commercial or financial relationships that could be constructed as a potential conflict of interest.

This study received funding from Sysmex Corporation. The funder had the following involvement with the study: conception and design, acquisition of data, analysis and interpretation of data, and writing and review of the manuscript.

Publisher's note

Supplementary material

The Supplementary Material for this article can be found online at: https://www.frontiersin.org/articles/10.3389/fimmu.2023.1325462/full#supplementary-material

SUPPLEMENTARY FIGURE 1
Scatter plot and linear regression for the plasma and serum concentrations of sPD-1 **(A)** or sPD-L1 **(B)** in matched paired samples. Correlation was evaluated with the Spearman correlation test.

SUPPLEMENTARY FIGURE 2
Kaplan-Meier curves of PFS **(A–C)** and OS **(D–F)** for patients with sPD-1^{high} or sPD-1^{low} levels among individuals with head and neck cancer **(A, D)**, urothelial cancer **(B, E)**, or renal cell cancer **(C, F)**.

SUPPLEMENTARY FIGURE 3
Kaplan-Meier curves of PFS **(A–C)** and OS **(D–F)** for patients with sPD-$L1^{high}$ or sPD-$L1^{low}$ levels among individuals with head and neck cancer **(A, D)**, urothelial cancer **(B, E)**, or renal cell cancer **(C, F)**.

SUPPLEMENTARY FIGURE 4
Kaplan-Meier curves of PFS **(A)** and OS **(B)** for all patients according to combined low or high levels of sPD-1 and sPD-L1.

References

1. Sung H, Ferlay J, Siegel RL, Laversanne M, Soerjomataram I, Jemal A, et al. Global cancer statistics 2020: GLOBOCAN estimates of incidence and mortality worldwide for 36 cancers in 185 countries. *CA Cancer J Clin* (2021) 71:209–49. doi: 10.3322/caac.21660

2. Joyce JA, Fearon DT. T cell exclusion, immune privilege, and the tumor microenvironment. *Science* (2015) 348:74–80. doi: 10.1126/science.aaa6204

3. Sharma P, Siddiqui BA, Anandhan S, Yadav SS, Subudhi SK, Gao J, et al. The next decade of immune checkpoint therapy. *Cancer Discovery* (2021) 11:838–57. doi: 10.1158/2159-8290.CD-20-1680

4. Darvin P, Toor SM, Sasidharan Nair V, Elkord E. Immune checkpoint inhibitors: recent progress and potential biomarkers. *Exp Mol Med* (2018) 50:1–11. doi: 10.1038/s12276-018-0191-1

5. Rosenberg JE, Hoffman-Censits J, Powles T, van der Heijden MS, Balar AV, Necchi A, et al. Atezolizumab in patients with locally advanced and metastatic urothelial carcinoma who have progressed following treatment with platinum-based chemotherapy: a single-arm, multicentre, phase 2 trial. *Lancet* (2016) 387:1909–20. doi: 10.1016/S0140-6736(16)00561-4

6. Antonia SJ, López-Martin JA, Bendell J, Ott PA, Taylor M, Eder JP, et al. Nivolumab alone and nivolumab plus ipilimumab in recurrent small-cell lung cancer (CheckMate 032): a multicentre, open-label, phase 1/2 trial. *Lancet Oncol* (2016) 17:883–95. doi: 10.1016/S1470-2045(16)30098-5

7. Yi M, Jiao D, Xu H, Liu Q, Zhao W, Han X, et al. Biomarkers for predicting efficacy of PD-1/PD-L1 inhibitors. *Mol Cancer* (2018) 17:129. doi: 10.1186/s12943-018-0864-3

8. Gu D, Ao X, Yang Y, Chen Z, Xu X. Soluble immune checkpoints in cancer: production, function and biological significance. *J Immunother Cancer* (2018) 6:132. doi: 10.1186/s40425-018-0449-0

9. Khan M, Arooj S, Wang H. Soluble B7-CD28 family inhibitory immune checkpoint proteins and anti-cancer immunotherapy. *Front Immunol* (2021) 12:651634. doi: 10.3389/fimmu.2021.651634

10. Murakami S, Shibaki R, Matsumoto Y, Yoshida T, Goto Y, Kanda S, et al. Association between serum level soluble programmed cell death ligand 1 and prognosis in patients with non-small cell lung cancer treated with anti-PD-1 antibody. *Thorac Cancer* (2020) 11:3585–95. doi: 10.1111/1759-7714.13721

11. Niu M, Liu Y, Yi M, Jiao D, Wu K. Biological characteristics and clinical significance of soluble PD-1/PD-L1 and exosomal PD-L1 in cancer. *Front Immunol* (2022) 13:827921. doi: 10.3389/fimmu.2022.827921

12. Sacdalan DB, Lucero JA, Sacdalan DL. Prognostic utility of baseline neutrophil-to-lymphocyte ratio in patients receiving immune checkpoint inhibitors: a review and meta-analysis. *Onco Targets Ther* (2018) 11:955–65. doi: 10.2147/OTT.S153290

13. Ogata T, Satake H, Ogata M, Hatachi Y, Inoue K, Hamada M, et al. Neutrophil-to-lymphocyte ratio as a predictive or prognostic factor for gastric cancer treated with nivolumab: a multicenter retrospective study. *Oncotarget* (2018) 9:34520–7. doi: 10.18632/oncotarget.26145

14. Bagley SJ, Kothari S, Aggarwal C, Bauml JM, Alley EW, Evans TL, et al. Pretreatment neutrophil-to-lymphocyte ratio as a marker of outcomes in nivolumab-treated patients with advanced non-small-cell lung cancer. *Lung Cancer* (2017) 106:1–7. doi: 10.1016/j.lungcan.2017.01.013

15. Eisenhauer EA, Therasse P, Bogaerts J, Schwartz LH, Sargent D, Ford R, et al. New response evaluation criteria in solid tumours: revised RECIST guideline (version 1.1). *Eur J Cancer* (2009) 45:228–47. doi: 10.1016/j.ejca.2008.10.026

16. Rohner F, Zeder C, Zimmermann MB, Hurrell RF. Comparison of manual and automated ELISA methods for serum ferritin analysis. *J Clin Lab Anal* (2005) 19:196–8. doi: 10.1002/jcla.20077

17. Goto M, Chamoto K, Higuchi K, Yamashita S, Noda K, Iino T, et al. Analytical performance of a new automated chemiluminescent magnetic immunoassays for soluble PD-1, PD-L1, and CTLA-4 in human plasma. *Sci Rep* (2019) 9:10144. doi: 10.1038/s41598-019-46548-3

18. Vecchiarelli S, Passiglia F, D'Incecco A, Gallo M, De Luca A, Rossi E, et al. Circulating programmed death ligand-1 (cPD-L1) in non-small-cell lung cancer (NSCLC). *Oncotarget* (2018) 9:17554–63. doi: 10.18632/oncotarget.24785

19. Frigola X, Inman BA, Krco CJ, Liu X, Harrington SM, Bulur PA, et al. Soluble B7-H1: differences in production between dendritic cells and T cells. *Immunol Lett* (2012) 142:78–82. doi: 10.1016/j.imlet.2011.11.001

20. Dezutter-Dambuyant C, Durand I, Alberti L, Bendriss-Vermare N, Valladeau-Guilemond J, Duc A, et al. A novel regulation of PD-1 ligands on mesenchymal stromal cells through MMP-mediated proteolytic cleavage. *Oncoimmunology* (2015) 5: e1091146. doi: 10.1080/2162402X.2015.1091146

21. Kawakami H, Sunakawa Y, Inoue E, Matoba R, Noda K, Sato T, et al. Soluble programmed cell death ligand 1 predicts prognosis for gastric cancer patients treated with nivolumab: blood-based biomarker analysis for the DELIVER trial. *Eur J Cancer* (2023) 184:10–20. doi: 10.1016/j.ejca.2023.02.003

22. Oh SY, Kim S, Keam B, Kim TM, Kim DW, Heo DS. Soluble PD-L1 is a predictive and prognostic biomarker in advanced cancer patients who receive immune checkpoint blockade treatment. *Sci Rep* (2021) 11:19712. doi: 10.1038/s41598-021-99311-y

23. Okuma Y, Wakui H, Utsumi H, Sagawa Y, Hosomi Y, Kuwano K, et al. Soluble programmed cell death ligand 1 as a novel biomarker for nivolumab therapy for non-small-cell lung cancer. *Clin Lung Cancer* (2018) 19:410–7.e1. doi: 10.1016/j.cllc.2018.04.014

24. Frigola X, Inman BA, Lohse CM, Krco CJ, Cheville JC, Thompson RH, et al. Identification of a soluble form of B7-H1 that retains immunosuppressive activity and is associated with aggressive renal cell carcinoma. *Clin Cancer Res* (2011) 17:1915–23. doi: 10.1158/1078-0432.CCR-10-0250

25. Hassounah NB, Malladi VS, Huang Y, Freeman SS, Beauchamp EM, Koyama S, et al. Identification and characterization of an alternative cancer-derived PD-L1 splice variant. *Cancer Immunol Immunother* (2019) 68:407–20. doi: 10.1007/s00262-018-2284-z

26. Liang Z, Tian Y, Cai W, Weng Z, Li Y, Zhang H, et al. High-affinity human PD-L1 variants attenuate the suppression of T cell activation. *Oncotarget* (2017) 8:88360–75. doi: 10.18632/oncotarget.21729

27. Nielsen C, Ohm-Laursen L, Barington T, Husby S, Lillevang ST. Alternative splice variants of the human PD-1 gene. *Cell Immunol* (2005) 235:109–16. doi: 10.1016/j.cellimm.2005.07.007

28. He L, Zhang G, He Y, Zhu H, Zhang H, Feng Z. Blockade of B7-H1 with sPD-1 improves immunity against murine hepatocarcinoma. *Anticancer Res* (2005) 25:3309–13.

29. Elhag OA, Hu XJ, Wen-Ying Z, Li X, Yuan YZ, Deng LF, et al. Reconstructed adeno-associated virus with the extracellular domain of murine PD-1 induces antitumor immunity. *Asian Pac J Cancer Prev* (2012) 13:4031–6. doi: 10.7314/apjcp.2012.13.8.4031

30. Tiako Meyo M, Jouinot A, Giroux-Leprieur E, Fabre E, Wislez M, Alifano M, et al. Predictive value of soluble PD-1, PD-L1, VEGFA, CD40 ligand and CD44 for nivolumab therapy in advanced non-small cell lung cancer: a case-control study. *Cancers (Basel)* (2020) 12:473. doi: 10.3390/cancers12020473

31. Himuro H, Nakahara Y, Igarashi Y, Kouro T, Higashijima N, Matsuo N, et al. Clinical roles of soluble PD-1 and PD-L1 in plasma of NSCLC patients treated with immune checkpoint inhibitors. *Cancer Immunol Immunother* (2023) 72:2829–40. doi: 10.1007/s00262-023-03464-w

32. Pedersen JG, Sokac M, Sørensen BS, Luczak AA, Aggerholm-Pedersen N, Birkbak NJ, et al. Increased soluble PD-1 predicts response to nivolumab plus ipilimumab in melanoma. *Cancers (Basel)* (2022) 14:3342. doi: 10.3390/cancers14143342

33. Lu L, Risch E, Halaban R, Zhen P, Bacchiocchi A, Risch HA. Dynamic changes of circulating soluble PD-1/PD-L1 and its association with patient survival in immune checkpoint blockade-treated melanoma. *Int Immunopharmacol* (2023) 118:110092. doi: 10.1016/j.intimp.2023.110092

frontiers | Frontiers in Immunology

TYPE Original Research
PUBLISHED 03 January 2024
DOI 10.3389/fimmu.2023.1325343

OPEN ACCESS

EDITED BY
Raquel Tarazona,
University of Extremadura, Spain

REVIEWED BY
Sabine Hombach-Klonisch,
University of Manitoba, Canada
Jaya Lakshmi Thangaraj,
University of California, San Diego,
United States

*CORRESPONDENCE
Mabel Ryder
ryder.mabel@mayo.edu

RECEIVED 21 October 2023
ACCEPTED 12 December 2023
PUBLISHED 03 January 2024

CITATION
Kotwal A, Gustafson MP, Bornschlegl S, Dietz AB, Delivanis D and Ryder M (2024) Circulating immunophenotypes are potentially prognostic in follicular cell-derived thyroid cancer.
Front. Immunol. 14:1325343.
doi: 10.3389/fimmu.2023.1325343

Circulating immunophenotypes are potentially prognostic in follicular cell-derived thyroid cancer

Anupam Kotwal[1,2], Michael P. Gustafson[3,4], Svetlana Bornschlegl[3], Allan B. Dietz[3,5,6], Danae Delivanis[2] and Mabel Ryder[2,7]*

[1]Division of Diabetes, Endocrinology and Metabolism, University of Nebraska Medical Center, Omaha, NE, United States, [2]Division of Endocrinology, Diabetes, Metabolism, and Nutrition, Mayo Clinic, Rochester, MN, United States, [3]Divisions of Experimental Pathology and Transfusion Medicine, Mayo Clinic, Rochester, MN, United States, [4]Division of Laboratory Medicine, Department of Laboratory Medicine and Pathology, Mayo Clinic Arizona, Phoenix, AZ, United States, [5]Department of Laboratory Medicine and Pathology, Mayo Clinic, Rochester, MN, United States, [6]Department of Immunology, Mayo Clinic, Rochester, MN, United States, [7]Division of Medical Oncology, Mayo Clinic, Rochester, MN, United States

Background: Exploring the immune interface of follicular cell-derived thyroid cancer has prognostic and therapeutic potential. The available literature is lacking for comprehensive immunophenotyping in relation to clinical outcomes. In this study, we identify circulating immunophenotypes associated with thyroid cancer prognosis.

Methods: We conducted a pilot observational study of adults with follicular cell-derived thyroid cancer who underwent surgery at our tertiary care referral center and had consented for flow cytometry on peripheral blood collected at the time of thyroidectomy.

Results: Of the 32 included subjects, 20 (62%) had well differentiated, 5 (16%) had poorly differentiated, and 7 (22%) had anaplastic thyroid cancer. The most frequent AJCC stage was 4 (59%) and the ATA risk of recurrence category was high (56%). Patients with AJCC stage 3/4 demonstrated fewer circulating mononuclear cells (CD45+), more monocytes (CD14+), fewer total lymphocytes (CD14-), fewer T cells (CD3+), fewer CD4+ T cells, fewer gamma-delta T cells, fewer natural killer (NK) T-like cells, more myeloid-derived suppressor cells (MDSCs; Lin-CD33+HLADR-), and more effector memory T cells but similar CD8+ T cells compared to stage1/2. Immunophenotype comparisons by ATA risk stratification and course of thyroid cancer were comparable to those observed for stage, except for significant differences in memory T cell subtypes. The median follow-up was 58 months.

Conclusions: Aggressive follicular cell-derived thyroid cancer either at presentation or during follow-up is associated with down-regulation of the

T cell populations specifically CD4+ T cells, gamma-delta T cells, and NK T-like cells but up-regulation of MDSCs and altered memory T cells. These immunophenotypes are potential prognostic biomarkers supporting future investigation for developing targeted immunotherapies against advanced thyroid cancer.

KEYWORDS

immune cell, flow cytometry, prognosis, thyroid carcinoma, T cell, immune markers

Background

The incidence of thyroid cancer has been steadily increasing. Follicular cell-derived differentiated thyroid cancers have a favorable prognosis with conventional treatment including thyroidectomy with or without radioactive iodine. However, at least 10% of patients develop radioactive iodine-refractory metastases to lung, bone, and other sites. In such cases, 5-year survival can be a dismal 15.3% (1). While aggressive multi-modality approaches and tyrosine kinase inhibitors have demonstrated improved outcomes, such therapies have toxicities and usually partial responses (2, 3). This has led to the exploration of immunotherapies for advanced thyroid cancer and stimulated an interest in understanding the effect of the immune system on thyroid cancer. The ligand for immune checkpoint programmed cell death protein 1 (PD-1) has been demonstrated on malignant thyroid cells (4, 5), thus leading to the trial of PD-1 inhibitors in anaplastic thyroid cancer (6). However, the effect of these therapies on advanced thyroid cancer has been unpredictable or poor (7). This could be due to the resurgence of an immunosuppressive tumor microenvironment as shown in a murine model of thyroid cancer (8).

The association between immune-mediated inflammation and follicular cell-derived thyroid cancer has been reported (9) as evidenced by a mixture of cytokines, chemokines, and immune cells in the tumor microenvironment. While an association between autoimmune thyroid disease and thyroid cancer has been reported in a database study (10), the impact of chronic lymphocytic thyroiditis on thyroid cancer prognosis remains unclear (11–14). To address this issue, studies have identified the increased immune suppressor cells, regulatory T cells (Tregs) (15), PD1+ T cells (15), myeloid-derived suppressor cells (MDSCs) (16), in circulation, and infiltrating the tumor of pathologically aggressive differentiated thyroid cancer (5, 17–19), while the association with effector CD8 + T cells has been mixed (20, 21). However, comprehensive examination of the relationship between circulating immunophenotypes and clinicopathologic outcomes in thyroid cancer patients remains limited. Our group has previously identified circulating immune cell profiles in thyroiditis caused by immune checkpoint inhibitors (ICIs) (22), as well as healthy and other malignancy patients (23, 24); and more immune activator T cell subpopulations in the thyroid glands of patients developing PD-1/PD-L1 inhibitor-induced thyroiditis (25). These studies highlight our ability to comprehensively analyze immunophenotypes in relation to clinically key factors. Based on the available literature and our previous work, we hypothesized that the circulating leukocyte populations, specifically suppressor (Tregs, MDSCs, effector memory T cells) and effector cells (CD4+ T cells, CD8+ T cells, gamma-delta T cells, NK cells, central memory T cells), in patients with high-risk thyroid cancer would be different from those in low-risk thyroid cancer. Hence, we aimed to identify immunophenotypes associated with follicular cell-derived thyroid cancer prognosis to recognize patients with aggressive thyroid cancer that could benefit from personalized management including novel immunotherapies.

Materials and methods

Study population and patient samples

We performed an institutional review board–approved pilot prospective cohort study of 32 adults with follicular cell-derived thyroid cancer who underwent initial or subsequent surgical management at a tertiary care cancer center. Informed consent was obtained from each participant and the research was completed in accordance with the Declaration of Helsinki as revised in 2013. We excluded patients with medullary thyroid cancer. Peripheral blood was collected at the time of surgery in tubes containing K_2EDTA anticoagulant. The electronic medical record was utilized to gather clinical, radiographic, laboratory, and pathologic data.

Outcomes

Participants were categorized into low, intermediate, and high risk for recurrence groups according to the 2015 revised American Thyroid Association (ATA) guidelines (26); into tumor node metastasis (TNM) stage 1, 2, 3 or 4 according to the 8th American Joint Committee on Cancer (AJCC) edition (27);

and according to the presence or absence of loco-regional and distant recurrence or progression during follow-up. Circulating immunophenotypes were compared among each of these groups.

Flow cytometry of peripheral blood

This was performed using a 10-color flow cytometer panel of antibodies for quantification of all major leukocyte populations (Supplementary Table 1) as previously published (22–25). Samples were run on the Beckman Coulter Gallios 3-laser, 10-color flow cytometer that was calibrated per the manufacturer's recommendations each day of use. List mode data (LMD) files were analyzed using Kaluza software version 1.2. Leukocyte populations of interest were colored by the representative gate or "backgated" using histograms of selected stained cell populations. Kaluza software was used to create radar plots. Leukocytes were quantified as: Cell count/microL = count ("Phenotype") X (Flow-Count Flourospheres/microL)/count. This allowed quantification of the absolute number and percentage of immune cells. The gating strategy is demonstrated in Figure 1.

Statistical analyses

Descriptive statistics were used to determine mean and standard deviation or median and range for continuous variables, and number and percentage for categorical variables. Comparisons of immune cells between different cohorts were evaluated for statistical significance via the student t-test. A p-value <0.05 was used to classify statistically significant, and a p-value <0.001 to classify highly statistically significant differences. All graphical representations and statistical analyses were performed in Prism 9.4.0 (GraphPad, San Diego, CA).

Results

Characteristics of thyroid cancer patients

In this cohort of 32 adult follicular cell-derived thyroid cancer patients followed for a median of 57.7 months from initial thyroid cancer surgery, the median age was 58 years (range 32, 85), all were non-Hispanic Caucasian, and 47% were females. Thyroid cancer was well-differentiated in 20 (62%), poorly differentiated in 5 (16%)

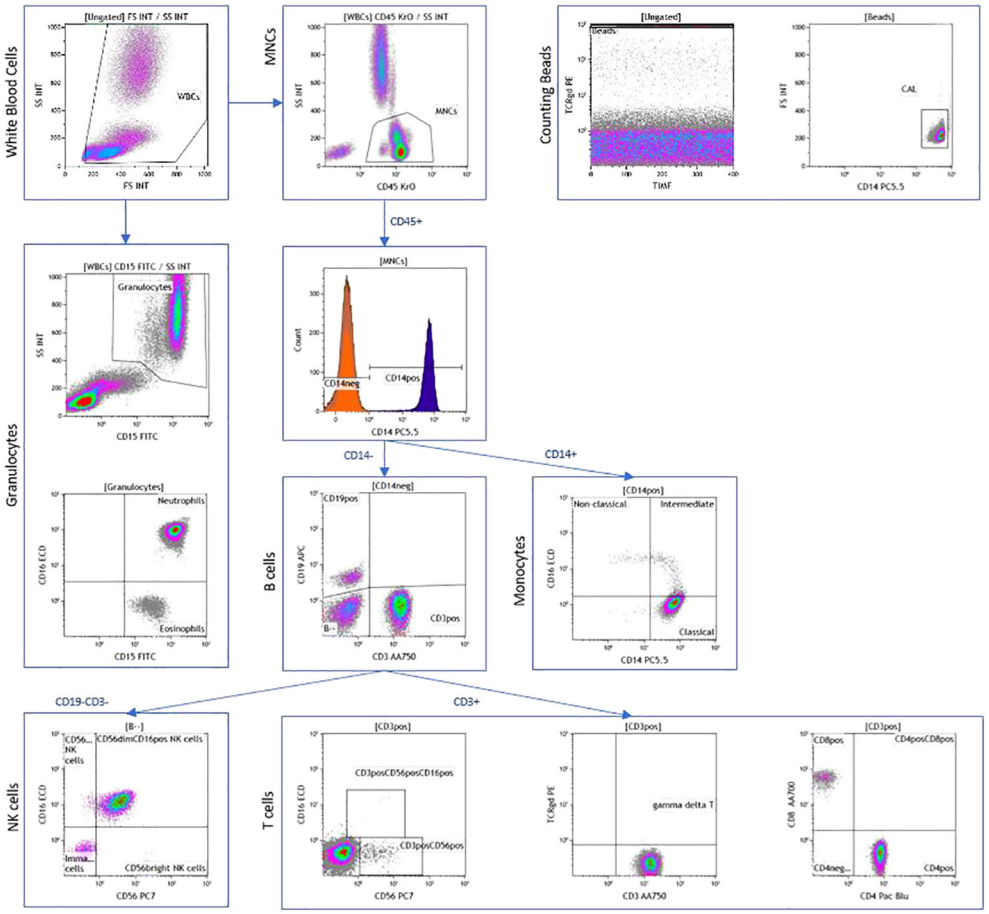

FIGURE 1
Peripheral blood immunophenotyping via flow cytometry demonstrating dot plots in a patient with AJCC TNM stage 4 and ATA high-risk follicular cell-derived thyroid cancer.

and anaplastic in 7 (22%). The most frequent AJCC stage was 4 (59%) and ATA risk of recurrence category was high in 18 (56%). Radioactive iodine (RAI) treatment was provided to 17 patients, and tyrosine kinase inhibitor (TKI) to 6 patients after the initial thyroid cancer surgery and blood draw for flow cytometry. The median overall survival was 20 years. The mortality rate was 19%, of which four had distant metastasis at presentation while the other two had distant spread during follow-up (Table 1). Due to few patients with ATA low risk cancer (n=4), we combined those with ATA low and intermediate risk when comparing immunophenotypes to high ATA risk group.

Circulating immunophenotype comparisons by AJCC stage of thyroid cancer

On immunophenotyping in the T cell, B cell, and NK cell panel, patients with AJCC stage 3/4 demonstrated overall fewer circulating mononuclear cells (CD45+) as compared to stage 1/2 (2210 vs. 2855 cells/microL; p=0.04). They also had more monocytes (CD14+) (579 cells/microL vs. 442 cells/microL; p=0.04) but fewer total lymphocytes (CD14-) (1632 cells/microL vs. 2413 cells/microL; p=0.01). Within the lymphocyte compartment, differences in lymphocyte populations were specific to the T cell compartment. Patients with stage 3/4 demonstrated fewer T cells (CD3+) (1111 cells/microL vs. 1770 cells/microL; p=0.007). In sub-populations of T cells, they exhibited fewer CD4+ T cells (646 cells/microL vs. 1165 cells/microL; p=0.002) gamma-delta T cells (40.8 cells/microL vs. 124 cells/microL; p=0.007) and natural killer (NK) T-like cells (CD3+CD56+) (3.43 cells/microL vs. 38.2 cells/microL; p=0.009), but there were no differences in CD8+ T cells or NK cells when compared to stage 1/2 (Figures 2A, B).

Upon further subtyping of T cells, there was a trend towards more Tregs (CD4+CD25hiCD127lo) among patients with AJCC stage 3/4 as compared to stage 1/2, but the difference was not statistically significant (p=0.06). We observed more circulating CD4+ effector memory T cells (CD4+CD45RO+CD62L-CCR7-) (23.9% vs. 9.7%; p=0.009) and CD8+ effector memory T cells (CD8+CD45RO+CD62L-CCR7-) (58.5% vs. 40.7%; p=0.02), but fewer CD4+ central memory T cells (CD4+CD45RO+CD62L+CCR7+) (49.6 vs. 69.5; p=0.002) and CD8+ central memory T cells (CD8+CD45RO+CD62L+CCR7+) in patients with stage 3/4 versus stage 1/2 disease (Figure 2C).

Stage 3/4 thyroid cancer patients also had more circulating myeloid-derived suppressor cells (MDSCs; Lin-CD33+HLADR-) as subset of mononuclear cells (2.63% vs. 1.54%; p=0.02) compared with stage1/2 (Figure 2D).

Circulating immunophenotype comparisons by ATA risk stratification of thyroid cancer

On immunophenotyping in the T cell, B cell, and NK cell panel, patients with ATA high-risk thyroid cancer demonstrated overall

TABLE 1 Demographic and clinical characteristics of 32 adult patients with follicular cell-derived thyroid cancer that underwent immunophenotyping by peripheral blood flow cytometry.

Characteristics (median, range or n, %)	Total sample = 32
Age, years	58.5 (32, 85)
Females	15 (46.9)
Caucasian race	32 (100)
Type of thyroid carcinoma	
Papillary	
Classic	11 (34.4)
Oncocytic variant	1 (3.1)
Follicular variant	2 (6.2)
Follicular	3 (9.4)
Hurthle cell	3 (9.4)
Poorly differentiated	5 (15.6)
Anaplastic	7 (21.9)
Autoimmune thyroid disease	
Hashimoto's (positive TPOAb or chronic lymphocytic thyroiditis on pathology)	4 (12.5)
Graves' (positive TRAb)	2 (6.2)
AJCC TNM stage*	
1	6 (18.7)
2	1 (3.1)
3	6 (18.7)
4a	6 (18.7)
4b	3 (9.4)
4c	10 (31.2)
T category*	
T1a	1 (3.1)
T1b	5 (15.6)
T2	3 (9.4)
T3	13 (40.6)
T4a	4 (12.5)
T4b	6 (18.7)
N category	
N0	3 (9.4)
N1a	6 (18.7)
N1b	23 (71.9)
M status	
M0	19 (59.4)
M1	14 (40.6)
ATA initial risk stratification	
Low	4 (12.5)
Intermediate	10 (31.2)
High	18 (56.3)
Radioactive iodine therapy	17 (53.1)*
Tyrosine kinase inhibitor therapy	6 (18.7) (n=4 also received RAI)
Duration from thyroidectomy to last follow-up or death (months)	57.7 (2, 491.8)
Disease status during follow-up	
Distant spread	21 (65.6)
Loco-regional stable	4 (12.5)
No evidence of disease	7 (21.9)
Mortality	6 (18.7)#
Median overall survival (months)	241.9

*n=8 ATA intermediate-risk and n=9 high-risk; n=11 M0 and n=6 M1; #all had distant spread and were ATA high-risk, n=4 of which also had M1 at surgery, all were AJCC TNM stage 4.

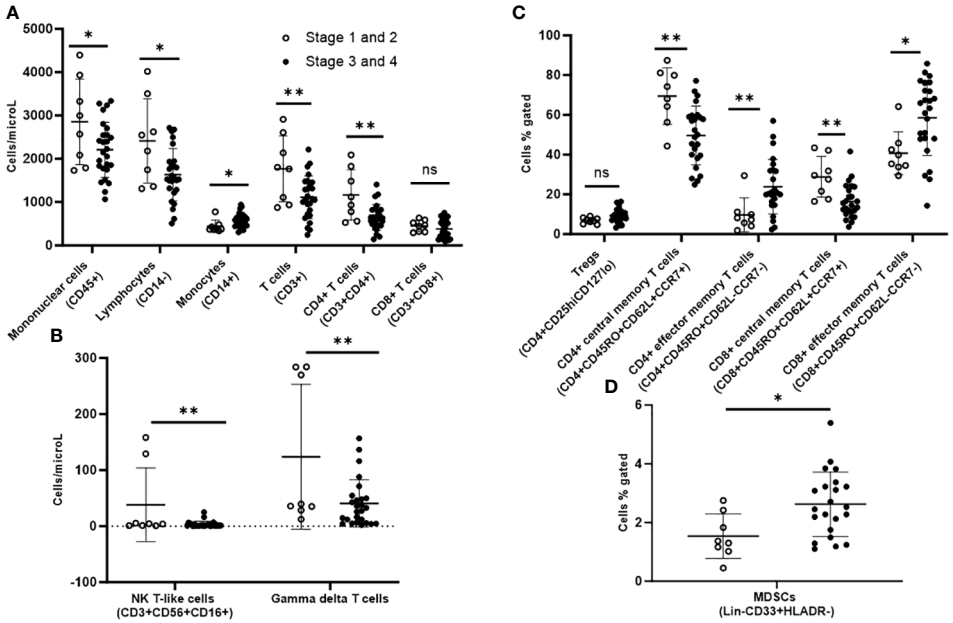

FIGURE 2
Peripheral blood immunophenotyping via flow cytometry comparing patients with AJCC TNM stages 3 and 4 versus stages 1 and 2 follicular cell-derived thyroid cancer. **(A)** shows immunophenotyping in the T cell, B cell and NK cell panel. **(B)** shows the NK T-like and gamma delta subpopulations of T cells. **(C)** shows further subtyping of T cells to characterize T regs and memory T cells. **(D)** shows MDSCs. *p<0.05; **p<0.01. NK cell: natural killer cell; Treg: T regulatory cell; MDSC: myeloid-derived suppressor cell.

fewer circulating mononuclear cells (CD45+) compared with ATA low/intermediate risk. They also had fewer total lymphocytes, and within the lymphocyte compartment, fewer T cells (CD3+) but no difference in B cells (CD19+). They also had fewer CD4+ T cells and gamma-delta T cells, but there were no differences in CD8+ T cells or NK cells compared with ATA low/intermediate-risk (Figures 3A, B).

Upon further subtyping of T cells, there was a trend towards more Tregs (CD4+CD25hiCD127lo) among patients with ATA

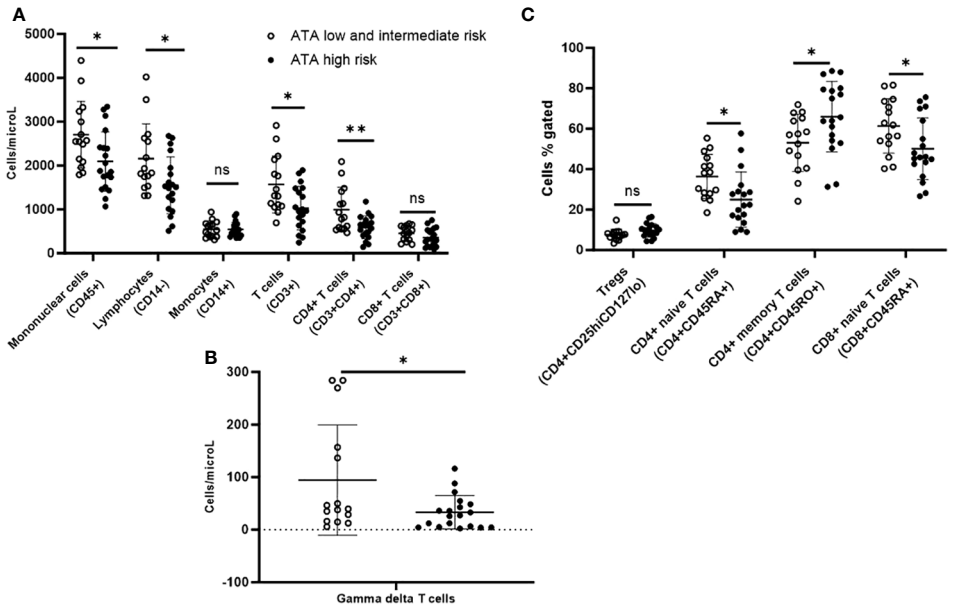

FIGURE 3
Peripheral blood immunophenotyping via flow cytometry comparing patients with ATA high-risk versus low/intermediate-risk of recurrence follicular cell-derived thyroid cancer. **(A)** shows immunophenotyping in the T cell, B cell and NK cell panel. **(B)** shows gamma delta subpopulation of T cells. **(C)** shows further subtyping of T cells to characterize T regs and memory T cells. *p<0.05; **p<0.01. NK cell: natural killer cell; Treg: T regulatory cell.

high compared to ATA low/intermediate risk, but the difference was not statistically significant (p=0.06). We observed more circulating CD4+ memory T cells (CD4+CD45RO+) (65.9% vs. 53.1%; p=0.03) and a non-significant trend for more CD8+ memory T cells (CD8+CD45RO+) (45.5% vs. 36.1%; p=0.06), but fewer CD4 + naive T cells (CD4+CD45RA+) (25% vs. 36.4%; p=0.014) and CD8+ naive T cells (CD8+CD45RA+) (50.1% vs. 61.4%; p=0.03) in ATA high-risk compared with ATA low/intermediate-risk patients (Figure 3C). There was a trend towards more MDSCs in ATA high-risk patients, but the difference was not statistically significant.

Circulating immunophenotype comparisons by course of thyroid cancer

During median follow-up of 57.7 years since initial thyroid cancer surgery, 21 patients demonstrated distant spread, of which 14 patients already had distant metastases during initial presentation. Due to the small sample of 6 patients that developed new distant metastases during follow-up, we compared 21 patients with any distant spread to 11 patients who had no evidence of disease or locoregional stable disease during this follow-up duration (Table 1). On immunophenotyping in the T cell, B cell, and NK cell panel, patients who demonstrated distant metastases during their disease course demonstrated overall fewer circulating mononuclear cells (CD45+) compared to those who had no evidence of disease or locoregional stable disease. They also had fewer total lymphocytes, and within the lymphocyte compartment, fewer T cells (CD3+) but no difference in B cells (CD19+). They had fewer CD4+ T cells and gamma-delta T cells, but there were no differences in CD8+ T cells or NK cells when compared to those with no evidence of disease or locoregional stable disease (Figures 4A, B).

Upon further subtyping of T cells, there was a trend towards more Tregs (CD4+CD25hiCD127lo) among patients who developed distant metastases during their disease course compared with those who had no evidence of disease or locoregional stable disease, but the difference was not statistically significant (p=0.06). We also observed more circulating CD4+ memory T cells (CD4+CD45RO+) (64.4% vs. 51.3%; p=0.03) but fewer CD4+ naive T cells (CD4+CD45RA+) (26.3% vs. 37.9%; p=0.02) in patients who developed distant metastases during their disease course compared with those who had no evidence of disease or locoregional stable disease (Figure 4C). There was a trend towards more MDSCs in these patients, but the difference was not statistically significant.

Additional circulating immunophenotype comparisons

There were no significant differences in the circulating immunophenotypes between patients treated when comparing patients based on age (55 years as cut-off), sex (male versus female), RAI treatment status (17 received versus the rest), TKI treatment status (6 received versus the rest). However, our sample of 32 subjects is not large enough to provide adequately powered conclusions from these negative results.

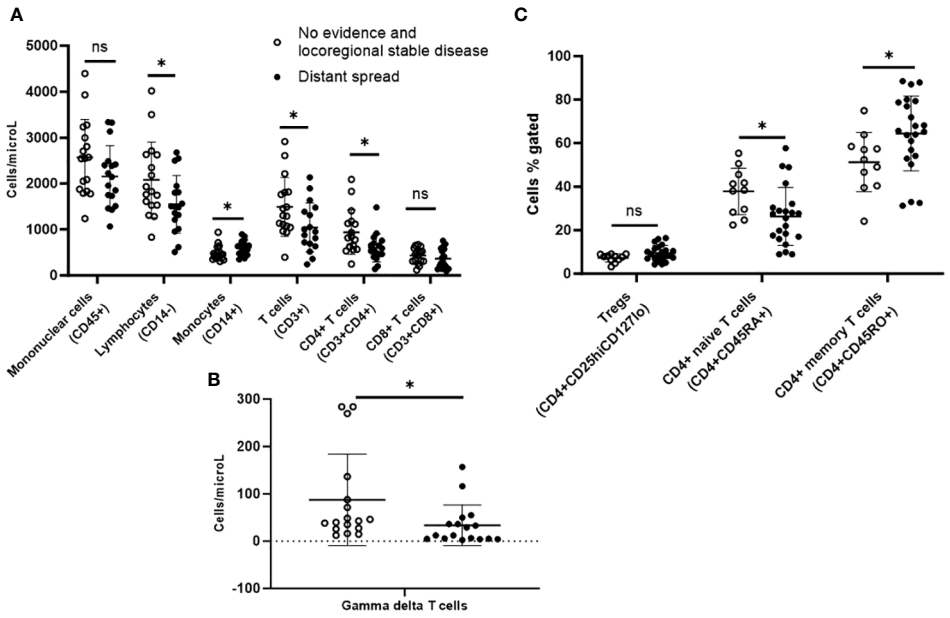

FIGURE 4
Peripheral blood immunophenotyping via flow cytometry comparing patients with distant metastases versus no recurrence or only loco-regional disease during follow-up follicular cell-derived thyroid cancer. *p<0.05; **p<0.01. **(A)** shows immunophenotyping in the T cell, B cell and NK cell panel. **(B)** gamma delta subpopulation of T cells. **(C)** shows further subtyping of T cells to characterize T regs and memory T cells. *p<0.05; **p<0.01. NK cell: natural killer cell; Treg: T regulatory cell.

Discussion

In this study of 32 adults with follicular cell-derived thyroid cancer, we demonstrated that circulating immunophenotypes serve as prognostic biomarkers. Overall, aggressive thyroid cancer at presentation or during follow-up was characterized by more immune suppressor cells (MDSCs and trend for Tregs) but fewer immune effector cells (CD4+ T cells, gamma-delta T cells and NK T-like cells) and altered memory T cell subtypes compared to less aggressive thyroid cancer. The immunophenotypes were not different based on sex or age of the patients. These findings prove our hypothesis that suppressor circulating immunophenotypes and altered T cell signaling portend a worse thyroid cancer prognosis.

Upon initial analysis, there was a down-regulation of T cell populations specifically in the CD4+ T cell compartment in patients with aggressive thyroid cancer defined as: i) AJCC TNM stage 3 or 4, ii) high risk of recurrence by ATA criteria, or iii) demonstrating distant metastases during follow-up. Available literature evaluating the presence of chronic lymphocytic thyroiditis in the tumor microenvironment without further identifying the specific cell types has demonstrated contradictory results in terms of its association with prognosis (11–14). Hence, we performed a more in-depth analysis of subsets of T cells and NK cells. There are conflicting data regarding the role of CD8+ cytotoxic T cells with one study demonstrating good (20) while another poor prognosis (21). In our study, the lower ratio of CD4/CD8, with significantly fewer CD4+ T cells but no significant difference in CD8+ T cells in patients with more aggressive disease supports the role of CD4+ cytotoxic and helper T cells in mediating immune response against cancer cells.

The lower number of circulating gamma-delta T cells in those with more aggressive thyroid cancer has not been reported in previous thyroid cancer studies of either the tumor microenvironment or peripheral blood. T lymphocytes expressing the gamma-delta form of the T-cell receptor are a distinct functional class whose physiologic role is not completely understood. Their activation results in cell proliferation, proinflammatory cytokine and chemokine secretion, and alteration of cell surface phenotypes (28). It has been postulated that they contribute more to immunoregulation and tissue repair than to immunoprotection (29). They contribute to the pathogenesis of autoimmune disorders, including autoimmune (Hashimoto's) thyroiditis (30). In addition, they have demonstrated an anti-tumor role via their antigen-presenting cell-like effects in gastric cancer (31) but to our knowledge, have not been evaluated in thyroid cancer. This significant finding of our study supports the hypothesis that the immune suppressor phenotype is associated with thyroid cancer aggressiveness. These cells should be investigated for avenues of immune upregulation.

Another important focus of our study was to identify MDSCs, which were significantly higher in those with stage 3 and 4 thyroid cancer and there was also a similar but non-significant trend in those with ATA high-risk and distant metastases on follow-up. MDSCs are a heterogeneous cell population that suppresses T cell and NK cell function. They arise from myeloid progenitor cells that do not differentiate into mature dendritic cells, granulocytes, or macrophages (32–34). They play a major role in immune evasion and tumor progression, however, a clear consensus on which phenotypes are most relevant in cancer patients has not been reached (34). Studies have demonstrated their immunosuppressive role in cancers including squamous head and neck cancer (35), breast cancer, and non-small cell lung cancer (36). We identified these cells as CD33+ and lineage negative (Lin-) meaning CD3-, CD14-, CD19-, and CD57- like previous studies (36). To our knowledge, only one study has evaluated circulating MDSCs in thyroid cancer patients demonstrating their association with clinicopathologically advanced thyroid cancer (16). Our results validate these findings suggesting that MDSCs are novel biomarkers for predicting aggressiveness of thyroid cancer at diagnosis and should be investigated as therapeutic targets in advanced thyroid cancer.

Tregs (CD4+CD25hiCD127lo) inhibit the anti-tumor response by producing IL-10 and expressing immune checkpoints CTLA-4 and PD-1, hence higher number of these cells in the circulation is associated with more aggressive thyroid cancer (15). The same study showed that PD-1+ T cells (15) were also elevated in more aggressive thyroid cancer. In our study, there was a trend towards more Tregs among patients with AJCC stage 3/4, ATA high-risk, and those that developed distant metastases, but the difference was not statistically significant. Due to the limited sample size, we cannot conclude if Tregs are associated with aggressive thyroid cancer or not. However, our findings support further investigation of their role in a larger cohort of thyroid cancer patients because they could be a potential target for immunotherapy that functions in an antagonistic manner.

In the literature, certain immunoregulatory subtypes of NK cells (CD3-CD16-CD56+)are reported to be associated with pathologically aggressive thyroid cancer (37), however, the main immune effector subtype of NK cells have been shown to clear cancerous cells with low MHC expression. We did not find significant differences in NK cells between the thyroid cancer subgroups; however, this could be a limitation of our sample size and characteristics. The NK T-like cells (CD3+CD56+) combine the characteristics of T (CD3+) and NK (CD56+) cells. The exact pathophysiological role of these cells remains unknown although literature has reported on their effector role in autoimmune diseases (38), and cytotoxic role against infectious diseases (39) and cancer (40, 41). They are reduced in circulation in patients with metastatic as compared to non-metastatic colorectal cancer (42) but have not been investigated in thyroid cancer. Their ability to clear cancerous cells with low MHC expression supports our investigation of their role in thyroid cancer. In our study, NK T-like cells were reduced in patients with advanced clinicopathologic thyroid cancer suggesting their cytotoxic role against tumor cells. Future studies should investigate ways for upregulating these cells as a novel form of therapy against advanced cancer.

In our study, advanced stage (III/IV) thyroid cancer at presentation was characterized by more effector memory T cells but fewer central memory T cells. These differences in subtypes of memory T cells were not significant when comparing by ATA risk or course during follow-up, but in general, there were more memory T cells and fewer naïve T cells in ATA high risk compared to low/intermediate risk and among patients who

developed distant metastases during their disease course compared with those who had no evidence of disease or locoregional stable disease. Since central memory T cells express the chemokine receptor CCR7, they traffic to lymph nodes and interact with dendritic cells. Effector memory T cells lacking CCR7 expression migrate to areas of inflamed tissue and display immediate effector function (43, 44). Studies have shown that in chronic infectious processes, there is a gradual shift in the composition of the memory T cell pool from an effector to a central memory phenotype (45, 46). Effector memory cells present an immediate, but not sustained, defense at pathogen sites of entry, whereas central memory T cells sustain the response by proliferating in the secondary lymphoid organs and producing a supply of new effectors (47–49) In addition, effector memory T cells are less efficient than central memory T cells at mediating recall responses in terms of proliferation and accumulation at inflammatory sites (46, 50). Hence, even though not definitively certain, the differences in these memory T cells observed in our study are consistent with the immune suppressor phenotype observed in aggressive thyroid cancer. CCR7 expression has been shown to be lower in poorly differentiated compared with differentiated thyroid cancer (51) which fits with more effector memory T cells (less CCR7) in advanced stages of thyroid cancer in our study. While previous studies have evaluated pathological aggressiveness, our study is novel in investigating this in a cohort predominantly comprised of differentiated thyroid cancer patients with adequate follow-up. Our results suggest that T cell trafficking is altered in advanced stages of thyroid cancer, thus shedding light on both the biology and potentially prognostic applications.

Our study is limited by its small sample size which precludes comparing immunophenotype differences between several types of follicular cell-derived thyroid cancer, stage 3 and 4 patients, and ATA intermediate and high-risk patients. The overall few events of distant progression do not allow us to evaluate the relationship between time to cancer progression and various immune phenotypes in this study. All patients being non-Hispanic Caucasian prevented us from analyzing differences by race or ethnicity. Additionally, the lack of significant differences in circulating immunophenotypes based on treatment with RAI or TKI, and lack of significant differences in Tregs or NK cells between various clinicopathologic subgroups could be due to inadequately powered sample size, hence should not be inferred as definitive lack of difference. Importantly, circulating immune phenotypes may not reflect the *in-situ* tumor microenvironment, including spatial relationships among immune cells. Tumor-associated macrophages are associated with poor outcomes such as lymph node metastases (52), larger tumor size (53) and reduced survival (54, 55), but are not enough in circulation to perform comparisons, hence these and other tumor-infiltrating immune cells should be the focus of further research on tumor and tumor-adjacent tissue to characterize the thyroid cancer tumor microenvironment. Also, we did not perform an investigation of intracellular factors or functionality of immune cells in our study, did not serially analyze the immunophenotypes over the course of disease or compare them to inflammatory thyroid diseases. The heterogeneity in our results and the overlap in immunophenotypes between the compared groups despite significant differences are also limitations. Hence, future studies with larger cohorts of thyroid cancer patients are required to investigate these important factors in thyroid cancer prognostication. Our pilot study's strengths include its prospective nature, comprehensiveness of immunophenotyping, evaluation of clinically important outcomes, being the first to demonstrate fewer gamma-delta T cells and NK T-like cells, and only the second to demonstrate more circulating MDSCs amongst patients with advanced thyroid cancer. These findings provide a strong basis for further investigation into the immune phenotypes in circulation and tumor microenvironment in a larger cohort of patients with thyroid cancer.

In conclusion, we have demonstrated that aggressive follicular cell-derived thyroid cancer either at presentation or during the disease course is associated with circulating suppressor immunophenotypes characterized by fewer CD4+ T cells, gamma-delta T cells, and NK T-like cells but more MDSCs; and altered memory T cell subtypes. These immunophenotypes serve as prognostic biomarkers for advanced thyroid cancer. Future studies with larger cohorts should evaluate the changes in circulating and tumor-infiltrating immunophenotypes with thyroid cancer progression and investigate the role of immunotherapies antagonistic to MDSCs and Tregs while upregulating NK T-like and gamma-delta T cells as well as influencing T cell signaling in advanced thyroid cancer.

Data availability statement

The original contributions presented in the study are included in the article/Supplementary Material. Further inquiries can be directed to the corresponding author.

Ethics statement

The studies involving humans were approved by Mayo Clinic Institutional Review Board. The studies were conducted in accordance with the local legislation and institutional requirements. The participants provided their written informed consent to participate in this study.

Author contributions

AK: Data curation, Formal analysis, Investigation, Methodology, Validation, Visualization, Writing – original draft, Writing – review & editing. MG: Data curation, Formal analysis, Investigation, Methodology, Resources, Software, Validation, Visualization, Writing – review & editing. SB: Formal analysis,

Investigation, Methodology, Project administration, Validation, Visualization, Writing – review & editing. AD: Conceptualization, Methodology, Resources, Supervision, Validation, Writing – review & editing. DD: Data curation, Methodology, Visualization, Writing – review & editing. MR: Conceptualization, Data curation, Formal analysis, Funding acquisition, Investigation, Methodology, Project administration, Resources, Software, Supervision, Validation, Visualization, Writing – original draft, Writing – review & editing.

Funding

The author(s) declare financial support was received for the research, authorship, and/or publication of this article. This publication was made possible by CTSA Grant Number UL1 TR002377 from the National Center for Advancing Translational Sciences (NCATS), a component of the National Institutes of Health (NIH); and Mayo Foundation Small Grants Program. The abstract of this study was presented as an oral presentation at ENDO 2021, the annual meeting of the Endocrine Society.

Conflict of interest

The authors declare that the research was conducted in the absence of any commercial or financial relationships that could be construed as a potential conflict of interest.

Publisher's note

Supplementary material

The Supplementary Material for this article can be found online at: https://www.frontiersin.org/articles/10.3389/fimmu.2023.1325343/full#supplementary-material

References

1. Wang LY, Palmer FL, Nixon IJ, Thomas D, Patel SG, Shaha AR, et al. Multi-organ distant metastases confer worse disease-specific survival in differentiated thyroid cancer. *Thyroid* (2014) 24(11):1594–9. doi: 10.1089/thy.2014.0173

2. Haugen BR, Alexander EK, Bible KC, Doherty GM, Mandel SJ, Nikiforov YE, et al. 2015 american thyroid association management guidelines for adult patients with thyroid nodules and differentiated thyroid cancer: the american thyroid association guidelines task force on thyroid nodules and differentiated thyroid cancer. *Thyroid* (2016) 26(1):1–133. doi: 10.1089/thy.2015.0020

3. Albero A, Lopéz JE, Torres A, de la Cruz L, Martín T. Effectiveness of chemotherapy in advanced differentiated thyroid cancer: a systematic review. *Endocr Relat Cancer* (2016) 23(2):R71–84. doi: 10.1530/ERC-15-0194

4. Lubin D, Baraban E, Lisby A, Jalali-Farahani S, Zhang P, Livolsi V. Papillary thyroid carcinoma emerging from hashimoto thyroiditis demonstrates increased PD-L1 expression, which persists with metastasis. *Endocr Pathol* (2018) 29(4):317–23. doi: 10.1007/s12022-018-9540-9

5. Ahn S, Kim TH, Kim SW, Ki CS, Jang HW, Kim JS, et al. Comprehensive screening for PD-L1 expression in thyroid cancer. *Endocr Relat Cancer* (2017) 24 (2):97–106. doi: 10.1530/ERC-16-0421

6. Iyer PC, Dadu R, Gule-Monroe M, Busaidy NL, Ferrarotto R, Habra MA, et al. Salvage pembrolizumab added to kinase inhibitor therapy for the treatment of anaplastic thyroid carcinoma. *J ImmunoTherapy Cancer* (2018) 6(1):68. doi: 10.1186/s40425-018-0378-y

7. Mehnert JM, Varga A, Brose MS, Aggarwal RR, Lin C-C, Prawira A, et al. Safety and antitumor activity of the anti-PD-1 antibody pembrolizumab in patients with advanced, PD-L1-positive papillary or follicular thyroid cancer. *BMC Cancer* (2019) 19 (1):196–6. doi: 10.1186/s12885-019-5380-3

8. Gunda V, Gigliotti B, Ndishabandi D, Ashry T, McCarthy M, Zhou Z, et al. Combinations of BRAF inhibitor and anti-PD-1/PD-L1 antibody improve survival and tumour immunity in an immunocompetent model of orthotopic murine anaplastic thyroid cancer. *Br J Cancer* (2018) 119(10):1223–32. doi: 10.1038/s41416-018-0296-2

9. Matsubayashi S, Kawai K, Matsumoto Y, Mukuta T, Morita T, Hirai K, et al. The correlation between papillary thyroid carcinoma and lymphocytic infiltration in the thyroid gland. *J Clin Endocrinol Metab* (1995) 80(12):3421–4.

10. McLeod DSA, Bedno SA, Cooper DS, Hutfless SM, Ippolito S, Jordan SJ, et al. Pre-existing thyroid autoimmunity and risk of papillary thyroid cancer: A nested case-control study of US active-duty personnel. *J Clin Oncol* (2022) 40(23):2578–87. doi: 10.1200/JCO.21.02618

11. Loh KC, Greenspan FS, Dong F, Miller TR, Yeo PP. Influence of lymphocytic thyroiditis on the prognostic outcome of patients with papillary thyroid carcinoma. *J Clin Endocrinol Metab* (1999) 84(2):458–63. doi: 10.1210/jcem.84.2.5443

12. Kashima K, Yokoyama S, Noguchi S, Murakami N, Yamashita H, Watanabe S, et al. Chronic thyroiditis as a favorable prognostic factor in papillary thyroid carcinoma. *Thyroid* (1998) 8(3):197–202. doi: 10.1089/thy.1998.8.197

13. Gupta S, Patel A, Folstad A, Fenton C, Dinauer CA, Tuttle RM, et al. Infiltration of differentiated thyroid carcinoma by proliferating lymphocytes is associated with improved disease-free survival for children and young adults. *J Clin Endocrinol Metab* (2001) 86(3):1346–54. doi: 10.1210/jc.86.3.1346

14. Pellegriti G, Belfiore A, Giuffrida D, Lupo L, Vigneri R. Outcome of differentiated thyroid cancer in Graves' patients. *J Clin Endocrinol Metab* (1998) 83(8):2805–9. doi: 10.1210/jc.83.8.2805

15. French JD, Kotnis GR, Said S, Raeburn CD, McIntyre RC Jr, Klopper JP, et al. Programmed death-1+ T cells and regulatory T cells are enriched in tumor-involved lymph nodes and associated with aggressive features in papillary thyroid cancer. *J Clin Endocrinol Metab* (2012) 97(6):E934–43. doi: 10.1210/jc.2011-3428

16. Angell TE, Lechner MG, Smith AM, Martin SE, Groshen SG, Maceri DR, et al. Circulating myeloid-derived suppressor cells predict differentiated thyroid cancer diagnosis and extent. *Thyroid* (2016) 26(3):381–9. doi: 10.1089/thy.2015.0289

17. Means C, Clayburgh DR, Maloney L, Sauer D, Taylor MH, Shindo ML, et al. Tumor immune microenvironment characteristics of papillary thyroid carcinoma are associated with histopathological aggressiveness and BRAF mutation status. *Head Neck* (2019) 41(8):2636–46. doi: 10.1002/hed.25740

18. Ahn J, Jin M, Song E, Ryu YM, Song DE, Kim SY, et al. Immune profiling of advanced thyroid cancers using fluorescent multiplex immunohistochemistry. *Thyroid* (2021) 31(1):61–7. doi: 10.1089/thy.2020.0312

19. Giannini R, Moretti S, Ugolini C, Macerola E, Menicali E, Nucci N, et al. Immune profiling of thyroid carcinomas suggests the existence of two major phenotypes: an ATC-like and a PDTC-like. *J Clin Endocrinol Metab* (2019) 104 (8):3557–75. doi: 10.1210/jc.2018-01167

20. Cunha LL, Morari EC, Guihen AC, Razolli D, Gerhard R, Nonogaki S, et al. Infiltration of a mixture of immune cells may be related to good prognosis in patients with differentiated thyroid carcinoma. *Clin Endocrinol (Oxf)* (2012) 77(6):918–25. doi: 10.1111/j.1365-2265.2012.04482.x

21. Cunha LL, Marcello MA, Nonogaki S, Morari EC, Soares FA, Vassallo J, et al. CD8+ tumour-infiltrating lymphocytes and COX2 expression may predict relapse in differentiated thyroid cancer. *Clin Endocrinol (Oxf)* (2015) 83(2):246–53. doi: 10.1111/cen.12586

22. Delivanis DA, Gustafson MP, Bornschlegl S, Merten MM, Kottschade L, Withers S, et al. Pembrolizumab-induced thyroiditis: comprehensive clinical review and insights into underlying involved mechanisms. *J Clin Endocrinol Metab* (2017) 102(8):2770–80. doi: 10.1210/jc.2017-00448

23. Gustafson MP, Lin Y, Maas ML, Van Keulen VP, Johnston PB, Peikert T, et al. A method for identification and analysis of non-overlapping myeloid immunophenotypes in humans. *PloS One* (2015) 10(3):e0121546. doi: 10.1371/journal.pone.0121546

24. Bornschlegl S, Gustafson MP, Delivanis DA, Ryder M, Liu MC, Vasmatzis G, et al. Categorisation of patients based on immune profiles: a new approach to identifying candidates for response to checkpoint inhibitors. *Clin Transl Immunol* (2021) 10(4):e1267. doi: 10.1002/cti2.1267

25. Kotwal A, Gustafson MP, Bornschlegl S, Kottschade L, Delivanis DA, Dietz AB, et al. Immune checkpoint inhibitor-induced thyroiditis is associated with increased intrathyroidal T lymphocyte subpopulations. *Thyroid* (2020) 30(10):1440–50. doi: 10.1089/thy.2020.0075

26. Wells SA Jr., Asa SL, Dralle H, Elisei R, Evans DB, Gagel RF, et al. Revised American Thyroid Association guidelines for the management of medullary thyroid carcinoma. *Thyroid Off J Am Thyroid Assoc* (2015) 25(6):567–610. doi: 10.1089/thy.2014.0335

27. Amin MB, Edge SB, Greene FL, Byrd DR, Brookland RK, Washington MK, et al. *AJCC cancer staging manual*. New York: Springer (2017).

28. Ribot JC, debarros A, Silva-Santos B. Searching for "signal 2": costimulation requirements of γδ T cells. *Cell Mol Life Sci* (2011) 68(14):2345–55. doi: 10.1007/s00018-011-0698-2

29. Hayday AC. [gamma][delta] cells: a right time and a right place for a conserved third way of protection. *Annu Rev Immunol* (2000) 18:975–1026. doi: 10.1146/annurev.immunol.18.1.975

30. Liu H, Zheng T, Mao Y, Xu C, Wu F, Bu L, et al. γδ T cells enhance B cells for antibody production in Hashimoto's thyroiditis, and retinoic acid induces apoptosis of the γδ T cell. *Endocrine* (2016) 51(1):113–22. doi: 10.1007/s12020-015-0631-9

31. Mao C, Mou X, Zhou Y, Yuan G, Xu C, Liu H, et al. Tumor-activated TCRγδ$^+$ T cells from gastric cancer patients induce the antitumor immune response of TCRαβ$^+$ T cells via their antigen-presenting cell-like effects. *J Immunol Res* (2014) 2014:593562. doi: 10.1155/2014/593562

32. Gabrilovich DI, Nagaraj S. Myeloid-derived suppressor cells as regulators of the immune system. *Nat Rev Immunol* (2009) 9(3):162–74. doi: 10.1038/nri2506

33. Gabrilovich DI, Ostrand-Rosenberg S, Bronte V. Coordinated regulation of myeloid cells by tumours. *Nat Rev Immunol* (2012) 12(4):253–68. doi: 10.1038/nri3175

34. Diaz-Montero CM, Finke J, Montero AJ. Myeloid-derived suppressor cells in cancer: therapeutic, predictive, and prognostic implications. *Semin Oncol* (2014) 41(2):174–84. doi: 10.1053/j.seminoncol.2014.02.003

35. Pak AS, Wright MA, Matthews JP, Collins SL, Petruzzelli GJ, Young MR. Mechanisms of immune suppression in patients with head and neck cancer: presence of CD34(+) cells which suppress immune functions within cancers that secrete granulocyte-macrophage colony-stimulating factor. *Clin Cancer Res* (1995) 1(1):95–103.

36. Almand B, Clark JI, Nikitina E, van Beynen J, English NR, Knight SC, et al. Increased production of immature myeloid cells in cancer patients: a mechanism of immunosuppression in cancer. *J Immunol* (2001) 166(1):678–89. doi: 10.4049/jimmunol.166.1.678

37. Gogali F, Paterakis G, Rassidakis GZ, Liakou CI, Liapi C. CD3(-)CD16(-)CD56(bright) immunoregulatory NK cells are increased in the tumor microenvironment and inversely correlate with advanced stages in patients with papillary thyroid cancer. *Thyroid* (2013) 23(12):1561–8. doi: 10.1089/thy.2012.0560

38. Lin S-J, Chen J-Y, Kuo M-L, Hsiao H-S, Lee P-T, Huang J-L. Effect of interleukin-15 on CD11b, CD54, and CD62L expression on natural killer cell and natural killer T-like cells in systemic lupus erythematosus. *Med Inflamm* (2016) 2016:9675861. doi: 10.1155/2016/9675861

39. Srivastava R, Aggarwal R, Bhagat MR, Chowdhury A, Naik S. Alterations in natural killer cells and natural killer T cells during acute viral hepatitis E. *J Viral Hepatitis* (2008) 15(12):910–6. doi: 10.1111/j.1365-2893.2008.01036.x

40. Almeida J-S, Couceiro P, López-Sejas N, Alves V, Růžičková L, Tarazona R, et al. NKT-like (CD3+CD56+) cells in chronic myeloid leukemia patients treated with tyrosine kinase inhibitors. *Front Immunol* (2019) 10. doi: 10.3389/fimmu.2019.02493

41. ZdrazilovaDubska L, Valik D, Budinska E, Frgala T, Bacikova L, Demlova R. NKT-like cells are expanded in solid tumour patients. *cytokines* (2012) 5:8.

42. Gharagozloo M, Rezaei A, Kalantari H, Bahador A, Hassannejad N, Maracy M, et al. Decline in peripheral blood NKG2D+CD3+CD56+ NKT cells in metastatic colorectal cancer patients. *Bratisl Lek Listy* (2018) 119(1):6–11. doi: 10.4149/BLL_2018_002

43. Marelli-Berg FM, Fu H, Vianello F, Tokoyoda K, Hamann A. Memory T-cell trafficking: new directions for busy commuters. *Immunology* (2010) 130(2):158–65. doi: 10.1111/j.1365-2567.2010.03278.x

44. Sallusto F, Lenig D, Förster R, Lipp M, Lanzavecchia A. Two subsets of memory T lymphocytes with distinct homing potentials and effector functions. *Nature* (1999) 401(6754):708–12. doi: 10.1038/44385

45. Usherwood EJ, Hogan RJ, Crowther G, Surman SL, Hogg TL, Altman JD, et al. Functionally heterogeneous CD8(+) T-cell memory is induced by Sendai virus infection of mice. *J Virol* (1999) 73(9):7278–86. doi: 10.1128/JVI.73.9.7278-7286.1999

46. Wherry EJ, Teichgräber V, Becker TC, Masopust D, Kaech SM, Antia R, et al. Lineage relationship and protective immunity of memory CD8 T cell subsets. *Nat Immunol* (2003) 4(3):225–34. doi: 10.1038/ni889

47. Berenzon D, Schwenk RJ, Letellier L, Guebre-Xabier M, Williams J, Krzych U. Protracted protection to Plasmodium berghei malaria is linked to functionally and phenotypically heterogeneous liver memory CD8+ T cells. *J Immunol* (2003) 171(4):2024–34. doi: 10.4049/jimmunol.171.4.2024

48. Harris NL, Watt V, Ronchese F, Le Gros G. Differential T cell function and fate in lymph node and nonlymphoid tissues. *J Exp Med* (2002) 195(3):317–26. doi: 10.1084/jem.20011558

49. Hengel RL, Thaker V, Pavlick MV, Metcalf JA, Dennis G, Yang J, et al. Cutting edge: L-selectin (CD62L) expression distinguishes small resting memory CD4+ T cells that preferentially respond to recall antigen. *J Immunol* (2003) 170(1):28–32. doi: 10.4049/jimmunol.170.1.28

50. Roberts AD, Ely KH, Woodland DL. Differential contributions of central and effector memory T cells to recall responses. *J Exp Med* (2005) 202(1):123–33. doi: 10.1084/jem.20050137

51. Sancho M, Vieira JM, Casalou C, Mesquita M, Pereira T, Cavaco BM, et al. Expression and function of the chemokine receptor CCR7 in thyroid carcinomas. *J Endocrinol* (2006) 191(1):229–38. doi: 10.1677/joe.1.06688

52. Fang W, Ye L, Shen L, Cai J, Huang F, Wei Q, et al. Tumor-associated macrophages promote the metastatic potential of thyroid papillary cancer by releasing CXCL8. *Carcinogenesis* (2014) 35(8):1780–7. doi: 10.1093/carcin/bgu060

53. Kim BH. The expression of tumor-associated macrophages in papillary thyroid carcinoma. *Endocrinol Metab (Seoul)* (2013) 28(3):178–9. doi: 10.3803/EnM.2013.28.3.178

54. Ryder M, Ghossein RA, Ricarte-Filho JC, Knauf JA, Fagin JA. Increased density of tumor-associated macrophages is associated with decreased survival in advanced thyroid cancer. *Endocr Relat Cancer* (2008) 15(4):1069–74. doi: 10.1677/ERC-08-0036

55. Jung KY, Cho SW, Kim YA, Kim D, Oh BC, Park DJ, et al. Cancers with higher density of tumor-associated macrophages were associated with poor survival rates. *J Pathol Transl Med* (2015) 49(4):318–24. doi: 10.4132/jptm.2015.06.01

frontiers | Frontiers in Oncology

TYPE Original Research
PUBLISHED 03 January 2024
DOI 10.3389/fonc.2023.1296948

OPEN ACCESS

EDITED BY
Paulo Rodrigues-Santos,
University of Coimbra, Portugal

REVIEWED BY
Angelika B. Riemer,
German Cancer Research Center (DKFZ), Germany
Rridha Oueslati,
University Carthage, Tunisia
Lindsay Grey Cowell,
University of Texas Southwestern Medical Center, United States

*CORRESPONDENCE
Shreerang A. Bhide
shreerang.bhide@icr.ac.uk

†These authors have contributed equally to this work and share senior authorship

RECEIVED 19 September 2023
ACCEPTED 28 November 2023
PUBLISHED 03 January 2024

CITATION
Nenclares P, Larkeryd A, Manodoro F, Lee JY, Lalondrelle S, Gilbert DC, Punta M, O'Leary B, Rullan A, Sadanandam A, Chain B, Melcher A, Harrington KJ and Bhide SA (2024) T-cell receptor determinants of response to chemoradiation in locally-advanced HPV16-driven malignancies. *Front. Oncol.* 13:1296948. doi: 10.3389/fonc.2023.1296948

T-cell receptor determinants of response to chemoradiation in locally-advanced HPV16-driven malignancies

Pablo Nenclares[1,2], Adrian Larkeryd[3], Floriana Manodoro[4], Jen Y. Lee[1], Susan Lalondrelle[1], Duncan C. Gilbert[5], Marco Punta[6], Ben O'Leary[1,2], Antonio Rullan[1,2], Anguraj Sadanandam[7], Benny Chain[8], Alan Melcher[1†], Kevin J. Harrington[1,2†] and Shreerang A. Bhide[1,2*†]

[1]Radiotherapy and Imaging Division, The Institute of Cancer Research, London, United Kingdom, [2]Head and Neck Unit, The Royal Marsden Hospital, London, United Kingdom, [3]Bioinformatics Unit, The Centre for Translational Immunotherapy, The Institute of Cancer Research, London, United Kingdom, [4]Genomics Facility, The Institute of Cancer Research, London, United Kingdom, [5]Sussex Cancer Centre, University Hospitals Sussex NHS Foundation Trust, Brighton, United Kingdom, [6]Unit of Immunogenetic, Leukemia Genomics and Immunobiology, IRCCS Ospedale San Raffaele, Milan, Italy, [7]Systems and Precision Cancer Medicine Team, The Institute of Cancer Research, London, United Kingdom, [8]Division of Infection and Immunity, University College London, London, United Kingdom

Background: The effect of chemoradiation on the anti-cancer immune response is being increasingly acknowledged; however, its clinical implications in treatment responses are yet to be fully understood. Human papillomavirus (HPV)-driven malignancies express viral oncogenic proteins which may serve as tumor-specific antigens and represent ideal candidates for monitoring the peripheral T-cell receptor (TCR) changes secondary to chemoradiotherapy (CRT).

Methods: We performed intra-tumoral and pre- and post-treatment peripheral TCR sequencing in a cohort of patients with locally-advanced HPV16-positive cancers treated with CRT. An in silico computational pipeline was used to cluster TCR repertoire based on epitope-specificity and to predict affinity between these clusters and HPV16-derived epitopes.

Results: Intra-tumoral repertoire diversity, intra-tumoral and post-treatment peripheral CDR3β similarity clustering were predictive of response. In responders, CRT triggered an increase peripheral TCR clonality and clonal relatedness. Post-treatment expansion of baseline peripheral dominant TCRs was associated with response. Responders showed more baseline clustered structures of TCRs maintained post-treatment and displayed significantly more maintained clustered structures. When applying clustering by TCR-specificity methods, responders displayed a higher proportion of intra-tumoral TCRs predicted to recognise HPV16 peptides.

Conclusions: Baseline TCR characteristics and changes in the peripheral T-cell clones triggered by CRT are associated with treatment outcome. Maintenance

and boosting of pre-existing clonotypes are key elements of an effective anti-cancer immune response driven by CRT, supporting a paradigm in which the immune system plays a central role in the success of CRT in current standard-of-care protocols.

KEYWORDS

human papillomavirus, radiotherapy, T-cell receptor, cervical cancer, anal cancer, head and neck cancer

1 Introduction

Chemoradiotherapy (CRT) is the cornerstone of treatment for locally-advanced malignancies related to human papillomavirus (HPV) infection, including head and neck squamous cell (HNSCC), anal squamous cell (ASCC) and cervical carcinomas (CC). Despite being a highly effective therapy for most patients, around 15 to 25% of those diagnosed with locoregionally advanced disease will relapse within 5 years of treatment (1–3). Increasing evidence suggests that CRT plays a role in the anti-cancer immune response, promoting a number of anti-tumor immune mechanisms such as improved antigen cross-presentation, increased type I interferon release, enhanced expression of major histocompatibility complex (MHC) class I on tumor cells, recruitment and maturation of dendritic cells, promotion of the infiltration of lymphocytes into the tumor and augmentation of cytotoxic T cell activation (4, 5). However, whether these processes have any clinical relevance in the response to CRT remains unclear. Several studies have investigated intra-tumoral and peripheral adaptive responses to immunotherapy, but there is a dearth of similar studies in the context of CRT (6–11).

T-cell receptor (TCR) sequencing has emerged as a powerful new method in the analysis of the host-tumor interaction, which partially enables the characterization of the dynamics of the adaptive anti-cancer immune response (12, 13). We hypothesized that, since anti-cancer immune responses, including those promoted by radiotherapy, can mirror normal defensive responses to pathogens, it might be possible to study patient responses to CRT by monitoring peripheral T-cell clonal dynamics during treatment (14). In this study, we used HPV16-driven cancers diagnosed at a locally-advanced stage and treated with curative-intent standard-of-care CRT as a model for investigating TCR metrics and dynamics that may be linked with patient response.

HPV-related malignancies are distinguished by the expression of viral oncoproteins, such as E2, E5, E6 and E7, which can serve as tumor-specific antigens (15–18). Within the different high-risk HPV subtypes, HPV16 is the most frequently associated with oropharyngeal (85%), cervical (55%) and anal carcinomas (90%) (19–21). Given the favorable prognosis associated with HPV-positive HNSCC, the concept of de-escalation strategies has been developed to reduce treatment-related long-term toxicities whilst maintaining excellent survival outcomes (22). However, there is mounting evidence that HPV-positive tumors are not uniform and that differences in the phenotype and immune response between distinct HPV-driven tumors subtypes have an impact on prognosis and survival, suggesting that different treatment approaches might be required (23, 24). Taking this into consideration, anti-PD-1/PDL-1 based therapies and therapeutic HPV vaccination in the neoadjuvant and adjuvant setting for HPV-mediated cancers have attracted research attention with the aim of improving responses to CRT (25). Nevertheless, published results of Phase III randomized trials tell a cautionary tale of treatment de-escalation, and negative results from Phase III randomized trials of anti-PD-1/PDL-1 based therapies in the concurrent and/or adjuvant setting, ultimately highlight the importance of further investigation into the effect of CRT on antigen-specific immune responses (26, 27).

In the current study, we set out to sequence the T-cell complementarity-determining region 3 of the β-chain (CDR3β) in both the pre-treatment tumor-infiltrating lymphocytes (TILs) and pre- and post-treatment peripheral blood mononuclear cells (PBMCs) among a cohort of patients with HPV-related cancers treated with standard-of-care radical CRT. We characterized the diversity, clonality and degree of sequence similarity of the TCR repertoire and looked for associations between different metrics and response to CRT. In addition, we performed in silico antigen-specificity clustering and bioinformatically tested for affinity between HPV16-derived antigens predicted to be presented according to the individual MHC complex of each patient and these clusters. Overall, the approach of TCR profiling presented here enables a comprehensive analysis of the T-cell repertoire and the identification of some relevant determinants of response to CRT. Our results identify several repertoire features which associate the response to therapy. These features provide further biological understanding of the anti-cancer T-cell immune responses in HPV-driven malignancies and may lead to improved selection of patients for de-escalation strategies or intensification with adjuvant immunotherapy.

2 Materials and methods

2.1 Study design

CCR4157 is a single-arm, translational, sample collection study of standard-of-care CRT in locally-advanced HPV-positive

malignancies including HNSCC, ASCC and CC. Informed consent was obtained from all eligible patients with stage III/IVB HNSCC, stage II/IIIB (AJCC 2007) ASCC and stage IIB/IVA (FIGO) CC. Institutional board and ethics committee (ref. no. 14/NE/1055) approved the study. In all cases, radiotherapy was delivered using simultaneous integrated boost-IMRT technique. All HNSCC patients were treated with doses of 65 Gy in 30 fractions (2.17 Gy/fraction) to the primary target and doses to the elective target were 54 Gy in 30 fractions (1.8 Gy/fraction) over 6 weeks. All HNSCC patients received concurrent cisplatin 100 mg/m^2 days 1 and 29). Radiotherapy for CC patients included external beam radiotherapy (total dose of 45 Gy in 28 fractions and boost to the involved nodes to total dose of 55-57 Gy) followed by intrauterine brachytherapy treatment to a total combined dose > 85 Gy EQD2. CC patients received weekly cisplatin (40 mg/m^2). Radiotherapy for the ASCC cohort was planned as per UK IMRT anal cancer guidelines and prescribed to a total dose of 53.2 Gy (50.4 Gy for stage II disease) to the primary disease, 50.4 Gy to the affected lymph nodes and 40 Gy to elective volume, administered in 28 days over 38 days. All patients diagnosed with ASCC received concurrent mitomycin C 12 mg/m^2 on day 1 and oral capecitabine 825 mg/m^2 BID on each radiotherapy day. At 12 weeks, response following treatment was assessed by clinical examination and ^{18}F-FDG PET-CT. Residual or equivocal uptake at primary and distant sites was confirmed with a biopsy.

Patients were classified as responders if they achieved a complete response (CR) in ^{18}F-FDG PET-CT 12 weeks following completion of radical CRT and there was no evidence of relapse within the next 5 years after treatment. Patients were considered non-responders if the ^{18}F-FDG PET-CT showed evidence of local and/or regional residual disease or progressive disease (which was subsequently histologically confirmed) and/or the patient showed histologically confirmed evidence of local, regional or distant relapse within the first year after completion of radical CRT. Patient with local, regional, or distant relapse within 2 to 5 years following completion of CRT were excluded from this sub-analysis.

Sample estimation was based on the hypothesis that both groups (responders and non-responders) would present a standard deviation (SD) in the clonality (1-normalised Shannon Index) of 0.4 and that the study would be able to detect a difference of 0.6 in the mean clonality values. This assumption was based on internal (not previously published) preliminary data of a small cohort of patients not included in this study. The required sample size based on these values was 8 patients for each group with a confidence level of 95%, a power of 80% and a two-sided contrast.

2.2 Sample collection

Tumor tissue was collected via biopsy at baseline. Serial blood samples were collected at baseline (pre-CRT), 6 weeks and 12 weeks following completion of CRT. Twenty milliliters of blood collected in Streck® tubes was centrifuge at 1,600 rpm for 10 min within 3 hours of collection and plasma and buffy coats were isolated and kept frozen at -80°C prior to DNA extraction.

2.3 Nucleic acid extraction

Five 10μm unstained slides and one hematoxylin and eosin-stained slides were obtained from representative formalin fixed paraffin embedded (FFPE) tumor blocks. Experienced pathologists assessed tumor content and suitable areas of tumor were marked for microdissection, if necessary. RNA and DNA were extracted from FFPE tumor blocks using AllPrep DNA/RNA FFPE kit (Qiagen). DNA from peripheral blood mononuclear cells (PBMC) was extracted using QIAamp DNA Blood mini kit (Qiagen) from the buffy coats. Nucleic acid yield and quality were assessed on Qubit Fluorometric quantification (ThermoFisher Scientific) and TapeStation4200 (Agilent).

2.4 HPV detection in tumor, TCR sequencing and HLA typing

P16 ^{INK4A} status of tumors was confirmed using immunohistochemistry and all immunohistochemical interpretations were made by consultant histopathologists. Diffuse strong nuclear expression of >70% of tumor nuclei for p16 was considered positive. RNA extracted from FFPE blocks was used for cDNA synthesis using the High-Capacity cDNA Reverse Transcriptase kit (Thermo Fisher). Evidence of HPV16 integration was assessed by detection of E7 expression using methods and primers described previously in a 7500 Sequence detection system (Applied Biosystems, Foster City, CA, USA/Thermo Fisher) (28). Any specimen producing dCt< 13 was consider positive for HPV integration. Detection of HPV16 DNA in tumor was performed using a "HPV16-detect" novel NGS assay with Ion AmpliSeq Designer (ThermoFisher Scientific) as previously described (29).

TCR β-chain sequencing was performed utilizing the genomic DNA extracted from FFPE tumor samples or from buffy coat samples by using Adaptive kit. Sequencing libraries were generated using the ImmunoSEQ kit (Adaptive Biotechnologies) according to the manufacturer's recommendations. The first round of PCR was carried out using the ImmunoSEQ proprietary PCR primer mix (32 μL per sample containing 25 uL of QIAGEN 2x Multiplex PCR Master Mix, 5μL of QIAGEN 5x Q-solution and 2 μL of primer mix). A positive control reaction, provided in the kit, and a negative control reaction were included with each sample batch. PCR cycling parameters were: heated lid (105°C), 95°C 5 min denaturation step, followed by 21 cycles of 94°C, 30 s denaturation, 65°C, 75 s annealing, and 72°C, 40 s extension; followed by 72°C, 10 min final extension, then hold at 4°C. Amplified libraries were diluted using the DNA suspension buffer (30 μL) provided. A second round of PCR was performed to generate uniquely barcoded sequencing libraries using the barcode primer plate included in the kit (17μL of working mix which include 12.5μL QIAGEN 2x Multiplex PCR master mix, 2.5μL QIAGEN 5x Q-solution and 2μL of QIAGEN RNase-free water; 4 μL of primers from the provided barcode plates and 4 μL of the first PCR product). Second PCR cycling parameters were: heated lid (105°C), 95°C 15 min denaturation step, followed by 21 cycles of 94°C, 30 s denaturation, 68°C, 40 s annealing, and 72°C, 60 s extension; followed

by 72°C, 10 min final extension, then hold at 12°C. The quality of the libraries was assessed using Agilent 4200 TapeStation High Sensitivity D1000 Screentape. Samples were pooled volumetrically and purified using MAGBIO HighPrep PCR beads (1x). The final pool was quantitated using a Kapa Library Quantification kit for Illumina. Libraries were sequenced on the Illumina MiSeq System following the manufacturer's instructions and using MiSeq Reagent Kit v3 (150-cycle) Single-Read. A total of 168 sequencing cycles were performed (Read 1:156 cycles, Read 2: 12 cycles), as recommended in the protocol, adding 5% PhiX. ImmunoSEQ platform was used for TCR identification and CDR3 extraction.

High-resolution HLA typing from genomic DNA extracted from blood was carried out by NGS at VH Bio (UK) for all patients.

2.5 TCR repertoire metrics

The clonality index was estimated for each sample by using the command clonality from the LymphoSeq R package (30). This score is derived from the Shannon entropy, which is calculated from the frequencies of all productive CDR3β sequences divided by the logarithm of the total number of productive sequences. This normalized entropy value is then inverted (1-normalised Shannon index) to produce the clonality metric.

Clonal relatedness was estimated using the "clonalRelatedness" command from the LymphoSeq R package with an edit distance of 3. Morisita index as a statistical method for overlap in a population, was calculated using the repOverlap(method="morisita") command from the immunarch package in R (31).

Expanded TCR clonotypes either in tumor or in blood were those present above a threshold of relative frequency of 2/1,000 (corresponding to the top 1% of the empirical TCR frequency distribution). At this threshold, which has been already described in previously published work, the correlation between clonality and proportion pf repertoire occupied by expanded TCRs is very strong and the number of TCRs labelled as expanded is greater than for higher thresholds for which this correlation is also significant (11).

The difference in abundance between pre- and post-treatment peripheral blood was calculated with the Fisher test function in LymphoSeq package in R. This function assumes that the repertoire contains S distinct clones and their proportional abundances in paired samples (sample 1 and sample 2) are given by the multinomial vectors $p^{(1)}=\{p_1{}^{(1)}, p_2{}^{(1)}, \ldots, p_S{}^{(1)}\}$ and $p^{(2)}=\{p_1{}^{(2)}, p_2{}^{(2)}, \ldots, p_S{}^{(2)}\}$ with $\sum_{i=1}^{S} p_i^{(j)}=1$. Supposing that n clones change in abundance between the two timepoints, these clones can be identified with the n element index vector Δ. Next, assuming that the aggregated change of a truly changed TCR abundance is small [i.e. $\sum_{i\in\Delta}(p_i^{(2)}-p_i^{(1)})\ll 1$] each observed clone can be independently tested for significance using a two-by-two contingency table and by employing a Fisher exact test to compute the p value for each clone across the two timepoints, against the null hypothesis that the abundance of the clone is identical in the two samples. To identify the set of significantly changed clones between the two timepoints, a positive false discovery rate (FDR) method of Storey is used (32, 33). TCRs with FDR q-values< 0.01 were labelled as statistically significant expanded or contracted.

2.6 CDR3β amino acid clustering

Pairwise similarity between pairs of TCRs was measured on the basis of amino acid triplet sharing. Sharing was quantified using the normalized string kernel function. The kernel is calculated as the number of amino acid triplets (sets of three consecutive amino acids) shared by two CDR3βs, normalized by the number of triplets in each CDR3β being compared. Two TCRs were considered connected if the similarity index was ≥0.7. Per (patient, timepoint) pair, the number of clusters containing an expanded CDR3β was counted.

For the maintained and replaced clustering methods, peripheral baseline expanded clonotypes that were shared with and expanded in tumor were selected and subsequently classified in either maintained or replaced clonotypes. Following this, the clustering was done as explained before using the same similarity index threshold. Per repertoire (maintained or replaced), the number of clonotypes that were part of a cluster at baseline were counted.

2.7 In silico antigen specificity clustering pipeline

The GLIPH version 2 algorithm was implemented for the establishment of T-cell specificity groups using the CDR3β sequences from tumor and peripheral blood at each timepoint and the HLA types (34, 35). The parameters used to run GLIPH2 were local minimum p value of 0.001, p depth of 1000, global convergence cutoff of 1, simulation depth of 1000, kmer minimum depth of 3, local minimum OVE of 10, and accepting all amino acids interchangeable. Briefly, by comparing the input with the reference dataset of 273,920 distinct CDR3β sequences (both CD4 and CD8) from 12 healthy individuals, GLIPH2 first discovered clusters of CDR3β sequences sharing either global or local motifs, as previously described (34). Previously used in a large cohort of non-small cell lung cancer (NSCLC) patients, GLIPH2 algorithm has shown to enable the analysis of shared TCR specificity and HLA prediction (35). The output of GLIPH2 include the CDR3β clusters with shared sequence motifs and is accompanied by multiple statistical measurements to facilitate the calling of high-confidence specificity groups, including biases in Vβ gene usage, CDR3β length distribution (only relevant for local motifs), cluster size, HLA allele usage, and clonal expansion.

A scaled count for each patient in each GLIPH2 convergence group containing sequences from more than 10 samples (n=30,222) was used as input to the UMAP. UMAP analysis was performed using the umap R package. The UMAP parameters that were changed from default were n_neighbours (parameter that control how UMAP balances local versus global structure of the data) was set to 302 (the GLIPH2 converge group count divided by 100) and min_dist (parameter that provide the minimum distance apart that points are allowed to be in the low dimensional representation) set to 0.25. Based on the UMAP components, HDBSCAN was used to cluster the

GLIPH2 convergence group (R package hdbscan) with min_cluster_size set to 100 (parameter set to smallest size grouping aimed to consider a cluster) and min_samples set to 0 (lowest conservative threshold as possible for clustering, since the input was previously obtained GLIPH2 convergence groups). For each HDBSCAN cluster, the distributions of the scaled counts were compared between responders and non-responders and across timepoints using a Wilcoxon rank sum test and a signed-rank test, respectively. Any clusters with an FDR *q*-value of< 0.01 is shown circled in the graph (it is a three SD ellipse, based on all the points in the cluster). Next, we used netMHCpan-4.1 to select those 8-11 mers derived from the HPV16 oncoproteins E2, E5, E6 and E7 that were binders (percentage elution rank<1) according to the HLA type of each patient (36). We used the UMAP clusters output (CDR3β amino acid sequence) and the netMHCpan-4.1 output as the input to run ERGO pipeline and estimate the TCR-epitope binding probability (37). Finally, binding probabilities for each UMAP cluster was compared against those for all other clusters combined using Fisher exact test. Clusters with FDR *q*-values< 0.01 were labelled as displaying statistically significant higher (if Fisher stat< 1) or lower (of Fisher stat > 1) binding probability compared to the other clusters. GLIPH2, UMAP, HDBSCAN, netMHCpan4.1., ERGO and clustering comparison code are available in github: https://github.com/instituteofcancerresearch/CCR4157.

2.8 Quantification and statistical analysis

Statistical analysis was performed in R and GraphPad Prism 8. We used the T-test two-tailed paired or non-paired (or Mann-Whitney non-parametric test as appropriate when normality was not passed using Shapiro-Wilk test) to test for statistical differences in the mean between two samples. We used one-way ANOVA paired or non-paired (or non-parametric tests as matched Friedman test, as appropriate) to compare means between more than two samples, or two-way ANOVA (or mixed model) for grouped analysis. Significant values were corrected for multiple testing using Sidak's or Dunn's correction when appropriate. A p value less than 0.05 was considered significant. TCRβ V and J gene usage comparisons were done using Kruskall-Wallis test with Holm method correction. Data visualization was performed in R and GraphPad Prism 8. All graphs show bars with median and 95% confidence interval (CI).

3 Results

3.1 Cohort overview and patient characteristics

A total of 19 patients were recruited into this sub-study. These included 6 HNSCC, 6 ASCC and 7 CC and patients were classified as responders (n=11) or non-responders (n=8). The median time to relapse for the non-responder group was 192 days following completion of CRT and the average follow-up for the responder group was 5.61 years. Responders included 4 HNSCC, 4 ASCC and 3 CC while non-responders included 2 HNSCC, 2 ASCC and 4 CC (z test p value = 0.6713). Details for all patients are shown in Table 1. Baseline tumor biopsies were available for all patients, baseline blood was available for 18 patients and post-treatment (6 and 12 weeks) blood samples were available for 18 and 19 patients, respectively. All patients were confirmed to be positive for $p16^{INK4A}$ and HPV16 E7 in tumor by immunohistochemistry and detection of HPV16 E7 mRNA and HPV16 DNA with "HPV-detect", respectively. When testing for HPV18, 31 and 33 DNA, no other HPV subtypes were detected.

3.2 CRT increases the peripheral T-cell clonality, which correlates with response to treatment

Cohort-wide, the median number of unique β-chain transcripts detected in tumor and blood samples was 8,820 and 11,200,

TABLE 1 Patient characteristics.

	N	%
Age, years, mean (SD)	45.82 (25.16)	-
Sex		
Male	6	31.5
Female	13	68.5
Type of cancer		
Head and neck (oropharynx)	6	31.5
Anal	6	31.5
Cervical	7	37
Histology		
Squamous cell carcinoma	17	89.5
Adenocarcinoma	2	10.5
Node status		
Positive	12	63
Negative	7	37
Stage *		
I	3	16
II	8	42
III	7	37
IV	1	5
Response		
Responders	11	58
Non-responders		
- PR/PD after CRT	4	21
- Early PD (<1 year)	4	21

*Stage by AJCC TNM 8th Edition for head and neck and anal carcinoma and FIGO 20th Edition for cervical cancer.
CR, complete response; PD, progressive disease; PR, partial response.

respectively. The number of unique PBMC clonotypes was significantly lower at 6- and 12-weeks post-treatment compared to baseline, but no difference was seen between the 6- and 12-week post-treatment repertoire (Figure 1A). On the contrary, the absolute number of peripheral TCRs across timepoints and the proportion of unique clonotypes in relation to the total number of TCRs detected per sample across timepoints were not significantly different (Figures 1B, C). The total number of both, intra-tumoral detected TCRs and unique T-cells were significantly higher in HNSCC compared to CC and ASCC, as expected from a mucosa-associated lymphoid tissue (Supplementary Figures 1A, B). However, the proportion of unique clonotypes in relation to the total number of TCRs retrieved per sample was not significantly different across tumour types (Supplementary Figure 1C). On the other hand, the number of unique clonotypes and detected TCRs in peripheral blood was similar across tumor entities (Supplementary Figures 1D, E). In order to assess potential biases stemming from fluctuation in clonotype number between different timepoints, which might influence the metric employed for the measurement of TCR clonality, the correlation between the 1- (normalized Shannon index) and the unique number of clonotypes was explored. However, no discernible correlation was ascertained between these variables (Supplementary Figure 1F). Thus, this was the metric used to quantify TCR clonality, where low scores correlate with a more diverse repertoire and higher scores with an expansion of dominant TCR clones. Overall, TCR clonality in tumor samples was similar compared to baseline peripheral blood (Figure 1D). Intra-tumoral TCR clonality was similar across the three tumor types (Supplementary Figure 1G) and we only found a significant higher peripheral clonality at baseline in ASCC compared to CC patients (Supplementary Figure 1H). We observed higher baseline intra-tumoral TCR clonality in non-responders compared to responders (Figure 1E), but peripheral TCR clonality was not associated with response at any of the sampled timepoints (Supplementary Figure 1I). The peripheral repertoire clonality significantly increased from baseline after CRT (Figure 1F). However, when patients were split according to response, only responders displayed a significant increase in peripheral TCR clonality 6 weeks post-treatment compared to baseline (Figure 1G). Next, we computed an intra-repertoire similarity score or clonal relatedness as a metric that takes into account sequence similarity without regard for clonal frequency, to evaluate the link between response to CRT and changes in the intra-repertoire peripheral clonotype similarity. We observed that only responders displayed a significant increase in clonal relatedness at 6 weeks compared to baseline (Figure 1H).

3.3 Early post-treatment expansion of previously expanded peripheral baseline clonotypes is associated with response to CRT

We next focused on the proportion of tumor-resident T-cell clones also present in the periphery. We classified CDR3β amino acid sequences as 'private' if they were only found in either tumor (TIL-private) or in peripheral blood (PBMC-private), or as 'migrated' PBMCs (mi-PBMCs) if they were shared between tumor and peripheral blood. As an example, at baseline, patient HN54 (responder) presented 47,501 unique CDR3β amino acid sequences in bulk PBMCs, 26,660 in TILs and 3,419 migrated sequences (Figure 2A). We computed the absolute number of mi-PBMCs that displayed statistically significant increase ("expansion") or decrease in frequency ("contraction") between two timepoints (baseline vs. 6 weeks post-treatment, and 6 vs. 12 weeks) using Fisher exact test with FDR< 0.01. We found that responders displayed a significantly higher absolute number of expanded than contracted mi-PBMCs at 6 weeks, and significantly more contracted than expanded mi-PBMCs at 12 weeks. In contrast, non-responders did not show any statistically significant difference between expanded and contracted mi-PBMCs at any timepoint (Figures 2B, C). In addition, subsequent contraction of previously expanded T-cell clones 12 weeks after completion of treatment was directly associated with response to treatment.

3.4 CRT increases peripheral TCR divergence and repertoire similarity correlates with response

We compared the clonal relatedness of the CDR3β sequences from the mi-PBMCs with the PBMC-private and TIL-private pools. At baseline, the mi-PBMCs displayed more clonal relatedness and higher clonality than both the PBMC-private and TIL-private CDR3β regions (Figures 2D, E), suggesting more TCR convergence and expansion in tumor-associated T cells that have potentially migrated into or from the peripheral blood, than in the bulk PBMC and TIL populations. Moreover, we consistently observed significantly higher CDR3β clonal relatedness and clonality in the mi-PBMC, compared to the PBMC-private pool, at 6 and 12 weeks post-treatment (Figures 2F, G). Next, we followed the mi-PBMC pools for each patient and, when comparing the relative frequency of T-cell clones across timepoints in all patients, we observed a significant increase in the proportion of the peripheral PBMC repertoire occupied by this mi-PBMC pool compared to baseline at 6 weeks and 12 weeks (Figure 2H). Critically however, this increase was only found to be statistically significant in the responder group (Figure 2I). In addition, when we classified patients by response, we only found a significant increase in the clonal relatedness of both the mi- and the private-PBMC pools in the responder group (Supplementary Figure 2A). Given these findings, we calculated the Morisita index as a measure of how similar pre-treatment intra-tumoral and bulk peripheral TCR repertoires were across different timepoints. The Morisita overlap index considers the relative frequency of different TCRs in two samples and it is widely used as a highly efficient estimator of dispersion. Thus, this also allowed us to evaluate the link between response to CRT and maintenance of pre-existing, or replacement with novel, TCR clonotypes. Tracking the bulk TCR pools, we observed a greater degree of TCR clonal maintenance in responders (greater TCR repertoire overlap between baseline and 12-week peripheral and intra-tumoral repertoires), compared to non-responders (Supplementary Figures 2B-D).

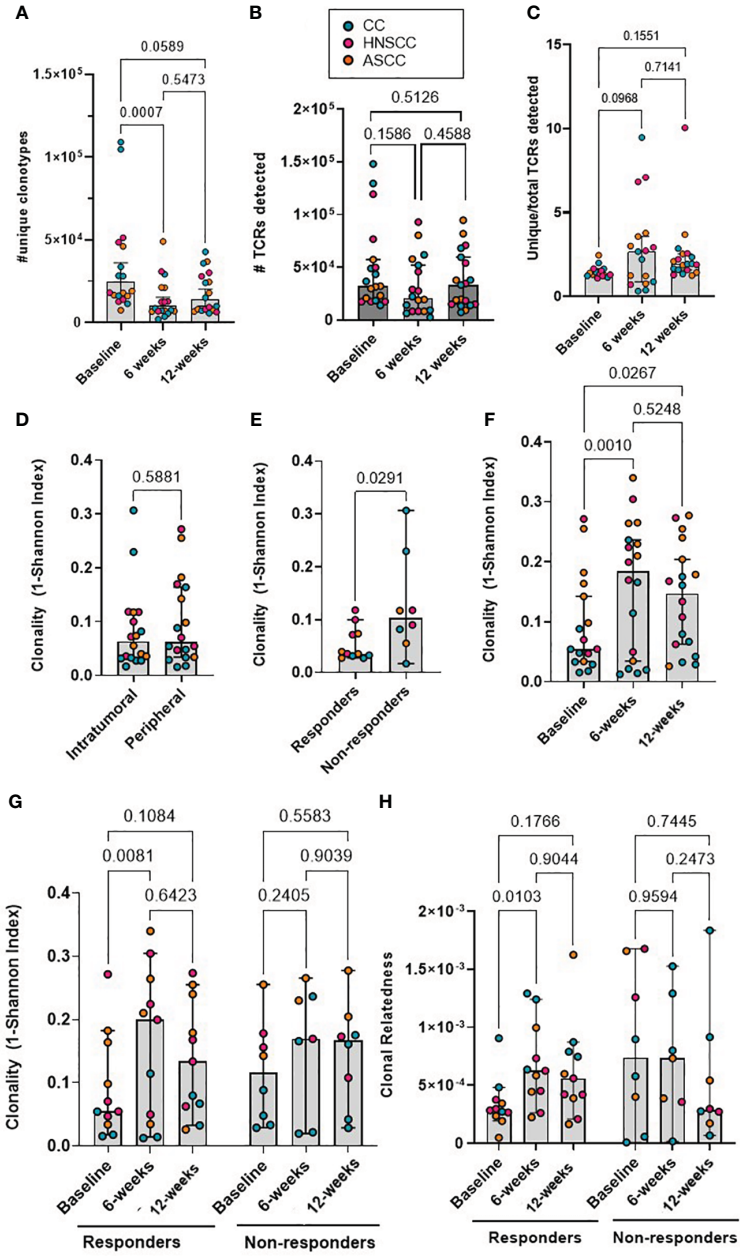

FIGURE 1
(A) The absolute number of unique peripheral TCR clonotypes are shown for each patient at each timepoint. **(B)** Absolute number of TCRs detected for each patient at each timepoint. Friedman test (paired samples) with Dunn's multiple comparisons p values are shown for figures A and B. **(C)** Proportion of unique clonotypes in relation to total TCRs detected in peripheral repertoire. Mixed-effect analysis with Dunnett's multiple comparisons p values are shown. **(D)** The intra-tumoral and baseline peripheral TCR repertoire clonality scores are shown for each patient. Paired t test p value shown. **(E)** The intra-tumoral TCR repertoire clonality scores are shown for each patient, categorized by response to CRT. Unpaired t test p value shown. **(F)** The matched peripheral TCR clonality scores are shown for each patient at each timepoint. **(G)** The peripheral TCR clonality scores are shown for each patient at each timepoint, categorized by response to CRT. **(H)** The peripheral TCR clonal relatedness scores are shown for each patient at each timepoint, categorized by response to CRT. Mixed-effect analysis with Sidak's multiple comparisons p values are shown for figures **F-H**. Graph bars show the median and 95%CI.

3.5 Pre-treatment intra-tumoral and post-treatment peripheral cluster structures are associated with response to CRT

Antigen-specific T-cell responses are often associated with the presence of clusters of TCRs with similar CDR3β peptide binding sequences. As previously described, we defined expanded TCRs as those present above a threshold frequency of 2/1,000, corresponding to the top 1% of the empirical TCR frequency distribution (11), and we performed clonotype clustering analysis in the expanded tumor-resident and peripheral TCR repertoires (Supplementary Figure 3). We observed that expanded TCR clones showed significantly increased clustering of similar CDR3β sequences (or "cluster structures") in responders compared with

10.3389/fonc.2023.1296948

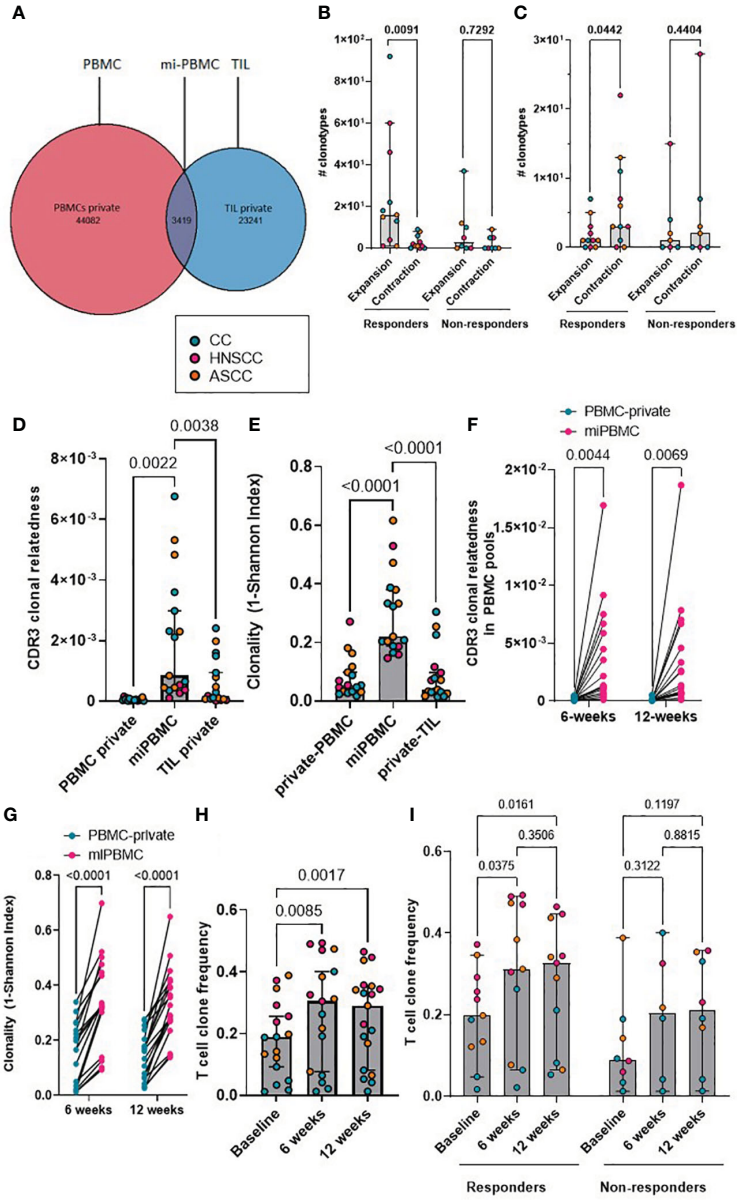

FIGURE 2
(A) Representative Venn diagram of a showing CDR3 sequences in PBMCs and TILs for patient HN54 (responder) at baseline. **(B, C)** Absolute number of expanded and contracted peripheral clonotypes of pre-expanded baseline clonotypes at 6 weeks **(B)** and 12 weeks **(C)** are shown for each patient categorized by response. Two-way ANOVA with Sidak's multiple comparison p values are shown. **(D)** Clonal relatedness (proportion of CDR3β amino acid sequences that were related by a maximum edit distance of 3) in the PBMC-private, mi-PBMC and TIL-private pools at baseline. **(E)** Clonality (1-normalised Shannon index) in the PBMC-private, mi-PBMC and TIL-private pools at baseline. One-way ANOVA with Dunnet's multiple comparisons test p values are shown for figured D and E. **(F, G)** Comparison of clonal relatedness (maximum edit distance = 3 amino acids) **(F)** and clonality (1-normalised Shannon index) **(G)** between the PBMC-private and the mi-PBMC pools at 6 and 12 weeks. Paired t-test p values are shown. **(H)** T-cell clone frequency in mi-PBMC pool at 6 and 12 weeks. Mixed-effect analysis with Sidak's multiple comparisons p values are shown. **(I)** Comparison T cell clone frequency in mi-PBMC pool across timepoints by response. Mixed-effect analysis with Tukey's multiple comparison corrected p values are shown. Bar graphs show median and 95% CI.

non-responders, both in the pre-treatment tumor-resident repertoire and in the post-treatment peripheral 12-week (but not earlier) repertoires (Figures 3A-D). In addition, when analyzing the proportion of intra-tumoral dominant clusters (where a dominant cluster was considered if it was formed by > 3 TCRs), we found a significantly higher proportion of them in the responder group, compared to non-responders (Figure 3E). These results are in line with the finding of a significantly higher clonal relatedness in the expanded tumor-resident TCR repertoire in the responder group compared to the non-responders (Supplementary Figure 4A). Next, we classified expanded TCRs in either maintained (if they were still expanded in the following timepoint) or replaced (if they were either not detected or not expanded in the following timepoint) and we applied same clustering methods (Figure 3I). We found that at baseline, expanded TCRs that were maintained at 6 weeks displayed significantly more clustered structures than expanded TCRs that

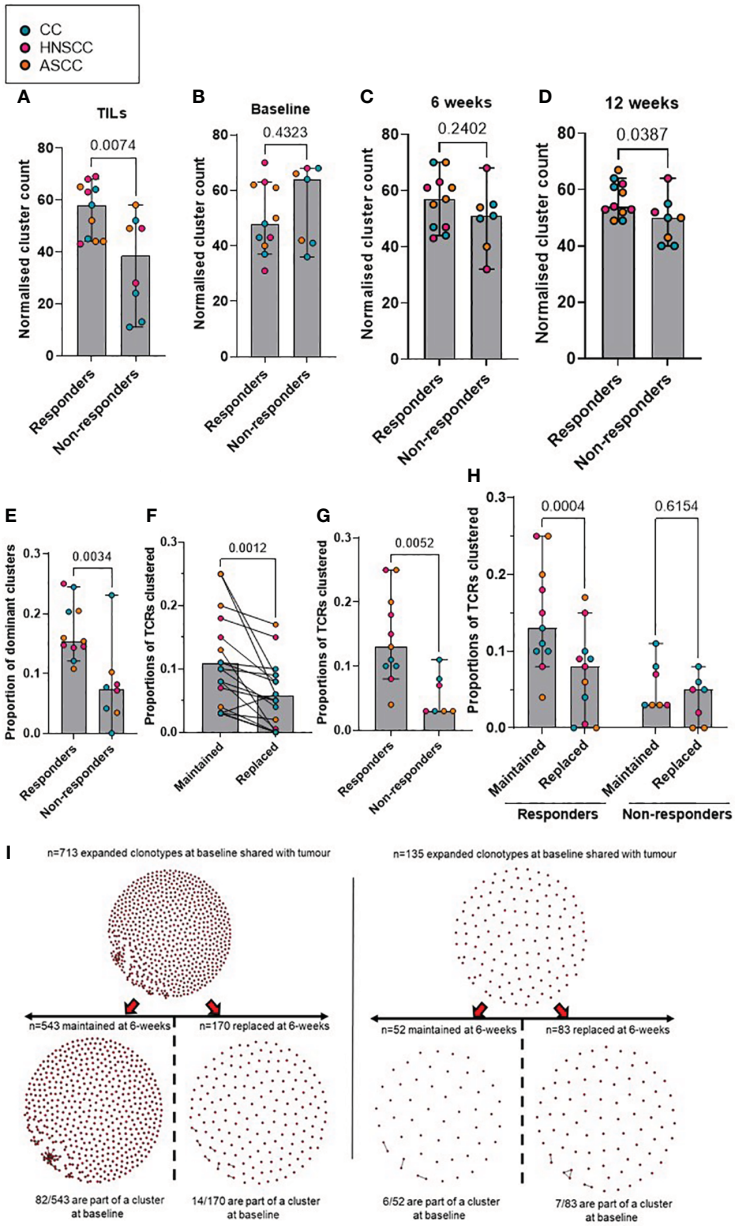

FIGURE 3
(A–D) Comparison according to response of normalised cluster count by CDR3β similarity for the networks containing expanded sequences in the intra-tumoral **(A)**, peripheral baseline **(B)**, 6 weeks **(C)** and 12 weeks **(D)** TCR repertoires. **(E)** Proportion of dominant TCR clusters in the intra-tumoural expanded repertoire according to response. Unpaired t test p values are shown for figures A-E. **(F)** Proportion of maintained versus replaced expanded clustered TCRs at 6 weeks from baseline which are present in the intra-tumoral repertoire. Paired t test p value is shown. **(G)** Proportion of baseline clustered structures of maintained TCRs at 6 weeks categorized by response to CRT. Unpaired t test p value is shown. **(H)** Proportion of maintained and replaced baseline clustered structured TCRs at 6-weeks categorized by response to CRT. Two-way ANOVA adjusted p values using Sidak's multiple comparison test are shown. **(I)**. Representative kernel network diagrams for peripheral baseline and 6-weeks CDR3β-chain sequences for a responder (left) and a non-responder (right). Clustering performed within the bulk TCR sequencing data around expanded TCRs, subdivided between clones that were maintained in the 6 weeks post-treatment (left) repertoire and clones that were replaced (right). Each dot represents an expanded T-cell clone and the vectors joining each dot represent a cluster of T-cell clones. Bar graphs show median and 95% CI.

were present at baseline and subsequently replaced (Figure 3F). When analyzing patients by response to CRT, we observed that responders showed significantly more baseline clustered TCR structures that were maintained at 6 weeks, compared to non-responders (Figure 3G). Moreover, only responders displayed statistically significantly more maintained than replaced clustered structures (Figure 3H). Similar results were found when comparing the 6- and 12-week expanded TCR repertoires: a significantly greater proportion of maintained, rather than replaced, clustered structures that were present at 6 weeks were still detected at 12 weeks, although this was only observed in responding patients (Supplementary Figures 4B-D).

3.6 Clustering peripheral T cell repertoire by antigen specificity using in silico models

As described previously (34), GLIPH2 identifies CDR3β sequences that are highly likely to share MHC-peptide specificities based on local motifs and/or global homology. To identify T-cells recognizing shared tumor antigens that may function as determinants of response, we applied GLIPH2 to the peripheral repertoire of all patients across all timepoints. A scaled count for each patient in each GLIPH2 convergence group containing sequences from more than 10 samples (n=30,222) was used as input to the UMAP and, based on the UMAP components, HDBSCAN was used to cluster the GLIPH2 convergence groups. For each HDBSCAN cluster, the distributions of the scaled counts were compared between responders and non-responders (Figure 4A) and across timepoints (baseline, 6 and 12 weeks) (Figure 4B). Interestingly, we found some clusters with significantly increased counts in either responders (i.e. clusters 1 and 2) or non-responders (i.e. clusters 6 and 39). In addition, despite most of the clusters showing a significantly higher count at baseline, some of them were more frequently represented at 6 weeks (i.e. clusters 1 and 2) and 12 weeks (i.e. clusters 21 and 30). Next, we used a previously described in silico pipeline for prediction of specific CDR3β amino acid sequences and peptide binding from large dictionaries of TCR-peptide pairs (ERGO) to predict the binding probability between the CDR3β that form each cluster and HPV16 peptides (37). Eight to 11-mer HPV16 peptides, derived from the E2, E5, E6 and E7 viral oncoproteins, were selected according to their percentage elution rank (equal or lower than 1) as strong binders according to the HLA type of each individual patient (Supplementary Table 1) using netMHCpan-4.1. Comparing the pooled TCR-peptide binding probabilities for each HDBSCAN cluster with all the others, we found that 3 clusters showed significantly higher HPV16-specific binding probability, whereas 6 clusters displayed significantly lower binding probability (Supplementary Table 2). We, therefore, focused on these 3 HPV16-specific TCR clusters (6, 2 and 25), and calculated their frequency in the TILs and PBMCs. We found that, despite the predicted HPV16-specific clones displaying similar relative abundance across all timepoints (Figure 4C), there was a significantly higher frequency in the pre-treatment TILs of the responder group (Figure 4D). These findings suggest that in the responding group there was a higher proportion of HPV16-specific T cells in the tumor prior to treatment, although the anti-HPV16 peripheral clones were equally abundant regardless of response.

4 Discussion

We present results of a translational study with sequential TCR analysis of samples from patients with locally advanced HPV16-driven malignancies treated with CRT. To our knowledge this is the first study investigating spatial (tumor versus peripheral) and temporal changes in T-cell repertoire to predict treatment outcomes in this setting. This study was proposed in the assumption that mean clonality would be different according to response to treatment. Although this was confirmed in the intra-tumoral TCR repertoire, the clonality index was lower than previously expected (mean clonality and SD difference of 0.07 and 0.06, respectively). This will serve for subsequent studies interrogating the TCR repertoire in this set of patients.

Some patterns of peripheral repertoire turnover (such as changes in the clonality and clonal relatedness) have been associated with an effective immune awakening in patients treated with immune checkpoint inhibitors (ICIs) (6–8, 38, 39). Our data identify some baseline intra-tumoral characteristics that may drive response to treatment, such as TIL high diversity and increased TIL clustering in the pre-treatment biopsy. The debate regarding the primary mechanism underlying ICI response focuses on two hypotheses: "T-cell clonal replacement," which involves the recruitment of novel T-cells into the tumor, and "T-cell clonal revival," which suggests the reinvigoration of pre-existing TILs (40). Clonal replacement mechanism has been supported in studies that included patients with skin cancer and NSCLC which showed that anti-PD-1 therapy promotes the infiltration of T-cells from the blood into the tumor by inducing recognition of neoantigens different from those recognized by expanded TCR clones at baseline, and that patients with major pathological response showed substantial overlap between intra-tumoral and peripheral blood TCR clonotypes, with most expanded clones shared between the two compartments (41, 42). An alternative perspective (clonal revival) suggests that ICI response arises from pre-existing intra-tumoral T-cells that are primed by neoantigens and capable of cytotoxic reinvigoration despite exhibiting exhaustion features. This has been supported in a recent study involving patients with metastatic renal clear-cell carcinoma treated with anti-PD-1 therapy which showed that responders had higher pre-treatment intra-tumoral TCR clonality and cluster structure compared to non-responders, indicating the presence of pre-existing adaptive immunity (7). Accordingly, our data show that the proportion of shared TIL-PBMC clonotypes increases with treatment, and that the responder group displays higher overlap between TIL and PBMCs and increased baseline intra-tumoral diversity and clustered structures than the non-responder group. To reconcile the seemingly conflicting reports supporting either clonal replacement or clonal revival, it is essential to consider that the mechanisms underlying ICIs response may be context-dependent and can vary among different malignancies, tumor samples (primary versus metastatic), on-treatment sampling timings, ICIs regimes and dosage. There is paucity of data regarding the effects that CRT has in the intra-tumoral and peripheral TCR repertoire and there is a high chance that these will be different to the ICI effects and will vary according to the irradiated site, the dose and the use of concurrent cytotoxic drugs. Our results point towards the fact that the expansion of tumor-infiltrating T-cell clones secondary to CRT is probably driven by pre-existing expanded and antigen-specific TILs which can be found and tracked in the peripheral blood, where they display different dynamics according to response to treatment. In this regard, we demonstrated that there is a population of peripheral expanded pre-treatment TCR clonotypes that are shared with tumor and are preferentially maintained and/or expanded by CRT, potentially reflecting enhanced stimulation by

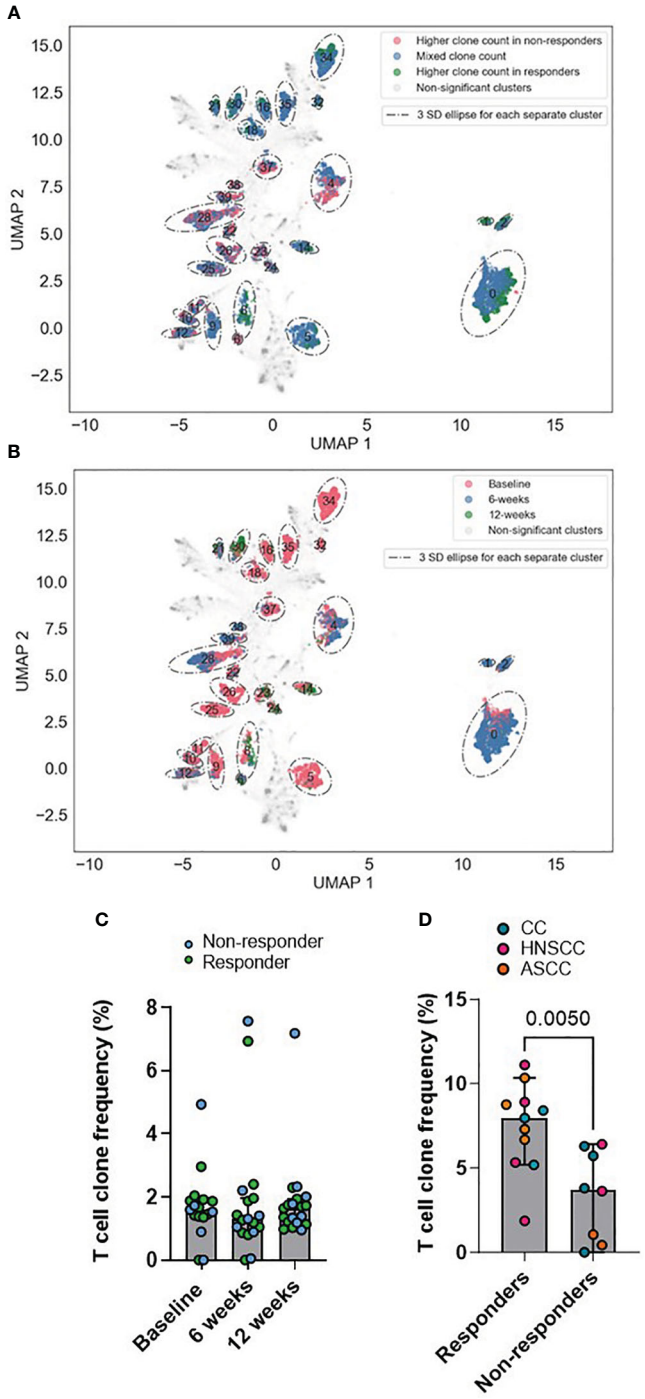

FIGURE 4
(A, B) UMAPs of GLIPH2 convergence groups by response **(A)** and by timepoint **(B)**. Based on the UMAP components, HDBSCAN was used to cluster the GLIPH2 clusters. For each HDBSCAN cluster, the distributions of the scaled counts were compared between responders and non-responders. Any clusters with a FDR q-value of< 0.01 is shown circled in the graph (it is a 3 SDs ellipse, based on all the points in the cluster). In A, those points belonging to a significant HDBSCAN cluster are also coloured by if the GLIPH2 convergence groups in question has a 4x higher clone count in responders, non-responders, or if the cluster is more mixed. In B, the points are coloured by which timepoint has the highest clone count in the GLIPH2 convergence groups, baseline, 6 or 12 weeks. **(C)** Peripheral frequency of the pools of T cell clones conforming clusters 6, 2 and 25 across all timepoints. **(D)** TIL frequency of the pools of T cell clones conforming the clusters 6, 2 and 25 in the pre-treatment biopsy. Unpaired t test p value is shown. Bar graphs show median and 95% CI.

increased antigen cross-presentation and priming, and/or the ability of CRT to promote the activation and expansion of T-cells which are already primed. These findings, whilst not previously demonstrated in patients treated with CRT, have been described in longitudinal samples of patients treated with ICIs and, importantly, support a role for anti-tumor immunity in the response to CRT as currently used in the clinic (7). In addition, this paradigm has long been supported by pre-clinical murine data,

but not by robust clinical evidence (43). Although the precise reason for the drop in their relative abundance 12-weeks following completion of CRT in the responder groups unknown, it may reflect that the resolution of active disease following therapy reduces the potential source of antigen required to maintain cancer-specific T cell immunity. However, another explanation for this may be sequestration of tumor-antigen reactive T cells from peripheral blood to the tumor. Indeed, this notion has been recently shown in a cohort of melanoma patients treated with anti-PD-1 therapy (44) and supported by Bhatt et al., who made the interesting observation that specific CD8+ and CD4+ anti-HPV T-cell reactivity dropped after radical CRT (45). On the other hand, the absence of either expansion or contraction of baseline TCR clones in non-responders reflects a failure of activation of effector anti-tumor T-cells during CRT, potentially associated with maintained presence of tumor antigens 12 weeks after completion of treatment.

The concept of mi-PBMCs allowed us to follow T cells that are shared between peripheral blood and tumor and that are presumed to have an anti-cancer immune function in the tumor microenvironment. The significant increase in the clonal relatedness of both the mi- and the private-PBMC pools in the responder group suggests a more pronounced reconfiguration in the peripheral TCR repertoire in responding, as opposed to non-responding, patients. Furthermore, our results imply that CRT induces TCR repertoire divergence, with an increase in the shared TIL-PBMC repertoire (mi-PBMC) frequency after treatment only in responders. Moreover, there is also a broader compartmental overlap (increased Morisita index between baseline tumor-resident and peripheral T-cell repertoire) and longitudinal sharing (increased clonal relatedness of mi-PBMCs) in the TCR repertoire in patients who responded.

Maintenance of early post-treatment (6 weeks) expanded clustered structures only in responders suggests that clonal preservation of pre-expanded T cells that share epitope-specificity functions as a pre-requisite of response to treatment, whereas loss or replacement of T cell clusters may reflect an ineffective anti-cancer immune response or tumor-induced tolerance in patients who do not respond. Furthermore, there is a population of closely related TCR clonotypes in responders that are expanded pre-treatment and detected in both tumor and peripheral blood and that these are preferentially maintained and/or expanded by CRT. This may reflect enhanced stimulation by increased antigen cross-presentation and T-cell priming, and/or the ability of CRT to promote primed T-cell activation and expansion.

Interestingly, our results also show that responding patients display similar predicted HPV16-specific peripheral T cell abundance to the non-responding patients, but a higher proportion of these in the TIL compartment pre-treatment. Moreover, although these tumor-infiltrating clonotypes show lower pre-treatment clonality in the responder group, they display increased clustering capacity, which suggests that a richer antigen-shared T cell repertoire is a key element of an effective anti-cancer immune response.

Our study sheds light on the determinants of response to standard-of-care CRT, and in particular the nature of the adaptive T cell response likely contributing to anti-tumor immunity. Despite the increased number of studies that have investigated possible predictive biomarkers of response to CRT in different HPV-driven malignancies, currently there are no markers of response used as standard-of-care in clinical practice (46). To date, most predictive markers of response have focused on the evaluation of pre-treatment tumor tissue. However, given the challenge of performing serial tissue biopsies during CRT, it is necessary to develop alternative strategies, that are reproducible and minimally invasive, to allow real-time monitoring of the clinical (and immune) response and disease evolution throughout treatment. In this regard, biomarkers such as circulating HPV DNA, or TCR repertoire analysis, can potentially be used for monitoring disease response during and following radical CRT (29, 47).

There are limitations to our study. First, the small number of patients limits data generalizability, and findings from this study would benefit from validation in larger datasets. We acknowledge that the differing group size, with smaller sample size in the non-responder group, suggests caution in missing an effect due to reduced power. However, our scope for translational discovery was supported by the extent of longitudinal tracking and in-depth analysis of the TCR repertoire changes under therapy. We acknowledge the fact that although all patients included in this study were diagnosed with locally-advanced HPV16-driven malignancies, they belong to three different tumor entities. Moreover, although the cornerstone treatment for all these three malignancies is radiotherapy, the total dose, fractionation, and concurrent chemotherapy agent used was different according to the tumor type. The potential influence of concurrent mitomycin C used for the treatment ASCC compared to cisplatin (used in HNSCC and CC) in the peripheral TCR repertoire is unknown. However, there is evidence that both cisplatin and mitomycin C are relatively inefficient in stimulating immunogenic cell death in the absence of radiation (48). Thus, one chemotherapy agent is not expected to be more immunogenic than the other. Since HPV genotype impacts the prognosis and response to CRT, especially in CC, only patients with confirmed HPV16 genotype (and no evidence of other HPV types) were included in this study. In addition, although these three entities display different biology, there is not enough evidence to assert that they display different TCR dynamics. Indeed, a recently published study which included cervical, vaginal, vulvar and anal carcinomas did not find differences in the antigen-specific immune response to CRT across these tumor types (49). Our results are consistent with this investigation and with the effects of radiation observed in preclinical models and human case reports across different types of malignancies (9, 50, 51). Although further studies are required to determine the mechanisms underpinning our observations and their specificity for CRT-induced responses, our research functions as a hypothesis generating study and provides a strategy to analyze immune cell evolution in patients treated with radiotherapy, chemotherapy, ICIs, or their combinations. This methodological strategy includes a novel pipeline which integrates the output from different and validated in silico predictions for MHC presentation, TCR clustering and TCR-epitope binding. We acknowledge that the use of TCR clonality metrics alone does not

provide a definitive assessment of anti-cancer T-cell responses. However, analysis TCR sequence similarity in the form of clusters (grouping TCRs with similar CDR3 peptide sequences) and networks (grouping closely related TCR clusters) provides insights into the antigenic specificity of TCRs. Indeed, in a recent analysis of TCR sequencing metrics from the TRACERX consortium which combined multi-region tumor samples and adjacent non-tumor tissue obtained from patients with early-stage NSCLC, authors showed the presence of clusters and networks of related TCR sequences within populations of TILs (11). Furthermore, whilst we acknowledge the limitations of the in silico strategies, they provide a first step towards a better understanding of the immune repertoire and its dynamics. Indeed, the proportion of our predicted HPV16-specific clonotypes in peripheral blood and tumor are consistent with previous publications (16). Looking forward, multiparameter flow cytometry, circulating tumor and HPV16 DNA, transcriptomic profiling techniques (including single cell) and additional ex vivo functional immune experiments to track T cell responses to HPV16 peptides, will be invaluable in studying baseline tumor microenvironment and peripheral immune changes to treatment. In this regard, previously published studies have interrogated the dynamics of circulating tumor and HPV16 DNA in plasma and the HPV viral load in tumor in HPV-driven malignancies treated with radical radiotherapy or CRT as an approach to predict disease progression and survival (29, 47, 52, 53).

In summary, in this translational study, we identified intra-tumoral and peripheral TCR metrics and in silico HPV16-specific T cell clones which hold promise for use as predictive markers of response to radical CRT and provide a template for future larger cohort immune-oncology biomarker studies in HPV-driven malignancies. Our findings advance the knowledge of immune responses to CRT and, critically, provide a potentially tractable tool to identify which patients will not respond or relapse early following radical CRT. This could eventually help clinicians to stratify patients more effectively and to consider poor-responder patients for adjuvant immunotherapeutic or other additional approaches, thereby improving personalization of therapeutic planning.

Data availability statement

TCR sequencing and HLA-typing datasets supporting the conclusions of this article are available in the figshare repository (DOI: 10.6084/m9.figshare.6025748.v1).

Ethics statement

The studies involving humans were approved by Institutional board and ethics committee 14/NE/1055. The studies were conducted in accordance with the local legislation and institutional requirements. The participants provided their written informed consent to participate in this study.

Author contributions

PN: Data curation, Formal analysis, Investigation, Methodology, Visualization, Writing – original draft, Writing – review & editing. AL: Formal analysis, Methodology, Writing – review & editing. FM: Formal analysis, Investigation, Methodology, Writing – review & editing. JL: Data curation, Formal analysis, Investigation, Methodology, Writing – review & editing. SL: Investigation, Writing – review & editing. DG: Investigation, Writing – review & editing. MP: Methodology, Software, Writing – review & editing. B'OL: Writing – review & editing. AR: Writing – review & editing. AS: Methodology, Writing – review & editing. BC: Formal analysis, Methodology, Resources, Writing – review & editing. AM: Supervision, Writing – review & editing. KH: Funding acquisition, Supervision, Writing – review & editing. SB: Conceptualization, Funding acquisition, Supervision, Writing – review & editing.

Funding

The author(s) declare financial support was received for the research, authorship, and/or publication of this article. This work was undertaken in The Royal Marsden NHS Foundation Trust and The Institute of Cancer Research. The Royal Marsden NHS Foundation Trust received a proportion of its funding from the NHS Executive. The CCR4157 trial was funded by the National Institute for Health Research Royal Marsden and Institute of Cancer Research Biomedical Research Centre and the Clinical Research Facility BRC grant nos. A67, B07, B002/ICiCPS3115 and B014. This work was supported by ICR/RMH NIHR Biomedical Research Centre, The Institute of Cancer Research/Royal Marsden Hospital Centre for Translational Immunotherapy, CRUK Head and Neck Program Grant (C7224/A23275), CRIS Foundation and ICR/RM CRUK RadNet Centre of Excellence (C7224/A28724).

Conflict of interest

The authors declare that the research was conducted in the absence of any commercial or financial relationships that could be construed as a potential conflict of interest.

Publisher's note

Supplementary material

The Supplementary Material for this article can be found online at: https://www.frontiersin.org/articles/10.3389/fonc.2023.1296948/full#supplementary-material

References

1. Ang KK, Harris J, Wheeler R, Weber R, Rosenthal DI, Nguyen-Tân PF, et al. Human papillomavirus and survival of patients with oropharyngeal cancer. *N Engl J Med* (2010) 363(1):24–35. doi: 10.1056/NEJMoa0912217

2. Eifel PJ, Winter K, Morris M, Levenback C, Grigsby PW, Cooper J, et al. Pelvic irradiation with concurrent chemotherapy versus pelvic and para-aortic irradiation for high-risk cervical cancer: an update of radiation therapy oncology group trial (RTOG) 90-01. *J Clin Oncol* (2004) 22(5):872–80. doi: 10.1200/JCO.2004.07.197

3. Meulendijks D, Dewit L, Tomasoa NB, van Tinteren H, Beijnen JH, Schellens JHM, et al. Chemoradiotherapy with capecitabine for locally advanced anal carcinoma: an alternative treatment option. *Br J Cancer* (2014) 111(9):1726–33. doi: 10.1038/bjc.2014.467

4. McLaughlin M, Patin EC, Pedersen M, Wilkins A, Dillon MT, Melcher AA, et al. Inflammatory microenvironment remodelling by tumour cells after radiotherapy. *Nat Rev Cancer* (2020) 20(4):203–17. doi: 10.1038/s41568-020-0246-1

5. Gameiro SR, Jammeh ML, Wattenberg MM, Tsang KY, Ferrone S, Hodge JW. Radiation-induced immunogenic modulation of tumor enhances antigen processing and calreticulin exposure, resulting in enhanced T-cell killing. *Oncotarget* (2013) 5 (2):403–16. doi: 10.18632/oncotarget.1719

6. Robert L, Tsoi J, Wang X, Emerson R, Homet B, Chodon T, et al. CTLA4 blockade broadens the peripheral T-cell receptor repertoire. *Clin Cancer Res Off J Am Assoc Cancer Res* (2014) 20(9):2424–32. doi: 10.1158/1078-0432.CCR-13-2648

7. Au L, Hatipoglu E, Robert de Massy M, Litchfield K, Beattie G, Rowan A, et al. Determinants of anti-PD-1 response and resistance in clear cell renal cell carcinoma. *Cancer Cell* (2021) 39(11):1497–518. doi: 10.1016/j.ccell.2021.10.001

8. Wieland A, Kamphorst AO, Adsay NV, Masor JJ, Sarmiento J, Nasti TH, et al. T cell receptor sequencing of activated CD8 T cells in the blood identifies tumorinfiltrating clones that expand after PD-1 therapy and radiation in a melanoma patient. *Cancer Immunol Immunother CII* (2018) 67(11):1767–76. doi: 10.1007/s00262-018-2228-7

9. Formenti SC, Rudqvist NP, Golden E, Cooper B, Wennerberg E, Lhuillier C, et al. Radiotherapy induces responses of lung cancer to CTLA-4 blockade. *Nat Med* (2018) 24(12):1845–51. doi: 10.1038/s41591-018-0232-2

10. Valpione S, Galvani E, Tweedy J, Mundra PA, Banyard A, Middlehurst P, et al. Immune awakening revealed by peripheral T cell dynamics after one cycle of immunotherapy. *Nat Cancer* (2020) 1(2):210–21. doi: 10.1038/s43018-019-0022-x

11. Joshi K, de Massy MR, Ismail M, Reading JL, Uddin I, Woolston A, et al. Spatial heterogeneity of the T cell receptor repertoire reflects the mutational landscape in lung cancer. *Nat Med* (2019) 25(10):1549–59. doi: 10.1038/s41591-019-0592-2

12. Rosati E, Dowds CM, Liaskou E, Henriksen EKK, Karlsen TH, Franke A. Overview of methodologies for T-cell receptor repertoire analysis. *BMC Biotechnol* (2017) 17(1):61. doi: 10.1186/s12896-017-0379-9

13. Jiang N, Schonnesen AA, Ma KY. Ushering in integrated T cell repertoire profiling in cancer. *Trends Cancer* (2019) 5(2):85–94. doi: 10.1016/j.trecan.2018.11.005

14. Wilkins A, Fontana E, Nyamundanda G, Ragulan C, Patil Y, Mansfield D, et al. Differential and longitudinal immune gene patterns associated with reprogrammed microenvironment and viral mimicry in response to neoadjuvant radiotherapy in rectal cancer. *J Immunother Cancer* (2021) 9(3):e001717. doi: 10.1136/jitc-2020-001717

15. Xiong C, Huang L, Kou H, Wang C, Zeng X, Sun H, et al. Identification of novel HLA-A*11:01-restricted HPV16 E6/E7 epitopes and T-cell receptors for HPV-related cancer immunotherapy. *J Immunother Cancer* (2022) 10(9):e004790. doi: 10.1136/jitc-2022-004790

16. Eberhardt CS, Kissick HT, Patel MR, Cardenas MA, Prokhnevska N, Obeng RC, et al. Functional HPV-specific PD-1+ stem-like CD8 T cells in head and neck cancer. *Nature* (2021) 597(7875):279–84. doi: 10.1038/s41586-021-03862-z

17. Keskin DB, Reinhold B, Lee SY, Zhang G, Lank S, O'Connor DH, et al. Direct identification of an HPV-16 tumor antigen from cervical cancer biopsy specimens. *Front Immunol* (2011) 2:75. doi: 10.3389/fimmu.2011.00075

18. Yee C, Krishnan-Hewlett I, Baker CC, Schlegel R, Howley PM. Presence and expression of human papillomavirus sequences in human cervical carcinoma cell lines. *Am J Pathol* (1985) 119(3):361–6.

19. Lechner M, Liu J, Masterson L, Fenton TR. HPV-associated oropharyngeal cancer: epidemiology, molecular biology and clinical management. *Nat Rev Clin Oncol* (2022) 19(5):306–27. doi: 10.1038/s41571-022-00603-7

20. Lin C, Franceschi S, Clifford GM. Human papillomavirus types from infection to cancer in the anus, according to sex and HIV status: a systematic review and meta-analysis. *Lancet Infect Dis* (2018) 18(2):198–206. doi: 10.1016/S1473-3099(17)30653-9

21. Schiffman M, Castle PE, Jeronimo J, Rodriguez AC, Wacholder S. Human papillomavirus and cervical cancer. *Lancet Lond Engl* (2007) 370(9590):890–907. doi: 10.1016/S0140-6736(07)61416-0

22. Golusinski P, Corry J, Poorten VV, Simo R, Sjögren E, Mäkitie A, et al. De-escalation studies in HPV-positive oropharyngeal cancer: How should we proceed? *Oral Oncol* (2021) 123:105620. doi: 10.1016/j.oraloncology.2021.105620

23. Keck MK, Zuo Z, Khattri A, Stricker TP, Brown CD, Imanguli M, et al. Integrative analysis of head and neck cancer identifies two biologically distinct HPV and three non-HPV subtypes. *Clin Cancer Res* (2015) 21(4):870–81. doi: 10.1158/1078-0432.CCR-14-2481

24. Ward MJ, Thirdborough SM, Mellows T, Riley C, Harris S, Suchak K, et al. Tumour-infiltrating lymphocytes predict for outcome in HPV-positive oropharyngeal cancer. *Br J Cancer* (2014) 110(2):489–500. doi: 10.1038/bjc.2013.639

25. Nenclares P, Rullan A, Tam K, Dunn LA, St. John M, Harrington KJ. Introducing checkpoint inhibitors into the curative setting of head and neck cancers: lessons learned, future considerations. *Am Soc Clin Oncol Educ Book* (2022) 42):511–26. doi: 10.1200/EDBK_351336

26. Mehanna H, Robinson M, Hartley A, Kong A, Foran B, Fulton-Lieuw T, et al. Radiotherapy plus cisplatin or cetuximab in low-risk human papillomavirus-positive oropharyngeal cancer (De-ESCALaTE HPV): an open-label randomised controlled phase 3 trial. *Lancet* (2019) 393(10166):51–60. doi: 10.1016/S0140-6736(18)32752-1

27. Lee NY, Ferris RL, Psyrri A, Haddad RI, Tahara M, Bourhis J, et al. Avelumab plus standard-of-care chemoradiotherapy versus chemoradiotherapy alone in patients with locally advanced squamous cell carcinoma of the head and neck: a randomised, double-blind, placebo-controlled, multicentre, phase 3 trial. *Lancet Oncol* (2021) 22 (4):450–62. doi: 10.1016/S1470-2045(20)30737-3

28. Lamarcq L, Deeds J, Ginzinger D, Perry J, Padmanabha S, Smith-McCune K. Measurements of human papillomavirus transcripts by real time quantitative reverse transcription-polymerase chain reaction in samples collected for cervical cancer screening. *J Mol Diagn JMD* (2002) 4(2):97–102. doi: 10.1016/S1525-1578(10)60687-3

29. Lee JY, Garcia-Murillas I, Cutts RJ, De Castro DG, Grove L, Hurley T, et al. Predicting response to radical (chemo)radiotherapy with circulating HPV DNA in locally advanced head and neck squamous carcinoma. *Br J Cancer* (2017) 117(6):876–83. doi: 10.1038/bjc.2017.258

30. Coffey D. LymphoSeq: Analyze high-throughput sequencing of T and B cell receptors. In: *Bioconductor version: Release (3.16)* (2023). Available at: https://bioconductor.org/packages/LymphoSeq/. fredhutch.org>.

31. Samokhina M, Popov A, ivan-immunomind, Nazarov VIimmunarch.bot, , Rumynskiy E, et al. immunomind/immunarch: immunarch 0.9.0 [Internet]. *Zenodo* (2022).

32. DeWitt WS, Emerson RO, Lindau P, Vignali M, Snyder TM, Desmarais C, et al. Dynamics of the cytotoxic T cell response to a model of acute viral infection. *J Virol* (2015) 89(8):4517–26. doi: 10.1128/JVI.03474-14

33. Pulendran B, Ahmed R. Immunological mechanisms of vaccination. *Nat Immunol* (2011) 12(6):509. doi: 10.1038/ni.2039

34. Huang H, Wang C, Rubelt F, Scriba TJ, Davis MM. Analyzing the Mycobacterium tuberculosis immune response by T-cell receptor clustering with GLIPH2 and genome-wide antigen screening. *Nat Biotechnol* (2020) 38(10):1194–202. doi: 10.1038/s41587-020-0505-4

35. Chiou SH, Tseng D, Reuben A, Mallajosyula V, Molina IS, Conley S, et al. Global analysis of shared T cell specificities in human non-small cell lung cancer enables HLA inference and antigen discovery. *Immunity* (2021) 54(3):586–602. doi: 10.1016/j.immuni.2021.02.014

36. Reynisson BV, Alvarez B, Paul S, Peters B, Nielsen M. NetMHCpan-4.1 and NetMHCIIpan-4.0: improved predictions of MHC antigen presentation by concurrent motif deconvolution and integration of MS MHC eluted ligand data. *Nucleic Acids Res* (2020) 48(1):449–54. doi: 10.1093/nar/gkaa379

37. Springer I, Besser H, Tickotsky-Moskovitz N, Dvorkin S, Louzoun Y. Prediction of specific TCR-peptide binding from large dictionaries of TCR-peptide pairs. *Front Immunol* (2020) 11:1803. doi: 10.3389/fimmu.2020.01803

38. Cha E, Klinger M, Hou Y, Cummings C, Ribas A, Faham M, et al. Improved survival with T cell clonotype stability after anti-CTLA-4 treatment in cancer patients. *Sci Transl Med* (2014) 6(238):238ra70. doi: 10.1126/scitranslmed.3008211

39. Wei SC, Levine JH, Cogdill AP, Zhao Y, Anang NAAS, Andrews MC, et al. Distinct cellular mechanisms underlie anti-CTLA-4 and anti-PD-1 checkpoint blockade. *Cell* (2017) 170(6):1120–33. doi: 10.1016/j.cell.2017.07.024

40. Sanromán ÁF, Joshi K, Au L, Chain B, Turajlic S. TCR sequencing: applications in immuno-oncology research. *Immuno-Oncol Technol* (2023) 17:100373. doi: 10.1016/j.iotech.2023.100373

41. Yost KE, Satpathy AT, Wells DK, Qi Y, Wang C, Kageyama R, et al. Clonal replacement of tumor-specific T cells following PD-1 blockade. *Nat Med* (2019) 25 (8):1251–9. doi: 10.1038/s41591-019-0522-3

42. Zhang J, Ji Z, Caushi JX, El Asmar M, Anagnostou V, Cottrell TR, et al. Compartmental analysis of T-cell clonal dynamics as a function of pathologic response to neoadjuvant PD-1 blockade in resectable non-small cell lung cancer. *Clin Cancer Res Off J Am Assoc Cancer Res* (2020) 26(6):1327–37. doi: 10.1158/1078-0432.CCR-19-2931

43. Stone HB, Peters LJ, Milas L. Effect of host immune capability on radiocurability and subsequent transplantability of a murine fibrosarcoma. *J Natl Cancer Inst* (1979) 63 (5):1229–35.

44. Bochem J, Zelba H, Spreuer J, Amaral T, Wagner NB, Gaissler A, et al. Early disappearance of tumor antigen-reactive T cells from peripheral blood correlates with superior clinical outcomes in melanoma under anti-PD-1 therapy. *J Immunother Cancer* (2021) 9(12):e003439. doi: 10.1136/jitc-2021-003439

45. Bhatt KH, Neller MA, Srihari S, Crooks P, Lekieffre L, Aftab BT, et al. Profiling HPV-16-specific T cell responses reveals broad antigen reactivities in oropharyngeal cancer patients. *J Exp Med* (2020) 217(10):e20200389. doi: 10.1084/jem.20200389

46. Balachandra S, Kusin SB, Lee R, Blackwell JM, Tiro JA, Cowell LG, et al. Blood-based biomarkers of human papillomavirus-associated cancers: A systematic review and meta-analysis. *Cancer* (2021) 127(6):850–64. doi: 10.1002/cncr.33221

47. Lee JY, Cutts RJ, White I, Augustin Y, Garcia-Murillas I, Fenwick K, et al. Next generation sequencing assay for detection of circulating HPV DNA (cHPV-DNA) in patients undergoing radical (Chemo)Radiotherapy in anal squamous cell carcinoma (ASCC). *Front Oncol* (2020) 10:505. doi: 10.3389/fonc.2020.00505

48. Galluzzi L, Buqué A, Kepp O, Zitvogel L, Kroemer G. Immunological effects of conventional chemotherapy and targeted anticancer agents. *Cancer Cell* (2015) 28 (6):690–714. doi: 10.1016/j.ccell.2015.10.012

49. Colbert LE, El MB, Lynn EJ, Bronk J, Karpinets TV, Wu X, et al. Expansion of candidate HPV-specific T cells in the tumor microenvironment during chemoradiotherapy is prognostic in HPV16+ Cancers. *Cancer Immunol Res* (2022) 10(2):259–71. doi: 10.1158/2326-6066.CIR-21-0119

50. Srivastava RM, Clump DA, Ferris RL. Anti-PD-1 mAb pre-radiotherapy (RT) loading dose and fractionated RT induce better tumor-specific immunity and tumor shrinkage than sequential administration in an HPV+ head and neck cancer model. *J Immunother Cancer* (2015) 3(Suppl 2):P314. doi: 10.1186/2051-1426-3-S2-P314

51. Chow J, Hoffend NC, Abrams SI, Schwaab T, Singh AK, Muhitch JB. Radiation induces dynamic changes to the T cell repertoire in renal cell carcinoma patients. *Proc Natl Acad Sci USA* (2020) 117(38):23721–9. doi: 10.1073/pnas.2001933117

52. Kahla S, Kochbati L, Sarraj S, Ben Daya I, Maalej M, Oueslati R. Molecular detection of human papillomavirus and viral DNA load after radiotherapy for cervical carcinomas. *Tumori J* (2016) 102(5):521–6. doi: 10.5301/tj.5000401

53. Honoré N, van Marcke C, Galot R, Helaers R, Ambroise J, van Maanen A, et al. Tumor-agnostic plasma assay for circulating tumor DNA detects minimal residual disease and predicts outcome in locally advanced squamous cell carcinoma of the head and neck. *Ann Oncol* (2023) 34(12):1175–86. doi: 10.1016/j.annonc.2023.09.3102

frontiers | Frontiers in Immunology

TYPE Original Research
PUBLISHED 11 January 2024
DOI 10.3389/fimmu.2023.1335546

OPEN ACCESS

EDITED BY
Raquel Tarazona,
University of Extremadura, Spain

REVIEWED BY
Nguyen Minh Duc,
Pham Ngoc Thach University of Medicine, Vietnam
Shuluan Li,
Chinese Academy of Medical Sciences and Peking Union Medical College, China

*CORRESPONDENCE
Shengchun Liu
liushengchun1968@163.com
Xiaohua Zeng
zxiaohuacqu@126.com

RECEIVED 09 November 2023
ACCEPTED 27 December 2023
PUBLISHED 11 January 2024

CITATION
Qu F, Luo Y, Peng Y, Yu H, Sun L, Liu S and Zeng X (2024) Construction and validation of a prognostic nutritional index-based nomogram for predicting pathological complete response in breast cancer: a two-center study of 1,170 patients.
Front. Immunol. 14:1335546.
doi: 10.3389/fimmu.2023.1335546

Construction and validation of a prognostic nutritional index-based nomogram for predicting pathological complete response in breast cancer: a two-center study of 1,170 patients

Fanli Qu[1,2], Yaxi Luo[3], Yang Peng[2], Haochen Yu[2], Lu Sun[4], Shengchun Liu[2]* and Xiaohua Zeng[1]*

[1]Department of Breast Cancer Center, Chongqing University Cancer Hospital, Chongqing, China, [2]Department of Breast and Thyroid Surgery, The First Affiliated Hospital of Chongqing Medical University, Chongqing, China, [3]Department of Rehabilitation, The Second Affiliated Hospital of Chongqing Medical University, Chongqing, China, [4]Department of Thyroid and Breast Surgery, The Eighth Affiliated Hospital, Sun Yat-sen University, Shenzhen, Guangdong, China

Background: Pathological complete response (pCR) after neoadjuvant chemotherapy (NAC) is associated with favorable outcomes in breast cancer patients. Identifying reliable predictors for pCR can assist in selecting patients who will derive the most benefit from NAC. The prognostic nutritional index (PNI) serves as an indicator of nutritional status and systemic immune competence. It has emerged as a prognostic biomarker in several malignancies; however, its predictive value for pCR in breast cancer remains uncertain. The objective of this study is to assess the predictive value of pretreatment PNI for pCR in breast cancer patients.

Methods: A total of 1170 patients who received NAC in two centers were retrospectively analyzed. The patients were divided into three cohorts: a training cohort (n=545), an internal validation cohort (n=233), and an external validation cohort (n=392). Univariate and multivariate analyses were performed to assess the predictive value of PNI and other clinicopathological factors. A stepwise logistic regression model for pCR based on the smallest Akaike information criterion was utilized to develop a nomogram. The C-index, calibration plots and decision curve analysis (DCA) were used to evaluate the discrimination, calibration and clinical value of the model.

Results: Patients with a high PNI (≥53) had a significantly increased pCR rate (OR 2.217, 95% CI 1.215-4.043, p=0.009). Tumor size, clinical nodal status, histological grade, ER, Ki67 and PNI were identified as independent predictors and included in the final model. A nomogram was developed as a graphical representation of the model, which incorporated the PNI and five other factors (AIC=356.13). The nomogram demonstrated satisfactory calibration and discrimination in the training cohort (C-index: 0.816, 95% CI 0.765-0.866), the internal validation cohort (C-index: 0.780, 95% CI 0.697-0.864) and external validation cohort (C-index: 0.714, 95% CI 0.660-0.769). Furthermore, DCA indicated a clinical net benefit from the nomogram.

Conclusion: The pretreatment PNI is a reliable predictor for pCR in breast cancer patients. The PNI-based nomogram is a low-cost, noninvasive tool with favorable predictive accuracy for pCR, which can assist in determining individualized treatment strategies for breast cancer patients.

KEYWORDS

breast cancer, prognostic nutritional index, neoadjuvant chemotherapy, nomogram, pathological complete response

1 Introduction

Breast cancer is the most common malignant tumor in females and is one of the leading causes of cancer morbidity and mortality in females worldwide. The incidence and mortality of breast cancer were estimated to be 279,100 and 42,690, respectively, in the United States in 2020 (1). There were an estimated 0.52 and 0.13 million new breast cancer cases and deaths in Europe in 2018 (2), whereas the numbers of Chinese patients were 0.27 and 0.07 million in 2015, respectively (3). Neoadjuvant chemotherapy (NAC) is a standard therapeutic option for most breast cancer patients, especially those with high-risk localized breast cancer. It aims to reduce the disease burden and decrease the extent of the operation. NAC can make breast cancer resectable for locally advanced patients and can make it possible to receive breast-conserving surgery for operable patients (4). Moreover, NAC provides an opportunity to assess breast cancer chemosensitivity *in vivo*. Tumor response to NAC is valuable for guiding individualized further systematic therapy (5). A large meta-analysis, including a total of 52 studies representing 27,895 patients, explored the significance of pathological complete response (pCR) following NAC. The results demonstrated that pCR was associated with better event-free survival and overall survival (OS) (6). However, breast cancer is a highly heterogeneous disease with different histological types, molecular classifications, and biological behaviors, leading to different responses to NAC (7). A portion of patients cannot benefit from NAC but are unnecessarily exposed to the toxicity of cytotoxic drugs. In addition, NAC may increase the risk of disease progression in these patients with chemoresistant tumors by delaying surgery. Thus, there is an urgent need to search for a reliable method to accurately predict pCR for screening patients who will benefit most from NAC.

Previous studies indicated that various methods could be utilized to predict pCR in breast cancer patients who received NAC, such as gene signatures, histomorphological factors, pathological parameters, and imaging features (8–13). Compared with the above factors, blood samples are easily accessible and can reflect the comprehensive state of cancer patients. Various serum tumor biomarkers have been identified as prognostic factors in breast cancer patients, including CEA, CA15-3, CA19-9, and CA125 (14, 15). In recent years, accumulating evidence has demonstrated that the nutrition status of a patient has a great impact on the prognosis of cancer (16–18). Albumin (ALB) is synthesized by the liver, which has been regarded as a biomarker of visceral protein and immunocompetence status, and is commonly used for nutritional assessment (19). Previous studies have suggested that ALB can be applied to predict prognosis in several malignancies, including gastric cancer, non-small-cell lung cancer, glioblastoma, and esophageal squamous cell carcinoma (20–23). It is known that systemic inflammation promotes tumor progression and metastasis (24). The prognostic values of inflammation-based prognostic scores, such as the C-reactive protein to albumin ratio, neutrophil to lymphocyte ratio, lymphocyte to monocyte ratio, platelet to lymphocyte ratio, and systemic-immune-inflammation index, have been reported in various malignancies, including breast cancer (25–29). The prognostic nutritional index (PNI) is a multiparametric index calculated as the serum albumin concentration and peripheral lymphocyte count and was first reported as an indicator to assess preoperative nutritional status and to estimate the risk of postoperative complications in gastrointestinal cancer patients (30). The PNI has been identified as an indicator of nutritional status and systemic immune competence with more accuracy than other variables (31, 32). Moreover, the PNI has been found to be an independent prognostic predictor in various malignant tumors, including breast cancer (33). However, whether the PNI can be used as a predictor for pCR in breast cancer patients who receive NAC has seldom been studied.

Therefore, in the current study, we evaluated the predictive role of the PNI for pCR in breast cancer patients. Furthermore, based on clinicopathological factors, including the PNI, a user-friendly nomogram was constructed and validated to predict the individual probability of pCR.

2 Materials and methods

2.1 Study population

A total of 1170 primary breast cancer patients of two medical centers, the First Affiliated Hospital of Chongqing Medical University and Chongqing University Cancer Hospital, were sequentially included. The inclusion criteria were as follow:

(a) histopathological examination confirmed the diagnosis of invasive breast cancer; (b) female; (c) received NAC and operation; (d) received at least 3 courses of treatment with TEC (docetaxel 75 mg/m^2, epirubicin 75 mg/m^2, and cyclophosphamide 500 mg/m^2) every 21 days before operation; (e) no history of other malignancies; and (f) serum ALB concentration and peripheral lymphocyte count were measured before treatment. Patients without complete information were excluded. Finally, 778 patients diagnosed at the First Affiliated Hospital of Chongqing Medical University from January 2012 to March 2018 were enrolled. They were randomly allocated into the training cohort and the internal validation cohort at a ratio of 7:3 (training cohort: n=545, internal validation cohort: n=233). Moreover, 392 primary breast cancer patients diagnosed at Chongqing University Cancer Hospital from January 2018 to June 2022 were included as external validation cohort. Representative images of diagnostic imaging were shown in Supplementary Figure 1. This study was reviewed and approved by the ethics committee of the First Affiliated Hospital of Chongqing Medical University and Chongqing University Cancer Hospital.

2.2 Data collection

Clinical characteristics, including age, menopausal status, courses of NAC, histological type of cancer, tumor size, clinical nodal status, histological grade, estrogen receptor (ER) status, progesterone receptor (PR) status, human epidermal growth factor receptor-2 (HER2) receptor status, Ki67 status, serum ALB concentration, and peripheral lymphocyte count, were collected for subsequent analysis. As shown in Supplementary Figure 2, ER and PR expression status were considered positive when more than 1% of the tumor cells showed nuclear immunohistochemical staining. HER2 status was defined as positive when the score of immunohistochemical staining was 3+ or a greater than 2.0-fold change compared to the expression of CEP17 in tumor cells by fluorescence *in situ* hybridization (34). Regarding Ki67, the percentage of Ki67-positive cells (500–1,000) among the total number of cancer cells in the invasive front of the tumor was defined as the Ki67 value (35).

Two pathologists assessed the status of ER, PR, HER2, and Ki67 independently. Based on the expression status of the above 4 molecules, tumors were divided into four subtypes: luminal subtype (ER positive and/or PR positive, HER2 negative), luminal/HER2 subtype (ER positive and/or PR positive, HER2 positive), HER2 enriched subtype (ER negative, PR negative, HER2 positive), and TNBC subtype (ER negative, PR negative, HER2 negative). The serum ALB concentration and peripheral lymphocyte count were measured along with routine plasma examinations at diagnosis. Blood samples were collected when patients had fasted for at least 6 hours. The serum ALB concentration was analyzed by a fully automatic biochemical analyzer (Roche c701, Basel, Switzerland). The peripheral lymphocyte count was analyzed by a fully automatic hematology analyzer (Sysmex XN-1000, Kobe, Japan). According to the Miller-Payne grading system, pathological complete response (pCR) was defined as no residual tumor lesion present in any excised breast tissue or lymph node (36).

2.3 Statistical analysis

The cutoff values of ALB and the lymphocyte count were 40 g/L and 800 per mm^3, respectively, which were established based on the normal reference values. According to the well-established formula, PNI = serum albumin (g/L) + 0.005 × peripheral lymphocytecount (per mm^3) (30). The optimal cutoff value of the PNI for pCR was determined by the maximum Youden index from receiver operating characteristic (ROC) curve analysis. The differences in clinicopathological variables between the training and validation cohorts were compared by the chi-square test or Fisher's exact test. Moreover, the relationships between the PNI and clinicopathological characteristics were analyzed by the chi-square test or Fisher's exact test. Similarly, the associations between pCR and clinicopathological characteristics were assessed. The primary goal of our study was to estimate the likelihood of breast cancer patients reaching pCR after NAC. Multivariate logistic regression analysis was performed to assess the associations between clinicopathological factors and the likelihood of pCR. Odds ratios were reported with corresponding 95% confidence intervals (CIs). A stepwise logistic regression model for pCR based on the smallest Akaike information criterion was employed to develop an individualized nomogram using the rms package (Version: 6.2-0, https://cran.r-project.org/web/packages/rms/index.html) in R software. Then, the performance of the logistic regression model was quantified by discrimination and calibration in the training, internal and external validation cohorts. The concordance index (C-index) was calculated by testing the concordance between the prediction probability and the actual status, which was utilized to assess the prediction and discrimination ability of the model. The bootstrapping method with 1000 resamples was used to generate the calibration curves to test the calibration of the nomogram. The fitness of the model was analyzed by the Hosmer–Lemeshow test. Furthermore, decision curve analysis (DCA) was applied to quantify the clinical usefulness of the nomogram, which is a method to estimate the net benefit of a model based on the relative value of benefits (true positives) and harms (false-positives).

All statistical analyses were performed using the Statistical Package for the Social Sciences version 25.0 software (IBM Corp., Armonk, USA) and R software (version 4.0.3; https://www.R-project.org/). A two-sided p value< 0.05 was considered statistically significant.

3 Results

3.1 Patient characteristics

According to the inclusion and exclusion criteria, a total of 778 breast cancer patients from the First Affiliated Hospital of Chongqing Medical University with a mean age of 49.0 ± 9.1 years (IQR: 43.0-56.0 years) were enrolled in the current study.

They were randomly allocated into the training cohort and the internal validation cohort at a ratio of 7:3 (training cohort: n=545, internal validation cohort: n=233) for constructing and internally validating the predictive model. Furthermore, 392 patients from Chongqing University Cancer Hospital were included in the external validation cohort. The clinicopathological characteristics are shown in Table 1. Among the 1170 patients, 802 (68.5%) were premenopausal, and 368 (31.5%) were postmenopausal at baseline.

TABLE 1 Baseline clinicopathological characteristics in training and validation cohorts.

Characteristics	Overall (n=1170)	Training cohort (n=545)	Internal validation cohort (n=233)	External validation cohort (n=392)
Age (y)				
<50	621(53.1)	301 (55.2)	127 (54.5)	193 (49.2)
≥50	549(46.9)	244 (44.8)	106 (45.5)	199 (50.8)
Menopause				
Yes	368(31.5)	218 (40.0)	93 (39.9)	57 (14.5)
No	802(68.5)	327 (60.0)	140 (60.1)	335 (85.5)
Chemotherapy courses				
3	34(2.9)	18 (3.3)	4 (1.7)	12 (3.1)
4	786(67.2)	486 (89.2)	207 (88.8)	93 (23.7)
5-8	350(29.2)	41 (7.5)	22 (9.4)	287 (73.2)
Histological type				
Ductal	1126(96.2)	523 (96.0)	225 (96.6)	378 (96.4)
Lobular	16(1.4)	7 (1.3)	3 (1.3)	6 (1.5)
Others	28(2.4)	15 (2.8)	5 (2.1)	8 (2.0)
Tumor size				
T1	130(11.1)	52 (9.5)	30 (12.9)	48 (12.2)
T2	833(71.2)	381 (69.9)	156 (67.0)	296 (75.5)
T3	207(17.7)	112 (20.6)	47 (20.2)	48 (12.2)
Clinical nodal status				
Negative	370(31.6)	211 (38.7)	107 (45.9)	52 (13.3)
Positive	800(68.4)	334 (61.3)	126 (54.1)	340 (86.7)
Histological grade				
I	71(6.1)	36 (6.6)	13 (5.6)	22 (5.6)
II	886(75.7)	407 (74.7)	167 (71.7)	312 (79.6)
III	213(18.2)	102 (18.7)	53 (22.7)	58 (14.8)
ER				
Negative	422(36.1)	198 (36.3)	92 (39.5)	132 (33.7)
Positive	748(63.9)	347 (63.7)	141 (60.5)	260 (66.3)
PR				
Negative	600(51.3)	275 (50.5)	122 (52.4)	203 (51.8)
Positive	570(48.7)	270 (49.5)	111 (47.6)	189 (48.2)
HER2 status				
Negative	800(68.4)	323 (59.3)	130 (55.8)	347 (88.5)
Positive	370(31.6)	222 (40.7)	103 (44.2)	45 (11.5)
Ki67 expression (%)				
<14	325(27.8)	171 (31.4)	70 (30.0)	84 (21.4)
≥14	845(72.2)	374 (68.6)	163 (70.0)	308 (78.6)
Molecular subtypes				
Luminal	573(49.0)	240 (44.0)	91 (39.1)	242 (61.7)
Luminal/HER2	197(16.8)	118 (21.7)	56 (24.0)	23 (5.9)
HER2	173(14.8)	104 (19.1)	47 (20.2)	22 (5.6)
TNBC	227(19.4)	83 (15.2)	39 (16.7)	105 (26.8)
ALB				
<40	393(33.6)	222 (40.7)	87 (37.3)	84 (78.6)
≥40	777(66.4)	323 (59.3)	146 (62.7)	308 (21.4)

(Continued)

TABLE 1 Continued

Characteristics	Overall (n=1170)	Training cohort (n=545)	Internal validation cohort (n=233)	External validation cohort (n=392)
Lymphocyte count				
<800	67(5.7)	34 (6.2)	15 (6.4)	18 (4.6)
≥800	1103(94.3)	511(93.8)	218 (93.6)	374 (95.4)
PNI				
<53	825(70.5)	413 (75.8)	176 (75.5)	236 (60.2)
≥53	345(29.5)	132 (24.2)	57 (24.5)	156 (39.8)
Response evaluation				
pCR	186(15.9)	70 (12.8)	32 (13.7)	84 (21.4)
Non-pCR	984(84.1)	475 (87.2)	201 (86.3)	308 (78.6)

ER, estrogen receptor; PR, progesterone receptor; HER2, human epidermal growth factor 2; ALB, albumin; PNI, prognostic nutritional index; pCR, pathologic complete response.

More than half of the patients (n=786, 67.2%) received 4 chemotherapy cycles before surgery. For the histological classification, 1126 (96.2%) patients were diagnosed with invasive lobular carcinoma; 16 patients (1.4%) were diagnosed with invasive lobular carcinoma; 28 patients (2.4%) were diagnosed with other special types. The most common tumor size was 2-5 cm (71.2%), followed by > 5 cm (17.7%) and ≤ 2 cm (11.1%). Moreover, the lymph nodes of 800 (68.4%) patients were involved. In terms of histological grade, 75.7% (n=886) of the tumors were categorized as Grade II. Most of the patients (n=845, 72.2%) had Ki67 expression ≥ 14%. The molecular subtype distribution was as follows: 49.0% (n=573) for the luminal subtype, 16.8% (n=197) for the luminal/HER2 subtype, 14.8% (n=173) for the HER2-enriched subtype and 19.4% (n=227) for the TNBC subtype. In addition, 66.4% (n=777) of patients had normal serum albumin concentrations, while 94.3% (n=1103) of patients had normal peripheral lymphocyte counts. According to the Miller-Payne grading system, 186 (15.9%) patients achieved pCR after NAC. No significant difference in the analyzed clinicopathological factors was observed between the training and validation cohorts.

3.2 Associations between the PNI and clinicopathological characteristics

The relationships between the PNI and clinicopathological characteristics were assessed in the training cohort. The optimal cutoff value of the PNI was 53 according to the ROC curve analysis and the Youden index. Based on the cutoff value, 413 (75.8%) patients were included in the low-PNI group (PNI< 53), while the other 132 (24.2%) patients were included in the high-PNI group (PNI ≥ 53). As shown in Table 2, the results demonstrated that the PNI level was significantly associated with pCR (p =0.007). The other clinicopathological factors were comparable between the two groups. No differences were observed in age, menopausal status, chemotherapy cycles, histological type, tumor size, clinical nodal status, histological grade, ER, PR, HER2, Ki67, or molecular subtypes between the high-PNI and low-PNI groups.

3.3 Predictors of pCR

As shown in Table 3, the univariate analysis of the training cohort demonstrated that pCR was significantly correlated with tumor size, clinical nodal status, histological grade, ER status, PR status, Ki67 expression, molecular subtypes, peripheral lymphocyte count, and PNI. Multivariate logistic regression models were applied to adjust for potential confounders. Variables with p< 0.1 in univariate analysis were included in multivariable models. To avoid the influence of multicollinearity between the lymphocyte count and PNI, only the PNI was included in further analysis. The results demonstrated that tumor size, clinical nodal status, histological grade, Ki67 expression, and PNI were independent predictors for pCR (Table 4). The probability of pCR in patients with a high PNI (PNI ≥ 53) was significantly higher (adjusted OR 2.217, 95% CI 1.215-4.043, p=0.009) than that in patients with a low PNI (PNI< 53). In addition, as expected, patients with larger, higher histological grade tumors and axillary lymph node-positive diseases had more difficulty achieving pCR (adjusted OR 0.167, 95% CI 0.076-0.370, p<0.001 for T2; adjusted OR 0.165, 95% CI 0.063-0.438, p<0.001 for T3; adjusted OR 0.094, 95% CI 0.031-0.290, p<0.001 for Grade II; adjusted OR 0.072, 95% CI 0.020-0.261, p<0.001 for Grade III; adjusted OR 0.326, 95% CI 0.179-0.591, p<0.001 for node-positive status). Moreover, the probability of pCR in patients with Ki67 expression ≥ 14% was 3.124-fold (95% CI 1.415-6.898, p=0.005) higher than that in patients with Ki67 expression< 14%.

3.4 Development and validation of the nomogram

A nomogram was constructed based on the stepwise logistic regression model for pCR with the training cohort. Ultimately, the following factors were incorporated into the nomogram: tumor size, clinical nodal status, histological grade, ER, Ki67, and PNI, which manifested the smallest AIC value (356.13). The nomogram determined the proportion of scores based on the regression

10.3389/fimmu.2023.1335546

TABLE 2 Correlations between PNI and clinicopathological characteristics in the training cohort.

Characteristics	PNI<53 (N=413)	PNI≥53 (N=132)	*p*-value
Age (y)			0.533
<50	225 (54.5)	76 (57.6)	
≥50	188 (45.5)	56 (42.4)	
Menopause			0.967
Yes	165 (40.0)	53 (40.2)	
No	248 (60.0)	79 (59.8)	
Chemotherapy cycles			0.120
3	15 (3.6)	3 (2.3)	
4	362 (87.7)	124 (93.9)	
5-8	36 (8.7)	5 (3.8)	
Histological type			0.478
Ductal	397 (96.1)	126 (95.5)	
Lobular	4 (1.0)	3 (2.3)	
Others	12 (2.9)	3 (2.3)	
Tumor size			0.593
T1	39 (9.4)	13 (9.8)	
T2	285 (69.0)	96 (72.7)	
T3	89 (21.5)	23 (17.4)	
Clinical nodal status			0.105
Negative	152 (36.8)	59 (44.7)	
Positive	261 (63.2)	73 (55.3)	
Histological Grade			0.958
I	28 (6.8)	8 (6.1)	
II	308 (74.6)	99 (75.0)	
III	77 (18.6)	25 (18.9)	
ER			0.842
Negative	151 (36.6)	47 (35.6)	
Positive	262 (63.4)	85 (64.4)	
PR			0.497
Negative	205 (49.6)	70 (53.0)	
Positive	208 (50.4)	62 (47.0)	
HER2 status			0.802
Negative	246 (59.6)	77 (58.3)	
Positive	167 (40.4)	55 (41.7)	
Ki67 expression (%)			0.928
<14	130 (31.5)	41 (31.1)	
≥14	283 (68.5)	91 (68.9)	
Molecular subtypes			0.630
Luminal	186 (45.0)	54 (40.9)	
Luminal/HER2	86 (20.8)	32 (24.2)	
HER2	81 (19.6)	23 (17.4)	
TNBC	60 (14.5)	23 (17.4)	
Response evaluation			0.007
pCR	44 (10.7)	26 (19.7)	
Non-pCR	369 (89.3)	106 (80.3)	

ER, estrogen receptor; PR, progesterone receptor; HER2, human epidermal growth factor 2; PNI, prognostic nutritional index; pCR, pathologic complete response.

coefficients of the included variables and assigned a score level for each variable. In Figure 1, the above factors were used to calculate points based on the points scale axis. By adding up these points, the total score was utilized to estimate the probability of pCR.

TABLE 3 Univariate analysis for factors associated with pCR in the training cohort.

Characteristics	Non-pCR (n=475)	pCR (n=70)	*p*-value
Age (y)			0.346
<50	266 (56.0)	35 (50.0)	
≥50	209 (44.0)	35 (50.0)	
Menopause			0.296
Yes	186 (39.2)	32 (45.7)	
No	289 (60.8)	38 (54.3)	
Chemotherapy cycles			0.801
3	16 (3.4)	2 (2.9)	
4	422 (88.8)	64 (91.4)	
5-8	37 (7.8)	4 (5.7)	
Histological type			0.055
Ductal	459 (96.6)	64 (91.4)	
Lobular	6 (1.3)	1 (1.4)	
Others	10 (2.1)	5 (7.1)	
Tumor size			<0.001
T1	36 (7.6)	16 (22.9)	
T2	338 (71.2)	43 (61.4)	
T3	101 (21.3)	11 (15.7)	
Clinical nodal status			<0.001
Negative	164 (34.5)	47 (67.1)	
Positive	311 (65.5)	23 (32.9)	
Histological Grade			<0.001
I	23 (4.8)	13 (18.6)	
II	361 (76.0)	46 (65.7)	
III	91 (19.2)	11 (15.7)	
ER			<0.001
Negative	159 (33.5)	39 (55.7)	
Positive	316 (66.5)	31 (44.3)	
PR			<0.001
Negative	226 (47.6)	49 (70.0)	
Positive	249 (52.4)	21 (30.0)	
HER2 status			0.517
Negative	284 (59.8)	39 (55.7)	
Positive	191 (40.2)	31 (44.3)	
Ki67 expression (%)			0.001
<14	161 (33.9)	10 (14.3)	
≥14	314 (66.1)	60 (85.7)	
Molecular subtypes			0.003
Luminal	220 (46.3)	20 (28.6)	
Luminal/HER2	105 (22.1)	13 (18.6)	
HER2	86 (18.1)	18 (25.7)	
TNBC	64 (13.5)	19 (27.1)	
ALB			0.894
<40	194 (40.8)	28 (40.0)	
≥40	281 (59.2)	42 (60.0)	
lymphocyte count			0.021
<800	34 (7.2)	0 (0)	
≥800	441 (92.8)	70 (100)	
PNI			0.007
<53	369 (77.7)	44 (62.9)	
≥53	106 (22.3)	26 (37.1)	

ER, estrogen receptor; PR, progesterone receptor; HER2, human epidermal growth factor 2; ALB, albumin; PNI, prognostic nutritional index; pCR, pathologic complete response.

10.3389/fimmu.2023.1335546

TABLE 4 Multivariate analysis for factors associated with pCR in the training cohort.

Characteristics	Crude OR (95%CI)	*p*-value	Adjusted OR (95%CI)	*p*-value
Histological type				
Ductal	Reference		Reference	
Lobular	1.195(0.142-10.090)	0.870	0.545 (0.052-5.686)	0.612
Others	3.586(1.188-10.826)	0.023	0.312(0.061-1.607)	0.164
Tumor size				
T1	Reference		Reference	
T2	0.286(0.147-0.559)	<0.001	0.167(0.076-0.370)	<0.001
T3	0.245(0.104-0.577)	0.001	0.165(0.063-0.438)	<0.001
Clinical nodal status				
Negative	Reference		Reference	
Positive	0.258(0.151-0.440)	<0.001	0.326(0.179-0.591)	<0.001
Histological grade				
I	Reference		Reference	
II	0.225(0.107-0.475)	<0.001	0.094(0.031-0.290)	<0.001
III	0.214(0.085-0.539)	0.001	0.072(0.020-0.261)	<0.001
ER				
Negative	Reference		Reference	
Positive	0.400(0.240-0.665)	<0.001	0.480(0.080-2.876)	0.421
PR				
Negative	Reference		Reference	
Positive	0.389(0.226-0.669)	0.001	0.579(0.244-1.374)	0.215
Ki67 expression (%)				
<14	Reference		Reference	
≥14	3.076(1.534-6.170)	0.002	3.124(1.415-6.898)	0.005
Molecular subtypes				
Luminal	Reference		Reference	
Luminal/HER2	1.362(0.652- 2.843)	0.411	1.096 (0.474- 2.531)	0.830
HER2	2.302(1.162- 4.562)	0.017	0.799 (0.103- 6.171)	0.829
TNBC	3.266 (1.643- 6.490)	0.001	0.740 (0.095- 5.765)	0.773
PNI				
<53	Reference		Reference	
≥53	2.057(1.210- 3.497)	0.008	2.217(1.215-4.043)	0.009

ER, estrogen receptor; PR, progesterone receptor; PNI, prognostic nutritional index; pCR, pathologic complete response.

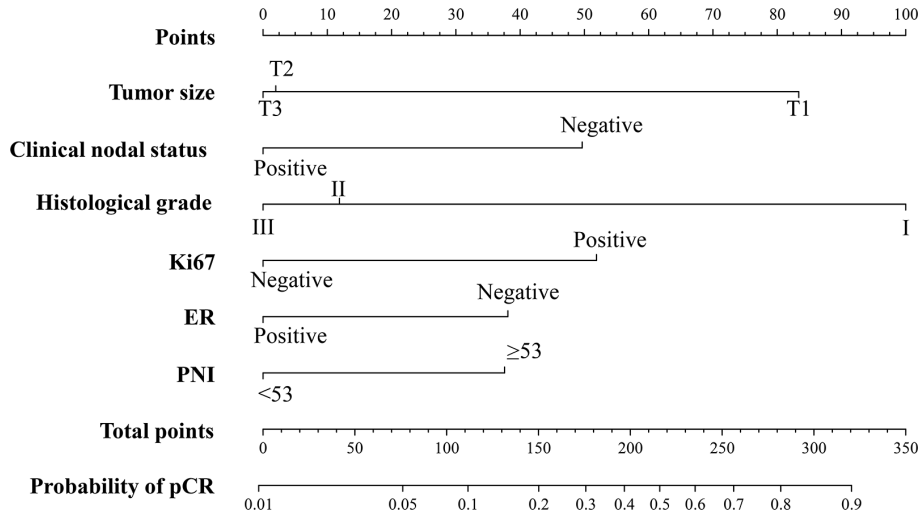

FIGURE 1
The PNI-based nomogram for predicting the probability of pCR after NAC in breast cancer patients. ER, estrogen receptor; PNI, Prognostic Nutritional Index; pCR, pathologic complete response.

The predictive accuracy of the nomogram for the pCR rate of breast cancer patients who underwent NAC was evaluated in the training and validation cohorts. The C-index was 0.816 (95% CI 0.765-0.866) in the training cohort, 0.780 (95% CI 0.697-0.864) in the internal validation cohort and 0.714 (95% CI 0.660-0.769) in the external validation cohort (Figures 2A–C). Moreover, the calibration plots for the probability of pCR indicated a satisfactory fit between prediction by nomogram and observation in the training and validation cohorts (Figures 2D–F). Decision curves of the training and validation cohorts were illustrated for the constructed nomogram to assess the clinical utility. It demonstrated that for predicted probability thresholds between 0 and 80%, the model-based decision was superior to either the treat-none or the treat-all-patients scheme (Figures 2G–I).

4 Discussion

Breast cancer is the most common malignant tumor among women and has resulted in a heavy disease burden worldwide (1). Currently, NAC is widely used in breast cancer patients, especially those with locally advanced diseases. Patients who achieve pCR

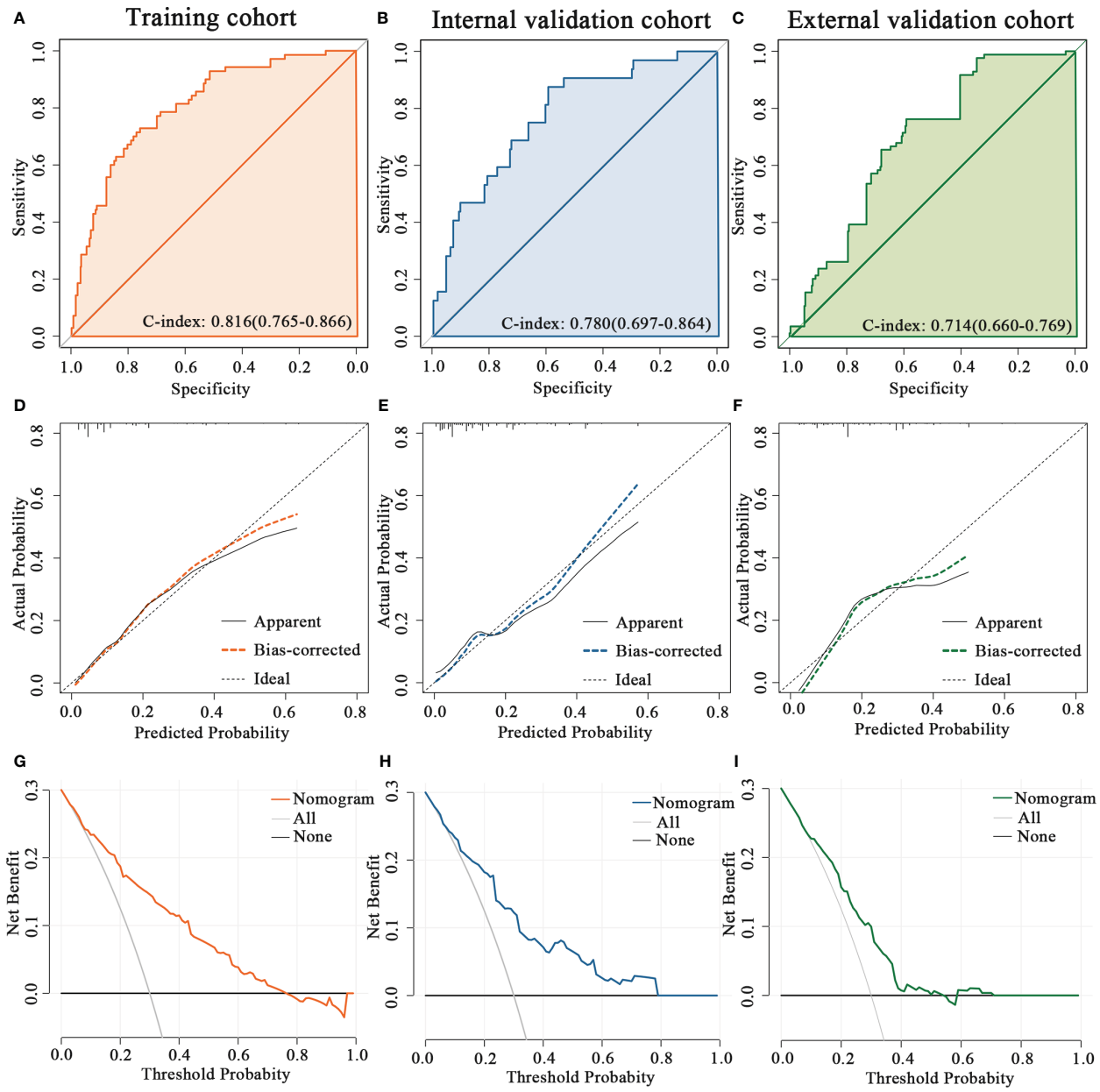

FIGURE 2
Validation the predictive value of the PNI-based nomogram. The ROC curves for the nomogram model in **(A)** the training cohort, **(B)** internal validation cohort and **(C)** external validation cohort. The calibration plots for the nomogram model in **(D)** the training cohort, **(E)** internal validation cohort and **(F)** external validation cohort. The decision curves show the net-benefit of using the nomogram in **(G)** the training cohort, **(H)** internal validation cohort and **(I)** external validation cohort.

after NAC have favorable survival outcomes regardless of molecular subtype; however, tumor response to NAC varies greatly from individual to individual (6). Consequently, an accurate prediction assessment for pCR after NAC would have great clinical significance for breast cancer patients. In the present study, the clinicopathological attributes of 1170 breast cancer patients who received NAC were analyzed. The results indicated that the PNI is an independent predictive factor for pCR. Patients with pretreatment PNI< 53 had a lower pCR rate. In addition, a novel PNI-based nomogram was developed to quantify the probability of pCR, which has promising prospects for clinical application.

To date, many studies have explored the prognostic role in predicting the outcome of breast cancer of hematological and serum biochemical parameters, such as fibrinogen, alkaline phosphatase, lactate dehydrogenase, and the lymphocyte to monocyte ratio (27, 37, 38). The serum ALB concentration and peripheral lymphocyte count are two accessible laboratory indices that are examined routinely at diagnosis. ALB, a globular, single band protein of 585 amino acids, is exclusively synthesized and secreted by the liver and accounts for approximately half of the total serum protein (39). In cancer patients, hypoalbuminemia may be caused by decreased synthesis, increased consumption, and loss of serum ALB, which is related to inflammation and malnutrition during cancer development and progression (40, 41). In addition, hypoproteinemia indicates impaired immune function and leads to poor anticancer treatment effects (42). Previous studies have reported that pretreatment serum ALB can be used as a prognostic indicator in several kinds of cancers, including lung, pancreatic, gastrointestinal, ovarian, and breast cancer (43). Lymphocytes can be divided into T lymphocytes, B lymphocytes, and natural killer cells according to their different phenotypes and biological functions. Moreover, lymphocytes are important cellular components of the host immune system, accounting for approximately 30% of the total number of normal human leukocytes, and are essential effector cells for the elimination of cancer cells (44). Previous studies have found that both pretreatment and treatment-related lymphopenia are associated with poor prognosis in cancers (45, 46). This phenomenon suggests that lymphopenia may be a manifestation of tumor-induced immunosuppression and a driver of tumor progression. The PNI is a noninvasive and easily assessable index that is calculated based on the serum ALB concentration and peripheral lymphocyte count, offering insights into both the immune and nutritional status of patients (31, 32). PNI was initially introduced as an index for evaluating postoperative complications in gastrointestinal surgery (30). Currently, it has emerged as a prognostic factor in various cancers, including breast cancer. Numerous studies have demonstrated that a higher PNI is associated with more favorable survival outcomes. Hua et al. (33) investigated the significance of the PNI as a predictor of OS for T1-2N1 breast cancer. The results revealed that patients with a high PNI had better OS than those with a low PNI. Similarly, Chen et al. (47) reported that the PNI was an independent predictive factor for disease-free survival (DFS) and OS in breast cancer patients treated with NAC. Oba et al. (48) found that a decrease in the PNI during NAC was related to poor DFS in breast cancer patients, but no significant difference in DFS was observed between the pre-NAC PNI high and low groups. In contrast, Wang et al. (49) obtained different results. They conducted a retrospective analysis including 202 locally advanced breast cancer patients who received NAC and found that patients with an excessively high PNI (>55) had more difficulty achieving pCR and had worse survival outcomes.

In the present study, the optimal cutoff value of the PNI was 53 according to ROC curve analysis and the maximum Youden index. This value is similar to the previously reported cutoff value of the pretreatment PNI in breast cancer patients (33, 47, 48). Initially, the associations between the PNI and clinicopathological characteristics were evaluated. Our results suggested that age, menopausal status, chemotherapy cycles, histological type, tumor size, clinical nodal status, histological grade, ER, PR, HER2, Ki67, or molecular subtypes were not related to the PNI, which was in line with previous studies (47, 49). Further analysis assessed the predictive value of clinicopathological factors for pCR after NAC. Univariate and multivariate analyses indicated that tumor size, clinical nodal status, histological grade, Ki67 expression, and PNI were independent predictors for pCR. Most of the above factors are consistent with published studies. A large-scale retrospective study from the Netherlands found that a lower T stage (T1-2 vs. T3-4) was a significant independent predictor of a higher pCR rate in breast cancer patients (50). Cortazar et al. conducted a pooled analysis including 11,955 patients and suggested that patients with positive lymph nodes and hormone receptors had lower pCR rates (51). Ki67 expression was associated with tumor cell proliferation, and several studies revealed that high Ki-67 was associated with more pCR events in breast cancer patients (52). Few studies have evaluated the predictive value of the PNI for pCR in breast cancer. We only found one study focused on it (49). However, this study suggested that a high PNI was less likely to achieve pCR, which differed from our results. The above inconsistent results may be associated with the differences in sample size, PNI cutoff value, and characteristics of tumors. Moreover, our results indicated no significant correlation between HER2 status and pCR, which is inconsistent with previous studies (6). The overall pCR rate of our study was 15.9%, which is relatively low compared with some previous large-scale studies (20.4-21.1%) (6, 53). Two randomized controlled trials (the NOAH trial and the NeoSphere trial) suggested that patients given neoadjuvant trastuzumab and pertuzumab plus NAC had a significantly improved pCR rate than those given NAC only, without substantial differences in tolerability (54, 55). In our study, 97% of HER2-positive patients refused neoadjuvant anti-HER2 therapy for economic reasons, which may result in a lower pCR rate and an insignificant correlation between HER2 status and pCR. A PNI-based nomogram was developed and validated to quantitatively estimate the pCR probability in breast cancer patients who received NAC to facilitate clinical application.

The main limitation of our study is that it is a retrospective study conducted at two medical centers. Additionally, the absence of neoadjuvant anti-HER2 therapy in 97% of HER2-positive patients greatly impacted the pCR rate. Consequently, large-scale multicenter prospective clinical trials are required to improve and validate the PNI-based nomogram in breast cancer patients. The

predictive role of the PNI in HER2-positive patients needs to be further analyzed in adequately treated patients.

5 Conclusions

In conclusion, this study demonstrated that the pretreatment PNI, tumor size, clinical nodal status, histological grade, and Ki67 expression could serve as independent predictive factors for pCR in breast cancer patients treated with NAC. The PNI-based nomogram can accurately estimate pCR probability and help to determine appropriate treatment strategies.

Data availability statement

The original data supporting the results of this study are available from the corresponding author upon request.

Ethics statement

The studies involving humans were approved by the First Affiliated Hospital of Chongqing Medical University and Chongqing University Cancer Hospital. The studies were conducted in accordance with the local legislation and institutional requirements. The participants provided their written informed consent to participate in this study.

Author contributions

FQ: Conceptualization, Data curation, Investigation, Methodology, Software, Writing – original draft. YL: Data curation, Formal analysis, Validation, Visualization, Writing – review & editing. YP: Data curation, Methodology, Validation, Visualization, Writing – review & editing. HY: Formal analysis, Resources, Writing – review & editing. LS: Data curation, Resources, Writing – review & editing. SL: Project administration, Supervision, Writing – review & editing. XZ: Funding acquisition, Project administration, Supervision, Writing – review & editing.

Funding

The author(s) declare financial support was received for the research, authorship, and/or publication of this article. This work was supported by the Talent Program of Chongqing (Grant No. CQYC20200303137), Chongqing Municipal Health and Health Commission (Grant No.2019NLTS005), Chongqing Research Institute Performance Incentive Guide Special Project and Beijing Science and Technology Innovation Medical Development Foundation (Grant No. KC2021-JF-0167-05).

Conflict of interest

The authors declare that the research was conducted in the absence of any commercial or financial relationships that could be construed as a potential conflict of interest.

Publisher's note

Supplementary material

The Supplementary Material for this article can be found online at: https://www.frontiersin.org/articles/10.3389/fimmu.2023.1335546/full#supplementary-material

References

1. Siegel RL, Miller KD, Jemal A. Cancer statistics, 2020. *CA Cancer J Clin* (2020) 70 (1):7–30. doi: 10.3322/caac.21590

2. Ferlay J, Colombet M, Soerjomataram I, Dyba T, Randi G, Bettio M, et al. Cancer incidence and mortality patterns in europe: estimates for 40 countries and 25 major cancers in 2018. *Eur J Cancer* (2018) 103:356–87. doi: 10.1016/j.ejca.2018.07.005

3. Chen W, Zheng R, Baade PD, Zhang S, Zeng H, Bray F, et al. Cancer statistics in China, 2015. *CA Cancer J Clin* (2016) 66(2):115–32. doi: 10.3322/caac.21338

4. Gralow J, Burstein H, Wood W, Hortobagyi G, Gianni L, von Minckwitz G, et al. Preoperative therapy in invasive breast cancer: pathologic assessment and systemic therapy issues in operable disease. *J Clin Oncol Off J Am Soc Clin Oncol* (2008) 26 (5):814–9. doi: 10.1200/jco.2007.15.3510

5. Bardia A, Baselga J. Neoadjuvant therapy as a platform for drug development and approval in breast cancer. *Clin Cancer Res an Off J Am Assoc Cancer Res* (2013) 19 (23):6360–70. doi: 10.1158/1078-0432.Ccr-13-0916

6. Spring L, Fell G, Arfe A, Sharma C, Greenup R, Reynolds K, et al. Pathologic complete response after neoadjuvant chemotherapy and impact on breast cancer recurrence and survival: A comprehensive meta-analysis. *Clin Cancer Res an Off J Am Assoc Cancer Res* (2020) 26(12):2838–48. doi: 10.1158/1078-0432.Ccr-19-3492

7. von Minckwitz G, Untch M, Blohmer J, Costa S, Eidtmann H, Fasching P, et al. Definition and impact of pathologic complete response on prognosis after neoadjuvant chemotherapy in various intrinsic breast cancer subtypes. *J Clin Oncol Off J Am Soc Clin Oncol* (2012) 30(15):1796–804. doi: 10.1200/jco.2011.38.8595

8. Li Z, Zhang Y, Zhang Z, Zhao Z, Lv Q. A four-gene signature predicts the efficacy of paclitaxel-based neoadjuvant therapy in human epidermal growth factor receptor 2-negative breast cancer. *J Cell Biochem* (2019) 120(4):6046–56. doi: 10.1002/jcb.27891

9. Jung Y, Hyun C, Jin M, Park I, Chung Y, Shim B, et al. Histomorphological factors predicting the response to neoadjuvant chemotherapy in triple-negative breast cancer. *J Breast Cancer* (2016) 19(3):261–7. doi: 10.4048/jbc.2016.19.3.261

10. Chen R, Ye Y, Yang C, Peng Y, Zong B, Qu F, et al. Assessment of the predictive role of pretreatment Ki-67 and Ki-67 changes in breast cancer patients receiving neoadjuvant chemotherapy according to the molecular classification: A retrospective study of 1010 patients. *Breast Cancer Res Treat* (2018) 170(1):35–43. doi: 10.1007/s10549-018-4730-1

11. Chen S, Shu Z, Li Y, Chen B, Tang L, Mo W, et al. Machine learning-based radiomics nomogram using magnetic resonance images for prediction of neoadjuvant chemotherapy efficacy in breast cancer patients. *Front Oncol* (2020) 10:1410. doi: 10.3389/fonc.2020.01410

12. Tuan Linh L, Minh Duc N, Tra My TT, Viet Bang L, Minh Thong P. Correlations between dynamic contrast-enhanced magnetic resonance imaging parameters and histopathologic factors in breast cancer. *Clin Ter* (2021) 172(5):453–60. doi: 10.7417/CT.2021.2358

13. Tuan Linh L, Minh Duc N, Minh Duc N, Tra My TT, Viet Bang L, Cong Tien N, et al. Correlations between apparent diffusion coefficient values and histopathologic factors in breast cancer. *Clin Ter* (2021) 172(3):218–24. doi: 10.7417/CT.2021.2318

14. Zhang F, Huang M, Zhou H, Chen K, Jin J, Wu Y, et al. A nomogram to predict the pathologic complete response of neoadjuvant chemotherapy in triple-negative breast cancer based on simple laboratory indicators. *Ann Surg Oncol* (2019) 26 (12):3912–9. doi: 10.1245/s10434-019-07655-7

15. Marín Hernández C, Piñero Madrona A, Gil Vázquez P, Galindo Fernández P, Ruiz Merino G, Alonso Romero J, et al. Usefulness of lymphocyte-to-monocyte, neutrophil-to-monocyte and neutrophil-to-lymphocyte ratios as prognostic markers in breast cancer patients treated with neoadjuvant chemotherapy. *Clin Trans Oncol Off Publ Fed Spanish Oncol Societies Natl Cancer Institute Mexico* (2018) 20(4):476–83. doi: 10.1007/s12094-017-1732-0

16. Chapek M, Martindale R. Nutrition in cancer therapy: overview for the cancer patient. *JPEN J parenteral enteral Nutr* (2021) 45(S2):33–40. doi: 10.1002/jpen.2259

17. Richards J, Arensberg M, Thomas S, Kerr K, Hegazi R, Bastasch M. Impact of early incorporation of nutrition interventions as a component of cancer therapy in adults: A review. *Nutrients* (2020) 12(11):3403. doi: 10.3390/nu12113403

18. Lee J, Leong L, Lim S. Nutrition intervention approaches to reduce malnutrition in oncology patients: A systematic review. *Supportive Care Cancer Off J Multinational Assoc Supportive Care Cancer* (2016) 24(1):469–80. doi: 10.1007/s00520-015-2958-4

19. Mukai H, Villafuerte H, Qureshi A, Lindholm B, Stenvinkel P. Serum albumin, inflammation, and nutrition in end-stage renal disease: C-reactive protein is needed for optimal assessment. *Semin Dialysis* (2018) 31(5):435–9. doi: 10.1111/sdi.12731

20. Kuroda D, Sawayama H, Kurashige J, Iwatsuki M, Eto T, Tokunaga R, et al. Controlling nutritional status (Conut) score is a prognostic marker for gastric cancer patients after curative resection. *Gastric Cancer Off J Int Gastric Cancer Assoc Japanese Gastric Cancer Assoc* (2018) 21(2):204–12. doi: 10.1007/s10120-017-0744-3

21. Miura K, Hamanaka K, Koizumi T, Kitaguchi Y, Terada Y, Nakamura D, et al. Clinical significance of preoperative serum albumin level for prognosis in surgically resected patients with non-small cell lung cancer: comparative study of normal lung, emphysema, and pulmonary fibrosis. *Lung Cancer (Amsterdam Netherlands)* (2017) 111:88–95. doi: 10.1016/j.lungcan.2017.07.003

22. Li J, Zuo M, Zhou X, Xiang Y, Zhang S, Feng W, et al. Prognostic significance of preoperative albumin to alkaline phosphatase ratio in patients with glioblastoma. *J Cancer* (2021) 12(19):5950–9. doi: 10.7150/jca.61866

23. Liu D, Li F, Jia W. Cumulative scores based on plasma D-dimer and serum albumin levels predict survival in esophageal squamous cell carcinoma patients treated with transthoracic esophagectomy. *Chin J Cancer* (2016) 35:11. doi: 10.1186/s40880-015-0062-2

24. Greten F, Grivennikov S. Inflammation and cancer: triggers, mechanisms, and consequences. *Immunity* (2019) 51(1):27–41. doi: 10.1016/j.immuni.2019.06.025

25. Yasukawa K, Shimizu A, Motoyama H, Kubota K, Notake T, Fukushima K, et al. Preoperative C-reactive protein-to-albumin ratio predicts long-term outcomes in extrahepatic cholangiocarcinoma patients. *J Surg Oncol* (2020) 122(6):1094–105. doi: 10.1002/jso.26109

26. Capone M, Giannarelli D, Mallardo D, Madonna G, Festino L, Grimaldi A, et al. Baseline neutrophil-to-lymphocyte ratio (Nlr) and derived nlr could predict overall survival in patients with advanced melanoma treated with nivolumab. *J immunotherapy Cancer* (2018) 6(1):74. doi: 10.1186/s40425-018-0383-1

27. Peng Y, Chen R, Qu F, Ye Y, Fu Y, Tang Z, et al. Low pretreatment lymphocyte/monocyte ratio is associated with the better efficacy of neoadjuvant chemotherapy in breast cancer patients. *Cancer Biol Ther* (2020) 21(2):189–96. doi: 10.1080/15384047.2019.1680057

28. Schobert I, Savic L, Chapiro J, Bousabarah K, Chen E, Laage-Gaupp F, et al. Neutrophil-to-lymphocyte and platelet-to-lymphocyte ratios as predictors of tumor response in hepatocellular carcinoma after deb-tace. *Eur Radiol* (2020) 30(10):5663–73. doi: 10.1007/s00330-020-06931-5

29. Zhang K, Hua Y, Wang D, Chen L, Wu C, Chen Z, et al. Systemic immune-inflammation index predicts prognosis of patients with advanced pancreatic cancer. *J Trans Med* (2019) 17(1):30. doi: 10.1186/s12967-019-1782-x

30. Onodera T, Goseki N, Kosaki G. [Prognostic nutritional index in gastrointestinal surgery of malnourished cancer patients]. *Nihon Geka Gakkai zasshi* (1984) 85(9):1001–5.

31. Morgan T, Tang D, Stratton K, Barocas D, Anderson C, Gregg J, et al. Preoperative nutritional status is an important predictor of survival in patients undergoing surgery for renal cell carcinoma. *Eur Urol* (2011) 59(6):923–8. doi: 10.1016/j.eururo.2011.01.034

32. Okadome K, Baba Y, Yagi T, Kiyozumi Y, Ishimoto T, Iwatsuki M, et al. Prognostic nutritional index, tumor-infiltrating lymphocytes, and prognosis in patients with esophageal cancer. *Ann Surg* (2020) 271(4):693–700. doi: 10.1097/SLA.0000000000002985

33. Hua X, Long Z, Huang X, Deng J, He Z, Guo L, et al. The value of prognostic nutritional index (Pni) in predicting survival and guiding radiotherapy of patients with T1-2n1 breast cancer. *Front Oncol* (2019) 9:1562. doi: 10.3389/fonc.2019.01562

34. Wolff A, Hammond M, Allison K, Harvey B, Mangu P, Bartlett J, et al. Human epidermal growth factor receptor 2 testing in breast cancer: American society of clinical oncology/college of American pathologists clinical practice guideline focused update. *J Clin Oncol Off J Am Soc Clin Oncol* (2018) 36(20):2105–22. doi: 10.1200/jco.2018.77.8738

35. Dowsett M, Nielsen T, A'Hern R, Bartlett J, Coombes R, Cuzick J, et al. Assessment of Ki67 in breast cancer: recommendations from the international ki67 in breast cancer working group. *J Natl Cancer Institute* (2011) 103(22):1656–64. doi: 10.1093/jnci/djr393

36. Ogston K, Miller I, Payne S, Hutcheon A, Sarkar T, Smith I, et al. A new histological grading system to assess response of breast cancers to primary chemotherapy: prognostic significance and survival. *Breast (Edinburgh Scotland)* (2003) 12(5):320–7. doi: 10.1016/s0960-9776(03)00106-1

37. Wang Y, Wang Y, Chen R, Tang Z, Peng Y, Jin Y, et al. Plasma fibrinogen acts as a predictive factor for pathological complete response to neoadjuvant chemotherapy in breast cancer: A retrospective study of 1004 Chinese breast cancer patients. *BMC Cancer* (2021) 21(1):542. doi: 10.1186/s12885-021-08284-8

38. Chen B, Dai D, Tang H, Chen X, Ai X, Huang X, et al. Pre-treatment serum alkaline phosphatase and lactate dehydrogenase as prognostic factors in triple negative breast cancer. *J Cancer* (2016) 7(15):2309–16. doi: 10.7150/jca.16622

39. Bernardi M, Angeli P, Claria J, Moreau R, Gines P, Jalan R, et al. Albumin in decompensated cirrhosis: new concepts and perspectives. *Gut* (2020) 69(6):1127–38. doi: 10.1136/gutjnl-2019-318843

40. Diakos C, Charles K, McMillan D, Clarke S. Cancer-related inflammation and treatment effectiveness. *Lancet Oncol* (2014) 15(11):e493–503. doi: 10.1016/s1470-2045(14)70263-3

41. Eckart A, Struja T, Kutz A, Baumgartner A, Baumgartner T, Zurfluh S, et al. Relationship of nutritional status, inflammation, and serum albumin levels during acute illness: A prospective study. *Am J Med* (2020) 133(6):713–22.e7. doi: 10.1016/j.amjmed.2019.10.031

42. Kim J, Keam B, Heo D, Han D, Rhee C, Kim J, et al. The prognostic value of albumin-to-alkaline phosphatase ratio before radical radiotherapy in patients with non-metastatic nasopharyngeal carcinoma: A propensity score matching analysis. *Cancer Res Treat Off J Korean Cancer Assoc* (2019) 51(4):1313–23. doi: 10.4143/crt.2018.503

43. Gupta D, Lis C. Pretreatment serum albumin as a predictor of cancer survival: A systematic review of the epidemiological literature. *Nutr J* (2010) 9:69. doi: 10.1186/1475-2891-9-69

44. Mellman I, Coukos G, Dranoff G. Cancer immunotherapy comes of age. *Nature* (2011) 480(7378):480–9. doi: 10.1038/nature10673

45. Joseph N, Dovedi S, Thompson C, Lyons J, Kennedy J, Elliott T, et al. Pre-treatment lymphocytopaenia is an adverse prognostic biomarker in muscle-invasive and advanced bladder cancer. *Ann Oncol Off J Eur Soc Med Oncol* (2016) 27(2):294–9. doi: 10.1093/annonc/mdv546

46. Grossman S, Ellsworth S, Campian J, Wild A, Herman J, Laheru D, et al. Survival in patients with severe lymphopenia following treatment with radiation and chemotherapy for newly diagnosed solid tumors. *J Natl Compr Cancer Network JNCCN* (2015) 13(10):1225–31. doi: 10.6004/jnccn.2015.0151

47. Chen L, Bai P, Kong X, Huang S, Wang Z, Wang X, et al. Prognostic nutritional index (Pni) in patients with breast cancer treated with neoadjuvant chemotherapy as a useful prognostic indicator. *Front Cell Dev Biol* (2021) 9:656741. doi: 10.3389/fcell.2021.656741

48. Oba T, Maeno K, Takekoshi D, Ono M, Ito T, Kanai T, et al. Neoadjuvant chemotherapy-induced decrease of prognostic nutrition index predicts poor prognosis in patients with breast cancer. *BMC Cancer* (2020) 20(1):160. doi: 10.1186/s12885-020-6647-4

49. Wang Y, Battseren B, Yin W, Lin Y, Zhou L, Yang F, et al. Predictive and prognostic value of prognostic nutritional index for locally advanced breast cancer. *Gland Surg* (2019) 8(6):618–26. doi: 10.21037/gs.2019.10.08

50. Goorts B, van Nijnatten T, de Munck L, Moossdorff M, Heuts E, de Boer M, et al. Clinical tumor stage is the most important predictor of pathological complete response rate after neoadjuvant chemotherapy in breast cancer patients. *Breast Cancer Res Treat* (2017) 163(1):83–91. doi: 10.1007/s10549-017-4155-2

51. Cortazar P, Zhang L, Untch M, Mehta K, Costantino J, Wolmark N, et al. Pathological complete response and long-term clinical benefit in breast cancer: the ctneobc pooled analysis. *Lancet (London England)* (2014) 384(9938):164–72. doi: 10.1016/s0140-6736(13)62422-8

52. Chen X, He C, Han D, Zhou M, Wang Q, Tian J, et al. The predictive value of ki-67 before neoadjuvant chemotherapy for breast cancer: A systematic review and meta-analysis. *Future Oncol (London England)* (2017) 13(9):843–57. doi: 10.2217/fon-2016-0420

53. Werutsky G, Untch M, Hanusch C, Fasching P, Blohmer J, Seiler S, et al. Locoregional recurrence risk after neoadjuvant chemotherapy: A pooled analysis of nine prospective neoadjuvant breast cancer trials. *Eur J Cancer (Oxford Engl 1990)* (2020) 130:92–101. doi: 10.1016/j.ejca.2020.02.015

54. Gianni L, Eiermann W, Semiglazov V, Manikhas A, Lluch A, Tjulandin S, et al. Neoadjuvant chemotherapy with trastuzumab followed by adjuvant trastuzumab versus neoadjuvant chemotherapy alone, in patients with Her2-positive locally advanced breast cancer (the noah trial): A randomised controlled superiority trial with a parallel her2-negative cohort. *Lancet (London England)* (2010) 375(9712):377–84. doi: 10.1016/s0140-6736(09)61964-4

55. Gianni L, Pienkowski T, Im Y, Roman L, Tseng L, Liu M, et al. Efficacy and safety of neoadjuvant pertuzumab and trastuzumab in women with locally advanced, inflammatory, or early her2-positive breast cancer (Neosphere): A randomised multicentre, open-label, phase 2 trial. *Lancet Oncol* (2012) 13(1):25–32. doi: 10.1016/s1470-2045(11)70336-9

frontiers | Frontiers in Immunology

TYPE Original Research
PUBLISHED 26 January 2024
DOI 10.3389/fimmu.2024.1287632

OPEN ACCESS

EDITED BY
Paulo Rodrigues-Santos,
University of Coimbra, Portugal

REVIEWED BY
Katherine Wendy Cook,
Scancell Ltd, United Kingdom
Markus Tschurtschenthaler,
Technical University of Munich, Germany
Sonia Ferkel,
Stanford University, United States
Arundhoti Das,
National Institutes of Health (NIH),
United States

*CORRESPONDENCE
Shigang Ding
dingshigang222@163.com
Weiwei Fu
fuweiwei@bjmu.edu.cn

†These authors have contributed equally to this work

RECEIVED 02 September 2023
ACCEPTED 10 January 2024
PUBLISHED 26 January 2024

CITATION
Meng Q, Zhao Y, Xu M, Wang P, Li J, Cui R, Fu W and Ding S (2024) Increased circulating regulatory T cells and decreased follicular T helper cells are associated with colorectal carcinogenesis. *Front. Immunol.* 15:1287632. doi: 10.3389/fimmu.2024.1287632

Increased circulating regulatory T cells and decreased follicular T helper cells are associated with colorectal carcinogenesis

Qiao Meng[1,2†], Yang Zhao[3†], Miao Xu[4], Pingzhang Wang[5], Jun Li[1], Rongli Cui[1], Weiwei Fu[1,2*†] and Shigang Ding[1,2*]

[1]Department of Gastroenterology, Peking University Third Hospital, Beijing, China, [2]Beijing Key Laboratory for Helicobacter Pylori Infection and Upper Gastrointestinal Diseases, Beijing, China, [3]Department of Laboratory Medicine, Peking University Third Hospital, Beijing, China, [4]Broad Institute of Harvard and Massachusetts Institute of Technology, Cambridge, MA, United States, [5]Department of Immunology, School of Basic Medical Sciences, Peking University Health Science Center, NHC Key Laboratory of Medical Immunology (Peking University), Beijing, China

Objective: Colorectal cancer (CRC) is the third most prevalent cancer worldwide and is associated with high morbidity and mortality rates. Colorectal carcinogenesis occurs via the conventional adenoma-to-carcinoma and serrated pathways. Conventional T helper (Th) and innate lymphoid cells (ILCs) play vital roles in maintaining intestinal homeostasis. However, the contribution of these two major lymphoid cell populations and their associated cytokines to CRC development is unclear. Therefore, we aimed to analyze peripheral lymphocyte profiles during colorectal carcinogenesis.

Methods: We collected 86 blood samples concurrently, and pathologists confirmed the presence of various pathological conditions (i.e., HPs, adenoma, and carcinoma) using hematoxylin and eosin staining. Ten healthy donors were recruited as healthy controls (HCs) from the physical examination center. We performed flow cytometry on peripheral blood mononuclear cells collected from patients with various pathological conditions and the HCs, and cytokines (interleukin-2, interleukin-4, interleukin-5, interleukin-13, interleukin-17A, interleukin-17F, interleukin-22, interferon-γ, and tumor necrosis factor-α) were quantified. We also analyzed the published single-cell RNA sequence data derived from tissue samples from different stages of colorectal carcinogenesis.

Results: The cytokine response in peripheral $CD4^+$ T cells was upregulated during the carcinoma process. The frequency of peripheral regulatory T cells (Tregs) increased in the adenoma and carcinoma stages. While the T follicular helper (Tfh) cell proportion was downregulated in the adenoma and carcinoma processes. Thus, Th cell subsets, especially Tregs and Tfh cells, were involved in colonic diseases. Moreover, the immunological profile characteristics in the HPs were clarified.

Conclusion: We comprehensively analyzed circulating ILCs and adaptive T-cell lymphocyte subtypes in colorectal carcinoma progression. Our results show the immunological profile characteristics and support the involvement of Th subsets, especially Treg and Tfh cell populations, in colonic diseases. These findings

significantly enhance our understanding of the immune mechanisms underlying CRC and its precancerous lesions. Further investigation of the Treg and Tfh cells' function in colorectal disease development will provide potential therapeutic targets for monitoring and preventing CRC development.

KEYWORDS

colorectal cancer, adenoma, hyperplastic polyps, T helper cell, innate lymphoid cells

Introduction

Colorectal cancer (CRC) is the third most prevalent cancer worldwide, with over 1.9 million new CRC cases and 0.93 million deaths estimated in 2020 (1). Although the death rate slightly decreased (2), CRC mortality still ranks second among all cancer-related death cases worldwide (3). Colorectal carcinogenesis can occur via the conventional adenoma-to-carcinoma and serrated pathways. The typical adenoma–carcinoma sequence is an established model for sporadic CRC development and causes approximately 60%–85% of colonic malignancies. Precursor lesions that display tubular, tubulovillous, or villous adenoma histology develop into low- or high-grade adenomas and CRC (4). However, the mechanisms underlying CRC onset and progression are not fully understood. Furthermore, over 15% of CRC cases arise through the serrated pathway (5). Hyperplastic polyps (HPs), classified as serrated lesions, have shown that cells only exhibit minimal cytological atypia in the upper two-thirds of the crypts (6). HPs often coexist with adenoma and adenocarcinoma and have distinct biological features in CRC (7, 8). Therefore, the characteristics of HPs must be clarified.

The tumor immune microenvironment plays a crucial role in CRC development (9), determines the durable response to immunotherapy, and may be a predictive biomarker (10–12). Progression from precancerous lesions to malignant CRC depends on a complex immune pathway involving activated T lymphocytes and cytotoxic cytokine production. Previous cancer immunological studies have primarily focused on $CD8^+$ T cells. However, recent studies highlighted the importance of $CD4^+$ T cells, considering that $CD4^+$ T cells are central coordinators of innate and antigen-specific immune responses (13). Innate lymphoid cells (ILCs) are heterogeneous immune cells with no antigen-specific receptors that produce cytokines similar to $CD4^+$ T helper (Th) subsets (14, 15). Conventional Th cells and ILCs play critical roles in maintaining intestinal homeostasis. However, Cui et al. have found that interleukin (IL)-17A plays important roles along the colorectal adenoma–carcinoma sequence (16–18). However, how these two major lymphoid cell populations and their related cytokines are involved in CRC development has not been determined systematically.

Recently, Zheng et al. dissected dynamic alterations in cell populations in the normal adenoma–carcinoma sequence using single-cell RNA-sequencing technology (19). Furthermore, using single-cell transcriptomic analysis, Chen et al. demonstrated the different immune microenvironmental features of conventional adenomas and serrated polyps (20). The occurrence and development of tumors are accompanied by systemic immune disturbance and peripheral immune cell alterations (21–24). Individual immunity is coordinated across tissues, and the colonic antitumor immune response depends on continuous communication with the peripheral blood (25, 26). Our previous study demonstrated peripheral adaptive and innate lymphocyte changes during human gastric cancer development (27). Considering the easily obtainable and non-invasive characteristics of peripheral blood samples, exploring changes in peripheral immune profiles is crucial and may help discover key functional cell subpopulations during CRC carcinogenesis. Therefore, novel target cells can be provided for the early screening of CRC patients.

This study comprehensively analyzed peripheral lymphocyte profiles in HPs and conventional adenoma–carcinoma sequences.

Materials and methods

Patients and controls

Patients were admitted to Peking University Third Hospital between December 2021 and August 2022. Eighty-six patients diagnosed with HPs (n = 10), adenomas (grade I, n = 19; grade II, n = 19; grade III, n = 19), or adenocarcinomas (n = 19) were enrolled. All patients were diagnosed based on histological examination results. Patients with active systemic infections or autoimmune diseases were excluded. Ten healthy donors were recruited as healthy controls (HCs) from the physical examination center. Two milliliters of the remaining blood samples from routine complete blood count tests were collected as peripheral blood samples for the experiment. The Medical

Abbreviations: CRC, colorectal cancer; Th cells, T helper cells; ILCs, innate lymphoid cells; HCs, healthy controls; HPs, hyperplastic polyps; PBMCs, peripheral blood mononuclear cells; Treg cells, regulatory T cells; Tfh cells, T follicular helper cells; TNF, tumor necrosis factor; IFN, interferon; IL, interleukin; CD, cluster of differentiation.

Science Research Ethics Committee of Peking University Third Hospital approved this study (2022 YLS No. 554-01).

Cell isolation and flow cytometry analysis

Peripheral blood mononuclear cells (PBMCs) were isolated from heparinized peripheral blood through Ficoll-Hypaque gradients as previously described (28). The collected PBMCs were resuspended and cryopreserved with freezing media, including 10% dimethylsulfoxide (DMSO) and 90% fetal bovine serum, and then stored in a freezing container at −80°C. For flow cytometry analysis, the cryopreserved PBMCs were placed in a 37°C water bath for rapid thawing and then transferred into a 15-mL conical centrifuge tube filled with prewarmed RPMI 1640. After the washing step, the cells were resuspended in a culture medium and incubated at 37°C for 2 h before staining or stimulation.

For staining, the Fixable Viability Dye eFluor 506 (Thermo Fisher Scientific, Waltham, MA, USA) was stained firstly to gate live cells, followed by 30 min of surface antibody staining at 4°C. The antibodies used for flow cytometry are listed in Supplementary Table 1. For cytokine detection, PBMCs were stimulated for 4.5 h with 50 ng/mL of phorbol 12-myristate 13-acetate and 500 ng/mL of ionomycin (Sigma-Aldrich, St. Louis, MO, USA) in the presence of GolgiStop (BD/PMG) in a 37°C incubator before staining. Cells were fixed, permeabilized, and stained using the Cytofix/Cytoperm Kit (BD). Flow cytometry was performed using a FACSCanto instrument (BD Biosciences, San Jose, CA, USA) and analyzed using FlowJo software 10.8.1. The cell type annotation and gating strategy were performed as shown previously (27–29).

Cytokine measurement

Cytokines [IL-2, IL-4, IL-5, IL-13, IL-17A, IL-17F, IL-22, interferon (IFN)-γ, and tumor necrosis factor (TNF)-α] in the plasma were measured using the LEGENDplex™ Multi-Analyte Flow Assay kit (BioLegend, San Diego, CA, USA) following the manufacturer's protocol and Canto flow cytometry.

Single-cell RNA sequence data analysis

A single-cell dataset derived from colorectal adenoma and carcinoma tissues was downloaded from the Gene Expression Omnibus database (GSE161277) (19). Standard analysis was performed using the R Seurat package (version 3.1.2) (29). Briefly, using the Read10X function to read the output results, the results were converted to Seurat objects using the CreateSeuratObject function. Each cell was normalized to 10,000 unique molecular identifier counts, and the top 2,000 highly variable genes (HVGs) were selected. After the data were scaled and centered, principal component analysis based on the HVGs was conducted. The uniform manifold approximation and projection method was used for dimensionality reduction in single-cell cluster visualization. Cell types were annotated according to marker gene expression, such as CD3 and CD4 for $CD4^+$ T cells. In $CD4^+$ T cells, dot plots were generated to show gene expression using the DotPlot function. The cell annotation strategy in DotPlot is according to the DICE database (https://dice-database.org/).

Statistical analyses

Differences between groups were analyzed using a one-way ANOVA if the data followed a normal distribution. Otherwise, we used the non-parametric Kruskal–Wallis test. Analyses were conducted using GraphPad Prism 8.0 (GraphPad Software, San Diego, CA, USA). All statistical tests were two-tailed. A value of $P < 0.05$ was considered significant.

Results

Cytokine profile analysis during colorectal carcinogenesis

To demonstrate the dynamic changes in the immune landscape during CRC development, we collected 86 blood samples to analyze the major lymphoid cell populations and their related cytokines (Figure 1A), and the pathological conditions were confirmed (Figure 1B). The clinical characteristics of the patients and HCs are shown in Table 1.

Firstly, we detected IL-2, IL-4, IL-5, IL-13, IL-17A, IL-17F, IL-22, IFN-γ, and TNF-α in the plasma to exclude the influence of infection or autoimmune disorders, and the standard curves were verified (Supplementary Figure 1). IL-2, IL-4, IL-5, IL-13, IL-17A, IL-17F, IL-22, IFN-γ, and TNF-α exhibited no apparent difference between each group, indicating the comparable inflammatory conditions between these samples (all $P > 0.05$) (Figures 2A–C). These results revealed that the plasma cytokine profile changed subtly, and their ability to indicate lesions was limited.

The cytokine response in peripheral $CD4^+$ T cells is upregulated during the carcinoma process

Firstly, we characterized the circulating Th cell subsets in the peripheral blood sample from healthy controls and patients with different colorectal lesions using surface markers. As shown in Figure 3A, $CD4^+CXCR3^+$ Th1 cells had no differences among the groups (Figure 3A). Compared with HPs, Th2 cells were decreased in adenoma grade II (31.6 vs. 24.7, $P = 0.0222$), adenoma grade III (31.6 *vs.* 22.2, $P = 0.0313$), and the CRC group (31.6 vs. 20.4, $P = 0.0029$) (Figure 3B). The percentage of Th2 cells was downregulated significantly from adenoma grade I to CRC (Figure 3B). As shown in Figure 3C, the $CD4^+CCR6^+$ Th17 cell proportion decreased in CRC when compared with the healthy control group (23.1 vs. 11.2, $P = 0.0279$) or adenoma grade I (24.3 vs. 11.2, $P = 0.0163$) or even adenoma grade II (21.7 vs. 11.2, $P = 0.0042$).

Moreover, we demonstrated the function of the peripheral Th cell subsets during carcinoma progression through key cytokine production analysis. IFN-gamma$^+$ Th1 cells increased in CRC

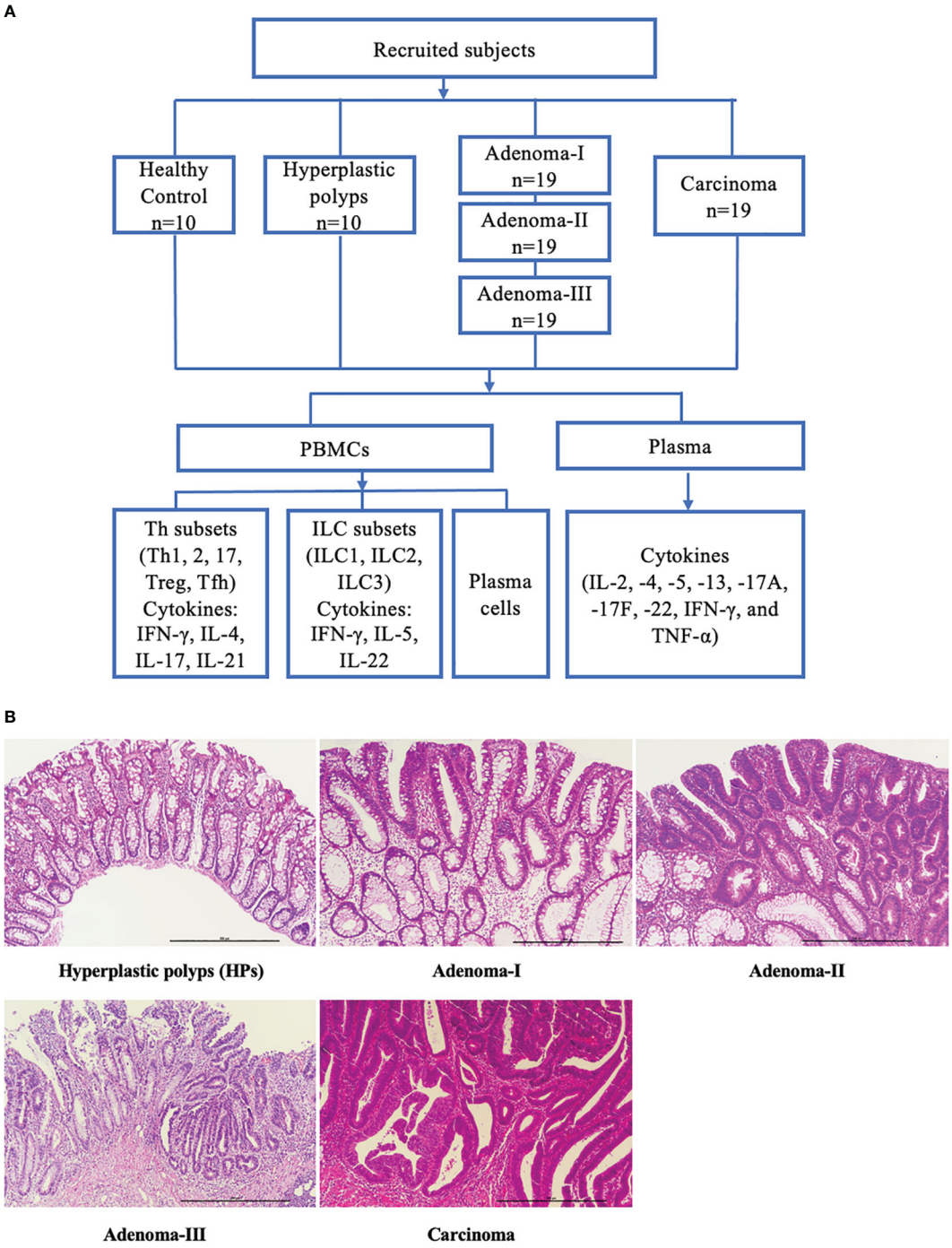

FIGURE 1
Study flowchart and pathologic diagnosis of enrolled patients. **(A)** Subdivision of enrolled subjects into health controls, hyperplastic polyps, adenoma (grades I, II, and III), and carcinoma. The peripheral blood samples were collected, and the key lymphocyte subpopulations in PBMCs and the plasma cytokines were analyzed. **(B)** Representative H&E-stained sections of a cascade of colonic lesions. Scale bar: 500 μm (×100 magnification).

compared with those in HPs (1.61 vs. 4.73, $P = 0.0267$) (Figure 3D). In addition, the Th1 cell response was upregulated significantly from adenoma grade I to CRC (Figure 3D). As shown in Figure 3E, $CD4^+IL\text{-}4^+$ Th2 cells were increased in the CRC group when compared with those in HPs and adenoma grade I (2.11 vs. 5.63, $P = 0.0027$; 2.20 vs. 5.63, $P = 0.0049$). Furthermore, the proportion of $CD4^+IL\text{-}17A^+$ Th17 cells was investigated during CRC development. As shown in Figure 3F, Th17 cells increased in CRC when compared with the healthy control group (2.32 vs. 6.06, $P = 0.0458$) or HPs (1.68 vs. 6.06, $P = 0.0014$) or even adenoma grade I (1.99 vs. 6.06, $P = 0.0130$).

Furthermore, we analyzed published single-cell RNA sequence data (GSE161277) from tissue samples of different colorectal carcinogenesis stages to confirm the effector Th cell response during the adenoma–carcinoma sequence. As shown in Supplementary Figure 2, $CD4^+$ T cells in tissue samples showed consistency only to the cytokine expression and

TABLE 1 Characteristics of enrolled patients with colonic lesions.

	Health control (*n* = 10)	Hyperplastic polyp (*n* = 10)	Tubular adenoma grade I (*n* = 19)	Tubular adenoma grade II (*n* = 19)	Tubular adenoma grade III (*n* = 19)	Colorectal carcinoma (*n* = 19)
Median age (years, range)	42 (39, 47)	61 (43, 68)	59 (30, 74)	64 (38, 77)	63 (42, 77)	67 (21, 90)
Gender						
Male	7 (70.0%)	8 (80.0%)	7 (36.8%)	7 (36.8%)	10 (52.6%)	15 (78.9%)
Female	3 (30.0%)	2 (20.0%)	12 (63.2%)	12 (63.2%)	9 (47.4%)	4 (21.1%)
Histological diagnosis	Untested	Hyperplastic polyp	Tubular adenoma grade I	Tubular adenoma grade II	Tubular adenoma grade III	Colorectal carcinoma

not to the protein surface markers with that of the peripheral effector Th cell response. Th1 cells, identified by the *CXCR3* or *IFN-gamma* expression in the tissue-derived $CD4^+$ T cells, were upregulated from adenoma to carcinoma (Supplementary Figure 2). Moreover, the upregulated Th2 cells, identified by the *CCR4* expression in the tissue-derived $CD4^+$T cells, from adenoma to CRC were consistent with the peripheral $CD4^+$IL-4^+ Th2 response (Supplementary Figure 2). Lastly, we also detected increased Th17 populations, identified by the *CCR6* expression in the tissue-derived $CD4^+$ T cells, in the CRC group when compared with the normal group, which was consistent with the peripheral $CD4^+$IL-$17A^+$ Th17 response (Supplementary Figure 2). These results demonstrate the upregulation of the effector $CD4^+$ T-cell response in colorectal carcinogenesis.

ILCs shift during the carcinoma development

ILC subsets were further clarified, and gating was performed as previously described (Supplementary Figure 3). The $CD45^+Lin^-CD127^+CRTH2^-CD117^-$ ILC1 cell frequency had no significant differences between the control and HPs (Figure 4A). The median level of ILC1s showed an increased and then a decreased tendency during the carcinoma development process. We also analyzed circulating $CD45^+Lin^-CD127^+CRTH2^+CD117^-$ ILC2s in patients with colonic diseases. Although an upward trend was found in the disease group compared with the HC group, no significant differences were detected in the frequency of ILC2 cells among all groups (Figure 4B).

Moreover, $CD45^+Lin^-CD127^+CRTH2^-CD117^+$ ILC3 was also analyzed in patients with a cascade of colonic disease, which also showed non-significantly increased frequency in colorectal precancerous lesions and CRC (Figure 4C).

We further demonstrated the key cytokine production in ILCs to identify their function variation during intestinal carcinogenesis. As shown in Figure 4D, the levels of IFN-gamma, mainly produced by ILC1, showed no difference among the groups.

We also measured IL-5 levels, primarily produced by ILC2, and found that there was also no difference between the groups (Figure 4E). The IL-22, which is primarily produced by ILC3 and plays a protective role in the intestinal mucosal barrier (30), was further measured to further confirm the involvement of ILC3 in colonic disease development. Compared with the control, IL-22 levels were lower in HPs (4.93 vs. 1.76, $P = 0.0163$), adenoma grade II (4.93 vs. 1.66, $P = 0.0059$), and CRC (4.93 vs. 1.28, $P = 0.0095$) (Figure 4F). These results suggest that ILC3s' function, especially IL-22 production, might be involved in both premalignant lesions, such as adenomas and HPs, and CRC.

Regulatory T-cell proportions increase from adenomas to carcinomas

The $CD4^+CD25^+$ regulatory T cell (Treg) percentage in PBMCs was investigated in all groups to further assess the frequency change in Tregs in colonic precancerous lesions and CRC (Figures 5A, B). The frequency of peripheral $CD4^+CD25^+$ Treg cells was comparable between the control and HP groups. However, compared with the control, a significantly increased percentage of circulating $CD4^+CD25^+$ Tregs was detected in the adenoma grade III (1.56 vs. 19.6, $P = 0.0032$) and CRC groups (1.56 vs. 29.9, $P < 0.0001$). The frequency of $CD4^+CD25^+$ Treg cells gradually increased from early to advanced adenomas and finally to CRC, suggesting that Treg cells increased to exert immunosuppressive effects as adenomas progressed toward CRC (grade I vs. grade II, 0.63 vs. 5.30, $P = 0.0400$; grade I vs. grade III, 0.63 vs. 19.6, $P < 0.0001$; grade I vs. CRC, 0.63 vs. 29.9, $P < 0.0001$; grade II vs. CRC, 5.30 vs. 5.30, $P = 0.0059$). Moreover, $CD4^+CD25^+$ Treg cells were decreased in HPs compared with grade III adenoma (1.96 vs. 19.6, $P = 0.0097$) or CRC (1.96 vs. 29.9, $P = 0.0001$). There was no difference between HPs and adenoma grade I or II.

Furthermore, single-cell RNA-sequencing data showed that the expression of *IL-2RA* (*CD25*) and *FOXP3*, the key markers of Treg cells, was increased from adenoma to carcinoma in the tissue-derived $CD4^+$ T cells (Figure 5C), which is consistent with the changes in peripheral Treg cells. This result further confirms the involvement of Tregs in colonic premalignant lesions and CRC.

T follicular helper cell response is downregulated during colorectal carcinogenesis

We further analyzed the T follicular helper (Tfh) response, and $CD4^+PD1^+CXCR5^+$ cells were significantly decreased in adenoma

10.3389/fimmu.2024.1287632

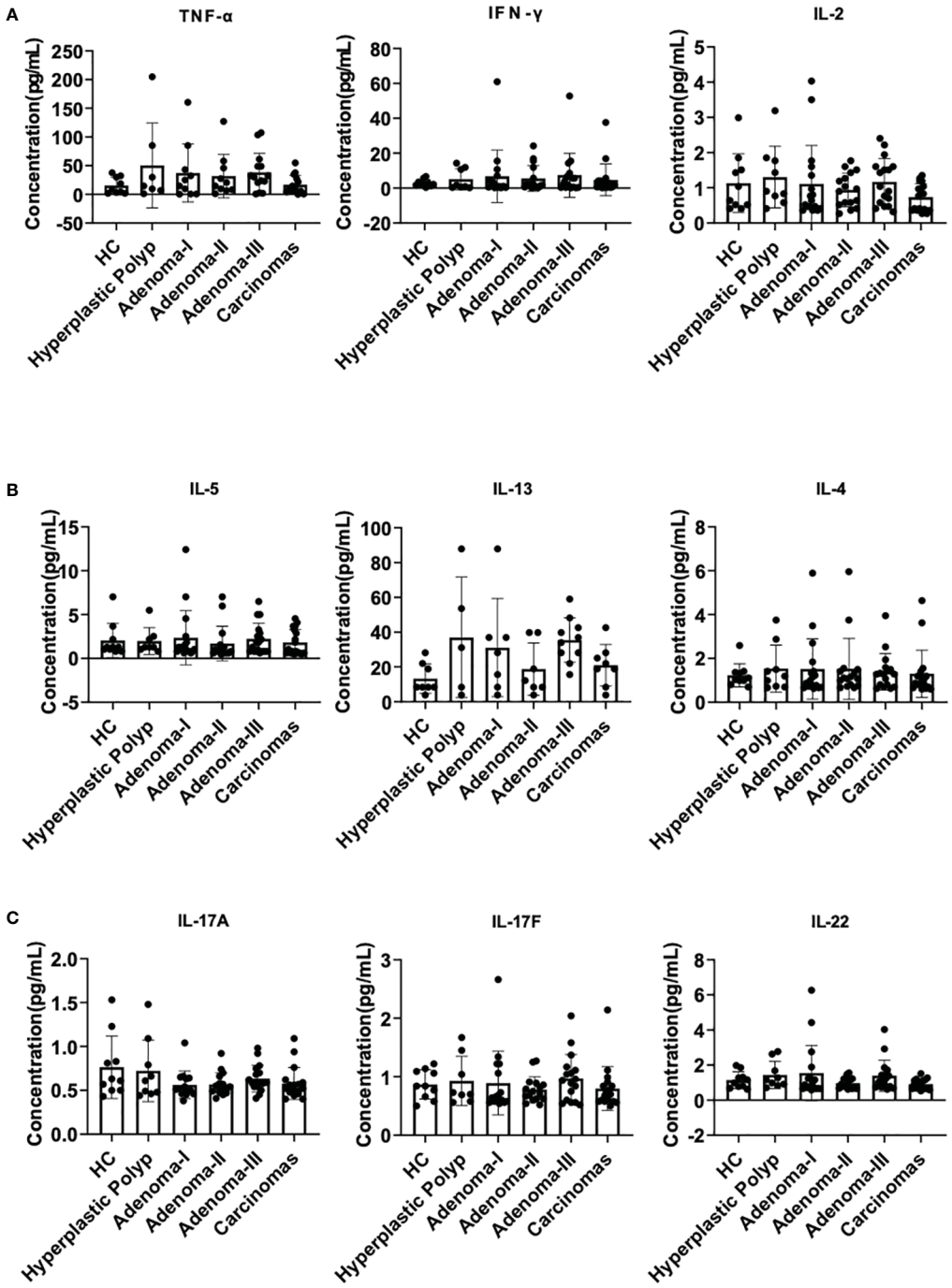

FIGURE 2
Plasma cytokine analysis during a cascade of colonic lesions. **(A)** The concentration of TNF-α, IFN-γ, and IL-2 in the plasma. **(B)** The concentration of IL-5, IL-13, and IL-4 in the plasma. **(C)** The concentration of IL-17A, 17F, and 22 in the plasma. Each dot represents one donor. HC, healthy control. Error bars represent the SEM. ANOVA or non-parametric test (Kruskal–Wallis test) as appropriate. All results are not significantly different. n = 10–19 in each group.

grade II (3.95 vs. 0.63, P = 0.0157), grade III (3.95 vs. 0.26, P = 0.0002), and CRC (3.95 vs. 0.16, $P < 0.0001$) compared with the control (Figure 6A). Moreover, the percentage of $CD4^+PD1^+CXCR5^+$ cells decreased from adenoma grade I to III and even in CRC (Figure 6A), primarily attributed to the change in programmed cell death protein 1 (PD1) but not CXCR5 (Supplementary Figures 4A, B). In addition, the expression of *PDCD1* and *CXCR5* in the tissue-derived $CD4^+$ T cells among different colonic lesions was analyzed using the single-cell RNA-sequencing data (GSE161277). As shown in Figure 6B, the Tfh cell markers *PDCD1* and *CXCR5* were decreased during the carcinoma progression, which is consistent with the change of t peripheral Tfh population. Furthermore, the percentage

10.3389/fimmu.2024.1287632

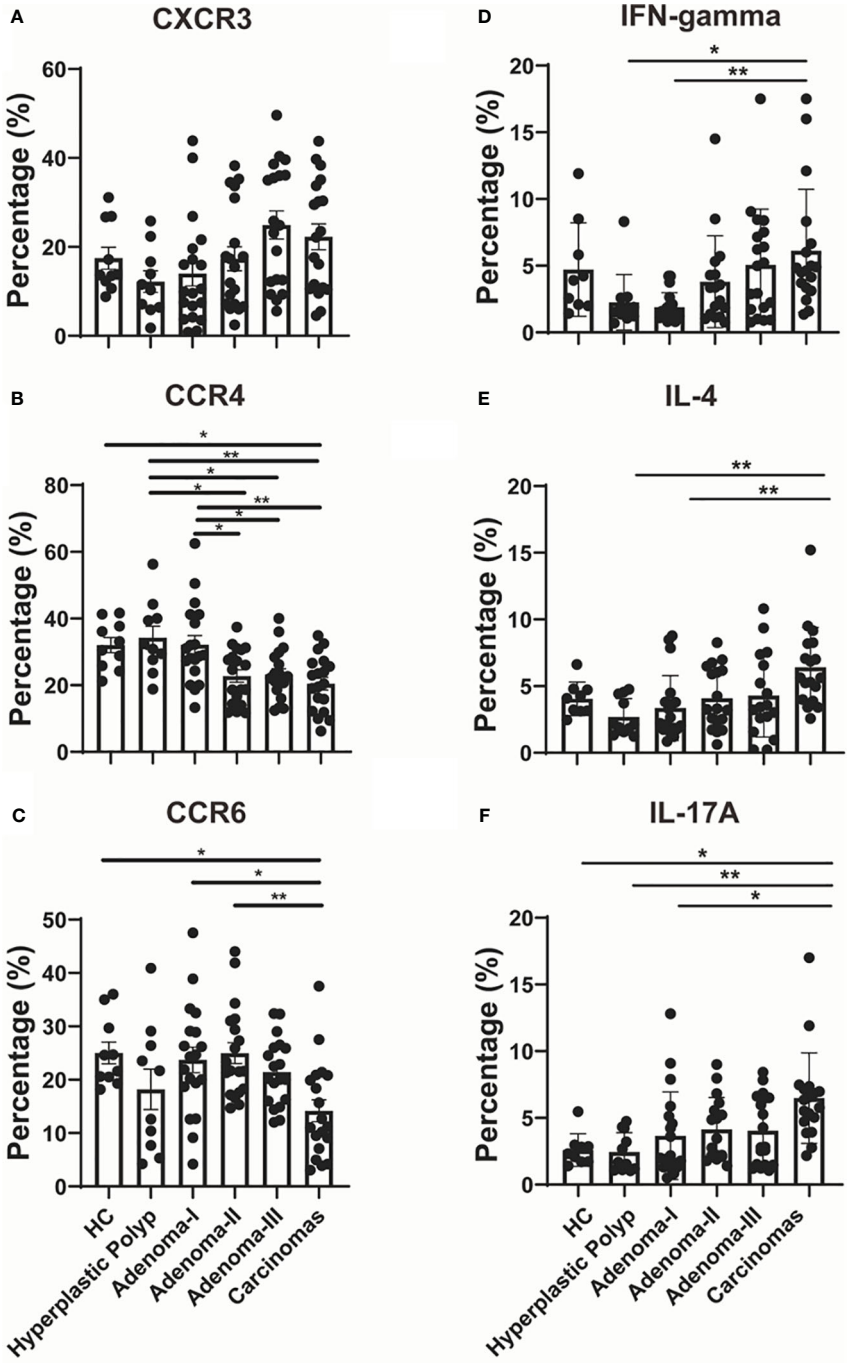

FIGURE 3
Th cell response analysis during a cascade of colonic lesions. **(A–C)** Flow cytometry quantification of the frequency of $CXCR3^+$ **(A)**, $CCR4^+$ **(B)**, and $CCR6^+$ **(C)** cells in $CD4^+$ T cells during a cascade of colonic lesions. **(D-F)** Flow cytometry quantification of the frequency of IFN-gamma$^+$ **(D)**, IL-4^+ **(E)**, and IL-$17A^+$ **(F)** cells in $CD4^+$ T cells during a cascade of colonic lesions. Each dot represents one donor. HC, healthy control. Error bars represent the SEM. *$P < 0.05$; **$P < 0.01$ (ANOVA or non-parametric test as appropriate). n = 10–19 in each group.

of antibody-secreting $CD19^+CD38^+CD27^+$ plasma cells also decreased in the adenoma grade II group (2.775 vs. 0.405, $P < 0.0001$), adenoma grade III group (2.775 vs. 1.230, $P = 0.0015$), and CRC group (2.775 vs. 1.280, $P = 0.0155$) compared with that in the control group (Figure 6C). However, IL-21^+ production in $CD4^+$ cells, the key cytokine of Tfh cells, showed no significant differences among the groups (Figure 6D). These results suggested a potential role of Tfh cells in both precancerous lesions and CRC.

Discussion

The ability of precancerous lesions to progress to cancer is related to the intrinsic phenotype and the contributions of the immune response. Therefore, an in-depth investigation of the immunological characteristics of colorectal carcinoma progression is crucial for understanding the mechanisms underlying CRC development. Tumor occurrence and development often result in

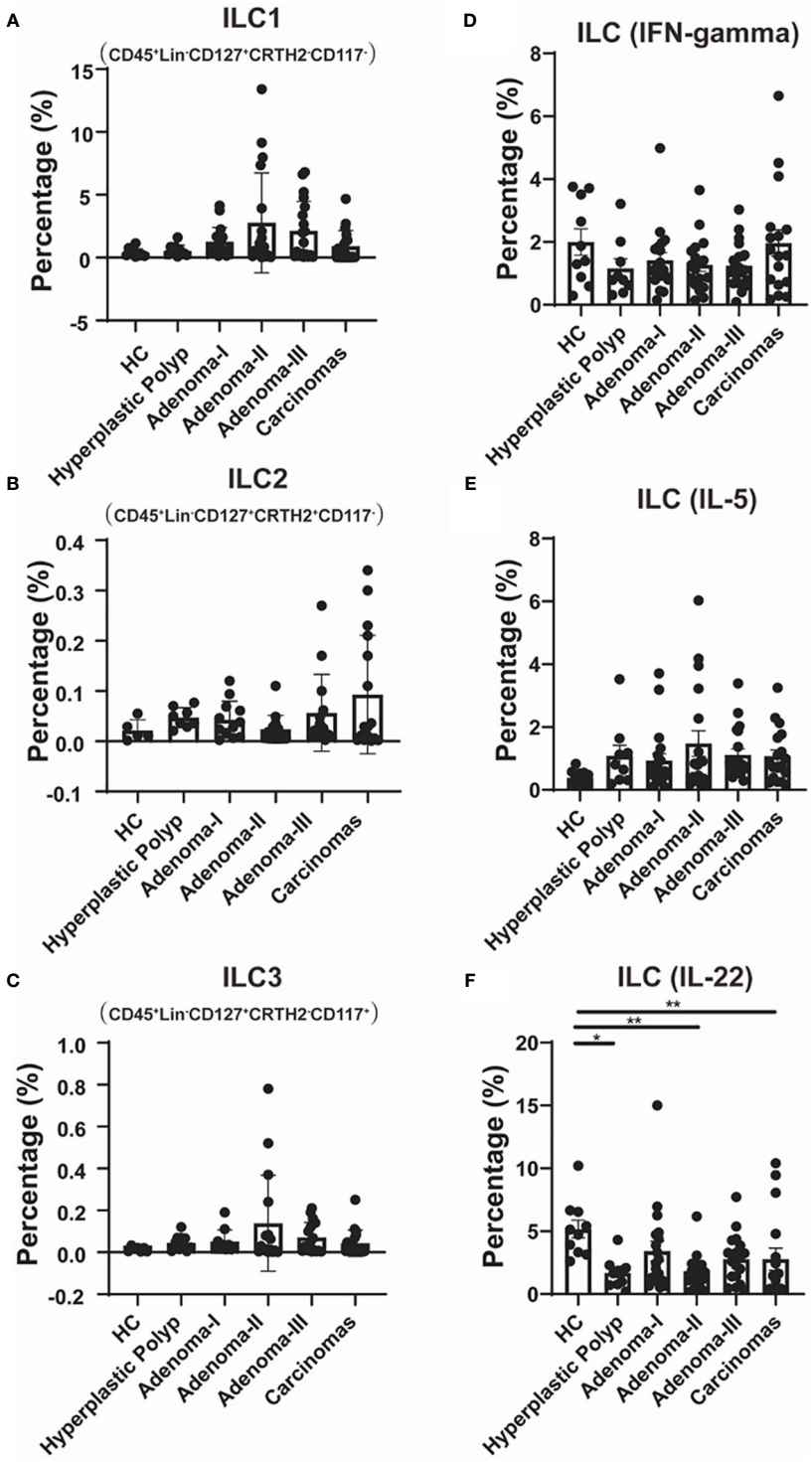

FIGURE 4
The change of ILC cell populations during a cascade of colonic lesions. **(A–C)** Flow cytometry quantification of the frequency of $Lin^-CD127^+CRTH2^-CD117^-$ ILC1 cells **(A)**, $Lin^-CD127^+CRTH2^+CD117^-$ ILC2 cells **(B)**, and $Lin^-CD127^+CRTH2^-CD117^+$ ILC3 cells **(C)** in $CD45^+$ PBMCs during a cascade of colonic lesions. **(D–F)** Flow cytometry quantification of the frequency of Lin^-CD127^+IFN-gamma$^+$ cells **(D)**, Lin^-CD127^+IL-5^+ cells **(E)**, and Lin^-CD127^+IL-22^+ cells **(F)** in $CD45^+$ PBMCs during a cascade of colonic lesions. Each dot represents one donor. HC, healthy control. Error bars represent the SEM. *$P < 0.05$; **$P < 0.01$ (ANOVA or non-parametric test as appropriate). n = 10–19 in each group.

systemic immune disturbances and alterations in peripheral immune cells through tissue communication with peripheral blood (21–24). Therefore, monitoring disease development through the peripheral immune response may be a better option. Dynamic changes in the peripheral immune profile, from colonic precancerous lesions to CRC lesions, have not been reported. In this study, we demonstrated the immune landscape of the CRC development process, including changes in Th cells, ILC cells, and

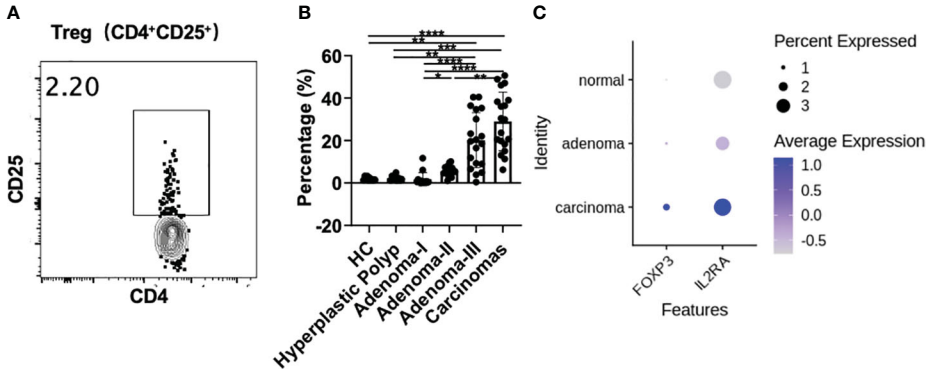

FIGURE 5
Treg cell analysis during a cascade of colonic lesions. **(A)** The representative flow plots about the gating strategy of CD25$^+$ Treg cells in CD4$^+$ T cells during a cascade of colonic lesions. **(B)** Flow cytometry quantification of the frequency of CD4$^+$CD25$^+$ Treg cells in CD4$^+$ T cells. Each dot represents one donor. HC, healthy control. Error bars represent the SEM. *P < 0.05; **P < 0.01; ***P < 0.001; ****P < 0.0001 (ANOVA or non-parametric test as appropriate). n = 10–19 in each group. **(C)** *IL-2RA* (*CD25*) and *FOXP3* expression analysis in the tissue-derived CD4$^+$ T cells among different colonic lesions by analyzing the single-cell RNA-sequencing data (GSE161277). The color depth represents the average expression, and the size of the dots represents the percentage expressed.

key cytokines that play critical roles in maintaining intestinal homeostasis.

Cytokines are a class of small molecular proteins or peptides with biological activities that can be divided into pro- and anti-inflammatory cytokines. The cytokines in our study exhibited non-significant subtle changes. IFN-γ, TNF-α, and IL-2 enhance cytotoxic and apoptotic effects in response to colon adenomas. IL-22 plays both protective and pathogenic roles in inflammation. At an early stage, IL-22 is protective, helps maintain barrier integrity, and reduces inflammation and tumors. However, during wound repair in the epithelium, IL-22 promotes tumor development (31). Our results were inconsistent with those of previous studies, and no changes were detected in the plasma cytokine spectrum, indicating that their ability to detect lesions might be limited.

We comprehensively analyzed lymphocyte profiles in premalignant and colorectal tumors. ILCs are central innate immune mediators in both gastrointestinal homeostasis and inflammatory pathologies (15) and exhibit striking similarities to the heterogeneity in CD4$^+$ T helper cells (14, 32). To our knowledge, our results are the first to demonstrate the characteristics of Th and ILC subsets in HPs. Though effector Th response increased during the carcinoma process, the ILC-derived IL-22 production was downregulated in the HP, adenoma, and CRC groups. The immunological characteristics of HP, adenoma, and CRC are generally consistent with the tissue-derived single-cell RNA-seq data from previously reported studies (20, 27). Interestingly, the peripheral CD4$^+$ T cells were contrary to the results of tumor-derived CD4$^+$ T cells in terms of their surface molecules. This might be due to the differences in methodology because the peripheral CD4$^+$ T cells were defined with surface molecules at the protein level while the tumor-derived CD4$^+$ T cells' surface molecules were analyzed at the RNA level. Moreover, the differences in localization might also contribute to that. The upregulation of these chemokines in the tumor-derived CD4$^+$ T cells was very likely associated with the migration toward tumor tissues. Considering the easily obtainable and non-invasive characteristics of peripheral blood samples, the circulating Th cell analysis might be used to monitor CRC development and discover key functional cell subpopulations during CRC carcinogenesis.

Maintaining the immune balance is critical for antitumor immunity. Foxp3$^+$ regulatory T cells secrete immunomodulatory cytokines and cytolytic molecules that regulate immune responses (33). Besides the effect of Th subsets, suppressive Treg cells also play an essential role in the tumor immune response. Elevated Treg cells are associated with promoting tumor development, immunotherapy failure, and poorer prognosis in CRC (34), suggesting that the immune balance is critical in antitumor immunity. In terms of tumor prognosis, a high number of Tregs are correlated with poor patient survival. Foxp3$^+$ Treg accumulation in the tumor microenvironment is an early event along the carcinoma development and may play a role in initiating CRC (35). Our study confirmed the upregulation of peripheral Tregs during carcinoma progression and showed a progressive increase from adenoma grade I to CRC. However, Treg activation induced CD25 upregulation in CD4$^+$ conventional T cells (36, 37). Therefore, we cannot exclude the involvement of activated T cells in the CD4$^+$CD25$^+$ population. We also investigated the changes in different effector CD4$^+$ cell subsets, and these populations did not show dramatic changes as the CD4$^+$CD25$^+$ populations. Thus, we speculated that the changes in CD4$^+$CD25$^+$ cells may be mainly attributed to Treg cells. In addition, the tendency of peripheral Treg cells to increase during CRC development was consistent with the results from colonic tissues, indicating the potential use of peripheral Treg cells to monitor CRC progression.

As a critical CD4$^+$ T-cell subset, Tfh cells primarily function by interacting with B cells and are essential for guiding immunoglobulin isotype switching, affinity maturation, and memory- and antibody-secreting B-cell differentiation (38). Tfh cells help B cells during effective antibody-mediated immune responses (38, 39). Recently, the role of Tfh cells in the antitumor immune response has attracted increasing attention (37, 39). Tfh

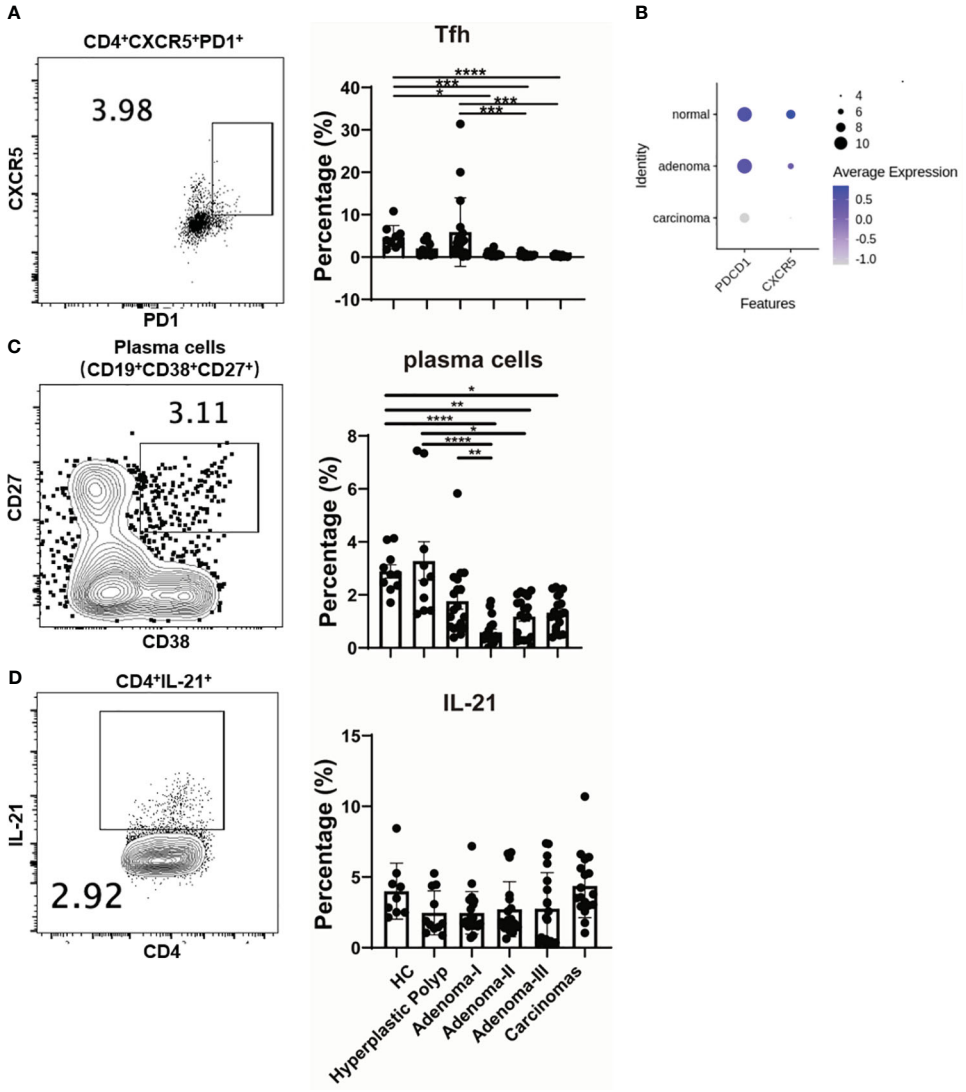

FIGURE 6
The change of Tfh cells during a cascade of colonic lesions. **(A)** The FACS staining (left) and frequency quantification (right) analysis of $CD4^+CXCR5^+$ $PD1^+$ cells in $CD4^+$ T cells during a cascade of colonic lesions. **(B)** The expression analysis of *PDCD1* and *CXCR5* in the tissue-derived $CD4^+$ T cells among different colonic lesions by analyzing the single-cell RNA-sequencing data (GSE161277). The color depth represents the average expression, and the size of the dots represents the percentage expressed. **(C)** The FACS staining (left) and frequency quantification (right) analysis of $CD19^+CD38^+CD27^+$ plasma cells during a cascade of colonic lesions. **(D)** The FACS staining (left) and frequency quantification (right) analysis of IL-21^+ cells in $CD4^+$ T cells during a cascade of colonic lesions. Each dot represents one donor. HC, healthy control. Error bars represent the SEM. $*P < 0.05$; $**P < 0.01$; $***P < 0.001$; $****P < 0.0001$ (ANOVA or non-parametric test as appropriate). n = 10–19 in each group.

indirectly enhances antitumor immunity mediated by $CD8^+$ T cells by secreting IL-21 (40). Furthermore, the specific intestinal bacterium *Helicobacter hepaticus* promotes Tfh-associated antitumor immunity in the colon (37). However, the involvement of Tfh cells and related antibody responses in CRC development is unclear. Our results further demonstrate that Tfh cells and related plasma cell populations decrease with disease progression, implying that Tfh cells are involved in precancerous and CRC stages.

However, our study has limitations, such as a small cohort of unpaired individuals. Considering this limitation and to further confirm the tissue specificity of the changed cell populations, we verified our PBMC results using published single-cell RNA-seq data by detecting the expression levels of Th cell subset markers in $CD4^+$ T cells from tissues. Tissue results showed the same variation tendency as that of the PBMCs. This finding verified our PBMC findings and further indicated that the changes in Th subsets may be primarily due to colorectal lesions. However, another model is needed to clarify whether this is a sequential effect, such as using paired tissue samples or collecting PBMCs at different pathological stages from the same patients. Moreover, the male/female ratios of the samples were inconsistent between the groups. The male/female ratio was lower in the adenoma group than in the control/CRC group. The small sample size also caused a potential bias during the short collection period, which may have confounded the results. Sexual dimorphisms have been described in innate and adaptive immune systems. Significantly elevated frequencies of Treg cells were reported in the peripheral blood of young postpubertal cisgender men compared with similarly aged cisgender women. Thus, sex chromosomes and hormones may drive

changes in Treg cell frequency and function, and young postpubertal men have a more anti-inflammatory Treg cell profile than women (41). A higher incidence of CRC is observed in men than in women (42). Although the control group had a high male ratio in our study, the percentage of Tregs was still lower than that in the adenoma and carcinoma groups. This finding indicates that changes in Tregs in colonic precancerous lesions and CRC may result from pathological changes. As for Tfh cells, no studies have reported the influence of sex on Tfh cells in colonic precancerous lesions and CRC. However, the relationship between elevated levels of circulating Tfh cells and female-biased autoimmune diseases has been verified (43). Accordingly, the decreased Tfh percentage may not be due to sex but to the lower female ratio in the control group. Since the exact influence of sex hormones on the immune phenotype during tumor development remains unclear, the effect of sex bias should be considered. Lastly, because ILC2s can also express CD117 (44), some ILC2s might be excluded from the analysis.

In summary, we analyzed the immunological profile characteristics and demonstrated the involvement of Th subsets, especially Treg and Tfh cell populations, during colorectal carcinogenesis. Our study is the first to demonstrate the lymphocyte profiles of HPs and the CRC development process by analyzing circulating PBMCs and the production of key cytokines. Further exploration of their functions is required to develop a precise treatment.

Conclusion

We analyzed circulating ILCs and adaptive T lymphocyte subtypes in colorectal carcinogenesis. We revealed the involvement of Th subsets, especially Treg and Tfh cells, in CRC development and clarified the immunological characteristics of HPs.

These findings significantly enhance our understanding of the immune mechanisms underlying CRC and its precancerous lesions. Further investigation of the Treg and Tfh cells' function in colorectal disease development will provide potential therapeutic targets for monitoring and preventing CRC development. Considering the easily obtainable and non-invasive characteristics of peripheral blood samples, demonstrating the change of peripheral functional cell subpopulations, like Treg and Tfh cells, during CRC carcinogenesis might provide novel target cells for the early screening of CRC patients.

Data availability statement

The raw data supporting the conclusions of this article will be made available by the authors, without undue reservation.

Ethics statement

The studies involving humans were approved by the Peking University Third Hospital Medical Science Research Ethics Committee. The studies were conducted in accordance with the local legislation and institutional requirements. The human samples used in this study were acquired from a by-product of routine care or industry. Written informed consent for participation was not required from the participants or the participants' legal guardians/next of kin in accordance with the national legislation and institutional requirements.

Author contributions

QM: Data curation, Methodology, Software, Validation, Visualization, Writing – original draft. YZ: Data curation, Writing – original draft. MX: Writing – review & editing. PW: Writing – review & editing. JL: Writing – original draft. RC: Writing – original draft. WF: Conceptualization, Formal analysis, Funding acquisition, Supervision, Writing – review & editing. SD: Funding acquisition, Project administration, Writing – review & editing.

Funding

The author(s) declare financial support was received for the research, authorship, and/or publication of this article. This work was supported by grants from the National Natural Science Foundation of China, grant number 82371771, 81870386 and China Health and Medical Development Foundation Cooperation Project (to WF and to SD).

Conflict of interest

The authors declare that the research was conducted in the absence of any commercial or financial relationships that could be construed as a potential conflict of interest.

Publisher's note

Supplementary material

The Supplementary Material for this article can be found online at: https://www.frontiersin.org/articles/10.3389/fimmu.2024.1287632/full#supplementary-material

References

1. Morgan E, Arnold M, Gini A, Lorenzoni V, Cabasag CJ, Laversanne M, et al. Global burden of colorectal cancer in 2020 and 2040: Incidence and mortality estimates from globocan. *Gut* (2023) 72:338–44. doi: 10.1136/gutjnl-2022-327736

2. Cronin KA, Scott S, Firth AU, Sung H, Henley SJ, Sherman RL, et al. Annual report to the nation on the status of cancer, part 1: National cancer statistics. *Cancer* (2022) 128:4251–84. doi: 10.1002/cncr.34479

3. Sung H, Ferlay J, Siegel RL, Laversanne M, Soerjomataram I, Jemal A, et al. Global cancer statistics 2020: Globocan estimates of incidence and mortality worldwide for 36 cancers in 185 countries. *CA Cancer J Clin* (2021) 71:209–49. doi: 10.3322/caac.21660

4. Nakanishi Y, Diaz-Meco MT, Moscat J. Serrated colorectal cancer: The road less travelled? *Trends Cancer* (2019) 5:742–54. doi: 10.1016/j.trecan.2019.09.004

5. IJ JE, Vermeulen L, Meijer GA, Dekker E. Serrated neoplasia-role in colorectal carcinogenesis and clinical implications. *Nat Rev Gastroenterol Hepatol* (2015) 12:401–9. doi: 10.1038/nrgastro.2015.73

6. Mezzapesa M, Losurdo G, Celiberto F, Rizzi S, d'Amati A, Piscitelli D, et al. Serrated colorectal lesions: An up-to-date review from histological pattern to molecular pathogenesis. *Int J Mol Sci* (2022) 23:4461. doi: 10.3390/ijms23084461

7. Hanby AM, Poulsom R, Singh S, Jankowski J, Hopwood D, Elia G, et al. Hyperplastic polyps: A cell lineage which both synthesizes and secretes trefoil-peptides and has phenotypic similarity with the ulcer-associated cell lineage. *Am J Pathol* (1993) 142:663–8.

8. Krishn SR, Kaur S, Smith LM, Johansson SL, Jain M, Patel A, et al. Mucins and associated glycan signatures in colon adenoma-carcinoma sequence: Prospective pathological implication(s) for early diagnosis of colon cancer. *Cancer Lett* (2016) 374:304–14. doi: 10.1016/j.canlet.2016.02.016

9. Chen J, Zhu H, Yin Y, Jia S, Luo X. Colorectal cancer: Metabolic interactions reshape the tumor microenvironment. *Biochim Biophys Acta Rev Cancer* (2022) 1877:188797. doi: 10.1016/j.bbcan.2022.188797

10. Zhang L, Zhao Y, Dai Y, Cheng JN, Gong Z, Feng Y, et al. Immune landscape of colorectal cancer tumor microenvironment from different primary tumor location. *Front Immunol* (2018) 9:1578. doi: 10.3389/fimmu.2018.01578

11. Grizzi F, Bianchi P, Malesci A, Laghi L. Prognostic value of innate and adaptive immunity in colorectal cancer. *World J Gastroenterol* (2013) 19:174–84. doi: 10.3748/wjg.v19.i2.174

12. Pernot S, Terme M, Voron T, Colussi O, Marcheteau E, Tartour E, et al. Colorectal cancer and immunity: What we know and perspectives. *World J Gastroenterol* (2014) 20:3738–50. doi: 10.3748/wjg.v20.i14.3738

13. Speiser DE, Chijioke O, Schaeuble K, Münz C. Cd4(+) t cells in cancer. *Nat Cancer* (2023) 4:317–29. doi: 10.1038/s43018-023-00521-2

14. Vivier E, Artis D, Colonna M, Diefenbach A, Di Santo JP, Eberl G, et al. Innate lymphoid cells: 10 years on. *Cell* (2018) 174:1054–66. doi: 10.1016/j.cell.2018.07.017

15. Atreya I, Kindermann M, Wirtz S. Innate lymphoid cells in intestinal cancer development. *Semin Immunol* (2019) 41:101267. doi: 10.1016/j.smim.2019.02.001

16. Cui G, Li Z, Florholmen J, Goll R. Dynamic stromal cellular reaction throughout human colorectal adenoma-carcinoma sequence: A role of th17/il-17a. *BioMed Pharmacother* (2021) 140:111761. doi: 10.1016/j.biopha.2021.111761

17. Cui G, Yuan A, Goll R, Florholmen J. Il-17a in the tumor microenvironment of the human colorectal adenoma-carcinoma sequence. *Scand J Gastroenterol* (2012) 47:1304–12. doi: 10.3109/00365521.2012.725089

18. Cui G, Yang H, Zhao J, Yuan A, Florholmen J. Elevated proinflammatory cytokine il-17a in the adjacent tissues along the adenoma-carcinoma sequence. *Pathol Oncol Res* (2015) 21:139–46. doi: 10.1007/s12253-014-9799-1

19. Zheng X, Song J, Yu C, Zhou Z, Liu X, Yu J, et al. Single-cell transcriptomic profiling unravels the adenoma-initiation role of protein tyrosine kinases during colorectal tumorigenesis. *Signal Transduct Target Ther* (2022) 7:60. doi: 10.1038/s41392-022-00881-8

20. Chen B, Scurrah CR, McKinley ET, Simmons AJ, Ramirez-Solano MA, Zhu X, et al. Differential pre-malignant programs and microenvironment chart distinct paths to Malignancy in human colorectal polyps. *Cell* (2021) 184:6262–6280.e6226. doi: 10.1016/j.cell.2021.11.031

21. Allen BM, Hiam KJ, Burnett CE, Venida A, DeBarge R, Tenvooren I, et al. Systemic dysfunction and plasticity of the immune macroenvironment in cancer models. *Nat Med* (2020) 26:1125–34. doi: 10.1038/s41591-020-0892-6

22. Wu WC, Sun HW, Chen HT, Liang J, Yu XJ, Wu C, et al. Circulating hematopoietic stem and progenitor cells are myeloid-biased in cancer patients. *Proc Natl Acad Sci U.S.A.* (2014) 111:4221–6. doi: 10.1073/pnas.1320753111

23. Templeton AJ, McNamara MG, Šeruga B, Vera-Badillo FE, Aneja P, Ocaña A, et al. Prognostic role of neutrophil-to-lymphocyte ratio in solid tumors: A systematic review and meta-analysis. *J Natl Cancer Inst* (2014) 106:dju124. doi: 10.1093/jnci/dju124

24. van Cruijsen H, van der Veldt AA, Vroling L, Oosterhoff D, Broxterman HJ, Scheper RJ, et al. Sunitinib-induced myeloid lineage redistribution in renal cell cancer patients: Cd1c+ dendritic cell frequency predicts progression-free survival. *Clin Cancer Res* (2008) 14:5884–92. doi: 10.1158/1078-0432.CCR-08-0656

25. Schultze JL, Mass E, Schlitzer A. Emerging principles in myelopoiesis at homeostasis and during infection and inflammation. *Immunity* (2019) 50:288–301. doi: 10.1016/j.immuni.2019.01.019

26. Masopust D, Schenkel JM. The integration of t cell migration, differentiation and function. *Nat Rev Immunol* (2013) 13:309–20. doi: 10.1038/nri3442

27. Fu W, Wang W, Zhang J, Zhao Y, Chen K, Wang Y, et al. Dynamic change of circulating innate and adaptive lymphocytes subtypes during a cascade of gastric lesions. *J Leukoc Biol* (2022) 112:931–8. doi: 10.1002/JLB.5MA0422-505R

28. Wang W, Xing Y, Chang Y, Wang Y, You Y, Chen Z, et al. The impaired development of innate lymphoid cells by preterm birth is associated with the infant disease. *Sci Bull (Beijing)* (2021) 66:421–4. doi: 10.1016/j.scib.2020.09.012

29. Butler A, Hoffman P, Smibert P, Papalexi E, Satija R. Integrating single-cell transcriptomic data across different conditions, technologies, and species. *Nat Biotechnol* (2018) 36:411–20. doi: 10.1038/nbt.4096

30. Penny HA, Hodge SH, Hepworth MR. Orchestration of intestinal homeostasis and tolerance by group 3 innate lymphoid cells. *Semin Immunopathol* (2018) 40:357–70. doi: 10.1007/s00281-018-0687-8

31. Huber S, Gagliani N, Zenewicz LA, Huber FJ, Bosurgi L, Hu B, et al. Il-22bp is regulated by the inflammasome and modulates tumorigenesis in the intestine. *Nature* (2012) 491:259–63. doi: 10.1038/nature11535

32. Artis D, Spits H. The biology of innate lymphoid cells. *Nature* (2015) 517:293–301. doi: 10.1038/nature14189

33. Vignali DA, Collison LW, Workman CJ. How regulatory t cells work. *Nat Rev Immunol* (2008) 8:523–32. doi: 10.1038/nri2343

34. Aristin Revilla S, Kranenburg O, Coffer PJ. Colorectal cancer-infiltrating regulatory t cells: Functional heterogeneity, metabolic adaptation, and therapeutic targeting. *Front Immunol* (2022) 13:903564. doi: 10.3389/fimmu.2022.903564

35. Hua W, Yuan A, Zheng W, Li C, Cui J, Pang Z, et al. Accumulation of foxp3+ t regulatory cells in the tumor microenvironment of human colorectal adenomas. *Pathol Res Pract* (2016) 212:106–12. doi: 10.1016/j.prp.2015.12.002

36. Gutiérrez-Melo N, Baumjohann D. T follicular helper cells in cancer. *Trends Cancer* (2023) 9:309–25. doi: 10.1016/j.trecan.2022.12.007

37. Overacre-Delgoffe AE, Bumgarner HJ, Cillo AR, Burr AHP, Tometich JT, Bhattacharjee A, et al. Microbiota-specific t follicular helper cells drive tertiary lymphoid structures and anti-tumor immunity against colorectal cancer. *Immunity* (2021) 54:2812–2824.e2814. doi: 10.1016/j.immuni.2021.11.003

38. Cui C, Craft J, Joshi NS. T follicular helper cells in cancer, tertiary lymphoid structures, and beyond. *Semin Immunol* (2023) 69:101797. doi: 10.1016/j.smim.2023.101797

39. Garaud S, Dieu-Nosjean MC, Willard-Gallo K. T follicular helper and b cell crosstalk in tertiary lymphoid structures and cancer immunotherapy. *Nat Commun* (2022) 13:2259. doi: 10.1038/s41467-022-29753-z

40. Shi W, Dong L, Sun Q, Ding H, Meng J, Dai G. Follicular helper t cells promote the effector functions of cd8(+) t cells via the provision of il-21, which is downregulated due to pd-1/pd-l1-mediated suppression in colorectal cancer. *Exp Cell Res* (2018) 372:35–42. doi: 10.1016/j.yexcr.2018.09.006

41. Robinson GA, Peng J, Peckham H, Butler G, Pineda-Torra I, Ciurtin C, et al. Investigating sex differences in t regulatory cells from cisgender and transgender healthy individuals and patients with autoimmune inflammatory disease: A cross-sectional study. *Lancet Rheumatol* (2022) 4:e710–24. doi: 10.1016/S2665-9913(22)00198-9

42. Abancens M, Bustos V, Harvey H, McBryan J, Harvey BJ. Sexual dimorphism in colon cancer. *Front Oncol* (2020) 10:607909. doi: 10.3389/fonc.2020.607909

43. Walker LSK. The link between circulating follicular helper t cells and autoimmunity. *Nat Rev Immunol* (2022) 22:567–75. doi: 10.1038/s41577-022-00693-5

44. Spits H, Artis D, Colonna M, Diefenbach A, Di Santo JP, Eberl G, et al. Innate lymphoid cells–a proposal for uniform nomenclature. *Nat Rev Immunol* (2013) 13:145–9. doi: 10.1038/nri3365

frontiers | Frontiers in Immunology

TYPE Original Research
PUBLISHED 09 February 2024
DOI 10.3389/fimmu.2024.1325330

OPEN ACCESS

EDITED BY
Raquel Tarazona,
University of Extremadura, Spain

REVIEWED BY
Ming Yi,
Zhejiang University, China
Xiaoping Zhong,
Second Affiliated Hospital of Shantou University Medical College, China

*CORRESPONDENCE
Wendao Liu
Liu_wendao_2023@163.com
Jiaping Li
jiapingli_2019@163.com

†These authors have contributed equally to this work

RECEIVED 21 October 2023
ACCEPTED 29 January 2024
PUBLISHED 09 February 2024

CITATION
Wang H, Huang H, Liu T, Chen Y, Li J, He M, Peng J, Liang E, Li J and Liu W (2024) Peripheral blood lymphocyte subsets predict the efficacy of TACE with or without PD-1 inhibitors in patients with hepatocellular carcinoma: a prospective clinical study. *Front. Immunol.* 15:1325330. doi: 10.3389/fimmu.2024.1325330

Peripheral blood lymphocyte subsets predict the efficacy of TACE with or without PD-1 inhibitors in patients with hepatocellular carcinoma: a prospective clinical study

Hongyu Wang[1,2†], Huijie Huang[3†], Ting Liu[3,4], Yaoming Chen[5], Jinwei Li[1], Min He[3], Jianxin Peng[6], Enyu Liang[3], Jiaping Li[7*] and Wendao Liu[1*]

[1]Department of Interventional Therapy, The Second Affiliated Hospital of Guangzhou University of Chinese Medicine, Guangzhou, China, [2]Guangdong Provincial Key laboratory of Chinese Medicine for Prevention and Treatment of Refractory Chronic Diseases, The Second Affiliated Hospital of Guangzhou University of Chinese Medicine, Guangzhou, China, [3]Department of Laboratory Medicine, The Second Clinical College of Guangzhou University of Chinese Medicine, Guangzhou, China, [4]State Key Laboratory of Traditional Chinese Medicine Syndrome, The Second Affiliated Hospital of Guangzhou University of Chinese Medicine, Guangzhou, China, [5]Department of Laboratory Medicine, The First Affiliated Hospital of Sun Yat-sen University, Guangzhou, China, [6]Department of Hepatobiliary Surgery, The Second Affiliated Hospital of Guangzhou University of Chinese Medicine, Guangzhou, China, [7]Department of Interventional Oncology, The First Affiliated Hospital of Sun Yat-Sen University, Guangzhou, China

Background: Although peripheral blood lymphocyte subsets, particularly PD-1+ T cells, are promising prognostic indicators for patients with cancer. However, their clinical significance remains unclear.

Methods: We prospectively enrolled 157 patients with hepatocellular carcinoma (HCC) treated with transcatheter arterial chemoembolization combined with or without PD-1 inhibitors. Twenty peripheral lymphocyte subsets and cytokines were analyzed. We analyzed the differences in PD-1+ T cells between patients treated with and without PD-1 inhibitors and their associations with tumor response, survival prognosis, and clinical features.

Results: We found that the baseline CD8+PD-1+ and CD4+PD-1+ T-cell frequencies in patients who had received PD-1 inhibitors were lower than those in patients who had not received PD-1 inhibitors ($p < 0.001$). In the former patients, there were no differences in PD-1+ T-cell frequencies between the responder and non-responder subgroups ($p > 0.05$), whereas in the latter patients, the levels of CD8+PD-1+ T cells, CD4+PD-1+ T cells, and CD8+PD-1+/CD4+PD-1+ ratio did not predict tumor response, progression-free survival (PFS), or overall survival (OS) ($p>0.05$). Furthermore, in multivariate analysis of patients treated with or without PD-1 inhibitors revealed that the levels of CD8+CD38+ T cells (OR = 2.806, $p = 0.006$) were associated with tumor response, whereas those of CD8+CD28+ T cells ($p = 0.038$, $p = 0.001$) and natural killer (NK) cells ($p = 0.001$, $p = 0.027$) were associated with PFS and OS. Although, these independent prognostic factors were associated with

progressive tumor characteristics ($p<0.05$), with the exception of CD8+CD28+ T cells, changes in these factors before and after treatment were unassociated with tumor response ($p > 0.05$).

Conclusion: Circulating CD8+CD38+ T cells, CD8+CD28+ T cells, and NK cells were identified as potential prognostic factors for tumor response and survival in patients with HCC. Contrastingly, although PD-1 inhibitors can effectively block the T cell PD-1 receptor, the baseline PD-1+ T-cell frequencies and changes in the frequency of these cells have limited prognostic value.

KEYWORDS

lymphocyte subsets, PD-1+ T cells, prognosis, hepatocellular carcinoma, PD-1 inhibitors

1 Introduction

Hepatocellular carcinoma (HCC), which accounts for 75%–85% of primary liver cancers, is among the most prevalent and fatal malignancies worldwide (1). Transcatheter arterial chemoembolization (TACE), the first-line treatment for patients with unresectable intermediate-stage HCC (2), is effective in patients with early- or advanced-stage HCC (3), and compared with monotherapy based on TACE or tyrosine kinase inhibitors (TKIs), TACE plus TKIs has been established to improve clinical outcomes for unresectable HCC (4, 5). Recent research has shown that the clinical benefit of triple combination therapy comprising TACE+TKIs+programmed cell death (PD)-1/programmed death-ligand 1 (PD-L1) inhibitors are significantly superior to those of dual combination therapy comprising TACE and TKIs (6–8). TKIs regulate the tumor immune microenvironment (9, 10). PD-1 inhibitors block the PD-1 receptors on the surface of T cells, prevent the binding of PD-1 to PD-L1 on the tumor surface, and activate the anti-tumor immunity of cytotoxic T cells (11). Although in recent years, predictive biomarkers based on PD-1/PD-L1 expression, tumor-infiltrating lymphocytes (TILs), and the genetic characteristics of tumor tissue have been reported (12, 13), these markers have yet to be widely validated or used to predict clinical benefits, and thus clinical risk factors still serve as a foundation for treatment choices.

Whereas most of the relevant studies conducted to date have tended to focus on PD-L1 expression in tumor cells and macrophages in the tumor microenvironment, the expression of PD-1 in peripheral T cells has been studied to a notably lesser extent. PD-1, an immune checkpoint receptor, is highly expressed on the surface of functionally exhausted T cells in response to persistent antigen stimulation in patients with tumors or chronic infections. This may explain the association between high levels of PD-1 expression on peripheral blood CD3+ T cells and CD8+ T cells and poor overall survival (OS) and progression-free survival (PFS) in patients with advanced-stage non-small cell lung cancer (NSCLC) treated with nivolumab (14). However, the findings of a further study have indicated that high levels of circulating CD8+PD-1+ T cells have a positive influence on the prognosis of patients with immune checkpoint inhibitor (ICI)-treated advanced NSCLC (15). Moreover, it has been demonstrated that HCC patients with high levels of circulating CD4+PD-1+ T cells are more likely to respond to tremelimumab therapy (16). Consequently, it has yet to be sufficiently established whether the circulating PD-1+ T-cell frequency and its change in response to ICI therapy have any prognostic value.

TILs influence the behavior of human tumors, and the relative abundance and phenotypes of specific subsets of TILs have been extensively investigated as potential biomarkers for ICI treatment (17–19). However, for many patients with advanced liver cancer, the detection of TILs is not feasible, owing to the limited availability of tumor tissues. In this regard, peripheral blood lymphocyte subsets have been identified as promising biomarkers for characterizing differences between cancer patients and healthy individuals, predicting patient prognosis, and determining treatment strategies. Nevertheless, the results of these studies have tended to be inconsistent. In theory, natural killer (NK) cells and CD8+ T cells are cytotoxic; however, the frequencies of circulating NK cells and CD8+ T cells are lower and higher, respectively, in patients with liver cancer than in healthy individuals (20, 21). Conversely, the findings of other studies have revealed reductions in the proportions of NK cells and CD8+ T cells in patients with cancer, whereas there is an increase in the CD4+/CD8+ T-cell ratio (22, 23). Although it is generally believed that high levels of NK, CD4+ T, and CD8+ T cells predict better tumor response and prolonged PFS in patients with NSCLC (23, 24), the findings of one study have indicated that high baseline NK cell levels in patients with advanced NSCLC treated with nivolumab are associated with a poor prognosis (14). These authors also reported that high levels of CD8+ T cells are associated with prolonged OS and PFS, whereas the frequency of CD8+ T cells in patients with tumor progression was higher than that in patients in a clinical benefit group (14). Moreover, different studies have reported variable predictive efficacies for T-cell functional subsets characterized by CD28 and CD38 expression (25–27).

In our previous study, we established that conventional circulating lymphocyte subsets were generally ineffective as prognostic predictors for HCC patients treated with TACE (28). In this prospective cohort study, we accordingly sought to characterize baseline circulating lymphocyte subsets and their changes in HCC patients treated with TACE administered with or without PD-1 inhibitors using high-dimensional flow cytometry and attempted to identify effective prognostic biomarkers.

2 Materials and methods

2.1 Patients

This study was approved by the Ethics Committee of the First Affiliated Hospital of Sun Yat-Sen University. All patients were informed of the study's aims and procedures and consented to enrollment. The cohort included as many patients as possible with a clinical or pathological diagnosis of HCC, covering patients with BCLC stages A, B, and C, as well as those who had received previous treatment. Patients with an Eastern Cooperative Oncology Group performance status score greater than 3, a Child-Pugh score greater than 13, or obvious infective symptoms were excluded. At enrollment, peripheral blood was drawn from patients prior to treatment to assess baseline levels of lymphocyte subsets and the cytokines IL-6 and IFN-γ. The outcomes of these preliminary analyses did not influence decisions regarding individual treatment plans.

2.2 Treatment and follow-up

On the basis of the characteristics and staging of tumors, we recommend TACE as the basic local treatment, and/or combination systemic therapy, such as TKIs and PD-1 inhibitors. TACE procedures were based on super-selective techniques and an operational protocol described in our previous study (28). The TKIs used at our research center included first-line drugs, such as sorafenib and lenvatinib, and second-line drugs, such as regorafenib and apatinib. PD-1 inhibitors include camrelizumab, sintilimab, tislelizumab. The treatment protocols adopted in this study all comply with Chinese clinical guidelines for the management of HCC (29); however, due to cost and poor compliance, some patients have received relatively conservative treatment or in some cases, the use of TKIs or ICIs bas been delayed.

To evaluate tumor response and determine subsequent treatment plans, patients underwent an initial enhanced CT or MRI examination 4 to 8 weeks after the preliminary treatment. Subsequent follow-up intervals were typically between 1 and 3 months. A tumor response 3 months after the initial treatment was evaluated based on modified RECIST (mRECIST). Responders were defined as those patients with a confirmed complete response (CR) or partial response (PR), whereas non-responders were defined as patients with confirmed stable disease (SD) or progressive disease (PD). PFS was defined from the date of initial lymphocyte subset detection initiation to tumor progression or death due to any cause in the absence of progression. OS was defined from the date of initial lymphocyte subset detection initiation to the data of death due to any cause.

2.3 Detection of lymphocyte subsets and cytokines

At enrollment, three samples of venous blood (two EDTA anticoagulant tubes, one separation gel coagulation promoting tube) were collected from patients prior treatment. Fresh blood samples were delivered to our clinical laboratory within 4 hours of collection. CD3+ T, CD4+ T, CD8+ T, CD19+ B, and CD16+ CD56 + NK cells were stained using BD Multitest 6-color TBNK reagent in Trucount tubes (Cat:662997). The inhibitory and activated T lymphocyte subsets were also analyzed based on a single-platform technique by ten-color flow cytometry. The data were collected and analyzed on a BD FACS Canto II flow cytometer. The main antibodies were CD45 KrO (B36294), CD3 PB (B49204), CD4 APC-cy7 (341115), CD8 PE-cy7 (664999), PD-1 Percp-cy5.5 (561273), CD28 PE (662797), CD38 APC (345807), HLA-DR FITC (652827). The gating strategy is shown in Supplementary Figure 1. The concentrations of the cytokines IL-6 and IFN-γ were determined using enzyme-linked immunosorbent assays (Hangzhou Clongene Biotech Co. Ltd., China). The procedures were performed in accordance with the manufacturer's protocols. Additionally, after 4-8 weeks of enrollment, the peripheral blood of patients was collected again to detect the aforementioned immune indicators and evaluate the clinical significance of any changes.

2.4 Statistical analysis

Continuous variables and categorical variables are presented as the means and standard deviations, or medians and interquartile ranges, and were compared between groups using Student's *t*-test, the Mann-Whitney U test, a paired *t*-test, or the chi-square test. The cutoff values for lymphocyte subsets and cytokines for predicting a tumor response were determined by receiver operating characteristic (ROC) curve analysis. Logistic regression was performed to identify variables associated with tumor response. Univariate and multivariate Cox analyses were also conducted to identify variables associated with survival outcomes, and only factors that reached a significance threshold of $p < 0.1$ in univariate analysis were selected for multivariate analysis. All presented p-values are two-sided, and a p-value < 0.05 was considered to indicate a statistical significance. IBM SPSS version 24.0 was used for statistical analysis, and GraphPad Prism version 8.0.1 was used for graphical presentation of the data.

3 Results

3.1 Patient characteristics

From September 2021, a total of 157 patients were enrolled within 6 months and followed up until June 2023. These included 115 previously treated patients and 42 newly diagnosed patients. At enrollment, compared with those patients who had not undergone

PD-1 inhibitor treatment (n = 96), those who had received this treatment (n=61) had advanced stage disease, multiple nodules, and extrahepatic metastasis characteristics (all $p < 0.05$) (Table 1). One patient with advanced-stage HCC opted to discontinue treatment, while the remaining patients received TACE-based treatment after enrollment. Among them, 84 patients received TKI+PD-1 inhibitor combination therapy, 30 patients received TKI combination therapy, 11 patients received PD-1 inhibitor combination therapy. Two patients died of liver failure and stroke following an initial TACE treatment. Therefore, the three patients had no assessable or acceptable tumor response or PFS. Additionally, 44 patients who were evaluated as PD at enrollment were lost to follow-up within 3 months or had no available imaging data. Accordingly, we were able to obtain OS data for 154 patients with an evaluable tumor response and evaluable PFS data for 110 patients. The patient distribution of clinical baseline characteristics and prognosis is shown in Figure 1.

TABLE 1 Clinical characteristics of patients who had or had not undergone PD-1 inhibitor treatment.

		PD-1 inhibitor treatment		p
		No	Yes	
Age	<56	42	34	0.143
	≥56	54	27	
Sex	Man	87	59	0.145
	Woman	9	2	
Current tumor response [a]	PR	27	30	0.93
	SD+PD	27	31	
Child-Pugh class	A	65	38	0.646
	B	25	20	
	C	6	3	
BCLC stage	A	22	5	0.01
	B	27	12	
	C	47	44	
Tumor boundary	Clear	50	31	0.877
	Obscure	46	30	
Tumor number	1	19	6	0.003
	2-3	41	15	
	≥4	36	40	
Tumor size (cm)	1-5	41	26	0.795
	5-10	29	21	
	≥10	26	14	
Vascular invasion	No	56	29	0.186
	Yes	40	32	
Extrahepatic metastasis	No	72	35	0.021
	Yes	24	26	

[a]One hundred and fifteen patients who had previously received treatment had evaluable tumor responses at enrollment.
PR, partial response; SD, stable disease; PD, progressive disease.

3.2 Clinical intergroup differences in PD-1+ T cells

Baseline PD-1+ T-cell frequency data was obtained for 156 patients. Compared with those in patients who had not received PD-1 inhibitor treatment (n=96), we detected approximately 20- to 30-fold reductions in the frequencies of CD4+PD-1+ T cells and CD8+PD-1+ T cells in patients who had received PD-1 inhibitor treatment ($n = 60$) ($p < 0.001$) (Supplementary Table 1, Figures 2A, C). However, we detected no differences among the subgroups with different ICI treatment courses ($p > 0.05$) (Figures 2B, D), which means that the PD-1 receptor on the surface of T cells can be effectively blocked after a single administration of PD-1 inhibitor. In patients who had been treated with PD-1 inhibitors, there were no significant differences in the percentages of CD4+PD-1+ T cells and CD8+PD-1+ T cells between the responder (n=30) and non-responder (n=30) groups at enrollment ($p > 0.05$) (Figure 3). This suggests that PD-1+ T cell levels did not rebound in patients who did not respond to PD-1 inhibitors.

In all 156 patients, we detected extremely high percentages of CD4+PD-1+ T cells and CD8+PD-1+ T cells in several patients (> median plus triple interquartile range; Figures 2, 3). We have known that PD-1 inhibitors can significantly reduce the level of PD-1 + T cells. Therefore, we first analyzed the reasons for the abnormal value of PD-1+ T cells in patients who have been treated with PD-1 inhibitors. In these patients, seven (4 responders and 3 non-responders) had an extremely high CD4+PD-1+ T-cell frequency (> 2.64%). Among the four responders, one patient had a 5-month interval from the final administration of sintilimab and the other three patients had a lower CD4+PD-1+ T-cell frequency than did those who had not undergone PD-1 inhibitor treatment. Among the three non-responders, two had a 2-/3-month interval from the final dose of camrelizumab. We also identified four patients with an extremely high CD8+PD-1+ T-cell frequency (> 1.95%), one of whom was a responder (with a 5-month interval from the final use of sintilimab), whereas the remaining three were non-responders

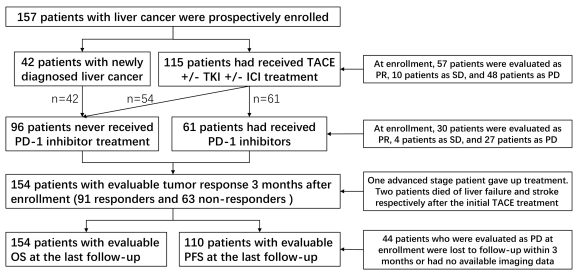

FIGURE 1
Patient distribution of clinical baseline characteristics and prognosis. TACE, transcatheter arterial chemoembolization; TKI, tyrosine kinase inhibitors; ICI, immune checkpoint inhibitor; PD-1, programmed cell death-1; PR, partial response; SD, stable disease; PD, progressive disease.

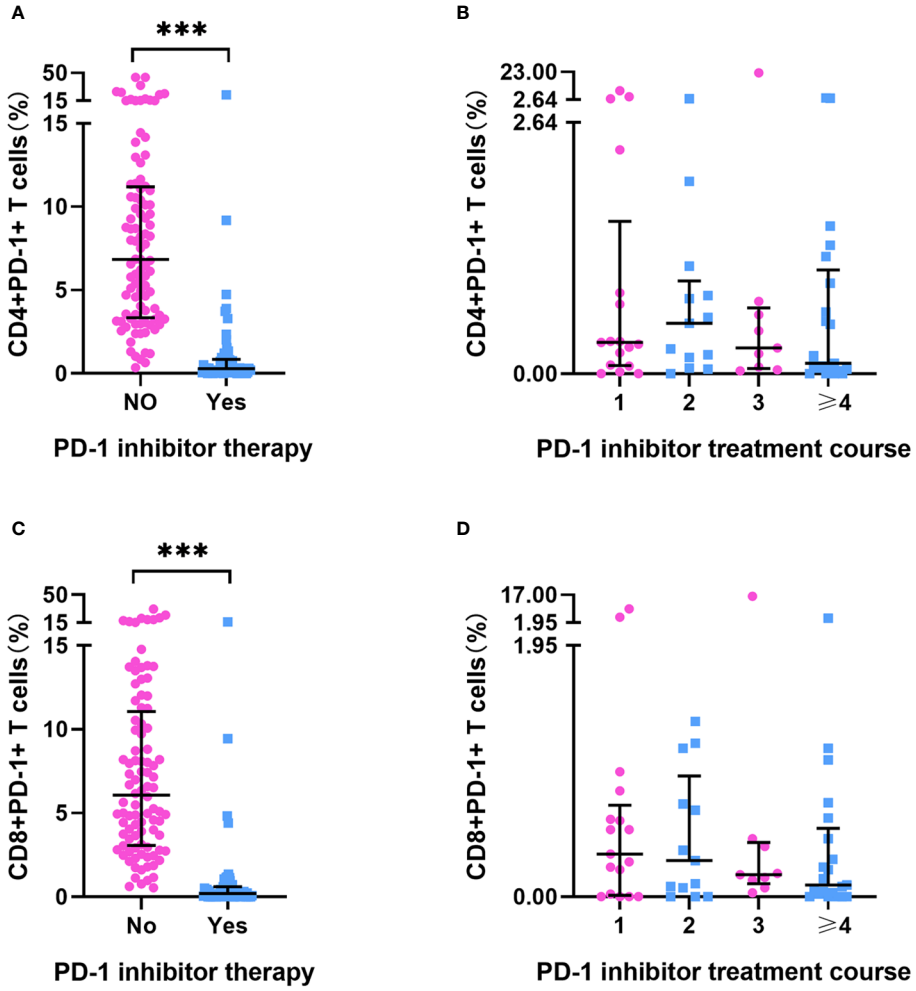

FIGURE 2
PD-1+ T cell frequency in HCC patients. **(A)** The frequency of CD4+PD-1+T cells in HCC patients treated with or without PD-1 inhibitor (No=96, Yes=60). **(B)** The frequency of CD4+PD-1+T cells in HCC patients after different PD-1 inhibitor treatment courses (once [n=17], twice [n=13], three times [n=9], ≥ four times [n=21]). **(C)** The frequency of CD8+PD-1+T cells in HCC patients treated with or without PD-1inhibitor treatment (No=96, Yes=60). **(D)** The frequency of CD8+PD-1+T cells in HCC patients after different PD-1 inhibitor treatment courses (once [n=17], twice [n=13], three times [n=9], ≥ four times [n=21]). ***p < 0.001.

(with one patient having a 3-month interval from the final use of camrelizumab). According to our case analysis, prolonged PD-1 inhibitor treatment intervals led to an increased rebound in the frequency of PD-1+ T cells. IL-6 and IFN-γ were reported to regulate the expression of PD-1 and PD-L1 in the tumor microenvironment. Therefore, we further analyzed their correlation with PD-1+ T cells in patients who did not receive PD-1 inhibitor treatment. In these patients, no significant correlations were detected between CD4+PD-1+ T cells and CD8+PD-1+ T cells and IL-6 or IFN-γ ($p < 0.05$) (Supplementary Table 2).

3.3 Prognostic analysis of tumor response in patients with different lymphocyte subsets and cytokines levels

When assessed at 3 months after enrollment, 154 patients (91 responders and 63 non-responders) had evaluable tumor responses. The tumor response (responder vs. non-responder) significantly differentiated the survival benefits with respect to PFS (hazard ratio [HR] = 2.968, 95% confidence interval [CI] = 1.710-5.150, $p < 0.001$) and OS (HR = 5.110, 95% CI = 3.111-8.392, $p < 0.001$) (Supplementary Figure 2). Subsequent ROC curve analysis of 20 lymphocyte subsets and the cytokines IL-6 and IFN-γ based on tumor response revealed significant differences in CD3+ T-cell counts, CD4+ T-cell counts, CD8+ T-cell counts, CD8+CD28+ T-cell frequency, CD8+CD38+ T-cell frequency, CD8+PD-1+/CD4+PD-1+ T-cell ratio, and the concentration of IL-6 in predicting tumor response (all $p < 0.05$) (Supplementary Table 3). The patients were divided into high and low groups based on the Youden indices of the aforementioned lymphocyte subsets and the cytokine IL-6, as well as the median of other previously widely assessed immune indicators, including NK cell counts, NK cell frequency, CD8+/CD4+ T-cell ratio, CD8+CD28− T-cell frequency, CD4+PD-1+ T-cell frequency, CD8+PD-1+ T-cell frequency, and IFN-γ.

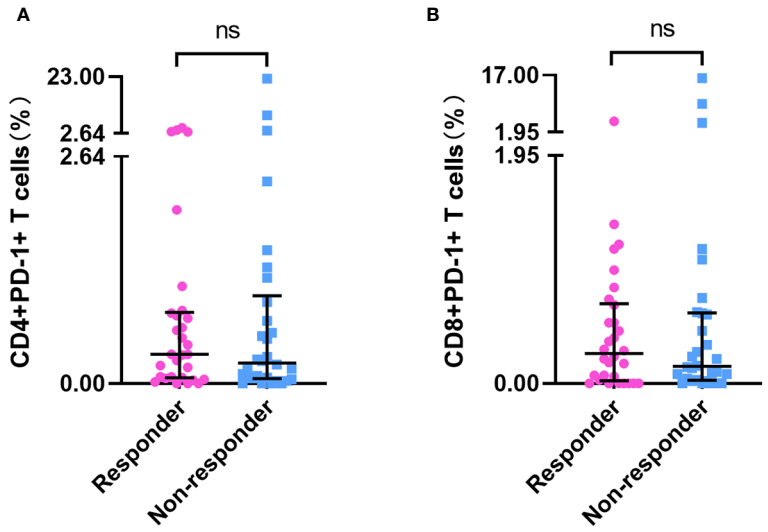

FIGURE 3
PD-1+ T cell frequency in responders and non-responders who had undergone PD-1 inhibitor treatment. The frequency of CD4+PD-1+ T cells **(A)** and CD8+PD-1+ T cells **(B)** in PD-1 inhibitor responders (n=30) and non-responders (n=30). 'ns' means No significance.

The predictive factors in the ROC curve analysis similarly revealed significant differences in the univariate logistic regression analysis (all p<0.05). Multivariate logistic regression analysis indicated significant differences in CD8+ T-cell counts (odds ratio [OR] = 0.409, 95% CI = 0.196-0.855, p = 0.018), CD8+CD38+ T-cell frequency (OR = 2.806, 95% CI = 1.335-5.898, p = 0.006), CD8+PD-1+/CD4+PD-1+ T-cell ratio (OR = 0.149, 95%CI = 0.05-0.451, p = 0.001), and IL-6 (OR = 2.527, 95%CI = 1.065-5.992, p = 0.035) (Figures 4A, B). Furthermore, univariate logistic regression analysis performed for the subgroup of patients who had undergone PD-1 inhibitor treatment, revealed that there were significant differences in CD8+CD28+ T-cell frequency, CD8+CD38+ T-cell frequency, and IL-6 (all p < 0.05), whereas multivariate analysis revealed significant differences in CD8+CD38+ T-cell frequency (OR = 5.997, 95%CI = 1.470-24.471, p = 0.013) and IL-6 (OR = 9.525, 95%CI = 1.509-60.127, p = 0.011) (Figures 4C, D). Moreover, we obtained evaluable tumor responses for 34 patients who commenced PD-1 inhibitor treatment following enrolment. On the basis of univariate analysis, we detected no significantly difference between responder and non-responder groups with respect to the baseline frequencies of CD4+PD-1+ T cells, CD8+PD-1+ T cells, or the ratio of CD8+PD-1+/CD4+PD-1+ T cells (all p > 0.05).

3.4 Survival analysis of RFS and OS in patients with different lymphocyte subsets and cytokines levels

Among the 110 patients with evaluable PFS, univariate survival analysis revealed a significant difference in the levels of six T-cell subsets and IL-6 (all p < 0.05), and multivariate analysis revealed significant differences in the levels of CD4+ T cells (≤ 268/μL vs. >268/μL) (HR = 0.357, 95%CI = 0.190-0.672, p = 0.01), NK cells (≤ 167/μL vs. >167/μL) (HR = 0.374, 95%CI = 0.209-0.670, p = 0.001), and CD8+CD28+ T cells (≤ 64% vs. >64%) (HR = 0.579, 95%CI = 0.345-0.971, p = 0.038) (Table 2). Among 35 patients who had undergone PD-1 inhibitors treatment, univariate analysis revealed significant differences in the levels of CD3+ T cells, CD4+ T cells, NK cells, and CD8+CD28+ T cells (all p < 0.05), whereas the multivariate analysis revealed differences in the levels of CD4+ T cells (≤ 268/μL vs. >268/μL) (HR = 0.242, 95%CI = 0.077-0.762, p = 0.015), NK cells (≤ 167/μL vs. >167/μL) (HR = 0.332, 95%CI = 0.106-1.042, p = 0.059), and CD8+CD28+ T cells (≤ 64% vs. >64%) (HR = 0.331, 95%CI = 0.113-0.971, p = 0.044) (Supplementary Table 4). Furthermore, among patients who commenced PD-1 inhibitor treatment following enrollment, 28 had evaluable PFS, and with the exception of CD4+PD-1+ T cell levels (HR: 2.401, 95% CI=1.000-5.770, p=0.05), univariate analysis revealed no significant differences among these patients with respect to the levels of CD8+PD-1+ T cells (HR = 1.326, p = 0.504) and CD8+PD-1+/CD4+PD-1+ T-cell ratio (HR = 0.658, p = 0.364).

Among the 154 patients with evaluable OS, univariate survival analysis revealed significant differences in the levels of 10 peripheral blood immune indicators, including CD8+/CD4+ T-cell ratio, CD8+PD-1+/CD4+PD-1+ T-cell ratio, and IL-6 (all p < 0.05), whereas multivariate analysis revealed significant differences in the levels of CD4+ T cells (≤ 268/μL vs. >268/μL) (HR = 0.433, 95%CI = 0.198-0.948, p = 0.036), CD8+ T cells (≤ 219/μL vs. >219/μL) (HR = 0.505, 95%CI = 0.312-0.814, p = 0.005), NK cells (≤ 167/μL vs. >167/μL) (HR = 0.569, 95%CI = 0.345-0.939, p = 0.027), CD8+CD28+ T cells (≤ 64% vs. >64%) (HR = 0.403, 95%CI = 0.241-0.675, p = 0.001), and IL-6 (≤ 25pg/mL vs. >25pg/mL) (HR = 2.036, 95%CI = 1.208-3.432, p = 0.008) (Table 3). Among 61 patients who had undergone PD-1 inhibitor treatment, univariate survival analysis of OS revealed significant differences in the levels of CD8+CD28+ T cells (p < 0.05), IL-6 (p < 0.05), and NK cells (p = 0.057), and, consistently, multivariate analysis revealed similar significant

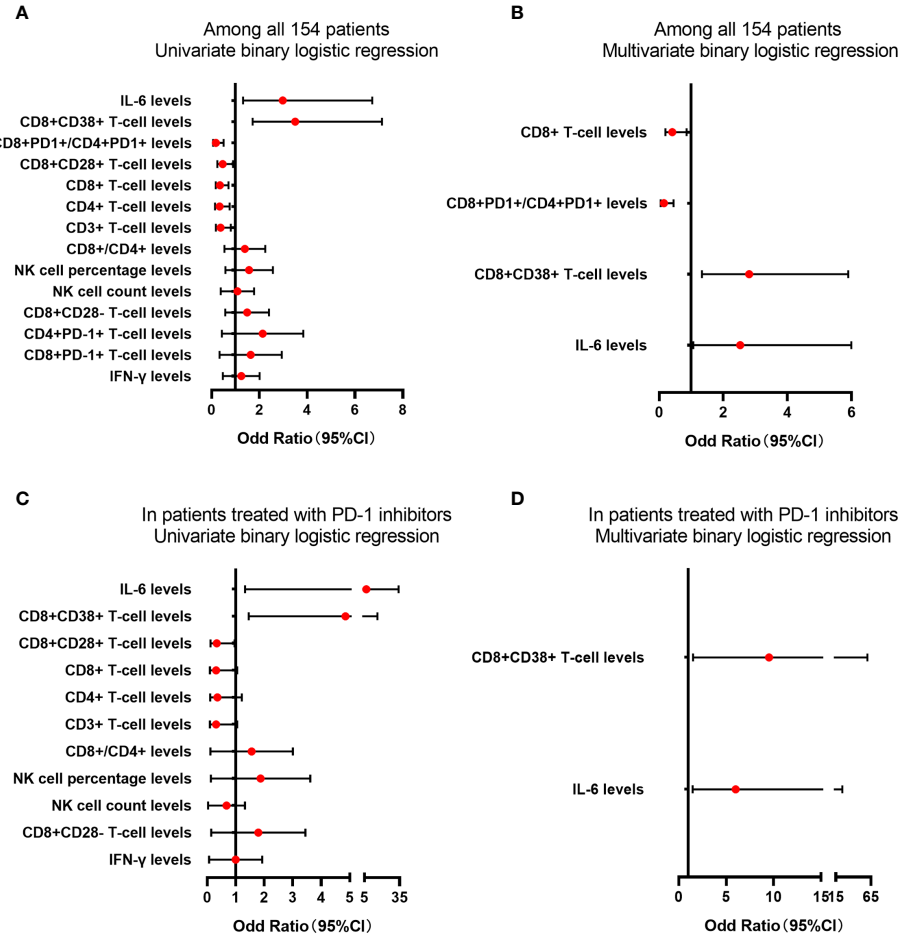

FIGURE 4
The analysis of lymphocyte subsets and cytokine levels in predicting the tumor response. The lymphocyte subsets and cytokines levels in predicting the tumor response for PD-1 treatment in univariate **(A)** or multivariate **(B)** binary logistic regression among all 154 patients. The lymphocyte subsets and cytokines levels in predicting the tumor response for PD-1 treatment in univariate **(C)** or multivariate **(D)** binary logistic regression in patients treated with PD-1 inhibitors.

differences in the three parameters (HR = 0.464, 95%CI = 0.216-1.000, p = 0.05; HR = 3.307, 95%CI = 1.500-7.287, p = 0.003; HR = 0.455, 95%CI = 0.207-0.997, p = 0.049) (Supplementary Table 5). Among patients who commenced PD-1 inhibitor treatment following enrollment, 34 had an evaluable OS, and for these individuals, univariate analysis revealed no significant differences in the levels of CD4+PD-1+ T cells, CD8+PD-1+ T cells, or CD8+PD-1+/CD4+PD-1+ T-cell ratio (all $p > 0.05$).

3.5 Correlation between independent prognostic factors and clinical characteristics

Among all patients and the subgroup of patients treated with PD-1 inhibitors, CD8+CD28+ T cells and NK cells were identified as the common independent prognostic factors for PFS and OS (Figure 5), whereas CD8+CD38+ T cells were common independent prognostic factors for tumor response. Correlation analysis performed to assess the significance of these three factors from a clinical perspective indicated associations with characteristic features of tumor progression, including advanced tumor stage, blurred boundaries, larger tumors, multiple nodules, extrahepatic metastasis, vascular invasion, and poor liver function (all $p < 0.05$) (Table 4).

3.6 Associations between changes in independent prognostic factors and tumor response

At 4 to 8 weeks post-enrollment, we re-assessed lymphocyte subsets in 33 patients and analyzed associations between the changes in the aforementioned three independent prognostic factors and tumor response. With respect to the non-responder subgroup (n=13), we accordingly detected a significant reduction in CD8+CD28+ T-cell frequency after 4–8 weeks ($p = 0.046$). Contrastingly, in neither subgroup did we detect any significant differences regarding comparisons of other indicators measured before and after treatment (Figure 6). In addition, there were no

10.3389/fimmu.2024.1325330

TABLE 2 Survival analysis for progression-free survival.

All patients	Groups	N	Univariate survival analysis		Multifactor survival analysis	
			HR (95% CI)	p	HR (95% CI)	p
CD3+ T cells (/μL)	≤ 533	21	1			
	>533	88	0.31 (0.176-0.545)	<0.001		
CD4+ T cells (/μL)	≤ 268	17	1		1	
	>268	92	0.214 (0.118-0.388)	<0.001	0.357 (0.190-0.672)	0.001
CD8+ T cells (/μL)	≤219	30	1			
	>219	79	0.390 (0.232-0.655)	<0.001		
CD8+/CD4+ ratio	≤ 0.63	58	1			
	>0.63	51	1.178 (0.713-1.947)	0.522		
NK cells (%)	≤ 17	56	1			
	>17	49	0.511 (0.299-0.872)	0.014		
NK cells (/μL)	≤ 167	49	1		1	
	>167	56	0.303 (0.176-0.520)	<0.001	0.374 (0.209-0.670)	0.001
CD8+CD28+ T cells (%)	≤ 64	48	1		1	
	>64	62	0.587 (0.356-0.967)	0.036	0.579 (0.345-0.971)	0.038
CD8+CD28− T cells (%)	≤ 9	59	1			
	>9	51	1.130 (0.686-1.863)	0.631		
CD8+CD38+ T cells (%)	≤ 59	54	1			
	>59	56	1.507 (0.906-2.504)	0.114		
CD4+PD-1+ T cells (%)	≤ 7	41	1			
	>7	34	1.511 (0.835-2.733)	0.172		
CD8+PD-1+ T cells (%)	≤ 6	38	1			
	>6	37	0.922 (0.510-1.667)	0.788		
CD8+PD-1+/CD4+PD-1+ ratio	≤ 0.55	13	1			
	>0.55	62	0.560 (0.276-1.135)	0.107		
IL-6 (pg/mL)	≤ 25	91	1			
	>25	19	2.351 (1.324-4.173)	0.004		
IFN-γ (pg/mL)	≤ 2	61	1			
	>2	49	0.915 (0.554-1.512)	0.728		

After ROC analysis, patients were divided into high and low groups based on the Youden index or median of lymphocyte subsets and cytokines (Supplementary Table 3). PD-1+ T cells were only analyzed in patients who had not undergone PD-1 inhibitor treatment.

significant differences between the responder and non-responder subgroups with respect to changes in the three independent prognostic factors (all $p > 0.05$) (Figure 7), thereby tending to indicate that changes in these factors would not be effective as predictors of a tumor response.

4 Discussion

To date, few studies have sought to verify the prognostic efficacy of peripheral blood lymphocyte subsets after TACE for liver cancer. However, given the significant heterogeneous responses of patients with advanced liver cancer treated with a combination of ICIs and an overall poor prognosis, accurate predictive markers are urgently needed. In this prospective study, we identified the levels of CD8+CD28+ T cells and NK cells as being independent prognostic factors for PFS and OS in all patients, as well as in subgroups of patients treated with PD-1 inhibitors. Furthermore, CD8+CD38+ T cells were found to be independent prognostic factors for tumor response. However, although PD-1 inhibitors can significantly block PD-1 receptors on the surface of T cells, we established that neither the baseline levels of CD8+PD-1+ and CD4+PD-1+ T cells nor the ratio or changes in these cells would serve as effective predictors of the prognosis of patients with liver cancer.

10.3389/fimmu.2024.1325330

TABLE 3 Survival analysis for overall survival.

All patients	Groups	N	Univariate survival analysis		Multifactor survival analysis	
			HR (95% CI)	p	HR (95% CI)	p
CD3+ T cells (/μL)	≤ 533	38	1			
	>533	114	0.421 (0.261-0.680)	<0.001		
CD4+ T cells (/μL)	≤ 268	31	1		1	
	>268	121	0.361 (0.220-0.591)	<0.001	0.433 (0.198-0.948)	0.036
CD8+ T cells (/μL)	≤219	51	1		1	
	>219	101	0.453 (0.285-0.718)	0.001	0.504 (0.312-0.814)	0.005
CD8+/CD4+ ratio	≤ 0.63	76	1			
	>0.63	77	1.631 (1.024-2.596)	0.039		
NK cells (%)	≤ 17	76	1			
	>17	70	0.776 (0.483-1.247)	0.295		
NK cells (/μL)	≤ 167	73	1		1	
	>167	73	0.489 (0.301-0.796)	0.004	0.569 (0.345-0.939)	0.027
CD8+CD28+ T cells (%)	≤ 64	79	1		1	
	>64	74	0.366 (0.223-0.600)	<0.001	0.403 (0.241-0.675)	0.001
CD8+CD28− T cells (%)	≤ 9	75	1			
	>9	78	1.661 (1.041-2.651)	0.033		
CD8+CD38+ T cells (%)	≤ 59	63	1			
	>59	90	1.782 (1.080-2.938)	0.024		
CD4+PD-1+ T cells (%)	≤ 7	47	1			
	>7	46	1.783 (0.933-3.408)	0.08		
CD8+PD-1+ T cells (%)	≤ 6	46	1			
	>6	47	0.884 (0.471-1.657)	0.7		
CD8+PD-1+/CD4+PD-1+ ratio	≤ 0.55	22	1			
	>0.55	71	0.376 (0.197-0.719)	0.003		
IL-6 (pg/mL)	≤ 25	121	1		1	
	>25	31	2.600 (1.592-4.245)	<0.001	2.036 (1.208-3.432)	0.008
IFN-γ (pg/mL)	≤ 2	84	1			
	>2	68	1.017 (0.641-1.615)	0.942		

After ROC analysis, patients were divided into high and low groups based on the Youden index or median of lymphocyte subsets and cytokines (Supplementary Table 3). PD-1+ T cells were only analyzed in patients who had not undergone PD-1 inhibitor treatment.

PD-1 receptors expressed on the surface of hematopoietic cells have an inhibitory function involving the negative regulation of immune responses, particularly in response to tumors. PD-1/PD-L1 blocking antibodies have been demonstrated to reverse these inhibitory effects and have accordingly shown clinical benefits in the treatment of tumors. However, in clinical practice, patients treated with PD-1 inhibitors often exhibit advanced tumor characteristics, making it difficult to predict their clinical benefit. Given that the expression of PD-1 on TILs has been established to be associated with prognosis in HCC, we sought to assess the utility of peripheral lymphocyte cells, including PD-1+ T cells, as biomarkers for predicting disease progression and prognosis in patients with HCC. We found that the baseline frequencies of circulating CD4+PD-1+ and CD8+PD-1+ T cells in HCC patients were 6.85% and 6.08%, respectively, whereas in patients treated with PD-1 inhibitors, we detected significantly reduced values of 0.30% and 0.21%, respectively, thereby indicating that PD-1 inhibitors can effectively block PD-1 receptors on the surface of T cells. The expression of PD-1 on circulating T cells in healthy individuals is lower than that in patients with NSCLC (30), and an increase in PD-1 expression is associated with tumor staging (31, 32). In the present study, however, we detected no significant correlation between PD-1 expression and tumor stage or liver function, except for patients with high levels of CD8+PD-1+ T cells

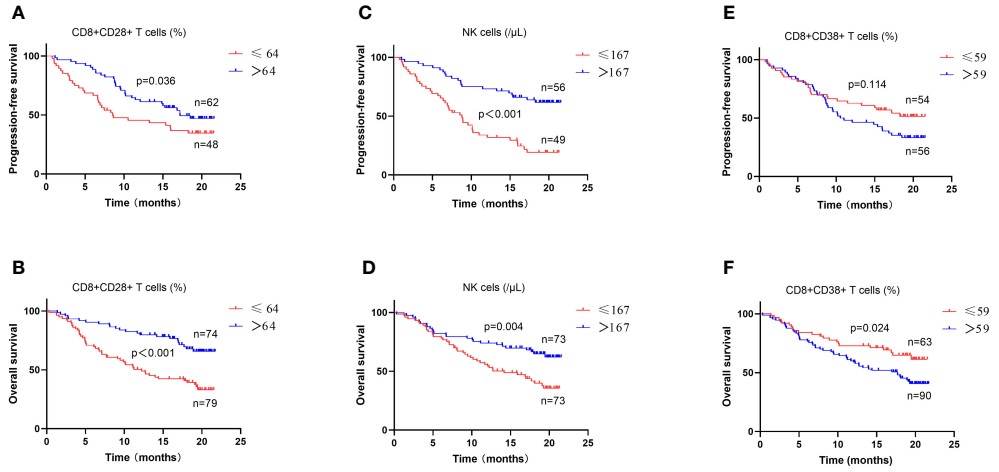

FIGURE 5
Survival analysis in patients with different lymphocyte subsets and cytokines levels. The levels of CD8+CD28+ T cells **(A, B)**, NK cells **(C, D)** and CD8+CD38+T cells **(E, F)** were analyzed for progression-free survival and overall survival in all patients.

associated with multiple tumors (data not shown). A high frequency of CD8+PD-1+TILs has previously been found to be a predictor of tumor responses in patients receiving ICI treatment. In contrast, a high frequency of circulating CD8+PD-1+ T cells is considered to be indicative of tumor progression in patients receiving sorafenib treatment (33). This indicates the contrasting predictive performance of PD-1+ T cells in relation to the therapeutic efficacy of ICI and TKI. The findings of a further study have revealed an increase in the expression of PD-1 in patients with recurrent NSCLC treated with PD-1 inhibitors (30). In the present study, however, we found that with the exception of the levels of CD4+PD-1+ T cells, which were shown to predict a worse OS in univariate analysis of the subgroup of patients treated with PD-1 inhibitors, there was no significant association between the baseline levels of PD-1+ T cells and patient prognosis. In patients treated with PD-1 inhibitors, we failed to detect any significant increase in the expression of PD-1 with tumor progression, and, consequently, we speculate that although PD-1 inhibitors can effectively block PD-1 receptors on the surface of T cells, they may not necessarily effectively activate T cell function in these non-responder patients. From another point of view, if the frequency of circulating PD-1+T cells in patients who fail to respond to PD-1 inhibitor treatment is significantly reduced (meaning the blood concentration of PD-1 inhibitor is high enough), we speculate that continuing medication may not be a wise choice. The abnormal increase in PD-1+ T-cell frequencies observed in patients treated with PD-1 inhibitors can partly be attributed to the extended treatment interval. Additionally, IL-6 and IFN-γ are considered to be the prominent stimulators that contribute to the expression of PD-1 and PD-L1 in the tumor microenvironment (34, 35); however, we were unable to detect any significant correlations between IL-6 or IFN-γ and PD-1 + T cells, which would thus tend to indicate that inflammatory cytokines are not associated with the abnormally high percentages of PD-1+ T cells.

Contrary to our expectations, we failed to detect any positive correlation between PD-1+ T cells and patient prognosis, which we assume could be attributable to one or more of the following factors. Firstly, there are differences regarding the expression of PD-1 on lymphocytes in peripheral blood and tumor tissues, and the expression of this protein does not fully reflect the immune status of the body. The frequency of PD-1+ TILs is significantly greater than that of peripheral PD-1+ T cells (33, 36), whereas in contrast, there is no significant difference in the frequency of circulating PD-1high T cells between healthy individuals and cancer patients (33). Secondly, PD-1+ T cells contain a group of cell subsets of differing functional status, and their co-expression with other molecules may represent a group of specific functional cell subsets, which may be more meaningful for identifying patient heterogeneity or predicting prognosis. For example, circulating PD-1+ early effector memory CD8+ T cells (CD28+CD27-CD45RO+) are characterized by early responses to anti-PD-1 therapy in patients with NSCLC (37). Moreover, circulating PD-1+TIGIT+CD8+ T cells are significantly upregulated in patients with HCC and are correlated with an advanced disease stage and poor prognosis (38). Thirdly, PD-1+ T cells are tumor-specific, and PD-1 is more highly expressed on tumor-associated antigen-specific CD8+ TILs than on other CD8+ TILs (36). In some cases, tumor-reactive peripheral blood lymphocytes are characterized by an overexpression of PD-1 receptors (39, 40). However, higher levels of PD-1+ T cells have also been established to be associated with other non-tumor factors, including aging, chronic inflammation, and infection. Consequently, the clinical significance of PD-1 expression on the peripheral lymphocytes of HCC patients needs further evaluation.

Theoretically, PD-1 inhibitors do not directly influence T cell surface receptors such as CD28, CD38, CD16, and CD56. In this study, we identified CD8+CD28+ T and NK cells as independent prognostic factors for PFS and OS in patients treated with TACE with or without the administration of PD-1 inhibitors. Similarly, CD38+ T cells were established to be an independent prognostic factor for tumor response. CD28 receptors are important co-stimulatory signals on the surface of T cells that in response to activation, exert anti-tumor effects when combined with B7

10.3389/fimmu.2024.1325330

TABLE 4 Correlations between independent prognostic factors and clinical characteristics.

		CD8+CD28+ T cell (%)			NK cell (cells/μL)			CD8+CD38+ T cell (%)		
		low	high	p	low	high	p	low	high	p
Age	<56	33	43	0.079	41	32	0.163	26	50	0.126
	≥ 56	46	34		34	42		37	43	
Sex	Man	76	69	0.108	68	71	0.198	61	84	0.12
	Woman	3	8		7	3		2	9	
Current tumor response [a]	PR	25	32	0.061	28	26	0.636	27	30	0.054
	SD+PD	35	22		31	24		17	40	
Child-Pugh class	A	45	58	0.036	40	58	0.005	48	55	0.083
	B	27	17		30	13		12	32	
	C	7	2		5	3		3	6	
BCLC stage	A	8	19	0.013	9	18	0.056	21	6	<0.001
	B	17	22		17	21		18	21	
	C	54	36		49	35		24	66	
Tumor boundary	Clear	34	46	0.037	31	46	0.011	38	42	0.063
	Obscure	45	31		44	28		25	51	
Tumor number	1	7	18	0.006	10	15	0.316	19	6	<0.001
	2-3	25	31		25	28		23	33	
	≥4	47	28		40	31		21	54	
Tumor size (cm)	1-5	29	37	0.046	26	38	0.079	38	28	0.001
	5-10	23	27		25	22		14	36	
	≥10	27	13		24	14		11	29	
Vascular invasion	No	34	50	0.006	35	48	0.025	45	39	<0.001
	Yes	45	27		40	26		18	54	
Extrahepatic metastasis	No	48	59	0.033	46	56	0.06	54	53	<0.001
	Yes	31	18		29	18		9	40	

[a]Patients who had previously received treatment had evaluable tumor responses at enrollment.
PR, partial response; SD, stable disease; PD, progressive disease.

molecules on antigen-presenting cells (41). On the basis of the expression of CD28+, CD8+ T cells were divided into CD8+CD28+ cytotoxic lymphocytes and CD8+CD28− senescent T cells. In this regard, it has previously been demonstrated that circulating levels of CD8+CD28+ T cells are lower in patients with ovarian cancer than in their benign counterparts (42), whereas the findings of a further study have indicated that high levels of circulating CD8+CD28+ T cells can serve as a predictor of immunotherapeutic responses and a more favorable prognosis in cancer patients (43). In the present study, we confirmed that high levels of circulating CD8+CD28+ T cells are associated with tumor response and prolonged PFS and OS. In contrast, the loss of CD28 is associated with a reduced proliferation of CD8+ T cells and a less efficient ability to recognize diverse antigens. It has also previously been found that in patients with lung cancer, circulating CD28−CD57+KLRG1 +CD8+ T cells were associated with a lack of benefit from ICIs (44). Our findings similarly indicate that elevated levels of CD8 +CD28− T-cell expression are associated with a poor OS in all patients, although are not predictive of tumor response or PFS, neither did they have an effective prognostic value in the PD-1 inhibitor treatment subgroup. In summary, CD8+CD28+ T cells are identified as an important functional subgroup that warrants further research.

CD38 was initially considered a biomarker for identifying activated T cells and thymocytes (45). In recent years, however, it has been established that CD38 is a member of the ribosyl cyclase family of proteins that is widely expressed on the surface of non-hematopoietic cells and several types of immune cells, in which it plays roles in adenosine synthesis, thereby contributing to immune escape (46). In HCC, a high frequency of CD38+PD-1+CD8+ T cells is associated with high histopathological grades (III and IV), thereby indicating that CD38, a T-cell co-exhaustion marker, is linked to tumor aggressiveness (27). A recent study has revealed that a heightened level of CD38 expression in TILs promotes

10.3389/fimmu.2024.1325330

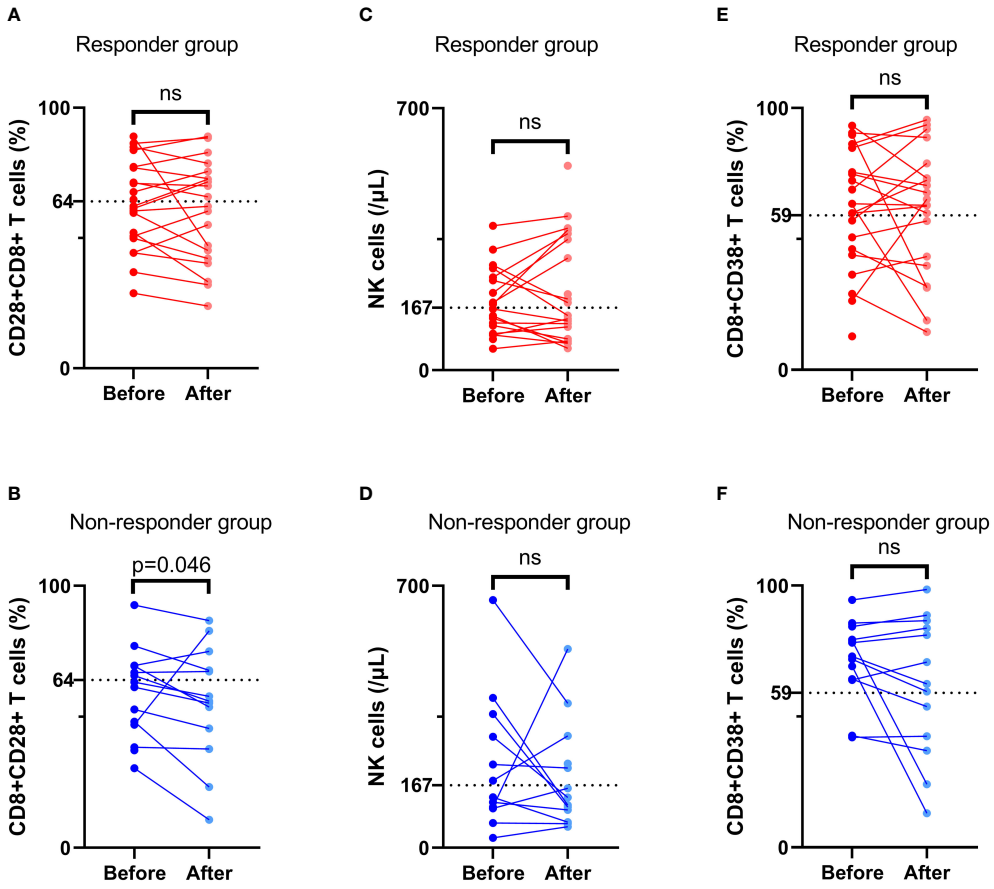

FIGURE 6
Comparison of lymphocyte subsets before and after treatment. The frequency of CD8+CD28+ T cells **(A, B)**, NK cell number **(C, D)**, and the frequency of CD8+CD38+ T cells **(E, F)** before and after treatment in the response group and non-response group. 'ns' means No significance.

increases in the levels of Ki-67 in tumor cells, and that highly expressed CD38+ TILs independently predict shorter OS and PFS (47). The findings of further studies have indicated that the progression of prostate cancer is associated with increases in CD38+ tumor-infiltrating immune cell density, which is independently associated with a worse OS (48). Moreover, anti-CD38 antibodies have been shown to enhance tumor inhibition, and in several clinical trials, have been found to have certain clinical benefits for patients with tumors (49, 50). Our findings in the present study also confirmed that high levels of CD38+CD8+ T cells are indicative of incomplete tumor response in patients with HCC treated with TACE with or without the administration of PD-1 inhibitors.

NK cells are part of the body's first line of defense against cancer cells and viral infection that can directly and non-specifically kill tumor cells and, as such, these cells have been extensively studied. The association between these lymphocytes and tumor prognosis has been reported in many clinical studies. For example, thermal ablation has been demonstrated to promote increases in the frequency and function of CD3-CD56+NK cells in the peripheral blood of patients with HCC, and is associated with recurrence-free survival (51), whereas radiation therapy has been found to have a significant effect on the levels of peripheral NK and NKT-like cells, with a higher percentage of NKT-like cells being found to be associated with a longer OS in HCC patients (52). Furthermore, sorafenib has been observed to modify the proportion and function of peripheral NK cells, which are associated with treatment outcomes in patients with HCC (53). However, whereas a high frequency of circulating NK cells has been established to be a predictor of tumor response in patients with NSCLC treated with immunotherapy (54), in the present study, although we found NK cells can serve as a predictor of long-term PFS and OS, they showed no significant association with a short-term tumor response. A plausible explanation for this contrasting performance is that circulating NK cells reflect systemic immunity and can predict long-term prognosis, whereas TACE has a significant influence on the tumor response, which may interfere with the short-term predictive performance of NK cells.

From a clinical perspective, we found that the levels of CD8+CD28+ T, NK, and CD8+CD38+ T cells were associated with tumor characteristics and liver function, which, to some extent, would explain their prognostic value. However, we also established that these dynamic changes were relatively ineffective as follow-up indicators for predicting a tumor response. In addition to these independent prognostic factors, IL-6 and CD4+ and CD8+ T cells have been reported as prognostic biomarkers in many studies. For

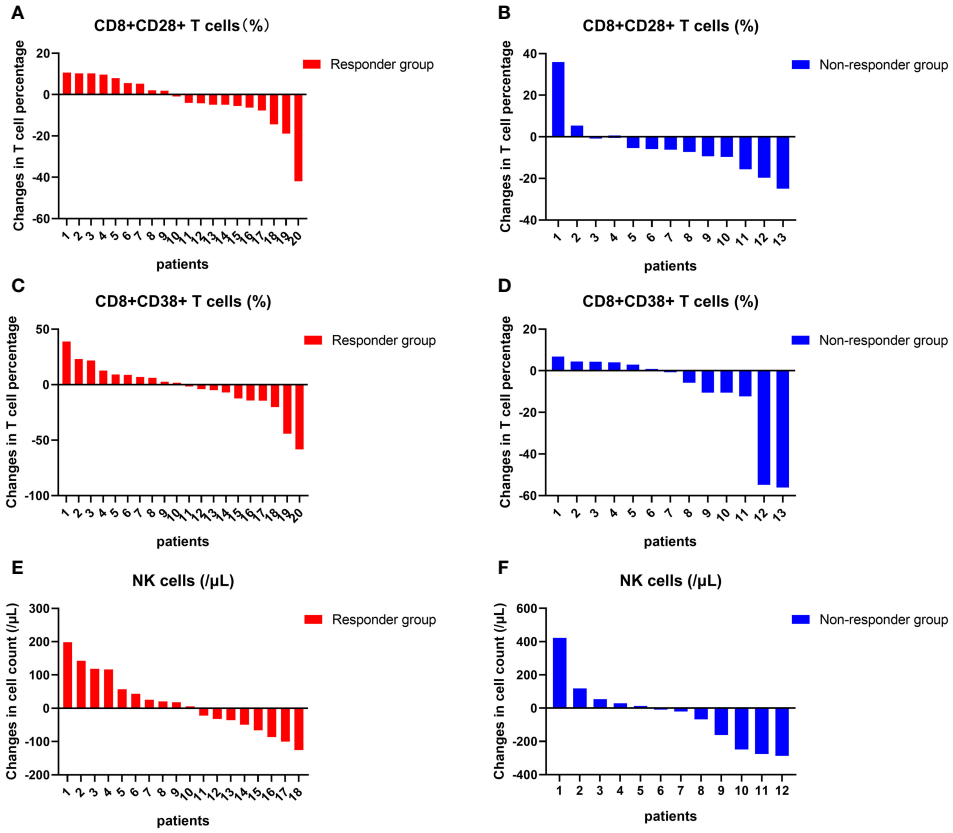

FIGURE 7
Changes in lymphocyte subsets in individuals. The changes in the frequency of CD8+CD28+ T cells **(A, B)**, NK cell counts **(C, D)**, and the frequency of CD8+CD38+ T cells **(E, F)** at the individual level before and after treatment in the response group and non-response group.

example, the baseline CD4+/CD8+ T-cell ratio and its changes have been identified as prognostic markers for cancer patients (33, 55), although the findings of a recent study have provided evidence to indicate that the CD8+PD-1+ to CD4+PD-1+ T-cell ratio, rather than the CD8+/CD4+ T-cell ratio, is associated with clinical benefits in advanced NSCLC patients treated with ICIs (56). The CD8+PD-1+/CD4+PD-1+ index proposed in this previous study was based on the premise that high CD8+PD-1+ T cell levels are associated with good prognosis in cancer patients, whereas high CD4+PD-1+ T cell levels are associated with poor clinical outcomes. In the present study, however, we were unable to detect any significant associations between PD-1+ T cells and survival, with the exceptions being CD8+PD-1+/CD4+PD-1+ in predicting tumor response and OS, and CD8+/CD4+ in predicting OS in the univariate analysis of all patients. Consequently, the clinical significance of peripheral blood lymphocyte subsets remains to be determined.

Although in this prospective study, we strived to enroll as many patients as possible who had undergone long-term follow-up, the study does have certain limitations. Firstly, we measured only lymphocyte subsets in peripheral blood. In future studies, to identify more reliable predictive biomarkers and elucidate the underlying mechanisms involved, we plan to evaluate both circulating and infiltrating lymphocytes in patients. Secondly, our flow cytometry antibody staining scheme may have produced negative results owing to its simplicity and insufficient accuracy in the detection of lymphocyte functional subsets. Finally, this was primarily an exploratory study based on real-world clinical practice. Many patients had already received treatment before enrollment, as well as different subsequent combination therapies, thereby introducing a certain level of heterogeneity within the study population.

5 Conclusion

Our findings in this study revealed that the levels of circulating CD8+CD38+ T cells, CD8+CD28+ T cells, and NK cells are potential prognostic factors for tumor response and long-term survival in patients with HCC treated with TACE, administered with or without PD-1 inhibitors. Although PD-1 inhibitors can effectively block PD-1 receptors on the surface of T cells, the baseline frequency of PD-1+ T cells and changes in the frequency of these cells were established to have limited prognostic value.

Data availability statement

The original contributions presented in the study are included in the article/Supplementary Material. Further inquiries can be directed to the corresponding authors.

Ethics statement

The studies involving humans were approved by the Ethics Committee of the First Affiliated Hospital of Sun Yat-Sen University. The studies were conducted in accordance with the local legislation and institutional requirements. The participants provided their written informed consent to participate in this study.

Author contributions

HW: Conceptualization, Data curation, Formal analysis, Funding acquisition, Investigation, Writing – original draft. HH: Conceptualization, Data curation, Investigation, Methodology, Writing – original draft. TL: Formal analysis, Funding acquisition, Methodology, Supervision, Writing – original draft. YC: Formal analysis, Investigation, Methodology, Writing – original draft. JWL: Data curation, Investigation, Writing – original draft. MH: Formal analysis, Methodology, Supervision, Writing – original draft. JP: Formal analysis, Funding acquisition, Supervision, Writing – original draft. EL: Formal analysis, Funding acquisition, Supervision, Writing – original draft. JPL: Conceptualization, Data curation, Formal analysis, Resources, Supervision, Writing – review & editing. WL: Conceptualization, Data curation, Formal analysis, Funding acquisition, Project administration, Resources, Supervision, Writing – review & editing.

Funding

The author(s) declare financial support was received for the research, authorship, and/or publication of this article. This study was supported by Major Program for Tackling Key Prob- lems of Guangzhou City (No. 202103000021); 2024 Guangzhou Basic and Applied Basic Research Scheme (Project for Maiden Voyage) (No. SL2024A04J00258); Medical Scientific Research Foundation of Guangdong Province, China (No. 202242915212755); National Natural Science Foundation of China (No. 82102169), the grants from outstanding young talents seedling program of Guangdong Hospital of Traditional Chinese Medicine (No. SZ2023QN03); Science and Technology Projects in Guangzhou (No. 202102021139); Guangdong Basic and Applied Basic Research Foundation (No. 2020A1515110329); Natural Science Foundation of Guangdong Province (No. 2022A1515011632).

Conflict of interest

The authors declare that the research was conducted in the absence of any commercial or financial relationships that could be construed as a potential conflict of interest.

Publisher's note

All claims expressed in this article are solely those of the authors and do not necessarily represent those of their affiliated organizations, or those of the publisher, the editors and the reviewers. Any product that may be evaluated in this article, or claim that may be made by its manufacturer, is not guaranteed or endorsed by the publisher.

Supplementary material

The Supplementary Material for this article can be found online at: https://www.frontiersin.org/articles/10.3389/fimmu.2024.1325330/full#supplementary-material

References

1. Sung H, Ferlay J, Siegel RL, Laversanne M, Soerjomataram I, Jemal A, et al. Global cancer statistics 2020: GLOBOCAN estimates of incidence and mortality worldwide for 36 cancers in 185 countries. *CA Cancer J Clin* (2021) 71(3):209–49. doi: 10.3322/caac.21660

2. Reig M, Forner A, Rimola J, Ferrer-Fàbrega J, Burrel M, Garcia-Criado Á, et al. BCLC strategy for prognosis prediction and treatment recommendation: The 2022 update. *J Hepatology.* (2022) 76(3):681–93. doi: 10.1016/j.jhep.2021.11.018

3. Raoul JL, Forner A, Bolondi L, Cheung TT, Kloeckner R, de Baere T. Updated use of TACE for hepatocellular carcinoma treatment: How and when to use it based on clinical evidence. *Cancer Treat Rev* (2019) 72:28–36. doi: 10.1016/j.ctrv.2018.11.002

4. Peng Z, Fan W, Zhu B, Wang G, Sun J, Xiao C, et al. Lenvatinib combined with transarterial chemoembolization as first-line treatment for advanced hepatocellular carcinoma: A phase III, randomized clinical trial (LAUNCH). *J Clin Oncol* (2023) 41 (1):117–27. doi: 10.1200/JCO.22.00392

5. Duan R, Gong F, Wang Y, Huang C, Wu J, Hu L, et al. Transarterial chemoembolization (TACE) plus tyrosine kinase inhibitors versus TACE in patients with hepatocellular carcinoma: a systematic review and meta-analysis. *World J Surg Oncol* (2023) 21(1):120. doi: 10.1186/s12957-023-02961-7

6. Qu W-F, Ding Z-B, Qu X-D, Tang Z, Zhu G-Q, Fu X-T, et al. Conversion therapy for initially unresectable hepatocellular carcinoma using a combination of toripalimab, lenvatinib plus TACE: real-world study. *BJS Open* (2022) 6(5):zrac114. doi: 10.1093/bjsopen/zrac114

7. Chen S, Wu Z, Shi F, Mai Q, Wang L, Wang F, et al. Lenvatinib plus TACE with or without pembrolizumab for the treatment of initially unresectable hepatocellular carcinoma harbouring PD-L1 expression: a retrospective study. *J Cancer Res Clin Oncol* (2022) 148(8):2115–25. doi: 10.1007/s00432-021-03767-4

8. Cai M, Huang W, Huang J, Shi W, Guo Y, Liang L, et al. Transarterial chemoembolization combined with lenvatinib plus PD-1 inhibitor for advanced hepatocellular carcinoma: A retrospective cohort study. *Front In Immunol* (2022) 13:848387. doi: 10.3389/fimmu.2022.848387

9. Yi C, Chen L, Lin Z, Liu L, Shao W, Zhang R, et al. Lenvatinib targets FGF receptor 4 to enhance antitumor immune response of anti-programmed cell death-1 in HCC. *Hepatology* (2021) 74(5):2544–60. doi: 10.1002/hep.31921

10. Adachi Y, Kamiyama H, Ichikawa K, Fukushima S, Ozawa Y, Yamaguchi S, et al. Inhibition of FGFR reactivates IFNγ Signaling in tumor cells to enhance the combined antitumor activity of lenvatinib with anti-PD-1 antibodies. *Cancer Res* (2022) 82 (2):292–306. doi: 10.1158/0008-5472.CAN-20-2426

11. Liu J, Chen Z, Li Y, Zhao W, Wu J, Zhang Z. PD-1/PD-L1 checkpoint inhibitors in tumor immunotherapy. *Front In Pharmacol* (2021) 12:731798. doi: 10.3389/fphar.2021.731798

12. Ji JH, Ha SY, Lee D, Sankar K, Koltsova EK, Abou-Alfa GK, et al. Predictive biomarkers for immune-checkpoint inhibitor treatment response in patients with hepatocellular carcinoma. *Int J Mol Sci* (2023) 24(8):7640. doi: 10.3390/ijms24087640

13. He P, Wan H, Wan J, Jiang H, Yang Y, Xie K, et al. Systemic therapies in hepatocellular carcinoma: Existing and emerging biomarkers for treatment response. *Front In Oncol* (2022) 12:1015527. doi: 10.3389/fonc.2022.1015527

14. Ottonello S, Genova C, Cossu I, Fontana V, Rijavec E, Rossi G, et al. Association between response to nivolumab treatment and peripheral blood lymphocyte subsets in patients with non-small cell lung cancer. *Front In Immunol* (2020) 11:125. doi: 10.3389/fimmu.2020.00125

15. Mazzaschi G, Minari R, Zecca A, Cavazzoni A, Ferri V, Mori C, et al. Soluble PD-L1 and circulating CD8+PD-1+ and NK cells enclose a prognostic and predictive immune effector score in immunotherapy treated NSCLC patients. *Lung Cancer* (2020) 148:1–11. doi: 10.1016/j.lungcan.2020.07.028

16. Agdashian D, ElGindi M, Xie C, Sandhu M, Pratt D, Kleiner DE, et al. The effect of anti-CTLA4 treatment on peripheral and intra-tumoral T cells in patients with hepatocellular carcinoma. *Cancer Immunol Immunother.* (2019) 68(4):599–608. doi: 10.1007/s00262-019-02299-8

17. Sangro B, Melero I, Wadhawan S, Finn RS, Abou-Alfa GK, Cheng A-L, et al. Association of inflammatory biomarkers with clinical outcomes in nivolumab-treated patients with advanced hepatocellular carcinoma. *J Hepatology.* (2020) 73(6):1460–9. doi: 10.1016/j.jhep.2020.07.026

18. Fridman WH, Pagès F, Sautès-Fridman C, Galon J. The immune contexture in human tumours: impact on clinical outcome. *Nat Rev Cancer.* (2012) 12(4):298–306. doi: 10.1038/nrc3245

19. Loupakis F, Depetris I, Biason P, Intini R, Prete AA, Leone F, et al. Prediction of benefit from checkpoint inhibitors in mismatch repair deficient metastatic colorectal cancer: role of tumor infiltrating lymphocytes. *Oncologist.* (2020) 25(6):481–7. doi: 10.1634/theoncologist.2019-0611

20. Huang M, Wang X, Bin H. Effect of transcatheter arterial chemoembolization combined with argon-helium cryosurgery system on the changes of NK cells and T cell subsets in peripheral blood of hepatocellular carcinoma patients. *Cell Biochem Biophys* (2015) 73(3):787–92. doi: 10.1007/s12013-015-0699-0

21. Liu HZ, Deng W, Li JL, Tang YM, Zhang LT, Cui Y, et al. Peripheral blood lymphocyte subset levels differ in patients with hepatocellular carcinoma. *Oncotarget* (2016) 7(47):77558–64. doi: 10.18632/oncotarget.13041

22. Wang YY, Zhou N, Liu Hs, Gong XL, Zhu R, Li XY, et al. Circulating activated lymphocyte subsets as potential blood biomarkers of cancer progression. *Cancer Med* (2020) 9(14):5086–94. doi: 10.1002/cam4.3150

23. Xia Y, Li W, Li Y, Liu Y, Ye S, Liu A, et al. The clinical value of the changes of peripheral lymphocyte subsets absolute counts in patients with non-small cell lung cancer. *Transl Oncol* (2020) 13(12):100849. doi: 10.1016/j.tranon.2020.100849

24. Li P, Qin P, Fu X, Zhang G, Yan X, Zhang M, et al. Associations between peripheral blood lymphocyte subsets and clinical outcomes in patients with lung cancer treated with immune checkpoint inhibitor. *Ann Palliat Med* (2021) 10(3):3039–49. doi: 10.21037/apm-21-163

25. Lian J, Yue Y, Yu W, Zhang Y. Immunosenescence: a key player in cancer development. *J Hematol Oncol* (2020) 13(1):151. doi: 10.1186/s13045-020-00986-z

26. Liu C, Zhu S, Dong Y, Shao J, Liu B, Shen J. The potential predictive biomarkers for advanced hepatocellular carcinoma treated with anti-angiogenic drugs in combination with PD-1 antibody. *Front In Immunol* (2022) 13:930096. doi: 10.3389/fimmu.2022.930096

27. Reolo MJY, Otsuka M, Seow JJW, Lee J, Lee YH, Nguyen PHD, et al. CD38 marks the exhausted CD8+ tissue-resident memory T cells in hepatocellular carcinoma. *Front In Immunol* (2023) 14:1182016. doi: 10.3389/fimmu.2023.1182016

28. Wang H, Zhang G, Fan W, Wu Y, Zhang J, Xue M, et al. Clinical significance of peripheral blood lymphocyte subtypes and cytokines in patients with hepatocellular carcinoma treated with TACE. *Cancer Manage Res* (2022) 14:451–64. doi: 10.2147/CMAR.S342527

29. Xie DY, Ren ZG, Zhou J, Fan J , Gao Q. 2019 Chinese clinical guidelines for the management of hepatocellular carcinoma: updates and insights. *Hepatobiliary Surg Nutr* (2020) 9(4):452–63. doi: 10.21037/hbsn-20-480

30. Chen T, Chen H, Lu W, Yao Y. T lymphocyte subsets and PD-1 expression on lymphocytes in peripheral blood of patients with non-small cell lung cancer. *Med (Baltimore).* (2022) 101(42):e31307. doi: 10.1097/MD.0000000000031307

31. MacFarlane AW, Jillab M, Plimack ER, Hudes GR, Uzzo RG, Litwin S, et al. PD-1 expression on peripheral blood cells increases with stage in renal cell carcinoma patients and is rapidly reduced after surgical tumor resection. *Cancer Immunol Res* (2014) 2(4):320–31. doi: 10.1158/2326-6066.CIR-13-0133

32. Núñez KG, Sandow T, Fort D, Hibino M, Wright P, Cohen AJ, et al. PD-1 expression in hepatocellular carcinoma predicts liver-directed therapy response and bridge-to-transplant survival. *Cancer Immunol Immunother.* (2022) 71(6):1453–65. doi: 10.1007/s00262-021-03087-z

33. Macek Jilkova Z, Aspord C, Kurma K, Granon A, Sengel C, Sturm N, et al. Immunologic features of patients with advanced hepatocellular carcinoma before and during sorafenib or anti-programmed death-1/programmed death-L1 treatment. *Clin Transl Gastroenterol* (2019) 10(7):e00058. doi: 10.14309/ctg.0000000000000058

34. Kuo IY, Yang Y-E, Yang P-S, Tsai Y-J, Tzeng H-T, Cheng H-C, et al. Converged Rab37/IL-6 trafficking and STAT3/PD-1 transcription axes elicit an immunosuppressive lung tumor microenvironment. *Theranostics* (2021) 11(14):7029–44. doi: 10.7150/thno.60040

35. Zerdes I, Matikas A, Bergh J, Rassidakis GZ, Foukakis T. Genetic, transcriptional and post-translational regulation of the programmed death protein ligand 1 in cancer: biology and clinical correlations. *Oncogene* (2018) 37(34):4639–61. doi: 10.1038/s41388-018-0303-3

36. Zhou GY, Sprengers D, Boor PPC, Doukas M, Schutz H, Mancham S, et al. Antibodies against immune checkpoint molecules restore functions of tumor-infiltrating T cells in hepatocellular carcinomas. *Gastroenterology* (2017) 153(4):1107. doi: 10.1053/j.gastro.2017.06.017

37. Khanniche A, Yang Y, Zhang J, Liu S, Xia L, Duan H, et al. Early-like differentiation status of systemic PD-1+CD8+ T cells predicts PD-1 blockade outcome in non-small cell lung cancer. *Clin Transl Immunol* (2022) 11(7):e1406. doi: 10.1002/cti2.1406

38. Liu X, Li M, Wang X, Dang Z, Jiang Y, Wang X, et al. PD-1+ TIGIT+ CD8+ T cells are associated with pathogenesis and progression of patients with hepatitis B virus-related hepatocellular carcinoma. *Cancer Immunol Immunother.* (2019) 68(12):2041–54. doi: 10.1007/s00262-019-02426-5

39. Gros A, Parkhurst MR, Tran E, Pasetto A, Robbins PF, Ilyas S, et al. Prospective identification of neoantigen-specific lymphocytes in the peripheral blood of melanoma patients. *Nat Med* (2016) 22(4):433–8. doi: 10.1038/nm.4051

40. Gros A, Robbins PF, Yao X, Li YF, Turcotte S, Tran E, et al. PD-1 identifies the patient-specific $CD8^+$ tumor-reactive repertoire infiltrating human tumors. *J Clin Invest* (2014) 124(5):2246–59. doi: 10.1172/JCI73639

41. Bour-Jordan H, Blueston JA. CD28 function: a balance of costimulatory and regulatory signals. *J Clin Immunol* (2002) 22(1):1–7. doi: 10.1023/a:1014256417651

42. Ye S, Chen W, Zheng Y, Wu Y, Xiang L, Li T, et al. Peripheral lymphocyte populations in ovarian cancer patients and correlations with clinicopathological features. *J Ovarian Res* (2022) 15(1):43. doi: 10.1186/s13048-022-00977-3

43. Geng R, Tang H, You T, Xu X, Li S, Li Z, et al. Peripheral CD8+CD28+ T lymphocytes predict the efficacy and safety of PD-1/PD-L1 inhibitors in cancer patients. *Front In Immunol* (2023) 14:1125876. doi: 10.3389/fimmu.2023.1125876

44. Ferrara R, Naigeon M, Auclin E, Duchemann B, Cassard L, Jouniaux J-M, et al. Circulating T-cell immunosenescence in patients with advanced non-small cell lung cancer treated with single-agent PD-1/PD-L1 inhibitors or platinum-based chemotherapy. *Clin Cancer Research: an Off J Am Assoc For Cancer Res* (2021) 27(2):492–503. doi: 10.1158/1078-0432.CCR-20-1420

45. Golden-Mason L, Curry MP, Nolan N, Traynor O, McEntee G, Kelly J, et al. Differential expression of lymphoid and myeloid markers on differentiating hematopoietic stem cells in normal and tumor-bearing adult human liver. *Hepatology* (2000) 31(6):1251–6. doi: 10.1053/jhep.2000.7713

46. Chatterjee S, Daenthanasanmak A, Chakraborty P, Wyatt MW, Dhar P, Selvam SP, et al. CD38-NAD+Axis regulates immunotherapeutic anti-tumor T cell response. *Cell Metab* (2018) 27(1). doi: 10.1016/j.cmet.2017.10.006

47. Ding Z, He Y, Fu Y, Zhu N, Zhao M, Song Y, et al. CD38 multi-functionality in oral squamous cell carcinoma: prognostic implications, immune balance, and immune checkpoint. *Front In Oncol* (2021) 11:687430. doi: 10.3389/fonc.2021.687430

48. Guo C, Crespo M, Gurel B, Dolling D, Rekowski J, Sharp A, et al. CD38 in advanced prostate cancers. *Eur Urol.* (2021) 79(6):736–46. doi: 10.1016/j.eururo.2021.01.017

49. Attal M, Richardson PG, Rajkumar SV, San-Miguel J, Beksac M, Spicka I, et al. Isatuximab plus pomalidomide and low-dose dexamethasone versus pomalidomide and low-dose dexamethasone in patients with relapsed and refractory multiple myeloma (ICARIA-MM): a randomised, multicentre, open-label, phase 3 study. *Lancet (London England).* (2019) 394(10214):2096–107. doi: 10.1016/S0140-6736(19)32556-5

50. Huang H, Zhu J, Yao M, Kim TM, Yoon DH, Cho S-G, et al. Daratumumab monotherapy for patients with relapsed or refractory natural killer/T-cell lymphoma, nasal type: an open-label, single-arm, multicenter, phase 2 study. *J Hematol Oncol* (2021) 14(1):25. doi: 10.1186/s13045-020-01020-y

51. Wang H-Y, Cui X-W, Zhang Y-H, Chen Y, Lu N-N, Bai L, et al. Dynamic changes of phenotype and function of natural killer cells in peripheral blood before and after thermal ablation of hepatitis B associated hepatocellular carcinoma and their correlation with tumor recurrence. *BMC Cancer.* (2023) 23(1):486. doi: 10.1186/s12885-023-10823-4

52. Li T-T, Sun J, Wang Q, Li W-G, He W-P, Yang R-C, et al. The effects of stereotactic body radiotherapy on peripheral natural killer and CD3+CD56+ NKT-like cells in patients with hepatocellular carcinoma. *Hepatobiliary Pancreat Dis Int* (2021) 20(3):240–50. doi: 10.1016/j.hbpd.2020.12.015

53. Hu J, Wang E, Liu L, Wang Q, Xia D, Bai W, et al. Sorafenib may enhance antitumour efficacy in hepatocellular carcinoma patients by modulating the proportions and functions of natural killer cells. *Invest New Drugs* (2020) 38(5):1247–56. doi: 10.1007/s10637-019-00885-2

54. Cho Y-H, Choi MG, Kim DH, Choi YJ, Kim SY, Sung KJ, et al. Natural killer cells as a potential biomarker for predicting immunotherapy efficacy in patients with non-small cell lung cancer. *Target Oncol* (2020) 15(2):241–7. doi: 10.1007/s11523-020-00712-2

55. Liu C, Cheng H, Luo G, Lu Y, Jin K, Guo M, et al. Circulating regulatory T cell subsets predict overall survival of patients with unresectable pancreatic cancer. *Int J Oncol* (2017) 51(2):686–94. doi: 10.3892/ijo.2017.4032

56. Duchemann B, Naigeon M, Auclin E, Ferrara R, Cassard L, Jouniaux J-M, et al. CD8+PD-1+ to CD4+PD-1+ ratio (PERLS) is associated with prognosis of patients with advanced NSCLC treated with PD-(L)1 blockers. *J For Immunotherapy Cancer* (2022) 10(2):e004012. doi: 10.1136/jitc-2021-004012

frontiers | Frontiers in Immunology

TYPE Systematic Review
PUBLISHED 26 February 2024
DOI 10.3389/fimmu.2024.1291840

OPEN ACCESS

EDITED BY
Paulo Rodrigues-Santos,
University of Coimbra, Portugal

REVIEWED BY
Xiaobin Gu,
First Affiliated Hospital of Zhengzhou University, China
Michal Michalak,
Poznan University of Medical Sciences, Poland

*CORRESPONDENCE
Zhining Tang
Tangzhining0203@163.com

RECEIVED 10 September 2023
ACCEPTED 05 February 2024
PUBLISHED 26 February 2024

CITATION
Zhang S and Tang Z (2024) Prognostic and clinicopathological significance of systemic inflammation response index in patients with hepatocellular carcinoma: a systematic review and meta-analysis.
Front. Immunol. 15:1291840.
doi: 10.3389/fimmu.2024.1291840

Prognostic and clinicopathological significance of systemic inflammation response index in patients with hepatocellular carcinoma: a systematic review and meta-analysis

Sunhuan Zhang and Zhining Tang*

Clinical Laboratory, Huzhou Central Hospital, Affiliated Central Hospital of Huzhou University, The Fifth School of Clinical Medicine of Zhejiang Chinese Medical University, Huzhou, Zhejiang, China

Background: It is unclear whether the systemic inflammation response index (SIRI) can predict the prognosis of patients with hepatocellular carcinoma (HCC). Consequently, the present study focused on systematically identifying the relationship between SIRI and the prognosis of patients with HCC through a meta-analysis.

Methods: Systematic and comprehensive studies were retrieved from PubMed, Web of Science, Embase, and the Cochrane Library from their inception to August 10, 2023. The role of SIRI in predicting overall survival (OS) and progression-free survival (PFS) in HCC was determined using pooled hazard ratios (HRs) and 95% confidence intervals (CIs). Odds ratios (ORs) and 95% CIs were pooled to analyze the correlations between SIRI and the clinicopathological features of HCC.

Results: Ten articles involving 2,439 patients were included. An elevated SIRI was significantly associated with dismal OS (HR=1.75, 95% CI=1.52–2.01, p<0.001) and inferior PFS (HR=1.66, 95% CI=1.34–2.05, p<0.001) in patients with HCC. Additionally, according to the combined results, the increased SIRI was significantly related to multiple tumor numbers (OR=1.42, 95% CI=1.09–1.85, p=0.009) and maximum tumor diameter >5 cm (OR=3.06, 95% CI=1.76–5.30, p<0.001). However, the SIRI did not show any significant relationship with sex, alpha-fetoprotein content, Child-Pugh class, or hepatitis B virus infection.

Conclusion: According to our results, elevated SIRI significantly predicted OS and PFS in patients with HCC. Moreover, the SIRI was significantly associated with tumor aggressiveness.

Systematic review registration: https://inplasy.com/inplasy-2023-9-0003/, identifier INPLASY202390003.

KEYWORDS

SIRI, meta-analysis, hepatocellular carcinoma, prognosis, evidence-based medicine

Introduction

Primary liver cancer ranks sixth among cancers in terms of morbidity and is the third most common cause of cancer-associated mortality worldwide (1). As estimated by GLOBCAN, 905,677 new liver cancer cases and 830,180 liver cancer-associated deaths were reported globally in 2020 (1). Hepatocellular carcinoma (HCC), the most frequent subtype of liver cancer, affects approximately 75% of patients worldwide (2). Approximately 72% of the HCC cases are reported in Asia (over 50% in China), and 10%, 7.8%, 5.1%, 4.6%, and 0.5% in Europe, Africa, North America, Latin America, and Oceania, respectively (3). In general, surgery, local thermal ablation, liver transplantation (LT), transcatheter arterial chemoembolization (TACE), and systemic therapy are the main treatments for HCC and have shown efficacy in reducing the mortality rates of HCC (4). Despite this, the long-term survival rates of patients remain unsatisfactory, and recurrence rates are high (5). Among patients with localized or metastatic HCC, the 5-year overall survival (OS) rate is < 10% (6). In addition, up to 70% of patients experience recurrence after undergoing treatment with a curative intent (6). Therefore, the identification of effective prognostic biomarkers is pivotal for risk stratification and adjunctive treatment development in patients with HCC.

Accumulating evidence suggests that immune responses and inflammation influence tumor progression and metastasis (7). Many inflammatory blood-based indices, such as the neutrophil-to-lymphocyte ratio (NLR) (8), platelet-to-lymphocyte ratio (PLR), albumin-to-globulin ratio (AGR) (9), lymphocyte-to-monocyte ratio (LMR) (10), and C-reactive protein-to-albumin ratio (CAR) (11), are significant prognostic markers of different cancer types. The systemic inflammation response index (SIRI) is a novel hematologic parameter that was first proposed in 2016 (12) and is determined using the following formula: SIRI = (neutrophil × monocyte)/lymphocyte count. SIRI has been widely suggested to exhibit a significant and powerful value in predicting solid tumors such as bladder cancer (13), non-small cell lung cancer (NSCLC) (14), gastric cancer (15), breast cancer (16), and ovarian cancer (17). The impact of the SIRI on predicting HCC prognosis has also been explored; however, no consistent findings have been found (18–27). In certain studies, elevated SIRI was found to be a significant prognostic marker of HCC (23–25), while other studies have shown no obvious relationship between SIRI and HCC survival (21, 27). This meta-analysis aimed to accurately identify the prognostic effects of SIRI in patients with HCC. Additionally, the relationship between SIRI and clinicopathological features of HCC was explored.

Abbreviations: SIRI, systemic inflammation response index; HCC, hepatocellular carcinoma; HR, hazard ratio; CI, confidence interval; OS, overall survival; PFS, progression-free survival; OR, odds ratio; AFP, alpha-fetoprotein; HBV, hepatitis B virus; LT, liver transplantation; TACE, transcatheter arterial chemoembolization; NLR, neutrophil-to-lymphocyte ratio; PLR, platelet-to-lymphocyte ratio; CAR, C-reactive protein-to-albumin ratio; AGR, albumin-to-globulin ratio; LMR, lymphocyte-to-monocyte ratio; NSCLC, non-small cell lung cancer; PRISMA, Preferred Reporting Items for Systematic Reviews and Meta-Analyses; DFS, disease-free survival; CSS, cancer-specific survival; NOS, Newcastle-Ottawa Scale; OR,odds ratio; RFA, radiofrequency ablation; ICIs, immune checkpoint inhibitors; TAMs, tumor-associated macrophages; TILs, tumor-infiltrating lymphocytes.

Materials and methods

Study guideline

The present meta-analysis was conducted in accordance with the guidelines of the Preferred Reporting Items for Systematic Reviews and Meta-Analyses (PRISMA) (28). Our meta-analysis protocol was registered in INPLASY (registration number: INPLASY202390003) and can be found at https://inplasy.com/inplasy-2023-9-0003/.

Ethics statement

Data in this study were extracted from publications, and, as a result, ethical approval or patient consent was waived.

Literature search

The PubMed, Web of Science, Embase, and Cochrane Library databases were comprehensively searched from their inception to August 10, 2023, using the following search terms: (systemic inflammation response index or systemic inflammatory response index) and (hepatocellular carcinoma, hepatocellular cancer, HCC, or liver cancer). A detailed search strategy for each database is provided in Supplementary Data Sheet 1. The language used in this study was English. To identify additional eligible articles, we manually searched the reference lists of each retrieved article.

Inclusion and exclusion criteria

Articles satisfying the following criteria were recruited: (1) HCC was diagnosed based on pathology or histology; (2) studies investigating the relationship between SIRI and prognosis of patients with HCC; (3) those with available or calculable hazard ratios (HRs) and 95% confidence intervals (CIs); (4) those mentioning threshold SIRI; (5) those reporting survival outcomes such as OS, disease-free survival (DFS), progression-free survival (PFS), or cancer-specific survival (CSS); and (6) English language articles. The following studies were excluded: (1) meeting abstracts, reviews, comments, letters, and case reports; (2) animal studies; and (3) those including overlapping patients.

Data extraction and quality assessment

The studies were reviewed and data were independently extracted from qualified studies by two reviewers (SZ and ZT). Any dispensaries were resolved through negotiation until a consensus was reached. The following information was collected: first author, publication year, country, study design, sample size, age, sex, study center, study period, Child-Pugh class, treatment, threshold, threshold selection method, survival outcomes, survival analysis type, follow-up, HRs, and 95%CIs for survival outcomes. If eligible studies underwent propensity score matching (PSM) analysis, the data for the entire population were extracted and analyzed to avoid selection bias. OS and PFS were defined as the primary and secondary survival outcomes, respectively. Two researchers (SZ and ZT) evaluated the literature quality using the Newcastle-Ottawa Scale (NOS) (29) and crosschecked our results. The NOS assesses literature quality from three perspectives: selection, comparability, and outcome measurement. The NOS score ranges from 0 to 9, with studies scoring ≥ 6 points considered to be of high quality.

Statistical analysis

The significance of the SIRI in predicting the OS and PFS of patients with HCC was evaluated based on the combined HRs and 95% CI. Interstudy heterogeneity was evaluated using the Higgins I^2 statistic and Cochran's Q test. The random-effects model was applied when I^2 was >50% or P was <0.1; otherwise, the fixed-effects model was used. Diverse factor-stratified subgroup analyses were conducted to identify sources of heterogeneity. The relationships between SIRI and the clinicopathological characteristics of HCC were analyzed using combined odds ratios (ORs) and 95% CIs. A sensitivity analysis was used to evaluate the consistency of the findings. Meta-regression was conducted to evaluate the effect of clinicopathological factors on the overall results. Begg's test, funnel plots, and Egger's test were used to examine possible publication bias. Stata software (version 12.0; Stata Corp., College Station, TX, USA) was used for graph generation and statistical analyses. Statistical significance was set at P<0.05.

Results

Study selection process

As shown in Figure 1, 529 studies were identified through primary literature retrieval, and 398 records were retained following the removal of duplicates. Subsequently, 360 articles were discarded by title and abstract screening owing to their irrelevance. Then, the full texts of 38 articles were examined, and another 28 were excluded because they did not focus on SIRI (n=24) or recruited overlapping patients (n=4). Finally, the present meta-analysis recruited 10 articles involving 2,439 patients (18–27) (Figure 1; Table 1).

Included study features

Table 1 presents the baseline characteristics of the selected articles. The publication years of these articles ranged between

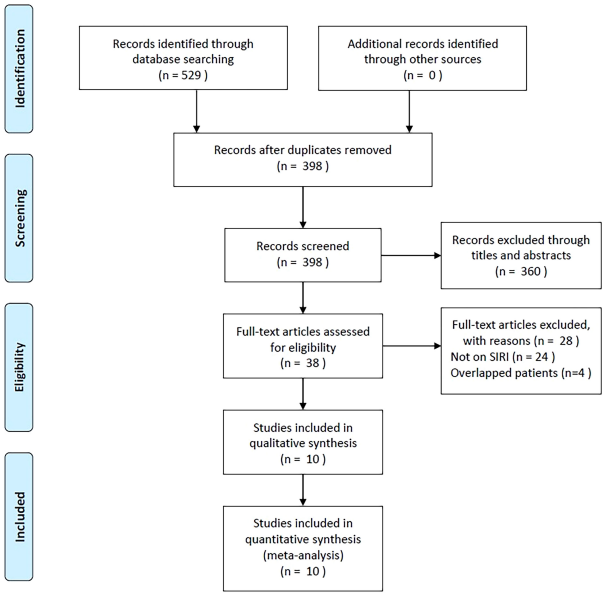

FIGURE 1
PRISMA flowchart of the established screening strategy.

TABLE 1 Baseline characteristics of included studies in this meta-analysis.

Study	Year	Country	Sample size	Study design	Study period	Gender (M/F)	Age (year) Median (range)	Treatment	Child-Pugh class	Study center	Cut-off value	Cut-off selecti-on	ROC methods	Survival outcomes	Survival analysis	Follow-up (month) Median (range)	NOS score
Xu, L.	2017	China	351	Retrospective	2006-2013	300/51	53.9	Surgery	A-B	Single center	1.05	ROC curve	NR	OS	Multivariate	1-100	8
Cinkir, H. Y.	2020	Twurkey	80	Retrospective	2011-2018	67/13	69 (29-83)	Sorafenib	A-B	Single center	2.2	ROC curve	Youden index	OS	Univariate	7.8 (1.2-38.7)	7
Wang, T. C.	2021	China	194	Retrospective	2014-2019	174/20	56.5	TACE	A-B	Multicenter	0.88	ROC curve	NR	OS, PFS	Univariate	1-80	9
Wu, Y.	2021	China	161	Retrospective	2011-2018	141/20	56.2	Surgery	A-B	Single center	1.03	ROC curve	Youden index	PFS	Multivariate	1-120	8
Zou, Y.	2021	China	370	Retrospective	2013-2019	325/45	54.2	Surgery	A-B	Single center	1.17	ROC curve	NR	PFS	Multivariate	1-96	8
Xin, Y.	2022	China	403	Retrospective	2012-2017	328/75	58 (30-80)	RFA	A-B	Single center	1.36	X-tile	NR	OS, PFS	Univariate	44.5 (12.6-95.0)	8
Zhao, M.	2022	China	352	Retrospective	2013-2020	290/62	58 (26-86)	Sorafenib/ ICIs	A-C	Single center	1.64	ROC curve	NR	OS, PFS	Univariate	1-100	7
Cui, S.	2023	China	218	Retrospective	2010-2020	197/21	53.9	LT	A-C	Single center	1.25	ROC curve	NR	OS, PFS	Multivariate	39.4	8
Mao, S.	2023	China	148	Retrospective	2016-2020	125/23	58.6	TACE	A-B	Single center	1.04	ROC curve	NR	PFS	Multivariate	13(1-36)	7
Wenpei, G.	2023	China	162	Retrospective	2013-2016	125/37	≤60 y: 107 >60 y: 55	Surgery	A-B	Single center	0.785	ROC curve	Youden index	PFS	Multivariate	1-24	8

M, male; F, female; TACE, transcatheter arterial chemoembolization; RFA, radiofrequency ablation; LT, liver transplantation; ICIs, immune checkpoint inhibitors; ROC, receiver operating characteristic; OS, overall survival; PFS, progression-free survival; NOS, Newcastle-Ottawa Scale.

10.3389/fimmu.2024.1291840

2017 and 2023 and all had a retrospective design. Nine studies were conducted in China (18, 20–27) while one was conducted in Turkey (19). The sample size across the selected articles ranged from 80 to 403 (median, 206). We therefore selected 200 for subgroup analysis of sample size. Four studies treated patients with HCC with surgery (18, 21, 22, 27), two studies used TACE treatment (20, 26), and one each used sorafenib (19), radiofrequency ablation (RFA) (23), sorafenib/immune checkpoint inhibitors (ICIs) (24), and LT (25). Nine studies were single-center studies (18, 19, 21–27) and one was a multicenter study (20). The threshold SIRI was 0.785–2.2 (median, 1.11). We, therefore, used 1.1 for subgroup analysis of cut-off value in the following analyses. Nine articles used the receiver operating characteristic (ROC) curve to determine the best threshold (18–22, 24–27) and one study applied the X-tile software (23). Six studies reported the significance of SIRI in the OS prediction of HCC (18–20, 23–25) and eight studies reported the association between SIRI and PFS (20–27). Six studies reported HRs and 95%CIs using multivariate analysis (18, 21, 22, 25–27) and four studies used univariate analysis (19, 20, 23, 24). The NOS scores of all eligible studies were 7–9, suggesting a high quality (Table 1).

SIRI and OS

Six studies involving 1,598 patients (18–20, 23–25) provided data on the significance of SIRI in predicting OS in HCC. There was no obvious heterogeneity (I^2 = 0, P=0.479); therefore, we adopted a fixed-effects model. As shown in Table 2 and Figure 2, the HR was

TABLE 2 Subgroups of the prognostic value of SIRI for OS in patients with HCC.

Subgroups	No. of studies	No. of patients	Effects model	HR (95%CI)	p	Heterogeneity I^2(%) Ph		Meta-regression p
Total	6	1,598	Fixed	1.75(1.52-2.01)	<0.001	0	0.479	
Country								0.305
Turkey	1	80	–	2.02(1.24-3.30)	0.005	–	–	
China	5	1,518	Fixed	1.72(1.49-1.99)	<0.001	3.4	0.387	
Sample size								0.649
<200	2	274	Fixed	1.81(1.38-2.38)	<0.001	0	0.602	
≥200	4	1,324	Fixed	1.72(1.47-2.03)	<0.001	27.5	0.247	
Treatment								0.827
Surgery	1	351	–	2.11(1.20-3.71)	0.009	–	–	
TACE	1	194	–	1.73(1.25-2.39)	0.001	–	–	
Sorafenib or Sorafenib/ICIs	2	432	Fixed	1.91(1.47-2.47)	<0.001	0	0.783	
LT	1	218	–	2.26(1.49-3.43)	<0.001	–	–	
RFA	1	403	–	1.47(1.17-1.85)	0.001	–	–	
Study center								0.528
Single center	5	1,404	Fixed	1.75(1.50-2.04)	<0.001	11.1	0.343	
Multicenter	1	194	–	1.73(1.25-2.39)	0.001	–	–	
Cut-off value								0.283
<1.1	2	545	Fixed	1.82(1.37-2.41)	<0.001	0	0.545	
≥1.1	4	1,053	Fixed	1.73(1.47-2.02)	<0.001	25.8	0.257	
Cut-off selection								0.714
ROC curve	5	1,195	Fixed	1.93(1.62-2.29)	<0.001	0	0.883	
X-tile	1	403	–	1.47(1.17-1.85)	0.001	–	–	
Survival analysis								0.927
Univariate	4	1,029	Fixed	1.67(1.43-1.94)	<0.001	0	0.522	
Multivariate	2	569	Fixed	2.20(1.58-3.09)	<0.001	0	0.851	

SIRI, systemic inflammation response index; OS, overall survival; HCC, hepatocellular carcinoma; TACE, transcatheter arterial chemoembolization; RFA, radiofrequency ablation; LT, liver transplantation; ICIs, immune checkpoint inhibitors; ROC, receiver operating characteristic.

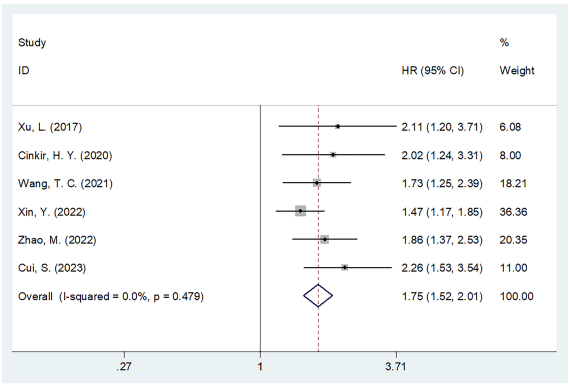

FIGURE 2
Forest plots of the prognostic role of SIRI for OS in patients with HCC.

1.75 (95% CI=1.52–2.01, p<0.001), suggesting a relationship between elevated SIRI and dismal OS in patients with HCC. Subgroup analysis revealed that the predictive role of SIRI in OS remained consistent across various factors including country, treatment, sample size, study center, threshold, threshold selection method, or survival analysis type (Table 2).

SIRI and PFS

Altogether, eight articles comprising 2,008 patients (20–27) reported a correlation between SIRI and PFS in patients with HCC. Because of significant heterogeneity, we employed the random-effects model (I^2 = 78.8%, P<0.001; Table 3 and Figure 3). Based on the pooled results, an increased SIRI significantly predicted inferior PFS in HCC (HR=1.66, 95% CI=1.34–2.05, p<0.001; Figure 3; Table 3).

TABLE 3 Subgroups of the prognostic value of SIRI for PFS in patients with HCC.

Subgroups	No. of studies	No. of patients	Effects model	HR (95%CI)	p	Heterogeneity I^2(%) Ph		Meta-regression p
Total	8	2,008	Random	1.66(1.34-2.05)	<0.001	78.8	<0.001	
Sample size								0.795
<200	4	665	Fixed	1.31(1.16-1.47)	<0.001	0	0.760	
≥200	4	1,343	Random	1.94(1.36-2.76)	<0.001	85.5	<0.001	
Treatment								0.891
Surgery	3	693	Fixed	1.55(1.35-1.79)	<0.001	0	0.810	
TACE	2	342	Fixed	1.29(1.14-1.47)	<0.001	0	0.433	
Sorafenib or Sorafenib/ICIs	1	352	–	1.51(1.11-2.05)	0.008	–	–	
LT	1	218	–	1.73(1.24-2.43)	0.001	–	–	
RFA	1	403	–	3.63(2.58-5.10)	<0.001	–	–	
Study center								0.460
Single center	7	1,814	Random	1.69(1.33-2.16)	<0.001	81.8	<0.001	
Multicenter	1	194	–	1.45(1.07-1.97)	0.018	–	–	
Cut-off value								0.615
<1.1	4	665	Fixed	1.31(1.16-1.47)	<0.001	0	0.760	
≥1.1	4	1,343	Random	1.94(1.36-2.76)	<0.001	85.5	<0.001	
Cut-off selection								0.339
ROC curve	7	1,605	Fixed	1.43(1.31-1.56)	<0.001	1.2	0.415	
X-tile	1	403	–	3.63(2.58-5.10)	<0.001	–	–	
Survival analysis								0.706
Univariate	3	949	Random	1.98(1.13-3.49)	0.017	89.5	<0.001	
Multivariate	5	1,059	Fixed	1.42(1.29-1.56)	<0.001	32.5	0.205	

SIRI, systemic inflammation response index; PFS, progression-free survival; HCC, hepatocellular carcinoma; TACE, transcatheter arterial chemoembolization; RFA, radiofrequency ablation; LT, liver transplantation; ICIs, immune checkpoint inhibitors; ROC, receiver operating characteristic.

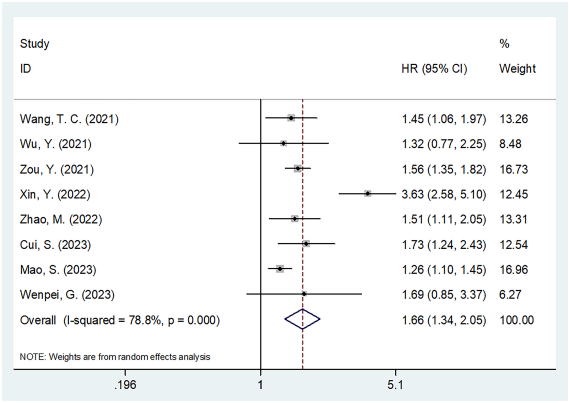

FIGURE 3
Forest plots of the prognostic role of SIRI for PFS in patients with HCC.

Subgroup analysis indicated that elevated SIRI still significantly predicted PFS in HCC, which was unaffected by country, treatment, sample size, study center, threshold, threshold selection method, or survival analysis type (Table 3).

The relationship of SIRI with clinicopathological characteristics of HCC

Four studies involving 1,111 patients investigated the relationship between the SIRI and the clinicopathological characteristics of HCC (20, 23, 24, 27). According to Figure 4 and Table 4, our combined results suggested a significant relationship between increased SIRI and multiple tumor numbers (OR=1.42, 95% CI=1.09–1.85, p=0.009) and maximum tumor diameter >5 cm (OR=3.06, 95% CI=1.76–5.30, p<0.001). Nonetheless, SIRI was not significantly related to sex (OR=1.10, 95% CI=0.88–1.51, p=0.559), Child-Pugh class (OR=1.46, 95% CI=0.52–4.11, p=0.476), alpha-fetoprotein (AFP) level (OR=1.02, 95% CI=0.80–1.30, p=0.880), or hepatitis B virus infection (OR=1.12, 95% CI=0.78–1.61, p=0.550) (Figure 4; Table 4).

Sensitivity analysis and meta-regression

By removing studies study-by-study, sensitivity analysis revealed that none of the studies had an effect on OS or PFS, suggesting that all results remained consistent (Figure 5). Meta-

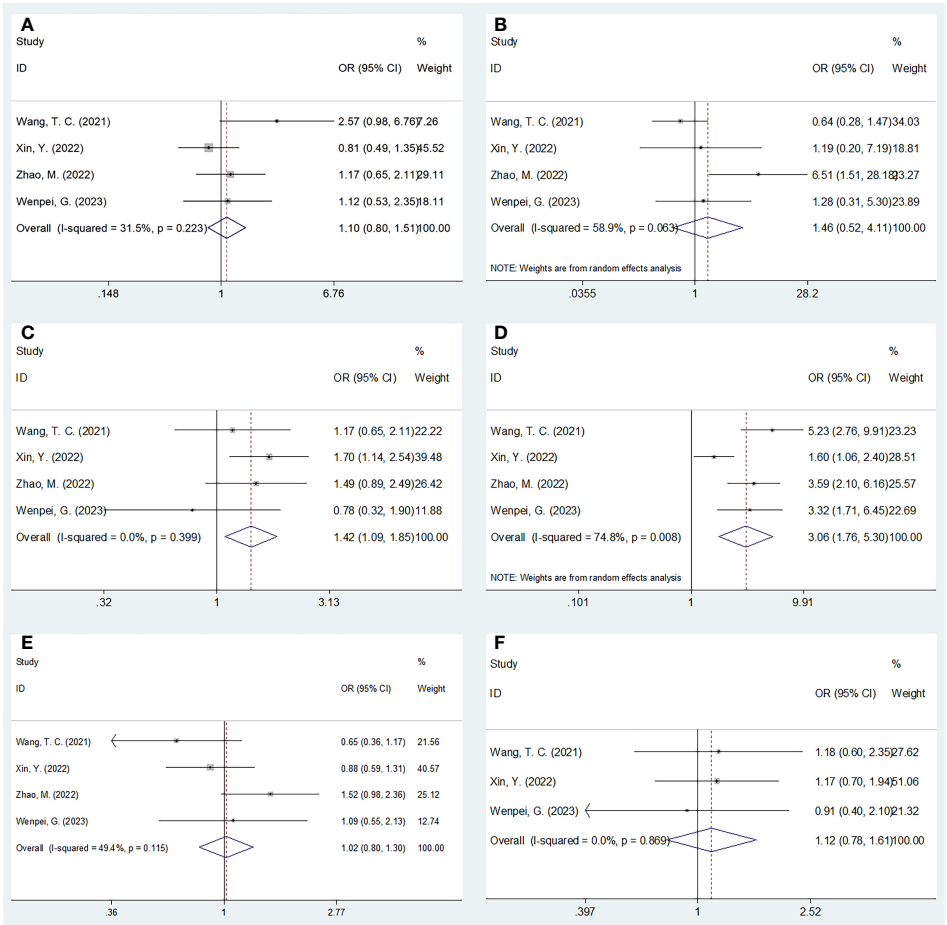

FIGURE 4
Forest plots of the associations between SIRI and clinicopathological factors in HCC. **(A)** Gender (male vs female); **(B)** Child-Pugh class (B-C vs A); **(C)** Tumor number (multiple vs solitary); **(D)** Maximum tumor diameter (>5 cm vs ≤5 cm); **(E)** AFP (ng/ml) (≥400 vs <400); and **(F)** HBV (+) (yes vs no).

TABLE 4 The association between SIRI and clinicopathological factors in patients with HCC. .

Variables	No. of studies	No. of patients	Effects model	OR (95%CI)	p	Heterogeneity I^2(%) Ph	
Gender (male vs female)	4	1,111	Fixed	1.10(0.88-1.51)	0.559	31.5	0.223
Child-Pugh class (B-C vs A)	4	1,111	Random	1.46(0.52-4.11)	0.476	58.9	0.063
Tumor number (multiple vs solitary)	4	1,111	Fixed	1.42(1.09-1.85)	0.009	0	0.399
Maximum tumor diameter (>5 cm vs ≤5 cm)	4	1,111	Random	3.06(1.76-5.30)	<0.001	74.8	0.008
AFP (ng/ml) (≥400 vs <400)	4	1,111	Fixed	1.02(0.80-1.30)	0.880	49.4	0.115
HBV (+) (yes vs no)	3	759	Fixed	1.12(0.78-1.61)	0.550	0	0.869

SIRI, systemic inflammation response index; HCC, hepatocellular carcinoma; AFP, alpha-fetoprotein; HBV, hepatitis B virus.

regression showed that none of the factors significantly influenced the overall results of OS and PFS (Tables 2, 3).

Publication bias

Begg's test, funnel plots, and Egger's test were used to assess potential publication bias. The funnel plot did not exhibit any significant asymmetry in the OS or PFS (Figure 6). Moreover, the results indicated no significant publication bias for OS (Begg's p=0.133; Egger's p=0.358) or PFS (Begg's p=0.536; Egger's p=0.302).

Discussion

The prognostic significance of SIRI in patients with HCC remains inconsistent. This meta-analysis collected data from 10 articles involving 2,439 patients. According to our results, elevated SIRI levels were markedly associated with shortened OS and inferior PFS in patients with HCC. Additionally, a high SIRI was significantly correlated with multiple tumor numbers and tumor size >5 cm in HCC. Publication bias tests and subgroup analyses were conducted to verify the reliability of the findings. Collectively, SIRI serves as a promising and cost-effective factor for predicting the short- and long-term prognoses of patients with HCC. To the best of our knowledge, this is the first meta-analysis to explore the potential of SIRI in predicting the prognosis of patients with HCC.

SIRI was calculated using the following formula: SIRI= neutrophil count × monocyte count/lymphocyte count. Therefore, a high SIRI could be the result of increased neutrophils, increased monocytes, and/or decreased lymphocytes. Currently, the accurate predictive mechanism of SIRI in HCC prognosis remains largely unclear and can be interpreted as follows: First, neutrophils recruited to a tumor site can produce inflammatory factors, such as interleukin-1 (IL-1) and IL-6, promoting the growth and metastasis of tumor cells (7). Activated neutrophils can suppress T cell proliferation and cytotoxicity by binding PD-L1 on the neutrophil surface to PD-1 on the T cell surface (30). This may promote tumor immune evasion and malignant growth, ultimately resulting in a shorter lifespan in cancer patients (31). Second, monocytes may differentiate into tumor-associated macrophages

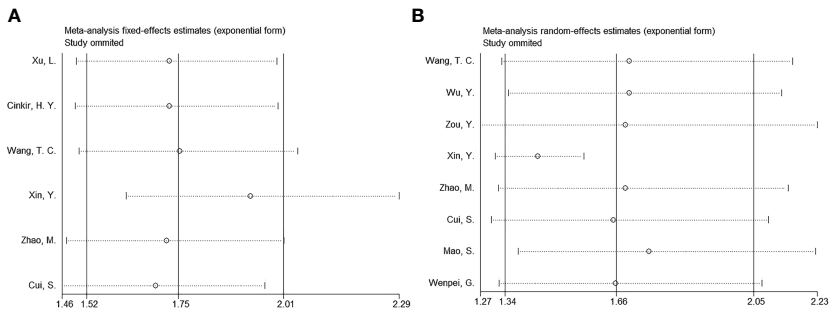

FIGURE 5
Sensitivity analysis. **(A)** OS and **(B)** PFS.

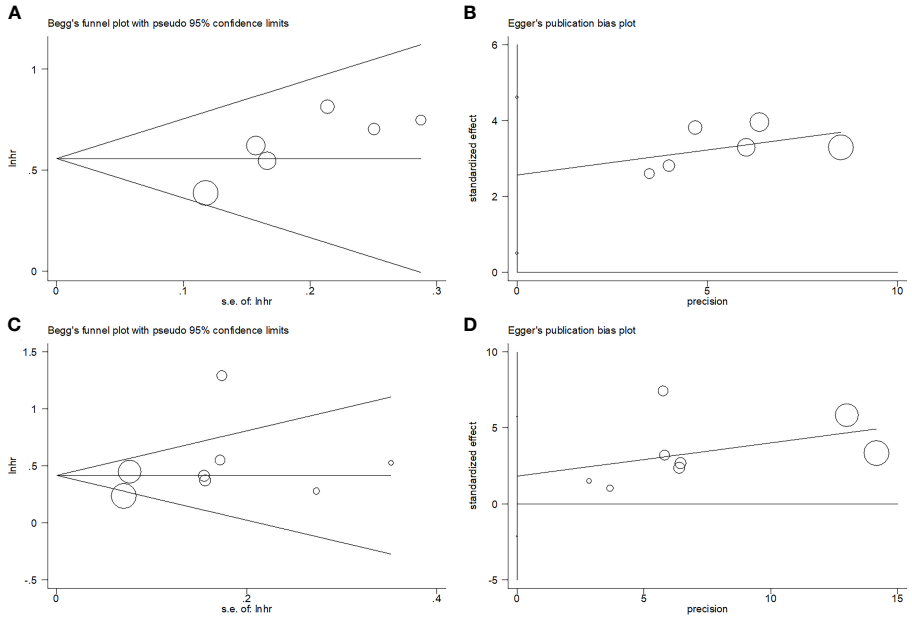

FIGURE 6
Publication test by Begg's test and Egger's test. **(A)** Begg's test for OS, p=0.133; **(B)** Egger's test for OS, p=0.358; **(C)** Begg's test for PFS, p=0.536; and **(D)** Egger's test for PFS, p=0.302.

(TAMs) (32). TAMs secrete several inflammatory factors that affect the tumor microenvironment, thereby promoting tumor occurrence, metastasis, and relapse (33). Many studies have demonstrated the presence of TAM infiltration in the HCC matrix, accelerating tumor angiogenesis, growth, metastasis, and immunosuppression (34, 35). Third, lymphocytes play a critical role in cellular anti-tumor responses. Tumor-infiltrating lymphocytes (TILs) have a pivotal impact on the anticancer immune microenvironment and are involved in multiple stages of tumor progression (36). The presence of lymphocyte infiltration in tumor tissues is associated with improved therapeutic outcomes. However, when the number of lymphocytes in the tumor microenvironment decreases, anti-tumor ability decreases, resulting in immune tolerance and tumor escape (37). Taken together, a high SIRI may significantly predict the prognosis of patients with HCC.

Notably, the degree of liver fibrosis may significantly affect SIRI. As these data were rarely evaluated in the included papers, they were not analyzed. However, the development of HCC in cirrhotic and non-cirrhotic livers differs significantly. Future studies are needed to investigate the prognostic value of SIRI for HCC in both cirrhotic and non-cirrhotic liver groups. Evaluating liver function is essential for determining the prognosis of HCC although the Child-Pugh score alone is not sufficient to do so. A major prognostic factor for HCC is portal hypertension, which may affect the SIRI; however, this has rarely been examined in the included studies. None of the included studies provided data on portal hypertension. Therefore, we expect future studies to evaluate the prognostic value of the SIRI under different circumstances of portal hypertension. Sarcopenia is another important prognostic factor in patients with solid tumors (38–42). Current evidence shows that sarcopenia is independently associated with a poor prognosis in various cancers (38–42). Previous studies have also indicated that many patients with HCC have sarcopenia (43–45). The SIRI is associated with tumor characteristics but may also be influenced by general health status, particularly sarcopenia. However, the included studies did not present data on sarcopenia. Therefore, we expect that the correlation between SIRI and sarcopenia in HCC can be investigated in future studies.

Recently, meta-analyses have been conducted to determine whether SIRI can be used to predict the prognosis of solid tumors. A meta-analysis conducted by Wang et al. found that the SIRI independently predicted the prognosis and survival status of nasopharyngeal carcinoma based on 3,187 patients (46). Another meta-analysis of 10,754 cases by Zhou et al. showed that a high SIRI was related to shorter OS and DFS/recurrence-free survival/PFS in various cancers (47). In addition, in a meta-analysis of 14 studies, Wei et al. demonstrated that the SIRI is a useful factor for predicting dismal prognostic outcomes during malignancy treatment (48). The present study identified an obvious relationship between SIRI and survival in HCC, which is in accordance with findings in other cancer types.

This study has certain limitations. First, the articles included were from Asian countries, particularly China. Although only articles in the English language were included, the applicability of our results should be noted. Second, the SIRI cut-off values differed, possibly inducing heterogeneity in the present study. Third, the sample size was relatively small. Therefore, large-scale prospective trials using standard SIRI cut-off values should be conducted for further validation.

Conclusions

In conclusion, the present study showed that elevated SIRI levels significantly predicted OS and PFS in patients with HCC. Moreover, the SIRI was significantly associated with tumor aggressiveness. The SIRI could be used as a promising prognostic index for HCC in clinical practice.

Data availability statement

The original contributions presented in the study are included in the article/Supplementary Material. Further inquiries can be directed to the corresponding author.

Author contributions

SZ: Conceptualization, Formal analysis, Investigation, Methodology, Project administration, Resources, Supervision, Validation, Writing – original draft. ZT: Conceptualization, Data curation, Formal analysis, Investigation, Methodology, Project administration, Resources, Supervision, Validation, Visualization, Writing – review & editing.

Funding

The author(s) declare that no financial support was received for the research, authorship, and/or publication of this article.

Acknowledgments

We would like to thank Editage (www.editage.com) for English language editing.

Conflict of interest

The authors declare that the research was conducted in the absence of any commercial or financial relationships that could be construed as a potential conflict of interest.

Publisher's note

Supplementary material

The Supplementary Material for this article can be found online at: https://www.frontiersin.org/articles/10.3389/fimmu.2024.1291840/full#supplementary-material

SUPPLEMENTARY DATA SHEET 1
The detailed search strategies of each database in this meta-analysis.

References

1. Sung H, Ferlay J, Siegel RL, Laversanne M, Soerjomataram I, Jemal A, et al. Global cancer statistics 2020: GLOBOCAN estimates of incidence and mortality worldwide for 36 cancers in 185 countries. *CA: Cancer J Clin* (2021) 71:209–49. doi: 10.3322/caac.21660

2. McGlynn KA, Petrick JL, El-Serag HB. Epidemiology of hepatocellular carcinoma. *Hepatology* (2021) 73 Suppl 1:4–13. doi: 10.1002/hep.31288

3. Torimura T, Iwamoto H. Treatment and the prognosis of hepatocellular carcinoma in Asia. *Liver Int* (2022) 42:2042–54. doi: 10.1111/liv.15130

4. Yang JD, Hainaut P, Gores GJ, Amadou A, Plymoth A, Roberts LR. A global view of hepatocellular carcinoma: trends, risk, prevention and management. *Nat Rev Gastroenterol Hepatol* (2019) 16:589–604. doi: 10.1038/s41575-019-0186-y

5. Villanueva A. Hepatocellular carcinoma. *N Engl J Med* (2019) 380:1450–62. doi: 10.1056/NEJMra1713263

6. Sperandio RC, Pestana RC, Miyamura BV, Kaseb AO. Hepatocellular carcinoma immunotherapy. *Annu Rev Med* (2022) 73:267–78. doi: 10.1146/annurev-med-042220-021121

7. Grivennikov SI, Greten FR, Karin M. Immunity, inflammation, and cancer. *Cell* (2010) 140:883–99. doi: 10.1016/j.cell.2010.01.025

8. Gao Y, Zhang Z, Li Y, Chen S, Lu J, Wu L, et al. Pretreatment neutrophil-to-lymphocyte ratio as a prognostic biomarker in unresectable or metastatic esophageal cancer patients with anti-PD-1 therapy. *Front Oncol* (2022) 12:834564. doi: 10.3389/fonc.2022.834564

9. Taguchi S, Kawai T, Nakagawa T, Nakamura Y, Kamei J, Obinata D, et al. Prognostic significance of the albumin-to-globulin ratio for advanced urothelial carcinoma treated with pembrolizumab: a multicenter retrospective study. *Sci Rep* (2021) 11:15623. doi: 10.1038/s41598-021-95061-z

10. Taha HF, Kamel LM, Embaby A, Abdelaziz LA. Prognostic significance of lymphocyte-to-monocyte ratio in patients with classical Hodgkin lymphoma before and after receiving first-line chemotherapy. *Contemp Oncol (Poznan Poland)* (2022) 26:69–77. doi: 10.5114/wo.2022.115459

11. Alkurt EG, Durak D, Turhan VB, Sahiner IT. Effect of C-reactive protein-to-albumin ratio on prognosis in gastric cancer patients. *Cureus* (2022) 14:e23972. doi: 10.7759/cureus.23972

12. Qi Q, Zhuang L, Shen Y, Geng Y, Yu S, Chen H, et al. A novel systemic inflammation response index (SIRI) for predicting the survival of patients with pancreatic cancer after chemotherapy. *Cancer* (2016) 122:2158–67. doi: 10.1002/cncr.30057

13. Yilmaz H, Cinar NB, Avci IE, Telli E, Uslubas AK, Teke K, et al. The systemic inflammation response index: An independent predictive factor for survival outcomes of bladder cancer stronger than other inflammatory markers. *Urol Oncol* (2023) 41:256. doi: 10.1016/j.urolonc.2022.11.011

14. Zuo R, Zhu F, Zhang C, Ma J, Chen J, Yue P, et al. The response prediction and prognostic values of systemic inflammation response index in patients with advanced lung adenocarcinoma. *Thorac Cancer* (2023) 14:1500–11. doi: 10.1111/1759-7714.14893

15. Yazici H, Yegen SC. Is systemic inflammatory response index (SIRI) a reliable tool for prognosis of gastric cancer patients without neoadjuvant therapy? *Cureus* (2023) 15:e36597. doi: 10.7759/cureus.36597

16. Zhu M, Chen L, Kong X, Wang X, Fang Y, Li X, et al. The systemic inflammation response index as an independent predictor of survival in breast cancer patients: A retrospective study. *Front Mol Biosci* (2022) 9:856064. doi: 10.3389/fmolb.2022.856064

17. Huang H, Wu K, Chen L, Lin X. Study on the application of systemic inflammation response index and platelet-lymphocyte ratio in ovarian Malignant tumors. *Int J Gen Med* (2021) 14:10015–22. doi: 10.2147/ijgm.S346610

18. Xu L, Yu S, Zhuang L, Wang P, Shen Y, Lin J, et al. Systemic inflammation response index (SIRI) predicts prognosis in hepatocellular carcinoma patients. *Oncotarget* (2017) 8:34954–60. doi: 10.18632/oncotarget.16865

19. Cinkir HY, Dogan I. Comparison of inflammatory indexes in patients treated with sorafenib in advanced hepatocellular carcinoma: A single-center observational study. *Erciyes Med J* (2020) 42:201–6. doi: 10.14744/etd.2020.82246

20. Wang TC, An TZ, Li JX, Pang PF. Systemic inflammation response index is a prognostic risk factor in patients with hepatocellular carcinoma undergoing TACE. *Risk Manag Healthc Policy* (2021) 14:2589–600. doi: 10.2147/rmhp.S316740

21. Wu Y, Tu C, Shao C. Inflammatory indexes in preoperative blood routine to predict early recurrence of hepatocellular carcinoma after curative hepatectomy. *BMC Surg* (2021) 21:178. doi: 10.1186/s12893-021-01180-9

22. Zou Y, Chen Z, Lou Q, Han H, Zhang Y, Chen Z, et al. A novel blood index-based model to predict hepatitis B virus-associated hepatocellular carcinoma recurrence after curative hepatectomy: guidance on adjuvant transcatheter arterial chemoembolization choice. *Front Oncol* (2021) 11:755235. doi: 10.3389/fonc.2021.755235

23. Xin Y, Zhang X, Li Y, Yang Y, Chen Y, Wang Y, et al. A systemic inflammation response index (SIRI)-based nomogram for predicting the recurrence of early stage hepatocellular carcinoma after radiofrequency ablation. *Cardiovasc interventional Radiol* (2022) 45:43–53. doi: 10.1007/s00270-021-02965-4

24. Zhao M, Duan X, Mi L, Shi J, Li N, Yin X, et al. Prognosis of hepatocellular carcinoma and its association with immune cells using systemic inflammatory response index. *Future Oncol (London England)* (2022) 18:2269–88. doi: 10.2217/fon-2021-1087

25. Cui S, Cao S, Chen Q, He Q, Lang R. Preoperative systemic inflammatory response index predicts the prognosis of patients with hepatocellular carcinoma after liver transplantation. *Front Immunol* (2023) 14:1118053. doi: 10.3389/fimmu.2023.1118053

26. Mao S, Shan Y, Yu X, Huang J, Fang J, Wang M, et al. A new prognostic model predicting hepatocellular carcinoma early recurrence in patients with microvascular invasion who received postoperative adjuvant transcatheter arterial chemoembolization. *Eur J Surg Oncol* (2023) 49:129–36. doi: 10.1016/j.ejso.2022.08.013

27. Wenpei G, Yuan L, Liangbo L, Jingjun M, Bo W, Zhiqiang N, et al. Predictive value of preoperative inflammatory indexes for postoperative early recurrence of hepatitis B-related hepatocellular carcinoma. *Front Oncol* (2023) 13:1142168. doi: 10.3389/fonc.2023.1142168

28. Moher D, Liberati A, Tetzlaff J, Altman DG, Grp P. Preferred reporting items for systematic reviews and meta-analyses: the PRISMA statement. *J Clin Epidemiol* (2009) 62:1006–12. doi: 10.1016/j.jclinepi.2009.06.005

29. Stang A. Critical evaluation of the Newcastle-Ottawa scale for the assessment of the quality of nonrandomized studies in meta-analyses. *Eur J Epidemiol* (2010) 25:603–5. doi: 10.1007/s10654-010-9491-z

30. Wang TT, Zhao YL, Peng LS, Chen N, Chen W, Lv YP, et al. Tumour-activated neutrophils in gastric cancer foster immune suppression and disease progression through GM-CSF-PD-L1 pathway. *Gut* (2017) 66:1900–11. doi: 10.1136/gutjnl-2016-313075

31. He G, Zhang H, Zhou J, Wang B, Chen Y, Kong Y, et al. Peritumoural neutrophils negatively regulate adaptive immunity *via* the PD-L1/PD-1 signalling pathway in hepatocellular carcinoma. *J Exp Clin Cancer Res CR* (2015) 34:141. doi: 10.1186/s13046-015-0256-0

32. Cavassani KA, Meza RJ, Habiel DM, Chen JF, Montes A, Tripathi M, et al. Circulating monocytes from prostate cancer patients promote invasion and motility of epithelial cells. *Cancer Med* (2018) 7:4639–49. doi: 10.1002/cam4.1695

33. Mano Y, Aishima S, Fujita N, Tanaka Y, Kubo Y, Motomura T, et al. Tumor-associated macrophage promotes tumor progression *via* STAT3 signaling in hepatocellular carcinoma. *Pathobiology J Immunopathol Mol Cell Biol* (2013) 80:146–54. doi: 10.1159/000346196

34. Yan C, Yang Q, Gong Z. Tumor-associated neutrophils and macrophages promote gender disparity in hepatocellular carcinoma in zebrafish. *Cancer Res* (2017) 77:1395–407. doi: 10.1158/0008-5472.Can-16-2200

35. Jackaman C, Tomay F, Duong L, Abdol Razak NB, Pixley FJ, Metharom P, et al. Aging and cancer: The role of macrophages and neutrophils. *Ageing Res Rev* (2017) 36:105–16. doi: 10.1016/j.arr.2017.03.008

36. Chen KJ, Zhou L, Xie HY, Ahmed TE, Feng XW, Zheng SS. Intratumoral regulatory T cells alone or in combination with cytotoxic T cells predict prognosis of hepatocellular carcinoma after resection. *Med Oncol (Northwood London England)* (2012) 29:1817–26. doi: 10.1007/s12032-011-0006-x

37. Gooden MJ, de Bock GH, Leffers N, Daemen T, Nijman HW. The prognostic influence of tumour-infiltrating lymphocytes in cancer: a systematic review with meta-analysis. *Br J Cancer* (2011) 105:93–103. doi: 10.1038/bjc.2011.189

38. Lin WL, Nguyen TH, Lin CY, Wu LM, Huang WT, Guo HR. Association between sarcopenia and survival in patients with gynecologic cancer: A systematic review and meta-analysis. *Front Oncol* (2022) 12:1037796. doi: 10.3389/fonc.2022.1037796

39. Gan H, Lan J, Bei H, Xu G. The impact of sarcopenia on prognosis of patients with pancreatic cancer: A systematic review and meta-analysis. *Scott Med J* (2023) 68:133–48. doi: 10.1177/00369330231187655

40. He J, Luo W, Huang Y, Song L, Mei Y. Sarcopenia as a prognostic indicator in colorectal cancer: an updated meta-analysis. *Front Oncol* (2023) 13:1247341. doi: 10.3389/fonc.2023.1247341

41. Park A, Orlandini MF, Szor DJ, Junior UR, Tustumi F. The impact of sarcopenia on esophagectomy for cancer: a systematic review and meta-analysis. *BMC Surg* (2023) 23:240. doi: 10.1186/s12893-023-02149-6

42. Xiong J, Chen K, Huang W, Huang M, Cao F, Wang Y, et al. Prevalence and effect on survival of pre-treatment sarcopenia in patients with hematological Malignancies: a meta-analysis. *Front Oncol* (2023) 13:1249353. doi: 10.3389/fonc.2023.1249353

43. Li X, Huang X, Lei L, Tong S. Impact of sarcopenia and sarcopenic obesity on survival in patients with primary liver cancer: a systematic review and meta-analysis. *Front Nutr* (2023) 10:1233973. doi: 10.3389/fnut.2023.1233973

44. Liu J, Luo H, Huang L, Wang J. Prevalence of sarcopenia among patients with hepatocellular carcinoma: A systematic review and meta–analysis. *Oncol Lett* (2023) 26:283. doi: 10.3892/ol.2023.13869

45. Prokopidis K, Affronti M, Testa GD, Ungar A, Cereda E, Smith L, et al. Sarcopenia increases mortality risk in liver transplantation: a systematic review and meta-analysis. *Panminerva Med* (2023). doi: 10.23736/s0031-0808.23.04863-2

46. Wang L, Qin X, Zhang Y, Xue S, Song X. The prognostic predictive value of systemic immune index and systemic inflammatory response index in nasopharyngeal carcinoma: A systematic review and meta-analysis. *Front Oncol* (2023) 13:1006233. doi: 10.3389/fonc.2023.1006233

47. Zhou Q, Su S, You W, Wang T, Ren T, Zhu L. Systemic inflammation response index as a prognostic marker in cancer patients: A systematic review and meta-analysis of 38 cohorts. *Dose-response Publ Int Hormesis Soc* (2021) 19:15593258211064744. doi: 10.1177/15593258211064744

48. Wei L, Xie H, Yan P. Prognostic value of the systemic inflammation response index in human Malignancy: A meta-analysis. *Med (Baltimore)* (2020) 99:e23486. doi: 10.1097/md.0000000000023486

frontiers | Frontiers in Immunology

TYPE Original Research
PUBLISHED 28 February 2024
DOI 10.3389/fimmu.2024.1316778

OPEN ACCESS

EDITED BY
Paulo Rodrigues-Santos,
University of Coimbra, Portugal

REVIEWED BY
Xiubao Ren,
Tianjin Medical University Cancer Institute and Hospital, China
Liang Qiao,
Loyola University Chicago, United States
Lingdi Zhao,
Henan Provincial Cancer Hospital, China

*CORRESPONDENCE
Yi Zhang
yizhang@zzu.edu.cn
Li Yang
fccyangl1@zzu.edu.cn
Taiying Lu
fccluty@zzu.edu.cn

†These authors have contributed equally to this work and share first authorship

RECEIVED 10 October 2023
ACCEPTED 14 February 2024
PUBLISHED 28 February 2024

CITATION
Zhen S, Wang W, Qin G, Lu T, Yang L and Zhang Y (2024) Dynamic surveillance of lymphocyte subsets in patients with non-small cell lung cancer during chemotherapy or combination immunotherapy for early prediction of efficacy.
Front. Immunol. 15:1316778.
doi: 10.3389/fimmu.2024.1316778

Dynamic surveillance of lymphocyte subsets in patients with non-small cell lung cancer during chemotherapy or combination immunotherapy for early prediction of efficacy

Shanshan Zhen[1,2†], Wenqian Wang[1,2†], Guohui Qin[1], Taiying Lu[2*], Li Yang[1,3,4*] and Yi Zhang[1,3,4*]

[1]Biotherapy Center, the First Affiliated Hospital of Zhengzhou University, Zhengzhou, Henan, China, [2]Department of Oncology, the First Affiliated Hospital of Zhengzhou University, Zhengzhou, Henan, China, [3]School of Life Sciences, Zhengzhou University, Zhengzhou, Henan, China, [4]State Key Laboratory of Esophageal Cancer Prevention & Treatment, Zhengzhou University, Zhengzhou, Henan, China

Background: Non-small cell lung cancer (NSCLC) remains the leading cause of cancer-related deaths worldwide. Lymphocytes are the primary executors of the immune system and play essential roles in tumorigenesis and development. We investigated the dynamic changes in peripheral blood lymphocyte subsets to predict the efficacy of chemotherapy or combination immunotherapy in NSCLC.

Methods: This retrospective study collected data from 81 patients with NSCLC who received treatments at the First Affiliated Hospital of Zhengzhou University from May 2021 to May 2023. Patients were divided into response and non-response groups, chemotherapy and combination immunotherapy groups, and first-line and multiline groups. We analyzed the absolute counts of each lymphocyte subset in the peripheral blood at baseline and after each treatment cycle. Within-group and between-group differences were analyzed using paired Wilcoxon signed-rank and Mann-Whitney U tests, respectively. The ability of lymphocyte subsets to predict treatment efficacy was analyzed using receiver operating characteristic curve and logistic regression.

Results: The absolute counts of lymphocyte subsets in the response group significantly increased after the first cycle of chemotherapy or combination immunotherapy, whereas those in the non-response group showed persistent decreases. Ratios of lymphocyte subsets after the first treatment cycle to those at baseline were able to predict treatment efficacy early. Combination immunotherapy could increase lymphocyte counts compared to chemotherapy alone. In addition, patients with NSCLC receiving chemotherapy or combination immunotherapy for the first time mainly presented with elevated lymphocyte levels, whereas multiline patients showed continuous reductions.

Conclusion: Dynamic surveillance of lymphocyte subsets could reflect a more actual immune status and predict efficacy early. Combination immunotherapy protected lymphocyte levels from rapid decrease and patients undergoing

multiline treatments were more prone to lymphopenia than those receiving first-line treatment. This study provides a reference for the early prediction of the efficacy of clinical tumor treatment for timely combination of immunotherapy or the improvement of immune status.

KEYWORDS

lymphocyte subsets, immunotherapy, chemotherapy, efficacy prediction, NSCLC

1 Introduction

Lung cancer is the most common cancer worldwide and the leading cause of cancer-related deaths (1). Non-small cell lung cancer (NSCLC) accounts for approximately 85% of all lung cancer cases (2). Although various clinical treatments, including chemotherapy, radiotherapy, and targeted therapy, have prolonged the survival of lung cancer patients, the five-year survival outcome of NSCLC remains unsatisfactory (3, 4). With the development of the tumor surveillance theory and continuous researches on the tumor immunity, scientists have increasingly realized the essential roles of the immune system in tumor control. The advent of immunotherapy has profoundly revolutionized cancer treatment because of its continuous therapeutic effects brought by immune memory (5–7). As the fourth modality of modern tumor treatment, immunotherapy, which controls tumors by mobilizing the immune system, is the only treatment that promises to eliminate tumor cells completely (8). The clinical effectiveness of anti-PD-1/PD-L1 therapy demonstrates the vital roles of the immune system in anti-tumor effects (9, 10). Immune status is closely related to tumorigenesis, progression and prognosis (11). Therefore, evaluating immune status of patients is of great significance in the clinical cancer treatment.

Classical lymphocyte subsets are classified into T cell, including $CD4^+$ T cell and $CD8^+$ T cell, B cell and natural killer (NK) cell. Abundant and active lymphocytes are important tumor resistant (8, 12). They are involved in innate and adaptive immunity and work together to exert anti-tumor effects (13). However, in clinical practice, assessing immune status by detecting tumor-infiltrating lymphocytes is not feasible for many patients with advanced cancer because of the difficulty in repeatedly obtaining tumor tissue. The use of easily available peripheral blood is less invasive and more convenient for clinical applications. Increasing evidence suggests that the absolute counts of peripheral blood lymphocytes are positively correlated with tumor prognosis and outcomes (14–16).

Currently, chemotherapy remains a vital treatment option for advanced NSCLC (17). Substances released during chemotherapy-induced tumor cell death may promote lymphocyte activation and proliferation, which are synergistically involved in tumor killing (18). However, long-term chemotherapy can lead to severe lymphopenia. The cytotoxicity of chemotherapeutic drugs and severe myelosuppression caused by chemotherapy affect the production and differentiation of lymphocytes (19). A low-lymphocyte environment affects tumor surveillance and killing, resulting in a highly susceptibility to the failure of tumor control. When there is an inadequate number of effective lymphocytes, the combination of anti-PD-1/PD-L1 therapy may not benefit cancer patients (20). Therefore, detecting dynamic changes in lymphocyte subsets is of great significance for early efficacy prediction, decisions on the replacement of ineffective treatments, the timely utilization of immunotherapy and the timely application of lymphocyte-improving drugs, such as thymosin in the clinic (21, 22).

The aim of this study was to explore the association between efficacies of chemotherapy or chemo-immunotherapy and the absolute counts of lymphocyte subsets in peripheral blood, and we expected to predict the efficacy in advance in order to provide a clinical reference. We also explored the effects of combined immunotherapy on lymphocyte counts. Besides, we noted significant differences in dynamic changes of lymphocyte subsets between patients receiving first-line and multiline treatments.

2 Methods

2.1 Clinical data collection

We collected data from NSCLC patients who received treatment at the First Affiliated Hospital of Zhengzhou University from May 2021 to May 2023. Eighty-one patients receiving first-line or multiline therapy with standard chemotherapy or chemoimmunotherapy were included in our study. Clinical and pathological data of all patients were collected, including age; sex; smoking history; pathological information; lymphocyte subsets; and imaging findings, such as

Abbreviations: NSCLC, non-small cell lung cancer; PD-1, programmed death 1; PD-L1, programmed cell death-ligand 1; NK cell, natural killer cell; CR, complete response; PR, partial response; SD, stable disease; PD, progressive disease; BL, baseline; ROC, receiver operating characteristic; AUC, area under the curve; CAR-T, chimeric antigen receptor T cell.

chest computed tomography (CT) and head magnetic resonance imaging (MRI). Baseline was collected before patients received their first treatment. Collection of lymphocyte subsets each cycle was before the next treatment (three weeks later). This study was approved by the Medical Ethics Committee of the First Affiliated Hospital of Zhengzhou University (2021-KY-1105-002).

2.2 Inclusion criteria

1. 18 to 80 years of age
2. Definite pathological diagnosis of non-small cell lung cancer
3. Eastern Cooperative Oncology Group score 0-1, expected survival > 6 months
4. No combination of other tumors, acute infections, blood system diseases, or immune system diseases
5. Received four consecutive cycles of chemotherapy or chemotherapy combined with anti-PD-1 therapy
6. Treated for the first time after diagnosis or treatment again after at least second-line failure

2.3 Exclusion criteria

1. Inability to trace personal or clinical date
2. Not followed up, lack of regular treatments or reviews, or inability to assess disease progression
3. The use of immunomodulators, such as thymopeptides or placental polypeptides, during treatment

2.4 Group design

1. First-line group: patients who received standard first-line therapy for the first time after diagnosis
2. Multiline group: patients who received retreatment after experiencing at least second-line failure
3. Chemotherapy group: patients who received a chemotherapy regimen during the four treatment cycles
4. Combination group: patients who received anti-PD-1 therapy in combination with four chemotherapy cycles

2.5 Efficacy evaluation

A comprehensive assessment of treatment efficacy after four treatment cycles was performed based on CT, MRI, bone scan, and other imaging methods. Complete response (CR), partial response (PR), stable disease (SD), and progressive disease (PD) were determined according to the Response Evaluation Criteria in Solid Tumors 1.1 criteria.

Response group: CR + PR + SD

Non-response group: PD

2.6 Statistical analysis

Differences in each basic characteristic between response and non-response groups were analyzed using Chi-square test. Dynamic changes in each lymphocyte subset within the groups in four treatment cycles were subjected to the paired Wilcoxon signed-rank test. The Mann-Whitney U test was used to analyze between-group differences. The receiver operator characteristic (ROC) curve was used to evaluate predictive capacity of lymphocyte subsets and choose the best cut-off values. Cut-off values were determined by calculating the Youden's Index = Sensitivity + Specificity-1. Combination indicators of two lymphocyte subsets for efficacy prediction as well as model evaluation were analyzed by binary logistic regression with SPSSPRO. Statistical analyses were performed using SPSS 22.0 (IBM, Armonk, NY, USA), and Prism 8.4.3 (GraphPad, San Diego, CA, USA) was used to construct figures.

3 Results

3.1 Patients' characteristics

A total of 81 patients were enrolled in this study, including 56 males and 25 females, with a mean age of 61 years old. Forty-eight of the patients had a history of smoking. According to the 8th edition of the American Joint Committee on Cancer staging criteria, 5 patients were in stage I, 9 patients were in stage II, 20 patients were in stage III, and 47 patients were in stage IV. Forty-two patients had identified gene mutation. In addition, immunohistochemistry showed KI67 expression. The expression of KI67 varied from 2 to 90 percent. All medical histories and pathological features were shown in Table 1. These characteristics were not significantly different between the response and non-response groups, according to the Chi-squared test ($P > 0.05$). In this study, 45 patients received first-line treatment and 36 patients received multiline treatment. The response rate was significantly higher in the first-line treatment group than the multiline treatment group ($P = 0.033$). Forty-seven patients were treated with chemotherapy alone and 34 received chemotherapy combined with immunotherapy. The response rates of the two treatments were not significantly different ($P = 0.752$).

3.2 Relationship between efficacy and dynamic changes in lymphocyte subsets

3.2.1 Significant differences in dynamic changes of lymphocyte subsets between the response and non-response groups

We respectively analyzed the dynamic changes in lymphocyte subsets in the response and non-response groups of patients who

10.3389/fimmu.2024.1316778

TABLE 1 The clinical and pathological characteristics of included 81 patients.

Characteristics	Case	Response	Non-response	$\chi 2$	*P* value
Age (years)				0.105	0.745
≤ 60	39 (48.1%)	30 (37.0%)	9 (11.1%)		
> 60	42 (51.9%)	31 (38.3%)	11 (13.6%)		
Sex				0.428	0.513
Male	56 (69.1%)	41 (50.6%)	15 (18.5%)		
Female	25 (30.9%)	20 (24.7%)	5 (6.2%)		
Smoking history				2.726	0.099
Yes	48 (59.3%)	33 (40.7%)	15 (18.5%)		
No	33 (40.7%)	28 (34.6%)	5 (6.2%)		
Histological type				0.199	1
AD	48 (59.3%)	36 (44.4%)	12 (14.8%)		
SQCC	27 (33.3%)	20 (24.7%)	7 (8.6%)		
Others	6 (7.4%)	5 (6.2%)	1 (1.2%)		
Clinical stage				2.008	0.565
I	5 (6.2%)	5 (6.2%)	0 (0%)		
II	9 (11.1%)	7 (8.6%)	2 (2.5%)		
III	20 (24.7%)	16 (19.8%)	4 (4.9%)		
IV	47 (58.0%)	33 (40.7%)	14 (17.3%)		
Gene mutation				1.74	0.419
Yes	42 (51.9%)	33 (40.7%)	9 (11.1%)		
No	12 (14.8%)	10 (12.3%)	2 (2.5%)		
Unknown	27 (33.3%)	18 (22.2%)	9 (11.1%)		
KI67 (%)				4.925	0.155
2 ≤ KI67 < 30	24 (29.6%)	21 (25.9%)	3 (3.7%)		
30 ≤ KI67 < 80	39 (48.1%)	25 (30.9%)	14 (17.3%)		
80 ≤ KI67 < 90	15 (18.5%)	12 (14.8%)	3 (3.7%)		
Unknown	3 (3.7%)	3 (3.7%)	0 (0%)		
Treatment					
First-line	45 (55.6%)	38 (46.9%)	7(8.6%)	4.545	0.033
Multiline	36 (44.4%)	23 (28.4%)	13(16.0%)		
Chemotherapy	47 (58.0%)	36 (44.4%)	11(13.6%)	0.1	0.752
Combination	34 (42.0%)	25 (30.9%)	9(11.1%)		

AD, adenocarcinoma; SQCC, squamous cell carcinoma. The numbers and percentages of each characteristic in the response and non-response groups were shown. Differences in each characteristic between the two groups were analyzed using the Chi-square Test, and P < 0.05 was considered statistically different.

received chemotherapy or combination immunotherapy during four consecutive treatment cycles. Box plots were used to display medians and interquartile ranges of lymphocyte subset counts in each treatment cycle. Significant differences within and between groups were analyzed and marked (Figure 1).

After the first chemotherapy cycle, the absolute counts of Lymphocyte (Figure 1A, P = 0.006), T cell (Figure 1B, P = 0.004), $CD4^+$ T cell (Figure 1C, P = 0.012) and $CD8^+$ T cell (Figure 1D, P = 0.004) showed significant increases in the response group, with B cell (Figure 1E, P = 0.134) and NK cell (Figure 1F, P = 0.177) showing numerical increases, in contrast to the remarkable decreases in the non-response group. The absolute counts of Lymphocyte (Figure 1A, P = 0.041), T cell (Figure 1B, P = 0.021), $CD4^+$ T cell (Figure 1C, P = 0.013), and B cell (Figure 1E, P = 0.037) significantly decreased in the non-response group after the first chemotherapy cycle. $CD8^+$ T cell (Figure 1D, P = 0.062) and NK cell (Figure 1F, P =

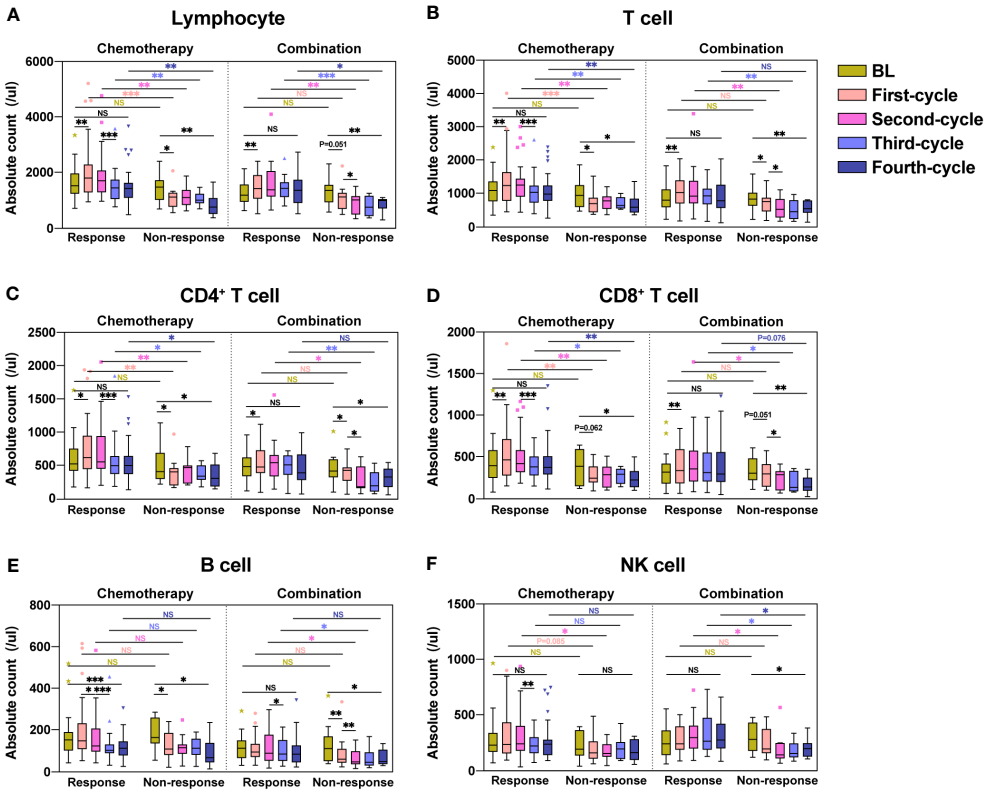

FIGURE 1
Dynamic changes in lymphocyte subsets during four treatment cycles in the response and non-response groups. Absolute counts of Lymphocyte **(A)**, T cell **(B)**, $CD4^+$ T cell **(C)**, $CD8^+$ T cell **(D)**, B cell **(E)**, and NK cell **(F)** in the response and non-response groups during four consecutive treatment cycles were shown as boxplots. The chemotherapy and combination immunotherapy groups were shown respectively. Within-group and between-group differences were analyzed using the paired Wilcoxon signed-rank test and Mann-Whitney U test, respectively. BL, Baseline; *, $P < 0.05$; **, $P < 0.01$; ***, $P < 0.001$; NS, not significant.

0.155) likewise decreased, although the difference was not statistically significant. Lymphocyte subsets in patients receiving the first combination immunotherapy cycle showed similar trends to chemotherapy in both response and non-response groups. During the four treatment cycles in the response group, lymphocyte subsets in patients receiving chemotherapy alone showed a trend of increasing counts first and then decreasing counts, whereas patients treated with combination immunotherapy showed an increase, followed by a maintenance of high lymphocyte counts. Except for B cell (Figure 1E, $P = 0.001$) in the chemotherapy group, lymphocyte subsets in the response group after four treatment cycles were not significantly different from those at baseline. Patients in the non-response group showed significant reduction in the counts of all lymphocyte subsets compared to baseline after four treatment cycles, regardless of whether they received chemotherapy or combination immunotherapy. Of note, the counts of lymphocyte subsets between the response and non-response groups were not significantly different at baseline, but significant differences were observed immediately after treatment. The counts of Lymphocyte (Figure 1A), especially T cell (Figure 1B), including $CD4^+$ T cell (Figure 1C) and $CD8^+$ T cells (Figure 1D), was significantly higher in the response group than those in the non-response group during chemotherapy or combination immunotherapy. B cell (Figure 1E) and NK cell (Figure 1F) in the response group also showed higher counts compared with the non-response group.

Overall, we found that lymphocyte subset reactions during treatment were strongly associated with the four-cycle treatment efficacy in patients with NSCLC who received chemotherapy or combination immunotherapy.

3.2.2 Predictive value of lymphocyte subsets on the efficacy in NSCLC patients

As shown in Figure 1, we found significant differences in lymphocyte subsets between the response and non-response groups. To better demonstrate the changes in lymphocytes, we used box plots to show the ratios of lymphocyte subset count after each treatment cycle to the counts at baseline (Figure 2). The ratios of each lymphocyte subset in the response group were almost greater than 1, especially in the first two chemotherapy or combination cycles, in contrast to the non-response group, in which the ratios were less than 1 throughout the treatment cycles. The ratios of Lymphocyte (Figure 2A), T cell (Figure 2B), $CD4^+$ T cell (Figure 2C), $CD8^+$ T cell (Figure 2D) and B cell (Figure 2E) were significantly higher in the response group than the non-response group ($P < 0.05$). Likewise, the ratios of NK cell were higher in the response group than the non-response group in some of the treatment cycles (Figure 2F, $P < 0.05$).

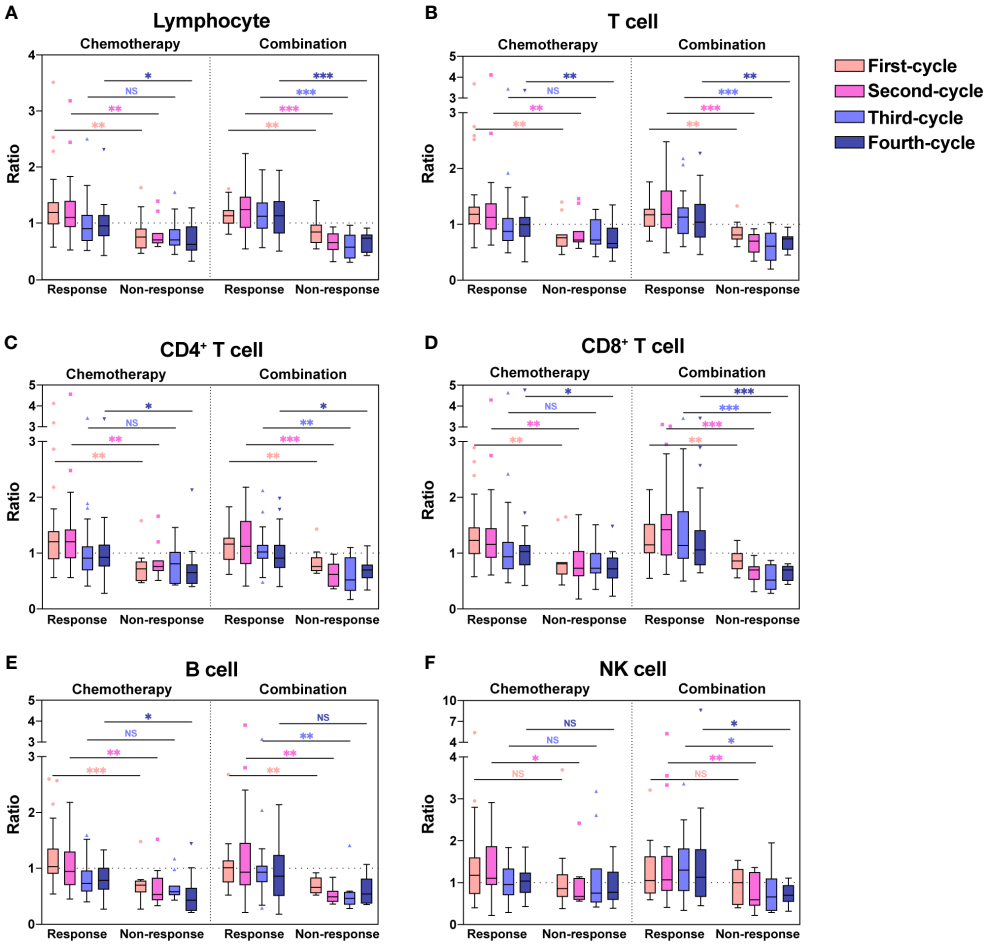

FIGURE 2
Ratios of absolute counts after each treatment to baseline for each lymphocyte subset. Ratios of absolute counts after each treatment cycle to baseline for Lymphocyte **(A)**, T cell **(B)**, $CD4^+$ T cell **(C)**, $CD8^+$ T cell **(D)**, B cell **(E)**, and NK cell **(F)** were shown as boxplots. The chemotherapy and combination immunotherapy groups were shown respectively. Between-group differences were analyzed statistically by Mann-Whitney U test. *, $P < 0.05$; **, $P < 0.01$; ***, $P < 0.001$; NS, not significant.

Regardless of whether patients received chemotherapy or combination immunotherapy, they showed similar differences in the ratios between the response and non-response groups. Owing to the cytotoxicity of chemotherapy, patients receiving chemotherapy alone in the response group experienced significant lymphopenia after the third chemotherapy cycle, leading to no significant difference in ratios between the response and non-response groups after the third chemotherapy cycle compared to baseline (Figures 2A-E, $P > 0.05$). While the protective effect of combination immunotherapy on lymphocytes reduced lymphopenia caused by long-term chemotherapy (Figures 2A–E).

The ratios were significantly higher in the response group than the non-response group for all chemotherapy cycles. Based on our previous analysis, lymphocyte levels in the response group and non-response groups did not demonstrate significant differences at baseline, whereas the ratios of lymphocyte count after the first chemotherapy cycle to baseline were significantly higher in the response group. This suggested that the response group possessed a more dynamic and more easily activated immune environment. Therefore, we hypothesized that the lymphocyte ratios after the first treatment cycle to baseline could predict the four-cycle treatment efficacy in patients with NSCLC. We analyzed the ROC curves in the response and non-response groups, and patients receiving chemotherapy alone or combination immunotherapy were analyzed separately (Figures 3A, B). The areas under the curve (AUCs) and cut-off values were displayed in Table 2. ROC curves showed that the ratios of Lymphocyte, T cell, $CD4^+$ T cell, $CD8^+$ T cell, and B cell counts after the first treatment cycle to baseline were good predictors of four-cycle treatment efficacy. B cell had the best predictive ability with AUCs of 0.857 (Figure 3A, $P = 0.002$) and 0.856 (Figure 3B, $P < 0.001$) for patients receiving chemotherapy and combination immunotherapy, respectively. Patients with NSCLC who received the first cycle of chemotherapy or combination immunotherapy had a peripheral blood B cell count to baseline ratio greater than 0.825 or 0.93, respectively, indicating that they were most likely to have good tumor control after four cycles of regular treatment. The AUCs for Lymphocyte, T cell, $CD4^+$ T cell and $CD8^+$ T cell were all greater than 0.75, indicating their predictive ability ($P < 0.002$). Based on these data, only NK cell was not an efficacy predictor (Figure 3A, $P = 0.109$, Figure 3B, $P = 0.238$). In addition, we attempted to construct models based on combined lymphocyte

10.3389/fimmu.2024.1316778

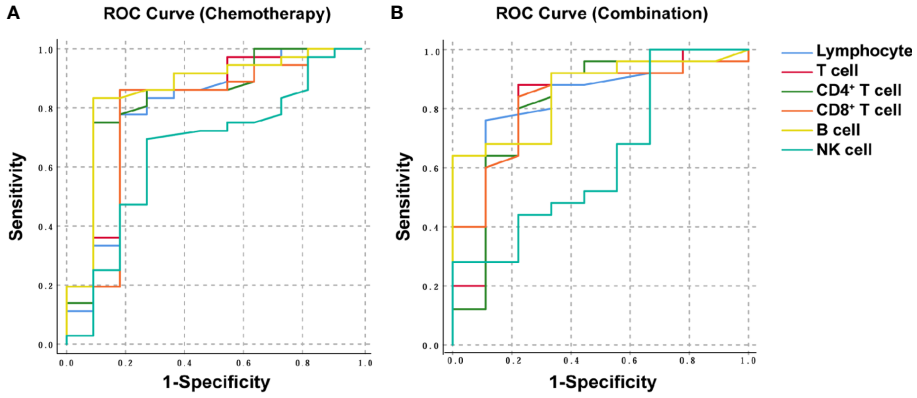

C

Combination Indicator	Regression Coefficient	OR (95%CI)	P_1 Value	Model Evaluation			
				Accuracy	F1	AUC	P_2 Value
T cell	0.03	1.031 (1.003-1.06)	0.032	0.864	0.863	0.88	<0.001
B cell	0.043	1.044 (1.009-1.08)	0.013				
CD8+ T cell	0.022	1.023 (1.002-1.044)	0.032	0.864	0.863	0.878	<0.001
B cell	0.049	1.05 (1.017-1.085)	0.003				

FIGURE 3
ROC analysis and Logistic regression of lymphocyte subsets for efficacy prediction. ROC curves were plotted for the ratios of each lymphocyte subset counts after the first treatment cycle to baseline in the response and non-response groups. The chemotherapy **(A)** and combination immunotherapy **(B)** groups were shown, respectively. AUC, significance, asymptotic 95% confidence interval, and cut-off values were shown in Table 2. **(C)** Logistic regression analysis of combined lymphocyte subsets for efficacy prediction. The two sets of combination indicators with the best predictive power and model evaluation were displayed. P_1 value represented the significance of each lymphocyte subset for efficacy prediction. Model evaluations were generated from logistic regression. F1 score combines the precision and recall to measure accuracy. ROC curves and AUC were used to measure the classification capacity of logistic regression. P_2 value was the likelihood ratio chi-square test to evaluate the validity of predictive models. $P < 0.05$ was considered statistically significant. OR: odds ratio, 95%CI: 95% confidence interval.

subsets through logistic regression for higher predictive power. Since there were only 21 non-response patients in this study, according to the rule of 10 events per variable in logistic model, we considered synthesizing two lymphocyte subsets in order to jointly predict efficacy. And we excluded total lymphocytes from the logistic regression due to the collinearity and correlation problems. By performing regression analyses on combinations of different two lymphocyte subsets, we determined that combinations of T cell plus B cell (AUC=0.88, P<0.001) and $CD8^+$ T cell plus B cell (AUC=0.878, P<0.001) showed excellent predictive power and were better than single lymphocyte subset. Regression analyses and forest plots were demonstrated in Figure 3C. And the reliability and accuracy of the predictive models were evaluated.

3.3 Combination immunotherapy improved lymphopenia caused by chemotherapy toxicity

In our study, each lymphocyte subset showed a significant reduction after the third cycle of chemotherapy, while this lymphopenia was significantly ameliorated with combination immunotherapy. We found that combination immunotherapy protected against decreased lymphocyte and increased the lymphocyte counts. To confirm our hypothesis, we analyzed each lymphocyte subset in the chemotherapy and combination immunotherapy groups (Figure 4). To exclude baseline differences due to previous treatment, first-line and multiline patients were analyzed respectively. Among patients receiving first-line treatment, both the chemotherapy and combination groups showed significant increases in Lymphocyte (Figure 4A), T cell (Figure 4B), $CD4^+$ T cell (Figure 4C), and $CD8^+$ T cell (Figure 4D) counts after the first treatment. The chemotherapy group showed a significant reduction in all lymphocyte subsets after the third treatment cycle, whereas no significant reduction was observed in the combination immunotherapy group (Figures 4A–F). Except for B cell (Figure 4E), there were no significant differences in lymphocytes counts before and after four cycles of treatment in first-line chemotherapy patients. Observably, lymphocyte subsets were significantly maintained at relatively higher levels in the combination immunotherapy group. In the multiline group, Lymphocyte (Figure 4A), T cell (Figure 4B), CD4+

TABLE 2 Predictive ability of lymphocyte subsets after the first treatment cycle.

	Variable	AUC	Asymptotic significance	Asymptotic 95% Confidence		Cut-off Value
				Lower Bound	Upper Bound	
Chemotherapy	Lymphocyte	0.789	0.001	0.612	0.966	0.93
	T cell	0.811	< 0.001	0.644	0.977	0.86
	$CD4^+$ T cell	0.831	< 0.001	0.677	0.985	0.92
	$CD8^+$ T cell	0.783	0.002	0.602	0.964	0.855
	B cell	0.857	< 0.001	0.714	1.001	0.825
	NK cell	0.657	0.109	0.465	0.848	
Combination	Lymphocyte	0.818	0.001	0.631	1.004	0.99
	T cell	0.822	< 0.001	0.644	1.000	0.895
	$CD4^+$ T cell	0.811	0.001	0.620	1.002	0.8
	$CD8^+$ T cell	0.831	< 0.001	0.677	0.985	0.955
	B cell	0.856	< 0.001	0.725	0.986	0.93
	NK cell	0.631	0.238	0.413	0.849	

The predictive ability of each lymphocyte subset for efficacy was analyzed using ROC curves and asymptotic significance at P < 0.05 was considered statistically significant.

T cell (Figure 4C), CD8+ T cell (Figure 4D), and B cell (Figure 4E) were significantly decreased after four chemotherapy cycles, whereas immunotherapy maintained lymphocytes at relatively high levels. There were no significant differences in the lymphocyte subsets before and after the four cycles of combination therapy. We further analyzed the ratios of each lymphocyte subset after four treatment cycles to baseline (Figures 4G, H). Lymphocyte subsets in the combination immunotherapy group demonstrated relatively higher levels overall in both the first-line and multiline patients, although the ratios between the chemotherapy and combination groups were not statistically significant, with only B cell in the multiline group exhibiting a significant increase following combination immunotherapy (Figure 4H, $P = 0.034$).

3.4 Significant differences in dynamic changes of lymphocyte subsets in the first-line and multiline treatments

According to our inclusion criteria, 45 patients in the first-line group were treated for the first time after diagnosis, and 36 patients in the multiline group were treated again after at least second-line failure. To explore the dynamic changes in lymphocyte subsets in patients receiving first-line and multiline treatments during chemotherapy or combination immunotherapy, within-group and between-group differences were analyzed, and different treatments were displayed respectively (Figure 5).

Lymphocyte (Figure 5A), especially T cell (Figure 5B), including $CD4^+$ T cell (Figure 5C) and $CD8^+$ T cell (Figure 5D), were significantly increased after the first cycle of chemotherapy or combination immunotherapy in the first-line group. Lymphocyte subsets began to decrease after the second treatment cycle, with a significant decrease after the third chemotherapy cycle. Those decreases were more significant in the chemotherapy group. Changes in lymphocyte subsets were unsatisfactory in the multiline group, with a rapid decrease, whereas combination immunotherapy significantly improved this problem. NK cell (Figure 5F) showed a similar trend, however, owing to the small number of cases included in this study and the large individual differences, no statistical differences were observed. However, abnormal behavior was observed for B cell (Figure 5E), which decreased significantly in the first-line patients who received combination therapy, but no significant decrease was observed in the multiline patients.

4 Discussion

PD-1 inhibitor in combination with chemotherapy has been the first-line standard treatment in advanced NSCLC. Although immunotherapy has pronounced excellent results, it is undeniable that some patients are insensitive to the treatment, resulting in a failure to benefit from it, which emphasizes the importance of early efficacy prediction in tumor treatment (23, 24). This prospective study aimed to analyze the differences in lymphocyte subsets with different efficacies to determine the potential predictive power of lymphocyte subsets. Our results showed that the counts of lymphocyte subsets in the response group significantly increased, in contrast to a rapid decline in the non-response group. Simultaneously, we found that patients who received anti-PD-1 based immunotherapy had higher lymphocyte levels relative to chemotherapy alone. We also noted the significant differences in the lymphocytes counts between patients who received first-line and multiline treatments.

Lymphocytes, including three major subsets of T, B, and NK cells, are the main executors of the adaptive immune system and

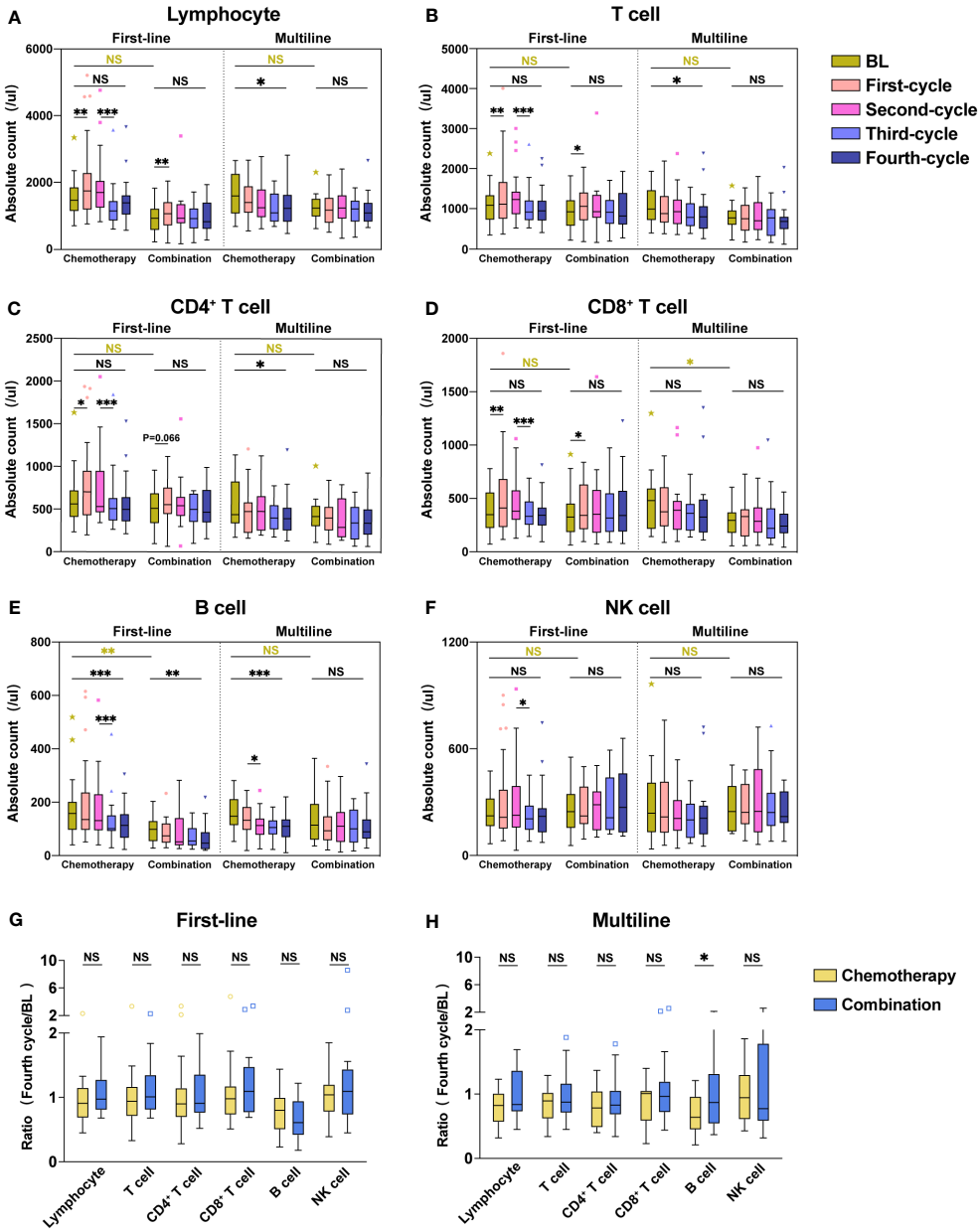

FIGURE 4
Combination immunotherapy improved absolute counts of lymphocyte subsets compared with chemotherapy alone. Absolute counts of Lymphocyte **(A)**, T cell **(B)**, $CD4^+$ T cell **(C)**, $CD8^+$ T cell **(D)**, B cell **(E)**, and NK cell **(F)** in the first-line group and multiline group during four consecutive treatment cycles were shown as boxplots. The ratios of each lymphocyte subset after four treatment cycles to baseline in the first-line **(G)** and multiline **(H)** patients. The chemotherapy and combination immunotherapy groups were shown, respectively. Within-group and between-group differences were analyzed using the paired Wilcoxon signed-rank test and Mann-Whitney U test, respectively. BL, Baseline; *, $P < 0.05$; **, $P < 0.01$; ***, $P < 0.001$; NS, not significant.

play vital roles in tumor control through surveillance and destruction (25). T cells, with the CD3 as the surface marker, are divided into helper T cells, marked by the CD4 molecule and cytotoxic T cells, marked by the CD8 molecule (26). $CD8^+$ T cells, the mainstay of adaptive immunity, can infiltrate tumor centers and directly target and kill tumor cells via cytotoxicity (27). Immunotherapy, especially chimeric antigen receptor T (CAR-T) cell therapy based on $CD8^+$ T cell, has shown excellent antitumor effects in many types of tumors owing to its targeting and durability (28–30). $CD4^+$ T cells are mainly considered as helper cells for the activation of $CD8^+$ T cells (31). They can also kill tumor cells directly or indirectly by secreting a variety of cytokines (32). A recent study has reported a new function of $CD4^+$ T cells for the first time, in which one specific subtype of $CD4^+$ T cells kills tumor cells that escape $CD8^+$ T cell attack (33). This suggests the potential to develop $CD4^+$ T cells as immunotherapy targets in the future, especially for the patients with cancer who have failed to respond to $CD8^+$ T cell therapy. B cells, with the CD19 as surface marker, mainly secrete antibodies against tumor-associated antigens and coactivate $CD8^+$ T cells in conjunction with $CD4^+$ T cells (34).

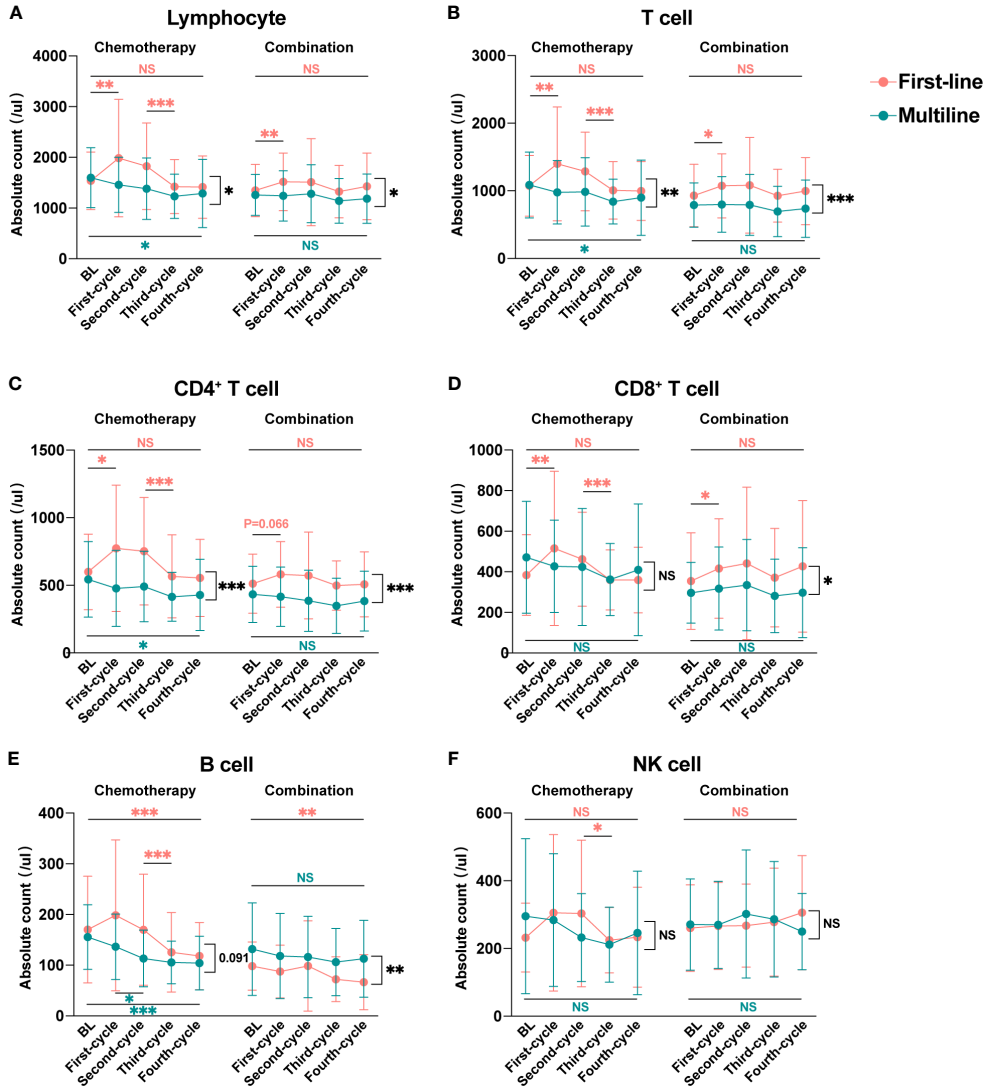

FIGURE 5
Dynamic changes in lymphocyte subsets during four treatment cycles in the first-line and multiline groups. Median absolute counts and interquartile ranges of Lymphocyte **(A)**, T cell **(B)**, $CD4^+$ T cell **(C)**, $CD8^+$ T cell **(D)**, B cell **(E)**, and NK cell **(F)** in the first-line group and multiline group during four consecutive treatment cycles were shown as folded line charts. The chemotherapy and combination immunotherapy groups were shown, respectively. Within-group differences and between-group differences were analyzed using the paired Wilcoxon signed-rank test and Mann-Whitney U test, respectively. BL, Baseline; *, $P < 0.05$; **, $P < 0.01$; ***, $P < 0.001$; NS, not significant.

However, studies have also reported that B cell infiltration in tumors is associated with poor prognosis (35, 36). NK cells are characterized by the surface molecule CD56. NK cells serve as the crucial first line of defense against tumors and pathogens (37). Their cytotoxic and immunomodulatory effects on the tumor microenvironment cannot be ignored (38). NK cell-based tumor immunotherapies have also been explored currently (39, 40). Lymphocytes, as multifunctional biomarkers, have been reported to be valuable for evaluating patient immunity and predicting outcomes (41–43). During chemotherapy, multiple substances released from tumor cells contribute to the activation and proliferation of lymphocytes, working together to kill tumors (44, 45). However, large numbers of inactive or "bystander" lymphocytes in the tumor immune microenvironment will compromise therapeutic efficacy (46). Thus, an assessment of the initial lymphocyte count merely may not accurately reflect the actual immune capacity. In this study, we respectively analyzed the dynamic changes in lymphocyte subsets in the peripheral blood of patients with NSCLC who received four consecutive cycles of chemotherapy or combination immunotherapy with ani-PD-1 antibody. We found the differences in lymphocyte subsets with different efficacies. Based on this, we propose that the ratios of lymphocyte absolute counts after the first chemotherapy or combination immunotherapy cycle to baseline are early and accurate predictors of efficacy.

The early prediction of clinical efficacy is an urgent problem for achieving precise and individualized treatment (47, 48). Early identification of patients with poor outcomes helps adjust treatment plans in a timely manner to improve treatment effects in the clinic, which is of great significance in prolonging the

progression-free survival and overall survival of cancer patients. In our study, the response and non-response groups, which showed no significant differences at baseline, exhibited extremely different performances after the first treatment. In contrast to the rapid decline observed in the non-response group, the absolute counts of lymphocyte subsets in the response group exhibited a marked increase. After four cycles of chemotherapy, all lymphocyte subsets in the non-response group were significantly reduced. ROC curve analysis showed that the ratios of absolute lymphocyte count after the first treatment cycle to baseline were good predictors of four-cycle treatment efficacy, except for NK cell. In addition, the combination of T cell and B cell or the combination of $CD8^+$ T cell and B cell had a better predictive power which provided a reference for timely identification of insensitive patients and the early prediction of outcomes in clinical practice. Although the counts of lymphocyte subsets at baseline in the non-response group were similar to those in the response group, there may be a higher proportion of anergic or bystander lymphocytes or even severe myelosuppression and an immunosuppressive microenvironment preventing lymphocyte activation and proliferation, which affects their ability towards tumor control (49). Our study highlights the importance of the dynamic detection of lymphocyte subsets in patients with cancer. Assessment of the initial immune environment alone cannot accurately predict treatment outcomes, and a dynamic assessment of the lymphocyte response during treatment may better represent immune function and predict the efficacy more reasonably.

In the response group, the absolute counts of each lymphocyte subset in the chemotherapy group first increased and then decreased, while in the combination group, they were maintained at a high level. We propose that chemotherapy combined with immunotherapy has a protective effect on lymphocytes and ameliorates the lymphopenia caused by prolonged chemotherapy. By analyzing all cases, we found that the persistent combination of anti-PD-1 therapy improved lymphocyte levels in patients receiving first-line or multiline therapy. This study provides a theoretical basis for early combination immunotherapy. On the one hand, lymphocytes in the early chemotherapy stage are in a state of massive proliferation, and high levels of lymphocytes allow anti-PD-1 antibody to work more effectively. On the other hand, combination immunotherapy is able to increase the count of lymphocytes and improve the activity of the tumor immune environment. Combined immunotherapy can provide tumor patients with greater benefits, and chemotherapy in combination with anti-PD-1/PD-L1 therapy has been included in Grade I recommendations for certain NSCLCs (50).

Finally, we found that lymphocyte performance in the multiline treatment group was unsatisfactory. Lymphocyte, especially T cell, were significantly reduced in the multiline group after reaccepting chemotherapy. Persistent lymphocyte count decrease may partly explain their poor efficacy in comparison to the favorable lymphocyte response in the first-line treatment group. This also indicates that lymphopenia may be involved in the resistance to tumor therapy. Severe myelosuppression after multiple chemotherapy treatments leads to a hypoactive immune environment, in which vulnerable lymphocytes are highly susceptible to chemotherapy toxicity, resulting in a rapid decrease in their numbers without a timely replenishment. Therefore, patients with low lymphoid levels or multiple chemotherapy treatments are recommended to be treated with immunostimulants, such as thymopeptides or placental polypeptides. Regularly evaluating the immunity level and improving immunity can collaborate with oncological treatments to achieve greater benefits for the patients. Of course, the abnormal performances of B cell after first-line and multiline treatments have also attracted attention. B cell, the smallest lymphocyte subset among three major subsets, accounts for approximately 10% of all lymphocytes (51). Both detection errors and individual differences significantly impacted on the analysis results. Therefore, the abnormality observed in this study was due to errors or unexplored mechanisms requiring multicenter large-sample data or scientific experiments for further verification.

However, this study has some limitations. Only 81 cases were included in this retrospective study. The small sample size was due to the impact of COVID-19 in recent years, which made it difficult to collect complete data covering four consecutive cycles. Factors, such as local treatment and loss to follow-up, influenced data collection. Besides, only the absolute counts of lymphocyte subsets in patients were analyzed in this study. The functions of lymphocytes and other complex tumor microenvironment components have not been considered. In the future, we plan to collect more cases and conduct prospective studies. Long-term dynamic monitoring of lymphocyte subsets in chemotherapy patients, not just limited to four cycles, will allows for a better prediction of efficacy. Importantly, in the future, we expect to build integrated models that combine immune, tumor, and personal characteristics to predict treatment efficacy more accurately.

Currently, the detection of absolute lymphocyte subset counts is largely limited to infectious and immunological diseases in practical clinic application. With the development of the immune surveillance theory, the efficacy of immunotherapy is directly affected by lymphocytes, suggesting a great application space in the field of cancer. Our study provides a reference for the prediction of tumor efficacy and confirms that this simple and easy clinical test can evaluate the real immune status, which is valuable for the timely application of immunostimulants or early replacement of insensitive chemotherapy regimens in clinical treatment. With the accumulation of relevant evidence, the detection of lymphocyte subsets will surely play an important role in the field of oncology. It is reasonable to expect that the rapid and effective detection of peripheral blood lymphocyte subsets will contribute to non-invasive early screening and accurate prognosis of cancer. The realization of this goal is of great significance for the survival of patients with cancer. However, more comprehensive clinical data are yet to be generated by large-scale clinical testing.

5 Conclusions

In this study, we identified an association between lymphocyte subsets and the prognosis of patients with NSCLC, which may contribute to the early prediction of the efficacy during

chemotherapy or combination immunotherapy. Combination anti-PD-1 therapy protected the immune microenvironment and increased the lymphocyte counts. Patients receiving multiline treatment showed a rapid decrease in lymphocytes, which may be related to the poor efficacy. In summary, dynamic surveillance of lymphocyte subsets allows for the effective assessment of the immune status and the prediction of outcomes in patients with NSCLC.

Data availability statement

The original contributions presented in the study are included in the article/supplementary material. Further inquiries can be directed to the corresponding authors.

Ethics statement

The studies involving humans were approved by medical ethics committee of the First Affiliated Hospital of Zhengzhou University. The studies were conducted in accordance with the local legislation and institutional requirements. Written informed consent for participation was not required from the participants or the participants' legal guardians/next of kin in accordance with the national legislation and institutional requirements.

Author contributions

SZ: Data curation, Formal analysis, Writing – original draft. WW: Data curation, Formal analysis, Writing – original draft. GQ: Funding acquisition, Investigation, Writing – review & editing. TL: Supervision, Writing – review & editing. LY: Supervision, Writing – review & editing. YZ: Supervision, Writing – review & editing.

Funding

The author(s) declare financial support was received for the research, authorship, and/or publication of this article. This work was supported by the Young Scientists Fund of the National Natural Science Foundation of China (Grant No. 82103427).

Conflict of interest

The authors declare that the research was conducted in the absence of any commercial or financial relationships that could be construed as a potential conflict of interest.

The reviewer LZ declared a shared parent affiliation with the authors, and the reviewer XR declared a past co-authorship with the author YZ at the time of the review.

The author(s) declared that they were an editorial board member of Frontiers, at the time of submission. This had no impact on the peer review process and the final decision.

Publisher's note

References

1. Sung H, Ferlay J, Siegel RL, Laversanne M, Soerjomataram I, Jemal A, et al. Global cancer statistics 2020: GLOBOCAN estimates of incidence and mortality worldwide for 36 cancers in 185 countries. *CA Cancer J Clin*. (2021) 71:209–49. doi: 10.3322/caac.21660

2. Duma N, Santana-Davila R, Molina JR. Non-small cell lung cancer: epidemiology, screening, diagnosis, and treatment. *Mayo Clin Proc*. (2019) 94:1623–40. doi: 10.1016/j.mayocp.2019.01.013

3. Brahmer JR, Lee JS, Ciuleanu TE, Bernabe Caro R, Nishio M, Urban L, et al. Five-year survival outcomes with nivolumab plus ipilimumab versus chemotherapy as first-line treatment for metastatic non-small-cell lung cancer in CheckMate 227. *J Clin Oncol*. (2023) 41:1200–12. doi: 10.1200/JCO.22.01503

4. Higgins KA, Puri S, Gray JE. Systemic and radiation therapy approaches for locally advanced non-small-cell lung cancer. *J Clin Oncol*. (2022) 40:576–85. doi: 10.1200/JCO.21.01707

5. Tang L, Huang Z, Mei H, Hu Y. Immunotherapy in hematologic Malignancies: achievements, challenges and future prospects. *Signal Transduct Target Ther*. (2023) 8:306. doi: 10.1038/s41392-023-01521-5

6. Zhu S, Zhang T, Zheng L, Liu H, Song W, Liu D, et al. Combination strategies to maximize the benefits of cancer immunotherapy. *J Hematol Oncol*. (2021) 14:156. doi: 10.1186/s13045-021-01164-5

7. Zhang L, Lin W, Tan F, Li N, Xue Q, Gao S, et al. Sintilimab for the treatment of non-small cell lung cancer. *biomark Res*. (2022) 10:23. doi: 10.1186/s40364-022-00363-7

8. Dagher OK, Schwab RD, Brookens SK, Posey AD Jr. Advances in cancer immunotherapies. *Cell*. (2023) 186:1814– e1. doi: 10.1016/j.cell.2023.02.039

9. Cao W, Ma X, Fischer JV, Sun C, Kong B, Zhang Q. Immunotherapy in endometrial cancer: rationale, practice and perspectives. *biomark Res*. (2021) 9:49. doi: 10.1186/s40364-021-00301-z

10. Huang MY, Jiang XM, Wang BL, Sun Y, Lu JJ. Combination therapy with PD-1/PD-L1 blockade in non-small cell lung cancer: strategies and mechanisms. *Pharmacol Ther*. (2021) 219:107694. doi: 10.1016/j.pharmthera.2020.107694

11. Ho WJ, Wood LD. Opposing roles of the immune system in tumors. *Science*. (2021) 373:1306–7. doi: 10.1126/science.abl5376

12. Pan Y, Fu Y, Zeng Y, Liu X, Peng Y, Hu C, et al. The key to immunotherapy: how to choose better therapeutic biomarkers for patients with non-small cell lung cancer. *biomark Res*. (2022) 10:9. doi: 10.1186/s40364-022-00355-7

13. Bedoui S, Gebhardt T, Gasteiger G, Kastenmuller W. Parallels and differences between innate and adaptive lymphocytes. *Nat Immunol*. (2016) 17:490–4. doi: 10.1038/ni.3432

14. Jorgensen N, Laenkholm AV, Saekmose SG, Hansen LB, Hviid TVF. Peripheral blood immune markers in breast cancer: Differences in regulatory T cell abundance are related to clinical parameters. *Clin Immunol*. (2021) 232:108847. doi: 10.1016/j.clim.2021.108847

15. Alessi JV, Ricciuti B, Alden SL, Bertram AA, Lin JJ, Sakhi M, et al. Low peripheral blood derived neutrophil-to-lymphocyte ratio (dNLR) is associated with increased tumor T-cell infiltration and favorable outcomes to first-line pembrolizumab in non-small cell lung cancer. *J Immunother Cancer*. (2021) 9:11. doi: 10.1136/jitc-2021-003536

16. Qin G, Liu J, Lian J, Zhang H, Lei Q, Yang H, et al. PMN-MDSCs-induced accumulation of CD8+CD39+ T cells predicts the efficacy of chemotherapy in

esophageal squamous cell carcinoma. *Clin Transl Med*. (2020) 10:e232. doi: 10.1002/ctm2.232

17. Pirker R. Conquering lung cancer: current status and prospects for the future. *Pulmonology*. (2020) 26:283–90. doi: 10.1016/j.pulmoe.2020.02.005

18. Lv J, Wei Y, Yin JH, Chen YP, Zhou GQ, Wei C, et al. The tumor immune microenvironment of nasopharyngeal carcinoma after gemcitabine plus cisplatin treatment. *Nat Med*. (2023) 29:1424–36. doi: 10.1038/s41591-023-02369-6

19. Velardi E, Tsai JJ, van den Brink MRM. T cell regeneration after immunological injury. *Nat Rev Immunol*. (2021) 21:277–91. doi: 10.1038/s41577-020-00457-z

20. Khan SM, Desai R, Coxon A, Livingstone A, Dunn GP, Petti A, et al. Impact of CD4 T cells on intratumoral CD8 T-cell exhaustion and responsiveness to PD-1 blockade therapy in mouse brain tumors. *J Immunother Cancer*. (2022) 10:12. doi: 10.1136/jitc-2022-005293

21. Ottonello S, Genova C, Cossu I, Fontana V, Rijavec E, Rossi G, et al. Association between response to nivolumab treatment and peripheral blood lymphocyte subsets in patients with non-small cell lung cancer. *Front Immunol*. (2020) 11:125. doi: 10.3389/fimmu.2020.00125

22. Mao F, Yang C, Luo W, Wang Y, Xie J, Wang H. Peripheral blood lymphocyte subsets are associated with the clinical outcomes of prostate cancer patients. *Int Immunopharmacol*. (2022) 113:109287. doi: 10.1016/j.intimp.2022.109287

23. Li H, Zu X, Hu J, Xiao Z, Cai Z, Gao N, et al. Cuproptosis depicts tumor microenvironment phenotypes and predicts precision immunotherapy and prognosis in bladder carcinoma. *Front Immunol*. (2022) 13:964393. doi: 10.3389/fimmu.2022.964393

24. Qin G, Liu S, Liu J, Hu H, Yang L, Zhao Q, et al. Overcoming resistance to immunotherapy by targeting GPR84 in myeloid-derived suppressor cells. *Signal Transduct Target Ther*. (2023) 8:164. doi: 10.1038/s41392-023-01388-6

25. Muenst S, Laubli H, Soysal SD, Zippelius A, Tzankov A, Hoeller S. The immune system and cancer evasion strategies: therapeutic concepts. *J Intern Med*. (2016) 279:541–62. doi: 10.1111/joim.12470

26. Sun L, Su Y, Jiao A, Wang X, Zhang B. T cells in health and disease. *Signal Transduct Target Ther*. (2023) 8:235. doi: 10.1038/s41392-023-01471-y

27. Li X, Gruosso T, Zuo D, Omeroglu A, Meterissian S, Guiot MC, et al. Infiltration of CD8(+) T cells into tumor cell clusters in triple-negative breast cancer. *Proc Natl Acad Sci U S A*. (2019) 116:3678–87. doi: 10.1073/pnas.1817652116

28. Cappell KM, Kochenderfer JN. Long-term outcomes following CAR T cell therapy: what we know so far. *Nat Rev Clin Oncol*. (2023) 20:359–71. doi: 10.1038/s41571-023-00754-1

29. Liu Y, An L, Huang R, Xiong J, Yang H, Wang X, et al. Strategies to enhance CAR-T persistence. *biomark Res*. (2022) 10:86. doi: 10.1186/s40364-022-00434-9

30. Li F, Zhang Z, Xuan Y, Zhang D, Liu J, Li A, et al. PD-1 abrogates the prolonged persistence of CD8(+) CAR-T cells with 4-1BB co-stimulation. *Signal Transduct Target Ther*. (2020) 5:164. doi: 10.1038/s41392-020-00277-6

31. Zander R, Kasmani MY, Chen Y, Topchyan P, Shen J, Zheng S, et al. Tfh-cell-derived interleukin 21 sustains effector CD8(+) T cell responses during chronic viral infection. *Immunity*. (2022) 55:475–93 e5. doi: 10.1016/j.immuni.2022.01.018

32. Nelson MH, Knochelmann HM, Bailey SR, Huff LW, Bowers JS, Majchrzak-Kuligowska K, et al. Identification of human CD4(+) T cell populations with distinct antitumor activity. *Sci Adv*. (2020) 6:27. doi: 10.1126/sciadv.aba7443

33. Kruse B, Buzzai AC, Shridhar N, Braun AD, Gellert S, Knauth K, et al. CD4(+) T cell-induced inflammatory cell death controls immune-evasive tumours. *Nature*. (2023) 618:1033–40. doi: 10.1038/s41586-023-06199-x

34. Sharonov GV, Serebrovskaya EO, Yuzhakova DV, Britanova OV, Chudakov DM. B cells, plasma cells and antibody repertoires in the tumour microenvironment. *Nat Rev Immunol*. (2020) 20:294–307. doi: 10.1038/s41577-019-0257-x

35. Nelson MA, Ngamcherdtrakul W, Luoh SW, Yantasee W. Prognostic and therapeutic role of tumor-infiltrating lymphocyte subtypes in breast cancer. *Cancer Metastasis Rev*. (2021) 40:519–36. doi: 10.1007/s10555-021-09968-0

36. Gu Y, Liu Y, Fu L, Zhai L, Zhu J, Han Y, et al. Tumor-educated B cells selectively promote breast cancer lymph node metastasis by HSPA4-targeting IgG. *Nat Med*. (2019) 25:312–22. doi: 10.1038/s41591-018-0309-y

37. Ran GH, Lin YQ, Tian L, Zhang T, Yan DM, Yu JH, et al. Natural killer cell homing and trafficking in tissues and tumors: from biology to application. *Signal Transduct Target Ther*. (2022) 7:205. doi: 10.1038/s41392-022-01058-z

38. Woan KV, Miller JS. Harnessing natural killer cell antitumor immunity: from the bench to bedside. *Cancer Immunol Res*. (2019) 7:1742–7. doi: 10.1158/2326-6066.CIR-19-0404

39. Liu S, Galat V, Galat Y, Lee YKA, Wainwright D, Wu J. NK cell-based cancer immunotherapy: from basic biology to clinical development. *J Hematol Oncol*. (2021) 14:7. doi: 10.1186/s13045-020-01014-w

40. Bald T, Krummel MF, Smyth MJ, Barry KC. The NK cell-cancer cycle: advances and new challenges in NK cell-based immunotherapies. *Nat Immunol*. (2020) 21:835–47. doi: 10.1038/s41590-020-0728-z

41. Yan Y, Wang X, Liu C, Jia J. Association of lymphocyte subsets with efficacy and prognosis of immune checkpoint inhibitor therapy in advanced non-small cell lung carcinoma: a retrospective study. *BMC Pulm Med*. (2022) 22:166. doi: 10.1186/s12890-022-01951-x

42. Xu L, Zou C, Zhang S, Chu TSM, Zhang Y, Chen W, et al. Reshaping the systemic tumor immune environment (STIE) and tumor immune microenvironment (TIME) to enhance immunotherapy efficacy in solid tumors. *J Hematol Oncol*. (2022) 15:87. doi: 10.1186/s13045-022-01307-2

43. Valero C, Lee M, Hoen D, Weiss K, Kelly DW, Adusumilli PS, et al. Pretreatment neutrophil-to-lymphocyte ratio and mutational burden as biomarkers of tumor response to immune checkpoint inhibitors. *Nat Commun*. (2021) 12:729. doi: 10.1038/s41467-021-20935-9

44. Marcus A, Mao AJ, Lensink-Vasan M, Wang L, Vance RE, Raulet DH. Tumor-derived cGAMP triggers a STING-mediated interferon response in non-tumor cells to activate the NK cell response. *Immunity*. (2018) 49:754–63 e4. doi: 10.1016/j.immuni.2018.09.016

45. Li K, Gong Y, Qiu D, Tang H, Zhang J, Yuan Z, et al. Hyperbaric oxygen facilitates teniposide-induced cGAS-STING activation to enhance the antitumor efficacy of PD-1 antibody in HCC. *J Immunother Cancer*. (2022) 10:8. doi: 10.1136/jitc-2021-004006

46. Meier SL, Satpathy AT, Wells DK. Bystander T cells in cancer immunology and therapy. *Nat Cancer*. (2022) 3:143–55. doi: 10.1038/s43018-022-00335-8

47. Li W, Liu JB, Hou LK, Yu F, Zhang J, Wu W, et al. Liquid biopsy in lung cancer: significance in diagnostics, prediction, and treatment monitoring. *Mol Cancer*. (2022) 21:25. doi: 10.1186/s12943-022-01505-z

48. Mino-Kenudson M, Schalper K, Cooper W, Dacic S, Hirsch FR, Jain D, et al. Predictive biomarkers for immunotherapy in lung cancer: perspective from the international association for the study of lung cancer pathology committee. *J Thorac Oncol*. (2022) 17:1335–54. doi: 10.1016/j.jtho.2022.09.109

49. Norman H, Lee KT, Stearns V, Alcorn SR, Mangini NS. Incidence and severity of myelosuppression with palbociclib after palliative bone radiation in advanced breast cancer: A single center experience and review of literature. *Clin Breast Cancer*. (2022) 22:e65–73. doi: 10.1016/j.clbc.2021.07.013

50. Lin A, Wei T, Meng H, Luo P, Zhang J. Role of the dynamic tumor microenvironment in controversies regarding immune checkpoint inhibitors for the treatment of non-small cell lung cancer (NSCLC) with EGFR mutations. *Mol Cancer*. (2019) 18:139. doi: 10.1186/s12943-019-1062-7

51. Carsetti R, Terreri S, Conti MG, Fernandez Salinas A, Corrente F, Capponi C, et al. Comprehensive phenotyping of human peripheral blood B lymphocytes in healthy conditions. *Cytometry A*. (2022) 101:131–9. doi: 10.1002/cyto.a.24507

frontiers | Frontiers in Immunology

TYPE Original Research
PUBLISHED 14 March 2024
DOI 10.3389/fimmu.2024.1363568

OPEN ACCESS

EDITED BY
Paulo Rodrigues-Santos,
University of Coimbra, Portugal

REVIEWED BY
Yongfeng He,
Cornell University, United States
Junjie Hang,
Chinese Academy of Medical Sciences and Peking Union Medical College, China
Kangchun Wang,
Southeast University, China

*CORRESPONDENCE
Takuya Yamamoto
yamamotot2@nibiohn.go.jp

†These authors have contributed equally to this work

RECEIVED 31 December 2023
ACCEPTED 22 February 2024
PUBLISHED 14 March 2024

CITATION
Murakami H, Takahama S, Akita H, Kobayashi S, Masuta Y, Nagatsuka Y, Higashiguchi M, Tomokuni A, Yoshida K, Takahashi H, Doki Y, Eguchi H, Matsuura N and Yamamoto T (2024) Circulating tumor-associated antigen-specific IFNγ$^+$4-1BB$^+$ CD8$^+$ T cells as peripheral biomarkers of treatment outcomes in patients with pancreatic cancer.
Front. Immunol. 15:1363568.
doi: 10.3389/fimmu.2024.1363568

Circulating tumor-associated antigen-specific IFNγ$^+$4-1BB$^+$ CD8$^+$ T cells as peripheral biomarkers of treatment outcomes in patients with pancreatic cancer

Hirotomo Murakami[1,2†], Shokichi Takahama[1†], Hirofumi Akita[1,3,4†], Shogo Kobayashi[2], Yuji Masuta[1], Yuta Nagatsuka[1,2], Masaya Higashiguchi[1,2], Akira Tomokuni[5], Keiichi Yoshida[4], Hidenori Takahashi[2], Yuichiro Doki[2], Hidetoshi Eguchi[2], Nariaki Matsuura[3] and Takuya Yamamoto[1,4,6,7*]

[1]Laboratory of Precision Immunology, Center for Intractable Diseases and ImmunoGenomics, National Institutes of Biomedical Innovation, Health and Nutrition, Osaka, Japan, [2]Department of Gastroenterological Surgery, Graduate School of Medicine, Osaka University, Osaka, Japan, [3]Department of Gastroenterological Surgery, Osaka International Cancer Institute, Osaka, Japan, [4]Next-Generation Precision Medicine Research Center, Osaka International Cancer Institute, Osaka, Japan, [5]Department of Gastroenterological Surgery, Osaka General Medical Center, Osaka, Japan, [6]Laboratory of Aging and Immune Regulation, Graduate School of Pharmaceutical Sciences, Osaka University, Osaka, Japan, [7]Department of Virology and Immunology, Graduate School of Medicine, Osaka University, Osaka, Japan

CD8$^+$ T cells affect the outcomes of pancreatic ductal adenocarcinoma (PDAC). Using tissue samples at pre-treatment to monitor the immune response is challenging, while blood samples are beneficial in overcoming this limitation. In this study, we measured peripheral antigen-specific CD8$^+$ T cell responses against four different tumor-associated antigens (TAAs) in PDAC using flow cytometry and investigated their relationships with clinical features. We analyzed the optimal timing within the treatment course for effective immune checkpoint inhibition *in vitro*. We demonstrated that the frequency of TAA-specific IFNγ$^+$4-1BB$^+$ CD8$^+$ T cells was correlated with a fold reduction in CA19-9 before and after neoadjuvant therapy. Moreover, patients with TAA-specific IFNγ$^+$4-1BB$^+$ CD8$^+$ T cells after surgery exhibited a significantly improved disease-free survival. Anti-PD-1 treatment *in vitro* increased the frequency of TAA-specific IFNγ$^+$4-1BB$^+$ CD8$^+$ T cells before neoadjuvant therapy in patients, suggesting the importance of the timing of anti-PD-1 inhibition during the treatment regimen. Our results indicate that peripheral immunophenotyping,

combined with highly sensitive identification of TAA-specific responses *in vitro* as well as detailed CD8$^+$ T cell subset profiling via *ex vivo* analysis, may serve as peripheral biomarkers to predict treatment outcomes and therapeutic efficacy of immunotherapy plus neoadjuvant chemotherapy.

KEYWORDS

pancreatic cancer, tumor-associated antigen-specific CD8 + T cells, PBMC, prognostic marker, immune checkpoint inhibition

1 Introduction

Pancreatic ductal adenocarcinoma (PDAC) has a poor prognosis, with a 5-year survival rate of approximately 12% (1). Resection is generally feasible in only 20% of PDAC cases (2), and the recurrence rate remains high (3). Therefore, multidisciplinary treatment with adjuvant therapies is employed to improve patient outcomes (4).

Cytotoxic chemotherapy and radiation therapy, which are commonly used for PDAC, affect immune cells, including CD8$^+$ T cells. For example, gemcitabine administration increases the peripheral blood and peritumoral CD8/CD4 ratios in a mouse model of liver metastasis and peritumoral dissemination (5). Furthermore, in patients with stage III–IV PDAC, elevated exhausted peripheral blood mononuclear cell (PBMC) CD8$^+$ T cells are associated with a poorer prognosis post-chemotherapy (6). Therefore, the characteristics of PBMC CD8$^+$ T cells may vary depending on the pathogenesis and treatment of PDAC. However, it remains unclear whether tumor-associated antigen (TAA)-specific CD8$^+$ T cells influence chemotherapy or surgery outcomes.

Recently, immunotherapy, including immune checkpoint inhibitors (ICIs), has been applied to the treatment of various cancers (7–11). However, its benefits for patients with PDAC are limited, as evidenced by the low objective response rates (3.1%) (12). The success of ICIs largely depends on the tumor microenvironment (TME); however, the use of tumor tissue biopsy samples before ICI initiation is challenging for monitoring the immunological condition of the TME. Thus, blood surrogate markers are valuable for assessing the anti-tumor efficacy of immunotherapeutic approaches. In lung cancer, correlations between the cytotoxic activity of tumor-infiltrating lymphocytes (TILs) and that of peripheral blood mononuclear cell (PBMC)-derived T cells have been reported, as have correlations between the cytotoxic activity of TILs and the percentage of PBMC-derived effector memory re-expressing CD45RA CD8$^+$ T cells. These findings suggest that certain phenotypes of peripheral blood CD8$^+$ T cells may reflect those of TILs (13).

In the present study, we examined the potential utility of antigen-specific CD8$^+$ T cell responses against TAAs detected in the blood of patients with PDAC. By analyzing PBMCs, we investigated the relationship between TAA-specific CD8$^+$ T cell responses and cytotoxic chemotherapy in patients with PDAC. Additionally, we evaluated the efficacy of immunotherapy by monitoring the TAA-specific responses of CD8$^+$ T cells. We also analyzed immune response enhancement by ICI *in vitro* to determine the optimal timing of treatment to maximize the efficacy of neoadjuvant chemotherapy.

2 Materials and methods

2.1 Patient and sample collection

Patients with pancreatic cancer were recruited from the Osaka University Hospital (Osaka, Japan) and Osaka International Cancer Institute (Osaka, Japan) from September 2019 to December 2021. All patients received neoadjuvant chemotherapy or chemoradiotherapy with the following regimens: gemcitabine + nab-paclitaxcel (n=9), gemcitabine + nab-paclitaxcel + radiation (n=7), gemcitabine + S-1 (n=20), gemcitabine + S-1 + radiation (n=13), FOLFIRINOX (n=1), gemcitabine + radiation (n=1), and multiple regimens (n=6). This study was approved by the local institutional ethics committees of Osaka University, Osaka International Cancer Center, and the National Institutes of Biomedical Innovation, Health, and Nutrition, Osaka, Japan, and was conducted in accordance with the Declaration of Helsinki (1975). All participants provided written informed consent. PBMCs were isolated from patients with PDAC within 6 h of blood sampling using BD Vacutainer CPT (BD Biosciences, Franklin Lakes, NJ, USA). PBMCs were cryopreserved in fetal bovine serum (FBS) containing 10% dimethyl sulfoxide (DMSO) and stored in liquid nitrogen vapor until analysis.

2.2 Pancreatic cancer cell lines, quantitative reverse transcription polymerase chain reaction, and cancer cell line encyclopedia analysis

Pancreatic cancer cell lines were cultured in an appropriate culture medium supplemented with 10% FBS and 1% penicillin–streptomycin (Gibco, Thermo Fisher Scientific, Waltham, MA,

USA). Dulbecco's modified Eagle medium (Sigma-Aldrich, St. Louis, MO, USA) was used for BxPC3, MiaPaCa2, Panc1, and PSN1 cells, and Eagle's minimal essential medium (Sigma-Aldrich) was used for SUIT-2 cells. TYPK1 cells were cultured in a 1:1 mixture of DMEM and Ham's F-12 medium supplemented with 5% FBS and 1% penicillin–streptomycin. Cells were cultured at 37°C and 5% CO_2 until reaching 80% confluency, at which point mRNA was extracted using an RNeasy mini kit (Qiagen, Hilden, Germany).

qRT-PCR was performed using SuperScript III Master Mix (Invitrogen, Thermo Fisher Scientific), RT enzyme, ROX, and TaqMan probes for candidate genes (*CEACAM5*, Hs00944025_m1; *CTAG1*, Hs00265824_m1; *DCT*, Hs01098278_m1; *MUC1*, Hs00159357_m1; *Telomerase reverse transcriptase (TERT)*, Hs00972656_m1; and *WT1*, Hs00240913_m1). The following thermal cycling conditions were used: 30 min at 45°C, 5 min at 95°C, 50 cycles of 1 s at 95°C, and 60 s at 50°C. qRT-PCR was replicated three times.

The CCLE (14) was used to evaluate the mRNA expression of six TAAs (*CEACAM5*, *NY-ESO-1* [*CTAG1A*], *TRP2* [*DCT*], *MUC1*, *TERT*, and *WT1*) in the pancreatic cancer cell lines. The normalized transcripts per kilobase million (TPM) dataset were downloaded from the Cancer Dependency Portal (DepMap) on 2022.12.14. The original log2 (TPM+1) values were plotted as a heatmap without scaling.

2.3 Overlapping peptides

Overlapping peptides covering four TAAs (all from JPT Peptide Technologies, Berlin, Germany) were used in this study: PepMix™ Human CEA (#PM-CEA) for CEACAM5; PepMix™ Human Mutin-1 (#PM-MUC1) for MUC1; PepMix™ Human TERT (#PM-TERT) for TERT; and PepMix™ Human WT1/WT33 (#PM-WT1) for WT1. The peptides consisted of 15 amino acids spanning the complete amino acid sequence of the indicated protein antigen, with 11 overlapping amino acids between adjacent peptides (Supplementary Table 1).

2.4 Amplification of TAA-specific $CD8^+$ T cells by *in vitro* culture

TAA-specific $CD8^+$ T cells were enriched from the PBMCs of patients with PDAC. Briefly, frozen PBMCs were thawed and treated with 1 mL of 50 unit/mL of benzonase (Merck, Rahway, NJ, USA) in R10 medium for 2 h at 37°C in 5% CO_2. Subsequently, 20% of the PBMCs (1.1×10^5 [0.2×10^5 – 3.5×10^5] cells) were pulsed with 2 μg/mL of each of the overlapping TAA peptides (CEA, MUC1, TERT, and WT1) for 1 h at 37°C. After washing, the pulsed PBMCs were co-cultured with the remaining 80% un-pulsed PBMCs in R10 in the presence of 20 U/mL of recombinant interleukin (IL)-2 (R&D Systems, Minneapolis, MN, USA) for 10 days; the medium was changed on days 4 and 7. For the ICI experiments, 1 mg/mL of anti-PD-1 (Cat# 621604, RRID: AB_2820105; BioLegend, San Diego, CA, USA), anti-TIGIT (Cat# 16-9500-82, RRID: AB_10718831; Thermo Fisher Scientific), or mouse IgG1 isotype control antibody (Cat# 400102, RRID: AB_2891079; BioLegend) was added to the culture medium at the beginning of the culture, and half of the medium was replaced with a culture medium without antibodies on days 4 and 7.

2.5 Flow cytometric detection of TAA-specific $CD8^+$ T cell responses

Ten days after culture, amplified cells were stimulated with 2 μg/mL of the TAA-derived overlapping peptides (CEA, MUC1, TERT, and WT1) for 30 min at 37°C with CD107A antibody (BD Biosciences). After 30 min of stimulation, 1 μL/mL BD GolgiPlug (containing Brefeldin A) (BD Biosciences) and 0.7 μL/mL of BD GolgiStop (containing Monensin) (BD Biosciences) were added to the media, and the cells were cultured for another 5.5 h. After incubation, the cells were washed with phosphate-buffered saline (PBS) and stained using a Live/Dead Fixable Aqua Dead Cell Stain Kit (L34957; Thermo Fisher Scientific) at 18-25°C for 5 min. Subsequently, the samples were probed with antibodies (Supplementary Table 2A) against cell surface markers for 15 min at 18-25°C. After washing, the cells were thoroughly resuspended in 200 μL BD Cytofix/Cytoperm solution per well and incubated for 20 min at 18-25°C. The cells were washed twice with BD Perm/Wash buffer and probed with intracellular staining antibodies for 25 min at 18-25°C. After staining, the cells were washed twice with BD Perm/Wash buffer and fixed with 1% paraformaldehyde. The data were collected using FACSymphony A5 (BD Biosciences).

2.6 HLA typing and analysis

Cryopreserved PBMCs were thawed, and genomic DNA was extracted from a portion of cells (approximately 100,000 cells) using a QIAamp DNA mini kit (Qiagen) and stored at −30°C until use. Isolated genomic DNA was used as a template to prepare cDNA libraries for HLA typing using the commercially available kit AlloSeq™ Tx 17.1 (CareDx) or WAKFlow® HLA DNA Typing (Wakunaga Pharmaceutical Co. Ltd., Osaka, Japan). The combination of each HLA was visualized using the "*circlize*" package (version 0.4.15) in the R software language (version 4.2.1). The frequency of HLA-A types among the donors was calculated based on the cumulative total number of alleles.

2.7 *Ex vivo* flow cytometry profiling of bulk $CD8^+$ T cells

Cryopreserved PBMCs were thawed, washed with PBS, and stained with Fixable Viable Stain UV440 (BD Biosciences) at 18-25°C for 5 min. CC-chemokine receptor 7 (CCR7) was stained at 37°C for 10 min and probed using antibodies against the remaining markers (Supplementary Table 2B) at 18-25°C for 15 min. After washing, the cells were thoroughly resuspended in 500 μL Fix/Perm solution per tube and incubated for 40 min at 4°C. The cells were washed twice with BD Perm/Wash solution and probed with anti-Ki67 antibodies for 40 min at 4°C. After staining, the cells were

washed twice with BD Perm/Wash solution and fixed with 1% paraformaldehyde, and the data were collected using FACSymphony A5 (BD Biosciences).

2.8 Flow cytometry data analysis

Flow cytometry FCS files were analyzed using FlowJo software (version 10.8.1; RRID: SCR_008520; BD Biosciences). The gating setting for settings for each population are described in result section and Figures. TAA-specific $CD8^+$ T cell responses were determined by subtracting the value obtained by peptide-free stimulation (DMSO; background) from that obtained by TAA stimulation. After background subtraction, values less than 0.01% were considered negative (no response). For the $IFN\gamma^+4\text{-}1BB^+$ criteria, values greater than 0.01% after background subtraction corresponded with responders, while those with values less than 0.01% corresponded with non-responders. For the $IFN\gamma^+$ and/or $4\text{-}1BB^+$ criteria, if the sum of the values after the background subtraction of $IFN\gamma^+4\text{-}1BB^+$, $IFN\gamma^+4\text{-}1BB^-$, and $IFN\gamma^-4\text{-}1BB^+$ was greater than 0.03%, it corresponded with a responder, while if it was less than 0.03%, it corresponded with a non-responder. For the $IFN\gamma^+$ and $4\text{-}1BB^+$ criteria, if the sum of the values after the background subtraction of two gates in each marker positive cells was greater than 0.02%, it corresponded with a responder, while if it was less than 0.02%, it corresponded with a non-responder.

2.9 Statistical analyses

Statistical analyses were performed using R/Bioconductor (R version 4.2.1) or GraphPad Prism (version 9.0.0; GraphPad Software, RRID: SCR_002798). Experiments and data analysis were performed by individuals blinded to the collection of blood samples and clinical information. For the HLA analysis, statistical significance of all combinations of four gating sets in each HLA type were obtained using Fisher's exact test, and are displayed in tile format.

3 Results

3.1 Selection of specific TAAs in pancreatic cancer cells

To detect major TAA-specific PBMC $CD8^+$ T cell responses in patients with PDAC, we selected TAAs based on their expression in PDAC cells. Of the 403 TAAs registered in the TAA database (TANTIGEN 2.0) (15), we selected four candidates that have been utilized in peptide vaccine clinical trials: CEACAM5 [carcinoembryonic antigen (CEA)] (16), MUC1 (17), TERT (18), and WT1 (19). Additionally, we selected two candidates used in peptide vaccine clinical trials for other cancers, NY-ESO-1 (CTAG1A) and TRP2 (DCT).

Using the RNAseq data of 1404 cell lines from the CCLE, we assessed the mRNA expression of six TAAs. Of these, *CEACAM5*, *MUC1*, *TERT*, and *WT1* were expressed in multiple PDAC cell lines, whereas *CTAG1A* and *DCT* were not expressed (Figure 1A and Supplementary Figure 1). Moreover, mRNA expression was further confirmed through qRT-PCR in six PDAC cell lines (four from primary tumors, one from liver metastasis, and one from lymph node metastasis), revealing upregulation of the expression of *CEACAM5*, *MUC1*, *TERT*, and *WT1* in several cell lines (Figures 1B, C).

3.2 Establishment of a detection system for TAA-specific PBMC $CD8^+$ T cell response from patients with PDAC

We then detected TAA-specific $CD8^+$ T cell responses in PBMCs derived from patients with PDAC at treatment initiation. As these cells are known to have a low frequency (20), to increase detection sensitivity, we stimulated PBMCs with overlapping peptides covering the full length of the four TAAs (Supplementary Table 1) and then cultured them in the presence of IL-2 for 10 days to amplify TAA-specific cells (21). Moreover, we aimed to increase detection sensitivity by stimulation with a mixture of four different TAAs. After culture, we re-stimulated the cells with the peptide pool and detected TAA-specific $CD8^+$ T cell responses using a flow cytometer. To evaluate antigen-specific responses, we measured the expression levels of interferon-gamma (IFNγ), a widely used marker for antigen-specific $CD8^+$ T cell responses, and 4-1BB, which is known as an activation-induced marker. IFNγ and 4-1BB have each been used as markers of antigen-specific responses (22, 23), and the antigen-specific response of the two in combination has been evaluated (24). However, it was unclear whether the and/or case, single positive, or double positive is more useful in controlling cancer, so we compared them in this study based on four criteria: $IFN\gamma^+$ and/or $4\text{-}1BB^+$, $IFN\gamma^+$, $4\text{-}1BB^+$, and double-positive ($IFN\gamma^+4\text{-}1BB^+$) (Figures 2A, B). Although there was a certain amount of bulk T cell amplification due to culture in the presence of IL-2, there was no increase in TAA-specific $CD8^+$ T cell responses due to TAA stimulation in healthy donors (Supplementary Figure 2).

3.3 Association of TAA-specific PBMC $IFN\gamma^+4\text{-}1BB^+$ $CD8^+$ T cell responses with neoadjuvant therapy efficacy in patients with PDAC

To investigate the relationship between TAA-specific $CD8^+$ T cell responses and clinical features of patients with PDAC (n=57), we stimulated PBMCs with a peptide pool containing four TAAs and determined the percentage of responders for TAA-specific $CD8^+$ T cell response using the four criteria described above (Figure 2C and Supplementary Figure 3).

We subsequently investigated if these cell responses were affected by specific HLA class 1 types. Among the 57 donors, 12 HLA-A types were detected with 25 allelic combinations (Supplementary Figures 4A, B), and TAA-specific $CD8^+$ T cell

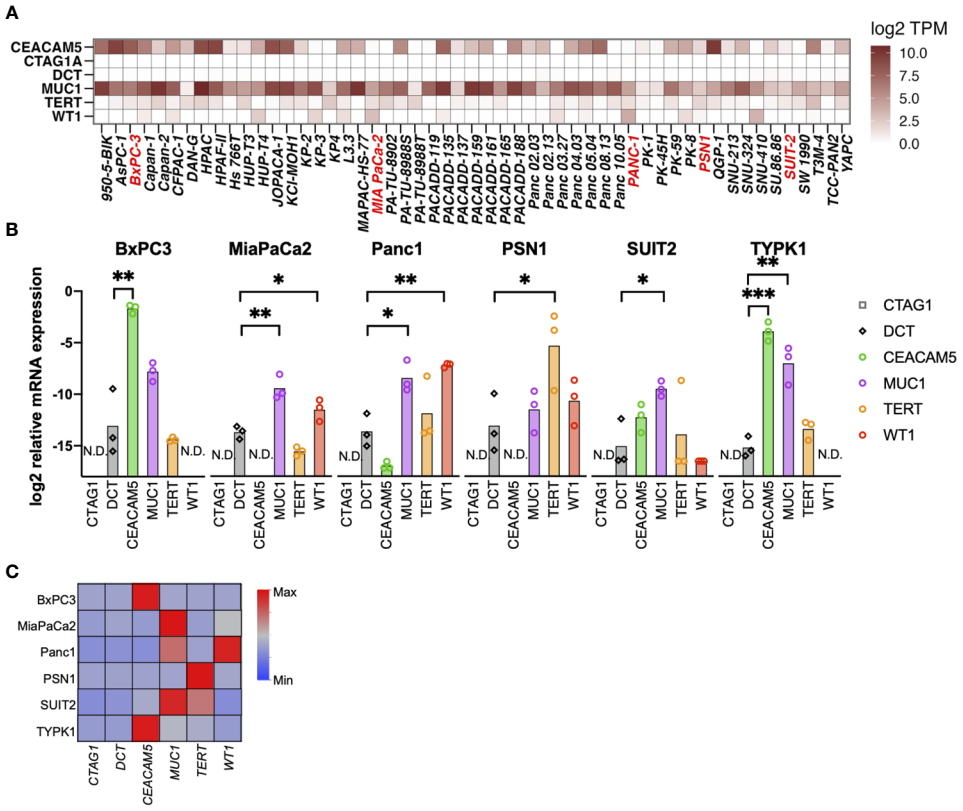

FIGURE 1
Selection of tumor-associated antigens (TAAs) specifically expressed in pancreatic cancer. **(A)** Gene expression of six TAAs (CEACAM5, NY-ESO-1 [CTAG1A], TRP2 [DCT], MUC1, TERT, and WT1) in pancreatic cancer cell lines. A public database (CCLE) was used to evaluate mRNA expression using RNA-sequencing. **(B, C)** mRNA expression of TAAs in pancreatic cancer cell lines determined by qRT-PCR. Relative expression levels of the housekeeping gene (hGUS) are shown as bar graphs **(B)**, and median values after min-max normalization are shown as heatmap **(C)**. Unpaired t-test was used for statistical analyses. *P<0.05, **P<0.01, ***P<0.001. "N.D" means "Not Detected".

responses were observed for all HLA-A types except A*30:01 (Supplementary Figure 4C). We then compared the HLA distribution of responders in each criterion to that of all donors to determine whether TAA-specific CD8$^+$ T cell responses were more prevalent in specific HLA-A types. However, we detected no differences in our cohort (Supplementary Figures 4D, E). Larger cohorts should be employed to investigate the association between HLA and TAA-specific responses.

We investigated the correlation between TAA-specific CD8$^+$ T cell responses and patient characteristics at the initiation of neoadjuvant therapy. The analysis revealed a significant association between TAA-specific IFNγ$^+$4-1BB$^+$ CD8$^+$ T cell response and pancreatic head and pancreatic body tail cancer (p = 0.0307; Supplementary Table 3). However, no significant correlations were observed for basic patient characteristics, such as age, sex, blood counts, and tumor factors (Supplementary Table 3). Moreover, there were no significant differences in the presence or absence of TAA-specific responses by treatment content (Supplementary Table 3).

To more comprehensively assess the relationship between clinical background information and total TAA-specific CD8$^+$ T cell responses, we generated a new index that may reflect the effects of neoadjuvant therapy. The index comprised ratios and differences of three tumor markers (CA19-9, CEA, and DUPAN-2), along with the tumor diameter on computed tomography (CT) images at the initiation of treatment, after neoadjuvant therapy, and after surgery. We then analyzed the parameters that were correlated with the frequency of TAA-specific CD8$^+$ T cell responses based on the four criteria.

The number of lymphocytes in the peripheral blood was positively correlated with TAA-specific 4-1BB$^+$ CD8$^+$ T cell and TAA-specific IFNγ$^+$4-1BB$^+$CD8$^+$ T cell frequencies (Figure 2D, columns 3 and 4). TAA-specific CD8$^+$ T cell frequency, characterized by IFNγ$^+$ and/or 4-1BB$^+$, was inversely correlated with both clinical progression (cStage) and tumor diameter on CT before treatment initiation. However, no inverse correlation was observed between the pathological progression (pStage) of the resected specimen and the difference in tumor diameter on CT after neoadjuvant therapy (Figure 2D, column 1). In contrast, the frequency of TAA-specific IFNγ$^+$4-1BB$^+$ CD8$^+$ T cell responses showed an inverse correlation with the rate of CA19-9 change during neoadjuvant therapy: the lower the rate, the better the therapeutic effect (R = −0.56, p = 0.011; Figure 2D, column 4 and Figure 2E). CA19-9 is a widely used serum biomarker in PDAC, and changes in its levels during neoadjuvant therapy are considered to be prognostic (25). The results suggest that patients with TAA-specific IFNγ$^+$4-1BB$^+$ CD8$^+$ T cell response observed prior to

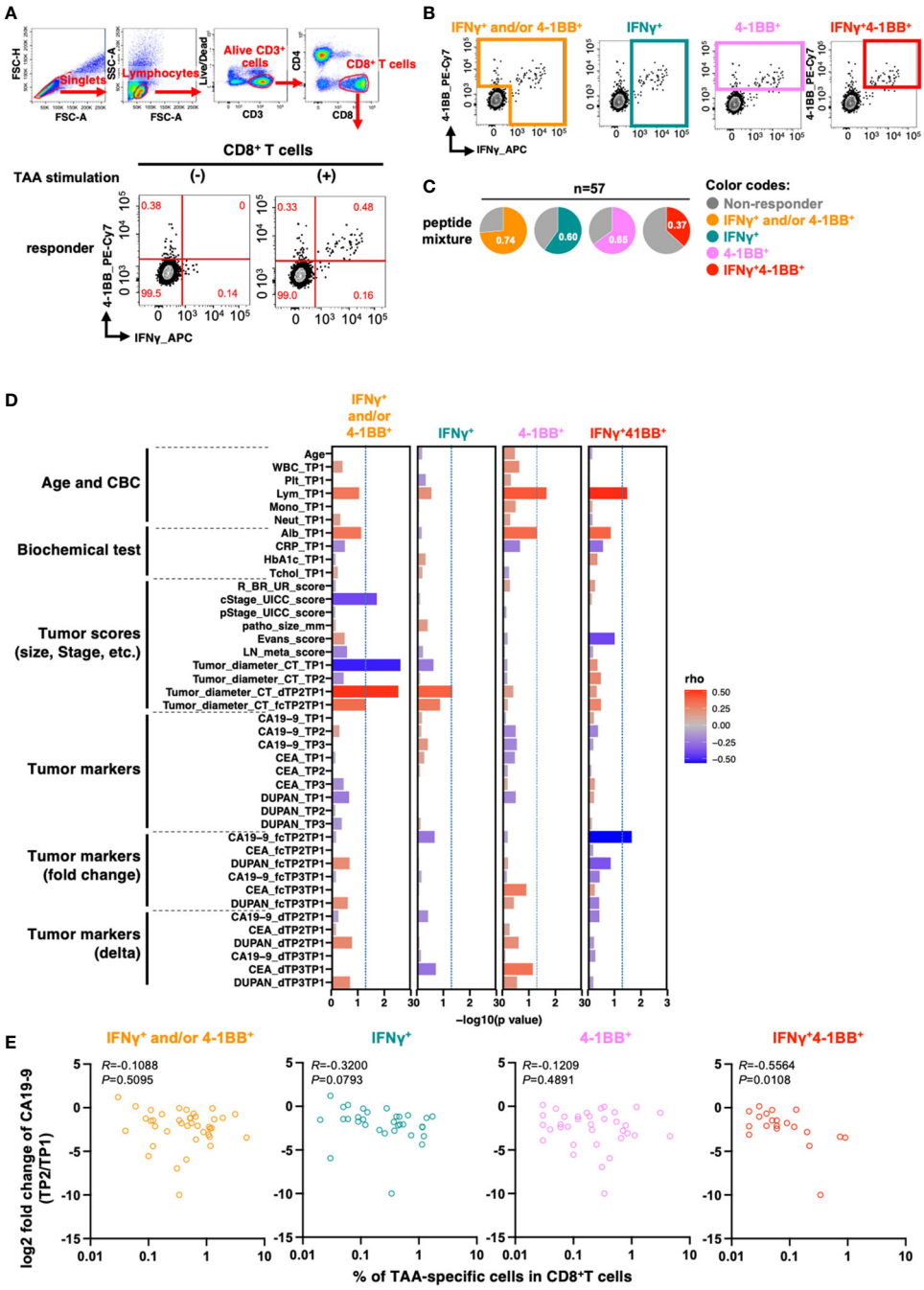

FIGURE 2
TAA-specific responses in CD8$^+$ T cells in PBMCs at the beginning of treatment are associated with changes in serum CA19-9 levels before and after treatment. **(A)** Flow cytometry gating for TAA-specific CD8$^+$ T cell response analysis and antigen-specific responses in CD8$^+$ T cells upon stimulation of PBMCs from patients with pancreatic cancer with the mixture of TAA peptides pool. Examples of TAA-specific response-positive specimens are shown. Numbers in the gates shown in red indicate frequencies (%). **(B)** Regions considered to have TAA-specific CD8$^+$ T-cell responses according to the four criteria are shown. **(C)** Percentage of patients with or without TAA-specific responses according to the four criteria (n=57). **(D)** Correlation between the percentage of TAAs-specific response in antigen-specific response-positive specimens according to the four criteria and the clinical information of the patients. The percentage of cells positive for each marker in CD8$^+$ T cells without peptide stimulation (as background) was subtracted from the percentage of each marker positive cells in CD8$^+$ T cells with TAA stimulation. **(E)** Correlation between the percentage of TAA-specific response in CD8$^+$ T cells and changes in pre- and post-treatment serum CA19-9 levels. Patients with CA19-9 levels below the detection sensitivity were excluded. Spearman's rank correlation test was used for statistical analysis.

10.3389/fimmu.2024.1363568

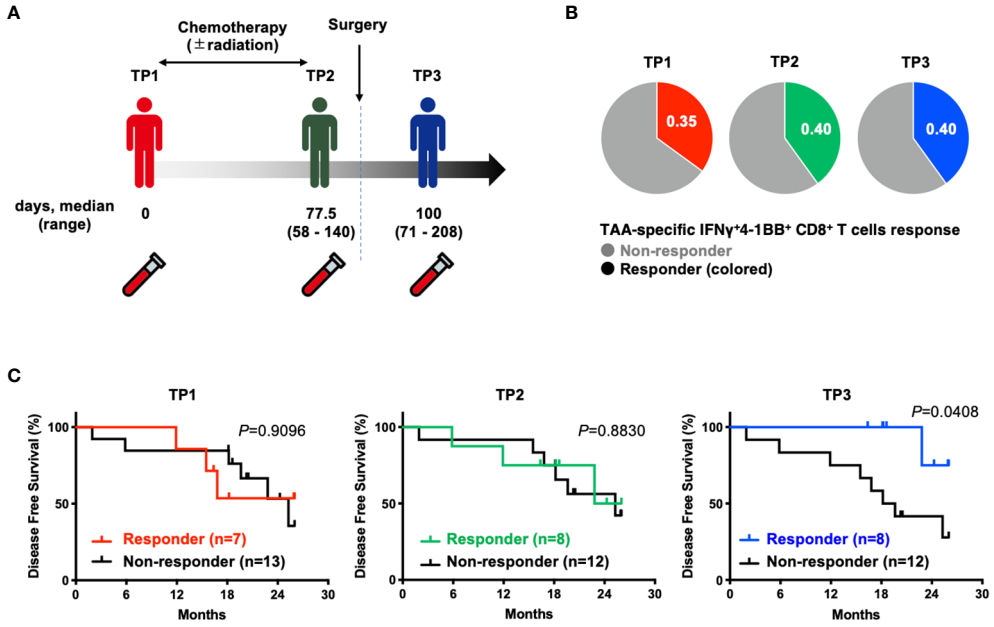

FIGURE 3
Patients with TAA-specific IFNγ+4-1BB$^+$ CD8$^+$ T cells responses in peripheral blood after surgery (TP3) had better disease free survival. **(A)** Schematic showing the timing of specimen collection. The numbers below each time point indicate the duration between each time point (days post TP1 at which TP2 or TP3 were sampled, median and range are indicated). **(B)** Ratio of responders evaluated by TAAs-specific IFNγ$^+$4-1 BB$^+$ CD8$^+$ T cells at TP1/TP2/TP3. The number of donors with all time points is n=20. **(C)** Kaplan-Meier survival curves compared disease free survival between the presence or absence of TAA-specific IFNγ$^+$4-1 BB$^+$ CD8$^+$ T cells at TP1/TP2/TP3. TP1, before the start of treatment; TP2, before surgical resection; TP3, after resection.

treatment initiation had a higher response to neoadjuvant therapy. Moreover, this criterion resulted in the lowest background; therefore, we used it for subsequent analyses.

3.4 Postoperative TAA-specific IFNγ$^+$4-1BB$^+$ CD8+ T cells and prognosis

To investigate the prognostic impact of TAA-specific IFNγ$^+$4-1BB$^+$ CD8$^+$ T cells at different time points (before treatment [TP1], after neoadjuvant therapy but before resection [TP2], and after resection [TP3]) using PBMCs collected from the same patients (Figure 3A), we compared the postoperative disease-free survival in the two groups according to the presence or absence of TAA-specific IFNγ$^+$4-1BB$^+$ CD8$^+$ T cells. There was no difference in the number of responders at each time point (Figure 3B). No difference was observed before treatment [TP1] or before surgery [TP2], whereas a significant difference was observed after surgery [TP3] (Figure 3C). The modulation of TAA-specific IFNγ$^+$4-1BB$^+$ responses over time did not exhibit a consistent trend, with some patients exhibiting a loss of response and others becoming new responders before and after treatment (Supplementary Figure 4). Notably, the four patients who had responded before treatment and maintained this response after surgery remained recurrence-free, whereas the three patients exhibiting loss of TAA-specific IFNγ$^+$4-1BB$^+$ responses experienced recurrence (data not shown). There were no significant differences in clinicopathologic factors (including treatment regimen) between the presence or absence of TAA-specific IFNγ$^+$4-1BB$^+$ reactions in TP3 (Supplementary Table 4).

3.5 ICIs enhance TAA-specific PBMC IFNγ$^+$4-1BB$^+$ CD8$^+$ T cell responses in cells derived from patients with PDAC

We investigated the impact of ICIs on TAA-specific IFNγ$^+$4-1BB$^+$ CD8$^+$ T cell response. To identify candidate immune checkpoint molecules as potential therapeutic targets, we compared the *ex vivo* expression profiles of PD-1, TIGIT, Tim-3, CD160, and BTLA on CD8$^+$ Tm cells in PBMCs derived from patients with PDAC via flow cytometry (Figure 4A; Supplementary Figure 6). Among these, only PD-1 was significantly more expressed in samples derived from patients with PDAC than in those from healthy participants (Figure 4B). Therefore, we selected PD-1 as the target molecule. We stimulated PBMCs with TAA peptide pools in the presence of ICIs and cultured them to analyze TAA-specific IFNγ$^+$4-1BB$^+$ CD8$^+$ T cells. We identified more responders in the anti-PD-1 antibody group than in the no-antibody and isotype groups, although this observation was not significant (Figure 4C; Supplementary Figure 7), suggesting that anti-PD-1 treatment detected new TAA-specific IFNγ$^+$4-1BB$^+$ CD8$^+$ T cells in some non-responders. Furthermore, anti-PD-1, but not anti-TIGIT, treatment significantly increased TAA-specific IFNγ$^+$4-1BB$^+$ CD8$^+$ T cell frequency (Figures 4C–E).

3.6 Timing of ICI intervention in PBMCs from patients with pancreatic cancer

To date, clinical trials of ICIs in patients with PDAC have included patients treated with cytotoxic anticancer drugs. Thus, we

10.3389/fimmu.2024.1363568

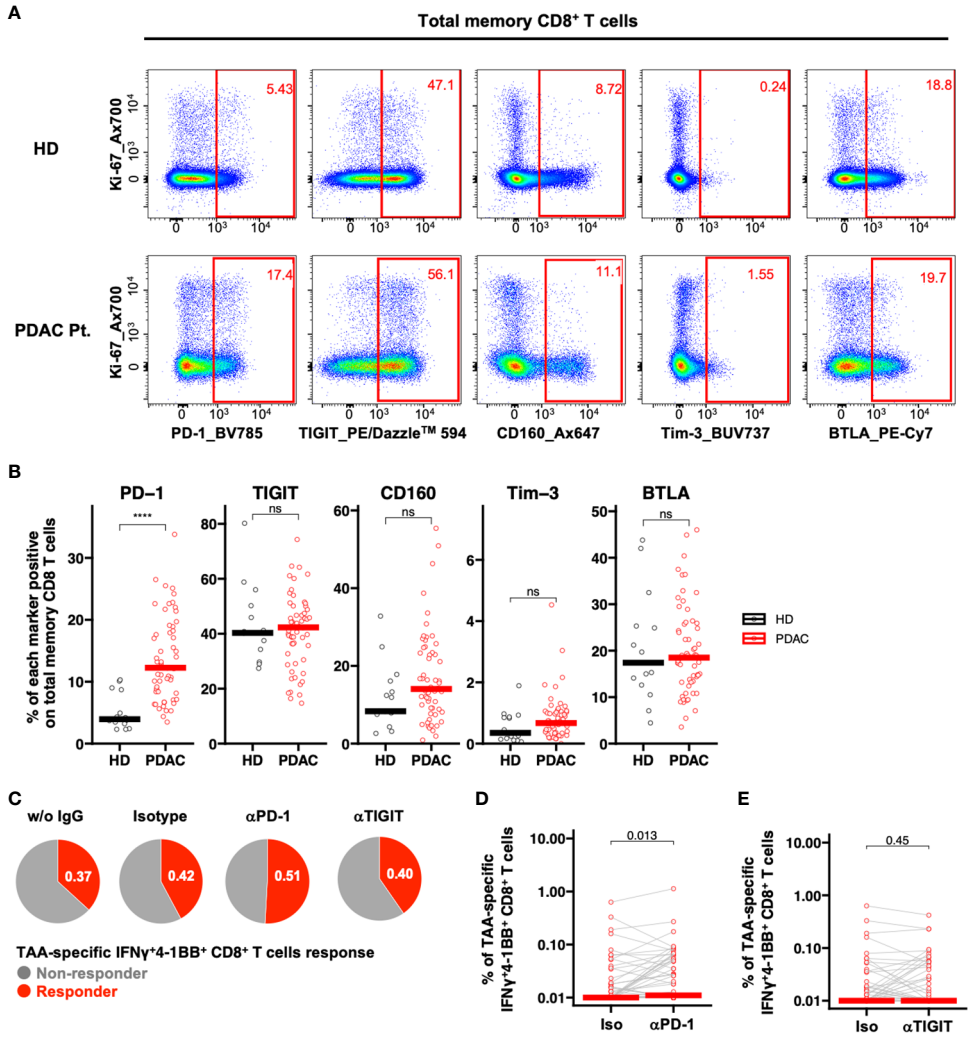

FIGURE 4
PD-1-positive memory CD8$^+$ T cells are increased in PBMCs from patients with pancreatic cancer, and PD-1 inhibition *in vitro* increased TAA-specific IFNγ$^+$4-1BB$^+$ CD8$^+$ T cells. **(A)** Representative flow cytometry plots of exhaustion markers expression in PBMCs from the healthy donor and the patient with pancreatic cancer. **(B)** PBMCs were analyzed *ex vivo* via flow cytometry, and the frequency of expression of five immune checkpoint molecules in memory CD8$^+$ T cells was compared between healthy donors (HD) (n=15) and pre-treatment (TP1) pancreatic cancer patients (PDAC Pt.) (n=57). Mann—Whitney U test was used for the statistical analysis. **(C)** Ratio of responders evaluated by TAA-specific IFNγ$^+$4-1BB$^+$ CD8$^+$ T cells in TP1 samples (n=57) treated without antibody, with isotype antibody, with anti-PD-1 antibody, or with anti-TIGIT antibody. **(D)** Comparison of TAA-specific IFNγ$^+$4-1BB$^+$ CD8$^+$ T cells frequencies in PDAC Pt. TP1 samples (n=57) upon isotype and anti-PD-1 antibody treatment. Wilcoxon signed-rank test was used for statistical analysis. **(E)** Comparison of TAA-specific IFNγ$^+$4-1BB$^+$ CD8$^+$ T cells frequencies in TP1 samples (n=57) treated with isotype or anti-TIGIT antibody. Wilcoxon signed-rank test was used for statistical analysis. ****P<0.0001. "ns" means "not significant".

next investigated whether chemotherapy, radiation therapy, or surgery would affect the efficacy of ICI in patients with PDAC. PD-1 inhibition was assessed at the TP1, TP2, and TP3 time points using PBMCs collected from the same patients. The efficacy of ICI in donors increased as follows: 50% at TP1, 25% at TP2, and 35% at TP3 (Figure 5A). PD-1 inhibition significantly increased the frequency of TAA-specific IFNγ$^+$4-1BB$^+$ CD8$^+$ T cells only at TP1 (Figure 5B), whereas TIGIT inhibition did not result in significant changes at any time point (Figure 5C). These results suggest that anti-PD-1 ICIs may be less effective after chemotherapy, either alone or in combination with radiotherapy, which could explain the poor outcomes reported in previous clinical trials.

4 Discussion

In the present study, we demonstrated that the frequency of TAA-specific IFNγ$^+$4-1BB$^+$ CD8$^+$ T cells in the blood before treatment was correlated with reduced CA19-9 levels, suggesting the potential utility of the proposed method for detecting TAA-specific IFNγ$^+$4-1BB$^+$ CD8$^+$ T cells as a surrogate marker to predict treatment efficacy. Additionally, we demonstrated that postoperative IFNγ$^+$4-1BB$^+$ TAA-specific IFNγ$^+$4-1BB$^+$ CD8$^+$ T cells may be predictive of postoperative recurrence. Although it remains unclear whether this peripheral *in vitro* response reflects *in vivo* suppression of cancer cells, patients exhibiting a TAA-specific IFNγ$^+$4-1BB$^+$ response after surgery exhibited a favorable

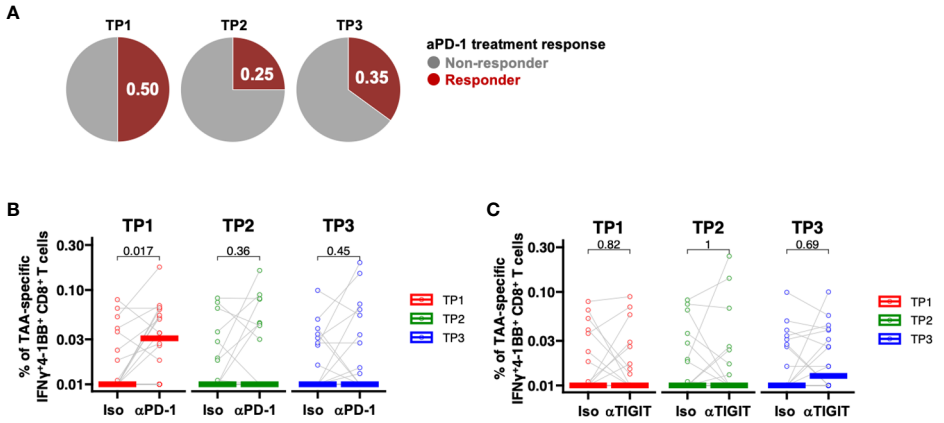

FIGURE 5
PD-1-positive memory CD8$^+$ T cells are increased in PBMCs from patients with pancreatic cancer, and PD-1 inhibition *in vitro* increased TAA-specific IFNγ$^+$4-1 BB$^+$ CD8$^+$ T cells. **(A)** Comparison of the percentage (%) of TAAs-specific IFNγ$^+$4-1BB$^+$ CD8$^+$ T cells during anti-PD-1 antibody treatment at TP1/TP2/TP3. The number of donors with all time points is n=20. **(B)** Comparison of the percentage (%) of TAA-specific IFNγ$^+$4-1BB$^+$ CD8$^+$ T cells during anti-PD-1 treatment at TP1/TP2/TP3. The number of donors with all time points is n=20. **(C)** Comparison of the percentage (%) of TAA-specific IFNγ$^+$4-1BB$^+$ CD8$^+$ T cells during anti-TIGIT treatment at TP1/TP2/TP3. The number of donors with all time points is n=20. Wilcoxon signed-rank test was used for statistical analysis. before the start of treatment; TP2, before surgical resection; TP3, after resection.

prognosis, whereas those exhibiting a response before treatment but not after surgery were more susceptible to recurrence.

TIL analysis requires invasive tissue collection, posing challenges to monitoring changes in patients. In contrast, liquid biopsies can be conducted multiple times with minimal invasiveness, and are considered a rich source of information that reflects biological status, therapeutic response, and clinical outcomes (26). Recently, a variety of biomolecules or particles in plasma such as cell free DNA (cfDNA), circulating tumor DNA (ctDNA), non-coding RNAs, and exome or extracellular vesicles have emerged as new probes to examine the biological status of tumors, therapeutic responses, and prognoses (27–32). In addition, certain types of cells, such as circulating tumor cells (CTCs), have been used to identify tumor status (33, 34). In general, cell-based analysis requires more labor than molecular-based analysis. However, the overall information it supplies is richer. Circulating immune cells would be as valuable a source of information as CTCs. Compared to the rare nature of CTCs and the specific tools needed to capture them, circulating T cells are easier to detect and more easily accessible using standard immunological instruments. Indeed, the transcriptomic analysis of bulk peripheral CD8$^+$ T cells in melanoma patients has revealed the association between peripheral CD8$^+$ T cell characteristics and ICI responses (35). Furthermore, in clinical trials investigating the use of atezolizumab and personalized RNA neoantigen vaccines, as well as mFOLFIRINOX as adjuvant chemotherapy in patients with pancreatic cancer, those with vaccine antigen-specific T cells in their PBMCs exhibited a significantly improved recurrence-free survival (36). While more patients are required for further validation, our study suggests a potential synergistic effect of immune response and neoadjuvant therapy, providing important insights for future combination therapies with anticancer drugs and ICIs.

In addition to conventional treatments such as surgery, chemotherapy, and radiation, immunotherapy has emerged as a new treatment strategy for cancer. However, the effectiveness of ICI monotherapy is limited in pancreatic cancer (10]. Therefore, various combination therapies are being investigated, including cytotoxic chemotherapy and radiotherapy (37). Moreover, a previous report has suggested that neoadjuvant chemotherapy activates the immune response (38). In cancers other than pancreatic cancer, ICI treatment is more effective when administered before surgery rather than after (39–42). Notably, a preoperative cytotoxic anticancer drug plus ICI therapy showed efficacy in a phase 3 trial for resectable non-small cell lung cancer (43). Based on these reports, clinical trials investigating ICI treatment in combination with neoadjuvant chemotherapy regimens are currently underway for pancreatic cancer. The results of these trials are anticipated to provide insights into the optimal timing of treatment. However, most of the study focuses on the neoadjuvant (preoperative) versus adjuvant (postoperative) difference, rather than the untreated versus neoadjuvant in a preoperative setting (44), or by comparing it with or without ICI in the neoadjuvant setting (45). Here, we directly investigated the three distinct timings of PD-1 inhibition *in vitro*. Contrary to the anticipated result from previous studies, our results indicated the effectiveness of PD-1 inhibition in TAA-specific IFNγ$^+$4-1BB$^+$ CD8$^+$ T cells before the start of neoadjuvant therapy, at least *in vitro*. There is one possible explanation for this discrepancy. The rationale for neoadjuvant ICI therapy is the following: increased priming of tumor-specific T cells due to immunogenic cell death in tissue that is induced by neoadjuvant increases the antigenic stimuli (46–49). In our analysis, in contrast, TAA-specific peripheral memory CD8$^+$ T cells were stimulated by an abundant amount of TAA peptides either in the presence or absence of PD-1 inhibition.

Another explanation is that the study design of previous reports was limited to fully delineate the optimal timing of ICI therapy. Consistently, one study focusing on the sequence of ICI before and after neoadjuvant suggested that the ICI before neoadjuvant was efficacious in BRAF-wildtype metastatic melanoma (50).

This study has some limitations. First, this study suggests the prognostic value of analyzing postoperative peripheral blood samples in patient follow-up. However, further investigations are warranted, owing to the small number of cases and short observation period. Second, given the interplay of peripheral $CD8^+$ cells with tissue-resident memory $CD8^+$ T cells against anti-tumoral immunity (51), TAA-specific $IFN\gamma^+4\text{-}1BB^+$ $CD8^+$ T cells in the blood may contribute to the efficacy of neoadjuvant therapy. However, our study did not directly analyze TILs, and it remains unclear if similar cells existed in the tissues.

In summary, we selected TAA-specific antigen molecules to stimulate $CD8^+$ T cells and we established a flow cytometry system to detect antigen-specific responses of these cells in peripheral blood derived from patients with PDAC, utilizing them as peripheral biomarkers for assessing the efficacy of neoadjuvant chemotherapy. Evaluation of the impact of immunotherapy by monitoring the TAA-specific $IFN\gamma^+4\text{-}1BB^+$ responses of $CD8^+$ T cells suggested that PD-1 inhibition may effectively increase TAA-specific $IFN\gamma^+4\text{-}1BB^+$ $CD8^+$ T cells when administered as a neoadjuvant therapy. Our findings suggest that a sequential treatment approach, involving initial ICI treatment followed by neoadjuvant chemotherapy, as opposed to a combination therapy where ICI and neoadjuvant chemotherapy are administered simultaneously, may optimize the efficacy of multidisciplinary treatment.

Data availability statement

The raw data supporting the conclusions of this article will be made available by the authors, without undue reservation.

Ethics statement

The studies involving humans were approved by Ethical Review Board Osaka University Hospital Osaka Prefectural Hospital Organization Osaka International Cancer Institute Certified Review Board Research Ethics Review Committee of National Institutes of Biomedical Innovation. The studies were conducted in accordance with the local legislation and institutional requirements. The participants provided their written informed consent to participate in this study.

Author contributions

HM: Conceptualization, Data curation, Formal analysis, Investigation, Visualization, Writing – original draft. ST: Conceptualization, Formal analysis, Investigation, Methodology, Visualization, Writing – original draft. HA: Conceptualization, Funding acquisition, Investigation, Resources, Validation, Writing – original draft, Writing – review & editing. SK: Resources, Writing – review & editing. YM: Data curation, Formal analysis, Writing – review & editing. YN: Data curation, Resources, Writing – review & editing. MH: Resources, Writing – review & editing. AT: Resources, Writing – review & editing. KY: Resources, Writing – review & editing. HT: Resources, Writing – review & editing. YD: Resources, Writing – review & editing. HE: Resources, Writing – review & editing. NM: Resources, Writing – review & editing. TY: Conceptualization, Funding acquisition, Investigation, Methodology, Project administration, Writing – original draft, Writing – review & editing.

Funding

The author(s) declare that financial support was received for the research, authorship, and/or publication of this article. This study was supported by the Japan Society for the Promotion of Science Grant-in-Aid for Scientific Research (B) (grant number 20H03728), Scientific Research (C) (grant number 19K09171), and the Uehara Memorial Foundation.

Acknowledgments

We would like to acknowledge the members of the Laboratory of Precision Immunology, Center for Intractable Diseases and ImmunoGenomics in NIBIOHN, the Laboratory of Translational Cancer Immunology and Biology at Osaka International Cancer Institute, and the Department of Gastroenterological Surgery at Osaka General Medical Center for their excellent technical support.

Conflict of interest

The authors declare that the research was conducted in the absence of any commercial or financial relationships that could be construed as a potential conflict of interest.

The author(s) declared that they were an editorial board member of Frontiers, at the time of submission. This had no impact on the peer review process and the final decision.

Publisher's note

Supplementary material

The Supplementary Material for this article can be found online at: https://www.frontiersin.org/articles/10.3389/fimmu.2024.1363568/full#supplementary-material

References

1. Siegel RL, Miller KD, Wagle NS, Jemal A. Cancer statistics, 2023. *CA Cancer J Clin*. (2023) 73:17–48. doi: 10.3322/caac.21763

2. Janssen QP, O'Reilly EM, van Eijck CHJ, Groot Koerkamp B. Neoadjuvant treatment in patients with resectable and borderline resectable pancreatic cancer. *Front Oncol*. (2020) 10:41. doi: 10.3389/fonc.2020.00041

3. Neoptolemos JP, Palmer DH, Ghaneh P, Psarelli EE, Valle JW, Halloran CM, et al. Comparison of adjuvant gemcitabine and capecitabine with gemcitabine monotherapy in patients with resected pancreatic cancer (ESPAC-4): a multicentre, open-label, randomised, phase 3 trial. *Lancet*. (2017) 389:1011–24. doi: 10.1016/S0140-6736(16)32409-6

4. Ahmad SA, Duong M, Sohal DPS, Gandhi NS, Beg MS, Wang-Gillam A, et al. Surgical outcome results from SWOG S1505: A randomized clinical trial of mFOLFIRINOX versus gemcitabine/nab-paclitaxel for perioperative treatment of resectable pancreatic ductal adenocarcinoma. *Ann Surg*. (2020) 272:481–6. doi: 10.1097/SLA.0000000000004155

5. Sakai Y, Miyazawa M, Komura T, Yamada T, Nasti A, Yoshida K, et al. Distinct chemotherapy-associated anti-cancer immunity by myeloid cells inhibition in murine pancreatic cancer models. *Cancer Sci*. (2019) 110:903–12. doi: 10.1111/cas.13944

6. Sams L, Kruger S, Heinemann V, Bararia D, Haebe S, Alig S, et al. Alterations in regulatory T cells and immune checkpoint molecules in pancreatic cancer patients receiving FOLFIRINOX or gemcitabine plus nab-paclitaxel. *Clin Transl Oncol*. (2021) 23:2394–401. doi: 10.1007/s12094-021-02620-x

7. Reck M, Rodriguez-Abreu D, Robinson AG, Hui R, Csoszi T, Fulop A, et al. Pembrolizumab versus chemotherapy for PD-L1-positive non-small-cell lung cancer. *N Engl J Med*. (2016) 375:1823–33. doi: 10.1056/NEJMoa1606774

8. Motzer RJ, Escudier B, McDermott DF, George S, Hammers HJ, Srinivas S, et al. Nivolumab versus everolimus in advanced renal-cell carcinoma. *N Engl J Med*. (2015) 373:1803–13. doi: 10.1056/NEJMoa1510665

9. El-Khoueiry AB, Sangro B, Yau T, Crocenzi TS, Kudo M, Hsu C, et al. Nivolumab in patients with advanced hepatocellular carcinoma (CheckMate 040): an open-label, non-comparative, phase 1/2 dose escalation and expansion trial. *Lancet*. (2017) 389:2492–502. doi: 10.1016/S0140-6736(17)31046-2

10. Robert C, Schachter J, Long GV, Arance A, Grob JJ, Mortier L, et al. Pembrolizumab versus ipilimumab in advanced melanoma. *N Engl J Med*. (2015) 372:2521–32. doi: 10.1056/NEJMoa1503093

11. Tang B, Yan X, Sheng X, Si L, Cui C, Kong Y, et al. Safety and clinical activity with an anti-PD-1 antibody JS001 in advanced melanoma or urologic cancer patients. *J Hematol Oncol*. (2019) 12:7. doi: 10.1186/s13045-018-0693-2

12. O'Reilly EM, Oh DY, Dhani N, Renouf DJ, Lee MA, Sun W, et al. Durvalumab with or without tremelimumab for patients with metastatic pancreatic ductal adenocarcinoma: A phase 2 randomized clinical trial. *JAMA Oncol*. (2019) 5:1431–8. doi: 10.1001/jamaoncol.2019.1588

13. Iwahori K, Shintani Y, Funaki S, Yamamoto Y, Matsumoto M, Yoshida T, et al. Peripheral T cell cytotoxicity predicts T cell function in the tumor microenvironment. *Sci Rep*. (2019) 9:2636. doi: 10.1038/s41598-019-39345-5

14. Li H, Ning S, Ghandi M, Kryukov GV, Gopal S, Deik A, et al. The landscape of cancer cell line metabolism. *Nat Med*. (2019) 25:850–60. doi: 10.1038/s41591-019-0404-8

15. Zhang G, Chitkushev L, Olsen LR, Keskin DB, Brusic V. TANTIGEN 2.0: a knowledge base of tumor T cell antigens and epitopes. *BMC Bioinf*. (2021) 22:40. doi: 10.1186/s12859-021-03962-7

16. Geynisman DM, Zha Y, Kunnavakkam R, Aklilu M, Catenacci DV, Polite BN, et al. A randomized pilot phase I study of modified carcinoembryonic antigen (CEA) peptide (CAP1-6D)/montanide/GM-CSF-vaccine in patients with pancreatic adenocarcinoma. *J Immunother Cancer*. (2013) 1:8. doi: 10.1186/2051-1426-1-8

17. Ramanathan RK, Lee KM, McKolanis J, Hitbold E, Schraut W, Moser AJ, et al. Phase I study of a MUC1 vaccine composed of different doses of MUC1 peptide with SB-AS2 adjuvant in resected and locally advanced pancreatic cancer. *Cancer Immunol Immunother*. (2005) 54:254–64. doi: 10.1007/s00262-004-0581-1

18. Kotsakis A, Vetsika EK, Christou S, Hatzidaki D, Vardakis N, Aggouraki D, et al. Clinical outcome of patients with various advanced cancer types vaccinated with an optimized cryptic human telomerase reverse transcriptase (TERT) peptide: results of an expanded phase II study. *Ann Oncol*. (2012) 23:442–9. doi: 10.1093/annonc/mdr396

19. Nishida S, Ishikawa T, Egawa S, Koido S, Yanagimoto H, Ishii J, et al. Combination gemcitabine and WT1 peptide vaccination improves progression-free survival in advanced pancreatic ductal adenocarcinoma: A phase II randomized study. *Cancer Immunol Res*. (2018) 6:320–31. doi: 10.1158/2326-6066.CIR-17-0386

20. Chen Y, Xue SA, Behboudi S, Mohammad GH, Pereira SP, Morris EC. *Ex vivo* PD-L1/PD-1 pathway blockade reverses dysfunction of circulating CEA-specific T cells in pancreatic cancer patients. *Clin Cancer Res*. (2017) 23:6178–89. doi: 10.1158/1078-0432.CCR-17-1185

21. Rivino L, Le Bert N, Gill US, Kunasegaran K, Cheng Y, Tan DZ, et al. Hepatitis B virus-specific T cells associate with viral control upon nucleos(t)ide-analogue therapy discontinuation. *J Clin Invest*. (2018) 128:668–81. doi: 10.1172/JCI92812

22. Lamoreaux L, Koup RA, Roederer M. OMIP-009: Characterization of antigen-specific human T-cells. *Cytometry A*. (2012) 81:362–3. doi: 10.1002/cyto.a.22042

23. Wolfl M, Kuball J, Ho WY, Nguyen H, Manley TJ, Bleakley M, et al. Activation-induced expression of CD137 permits detection, isolation, and expansion of the full repertoire of CD8+ T cells responding to antigen without requiring knowledge of epitope specificities. *Blood*. (2007) 110:201–10. doi: 10.1182/blood-2006-11-056168

24. Takahama S, Yoshio S, Masuta Y, Murakami H, Sakamori R, Kaneko S, et al. Hepatitis B surface antigen reduction is associated with hepatitis B core-specific CD8+ T cell quality. *Front Immunol*. (2023) 14:1257113. doi: 10.3389/fimmu.2023.1257113

25. Akita H, Takahashi H, Eguchi H, Asukai K, Hasegawa S, Wada H, et al. Difference between carbohydrate antigen 19-9 and fluorine-18 fluorodeoxyglucose positron emission tomography in evaluating the treatment efficacy of neoadjuvant treatment in patients with resectable and borderline resectable pancreatic ductal adenocarcinoma: Results of a dual-center study. *Ann Gastroenterol Surg*. (2021) 5:381–9. doi: 10.1002/ags3.12418

26. Heitzer E, Haque IS, Roberts CES, Speicher MR. Current and future perspectives of liquid biopsies in genomics-driven oncology. *Nat Rev Genet*. (2019) 20:71–88. doi: 10.1038/s41576-018-0071-5

27. Wan JCM, Massie C, Garcia-Corbacho J, Mouliere F, Brenton JD, Caldas C, et al. Liquid biopsies come of age: towards implementation of circulating tumour DNA. *Nat Rev Cancer*. (2017) 17:223–38. doi: 10.1038/nrc.2017.7

28. Budhraja KK, McDonald BR, Stephens MD, Contente-Cuomo T, Markus H, Farooq M, et al. Genome-wide analysis of aberrant position and sequence of plasma DNA fragment ends in patients with cancer. *Sci Transl Med*. (2023) 15:eabm6863. doi: 10.1126/scitranslmed.abm6863

29. Cristiano S, Leal A, Phallen J, Fiksel J, Adleff V, Bruhm DC, et al. Genome-wide cell-free DNA fragmentation in patients with cancer. *Nature*. (2019) 570:385–9. doi: 10.1038/s41586-019-1272-6

30. Toden S, Goel A. Non-coding RNAs as liquid biopsy biomarkers in cancer. *Br J Cancer*. (2022) 126:351–60. doi: 10.1038/s41416-021-01672-8

31. Lee JS, Park SS, Lee YK, Norton JA, Jeffrey SS. Liquid biopsy in pancreatic ductal adenocarcinoma: current status of circulating tumor cells and circulating tumor DNA. *Mol Oncol*. (2019) 13:1623–50. doi: 10.1002/1878-0261.12537

32. Möller A, Lobb RJ. The evolving translational potential of small extracellular vesicles in cancer. *Nat Rev Cancer*. (2020) 20:697–709. doi: 10.1038/s41568-020-00299-w

33. Ring A, Nguyen-Sträuli BD, Wicki A, Aceto N. Biology, vulnerabilities and clinical applications of circulating tumour cells. *Nat Rev Cancer*. (2023) 23:95–111. doi: 10.1038/s41568-022-00536-4

34. Chen J, Wang H, Zhou L, Liu Z, Tan X. A combination of circulating tumor cells and CA199 improves the diagnosis of pancreatic cancer. *J Clin Lab Anal*. (2022) 36:e24341. doi: 10.1002/jcla.24341

35. Fairfax BP, Taylor CA, Watson RA, Nassiri I, Danielli S, Fang H, et al. Peripheral CD8+ T cell characteristics associated with durable responses to immune checkpoint blockade in patients with metastatic melanoma. *Nat Med*. (2020) 26:193–9. doi: 10.1038/s41591-019-0734-6

36. Rojas LA, Sethna Z, Soares KC, Olcese C, Pang N, Patterson E, et al. Personalized RNA neoantigen vaccines stimulate T cells in pancreatic cancer. *Nature*. (2023) 618:144–50. doi: 10.1038/s41586-023-06063-y

37. Wainberg ZA, Hochster HS, Kim EJ, George B, Kaylan A, Chiorean EG, et al. Open-label, phase I study of nivolumab combined with nab-paclitaxel plus gemcitabine in advanced pancreatic cancer. *Clin Cancer Res*. (2020) 26:4814–22. doi: 10.1158/1078-0432.CCR-20-0099

38. Peng H, James CA, Cullinan DR, Hogg GD, Mudd JL, Zuo C, et al. Neoadjuvant FOLFIRINOX therapy is associated with increased effector T cells and reduced suppressor cells in patients with pancreatic cancer. *Clin Cancer Res*. (2021) 27:6761–71. doi: 10.1158/1078-0432.CCR-21-0998

39. Amaria RN, Reddy SM, Tawbi HA, Davies MA, Ross MI, Glitza IC, et al. Neoadjuvant immune checkpoint blockade in high-risk resectable melanoma. *Nat Med*. (2018) 24:1649–54. doi: 10.1038/s41591-018-0197-1

40. Keung EZ, Lazar AJ, Torres KE, Wang WL, Cormier JN, Ashleigh Guadagnolo B, et al. Phase II study of neoadjuvant checkpoint blockade in patients with surgically resectable undifferentiated pleomorphic sarcoma and dedifferentiated liposarcoma. *BMC Cancer*. (2018) 18:913. doi: 10.1186/s12885-018-4829-0

41. Cloughesy TF, Mochizuki AY, Orpilla JR, Hugo W, Lee AH, Davidson TB, et al. Neoadjuvant anti-PD-1 immunotherapy promotes a survival benefit with intratumoral and systemic immune responses in recurrent glioblastoma. *Nat Med*. (2019) 25:477–86. doi: 10.1038/s41591-018-0337-7

42. Schmid P, Cortes J, Pusztai L, McArthur H, Kummel S, Bergh J, et al. Pembrolizumab for early triple-negative breast cancer. *N Engl J Med*. (2020) 382:810–21. doi: 10.1056/NEJMoa1910549

43. Forde PM, Spicer J, Lu S, Provencio M, Mitsudomi T, Awad MM, et al. Neoadjuvant nivolumab plus chemotherapy in resectable lung cancer. *N Engl J Med*. (2022) 386:1973–85. doi: 10.1056/NEJMoa2202170

44. Topalian SL, Forde PM, Emens LA, Yarchoan M, Smith KN, Pardoll DM. Neoadjuvant immune checkpoint blockade: A window of opportunity to advance cancer immunotherapy. *Cancer Cell*. (2023) 41:1551–66. doi: 10.1016/j.ccell.2023.07.011

45. Katz MHG, Petroni GR, Bauer T, Reilley MJ, Wolpin BM, Stucky C, et al. Multicenter randomized controlled trial of neoadjuvant chemoradiotherapy alone or in combination with pembrolizumab in patients with resectable or borderline resectable pancreatic adenocarcinoma. *J Immunother Cancer*. (2023) 11:e007586. doi: 10.1136/jitc-2023-007586

46. O'Donnell JS, Hoefsmit EP, Smyth MJ, Blank CU, Teng MWL. The promise of neoadjuvant immunotherapy and surgery for cancer treatment. *Clin Cancer Res*. (2019) 25:5743–51. doi: 10.1158/1078-0432.CCR-18-2641

47. Galluzzi L, Buqué A, Kepp O, Zitvogel L, Kroemer G. Immunological effects of conventional chemotherapy and targeted anticancer agents. *Cancer Cell*. (2015) 28:690–714. doi: 10.1016/j.ccell.2015.10.012

48. Liu J, O'Donnell JS, Yan J, Madore J, Allen S, Smyth MJ, et al. Timing of neoadjuvant immunotherapy in relation to surgery is crucial for outcome. *Oncoimmunology*. (2019) 8:e1581530. doi: 10.1080/2162402X.2019.1581530

49. Topalian SL, Taube JM, Pardoll DM. Neoadjuvant checkpoint blockade for cancer immunotherapy. *Science*. (2020) 367:eaax0182. doi: 10.1126/science.aax0182

50. Markovic SN, Suman VJ, Javed A, Reid JM, Wall DJ, Erickson LA, et al. Sequencing ipilimumab immunotherapy before or after chemotherapy (Nab-paclitaxel and bevacizumab) for the treatment of BRAFwt (BRAF wild-type) metastatic Malignant melanoma: results of a study of academic and community cancer research united (ACCRU) RU261206I. *Am J Clin Oncol*. (2020) 43:115–21. doi: 10.1097/COC.0000000000000644

51. Enamorado M, Iborra S, Priego E, Cueto FJ, Quintana JA, Martinez-Cano S, et al. Enhanced anti-tumour immunity requires the interplay between resident and circulating memory $CD8^+$ T cells. *Nat Commun*. (2017) 8:16073. doi: 10.1038/ncomms16073

frontiers | Frontiers in Immunology

TYPE Review
PUBLISHED 15 March 2024
DOI 10.3389/fimmu.2024.1378944

OPEN ACCESS

EDITED BY
Raquel Tarazona,
University of Extremadura, Spain

REVIEWED BY
Anu Sharma,
St. Jude Children's Research Hospital, United States
Remya Raja,
Mayo Clinic Arizona, United States

*CORRESPONDENCE
Andreja Nataša Kopitar
andreja-natasa.kopitar@mf.uni-lj.si

RECEIVED 30 January 2024
ACCEPTED 04 March 2024
PUBLISHED 15 March 2024

CITATION
Levstek L, Janžič L, Ihan A and Kopitar AN (2024) Biomarkers for prediction of CAR T therapy outcomes: current and future perspectives.
Front. Immunol. 15:1378944.
doi: 10.3389/fimmu.2024.1378944

Biomarkers for prediction of CAR T therapy outcomes: current and future perspectives

Lucija Levstek, Larisa Janžič, Alojz Ihan and Andreja Nataša Kopitar*

Institute of Microbiology and Immunology, Faculty of Medicine, University of Ljubljana, Ljubljana, Slovenia

Chimeric antigen receptor (CAR) T cell therapy holds enormous potential for the treatment of hematologic malignancies. Despite its benefits, it is still used as a second line of therapy, mainly because of its severe side effects and patient unresponsiveness. Numerous researchers worldwide have attempted to identify effective predictive biomarkers for early prediction of treatment outcomes and adverse effects in CAR T cell therapy, albeit so far only with limited success. This review provides a comprehensive overview of the current state of predictive biomarkers. Although existing predictive metrics correlate to some extent with treatment outcomes, they fail to encapsulate the complexity of the immune system dynamics. The aim of this review is to identify six major groups of predictive biomarkers and propose their use in developing improved and efficient prediction models. These groups include changes in mitochondrial dynamics, endothelial activation, central nervous system impairment, immune system markers, extracellular vesicles, and the inhibitory tumor microenvironment. A comprehensive understanding of the multiple factors that influence therapeutic efficacy has the potential to significantly improve the course of CAR T cell therapy and patient care, thereby making this advanced immunotherapy more appealing and the course of therapy more convenient and favorable for patients.

KEYWORDS

CAR T cells, adoptive cell immunotherapy, predictive biomarkers, therapeutic response, cytokine release syndrome, immune effector cell-associated neurotoxicity syndrome

1 Introduction

Chimeric antigen receptor (CAR) T cell therapy holds enormous potential for the treatment of hematologic malignancies and shows promise for solid tumors treatment as well. This innovative approach involves reprogramming patient's T cells to recognize and attack cancer cells through engineered receptors known as CARs. As research and clinical applications evolve, CAR T cell therapies have been developed across multiple generations, each with distinct features aimed at enhancing therapeutic efficacy and safety. The first generation of CAR T cells laid the groundwork by introducing a singular signaling domain,

typically CD3ζ, to activate T cells upon antigen recognition. However, their clinical impact was limited due to modest T cell proliferation and persistence (1). Second-generation CAR T cells improved upon this by incorporating an additional costimulatory domain (such as CD28 or 4-1BB) alongside CD3ζ. This enhancement significantly boosted T cell expansion, lifespan, and antitumor activity, representing a leap forward in therapeutic effectiveness (2). Third-generation CARs further advanced the design by including two costimulatory domains, aiming to amplify T cell activation and antitumor responses even more (2). The fourth generation, often referred to as TRUCKs (T cells redirected for universal cytokine killing), are engineered to secrete proinflammatory cytokines upon engaging with tumor antigens. This feature is intended to recruit additional immune effector cells to the tumor site, intensifying the immune response (3). The fifth-generation CAR T cells, which incorporate novel signaling domains, are designed to mimic the complete activation pathway of natural T cells, offering the promise of even more potent and selective cancer targeting capabilities (4).

Despite their potential, CAR T cell therapies are associated with significant adverse events. Cytokine release syndrome (CRS) is often considered the most common side effect of CAR T cell therapy, which results from the massive release of cytokines by activated T cells and other immune cells. Symptoms can range from mild flu-like symptoms, such as fever, fatigue, and myalgia, to severe life-threatening conditions, including hypotension, high fever, and multi-organ dysfunction (5). Immune effector cell-associated neurotoxicity syndrome (ICANS) is another common side effect of CAR T cell therapy, characteristic of a wide range of neurological symptoms. These can include headache, confusion, aphasia, tremors, seizures, and in severe cases, cerebral edema (6). Other common side effects include B-cell aplasia, off-tumor cytotoxicity, tumor lysis syndrome (TLS), macrophage activation syndrome (MAS), and other less frequent adverse events (7, 8).

Despite the benefits of this promising treatment approach, it is still used as a second line of therapy for patients who relapsed after at least two previous lines of cancer therapy, or for whom for any reason other therapies can no longer be considered effective (9). The limitations of CAR T cell therapy arise primarily from severe side effects during treatment course, mainly CRS and ICANS, which can result in multiple organ dysfunction and even death. Overview of incidence of CRS and ICANS and their severity in patients treated with CAR T cell therapies is shown in Table 1. Accurate monitoring and efficient response times for intervention after the onset of side effect symptoms are seldom achieved because side effect symptoms usually occur rapidly and share many similarities with the regular therapy progression (inflammation, fever, fatigue, confusion, nausea, headache, rapid heart rate, etc.). Another substantial challenge in the field of CAR T cell therapy lies in addressing the issue of patient unresponsiveness. It has been observed that up to 36% of patients eligible for CAR T cell therapy undergo treatment, only to be later identified as non-responders (10). For these non-responders, the aftermath of an unsuccessful CAR T treatment can be particularly dire; it often becomes too late to pursue alternative treatments, leading to deteriorating outcomes or even death. This predicament necessitates significant research aimed at identifying potential non-responders prior to initiating CAR T cell therapy. This would enable these patients to be redirected toward alternative, more appropriate cancer therapies. Furthermore, it has the potential to alleviate the financial burden associated with unsuccessful treatment attempts. Given that the cost of CAR T therapy can range from 50,000 to several hundred thousand euros, its ineffectiveness in non-responders represents not only a therapeutic failure but also a substantial economic setback. Hence, efforts to preemptively distinguish responders from non-responders could significantly improve the cost-effectiveness and overall success rate of this innovative treatment approach. The therapy exploits the patient's own immune system as a tool to fight cancer and, due to the heterogeneous immune traits of each individual, more personalized approaches are needed to improve therapeutic outcomes and patient care. In order to improve therapeutic efficacy, it is necessary to develop better biomarker models for predicting immune system response to CAR T cell infusion, cytotoxic efficacy of the infusion product, side effect susceptibility of each patient, therapeutic outcomes, and long-term remission.

Numerous researchers worldwide have sought to identify effective predictive biomarkers, albeit so far only with limited success. The Eastern Cooperative Oncology Group (ECOG) performance status is a general scale used to evaluate disease progression and the patient's abilities in daily living (11, 12). Considerable attention has been paid to estimating tumor burden prior to CAR T cell therapy, as lower tumor burden and biomass are preferred for an effective antitumor response by CAR T cells. Although tumor burden is a critical factor influencing the success of CAR T therapy (13–15), the presence of disseminated tumor already serves as a primary exclusion criterion for this treatment. Some researchers propose that assessing the tumor burden prior to CAR T cell therapy may predict therapy's outcome (14, 16, 17). However, given the stringent inclusion criteria and the complex mechanisms affecting the therapy's outcome and the onset of side effects, this strategy alone is not comprehensive enough for effective prediction of therapy progression (18). Clinical evidence also suggests that ≥ 3 prior lines of therapy may predict inferior survival, suggesting that CAR T therapy may be more effective if given earlier (19).

Another commonly used predictive model is the CAR-HEMATOTOX score, which captures cytopenias (thrombocytopenia, anemia, neutropenia, etc.) and inflammatory markers (C-reactive protein (CRP), ferritin, etc.) at baseline condition (20, 21). Factors included in the CAR-HEMATOTOX score are associated with prolonged cytopenias following CAR T cell therapy (20). Even though studies cite that CAR-HEMATOTOX score represents an easy-to-use risk-stratification tool that is helpful in ruling out patients at risk of hematotoxicity, the baseline CAR-HEMATOTOX score alone did not prove to be an accurate predictor of CAR T therapy progression (21, 22).

The Inflammation-Based Prognostic Score (IBPS) is a validated approach assessing systemic immune inflammation as well as a prognostic nutritional index which might prove useful in predicting CAR T therapy outcomes, however, further research is needed (23). Furthermore, the Endothelial Activation and Stress Index (EASIX)

10.3389/fimmu.2024.1378944

TABLE 1 Overview of incidence of CRS and ICANS and their severity in patients treated with CAR T cell therapies.

Target Antigen	N	CR (%)	CRS (%)	Severe CRS* (%)	ICANS (%)	Severe ICANS* (%)	Ref.
ALL							
CD19	30	90	100	27	43	NA	(182)
	75	81	77	46	40	13	(183)
	53	83	85	26	44	42	(15)
	43	93	93	23	49	21	(184)
	35	69	94	17	40	6	(185)
	Average:	**83**	**90**	**28**	**43**	**21**	
NHL							
CD19	32	34	63	13	28	28	(186)
	28	57	57	18	39	11	(187)
	101	54	93	13	64	28	(188)
	111	40	58	22	21	12	(189)
	269	53	42	2	30	10	(190)
	Average:	**48**	**63**	**14**	**36**	**18**	
CLL							
CD19	14	29	64	43	43	7	(191)
	24	21	83	8	33	25	(192)
	38	28	63	24	8	0	(193)
	Average:	**26**	**70**	**25**	**28**	**11**	
MM							
BCMA	16	63	94	38	NA	NA	(194)
	57	68	90	7	2	0	(195)
	25	8	88	32	32	12	(196)
	33	45	76	6	42	3	(197)
	128	33	84	5	18	3	(198)
	Average:	**43**	**86**	**18**	**24**	**5**	
MCL							
CD19	68	67	91	15	63	31	(199)

N, Number of patients; CR, Complete response; CRS, Cytokine release syndrome; ICANS, Immune effector cell-associated neurotoxicity syndrome; ALL, B-cell acute lymphoblastic leukemia; NHL, Non-Hodgkin lymphoma; CLL, B-cell chronic lymphocytic leukemia; MM, Multiple myeloma; MCL, Mantle cell lymphoma.
*Grade 2-4. NA, Not analysed.

score, a marker of endothelial damage, was tested to predict the occurrence of CAR T therapy side effects. However, the major limitation of the EASIX score arises from the use of surrogate blood biomarkers that do not directly indicate endothelial damage but could also be associated with other pathologic conditions. The EASIX score is based on baseline blood levels of lactate dehydrogenase (LDH), creatinine, platelets, and additionally CRP and ferritin (24–26).

Another prediction score called the modified Cumulative Illness Rating Scale (CIRS), is used to assess comorbidities in patients with hematologic malignancies. The comorbidities with the highest impact on therapy prognosis have been classified into four main categories, referred to as the ″Severe4″ (encompassing the respiratory, upper gastrointestinal, hepatic, and renal systems). Patients with an overall CIRS score ≥ 7 before CAR T cell therapy, indicating severe or life-threatening comorbidities, were associated with worse CAR T therapy progression and overall survival (19, 27, 28). Although severe comorbidities serve as a prediction of poor therapy response, not many patients bear other severe illnesses. Therefore, the CIRS score is only useful for distinguishing between therapy responders and non-responders in this small group of critically ill patients, but not in patients without comorbidities or for identifying patients at increased risk for developing severe side effects (29).

Other studies have demonstrated statistically significant correlations of specific single biomarkers (e.g., LDH, programmed

cell death protein 1 (PD-1), ferritin, CRP, interleukin 6 (IL-6), interleukin 15 (IL-15), etc.) with therapy progression prior to CAR T cell infusion, but failed to encapsulate the complexity of the immunologic response to CAR T cells and their antitumor effect (30–35). While many of the aforementioned prediction scores show correlations with CAR T therapy outcomes and the occurrence of adverse effects, they are unable to capture the intricate combinations of various factors involved in the antitumor activity of the infused CAR T cells and the immune system response. Therefore, more robust and complex prediction scores are needed.

The aim of this review is to identify six principal groups of predictive biomarkers and propose their use in the development of improved and efficient models for early prediction of outcomes and adverse effects in CAR T cell therapy. This approach captures various aspects of the immune response, which is a critical factor in developing robust predictive models intended for a broader population. Our review focuses on potential blood markers that can be measured using common methods, as well as advanced immunological techniques. The main focus is on markers where even minor changes in blood concentrations could have a significant value in accurately predicting the therapy progression. This is an innovative new concept that has never been explored before into such detail. It has the potential to significantly improve the course of CAR T cell therapy and patient care, thereby making this advanced immunotherapy more appealing and the course of therapy more convenient and favorable for patients.

2 Prospective groups of biomarkers to predict progression of CAR T cell therapy

2.1 Changes in mitochondrial dynamics

To better understand the state of immune cells during the process of CAR T cell therapy, it is important to note that at the time of leukapheresis, the patient's T lymphocytes have usually already undergone at least two lines of other cancer therapies (9). These cells, influenced by the previous lines of immunosuppressive medication and the inhibitory tumor microenvironment (persistent antigen stimulation, inhibitory signaling, hypoxia, acidosis, etc.), often enter the CAR T production process already exhausted, terminally differentiated, and with impaired mitochondrial function (36, 37). During the production process, the cells are activated, genetically modified, proliferated, kept, and stored in *in vitro* conditions (38, 39). Upon infusion into the patient, it is desired that the CAR T cells further clonally expand, migrate rapidly to the tumor site, recognize, and efficiently kill tumor cells, with each CAR T cell eliminating as many tumor cells as possible (40, 41). Since all of these processes are extremely energy consuming, adequate energy production and cellular energy metabolism are crucial for an effective and successful therapy course. In this context, mitochondria play a key role as cellular organelles, responsible for energy production and metabolism (42, 43), constantly adapting to environmental stimuli and the energy demands of the cell. A simplified schematization of mitochondrial dynamics during different phases of CAR T cell therapy is presented in Figure 1.

For successful therapeutic outcomes at each phase of the process, it is imperative that mitochondrial function remains robust and demonstrates rapid adaptability to alterations in the cellular milieu and metabolic demands. Five main groups of mitochondrial processes and their potential impact on CAR T cell therapy are further discussed. These are metabolic reprogramming, mitochondrial mass and biogenesis, mitochondrial membrane potential, production and neutralization of reactive oxygen species (ROS), and mitophagy.

Metabolic reprogramming in T lymphocytes refers to the shift in cellular metabolic pathways in response to changes in cellular energy requirements. The primary cellular metabolism in naive, non-activated T cells is oxidative phosphorylation, in which ATP is generated by the transfer of electrons through the electron transport chain at the inner mitochondrial membrane, producing few toxic byproducts and efficiently utilizing glucose (44, 45). However, when cells' energy demands increase (e.g., during activation, proliferation, cytotoxic activity, or other complex cellular processes), cells shift their metabolism toward glycolysis (46). The latter produces ATP molecules faster, but less efficiently and with the production of toxic byproducts, such as excessive lactate, which can lead to acidification of the cellular environment and loss of cellular functions (47). In addition to glucose metabolism, other catabolic pathways, such as efficient fatty acid oxidation, play critical roles in T cell development, central memory differentiation, cell survival, and long-term remission (48). While shifts in metabolic pathways in healthy cells occur regularly in response to stimuli for altered energy demands, it has been shown that the most effective CAR T cells possess a balanced metabolic profile and are characterized by the ability to quickly shift from one metabolic type to another and vice versa. Inefficient metabolic shifts can result in prolonged glycolysis, inefficient energy production, and consequently ineffective and short-lived CAR T cells (42, 49–51).

Adequate mitochondrial mass is another critical factor defining cellular energy production capacity (52). Along with the increased energy demands and metabolic switch to glycolysis in T lymphocytes or CAR T cells, these cells enhance their mitochondrial biogenesis, resulting in elevated number of mitochondria per cell, and increased mitochondrial size and mass to increase the energy production capacity (53). For the CAR T production process, it is desired that the input T cells have intact mitochondrial function and high mitochondrial biomass (49). After T cell selection, the cells first undergo activation characterized by mitochondrial fission and multiplication. This leads to the formation of punctate mitochondria with loose cristae, reducing the efficiency of oxidative phosphorylation and triggering the initiation of glycolytic metabolism characteristic of effector T cells (42, 53). After effector function, a small proportion of T lymphocytes transform into a memory phenotype with large, elongated mitochondria. These mitochondria possess a high capacity for energy production, which enables them to maintain oxidative phosphorylation and allows the cells to persist in the organism for prolonged time periods (42, 52). However, most effector T lymphocytes become

10.3389/fimmu.2024.1378944

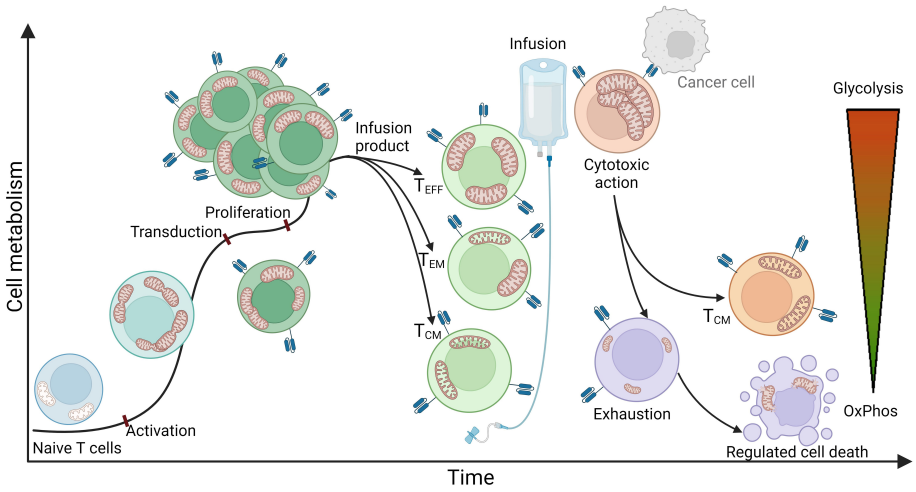

FIGURE 1
An idealized representation of T cell metabolism and mitochondrial dynamics in CAR T cell therapy. The figure illustrates a simplified representation of T cell metabolism and mitochondrial dynamics during the stages of CAR T cell therapy. The process begins with naive T cells characterized by quiescent mitochondria that mainly use oxidative phosphorylation (OxPhos) as a metabolic pathway. The obtained T cells are transferred to the CAR T production process, where they first undergo activation. This stage is characterized by a significant increase in energy demand and consequently a shift in metabolism towards glycolysis. At the same time, mitochondria undergo fission, multiplication, and formation of cristae - intricate invaginations of the inner membrane that serve to expand the surface area of the inner membrane to increase energy production capacity. After activation, the cells are genetically modified, usually by exploiting viral vectors such as lentiviral or retroviral vectors encoding for a CAR receptor. This modification normally has no significant effect on cellular metabolism or mitochondrial dynamics. Once the genetically modified CAR T cells are produced, they enter a stage of proliferation in which they further multiply their mitochondria and continue to rely on glycolysis to meet their increased energy demands. Subsequent steps include purification and quality control, culminating in the production of the infusion product, which consists mainly of effector T cells (Teff), effector memory T cells (Tem), and central memory T cells (Tcm). Effector T cells are characterized by a high rate of glycolysis and increased mitochondrial biomass, which enables the cells to respond rapidly to target cells and effectively perform their cytotoxic function within a short period of time. Central memory T cells, on the other hand, typically possess elongated mitochondrial structures and primarily utilize oxidative phosphorylation, allowing them to extend their lifespan and persist in the organism. The phenotype of effector memory T cells can be simplistically viewed as a combination of both and therefore exhibits both glycolytic and oxidative phosphorylating metabolism. Once infused into the patient, CAR T cells rapidly recognize tumor cells and exert a cytotoxic effect on them. Cytotoxicity is a highly energy-consuming process characterized by a high rate of glycolysis and increased mitochondrial biomass. Mitochondria are polarized along the cellular cytoskeleton toward the immunological synapse, providing the energy required for production, polarization, and formation of the immunological synapse, as well as for transfer of lytic granules into target cells to induce apoptosis - in the case of CAR T cells, apoptosis of target cancer cells. Remarkably, a single CAR T cell can eliminate multiple cancer cells. Following the cytotoxic effect, the majority of T cells become exhausted, with mitochondria undergoing mitophagy and the cells losing their effector function as all types of metabolism diminish. These cells may undergo apoptosis, initiated by the mitochondria, leading to rupture of cell structures and cell death. However, a small subset of cytotoxic cells transforms into central memory T cells, forming a permanent immunological memory for the specific antigen.

exhausted, the mitochondria disintegrate, shrink, and all metabolic types vanish, leading to cell apoptosis (53). In the context of predicting CAR T therapy progression, Rostamian et al. (42) found that impaired mitochondrial function with low mitochondrial biomass prior to infusion of CAR T cell product leads to poor therapeutic outcomes.

The mitochondrial membrane potential ($\Delta\Psi m$), generated by pumping protons from the mitochondrial matrix into the intermembrane space, is another indicator of mitochondrial function and the antitumor efficacy of CAR T cells and is crucial for efficient ATP synthesis (54). High mitochondrial membrane potential characterizes the effector phenotype of T lymphocytes, along with increased glycolysis, ROS production, and cellular impairment. In contrast, low mitochondrial membrane potential is characteristic of naive and memory T lymphocytes and is favored in input cells in the CAR T production process for better energy production capacity of the final product (42, 50). In terms of cytotoxic T lymphocytes, lower $\Delta\Psi m$ levels are desirable, as they indicate a better metabolic capacity of the cells, less exhaustion, correspondingly low glycolysis levels, better persistence *in vivo*, better migratory capacity, and antitumor efficacy (50).

Reactive oxygen species (ROS) are oxygen-containing molecules that are mainly generated in the mitochondria (55). Due to their instability, they react rapidly, causing cellular defects at the DNA, RNA, or cellular structure levels, and can even induce cell death (43). Small amounts of ROS are continuously produced and act as signaling molecules, which are then neutralized by cellular antioxidant mechanisms (56). However, under pathological conditions (e.g., cancer) and in exhausted cells, ROS concentrations can greatly increase (53, 57) and damage cellular structures to the point of irreparability (53), impair T cells function (58), and induce T cells senescence (59). Elevated ROS concentrations and impaired antioxidant mechanisms for ROS neutralization in T lymphocytes

and CAR T cells prior to infusion of CAR T cell product are indicative of a poor prognosis for effector cell function upon infusion into the patient (42).

Mitophagy is a multistep process that involves recognition of damaged or dysfunctional mitochondria, their uptake into autophagosomes, and subsequent degradation by fusion with lysosomes (60). The process is tightly regulated at multiple levels, including activation of specific mitophagy receptors, recruitment of autophagic machinery components, and coordination of autophagosome-lysosome fusion (61). Mitophagy is essential for proper mitochondrial function in CAR T cells, as it helps to prevent the accumulation of damaged mitochondria that otherwise accumulate excessive amounts of ROS and impair energy production throughout the CAR T production process as well as the therapy course (49, 62).

Mitochondria therefore hold great potential as therapeutic targets to aid the antitumor therapies and as predictive biomarkers for assessing the therapy course prior to CAR T cell infusion (42, 43, 46, 49, 57, 62).

As research continues to illuminate the dynamic role of mitochondria in CAR T cell therapy, understanding and monitoring mitochondrial processes may lead to more effective therapeutic outcomes. Methods to assess mitochondrial function can be categorized at the genomic, transcriptomic, proteomic, and metabolomic levels (63). Primary mitochondrial genetic disorders arise from cellular or mitochondrial pathological mutations (63) that can be identified by genome sequencing analyses (64). At the transcriptomic level, gene expression can be assessed using techniques such as RNA sequencing, polymerase chain reaction (PCR), Northern blotting, microarrays, and many others (65). Epigenetic regulation and post-translational modifications also play an important role in modulating mitochondrial dynamics (66). A variety of techniques are available for proteomic analysis. For example, fluorescently labeled dyes can be used to stain target molecules, allowing determination of their concentration, localization, and dynamics. Such measurements can be performed with fluorescence microscopy (i.e., flow cytometry) and allow visualization and quantification of mitochondrial membrane potential, mass, and other parameters (67). Other common methods for analyzing protein content include Western blotting, electrophoresis, ELISA, chromatography, mass spectrometry, protein microarrays, etc. (63, 65, 66) The Seahorse analyzer is an excellent tool for determining the metabolic status of target cells (68). In addition, high-resolution respirometry, isotope tracking, and other methods have proven useful in this field (69). Other microscopy techniques, such as transmission electron microscopy (TEM), provide high-resolution images of mitochondria that allow direct observation of changes in mitochondrial morphology and structure (70). The analysis of mitochondrial characteristics offers an insight into the cell's functional state, potentially serving as a biomarker for predicting cell behavior and progression during the CAR T production process. Since mitochondrial characteristics are indicative of cells' energy capacity, apoptotic susceptibility, and cytotoxic functionality, they could be utilized to forecast the anti-tumor cytotoxicity of CAR T cells before therapy initiation. This prospective approach may allow for the early identification of therapeutic potential of CAR T cells, enhancing patient-specific treatment strategy.

2.2 Endothelial activation

The endothelium is a layer of endothelial cells that form the inner lining of blood and lymphatic vessels and play a crucial role in many bodily functions, including the regulation of inflammation, blood clotting, and the formation of new blood vessels (angiogenesis) (71). Upon infusion of CAR T cells, the infused cells migrate to the tumor site and induce apoptosis of tumor cells. In addition to the cytotoxic effect, they secrete cytokines that trigger inflammation and activation of endogenous immune cells (such as macrophages, dendritic cells, natural killer cells, B cells, etc.), fibroblasts, and endothelial cells (72–76). Activated endogenous cells also secrete proinflammatory cytokines and chemokines, which can lead to overactivation of the immune system, endothelial damage, and increased vascular permeability (5, 77). Among these inflammatory cytokines and chemokines, IL-6 is considered the critical cytokine involved in endothelial permeabilization and induction of CRS (5, 78, 79). After endothelial activation and permeabilization, activated endothelial cells also begin to secrete inflammatory signals (such as IL-6). This further leads to increased permeability of the blood-brain barrier, infiltration of inflammatory molecules and immune cells into the central nervous system, and onset of ICANS symptoms such as headache, nausea, confusion, blurred vision, delirium, coma, or even death (80, 81). IL-6 antagonists (such as tocilizumab) are used as intervention drugs to treat severe CRS and ICANS symptoms (78, 79, 82). The stages of endothelial activation and blood-brain barrier permeabilization in CAR T cell therapy leading to the occurrence of CRS and ICANS are shown in Figure 2.

In CAR T cell therapy, endothelial activation plays a crucial role in inflammation, regulation of the immune response, and development of side effects (CRS, ICANS, etc.) (5, 83). After administration of the cell product and migration of CAR T cells to the tumor site, the antitumor immune response is initiated. At this time, it is desired that endothelial activation and vascular permeability remain low to moderate to allow for an effective immune response and inflammatory signaling without causing severe inflammation or vascular injury (5). It is important to note that increased endothelial activation and vascular permeability can lead to severe inflammation and high-grade side effects, resulting in less efficient tumor cell killing, unsuccessful therapeutic outcomes, and unmanageable development of side effects that can result in long-lasting consequences and even death (83). Not only does the endothelial activation play a crucial role after administration of the cell product and therapy progression, but studies have also shown that endothelial activation prior to CAR T cell infusion may also contribute to therapy progression and have a negative prognostic effect on CAR T therapy outcome and the occurrence of CRS and ICANS (6). There are many reasons for endothelial activation prior

10.3389/fimmu.2024.1378944

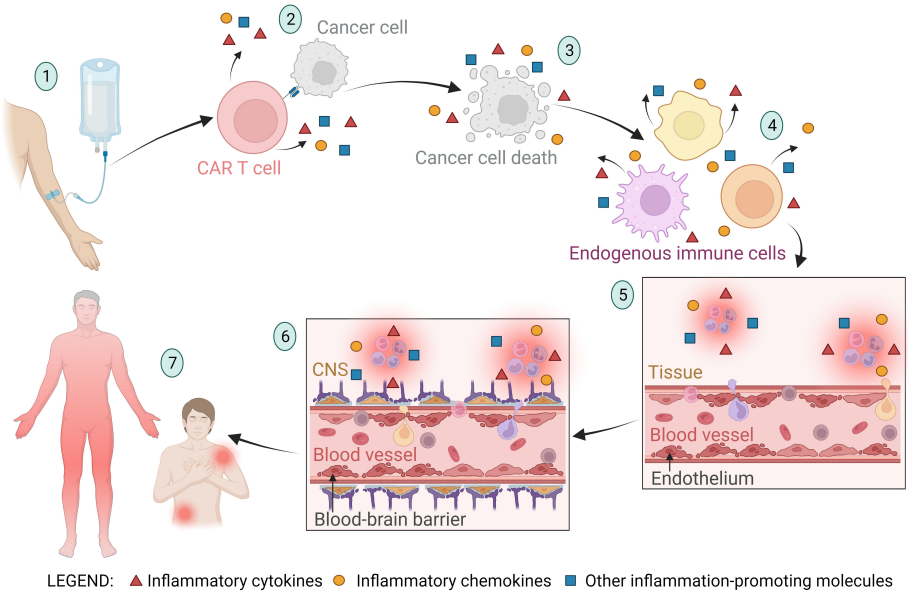

FIGURE 2
A schematic representation of the stages of endothelial activation and blood-brain barrier permeabilization in CAR T cell therapy leading to the occurrence of cytokine release syndrome (CRS) and immune effector cell-associated neurotoxicity syndrome (ICANS). (1) The CAR T cell product is infused into the patient, and the CAR T cells migrate to the tumor site. (2) CAR T cells recognize the tumor cells and exert a cytotoxic effect on them, triggering the release of inflammatory molecules. (3) Apoptosis and pyroptosis of tumor cells lead to tumor cell death and release of large amounts of cellular components and apoptotic bodies into the bloodstream. The byproducts of tumor cell death trigger the activation of neighboring cells and further stimulate the secretion of inflammatory molecules. (4) The inflammatory molecules from the previously described stages of the CAR T therapy process cause activation of endogenous immune cells (such as macrophages, dendritic cells, neutrophils, natural killer cells, healthy B cells, T cells, and others), resulting in further secretion of inflammatory molecules. (5) Cytokines (primarily IL-6) and other inflammatory molecules stimulate activation and permeabilization of the endothelium, leading to migration of immune cells into the tissue and initiation of inflammation. Activated endothelial cells also begin to secrete inflammatory molecules (such as IL-6), further promoting endothelial activation. (6) Along with endothelial activation, the blood-brain barrier (BBB) is also activated and its integrity is compromised. This allows immune cells and inflammatory molecules to enter the central nervous system (CNS), culminating in CNS inflammation and subsequently the onset of immune effector cell-associated neurotoxicity syndrome (ICANS). (7) Endothelial activation and increased permeability allow immune cells and inflammatory molecules to infiltrate tissues and cause local or systemic inflammation, characteristic of CRS.

to CAR T cell infusion. On the one hand, it may be a consequence of previous cancer therapies (chemo- or immunotherapy) and the lymphodepleting regimen. Tumor burden with inhibitory tumor microenvironment (TME), hypoxia, and permanent antigen stimulation may also trigger endothelial activation. On the other hand, factors may be un-related to the tumor, such as other medical conditions (diabetes, hypertension, etc.), infections and inflammations, or the physiological state of the patient (obesity, physical performance, age, stress, injuries, etc.) (37, 80, 84). It is usually impossible to select a single factor, but a combination of the listed reasons typically results in excessive activation of the endothelium.

In the context of predicting the outcome of CAR T cell therapy, the Endothelial Activation and Stress Index (EASIX) score has been proposed. It is defined as (creatinine [mg/dL] × lactate dehydrogenase [LDH; U/L])/platelets [10^9 cells/L] or modified EASIX score combined with CRP × ferritin (EASIX-FC) (24, 25, 85). The correlation between the EASIX score prior to CAR T cell infusion and the occurrence of CRS and ICANS was confirmed (26, 85). However, while EASIX can be a useful predictive tool, it does not directly measure endothelial activation. Instead, it uses surrogate biomarkers that may be influenced by various other factors and accompanying pathological conditions.

In the search for better biomarkers of endothelial activation, the candidates can be classified into three groups based on their effect on the endothelium. The first are endothelial stabilizers, which are mainly synthesized by the endothelium and released into the bloodstream. They are responsible for maintaining endothelial homeostasis and stability and are absent or under-expressed in pathological conditions with endothelial overactivation. Common examples of endothelial stabilizers are nitric oxide (NO) (86), VE-cadherin (87), antioxidant compounds such as superoxide dismutase (SOD) and catalase to combat oxidative stress and maintain endothelial stability (88), extracellular matrix (ECM) components such as collagens, laminins, fibronectins, etc., that structurally support the endothelium and are responsible for maintaining endothelial barrier function (89), and many others. The next group of biomarkers for endothelial activation are endothelial destabilizers, which can be secreted from various cell types and are typically elevated in pathological conditions such as inflammation, stress, cancer, injury, and others. Some common examples of endothelial destabilizers are inflammatory cytokines, such as tumor necrosis factor-alpha (TNF-α) and IL-6 (90, 91), ROS that can cause oxidative stress and damage to the endothelium (92, 93), matrix metalloproteinases (MMPs) that can degrade the ECM and impair endothelial structural support and barrier

function (89, 90), and many others. The next important group of endothelial activation biomarkers are endothelial adhesion molecules, which are expressed on the surface of endothelial and other cells and play a crucial role in the interaction and adhesion of leukocytes, other cells, and the ECM to the endothelium (94, 95). Endothelial adhesion molecules play dual roles in stabilizing and destabilizing the endothelium and also in controlling the contact between CAR T cells and their targets (96). Under normal physiological conditions, they contribute to the maintenance of vascular integrity and homeostasis by regulating leukocyte recruitment and transendothelial migration. However, in pathological conditions such as inflammation, infection, or cancer, excessive or prolonged expression of adhesion molecules can lead to endothelial destabilization, increased vascular permeability, and leukocyte infiltration (96, 97). To highlight only a few of the important examples of adhesion molecules, Intercellular Adhesion Molecule-1 (ICAM-1), angiopoietin-2 (Ang-2), Vascular Cell Adhesion Molecule-1 (VCAM-1), and others contribute to endothelial permeabilization. In elevated concentrations, they exhibit a poor prognostic effect and may immunosuppress CAR T cells (98, 99).

It is important to note that to maintain endothelial homeostasis, a precise balance between stabilizing and destabilizing signals must be maintained. Many of the endothelium-related molecules are released into the circulation and can be easily measured from blood samples. They therefore represent a great source of potential biomarkers for predicting CAR T cell therapy outcomes and side effects susceptibility. Moreover, endothelial markers, reflecting the state of vascular health, could serve as valuable tools for predicting therapeutic outcomes even before the initiation of CAR T cell therapy process. Their role in vascular integrity and reaction to inflammatory stimuli makes them promising indicators for assessing the efficacy and potential side effects of treatments in advance.

2.3 Central nervous system impairment

The term central nervous system (CNS) includes the brain, spinal cord, nerves, and associated cells. The causes of CNS impairment and injury may be due to concomitant diseases and disorders (autoimmune diseases, neurodegenerative diseases, stroke, etc.), neurological diseases of exogenous origin (toxins, inflammation, infection, injury, etc.), or tumor burden and the TME. The malignancy itself can promote inflammation, tissue damage, and CNS impairment, but prior cancer therapies (chemo- or immunotherapy) and the lymphodepleting regimen may also have an impact (6, 9, 100, 101).

The connection between CNS impairment and the outcome of CAR T cell therapy is an emerging area of research. Focusing on even the smallest changes in markers of blood-brain barrier disruption and markers of neuronal and glial injury could help in predicting and monitoring the progression of ICANS (6, 101–103). Schoeberl et al. (104) observed that efficient ICANS prediction could be achieved in patients without a history of neurological disorders, while patients with accompanying neurological disorders and diseases show signs of previous and/or chronic neuronal damage and respond very heterogeneously to the treatment. Therefore, the predictive accuracy for therapy outcomes and ICANS is limited to individuals without prior neuronal injuries (104).

Biomarkers for determining CNS impairment can be monitored after cell infusion to observe disruptions in CNS homeostasis. The measured values can serve as early indicators of ICANS. However, an emerging field is the use of biomarkers of CNS impairment prior to infusion of CAR T cells. These markers reflect impaired CNS homeostasis and possible CNS injury that may later lead to the development of high-grade ICANS (100). Recent studies have shown that levels of CNS impairment markers prior to CAR T cell infusion correlate with the development of ICANS after CAR T cells administration (103, 105, 106). Several notable biomarkers of neuronal or glial injury have been identified that show considerable promise for predicting the occurrence of ICANS with CAR T cell therapy. Such examples include neurofilament light chain (NfL), a protein originally located in neurons and released into the cerebrospinal fluid (CSF) and into the bloodstream during neuronal injury (100, 104); glial fibrillary acidic protein (GFAP) which indicates astrocyte activation and astrogliosis, often associated with neuroinflammation (105, 106); S100 calcium-binding protein B (S100B), which is released by activated astrocytes and indicates CNS injury (106), and many others. These markers are secreted into the CSF upon CNS injury, but their concentrations in the CSF correlate directly with their concentrations in the blood and can therefore be easily measured from a blood sample (104, 107, 108). Furthermore, the predictive value of CNS impairment markers prior to therapy initiation is gaining attention. By assessing these markers before starting CAR T cell therapy, clinicians might better anticipate therapeutic outcomes and the risk of ICANS, enabling more tailored and proactive management strategies. This approach leverages the correlation between pre-treatment levels of CNS markers and the likelihood of subsequent ICANS, highlighting their utility in enhancing patient-specific therapeutic strategies.

2.4 Markers of the immune system

The concept of "immune system markers" encompasses diverse facets of a patient's heterogeneous immune system. Such aspects include the patient's baseline characteristics such as age, performance status, organ function, comorbidities, immune system characteristics, immune cells function and exhaustion, and other factors. These characteristics may influence the course and outcome of CAR T cell therapy (19, 27, 29, 37, 84, 109, 110). Moreover, immune system function markers may denote cell markers that differentiate between subpopulations of immune cells and define their phenotypic characteristics (29, 111). This has notable implications for the production process of CAR T cells and their subsequent antitumor efficacy post-administration (29, 37). Therefore, an in-depth understanding of individual immune systems and immune cells characteristics could potentially pave the way for improved prediction of response to CAR T cell therapy and resulting therapeutic outcomes.

Various baseline characteristics and blood biomarkers have been identified that might predict the outcomes of CAR T cell

therapy, thus highlighting their importance for therapy selection and management. Among physiological measures, parameters such as age, heart rate, body temperature, comorbidities, and blood pressure have displayed the highest predictive values (29, 110, 112). Among blood biomarkers, leukocyte count, inflammatory cytokines, hemoglobin, creatinine, CRP, ferritin, fibrinogen, and platelets have been shown to predict the development of severe CRS (10, 34, 113, 114). However, consideration of these patient characteristics alone does not provide a sufficiently specific and robust predictive model for application in a broader population. Given their high variability, which may be influenced by previous therapies, patient lifestyle, and disease burden, baseline patient characteristics should be used in conjunction with more robust biomarker systems (29, 37).

Given the nature of CAR T as a T cell therapy, T cell biomarkers are frequently being monitored throughout the process. For instance, studies have shown that a defined CD4:CD8 ratio of T lymphocytes at the time of leukapheresis (ranging from 1:1 to 3:1) is associated with a better proliferative capacity for the CAR T production process (111, 115, 116). A higher CD45RA : CD45RO ratio at the time of leukapheresis indicates an increased proportion of naive, less differentiated T cells correlated with improved proliferative capacity and therapeutic outcome (49). CAR T cell subsets can be distinguished as naive T cells (CD45RO−/CD62L+/CD27+), central memory T cells (CD45RO+/CD62L+/CD27+), effector memory T cells (CD45RO+/CD62L−/CD27−), and effector T cells (CD45RO+/CD62L−/CD27−). Activated CAR T cells express activation markers such as CD25, CD69, and CD137 (76, 117, 118). Furthermore, studies indicate that higher levels of central memory T cells (Tcm) and lower levels of effector T cells (Tef) in the infusion product are associated with improved therapeutic outcomes (32, 76, 111, 118, 119). Elevated levels of exhausted and senescent (CD57+) T cells in the infusion product correlate with poor therapy progression (76, 120). To achieve long-term remission, it is therefore advantageous to have memory CAR T cells that persist over time and provide an efficient antitumor response in the event of relapse (121). New phenotyping biomarkers with higher predictive capacity for CAR T therapy progression are being extensively investigated.

Another significant component of biomarkers of the immune system pertains to the antitumor cytotoxic activity of the CAR T cells. The mechanisms entailing migration, tumor cell recognition, cytokine release, and target cell killing are highly complex and play key roles in successful antitumor efficacy of CAR T cells after administration of the cell product into the patient (10, 96, 122, 123). The specific steps of the cytotoxic function are shown in Figure 3. Any malfunctions within these cytotoxic mechanisms can lead to unsuccessful therapy and severe inflammation. Such malfunctions

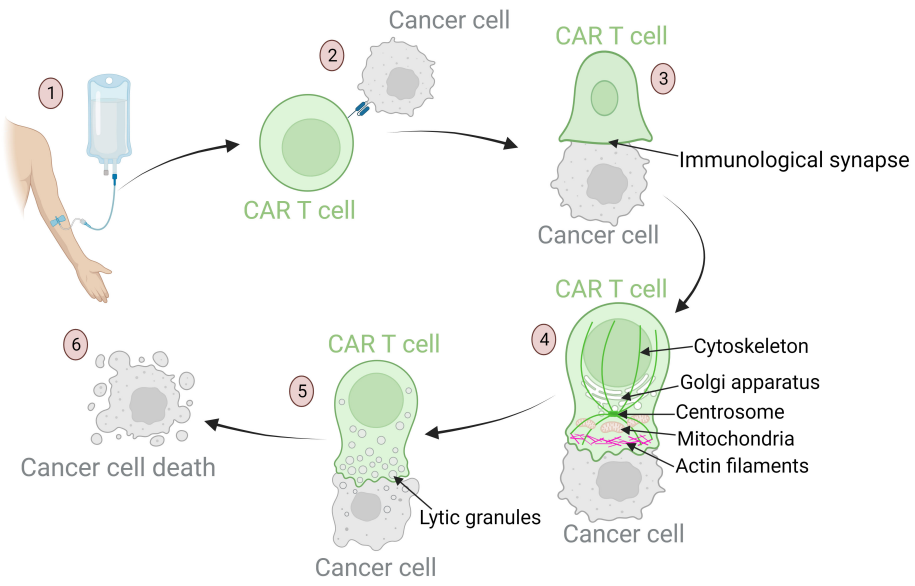

FIGURE 3
Mechanisms of anti-tumor response of CAR T cells: from target recognition to tumor cell apoptosis. (1) Upon infusion into the patient, CAR T cells migrate through the bloodstream to tumor sites. Their homing ability is influenced by chemokines and adhesion molecules that ensure these cells reach the designated area. (2) Once in the tumor vicinity, CAR T cells recognize specific tumor-associated antigens. This recognition is crucial for precision in targeting. Defects in this process can result in off-tumor toxicities and the development of severe side effects. (3) After recognition of the target antigen, the CAR T cell binds to the tumor cell, leading to cytoskeletal reorganization and formation of the immunological synapse – a specialized interface between the CAR T cell and its target. (4) Dynamic reorganization of CAR T cell components is required to achieve a cytotoxic effect. The cellular organelles responsible for cytotoxic processes travel along the reorganizing cytoskeleton toward the immunological synapse: actin filaments provide structural support for the lamellipodium near the synapse; the centrosome guides cytoskeletal reorganization; the Golgi apparatus aids in the formation of cytotoxic vesicles; mitochondria provide the energy required for cytotoxic processes. (5) These mechanisms culminate in the formation of lytic granules. These granules are transported into the target cell through the immunological synapse. (6) Lytic granules induce apoptosis of tumor cells.

may stem from relatively rare genetic disorders or from T cells dysfunction, which may be a consequence of disease burden, patient characteristics, and exhausted and senescent T cell phenotypes prior to the CAR T production process (10, 37, 84, 124). The malfunctions may also arise during the production process, as cells respond differently to *ex vivo* manipulation due to their individual characteristics (37). The vector encoding the CAR receptor is integrated semi-randomly into the genome, leading to variable expression and consequently variable efficacy of the CAR T cells. The receptors can also be expressed constitutively for extended periods or inductively for a brief duration (125, 126).

Furthermore, the integration of transgenes via viral vectors raises concerns about potential risks, including insertional oncogenesis, gene inactivation or dysregulation, and impairment of cell functions (126). Early detection of such integration events is crucial for ensuring the safety of CAR T cell therapies. Potential biomarkers, such as abnormal gene expression levels, novel fusion transcripts, epigenetic changes, etc., and assays, such as linear amplification-mediated PCR (LAM-PCR), high-throughput sequencing (i.e. integration site sequencing), whole-genome sequencing (WGS), etc. could serve to identify transgene integration sites (127). Advanced bioinformatics tools are further used to analyze the data to assess the potential impact of transgene integration on gene expression (127). Monitoring these integration events could provide insights into the safety profile of CAR T cell products and help mitigate risks associated with gene therapy.

After infusion of the CAR T cell product, the modified cells first migrate to the tumor site. The migration and infiltration into tumor tissue are the main obstacles of CAR T efficiency in solid tumors (128) but also play an important role in hematologic malignancies (81, 97). Adequate expression of adhesion molecules (e.g., LFA-1, VCAM-1, ICAM-1, VEGFA, and others), chemokines (e.g., CCL3, CCL4, CXCL9, CXCL10, CXCL11, CXCL12, and others), and other guidance molecules are of paramount importance for effective CAR T cell homing (96, 129–135). Therefore, inadequate expression of these navigation-related molecules could serve as a negative predictive factor for the progression and outcome of CAR T cell therapy (96, 131, 132). For successful effector functions, it is imperative for CAR T cells to rapidly recognize tumor cells and facilitate CAR receptor binding with the CAR antigen (e.g., CD19, CD20, CD22, BCMA, etc.) expressed on tumor cells (136). Recent clinical evidence indicates that antigen downregulation and escape have arisen as major obstacles that affect the overall efficacy, success rate, and long-term remission after CAR T cell therapy (137). Therefore, sufficient antigen expression on tumor cells may serve as a prognostic tool for therapy outcomes and may even influence patient eligibility for CAR T cell therapy. Upon recognition of target cells, CAR T cells trigger a series of cytotoxic reactions aimed at inducing target cells apoptosis.

In the event of abnormalities within cytotoxic mechanisms or prolonged duration of the immunological synapses leading to an extended effector function timeframe, this could escalate the release of cytokines and chemokines, thus increasing inflammation, compromising the efficacy of the therapeutic response, and potentially causing a relapse of antigen-free malignancy (10, 122, 124, 129, 138–140). Methods for *ex vivo* examination of cytotoxic efficiency of CAR T cells are described in Table 2. A careful examination of cytotoxic mechanisms of T cells prior to CAR T cell infusion may provide insight into potential defects and serve as an initial indication of therapy prognosis and the probability of severe inflammation occurrence. This information is crucial for predicting the course of CAR T cell therapy prior to cell infusion.

TABLE 2 Methods for *ex vivo* investigation of the cytotoxic efficacy of CAR T cells.

Technique	Methodology	Indices	Ref.
Co-culture of CAR T cells with fluorescently-labeled tumor cells	Fluorescence microscopy	Decrease in fluorescence indicates tumor cell lysis	(129)
Chromium release assay	Detection of released radioactive chromium isotope from target cells	Elevated levels of released chromium isotope indicate higher level of target cell apoptosis	(138)
LDH release assay	Colorimetric assay	Elevated levels of released LDH indicate higher level of target cell lysis	(139)
Release of effector cytokines	ELISA	Sufficient levels of effector cytokines are released during successful target cell killing	(121, 123)
Release of degranulation markers	Flow cytometry	Effective release of cytotoxic granules leads to effective target cell killing	(123)
Expression of cytotoxicity-related proteins	qPCR	Elevated levels indicate better cytotoxic reactivity	(10)
Real-time impedance-based assays	Electrical impedance measurements	Monitoring cellular interactions, cytotoxicity, and cell lysis	(140)
Tumor spheroids or organoids	Modeling tumor cell killing	Tumor spheroids or organoids can serve as targets of tumor cell killing	(121)
Multiparametric flow cytometry	Flow cytometry	evaluation of different markers of activation, exhaustion, and cytotoxicity	(138)
Time-lapse microscopy	Live-cell imaging platforms	Visualizing CAR T cell interactions with tumor cells and monitoring tumor cell elimination kinetics	(122)
Polyfunctionality measurement	Various methodologies assessing multiple functions simultaneously (cytokine production, proliferation, target cell killing, etc.)	A more comprehensive indication of CAR T cell cytotoxic efficacy	(200)

2.5 Extracellular vesicles

Extracellular vesicles (EVs) are small membrane-derived particles that are released by cells into the extracellular space and can be transported throughout the body. These vesicles play an important role in cell-to-cell communication and transport a variety of biological molecules from their cell of origin to target cells (141, 142). Because they are derived from parent cells, the EVs carry markers of parent cell that allow the origin of the vesicles and their contents to be determined (143). By analyzing the vesicles content, cellular signaling can be monitored, providing insight into cell-to-cell communications (144). Their usual cargo is proteins, lipids, DNA, messenger RNAs (mRNAs), microRNAs (miRNAs), and other molecules (145).

Because EVs are involved in many physiological and pathological processes, their content provides valuable insights into the signaling of specific cell populations. For example, they can mediate immune responses, facilitate blood clotting, and contribute to the spread of cancer (141, 146, 147). In the case of CAR T immunotherapy, this could prove useful in assessing the immune system status, immune cell exhaustion and functionality, and antitumor response. On the other hand, by studying tumor cell-derived extracellular vesicles (oncosomes), the information on tumor invasiveness, antigen escape, and inhibitory signaling toward cells of the immune system, including CAR T cells, could be better understood (144, 148). EVs were shown to exhibit an effect on CAR T cells (149, 150). Due to their ability to transport molecules from one cell to another, EVs are being extensively studied for their potential use as drug delivery systems and as biomarkers for disease prognosis and immunotherapy progression (151–153).

To discuss some examples of EVs that could potentially predict response to CAR T cell therapy and the development of high-grade CRS and ICANS, the origin of the vesicles must be taken into consideration. First, the vesicles can be derived from endogenous immune cells. They can exhibit stimulatory or inhibitory functions toward CAR T cells and therapy response (154, 155). For example, an increased number of CD69 positive T cell vesicles can indicate increased T cell activation and act as a negative feedback loop that inhibits further T cell activation (156). Increased numbers of T cell EVs expressing inhibitory molecules such as PD-1, CTLA-4, TIM-3, LAG-3, and others reflect an ineffective and exhausted immune system and could consequently be used to predict poor response to therapy (150, 155, 157).

Possible sources of EVs are also CAR T cells. Studies have shown that persistent concentrations of CAR-positive EVs in the bloodstream of patients after CAR T cell infusion exhibit predictive impact on long-lasting remission (158). Evidence also suggests that CAR-positive EVs assist the antitumor function of CAR T cells by overcoming obstacles and barriers that otherwise limit the effect of the immunotherapy (159–161). The next example is increased levels of endothelial vesicles and apoptotic bodies, which indicate excessive endothelial activation and damage, which may predict the development of severe CRS and ICANS even before infusion of the cell product (151). Tumor-derived vesicles often express inhibitory molecules and reduce the antitumor effect of CAR T cells (150). Elevated levels of circulating tumor DNA correlate with poor therapeutic efficacy and higher CRS levels (162), which can also be applied to circulating oncosomes containing tumor DNA. CD19+ vesicles were shown to cause activation and exhaustion of CAR T cells with decreased antitumor activity and trigger CRS (156).

Stated here are just some common examples of EVs and their potential impact on immunotherapy. The EVs show great potential for predicting the immune response to CAR T cell therapy. However, this field is relatively young and poses many challenges. The first is the development of standardized and optimized extraction procedures for isolation of heterogeneous vesicles from cancer patients' samples. Because vesicles vary in density, structure, and size, robust isolation techniques with minimal sample loss need to be established (146). Another challenge currently being investigated by many research groups is the development of biomarkers to efficiently differentiate B-cell leukemia or lymphoma from other types of vesicles. Some studies suggest examples such as CD5, CD19, CD31, CD44, CD55, CD62L, CD82, and CD123 (150, 163, 164). Further research on this topic is needed to develop efficient biomarkers and predictive models. EVs could serve as predictors before CAR T cell infusion to provide an impression of cellular signaling and information circulating in the patient's bloodstream.

2.6 Inhibitory tumor microenvironment

The tumor microenvironment (TME) is a complex mixture of various components, including different cell types, signaling molecules, and extracellular matrix components. The TME can contribute to tumor growth, progression, and inhibition of the antitumor immune responses (165, 166). Consequently, the TME components may undermine the cytotoxic potency of CAR T cells, thereby limiting the efficacy of CAR T cell therapy. Accordingly, assessment of individual patient TME characteristics and the inhibitory properties of the TME components on CAR T cells prior to CAR T cell infusion may serve as predictive parameters for determining the potential extent of CAR T cell effector function inhibition after infusion. This could allow the prediction of inflammation development associated with immune cell inhibition.

The TME constituents are divided into six main categories based on their composition and function. First are immunosuppressive cells, which include regulatory T cells (Tregs), myeloid-derived suppressor cells (MDSCs), tumor-associated macrophages (TAMs), and other (95, 167–170). The TME immunosuppressive cells can inhibit the antitumor response in several ways: by inducing anergy, exhaustion, or even apoptosis of T cells (171, 172), by inducing expression of immunosuppressive cell markers (such as immune checkpoint molecules) (168, 170, 173), by signaling proliferation and recruitment of other immunosuppressive cells (170, 173), by altering antigen presentation, which impairs recognition of the tumor by the immune system (168), by altering metabolic pathways to deplete energy sources and produce toxic metabolites (171), and by secretion of immunosuppressive molecules such as cytokines, chemokines, and others (168, 169, 173). The TME can induce expression of inhibitory immune checkpoints, typically expressed on various immune cell

types. Normally, these molecules regulate and control the immune response to prevent over-activation. However, in the context of cancer, tumor cells can exploit their mechanisms to downregulate the immune system response, thereby facilitating evasion of the immune system. Prominent examples of inhibitory immune checkpoints include PD-1, CTLA-4, TIM-3, LAG-3, etc. (174, 175) Moreover, these inhibitory checkpoint molecules can hinder the activation and functionality of CAR T cells after infusion (174), and their quantitative expression serves as an estimate of their inhibitory effect on CAR T cells (176). Albeit more common in solid tumors, hypoxia may also manifest in the bone marrow microenvironment and contribute to immunosuppression in hematologic malignancies (168, 171). Hypoxic conditions can induce accumulation of immunosuppressive cells and molecules, inhibit the effector function of T cells, and promote immune evasion by tumor cells (95, 177). Tumor cells also expedite metabolic pathways to produce sufficient energy for tumor growth, depriving tissues of nutrients such as glucose, glutamine, amino acids, O_2, etc. (95, 171, 178) This increased metabolic activity generates toxic or acidic metabolic byproducts (such as lactate) (94, 171) that contribute to acidification of the tumor microenvironment and subsequently suppress the immune response and CAR T cell function (94, 95, 177). The dysregulation of metabolic pathways and the imbalance of metabolites can result in the production of ROS, causing further damage to immune cells and tissues, inhibiting the antitumor effect of T lymphocytes and CAR T cells, and promoting tumor growth (95, 172). Another significant impact of the TME is the degradation and alteration of the ECM by degradative enzymes secreted by tumor cells (e.g., metalloproteinases, collagenases, oxidases) (173, 179). Degradation and alteration of the ECM can lead to impaired tissue integrity, accumulation of metabolic byproducts, and promotion of tumor spread and growth (94, 180). The main components of the inhibitory TME associated with hematologic malignancies are shown in Figure 4.

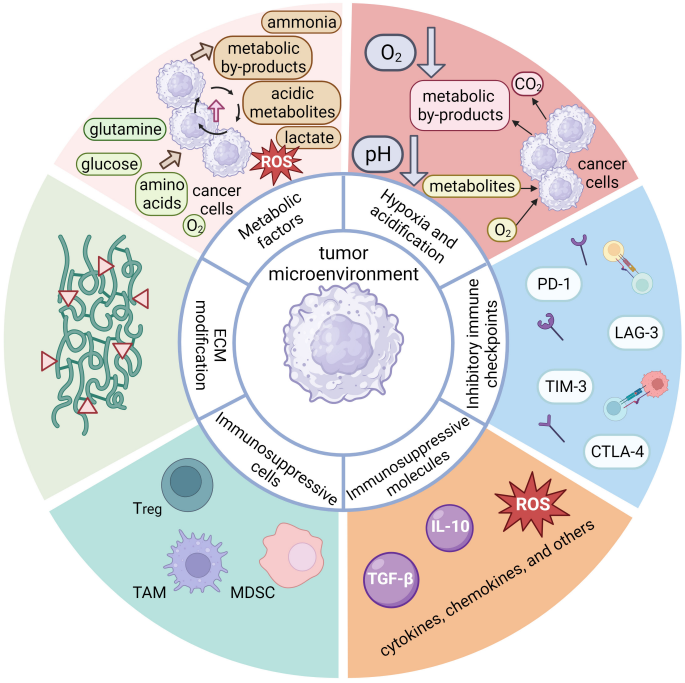

FIGURE 4
A schematic representation of the main components of the inhibitory tumor microenvironment (TME) associated with hematologic malignancies, which possess inhibitory properties toward the anti-tumor response of the immune system. The components of hematologic TME can be divided into six main groups. One important component are the immunosuppressive cells, which include regulatory T cells (Tregs), tumor-associated macrophages (TAMs), myeloid-derived suppressor cells (MDSCs), tumor cells, and others. These immunosuppressive cells can secrete immunosuppressive molecules, along with other patient cells. These molecules are cytokines (IL-10, TGF-β, etc.), chemokines, or others (e.g., reactive oxygen species), all of which may exert an inhibitory effect on the anti-tumor functions of the immune system. The expression of inhibitory immune checkpoint molecules (PD-1, CTLA-4, TIM-3, LAG-3, etc.) is another important aspect of inhibitory TME that leads to cellular exhaustion and ineffectiveness of immune cells. Although hypoxia is more characteristic of solid tumors due to poor perfusion of tumor tissue and metabolic processes, it also plays an important role in hematologic diseases. Its effect is more pronounced in the bone marrow and can lead to accumulation of immunosuppressive cells and molecules that inhibit the effector function of T cells. Tumor cells are characterized by enhanced metabolic processes leading to excessive uptake of glucose, glutamine, amino acids and O_2. The high nutrient uptake by tumor cells can deprive immune cells of nutrients, thereby impairing their metabolic processes and overall fitness. Excessive metabolic byproducts, such as lactate, CO_2, other acidic metabolites, ammonia, and ROS are also produced and secreted into the TME, often leading to a drop in pH and subsequent immunosuppression. Finally, tumor cells can secrete various enzymes (e.g., metalloproteinases, collagenases, oxidases, etc.) that can degrade or alter the components of the extracellular matrix (ECM), which is critical for maintaining tissue integrity. The thickening and alteration of the ECM can inhibit the anti-tumor immune response, facilitate tumor growth and spread, and promote inflammatory processes.

Considering the factors described above, the characteristics of the TME are increasingly recognized as potential predictive biomarkers for CAR T cell therapy progression even before infusion of the cell product into the patient. For instance, the presence of specific immunosuppressive cell types (such as CD4+/CD25+/FOXP3+ Tregs) (81, 176), the expression of certain inhibitory molecules (e.g., PDL-1, TGF-β, IL-10, ROS, etc.) (37, 94, 181), and the overall metabolic state of the TME (e.g., lactate, LDH, etc.) (84, 94, 176) could provide insight into the ability of CAR T cells to function effectively after infusion. A thorough understanding of the interplay between CAR T cells and the TME will also aid in development of strategies to overcome the inhibitory environment. Approaches such as co-administration of immune checkpoint inhibitors, supplementation of cytokines, or genetic modification of CAR T cells to resist the immunosuppressive environment are currently being investigated to increase the efficacy of CAR T cell therapy (94, 155, 176, 177). Given the dynamic nature of the tumor immunological microenvironment,

TABLE 3 Examples of common techniques for *ex vivo* biomarker analysis for predicting treatment response and side effects in CAR T cell therapy.

Category	Biomarkers	Methodology	Indices	Ref.
Mitochondrial dynamics	Mitochondrial membrane potential	Flow cytometry	Indicator of mitochondrial function	(50, 67)
	Oxidative phosphorylation and glycolysis	Seahorse XF Analyzer	Indicator of cellular respiration and energy metabolism	(49)
	GAPDH and LDHA	PCR	Upregulated expression indicates high levels of glycolysis	(46)
	Visualization of mitochondrial morphology and structure	TEM	Indicator of potential mitochondrial impairment	(70)
	ROS	Mass Spectrometry	Elevated levels indicate poor prognosis for T cell effector function	(49)
Endothelial activation	IL-6	Multiplex Bead Array	Induction of CRS	(78)
	Ang2/Ang1	ELISA	Indication of endothelial stability and function	(99)
	ICAM-1, VCAM-1	PCR	Elevated endothelial expression levels exhibit poor prognostic effect on CAR T cells	(83)
	Endothelial EVs (e.g., CD31-positive EVs)	Flow cytometry	Indication of excessive endothelial activation and damage	(151)
	NO	Spectroscopy	Endothelial stabilizer, which may indicate inflammatory processes	(25, 86)
	von Willebrand Factor (vWF)	Immunoturbidimetry	Elevated blood levels of vWF can indicate endothelial damage or dysfunction	(98)
Central nervous system impairment	GFAP	ELISA	Indicates astrocyte activation and neuroinflammation	(100, 105)
	NfL	Single-molecule array assay	Marker of neuronal injury	(103, 104)
	MMP-9	Multiplex assays	Indicates inflammation and disruption of the blood-brain barrier	(89, 90)
	S100B	Chemiluminescence immunoassay	Indicates astrocyte injury and BBB impairment	(108)
Markers of the immune system	PD-1, CTLA-4, LAG-3, TIM-3	Flow cytometry	T cell exhaustion	(138, 175)
	Target cell death	Impedance-based assays	Effective cytotoxicity of T and CAR T cells	(140)
	CRP	High-sensitivity CRP test	Indicates systemic inflammation, usually leading to development of more severe CRS	(30, 85)
	GZMB, GZMA, and PRF1	PCR	Sufficient expression in T cells for successful induction of target cell apoptosis	(138)
	TGF-β and IL-10	Multiplex Bead Array	Inhibition of T and CAR T cell function	(121)
	CCL3, CCL4, CXCL9, CXCL10, CXCL11	ELISA	Homing of CAR T cells to tumor sites	(132, 134)
	CAR T cells and target cells	Live Cell Imaging		

(Continued)

TABLE 3 Continued

Category	Biomarkers	Methodology	Indices	Ref.
			Formation of immunological synapse and release of lytic granules to induce target cell apoptosis	(122, 129)
Monitoring extracellular vesicles	miRNA	RNAseq	Inhibition of T and CAR T cell function	(145)
	CD19-positive Evs	Flow cytometry	Unspecific activation and exhaustion of CAR T cells with reduced antitumor activity and triggering CRS	(154, 156)
	CAR-positive EVs	ELISA	Long-lasting remission	(158)
	Leukemia cells derived EVs	Nanoparticle tracking analysis	Potential inhibition of leukemia-derived vesicles on CAR T cells	(150, 156)
Inhibitory tumor micro-environment	Suppressor cells of the TME	Flow cytometry	Inhibition of T and CAR T cell function and induction of apoptosis	(167)
	PDL-1 expression	PCR	Inhibitory signaling resulting in T and CAR T cell exhaustion	(181)
	Lactate	Lactate Test Strips	Metabolic byproduct of cancer cells with inhibitory properties on T (CAR T) cell effector function	(177)
	Tumor-infiltrating CAR T cells	Immunohistochemistry (IHC)	Infiltration and persistence of CAR T cells indicate better therapy response	(122)
	ROS	Chemiluminescence	High levels indicate less favourable environment for T (CAR T) cell function	(177)

which exhibits variations over time, it is of paramount importance to personalize and monitor immunotherapies to maximize the therapeutic efficacy (177). An overview of common techniques for *ex vivo* biomarker analysis of the discussed biomarkers for predicting treatment response and side effects in CAR T cell therapy is presented in Table 3.

3 Conclusions and future directions

The emergence of CAR T cell therapy has ushered in a new era of cancer treatment, offering the potential to overcome many of the limitations associated with conventional therapies. However, better approaches for understanding and predicting the therapy progression are needed. This review emphasizes the multifactorial nature of therapeutic outcomes that extend beyond the CAR T cells themselves to include the intrinsic characteristics of the patient's immune system and the dynamic interplay with the tumor microenvironment. The findings highlight the complexity and variability of the determinants of therapeutic success and suggest that a shift away from a reductionist approach focusing on single biomarkers toward a more integrative perspective is needed. Here, we propose the use of advanced biomarker models that incorporate various aspects of individual immune characteristics as well as the interplay and signaling between the immune system and the malignancy at both the cellular and systemic levels, as discussed in this review. In this way, predictive models could more accurately reflect the complex interactions that occur within the human body, potentially leading to more precise and robust predictions of therapy outcomes and more personalized therapeutic strategies. In conclusion, to realize the full potential of CAR T cell therapy, a comprehensive understanding of the numerous factors influencing its efficacy is needed. Further investigation of the impact and correlation of the discussed factors with therapy progression may lead toward a more personalized approach, which could offer reduced side effects and hold promise for the future use of this advanced immunotherapy.

Author contributions

LL: Conceptualization, Visualization, Writing – original draft, Writing – review & editing. LJ: Writing – review & editing. AI: Writing – review & editing. AK: Conceptualization, Visualization, Writing – original draft, Writing – review & editing.

Funding

The author(s) declare that financial support was received for the research, authorship, and/or publication of this article. This work was founded by the Slovenian Research Agency (ARIS) under postgraduate program and grant number P3-0083.

Conflict of interest

The authors declare that the research was conducted in the absence of any commercial or financial relationships that could be construed as a potential conflict of interest.

Publisher's note

References

1. Brentjens RJ, Curran KJ. Novel cellular therapies for leukemia: CAR-modified T cells targeted to the CD19 antigen. *Hematol Am Soc Hematol Educ Program*. (2012) 2012:143–51. doi: 10.1182/asheducation.V2012.1.143.3798224

2. Weinkove R, George P, Dasyam N, McLellan AD. Selecting costimulatory domains for chimeric antigen receptors: functional and clinical considerations. *Clin Transl Immunol*. (2019) 8:e1049. doi: 10.1002/cti2.1049

3. Chmielewski M, Abken H. TRUCKs: the fourth generation of CARs. *Expert Opin Biol Ther*. (2015) 15:1145–54. doi: 10.1517/14712598.2015.1046430

4. Tokarew N, Ogonek J, Endres S, von Bergwelt-Baildon M, Kobold S. Teaching an old dog new tricks: next-generation CAR T cells. *Br J Cancer*. (2019) 120:26–37. doi: 10.1038/s41416-018-0325-1

5. Morris EC, Neelapu SS, Giavridis T, Sadelain M. Cytokine release syndrome and associated neurotoxicity in cancer immunotherapy. *Nat Rev Immunol*. (2022) 22:85–96. doi: 10.1038/s41577-021-00547-6

6. Xiao X, Huang S, Chen S, Wang Y, Sun Q, Xu X, et al. Mechanisms of cytokine release syndrome and neurotoxicity of CAR T-cell therapy and associated prevention and management strategies. *J Exp Clin Cancer Res*. (2021) 40:367. doi: 10.1186/s13046-021-02148-6

7. Zhang Q, Zu C, Meng Y, Lyu Y, Hu Y, Huang H. Risk factors of tumor lysis syndrome in relapsed/refractory multiple myeloma patients undergoing BCMA CAR-T cell therapy. *Zhejiang Da Xue Xue Bao Yi Xue Ban*. (2022) 51:144–50. doi: 10.3724/zdxbyxb-2022-0038

8. Miao L, Zhang Z, Ren Z, Li Y. Reactions related to CAR-T cell therapy. *Front Immunol*. (2021) 12:663201. doi: 10.3389/fimmu.2021.663201

9. Amini L, Silbert SK, Maude SL, Nastoupil LJ, Ramos CA, Brentjens RJ, et al. Preparing for CAR T cell therapy: patient selection, bridging therapies and lymphodepletion. *Nat Rev Clin Oncol*. (2022) 19:342–55. doi: 10.1038/s41571-022-00607-3

10. Liu D, Badeti S, Dotti G, Jiang JG, Wang H, Dermody J, et al. The role of immunological synapse in predicting the efficacy of chimeric antigen receptor (CAR) immunotherapy. *Cell Commun Signal*. (2020) 18:134. doi: 10.1186/s12964-020-00617-7

11. Jie J, Hao S, Jiang S, Li Z, Yang M, Zhang W, et al. Phase 1 trial of the safety and efficacy of fully human anti-bcma CAR T cells in relapsed/refractory multiple myeloma. *Blood*. (2019) 134:4435–. doi: 10.1182/blood-2019-126104

12. Dwivedy Nasta S, Hughes ME, Namoglu EC, Landsburg DJ, Chong EA, Barta SK, et al. A characterization of bridging therapies leading up to commercial CAR T-cell therapy. *Blood*. (2019) 134:4108–. doi: 10.1182/blood-2019-131399

13. Kuhnl A, Roddie C, Kirkwood AA, Menne T, Cuadrado M, Marzolini MAV, et al. Early FDG-PET response predicts CAR-T failure in large B-cell lymphoma. *Blood Adv*. (2022) 6:321–6. doi: 10.1182/bloodadvances.2021005807

14. Hong R, Tan Su Yin E, Wang L, Zhao X, Zhou L, Wang G, et al. Tumor burden measured by 18F-FDG PET/CT in predicting efficacy and adverse effects of chimeric antigen receptor T-cell therapy in non-hodgkin lymphoma. *Front Oncol*. (2021) 11:713577. doi: 10.3389/fonc.2021.713577

15. Park JH, Rivière I, Gonen M, Wang X, Sénéchal B, Curran KJ, et al. Long-term follow-up of CD19 CAR therapy in acute lymphoblastic leukemia. *N Engl J Med*. (2018) 378(5):449–59. doi: 10.1056/NEJMoa1709919

16. Reinert CP, Perl RM, Faul C, Lengerke C, Nikolaou K, Dittmann H, et al. Value of CT-textural features and volume-based PET parameters in comparison to serologic markers for response prediction in patients with diffuse large B-cell lymphoma undergoing CD19-CAR-T cell therapy. *J Clin Med*. (2022) 11(6):1522. doi: 10.3390/jcm11061522

17. Sjöholm T, Korenyushkin A, Gammelgård G, Sarén T, Lövgren T, Loskog A, et al. Whole body FDG PET/MR for progression free and overall survival prediction in patients with relapsed/refractory large B-cell lymphomas undergoing CAR T-cell therapy. *Cancer Imaging*. (2022) 22:76. doi: 10.1186/s40644-022-00513-y

18. Cohen D, Luttwak E, Beyar-Katz O, Hazut Krauthammer S, Bar-On Y, Amit O, et al. [(18)F]FDG PET-CT in patients with DLBCL treated with CAR-T cell therapy: a practical approach of reporting pre- and post-treatment studies. *Eur J Nucl Med Mol Imaging*. (2022) 49:953–62. doi: 10.1007/s00259-021-05551-5

19. Shouse G, Kaempf A, Gordon MJ, Artz A, Yashar D, Sigmund AM, et al. A validated composite comorbidity index predicts outcomes of CAR T-cell therapy in patients with diffuse large B-cell lymphoma. *Blood Adv*. (2023) 7:3516–29. doi: 10.1182/bloodadvances.2022009309

20. Rejeski K, Perez A, Sesques P, Hoster E, Berger C, Jentzsch L, et al. CAR-HEMATOTOX: a model for CAR T-cell–related hematologic toxicity in relapsed/refractory large B-cell lymphoma. *Blood*. (2021) 138:2499–513. doi: 10.1182/blood.2020010543

21. Corona M, Shouval R, Alarcon A, Flynn J, Devlin S, Batlevi C, et al. Management of prolonged cytopenia following CAR T-cell therapy. *Bone Marrow Transplant*. (2022) 57:1839–41. doi: 10.1038/s41409-022-01771-x

22. Oliver-Caldes A, Rodríguez-Lobato LG, Gonzalez-Calle V, Tovar N, Cabañas V, Rodríguez-Otero P, et al. CAR-T related cytopenia profile in relapsed/refractory multiple myeloma: results of patients treated with ARI0002h, an academic BCMA-directed CAR-T cell. *Blood*. (2022) 140:10347–9. doi: 10.1182/blood-2022-166525

23. Liu Y, Sheng L, Hua H, Zhou J, Zhao Y, Wang B. A novel and validated inflammation-based prognosis score (IBPS) predicts outcomes in patients with diffuse large B-cell lymphoma. *Cancer Manage Res*. (2023) 15:651–66. doi: 10.2147/CMAR.S408100

24. Pennisi M, Sanchez-Escamilla M, Flynn JR, Shouval R, Alarcon Tomas A, Silverberg ML, et al. Modified EASIX predicts severe cytokine release syndrome and neurotoxicity after chimeric antigen receptor T cells. *Blood Adv*. (2021) 5:3397–406. doi: 10.1182/bloodadvances.2020003885

25. Acosta-Medina AA, Johnson IM, Bansal R, Hathcock M, Kenderian SJ, Durani U, et al. Pre-lymphodepletion & infusion endothelial activation and stress index as predictors of clinical outcomes in CAR-T therapy for B-cell lymphoma. *Blood Cancer J*. (2023) 13(1):7. doi: 10.1038/s41408-022-00777-4

26. Greenbaum U, Strati P, Saliba RM, Torres J, Rondon G, Nieto Y, et al. The easix (Endothelial activation and stress index) score predicts for CAR T related toxicity in patients receiving axicabtagene ciloleucel (axi-cel) for non-hodgkin lymphoma (NHL). *Blood*. (2020) 136:17–8. doi: 10.1182/blood-2020-141388

27. Rotbain EC, Gordon MJ, Vainer N, Frederiksen H, Hjalgrim H, Danilov AV, et al. The CLL comorbidity index in a population-based cohort: a tool for clinical care and research. *Blood Adv*. (2022) 6:2701–6. doi: 10.1182/bloodadvances.2021005716

28. Qualls D, Jacobson CA. Comorbidities in DLBCL: too "Severe4" CAR-T therapy? *Blood Adv*. (2023) 7:3469–71. doi: 10.1182/bloodadvances.2023009834

29. Caballero AC, Escribà-Garcia L, Alvarez-Fernández C, Briones J. CAR T-cell therapy predictive response markers in diffuse large B-cell lymphoma and therapeutic options after CART19 failure. *Front Immunol*. (2022) 13:904497. doi: 10.3389/fimmu.2022.904497

30. Liu Y, Jie X, Nian L, Wang Y, Wang C, Ma J, et al. A combination of pre-infusion serum ferritin, CRP and IL-6 predicts outcome in relapsed/refractory multiple myeloma patients treated with CAR-T cells. *Front Immunol*. (2023) 14:1169071. doi: 10.3389/fimmu.2023.1169071

31. Vercellino L, Di Blasi R, Kanoun S, Tessoulin B, Rossi C, D'Aveni-Piney M, et al. Predictive factors of early progression after CAR T-cell therapy in relapsed/refractory diffuse large B-cell lymphoma. *Blood Adv*. (2020) 4:5607–15. doi: 10.1182/bloodadvances.2020003001

32. Dancy E, Garfall AL, Cohen AD, Fraietta JA, Davis M, Levine BL, et al. Clinical predictors of T cell fitness for CAR T cell manufacturing and efficacy in multiple myeloma. *Blood*. (2018) 132:1886–. doi: 10.1182/blood-2018-99-115319

33. Ding J, Karp JE, Emadi A. Elevated lactate dehydrogenase (LDH) can be a marker of immune suppression in cancer: Interplay between hematologic and solid neoplastic clones and their microenvironments. *Cancer biomark*. (2017) 19:353–63. doi: 10.3233/CBM-160336

34. Hay KA, Hanafi LA, Li D, Gust J, Liles WC, Wurfel MM, et al. Kinetics and biomarkers of severe cytokine release syndrome after CD19 chimeric antigen receptor-modified T-cell therapy. *Blood*. (2017) 130:2295–306. doi: 10.1182/blood-2017-06-793141

35. Kochenderfer JN, Somerville RPT, Lu T, Shi V, Bot A, Rossi J, et al. Lymphoma remissions caused by anti-CD19 chimeric antigen receptor T cells are associated with high serum interleukin-15 levels. *J Clin Oncol*. (2017) 35:1803–13. doi: 10.1200/JCO.2016.71.3024

36. Mehta PH, Fiorenza S, Koldej RM, Jaworowski A, Ritchie DS, Quinn KM. T cell fitness and autologous CAR T cell therapy in haematologic Malignancy. *Front Immunol*. (2021) 12:780442. doi: 10.3389/fimmu.2021.780442

37. Jiang J, Ahuja S. Addressing patient to patient variability for autologous CAR T therapies. *J Pharm Sci*. (2021) 110:1871–6. doi: 10.1016/j.xphs.2020.12.015

38. Wang X, Rivière I. Clinical manufacturing of CAR T cells: foundation of a promising therapy. *Mol Ther Oncolytics*. (2016) 3:16015. doi: 10.1038/mto.2016.15

39. Levine BL, Miskin J, Wonnacott K, Keir C. Global manufacturing of CAR T cell therapy. *Mol Ther Methods Clin Dev*. (2017) 4:92–101. doi: 10.1016/j.omtm.2016.12.006

40. June CH, Sadelain M. Chimeric antigen receptor therapy. *N Engl J Med*. (2018) 379:64–73. doi: 10.1056/NEJMra1706169

41. Davenport AJ, Jenkins MR, Cross RS, Yong CS, Prince HM, Ritchie DS, et al. CAR-T cells inflict sequential killing of multiple tumor target cells. *Cancer Immunol Res*. (2015) 3:483–94. doi: 10.1158/2326-6066.CIR-15-0048

42. Rostamian H, Khakpoor-Koosheh M, Fallah-Mehrjardi K, Mirzaei HR, Brown CE. Mitochondria as playmakers of CAR T-cell fate and longevity. *Cancer Immunol Res*. (2021) 9:856–61. doi: 10.1158/2326-6066.CIR-21-0110

43. Rad SMA, Halpin JC, Mollaei M, Smith Bell SWJ, Hirankarn N, McLellan AD. Metabolic and mitochondrial functioning in chimeric antigen receptor (CAR)-T cells. *Cancers (Basel)*. (2021) 13(6):1229. doi: 10.3390/cancers13061229

44. Vardhana SA, Hwee MA, Berisa M, Wells DK, Yost KE, King B, et al. Impaired mitochondrial oxidative phosphorylation limits the self-renewal of T cells exposed to persistent antigen. *Nat Immunol*. (2020) 21:1022–33. doi: 10.1038/s41590-020-0725-2

45. Jiang S. Mitochondrial oxidative phosphorylation is linked to T-cell exhaustion. *Aging (Albany NY)*. (2020) 12:16665–6. doi: 10.18632/aging.v12i17

46. Rangel Rivera GO, Knochelmann HM, Dwyer CJ, Smith AS, Wyatt MM, Rivera-Reyes AM, et al. Fundamentals of T cell metabolism and strategies to enhance cancer immunotherapy. *Front Immunol*. (2021) 12:645242. doi: 10.3389/fimmu.2021.645242

47. Maciolek JA, Pasternak JA, Wilson HL. Metabolism of activated T lymphocytes. *Curr Opin Immunol*. (2014) 27:60–74. doi: 10.1016/j.coi.2014.01.006

48. Kawalekar OU, O'Connor RS, Fraietta JA, Guo L, McGettigan SE, Posey AD Jr., et al. Distinct signaling of coreceptors regulates specific metabolism pathways and impacts memory development in CAR T cells. *Immunity*. (2016) 44:380–90. doi: 10.1016/j.immuni.2016.01.021

49. Huang Y, Si X, Shao M, Teng X, Xiao G, Huang H. Rewiring mitochondrial metabolism to counteract exhaustion of CAR-T cells. *J Hematol Oncol*. (2022) 15:38. doi: 10.1186/s13045-022-01255-x

50. Sukumar M, Liu J, Mehta GU, Patel SJ, Roychoudhuri R, Crompton JG, et al. Mitochondrial membrane potential identifies cells with enhanced stemness for cellular therapy. *Cell Metab*. (2016) 23:63–76. doi: 10.1016/j.cmet.2015.11.002

51. van Bruggen JAC, Martens AWJ, Fraietta JA, Hofland T, Tonino SH, Eldering E, et al. Chronic lymphocytic leukemia cells impair mitochondrial fitness in CD8(+) T cells and impede CAR T-cell efficacy. *Blood*. (2019) 134:44–58. doi: 10.1182/blood.2018885863

52. Buck MD, O'Sullivan D, Pearce EL. T cell metabolism drives immunity. *J Exp Med*. (2015) 212:1345–60. doi: 10.1084/jem.20151159

53. Aksoylar HI, Tijaro-Ovalle NM, Boussiotis VA, Patsoukis N. T cell metabolism in cancer immunotherapy. *Immunometabolism*. (2020) 2(3):e200020. doi: 10.20900/immunometab20200020

54. Zorova LD, Popkov VA, Plotnikov EY, Silachev DN, Pevzner IB, Jankauskas SS, et al. Mitochondrial membrane potential. *Anal Biochem*. (2018) 552:50–9. doi: 10.1016/j.ab.2017.07.009

55. Austin S, St-Pierre J. PGC1α and mitochondrial metabolism–emerging concepts and relevance in ageing and neurodegenerative disorders. *J Cell Sci*. (2012) 125:4963–71:Pt 21). doi: 10.1242/jcs.113662

56. Poorebrahim M, Melief J, Pico de Coaña Y, LW S, Cid-Arregui A, Kiessling R. Counteracting CAR T cell dysfunction. *Oncogene*. (2021) 40:421–35. doi: 10.1038/s41388-020-01501-x

57. Pellegrino M, Del Bufalo F, De Angelis B, Quintarelli C, Caruana I, de Billy E. Manipulating the metabolism to improve the efficacy of CAR T-cell immunotherapy. *Cells*. (2020) 10(1):4. doi: 10.3390/cells10010014

58. FranChina DG, Dostert C, Brenner D. Reactive oxygen species: involvement in T cell signaling and metabolism. *Trends Immunol*. (2018) 39:489–502. doi: 10.1016/j.it.2018.01.005

59. Zhang L, Zhang W, Li Z, Lin S, Zheng T, Hao B, et al. Mitochondria dysfunction in CD8+ T cells as an important contributing factor for cancer development and a potential target for cancer treatment: a review. *J Exp Clin Cancer Res*. (2022) 41:227. doi: 10.1186/s13046-022-02439-6

60. Um JH, Yun J. Emerging role of mitophagy in human diseases and physiology. *BMB Rep*. (2017) 50:299–307. doi: 10.5483/BMBRep.2017.50.6.056

61. Pickles S, Vigié P, Youle RJ. Mitophagy and quality control mechanisms in mitochondrial maintenance. *Curr Biol*. (2018) 28:R170–r85. doi: 10.1016/j.cub.2018.01.004

62. Zhang M, Jin X, Sun R, Xiong X, Wang J, Xie D, et al. Optimization of metabolism to improve efficacy during CAR-T cell manufacturing. *J Transl Med*. (2021) 19:499. doi: 10.1186/s12967-021-03165-x

63. Khan S, Ince-Dunn G, Suomalainen A, Elo LL. Integrative omics approaches provide biological and clinical insights: examples from mitochondrial diseases. *J Clin Invest*. (2020) 130:20–8. doi: 10.1172/JCI129202

64. Cui H, Li F, Chen D, Wang G, Truong CK, Enns GM, et al. Comprehensive next-generation sequence analyses of the entire mitochondrial genome reveal new insights into the molecular diagnosis of mitochondrial DNA disorders. *Genet Med*. (2013) 15:388–94. doi: 10.1038/gim.2012.144

65. Abdelkader Y, Perez-Davalos L, LeDuc R, Zahedi RP, Labouta HI. Omics approaches for the assessment of biological responses to nanoparticles. *Adv Drug Delivery Rev*. (2023) 200:114992. doi: 10.1016/j.addr.2023.114992

66. Palmfeldt J, Bross P. Proteomics of human mitochondria. *Mitochondrion*. (2017) 33:2–14. doi: 10.1016/j.mito.2016.07.006

67. Buck MD, O'Sullivan D, Klein Geltink RI, Curtis JD, Chang CH, Sanin DE, et al. Mitochondrial dynamics controls T cell fate through metabolic programming. *Cell*. (2016) 166:63–76. doi: 10.1016/j.cell.2016.05.035

68. Rogers GW, Brand MD, Petrosyan S, Ashok D, Elorza AA, Ferrick DA, et al. High throughput microplate respiratory measurements using minimal quantities of isolated mitochondria. *PloS One*. (2011) 6:e21746. doi: 10.1371/journal.pone.0021746

69. Brand MD, Nicholls DG. Assessing mitochondrial dysfunction in cells. *Biochem J*. (2011) 435:297–312. doi: 10.1042/BJ20110162

70. Chakraborty J, Caicci F, Roy M, Ziviani E. Investigating mitochondrial autophagy by routine transmission electron microscopy: Seeing is believing? *Pharmacol Res*. (2020) 160:105097. doi: 10.1016/j.phrs.2020.105097

71. Pober JS, Tellides G. Participation of blood vessel cells in human adaptive immune responses. *Trends Immunol*. (2012) 33:49–57. doi: 10.1016/j.it.2011.09.006

72. Hosseinkhani N, Derakhshani A, Kooshkaki O, Abdoli Shadbad M, Hajiasgharzadeh K, Baghbanzadeh A, et al. Immune checkpoints and CAR-T cells: the pioneers in future cancer therapies? *Int J Mol Sci*. (2020) 21(21):8305. doi: 10.3390/ijms21218305

73. Becht E, Giraldo NA, Dieu-Nosjean MC, Sautès-Fridman C, Fridman WH. Cancer immune contexture and immunotherapy. *Curr Opin Immunol*. (2016) 39:7–13. doi: 10.1016/j.coi.2015.11.009

74. Slaney CY, Kershaw MH, Darcy PK. Trafficking of T cells into tumors. *Cancer Res*. (2014) 74:7168–74. doi: 10.1158/0008-5472.CAN-14-2458

75. Kaufman HL, Disis ML. Immune system versus tumor: shifting the balance in favor of DCs and effective immunity. *J Clin Invest*. (2004) 113:664–7. doi: 10.1172/JCI200421148

76. Hong R, Hu Y, Huang H. Biomarkers for chimeric antigen receptor T cell therapy in acute lymphoblastic leukemia: prospects for personalized management and prognostic prediction. *Front Immunol*. (2021) 12:627764. doi: 10.3389/fimmu.2021.627764

77. Lindo L, Wilkinson LH, Hay KA. Befriending the hostile tumor microenvironment in CAR T-cell therapy. *Front Immunol*. (2020) 11:618387. doi: 10.3389/fimmu.2020.618387

78. Chen F, Teachey DT, Pequignot E, Frey N, Porter D, Maude SL, et al. Measuring IL-6 and sIL-6R in serum from patients treated with tocilizumab and/or siltuximab following CAR T cell therapy. *J Immunol Methods*. (2016) 434:1–8. doi: 10.1016/j.jim.2016.03.005

79. Kang S, Kishimoto T. Interplay between interleukin-6 signaling and the vascular endothelium in cytokine storms. *Exp Mol Med*. (2021) 53:1116–23. doi: 10.1038/s12276-021-00649-0

80. Gust J, Hay KA, Hanafi LA, Li D, Myerson D, Gonzalez-Cuyar LF, et al. Endothelial activation and blood-brain barrier disruption in neurotoxicity after adoptive immunotherapy with CD19 CAR-T cells. *Cancer Discovery*. (2017) 7:1404–19. doi: 10.1158/2159-8290.CD-17-0698

81. Tan JY, Low MH, Chen Y, Lim F. CAR T cell therapy in hematological Malignancies: implications of the tumor microenvironment and biomarkers on efficacy and toxicity. *Int J Mol Sci*. (2022) 23(13):6931. doi: 10.3390/ijms23136931

82. Si S, Teachey DT. Spotlight on tocilizumab in the treatment of CAR-T-cell-induced cytokine release syndrome: clinical evidence to date. *Ther Clin Risk Manage*. (2020) 16:705–14. doi: 10.2147/TCRM.S223468

83. Chen Y, Li R, Shang S, Yang X, Li L, Wang W, et al. Therapeutic potential of TNFα and IL1β Blockade for CRS/ICANS in CAR-T therapy via ameliorating endothelial activation. *Front Immunol*. (2021) 12:623610. doi: 10.3389/fimmu.2021.623610

84. Jain MD, Zhao H, Wang X, Atkins R, Menges M, Reid K, et al. Tumor interferon signaling and suppressive myeloid cells are associated with CAR T-cell failure in large B-cell lymphoma. *Blood*. (2021) 137:2621–33. doi: 10.1182/blood.2020007445

85. Greenbaum U, Strati P, Saliba RM, Torres J, Rondon G, Nieto Y, et al. CRP and ferritin in addition to the EASIX score predict CAR-T-related toxicity. *Blood Adv*. (2021) 5:2799–806. doi: 10.1182/bloodadvances.2021004575

86. Cyr AR, Huckaby LV, Shiva SS, Zuckerbraun BS. Nitric oxide and endothelial dysfunction. *Crit Care Clin*. (2020) 36:307–21. doi: 10.1016/j.ccc.2019.12.009

87. Carmeliet P, Jain RK. Molecular mechanisms and clinical applications of angiogenesis. *Nature*. (2011) 473:298–307. doi: 10.1038/nature10144

88. Rabbani R, Topol EJ. Strategies to achieve coronary arterial plaque stabilization. *Cardiovasc Res*. (1999) 41:402–17. doi: 10.1016/S0008-6363(98)00279-X

89. Davis GE, Senger DR. Endothelial extracellular matrix: biosynthesis, remodeling, and functions during vascular morphogenesis and neovessel stabilization. *Circ Res*. (2005) 97:1093–107. doi: 10.1161/01.RES.0000191547.64391.e3

90. Stoll G, Bendszus M. Inflammation and atherosclerosis: novel insights into plaque formation and destabilization. *Stroke*. (2006) 37:1923–32. doi: 10.1161/01.STR.0000226901.34927.10

91. Rochfort KD, Cummins PM. The blood-brain barrier endothelium: a target for pro-inflammatory cytokines. *Biochem Soc Trans*. (2015) 43:702–6. doi: 10.1042/BST20140319

92. Di A, Mehta D, Malik AB. ROS-activated calcium signaling mechanisms regulating endothelial barrier function. *Cell Calcium*. (2016) 60:163–71. doi: 10.1016/j.ceca.2016.02.002

93. Apopa PL, Qian Y, Shao R, Guo NL, Schwegler-Berry D, Pacurari M, et al. Iron oxide nanoparticles induce human microvascular endothelial cell permeability through reactive oxygen species production and microtubule remodeling. *Part Fibre Toxicol*. (2009) 6:1. doi: 10.1186/1743-8977-6-1

94. Tiwari A, Trivedi R, Lin SY. Tumor microenvironment: barrier or opportunity towards effective cancer therapy. *J BioMed Sci*. (2022) 29:83. doi: 10.1186/s12929-022-00866-3

95. Yang Y, Li C, Liu T, Dai X, Bazhin AV. Myeloid-derived suppressor cells in tumors: from mechanisms to antigen specificity and microenvironmental regulation. *Front Immunol*. (2020) 11:1371. doi: 10.3389/fimmu.2020.01371

96. Simula L, Ollivier E, Icard P, Donnadieu E. Immune checkpoint proteins, metabolism and adhesion molecules: overlooked determinants of CAR T-cell migration? *Cells*. (2022) 11(11):1854. doi: 10.3390/cells11111854

97. Liu G, Rui W, Zhao X, Lin X. Enhancing CAR-T cell efficacy in solid tumors by targeting the tumor microenvironment. *Cell Mol Immunol*. (2021) 18:1085–95. doi: 10.1038/s41423-021-00655-2

98. Ren G, Roberts AI, Shi Y. Adhesion molecules: key players in Mesenchymal stem cell-mediated immunosuppression. *Cell Adh Migr*. (2011) 5:20–2. doi: 10.4161/cam.5.1.13491

99. Moreno-Castaño AB, Fernández S, Ventosa H, Palomo M, Martinez-Sanchez J, Ramos A, et al. Characterization of the endotheliopathy, innate-immune activation and hemostatic imbalance underlying CAR-T cell toxicities: laboratory tools for an early and differential diagnosis. *J Immunother Cancer*. (2023) 11(4):e006365. doi: 10.1136/jitc-2022-006365

100. Gust J, Rawlings-Rhea SD, Wilson AL, Tulberg NM, Sherman AL, Seidel KD, et al. GFAP and NfL increase during neurotoxicity from high baseline levels in pediatric CD19-CAR T-cell patients. *Blood Adv*. (2022) 7(6):1001–10. doi: 10.1182/bloodadvances.2022008119

101. Leahy AB, Newman H, Li Y, Liu H, Myers R, DiNofia A, et al. CD19-targeted chimeric antigen receptor T-cell therapy for CNS relapsed or refractory acute lymphocytic leukaemia: a post-hoc analysis of pooled data from five clinical trials. *Lancet Haematol*. (2021) 8:e711–e22. doi: 10.1016/S2352-3026(21)00238-6

102. Torre M, Solomon IH, Sutherland CL, Nikiforow S, DeAngelo DJ, Stone RM, et al. Neuropathology of a case with fatal CAR T-cell-associated cerebral edema. *J Neuropathol Exp Neurol*. (2018) 77:877–82. doi: 10.1093/jnen/nly064

103. Butt OH, Zhou AY, Caimi PF, Derenoncour P-R, Lee K, Wu GF, et al. Pre-infusion neurofilament light chain (NfL) levels predict the development of immune effector cell-associated neurotoxicity syndrome (ICANS) - a multicenter retrospective study. *Blood*. (2021) 138:2841–. doi: 10.1182/blood-2021-149674

104. Schoeberl F, Tiedt S, Schmitt A, Blumenberg V, Karschnia P, Burbano VG, et al. Neurofilament light chain serum levels correlate with the severity of neurotoxicity after CAR T-cell treatment. *Blood Adv*. (2022) 6:3022–6. doi: 10.1182/bloodadvances.2021006144

105. Abdelhak A, Foschi M, Abu-Rumeileh S, Yue JK, D'Anna L, Huss A, et al. Blood GFAP as an emerging biomarker in brain and spinal cord disorders. *Nat Rev Neurol*. (2022) 18:158–72. doi: 10.1038/s41582-021-00616-3

106. Gust J, Finney OC, Li D, Brakke HM, Hicks RM, Futrell RB, et al. Glial injury in neurotoxicity after pediatric CD19-directed chimeric antigen receptor T cell therapy. *Ann Neurol*. (2019) 86:42–54. doi: 10.1002/ana.25502

107. Flanagan EP, Hinson SR, Lennon VA, Fang B, Aksamit AJ, Morris PP, et al. Glial fibrillary acidic protein immunoglobulin G as biomarker of autoimmune astrocytopathy: Analysis of 102 patients. *Ann Neurol*. (2017) 81:298–309. doi: 10.1002/ana.24881

108. Haselmann V, Schamberger C, Trifonova F, Ast V, Froelich MF, Strauss M, et al. Plasma-based S100B testing for management of traumatic brain injury in emergency setting. *Pract Lab Med*. (2021) 26:e00236. doi: 10.1016/j.plabm.2021.e00236

109. Al Hadidi S, Szabo A, Esselmann J, Hammons L, Hussain M, Ogunsesan Y, et al. Clinical outcome of patients with relapsed refractory multiple myeloma listed for BCMA directed commercial CAR-T therapy. *Bone Marrow Transplant*. (2023) 58:443–5. doi: 10.1038/s41409-022-01905-1

110. Westin JR, Kersten MJ, Salles G, Abramson JS, Schuster SJ, Locke FL, et al. Efficacy and safety of CD19-directed CAR-T cell therapies in patients with relapsed/refractory aggressive B-cell lymphomas: Observations from the JULIET, ZUMA-1, and TRANSCEND trials. *Am J Hematol*. (2021) 96:1295–312. doi: 10.1002/ajh.26301

111. Garfall AL, Dancy EK, Cohen AD, Hwang WT, Fraietta JA, Davis MM, et al. T-cell phenotypes associated with effective CAR T-cell therapy in postinduction vs relapsed multiple myeloma. *Blood Adv*. (2019) 3:2812–5. doi: 10.1182/bloodadvances.2019000600

112. Atar O, Ram R, Avivi I, Amit O, Vitkon R, Luttwak E, et al. Vagal nerve activity predicts prognosis in diffused large B-cell lymphoma and multiple myeloma. *J Clin Med*. (2023) 12(3):908. doi: 10.3390/jcm12030908

113. Agarwal V, Aptekar J, Fajgenbaum DC, Lafeuille P. Deriving predictive features of severe CRS from pre-infusion clinical data in CAR T-cell therapies. *Blood*. (2022) 140:7838–9. doi: 10.1182/blood-2022-169287

114. Holtzman NG, Bentzen SM, Kesari V, Bukhari A, El Chaer F, Hutnick E, et al. Immune effector cell-associated neurotoxicity syndrome (ICANS) after CD19-directed chimeric antigen receptor T-cell therapy (CAR-T) for large B-cell lymphoma: predictive biomarkers and clinical outcomes. *Blood*. (2019) 134:3239–. doi: 10.1182/blood-2019-125400

115. Lee DH, Cervantes-Contreras F, Lee SY, Green DJ, Till BG. Improved expansion and function of CAR T cell products from cultures initiated at defined CD4:CD8 ratios. *Blood*. (2018) 132:3334–. doi: 10.1182/blood-2018-99-111576

116. Turtle CJ, Hanafi LA, Berger C, Gooley TA, Cherian S, Hudecek M, et al. CD19 CAR-T cells of defined CD4+:CD8+ composition in adult B cell ALL patients. *J Clin Invest*. (2016) 126:2123–38. doi: 10.1172/JCI85309

117. Jiang P, Zhang Z, Hu Y, Liang Z, Han Y, Li X, et al. Single-cell ATAC-seq maps the comprehensive and dynamic chromatin accessibility landscape of CAR-T cell dysfunction. *Leukemia*. (2022) 36:2656–68. doi: 10.1038/s41375-022-01676-0

118. Fraietta JA, Lacey SF, Orlando EJ, Pruteanu-Malinici I, Gohil M, Lundh S, et al. Determinants of response and resistance to CD19 chimeric antigen receptor (CAR) T cell therapy of chronic lymphocytic leukemia. *Nat Med*. (2018) 24:563–71. doi: 10.1038/s41591-018-0010-1

119. Sommermeyer D, Hudecek M, Kosasih PL, Gogishvili T, Maloney DG, Turtle CJ, et al. Chimeric antigen receptor-modified T cells derived from defined CD8+ and CD4+ subsets confer superior antitumor reactivity *in vivo*. *Leukemia*. (2016) 30:492–500. doi: 10.1038/leu.2015.247

120. Beider K, Besser MJ, Schachter J, Grushchenko-Polaq AH, Voevoda V, Wolf I, et al. Upregulation of senescent/exhausted phenotype of CAR T cells and induction of both treg and myeloid suppressive cells correlate with reduced response to CAR T cell therapy in relapsed/refractory B cell Malignancies. *Blood*. (2019) 134:3234–. doi: 10.1182/blood-2019-128068

121. Kumari R, Ouyang X, Wang J, Xu X, Zheng M, An X, et al. Preclinical pharmacology modeling of chimeric antigen receptor T therapies. *Curr Opin Pharmacol*. (2021) 61:49–61. doi: 10.1016/j.coph.2021.08.008

122. Xiong W, Chen Y, Kang X, Chen Z, Zheng P, Hsu YH, et al. Immunological synapse predicts effectiveness of chimeric antigen receptor cells. *Mol Ther*. (2018) 26:963–75. doi: 10.1016/j.ymthe.2018.01.020

123. Guedan S, Luu M, Ammar D, Barbao P, Bonini C, Bousso P, et al. Time 2EVOLVE: predicting efficacy of engineered T-cells - how far is the bench from the bedside? *J Immunother Cancer*. (2022) 10(5):e003487. doi: 10.1136/jitc-2021-003487

124. Jenkins MR, Rudd-Schmidt JA, Lopez JA, Ramsbottom KM, Mannering SI, Andrews DM, et al. Failed CTL/NK cell killing and cytokine hypersecretion are directly linked through prolonged synapse time. *J Exp Med*. (2015) 212:307–17. doi: 10.1084/jem.20140964

125. Wang W, Fasolino M, Cattau B, Goldman N, Kong W, Frederick MA, et al. Joint profiling of chromatin accessibility and CAR-T integration site analysis at population and single-cell levels. *Proc Natl Acad Sci U S A*. (2020) 117:5442–52. doi: 10.1073/pnas.1919259117

126. Dabiri H, Safarzadeh Kozani P, Habibi Anbouhi M, Mirzaee Godarzee M, Haddadi MH, Basiri M, et al. Site-specific transgene integration in chimeric antigen receptor (CAR) T cell therapies. *biomark Res*. (2023) 11:67. doi: 10.1186/s40364-023-00509-1

127. Hamada M, Nishio N, Okuno Y, Suzuki S, Kawashima N, Muramatsu H, et al. Integration mapping of piggyBac-mediated CD19 chimeric antigen receptor T cells analyzed by novel tagmentation-assisted PCR. *EBioMedicine*. (2018) 34:18–26. doi: 10.1016/j.ebiom.2018.07.008

128. Donnadieu E, Dupré L, Pinho LG, Cotta-de-Almeida V. Surmounting the obstacles that impede effective CAR T cell trafficking to solid tumors. *J Leukoc Biol*. (2020) 108:1067–79. doi: 10.1002/JLB.1MR0520-746R

129. Davenport AJ, Cross RS, Watson KA, Liao Y, Shi W, Prince HM, et al. Chimeric antigen receptor T cells form nonclassical and potent immune synapses driving rapid cytotoxicity. *Proc Natl Acad Sci U S A*. (2018) 115:E2068–E76. doi: 10.1073/pnas.1716266115

130. Bui TM, Wiesolek HL, Sumagin R. ICAM-1: A master regulator of cellular responses in inflammation, injury resolution, and tumorigenesis. *J Leukoc Biol*. (2020) 108:787–99. doi: 10.1002/JLB.2MR0220-549R

131. Wei Z, Cheng Q, Xu N, Zhao C, Xu J, Kang L, et al. Investigation of CRS-associated cytokines in CAR-T therapy with meta-GNN and pathway crosstalk. *BMC Bioinf*. (2022) 23:373. doi: 10.1186/s12859-022-04917-2

132. Ansell SM, Maurer MJ, Ziesmer SC, Slager SL, Habermann TM, Link BK, et al. Elevated pretreatment serum levels of interferon-inducible protein-10 (CXCL10) predict disease relapse and prognosis in diffuse large B-cell lymphoma patients. *Am J Hematol*. (2012) 87:865–9. doi: 10.1002/ajh.23259

133. LaSalle T, Austin EE, Rigney G, Wehrenberg-Klee E, Nesti S, Larimer B, et al. Granzyme B PET imaging of immune-mediated tumor killing as a tool for understanding immunotherapy response. *J Immunother Cancer*. (2020) 8(1):e000291. doi: 10.1136/jitc-2019-000291

134. Tian Y, Wen C, Zhang Z, Liu Y, Li F, Zhao Q, et al. CXCL9-modified CAR T cells improve immune cell infiltration and antitumor efficacy. *Cancer Immunol Immunother*. (2022) 71:2663–75. doi: 10.1007/s00262-022-03193-6

135. Wang G, Zhang Z, Zhong K, Wang Z, Yang N, Tang X, et al. CXCL11-armed oncolytic adenoviruses enhance CAR-T cell therapeutic efficacy and reprogram tumor microenvironment in glioblastoma. *Mol Ther*. (2023) 31:134–53. doi: 10.1016/j.ymthe.2022.08.021

136. Savani M, Oluwole O, Dholaria B. New targets for CAR T therapy in hematologic Malignancies. *Best Pract Res Clin Haematol*. (2021) 34:101277. doi: 10.1016/j.beha.2021.101277

137. Majzner RG, Mackall CL. Tumor antigen escape from CAR T-cell therapy. *Cancer Discovery*. (2018) 8:1219–26. doi: 10.1158/2159-8290.CD-18-0442

138. Kiesgen S, Messinger JC, Chintala NK, Tano Z, Adusumilli PS. Comparative analysis of assays to measure CAR T-cell-mediated cytotoxicity. *Nat Protoc*. (2021) 16:1331–42. doi: 10.1038/s41596-020-00467-0

139. La Muraglia GM 2nd, O'Neil MJ, Madariaga ML, Michel SG, Mordecai KS, Allan JS, et al. A novel approach to measuring cell-mediated lympholysis using quantitative flow and imaging cytometry. *J Immunol Methods*. (2015) 427:85–93. doi: 10.1016/j.jim.2015.10.005

140. Zhong J, Yang D, Zhou Y, Liang M, Ai Y. Multi-frequency single cell electrical impedance measurement for label-free cell viability analysis. *Analyst*. (2021) 146:1848–58. doi: 10.1039/D0AN02476G

141. Cheng L, Hill AF. Therapeutically harnessing extracellular vesicles. *Nat Rev Drug Discovery*. (2022) 21:379–99. doi: 10.1038/s41573-022-00410-w

142. Mathieu M, Martin-Jaular L, Lavieu G, Théry C. Specificities of secretion and uptake of exosomes and other extracellular vesicles for cell-to-cell communication. *Nat Cell Biol*. (2019) 21:9–17. doi: 10.1038/s41556-018-0250-9

143. van Niel G, D'Angelo G, Raposo G. Shedding light on the cell biology of extracellular vesicles. *Nat Rev Mol Cell Biol*. (2018) 19:213–28. doi: 10.1038/nrm.2017.125

144. Navarro-Tableros V, Gomez Y, Camussi G, Brizzi MF. Extracellular vesicles: new players in lymphomas. *Int J Mol Sci*. (2018) 20(1):41. doi: 10.3390/ijms20010041

145. Wen C, Seeger RC, Fabbri M, Wang L, Wayne AS, Jong AY. Biological roles and potential applications of immune cell-derived extracellular vesicles. *J Extracell Vesicles*. (2017) 6:1400370. doi: 10.1080/20013078.2017.1400370

146. Marar C, Starich B, Wirtz D. Extracellular vesicles in immunomodulation and tumor progression. *Nat Immunol*. (2021) 22:560–70. doi: 10.1038/s41590-021-00899-0

147. Zhang X, Liu D, Gao Y, Lin C, An Q, Feng Y, et al. The biology and function of extracellular vesicles in cancer development. *Front Cell Dev Biol*. (2021) 9:777441. doi: 10.3389/fcell.2021.777441

148. Jaiswal R, Sedger LM. Intercellular vesicular transfer by exosomes, microparticles and oncosomes - implications for cancer biology and treatments. *Front Oncol*. (2019) 9:125. doi: 10.3389/fonc.2019.00125

149. Ukrainskaya VM, Musatova OE, Volkov DV, Osipova DS, Pershin DS, Moysenovich AM, et al. CAR-tropic extracellular vesicles carry tumor-associated antigens and modulate CAR T cell functionality. *Sci Rep*. (2023) 13:463. doi: 10.1038/s41598-023-27604-5

150. Cox MJ, Lucien F, Sakemura R, Boysen JC, Kim Y, Horvei P, et al. Leukemic extracellular vesicles induce chimeric antigen receptor T cell dysfunction in chronic lymphocytic leukemia. *Mol Ther*. (2021) 29:1529–40. doi: 10.1016/j.ymthe.2020.12.033

151. Calvo V, Izquierdo M. T lymphocyte and CAR-T cell-derived extracellular vesicles and their applications in cancer therapy. *Cells*. (2022) 11(5):790. doi: 10.3390/cells11050790

152. Ruan S, Greenberg Z, Pan X, Zhuang P, Erwin N, He M. Extracellular vesicles as an advanced delivery biomaterial for precision cancer immunotherapy. *Adv Healthc Mater*. (2022) 11:e2100650. doi: 10.1002/adhm.202100650

153. Pagotto S, Simeone P, Brocco D, Catitti G, De Bellis D, Vespa S, et al. CAR-T-derived extracellular vesicles: A promising development of CAR-T anti-tumor therapy. *Cancers (Basel)*. (2023) 15(4):1052. doi: 10.3390/cancers15041052

154. Crompot E, Van Damme M, Pieters K, Vermeersch M, Perez-Morga D, Mineur P, et al. Extracellular vesicles of bone marrow stromal cells rescue chronic lymphocytic leukemia B cells from apoptosis, enhance their migration and induce gene expression modifications. *Haematologica*. (2017) 102:1594–604. doi: 10.3324/haematol.2016.163337

155. Ramos RN, Amano MT, Paes Leme AF, Fox JW, de Oliveira AK. Editorial: Tumor microenvironment (TME) and tumor immune microenvironment (TIME): New perspectives for prognosis and therapy. *Front Cell Dev Biol*. (2022) 10:971275. doi: 10.3389/fcell.2022.971275

156. Zhu X, Hu H, Xiao Y, Li Q, Zhong Z, Yang J, et al. Tumor-derived extracellular vesicles induce invalid cytokine release and exhaustion of CD19 CAR-T Cells. *Cancer Lett*. (2022) 536:215668. doi: 10.1016/j.canlet.2022.215668

157. Lazana I. Extracellular vesicles in haematological disorders: A friend or a foe? *Int J Mol Sci*. (2022) 23(17):10118. doi: 10.3390/ijms231710118

158. Fu W, Lei C, Liu S, Cui Y, Wang C, Qian K, et al. CAR exosomes derived from effector CAR-T cells have potent antitumour effects and low toxicity. *Nat Commun*. (2019) 10:4355. doi: 10.1038/s41467-019-12321-3

159. Aharon A, Horn G, Bar-Lev TH, Zagagi Yohay E, Waks T, Levin M, et al. Extracellular vesicles derived from chimeric antigen receptor-T cells: A potential therapy for cancer. *Hum Gene Ther*. (2021) 32:1224–41. doi: 10.1089/hum.2021.192

160. Zhang Y, Ge T, Huang M, Qin Y, Liu T, Mu W, et al. Extracellular vesicles expressing CD19 antigen improve expansion and efficacy of CD19-targeted CAR-T cells. *Int J Nanomed*. (2023) 18:49–63. doi: 10.2147/IJN.S390720

161. Tang XJ, Sun XY, Huang KM, Zhang L, Yang ZS, Zou DD, et al. Therapeutic potential of CAR-T cell-derived exosomes: a cell-free modality for targeted cancer therapy. *Oncotarget*. (2015) 6:44179–90. doi: 10.18632/oncotarget.v6i42

162. Sworder B, Alizadeh AA, Miklos DB, Diehn M, Mackall CL, Majzner RG, et al. Circulating DNA for molecular response prediction, characterization of resistance mechanisms and quantification of CAR T-cells during axicabtagene ciloleucel therapy. *Blood*. (2019) 134:550–. doi: 10.1182/blood-2019-129015

163. Belov L, Matic KJ, Hallal S, Best OG, Mulligan SP, Christopherson RI. Extensive surface protein profiles of extracellular vesicles from cancer cells may provide diagnostic signatures from blood samples. *J Extracell Vesicles*. (2016) 5:25355. doi: 10.3402/jev.v5.25355

164. Gargiulo E, Morande PE, Largeot A, Moussay E, Paggetti J. Diagnostic and therapeutic potential of extracellular vesicles in B-cell Malignancies. *Front Oncol*. (2020) 10:580874. doi: 10.3389/fonc.2020.580874

165. Hinshaw DC, Shevde LA. The tumor microenvironment innately modulates cancer progression. *Cancer Res*. (2019) 79:4557–66. doi: 10.1158/0008-5472.CAN-18-3962

166. Pitt JM, Marabelle A, Eggermont A, Soria JC, Kroemer G, Zitvogel L. Targeting the tumor microenvironment: removing obstruction to anticancer immune responses and immunotherapy. *Ann Oncol*. (2016) 27:1482–92. doi: 10.1093/annonc/mdw168

167. Haist M, Stege H, Grabbe S, Bros M. The functional crosstalk between myeloid-derived suppressor cells and regulatory T cells within the immunosuppressive tumor microenvironment. *Cancers (Basel)*. (2021) 13(2):210. doi: 10.3390/cancers13020210

168. Kumar V, Patel S, Tcyganov E, Gabrilovich DI. The nature of myeloid-derived suppressor cells in the tumor microenvironment. *Trends Immunol*. (2016) 37:208–20. doi: 10.1016/j.it.2016.01.004

169. Vasievich EA, Huang L. The suppressive tumor microenvironment: a challenge in cancer immunotherapy. *Mol Pharm*. (2011) 8:635–41. doi: 10.1021/mp1004228

170. Najafi M, Hashemi Goradel N, Farhood B, Salehi E, Nashtaei MS, Khanlarkhani N, et al. Macrophage polarity in cancer: A review. *J Cell Biochem*. (2019) 120:2756–65. doi: 10.1002/jcb.27646

171. Davoodzadeh Gholami M, Kardar GA, Saeedi Y, Heydari S, Garssen J, Falak R. Exhaustion of T lymphocytes in the tumor microenvironment: Significance and effective mechanisms. *Cell Immunol*. (2017) 322:1–14. doi: 10.1016/j.cellimm.2017.10.002

172. Zhang Z, Liu S, Zhang B, Qiao L, Zhang Y, Zhang Y. T cell dysfunction and exhaustion in cancer. *Front Cell Dev Biol*. (2020) 8:17. doi: 10.3389/fcell.2020.00017

173. Komohara Y, Fujiwara Y, Ohnishi K, Takeya M. Tumor-associated macrophages: Potential therapeutic targets for anti-cancer therapy. *Adv Drug Delivery Rev*. (2016) 99:180–5. doi: 10.1016/j.addr.2015.11.009

174. Lei X, Lei Y, Li JK, Du WX, Li RG, Yang J, et al. Immune cells within the tumor microenvironment: Biological functions and roles in cancer immunotherapy. *Cancer Lett*. (2020) 470:126–33. doi: 10.1016/j.canlet.2019.11.009

175. Menter T, Tzankov A, Dirnhofer S. The tumor microenvironment of lymphomas: Insights into the potential role and modes of actions of checkpoint inhibitors. *Hematol Oncol*. (2021) 39:3–10. doi: 10.1002/hon.2821

176. Deng Z, Sun X, Cao J, Xiao Q. Editorial: Immune modulation in tumor microenvironment: New perspectives for cancer immunotherapy. *Front Cell Dev Biol*. (2022) 10:1103705. doi: 10.3389/fcell.2022.1103705

177. Peng S, Xiao F, Chen M, Gao H. Tumor-microenvironment-responsive nanomedicine for enhanced cancer immunotherapy. *Adv Sci (Weinh)*. (2022) 9:e2103836. doi: 10.1002/advs.202103836

178. Renner K, Singer K, Koehl GE, Geissler EK, Peter K, Siska PJ, et al. Metabolic hallmarks of tumor and immune cells in the tumor microenvironment. *Front Immunol*. (2017) 8:248. doi: 10.3389/fimmu.2017.00248

179. Niland S, Eble JA. Hold on or cut? Integrin- and MMP-mediated cell-matrix interactions in the tumor microenvironment. *Int J Mol Sci*. (2020) 22(1):238. doi: 10.3390/ijms22010238

180. Winkler J, Abisoye-Ogunniyan A, Metcalf KJ, Werb Z. Concepts of extracellular matrix remodelling in tumour progression and metastasis. *Nat Commun*. (2020) 11:5120. doi: 10.1038/s41467-020-18794-x

181. Lotfinejad P, Kazemi T, Mokhtarzadeh A, Shanehbandi D, Jadidi Niaragh F, Safaei S, et al. PD-1/PD-L1 axis importance and tumor microenvironment immune cells. *Life Sci*. (2020) 259:118297. doi: 10.1016/j.lfs.2020.118297

182. Maude SL, Frey N, Shaw PA, Aplenc R, Barrett DM, Bunin NJ, et al. Chimeric antigen receptor T cells for sustained remissions in leukemia. *N Engl J Med*. (2014) 371:1507–17. doi: 10.1056/NEJMoa1407222

183. Maude SL, Laetsch TW, Buechner J, Rives S, Boyer M, Bittencourt H, et al. Tisagenlecleucel in children and young adults with B-cell lymphoblastic leukemia. *N Engl J Med*. (2018) 378:439–48. doi: 10.1056/NEJMoa1709866

184. Gardner RA, Finney O, Annesley C, Brakke H, Summers C, Leger K, et al. Intent-to-treat leukemia remission by CD19 CAR T cells of defined formulation and dose in children and young adults. *Blood*. (2017) 129:3322–31. doi: 10.1182/blood-2017-02-769208

185. Frey NV, Shaw PA, Hexner EO, Pequignot E, Gill S, Luger SM, et al. Optimizing chimeric antigen receptor T-cell therapy for adults with acute lymphoblastic leukemia. *J Clin Oncol*. (2020) 38:415–22. doi: 10.1200/JCO.19.01892

186. Turtle CJ, Hanafi LA, Berger C, Hudecek M, Pender B, Robinson E, et al. Immunotherapy of non-Hodgkin's lymphoma with a defined ratio of CD8+ and CD4+ CD19-specific chimeric antigen receptor-modified T cells. *Sci Transl Med*. (2016) 8:355ra116. doi: 10.1126/scitranslmed.aaf8621

187. Schuster SJ, Svoboda J, Chong EA, Nasta SD, Mato AR, Anak Ö, et al. Chimeric antigen receptor T cells in refractory B-cell lymphomas. *N Engl J Med*. (2017) 377:2545–54. doi: 10.1056/NEJMoa1708566

188. Neelapu SS, Locke FL, Bartlett NL, Lekakis LJ, Miklos DB, Jacobson CA, et al. Axicabtagene ciloleucel CAR T-cell therapy in refractory large B-cell lymphoma. *N Engl J Med*. (2017) 377(26):2531–44. doi: 10.1056/NEJMoa1707447

189. Schuster SJ, Bishop MR, Tam CS, Waller EK, Borchmann P, McGuirk JP, et al. Tisagenlecleucel in adult relapsed or refractory diffuse large B-cell lymphoma. *N Engl J Med*. (2019) 380:45–56. doi: 10.1056/NEJMoa1804980

190. Abramson JS, Palomba ML, Gordon LI, Lunning MA, Wang M, Arnason J, et al. Lisocabtagene maraleucel for patients with relapsed or refractory large B-cell lymphomas (TRANSCEND NHL 001): a multicentre seamless design study. *Lancet*. (2020) 396:839–52. doi: 10.1016/S0140-6736(20)31366-0

191. Porter DL, Hwang WT, Frey NV, Lacey SF, Shaw PA, Loren AW, et al. Chimeric antigen receptor T cells persist and induce sustained remissions in relapsed refractory chronic lymphocytic leukemia. *Sci Transl Med*. (2015) 7:303ra139. doi: 10.1126/scitranslmed.aac5415

192. Turtle CJ, Hay KA, Hanafi LA, Li D, Cherian S, Chen X, et al. Durable molecular remissions in chronic lymphocytic leukemia treated with CD19-specific chimeric antigen receptor-modified T cells after failure of ibrutinib. *J Clin Oncol*. (2017) 35:3010–20. doi: 10.1200/JCO.2017.72.8519

193. Frey NV, Gill S, Hexner EO, Schuster S, Nasta S, Loren A, et al. Long-term outcomes from a randomized dose optimization study of chimeric antigen receptor modified T cells in relapsed chronic lymphocytic leukemia. *J Clin Oncol*. (2020) 38:2862–71. doi: 10.1200/JCO.19.03237

194. Brudno JN, Maric I, Hartman SD, Rose JJ, Wang M, Lam N, et al. T cells genetically modified to express an anti-B-cell maturation antigen chimeric antigen receptor cause remissions of poor-prognosis relapsed multiple myeloma. *J Clin Oncol*. (2018) 36:2267–80. doi: 10.1200/JCO.2018.77.8084

195. Zhao WH, Liu J, Wang BY, Chen YX, Cao XM, Yang Y, et al. A phase 1, open-label study of LCAR-B38M, a chimeric antigen receptor T cell therapy directed against B cell maturation antigen, in patients with relapsed or refractory multiple myeloma. *J Hematol Oncol*. (2018) 11:141. doi: 10.1186/s13045-018-0681-6

196. Cohen AD, Garfall AL, Stadtmauer EA, Melenhorst JJ, Lacey SF, Lancaster E, et al. B cell maturation antigen-specific CAR T cells are clinically active in multiple myeloma. *J Clin Invest*. (2019) 129:2210–21. doi: 10.1172/JCI126397

197. Raje N, Berdeja J, Lin Y, Siegel D, Jagannath S, Madduri D, et al. Anti-BCMA CAR T-cell therapy bb2121 in relapsed or refractory multiple myeloma. *N Engl J Med*. (2019) 380:1726–37. doi: 10.1056/NEJMoa1817226

198. Munshi NC, Anderson LD Jr., Shah N, Madduri D, Berdeja J, et al. Idecabtagene vicleucel in relapsed and refractory multiple myeloma. *N Engl J Med*. (2021) 384:705–16. doi: 10.1056/NEJMoa2024850

199. Wang M, Munoz J, Goy A, Locke FL, Jacobson CA, Hill BT, et al. KTE-X19 CAR T-cell therapy in relapsed or refractory mantle-cell lymphoma. *N Engl J Med*. (2020) 382:1331–42. doi: 10.1056/NEJMoa1914347

200. Michelozzi IM, Gomez-Castaneda E, Pohle RVC, Cardoso Rodriguez F, Sufi J, Puigdevall Costa P, et al. Activation priming and cytokine polyfunctionality modulate the enhanced functionality of low-affinity CD19 CAR T cells. *Blood Adv*. (2023) 7:1725–38. doi: 10.1182/bloodadvances.2022008490

frontiers | Frontiers in Immunology

TYPE Original Research
PUBLISHED 08 April 2024
DOI 10.3389/fimmu.2024.1364507

OPEN ACCESS

EDITED BY
Raquel Tarazona,
University of Extremadura, Spain

REVIEWED BY
Mehrdad Rakaee,
Oslo University Hospital, Norway
Julien Faget,
INSERM U1194 Institut de Recherche en Cancérologie de Montpellier (IRCM), France

*CORRESPONDENCE
Tianyang Zeng
z_ty1991@163.com

†These authors have contributed equally to this work and share first authorship

RECEIVED 02 January 2024
ACCEPTED 26 March 2024
PUBLISHED 08 April 2024

CITATION
Yang X, Li Q and Zeng T (2024) Peripheral CD4$^+$ T cells correlate with response and survival in patients with advanced non-small cell lung cancer receiving chemo-immunotherapy.
Front. Immunol. 15:1364507.
doi: 10.3389/fimmu.2024.1364507

Peripheral CD4$^+$ T cells correlate with response and survival in patients with advanced non-small cell lung cancer receiving chemo-immunotherapy

Xin Yang[1†], Qiao Li[2†] and Tianyang Zeng[3*]

[1]Department of Cardio-Thoracic Surgery, Deyang People's Hospital, Deyang, Sichuan, China, [2]Department of Pathology, Deyang People's Hospital, Deyang, Sichuan, China, [3]Department of Thoracic Surgery, The First Affiliated Hospital of Chongqing Medical University, Chongqing, China

Background: The aim of the present study was to explore the potential of peripheral immune cells in predicting the response and prognosis of patients with advanced non-small cell lung cancer (NSCLC) receiving anti-PD-1 immunotherapy and platinum-based chemotherapy.

Participants and Methods: We utilized flow cytometry to examine the levels and dynamics of blood immune cells in 79 advanced NSCLC patients treated with the chemoimmunotherapy between December 2019 and January 2022. The pre- and post-treatment blood samples were collected within 3 days prior to the initiation of the first and third cycle of combination treatment, respectively. Progression-free survival (PFS) and overall survival (OS) analyses were conducted using Kaplan-Meier method and Cox regression models.

Results: The pre-treatment CD4$^+$/Total T cells ratio was significantly higher in responders than non-responders ($P < 0.05$). The levels of pre-treatment total lymphocytes ($P = 0.012$), total B lymphocytes ($P = 0.025$), and NK cells ($P = 0.022$), and post-treatment NK cells ($P = 0.011$) and NKT cells ($P = 0.035$) were significantly associated with OS. Post-treatment CD8$^+$/Total T cells ratio was positively correlated with OS ($P = 0.038$). In multivariate analysis, post-treatment NK cells and post-treatment CD4$^+$CD8$^+$/Total T cells ratio were negatively associated with OS (hazard ratio [HR] = 10.30, $P = 0.038$) and PFS (HR = 1.95, $P = 0.022$), respectively. Notably, significantly positive correlations were observed between CD4$^+$/Total T cells ratio and prognosis both before and after treatment ($P < 0.05$).

Conclusion: To summarize, our finding reveals that high CD4$^+$/total T cells ratio was associated with favorable response and prognosis, highlighting its potential as a predictive biomarker to guide the selection of likely responders to platinum and anti-PD-1 combination therapy.

KEYWORDS

chemoimmunotherapy, lymphocyte subsets, biomarker, prognosis, non-small cell lung cancer

Introduction

Non-small cell lung cancer (NSCLC) is among the leading cause of cancer-related deaths worldwide, greatly endangering public health (1). Cytotoxic therapies, such as platinum-based chemotherapy, in combination with immune checkpoint inhibitors (ICIs) targeting PD-1/PD-L1 axis have been shown to profoundly improve efficacies of NSCLC treatment by synergizing to enhance anti-cancer immunity (2–4). Of note, only a limited range of NSCLC patients could derive significant survival benefits from the combination therapy (5, 6). However, specific biomarkers that were capable of predicting responses to the chemoimmunotherapy (chemoIO) remain to be identified (7–9). Therefore, it is paramount to identify feasible biomarkers to discriminate responders to the chemoIO from non-responders (10).

Peripheral blood might contain immune cells that were derived from the sites of tumor tissues, and therefore might have been recently recognized to possess predictive values for tumor infiltration and therapy response across multiple cancers, such as NSCLC, colorectal adenocarcinoma, endometrial adenocarcinoma and renal clear cell carcinoma (11). For example, increased lymphocyte-to-monocyte ratio in the peripheral blood was associated with improved clinical outcome in patients with metastatic nasopharyngeal carcinoma (12). High circulating NK cell counts forecasted a better overall survival in patients with untreated advanced gastric cancer (13). In addition, enhanced proliferation of peripheral PD-1^{+}CD8^{+} T cells was linked with improved prognosis (14), while relative B cell levels in the blood predicted a poor overall survival in patients with NSCLC receiving immune checkpoint inhibitors-based therapy (15). However, the association between peripheral immune cells and clinical outcome remains to be explored in NSCLC patients treated with chemoIO.

Here, we present the first research centering on evaluating the relationship of the compositions of peripheral immune cells with the response and prognosis in patients with inoperable advanced NSCLC receiving chemoIO, with the aim of characterizing potential response biomarkers to chemoIO. Overall, our findings may pave the way for further research on identifying novel biomarkers in the peripheral blood to promote the implementation of chemo-immunotherapy in clinical practice for treating NSCLC.

Abbreviations: NSCLC, non-small-cell lung cancer; ICIs, immune checkpoint inhibitors; ChemoIO, chemoimmunotherapy; PD-1, programmed cell death protein 1; PD-L1, programmed cell death 1 ligand 1; CT, computed tomography; EGFR, epidermal growth factor receptor; ALK, anaplastic lymphoma kinase; ROS1, ROS proto-oncogene 1, receptor tyrosine kinase; NK cell, natural killer cell; NKT cell, natural killer T cell; CR, complete response; PR, partial response; SD, stable disease; PD, progressive disease; OS, overall survival; PFS, Progression-free survival; ctDNA, circulating tumor DNA; HR, hazard ratio; CI, confidence intervals; ORR, objective response rate.

Patients and methods

Study population

A total of 79 advanced NSCLC patients (stage III and IV at diagnosis according to IASLC 8th version) receiving platinum-based chemotherapy in combination with PD-1 checkpoint inhibitors at the First Affiliated Hospital of Chongqing Medical University (Chongqing, China) between September 2019 and January 2022 were enrolled in this study. Survival follow-up was carried out through multiple ways, mainly including clinic visits, reaching patients through monthly phone calls, and surveying death reports. Overall survival (OS) and Progression-free survival (PFS) were used as the endpoints for survival outcomes. OS was defined as the duration time starting from the initiation of chemoIO treatment to death from any cause. PFS was defined as the duration time starting from the initiation of chemoIO treatment to disease progression or death from any cause, whichever happened first. The follow-up period of OS and PFS ended December 11, 2022, or death.

Criteria of inclusion and exclusion

The inclusion of patients was based on the following criteria: 1) stage III-IV NSCLC patients with diagnostic biopsy; 2) patients treated with platinum-based chemotherapy in combination with immune checkpoint inhibitors targeting PD-1; 3) patients without autoimmune diseases; 4) patients with normal functions of liver and kidney; 5) patients with good tolerance to chemotherapy plus immunotherapy, as indicated by Karnofsky performance status (KPS) score ≥ 80.

The exclusion criteria were as follows: 1) patients receiving adjuvant therapy after undergoing radical surgery of lung cancer; 2) patients treated with neoadjuvant therapy; 3) patients with severe organ dysfunctions; 3) patients with incomplete clinical data (for example, only tested for blood immune cells once); 4) patients with recent use of immunosuppressive medications; 5) patients lost to follow up; 6) positive for EGFR mutation, ALK fusion, and ROS1 fusion.

The following data were sourced from the medical records: age, gender, smoking history, histopathological features, disease stage, use of PD-1 inhibitors and comorbidity. Platinum-based chemotherapy was applied following the standard first-line chemotherapy regimen for advanced NSCLC. The immunotherapy drugs contained camrelizumab, tislelizumab, and pembrolizumab. Patients achieving complete response (CR) or partial response (PR) were grouped as responders, whereas patients showing stable disease (SD) or progressive disease (PD) were defined as non-responders, according to RECIST criteria v1.1.

Patient sample collection

Fasting blood (> 200 μL) was aseptically collected through venipuncture within 3 days before the initiation of the first and third cycle of chemoIO treatment to examine pre- and post-

treatment blood samples, respectively. Then, the blood was immediately transported in vacutainer blood collection tubes to the laboratory at room temperature and processed within 24 hours of draw.

Flow cytometry analysis

The flow cytometry was performed to determine the percentages and absolute counts of T lymphocytes ($CD3^+$), B lymphocytes ($CD19^+$), natural killer (NK) lymphocytes ($CD3^-$ $CD16^+$ and/or $CD56^+$), helper/inducer T lymphocytes ($CD3^+CD4^+$), and suppressor/cytotoxic T lymphocytes ($CD3^+CD8^+$) in the peripheral whole blood samples, using a 6-Color TBNK Reagent (QuantoBio, China, Z8610002) following the manufacturer's instructions. Whole blood samples were stained within 24 hours of draw. The representative gating strategy for these cells from one representative patient was shown in Figure 1. Briefly, 50 µL of well-mixed, anticoagulated whole blood and 20 µL of CD3/CD16 + 56/CD45/CD4/CD19/CD8 reagent containing a mixture of fluorophore conjugated antibodies (fluorescein isothiocyanate (FITC)-labeled CD3 (UCHT1), phycoerythrin (PE)-labeled CD16 (CB16), PE-labeled CD56 (MEM-188), PerCP-Cy5.5–labeled CD45 (2D1), PC7–labeled CD4 (RPA-T4), allophycocyanin (APC)-labeled CD19 (HIB19), and APC-Cy7–labeled CD8 (HIT8a)) were pipetted into the bottom of the collection tubes, and vortexed gently to mix, followed by incubation in the dark at room temperature for 15–30 minutes. Next, to lyse red blood cells, 450 µL lysing solution were added to the tubes and incubated for 15–30 minutes in the dark at room temperature. Then, the samples were acquired on the flow cytometer (BD FACSCantoTMII, USA) and the data were analyzed using the BD FACSCantoTM clinical software.

To simply introduce the gating strategies, nucleated cells (R1) were first revealed by CD45 expression and side scatter (SSC) size. Then, the sum of lymphocytes and monocytes (A) were gated by $CD45^{high}$ and SSC^{low} populations. Within the gate (A), the total lymphocytes (Lym) were identified by gating out monocytes in (q). The lymphocytes (Lym) could be split into CD3 positive T cells and CD3 negative cells (G) by the CD3 expression. CD3 positive T cells were then further identified and gated by the expression of CD4 and CD8 to identify helper and cytotoxic cells. Within the gate (G), CD3 negative cells were split into B cells and NK cells by the expression of CD19 and CD16 + 56. All information on antibodies was presented in Supplementary Table S1.

Statistical analyses

GraphPad Prism version 10.0 and R software 3.6.2 were used for statistical analysis. Data were presented as mean ± SEM. Fisher's exact test was used to analyze the categorical variables that were processed as percentages and frequencies. Survival analyses were performed using the Kaplan-Meier method with log-rank test and Cox proportional hazards regression model. The optimal cutpoints of different lymphocyte subsets for survival analysis were determined using the maximally selected test statistics from survminer R package. PFS used the same cutpoints as those of OS for corresponding immune cell subset. Hazard ratio (HR) and 95% confidence interval (CI) were calculated for Cox regression analysis. The variables that showed statistical significance in the univariate analyses were selected to be further analyzed in the multivariate models. The continuous variables were analyzed using Mann–Whitney U test and paired t-test, and the categorical variables using Fisher's exact test. The two-sided probability of type I error was 0.05 in the analysis. $P < 0.05$ was determined to be with statistical difference.

Results

Patient demographic and clinical characteristics

159 NSCLC patients who were not eligible for curative surgery and received combination treatment of platinum-based chemotherapy plus PD-1 checkpoint inhibitors were retrospectively enrolled from September 2019 to January 2022 at the Department of Thoracic Surgery, the First Affiliated Hospital of Chongqing Medical University. Thirty patients with stage I-II NSCLC were excluded due to severe cardiopulmonary functions. Next, 38 patients with incomplete clinical data were excluded. Twelve additional patients lost to follow up were excluded. Therefore, the study cohort comprised of 79 advanced NSCLC patients qualified for peripheral immune cell analysis (Figure 2). The detailed clinical characteristics of the included patients were displayed in Table 1. Across the 79 patients, 47 (59.5%) and 32 (40.5%) were lung squamous carcinoma and lung adenocarcinoma, respectively. The cohort has a median age of 59 years old (range, 30-74 years old), and 52 (65.8%) patients have a smoking history or currently smoke. Males, being a major part of the cohort, account for 89% of the cohort. According to the Fisher's exact test, no significant differences of histology type, PD-1 inhibitors types, comorbidity, smoking history, age, and gender were observed between the two groups (CR/PR vs SD/PD) (Table 1). Overall, with 39 and 40 patients achieving CR/PR and SD/PD respectively, the objective response rate (ORR) was 49.4% (39/79) in advanced NSCLC patients treated with the chemoimmunotherapy.

Correlations between peripheral immune cells and response

The patients were stratified into two groups, responders (CR/PR) and non-responders (SD/PD) based on their response to platinum-based chemotherapy plus immunotherapy, as clarified by RECIST criteria v1.1. To investigate the association between clinical hematological parameters and patients' response to therapy, the levels of peripheral total lymphocytes, total B lymphocytes, total T lymphocytes, NK cells and NKT cells were compared between CR/PR and SD/PD. The pre-treatment $CD4^+$/Total T cells ratio (*P*

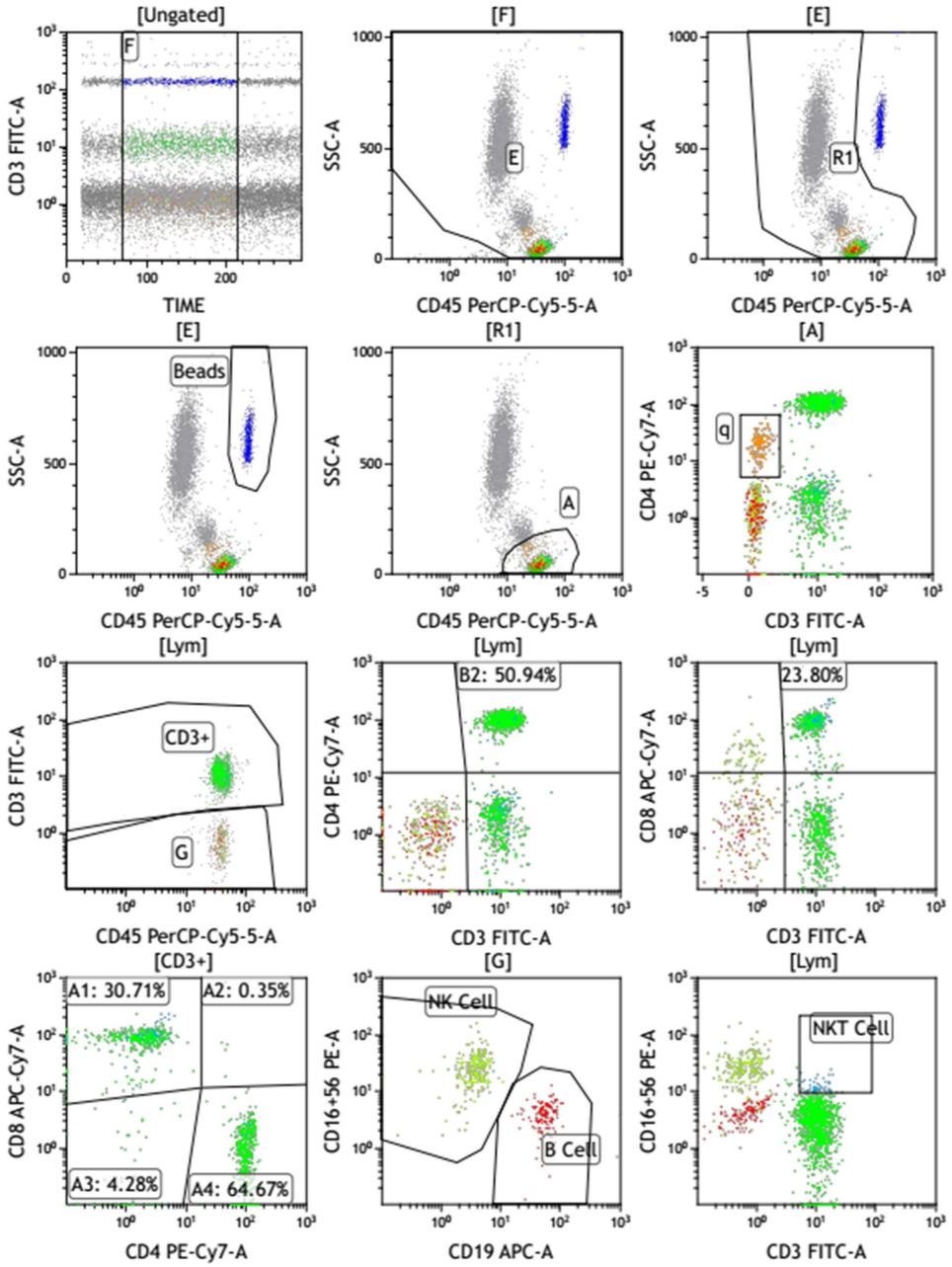

FIGURE 1
The gating strategy of a representative sample.

= 0.003, Fisher's exact test) and post-treatment $CD4^-CD8^-$ T cell frequency (P = 0.029, Fisher's exact test) were significantly different between CR/PR group and SD/PD group (Tables 2, 3). The level of peripheral total B lymphocytes was significantly decreased after treatment in non-responders as compared with pre-treatment (Figure 3A). Furthermore, the ratios of respective T cell subset to total or $CD8^+$ T cells were analyzed. According to Figure 3B, pre-treatment $CD4^+$/Total T cells ratio was significantly higher in responders than non-responders. In addition, $CD4^-CD8^-$/Total T cells ratio and the $CD4^+/CD8^+$ T cells ratio before treatment was significantly increased and decreased compared to their counterparts after treatment in responders, respectively (Figure 3B).

Correlations between peripheral immune cells and clinical outcomes

Next, we comparatively analyzed the differences between the pre- and post-treatment peripheral immune cells compositions in NSCLC patients treated with chemoIO. Low pre-treatment levels of total lymphocytes (P = 0.012), total B lymphocytes (P = 0.025), and low pre- and post-treatment levels of NK cells (P = 0.0215; P = 0.011) were associated with significantly better overall survival than high-level groups, while higher levels of post-treatment NKT cells were correlated with longer overall survival (P = 0.035) (Figure 4, Supplementary Figure S1). However, no association was observed

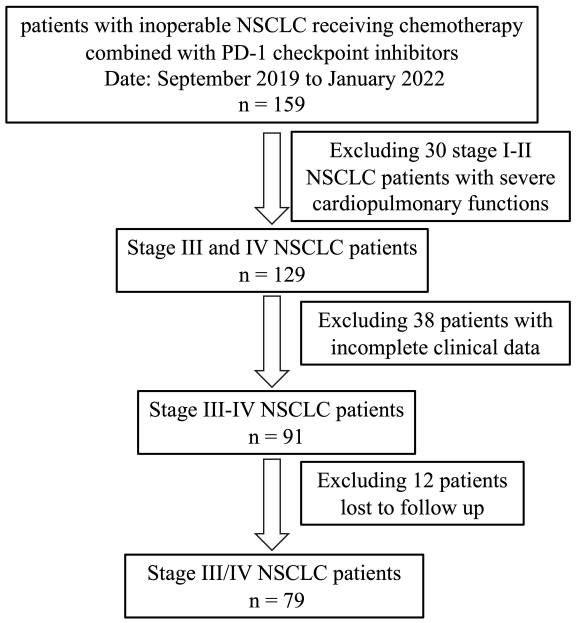

FIGURE 2
The flowchart of patient selection.

between peripheral immune cell levels and progression-free survival (Supplementary Figure S2). Next, the correlations between the relative abundances of immune cell subsets among the total T cells and patients' prognosis were also analyzed. Both before and after chemoIO treatment, the $CD4^+$/total T cells ratio was positively associated with improved OS (before: $P < 0.001$; after: $P = 0.0015$) and PFS (pre: $P = 0.0002$; post: $P < 0.0001$) (Figure 5A). And post-treatment $CD8^+$/Total T cells ratio and $CD4^+CD8^+$/Total T cells ratio were significantly associated with OS and PFS, respectively (Figures 5B, C, Supplementary Figures S3, S4).

We next conducted univariate and multivariate cox regression analysis to analyze the potential of peripheral lymphocyte subsets as independent prognostic factors. As illustrated by the forest plot, high level of post-treatment NK cells was significantly associated with shorter OS ($P = 0.038$, HR = 10.30). Conversely, pre-treatment $CD4^+$/Total T cells ratio ($P = 0.004$, HR = 0.28) and post-treatment $CD4^+$/Total T cells ratio ($P = 0.006$, HR = 0.17) were significantly associated with improved OS (Figure 6A, Table 4). Furthermore, an increased ratio of $CD4^+$ to Total T cells before ($P = 0.025$, HR = 0.45) and after treatment ($P = 0.002$, HR = 0.25) was associated with favorable prognosis, while post-treatment $CD4^+CD8^+$/Total T cells ratio ($P = 0.022$, HR = 1.95) was independently associated with shorter PFS (Figure 6B, Table 5). Collectively, these results suggested that $CD4^+$ T cells was associated with better clinical outcome in advanced NSCLC patients receiving the chemoIO treatment.

Discussion

Chemotherapy in combination with anti PD-1/PD-L1 antibodies has become a mainstay for patients with advanced non-small cell lung cancer (16). However, accurate selection of potential responders to the chemoIO remains challenging due to the wide variations in patients' clinical responses to immunotherapy due to tumor heterogeneity. Here, we demonstrated that $CD4^+$/total T cells ratio was significantly higher in CR/PR group than in SD/PD group. In addition, our study uncovered that the frequencies of circulating immune cells, including $CD4^+$ T cells, $CD8^+$ T cells and NK cells, were significantly associated with the overall survival and progression-free survival. Notably, this is the first study to support the characterization of $CD4^+$ T cells as a potential prognostic parameter in inoperable advanced NSCLC patients receiving chemoimmunotherapy.

Combining chemotherapy with ICIs could enhance immunotherapy efficacy by exposing tumor neoantigens and priming immune cells, thus inducing immunogenic cell death (17–19). For example, chemotherapy could enhance cytotoxic T lymphocytes-mediated killing of cancer cells through immunogenic modulation (20). However, no available blood-based biomarkers associated with clinical outcome have been investigated as of now. Therefore, there is a pressing need to identify effective biomarkers to guide selection of

TABLE 1 Baseline characteristics of 79 patients with advanced NSCLC.

Characteristic	Total (n =79)	CR/PR (n = 39)	SD/PD (n = 40)	*P*-value
Age				
< 59 years	38 (48%)	20	18	0.655
≥ 59 years	41 (52%)	19	22	
Gender				
Female	9 (11%)	4	5	1.000
Male	70 (89%)	35	35	
Smoking status				
History of smoking	52 (66%)	26	26	1.000
No history of smoking	27 (34%)	13	14	
Histopathological features				
Non-squamous	32 (41%)	15	17	0.820
Squamous cell carcinoma	47 (59%)	24	23	
Disease stage				
Stage III	48 (61%)	25	23	0.647
Stage IV	31 (39%)	14	17	
PD-1 inhibitors				
Camrelizumab	66 (83%)	32	34	0.876
Tislelizumab	11 (14%)	6	5	
Pembrolizumab	2 (3%)	1	1	
Comorbidity				
Hypertension	12 (15%)	7	5	0.688
Diabetes mellitus	10 (13%)	4	6	
Viral hepatitis B	5 (6%)	3	2	

p-values were estimated by Fisher's exact test.

TABLE 2 Association of lymphocyte subsets before treatment with objective response rate.

Characteristics	Total (n =79)	CR/PR (n = 39)	SD/PD (n = 40)	*p*-value[a]
Total lymphocytes (cells/μL)	1714 (464, 3772)	1725 (464, 3772)	1561 (746, 3359)	0.551
> 1218		8	9	0.83
≤ 1218		31	31	
Total T lymphocytes (cells/μL)	1170 (399, 2854)	1278 (399, 2854)	1082.5 (480, 2241)	0.229
> 783		34	35	1
≤ 783		5	5	
B lymphocytes (cells/μL)	161 (27, 902)	179 (42, 653)	153 (27, 902)	0.943
> 128		26	26	0.876
≤ 128		13	14	
NK cells (cells/μL)	260 (21, 1376)	228 (21, 1017)	265.5 (60, 1376)	0.540
> 112		33	37	0.311
≤ 112		6	3	
NKT cells (cells/μL)	39 (6, 216)	44 (8, 216)	31 (6, 199)	0.432
> 69		8	9	0.83
≤ 69		31	31	
$CD4^+/CD8^+$ T cells ratio	1.6 (0.3, 3.53)	1.61 (0.93, 3.25)	1.585 (0.3, 3.53)	0.187
> 1.23		30	29	0.651
≤ 1.23		9	11	
$CD4^+$/Total T cells ratio	41.77 (19.79, 60.7)	42.71 (30.25, 57.43)	38.61 (19.79, 60.7)	0.047
> 31.44		38	29	0.003
≤ 31.44		1	11	
$CD8^+$/Total T cells ratio	25 (13.37, 65.15)	24.26 (13.37, 50.72)	25.355 (14.82, 65.15)	0.541
> 26.81		15	17	0.715
≤ 26.81		24	23	
$CD4^+CD8^+$/Total T cells ratio	0.44 (0, 15.51)	0.4 (0, 15.51)	0.445 (0.07, 1.72)	0.382
> 0.15		34	33	0.562
≤ 0.15		5	7	

(Continued)

TABLE 2 Continued

Characteristics	Total (n =79)	CR/PR (n = 39)	SD/PD (n = 40)	*p*-value[a]
$CD4^-CD8^-$/Total T cells ratio	3.91 (0.91, 23.99)	4.36 (0.91, 23.99)	3.575 (1.18, 15.46)	0.257
> 5.62		11	7	0.257
≤ 5.62		28	33	

[a]p-Values were estimated by Fisher's exact test and Mann–Whitney U test for categorical variables and continuous variables, respectively.

TABLE 3 Association of lymphocyte subsets with objective response rates after treatment.

Characteristics	Total (n =79)	CR/PR (n = 39)	SD/PD (n = 40)	*p*-value[a]
Total lymphocytes (cells/μL)	1577 (311, 2954)	1608 (311, 2954)	1489.5 (879, 2896)	0.554
> 1885		15	10	0.198
≤ 1885		24	30	
Total T lymphocytes (cells/μL)	1127 (222, 2376)	1187 (222, 2376)	1105 (437, 2026)	0.508
> 1090		23	20	0.423
≤ 1090		16	20	
B lymphocytes (cells/μL)	127 (9, 749)	149 (9, 749)	116 (23, 450)	0.294
> 95		30	26	0.243
≤ 95		9	14	
NK cells (cells/μL)	249 (73, 928)	240 (78, 928)	264.5 (73, 672)	0.903
> 147		27	34	0.095
≤ 147		12	6	
NKT cells (cells/μL)	32 (5, 509)	33 (8, 112)	28.5 (5, 509)	0.306
> 21		28	22	0.122
≤ 21		11	18	
$CD4^+/CD8^+$ T cells ratio	1.57 (0.48, 3.7)	1.57 (0.61, 3.62)	1.475 (0.48, 3.7)	0.483
> 1.20		30	23	0.066
≤ 1.20		9	17	
$CD4^+$/Total T cells ratio	39.58 (20.53, 60.92)	40.11 (26.65, 55.57)	39.555 (20.53, 60.92)	0.540
> 27.71		38	34	0.108
≤ 27.71		1	6	
$CD8^+$/Total T cells ratio	26.28 (13.38, 51.91)	25.43 (13.38, 49.11)	27.65 (15, 51.91)	0.399

(Continued)

TABLE 3 Continued

Characteristics	Total (n =79)	CR/PR (n = 39)	SD/PD (n = 40)	*p*-value[a]
> 23.46		25	26	0.933
≤ 23.46		14	14	
$CD4^+CD8^+$/Total T cells ratio	0.4 (0.06, 8.02)	0.35 (0.06, 8.02)	0.415 (0.06, 1.83)	0.714
> 0.51		11	17	0.184
≤ 0.51		28	23	
$CD4^-CD8^-$/Total T cells ratio	4.05 (1.05,23.49)	4.67 (1.23,23.49)	3.915 (1.05,16.75)	0.123
> 5.00		19	10	0.029
≤ 5.00		20	30	

[a]p-Values were estimated by Fisher's exact test Mann–Whitney U test for categorical variables and continuous variables, respectively.

NSCLC patients that might derive survival benefit from chemoIO treatment. Due to the invasive and time-consuming nature of histopathological evaluation which is currently a standard disease monitoring approach, identifying a novel blood-based biomarker that is non-invasive and easily accessible is of great clinical significance (21). In contrast with tumor tissues, the immune cells in the peripheral blood would provide a far more convenient sample source for patient selection and might offer a more comprehensive immune landscape of the whole tumor since they are circulated systemically (22, 23). Moreover, durable antitumor immune responses also require unrelenting immune cell recruitment from the peripheral blood (24, 25). However, the association between peripheral immune cell subsets and clinical outcomes in NSCLC patients receiving chemoimmunotherapy has remained elusive yet. A previous study showed that the levels of peripheral T cells and NK cells were closely related to the pathological response in 59 patients with resectable stage IIA-IIIB NSCLC treated with neoadjuvant chemoIO (26). Here, we demonstrated that the peripheral $CD4^+$/Total T cells ratio was significantly higher in responders (CR and PR) as compared to non-responders (SD and PD). Consistently, a previous study demonstrated that the activated $CD4^+$ T cell subset in the peripheral blood was a potent mediator of anti-tumor immunity (27). Collectively, the present study demonstrated the association between peripheral $CD4^+$ T cells and response to chemoIO in inoperable NSCLC patients for the first time.

The immune contexture is a major determinant of tumor progression and clinical outcomes in patients with solid tumors (28). For example, increased tumor-infiltrating lymphocytes (TILs) were associated with survival in patients with breast cancer (29). Besides, it has been reported that long-term responders showed significantly higher levels of peripheral $CD62L^{low}CD4^+$ T cells before PD-1 blockade therapy in patients with NSCLC (30). Moreover, the prognostic impact of the peripheral neutrophils-to-lymphocytes ratio has also been recognized across different cancers (31). Hematological biomarkers, which allow for longitudinal monitoring of real-time disease status by safe venipuncture, present an informative surrogate of histopathological examination for risk stratification and treatment guidance (32). For instance, as one of the most prevalent biomarkers used in liquid biopsy, ctDNA is now widely used to aid in the selection of NSCLC patients who might benefit from epidermal growth factor receptor (EGFR)-targeted therapy (33). Here, we demonstrated the association of lymphocytes and NK cells with prognosis in NSCLC patients receiving chemoimmunotherapy for the first time. Our study revealed that higher percentages of pre- and post-chemoIO $CD4^+$ T cells were independently associated with improved OS and PFS in patients with NSCLC, which was in line with our finding that $CD4^+$/Total T cells ratio before chemoIO therapy was higher in responders

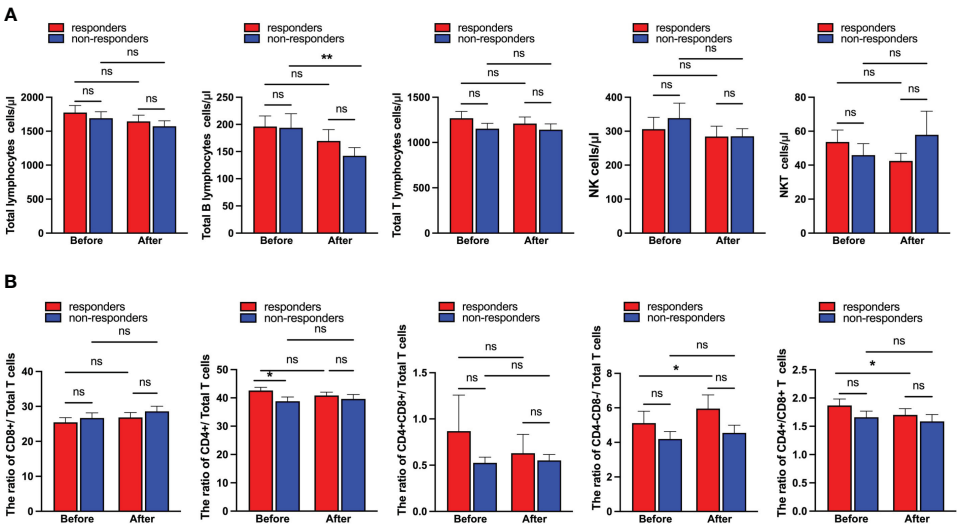

FIGURE 3
The correlations between pre- and post-treatment peripheral immune cell levels and responses. **(A)** The differneces of the abundances and **(B)** ratios of peripheral immune cell subsets between responders and non-responders. Responders group corresponds to complete response (CR) and partial response (PR), while non-responders group refers to stable disease (SD) and progressive disease (PD). The data were analyzed by paired t-test and Mann–Whitney U test. Data were presented as mean ± SEM. *p<0.05 and **p<0.01. ns, not significant.

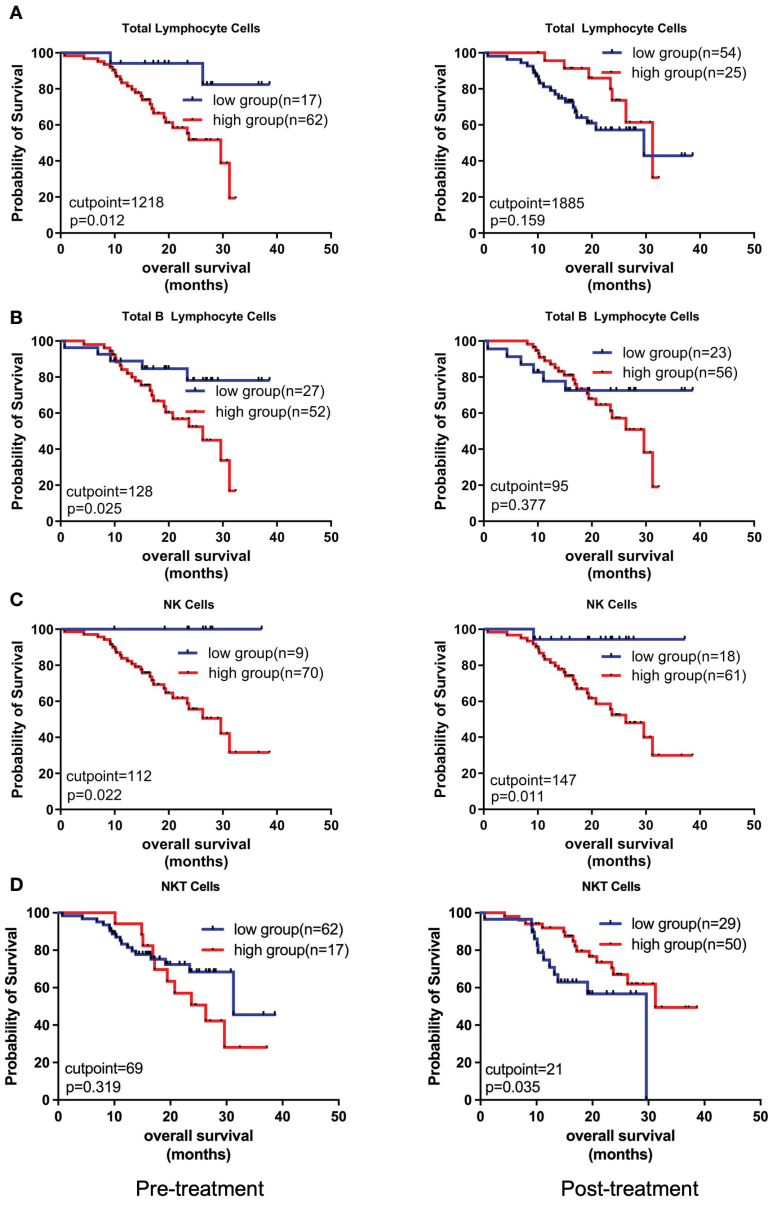

FIGURE 4
Kaplan-Meier analysis on the overall survival with regard to different peripheral immune cell subsets. The Kaplan-Meier curves of OS of patients stratified by total lymphocyte cells **(A)**, total B lymphocyte cells **(B)**, NK cells **(C)**, and NKT cells **(D)** at pre- and post-treatment according to the optimal cutpoints of respective lymphocyte subsets. The high and low groups were stratified by the cutpoints that were determined using the maximally selected test statistics for OS. The log-rank test was conducted to evaluate the significance of patients' survival.

than non-responders. Taken together, these results suggested that peripheral $CD4^+$ T cell subset might exert protective functions in response to chemoIO treatment, thus underscoring its potential as a predictive biomarker for screening beneficiaries before chemoIO treatment and evaluating efficacy after the chemoIO treatment. Despite less understood than $CD8^+$ T cells in anti-cancer function, the $CD4^+$ T cell subset has been recently demonstrated to be protective against cancer progression likely by enhancing tumoricidal activity of other antitumor effector cells subsets (34). For example, $CD4^+$ T cell depletion retarded tumor growth by increasing effector T cell function (35). Moreover, it was lately demonstrated that a novel $CD62L^{low}CCR4^-CCR6^+$ $CD4^+$ T cell metacluster exhibited predictive potential of the immune status and sensitivity to PD-1 blockade (36). It should be noted though that effective prediction will most likely be satisfactorily achieved by comprehensively implementing multiple biomarkers instead of a single one, thus highlighting the importance of combining peripheral CD4+ T cells with other parameters to effectively evaluate efficacy and prognosis in response to chemoIO. Overall, this is the first study to suggest a positive correlation of peripheral $CD4^+$ T cells with OS and PFS in patients with inoperable advanced NSCLC treated with chemoimmunotherapy.

However, there are several limits to the present study. Firstly, a prospective study should be conducted in the future to validate the relationships of the peripheral blood immune cell subsets to the

10.3389/fimmu.2024.1364507

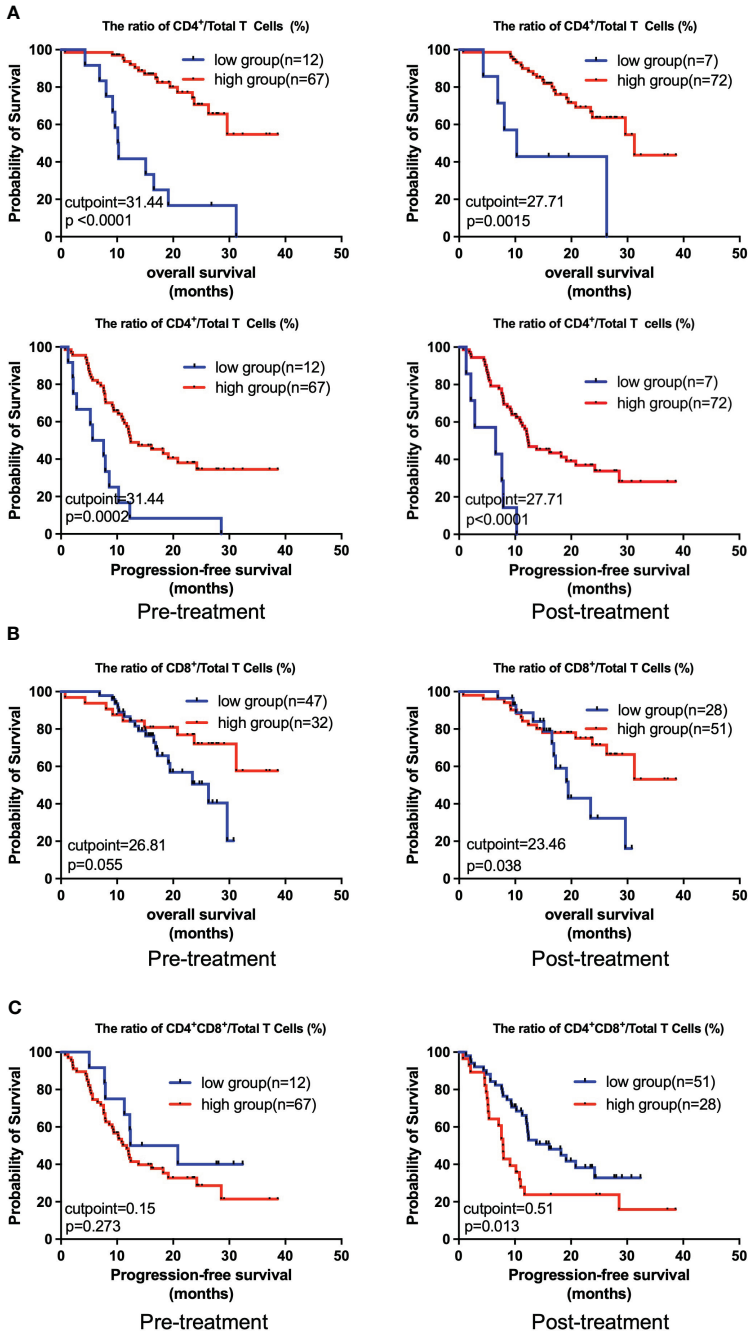

FIGURE 5
Kaplan-Meier analysis on the overall survival and progression-free survival with regard to the relative levels of different peripheral immune cells. The Kaplan-Meier curves of OS and PFS of patients stratified by CD4+/Total T cells ratio **(A)**, OS of patients stratified by CD4+/Total T cells ratio **(B)**, and PFS of patients stratified by $CD4^+CD8^+$/Total T cells ratio **(C)** at pre- and post-treatment according to the best cutpoints of respective immune cell ratios. The high and low groups in both OS and PFS analysis were stratified by the cutpoints that were determined using the maximally selected test statistics for OS. The log-rank test was conducted to evaluate the significance of patients' survival.

response and prognostic outcomes in a larger cohort of NSCLC patients receiving chemoIO. Secondly, the functions of each immune cell subset are multifaceted, therefore a more detailed landscape of the immune composition need to be further profiled to investigate the specific immune subpopulation that is involved in cancer-related immunity. Lastly, with only relevance analysis being performed in the current study, experiments *in vitro* and *in vivo* will also be our next step to explore the molecular mechanisms underlying the protective roles of $CD4^+$ T cells in patients with advanced NSCLC receiving chemo-immunotherapy.

In conclusion, with the prospects for long-time survival greatly improved by immunotherapy, our results provide timely and valuable information on the prognostic roles of $CD4^+$ T cells in advanced NSCLC patients treated with chemoIO. Dynamic and longitudinal monitoring of the peripheral $CD4^+$ T cells might aid in selection of likely responders to the treatment. A prospective study in a larger cohort of advanced NSCLC

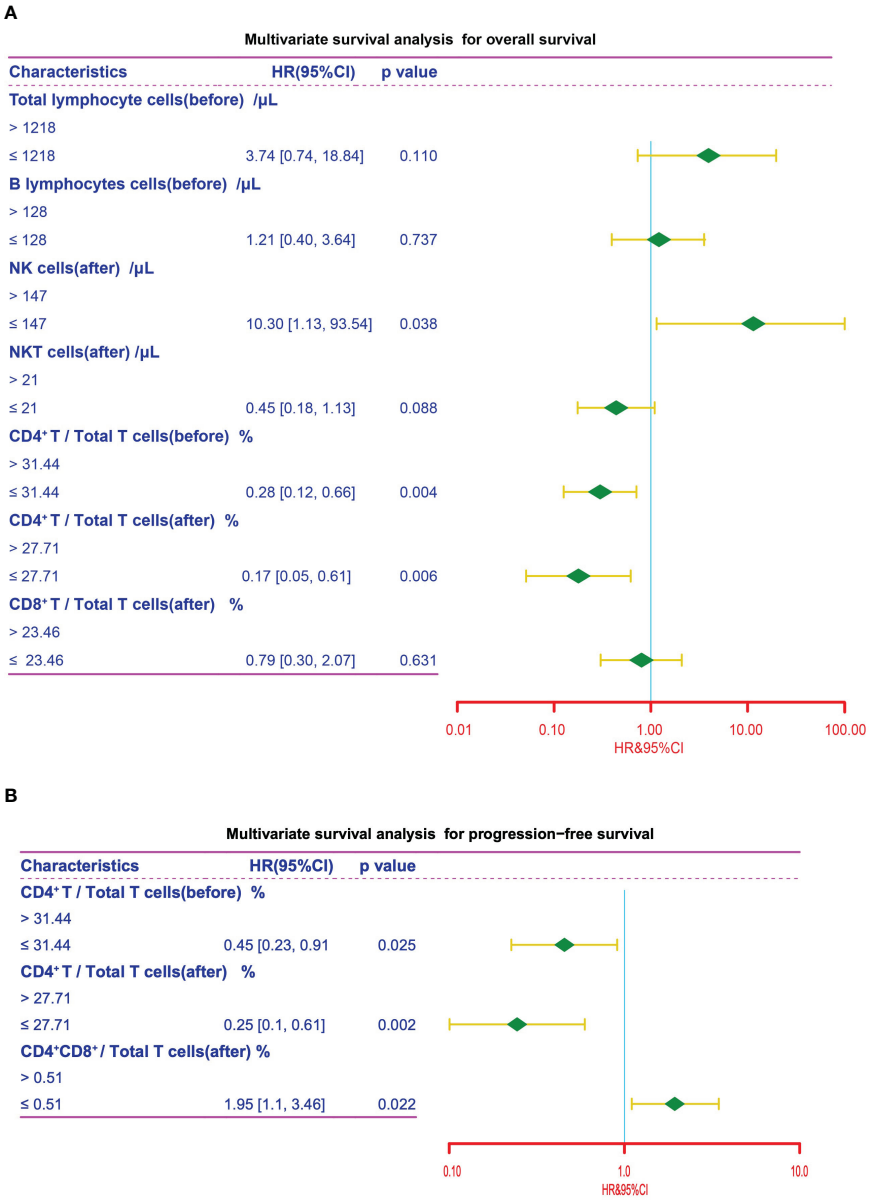

FIGURE 6
Multivariate survival analysis. Multivariate survival analysis of the peripheral immune cell subsets for OS **(A)** and PFS **(B)** in NSCLC patients for variables that showed statistical significance in univariate survival analysis. The cutpoints that were determined using the maximally selected test statistics.

TABLE 4 Cox proportional analysis for overall survival.

Characteristics	Univariate			Multivariate		
	HR	95% CI	*p*-value	HR	95% CI	*p*-value
Total lymphocytes (before)	5.43	1.27 – 23.25	0.023	3.74	0.74 – 18.84	0.110
Total lymphocytes (after)	0.54	0.23 – 1.29	0.165			
Total T lymphocytes (before)	5.04	0.68 – 37.27	0.113			
Total T lymphocytes (after)	0.57	0.27 – 1.24	0.157			
Total B lymphocytes (before)	2.91	1.09 – 7.73	0.033	1.21	0.40 – 3.64	0.737
Total B lymphocytes (after)	1.51	0.60 – 3.78	0.381			

(Continued)

10.3389/fimmu.2024.1364507

TABLE 4 Continued

Characteristics	Univariate			Multivariate		
	HR	95% CI	*p*-value	HR	95% CI	*p*-value
NK cells (before)	Inf	0 - Inf	0.998			
NK cells (after)	8.71	1.18 – 64.28	0.034	10.3	1.13 – 93.54	0.038
NKT cells (before)	1.49	0.68 – 3.28	0.322			
NKT cells (after)	0.44	0.20 – 0.96	0.04	0.45	0.18 – 1.13	0.088
$CD4^+/CD8^+$ T cells ratio (before)	1.77	0.69 – 4.53	0.236			
$CD4^+/CD8^+$ T cells ratio (after)	0.61	0.28 – 1.33	0.217			
$CD4^+$/Total T cells (before)	0.16	0.07 – 0.035	0.000	0.28	0.12 – 0.66	0.004
$CD4^+$/Total T cells (after)	0.23	0.09 – 0.62	0.004	0.17	0.05 – 0.61	0.006
$CD8^+$/Total T cells (before)	0.44	0.19 – 1.04	0.061			
$CD8^+$/Total T cells (after)	0.44	0.20 – 0.98	0.043	0.79	0.30 – 2.07	0.631
$CD4^+CD8^+$/Total T cells (before)	2.84	0.67 – 12.07	0.157			
$CD4^+CD8^+$/Total T cells (after)	1.68	0.79 – 3.59	0.181			
$CD4^-CD8^-$/Total T cells (before)	0.47	0.16 – 1.39	0.173			
$CD4^-CD8^-$/Total T cells (after)	0.51	0.22 – 1.22	0.13			

TABLE 5 Cox proportional analysis for progression-free survival.

Characteristics	Univariate			Multivariate		
	HR	95% CI	*p*-value	HR	95% CI	*p*-value
Total lymphocytes (before)	1.29	0.66 – 2.51	0.462			
Total lymphocytes (after)	0.57	0.30 – 1.09	0.089			
Total T lymphocytes (before)	1.07	0.48 - 2.38	0.87			
Total T lymphocytes (after)	0.58	0.33 – 1.02	0.057			
Total B lymphocytes (before)	1.09	0.61 - 1.94	0.768			
Total B lymphocytes (after)	0.99	0.54 - 1.81	0.981			
NK cells (before)	2.40	0.86 – 6.70	0.094			
NK cells (after)	1.51	0.76 - 3.02	0.244			
NKT cells (before)	0.93	0.49 – 1.79	0.838			
NKT cells (after)	0.57	0.32 – 1.01	0.054			
$CD4^+/CD8^+$ T cells ratio (before)	1.03	0.55 - 1.93	0.92			
$CD4^+/CD8^+$ T cells ratio (after)	0.64	0.36 – 1.13	0.121			
$CD4^+$/Total T cells (before)	0.31	0.16 – 0.60	0.001	0.45	0.23 - 0.91	0.025
$CD4^+$/Total T cells (after)	0.20	0.09 – 0.47	0.000	0.25	0.10 – 0.61	0.002
$CD8^+$/Total T cells (before)	0.79	0.44 – 1.41	0.431			
$CD8^+$/Total T cells (after)	0.84	0.47 – 1.50	0.557			
$CD4^+CD8^+$/Total T cells (before)	1.56	0.70 – 3.48	0.276			
$CD4^+CD8^+$/Total T cells (after)	2.01	1.15 – 3.53	0.015	1.95	1.10 – 3.46	0.022
$CD4^-CD8^-$/Total T cells (before)	0.68	0.34 – 1.36	0.272			
$CD4^-CD8^-$/Total T cells (after)	0.76	0.43 – 1.35	0.352			

patients treated with chemoimmunotherapy is further warranted to validate the use of peripheral $CD4^+$ T cells as biomarkers that are truly predictive of prognosis.

Data availability statement

The original contributions presented in the study are included in the article/Supplementary Material. Further inquiries can be directed to the corresponding author.

Ethics statement

The studies involving humans were approved by the Ethics Committee in the First Affiliated Hospital of Chongqing Medical University. The studies were conducted in accordance with the local legislation and institutional requirements. The participants provided their written informed consent to participate in this study.

Author contributions

QL: Funding acquisition, Investigation, Writing – original draft, Data curation, Formal analysis, Writing – review & editing. XY: Conceptualization, Data curation, Formal analysis, Investigation, Methodology, Software, Visualization, Writing – review & editing, Writing – original draft. TZ: Conceptualization, Funding acquisition, Supervision, Writing – review & editing.

Funding

The author(s) declare that financial support was received for the research, authorship, and/or publication of this article. This work was supported in part by grants from Innovation Fund for Project of innovation team for Graduate Teaching (CYYY-YJSJXCX-202318); and Xinglin scholars program (YYZX2022065).

Conflict of interest

The authors declare that the research was conducted in the absence of any commercial or financial relationships that could be construed as a potential conflict of interest.

Publisher's note

Supplementary material

The Supplementary Material for this article can be found online at: https://www.frontiersin.org/articles/10.3389/fimmu.2024.1364507/full#supplementary-material

SUPPLEMENTARY FIGURE S1
Kaplan-Meier analysis on the overall survival. The Kaplan-Meier curves of OS of patients stratified by the optimal cutpoint of total T lymphocyte cells at pre- and post-treatment.

SUPPLEMENTARY FIGURE S2
Kaplan-Meier analysis on the progression-free survival. The Kaplan-Meier curves of PFS of patients stratified by the optimal cutpoints of OS at pre- and post-treatment.

SUPPLEMENTARY FIGURE S3
Kaplan-Meier analysis on the overall survival. The Kaplan-Meier curves of OS of patients stratified by the optimal cutpoints of OS at pre- and post-treatment.

SUPPLEMENTARY FIGURE S4
Kaplan-Meier analysis on the progression-free survival. The Kaplan-Meier curves of PFS at pre- and post-treatment. The cutpoints for PFS were determined by the optimal cutpoints of OS.

References

1. Siegel R, Miller K, Wagle N, Jemal A. Cancer statistics 2023. *CA: Cancer J Clin.* (2023) 73:17–48. doi: 10.3322/caac.21763

2. Kanda S, Goto K, Shiraishi H, Kubo E, Tanaka A, Utsumi H, et al. Safety and efficacy of nivolumab and standard chemotherapy drug combination in patients with advanced non-small-cell lung cancer: a four arms phase Ib study. *Ann Oncol.* (2016) 27:2242–50. doi: 10.1093/annonc/mdw416

3. Mathew M, Enzler T, Shu C, Rizvi N. Combining chemotherapy with PD-1 blockade in NSCLC. *Pharmacol Ther.* (2018) 186:130–7. doi: 10.1016/j.pharmthera.2018.01.003

4. Ribas A, Wolchok J. Cancer immunotherapy using checkpoint blockade. *Sci (New York N.Y.).* (2018) 359:1350–5. doi: 10.1126/science.aar4060

5. Ren D, Hua Y, Yu B, Ye X, He Z, Li C, et al. Predictive biomarkers and mechanisms underlying resistance to PD1/PD-L1 blockade cancer immunotherapy. *Mol Cancer.* (2020) 19:19. doi: 10.1186/s12943-020-1144-6

6. Passaro A, Brahmer J, Antonia S, Mok T, Peters S. Managing resistance to immune checkpoint inhibitors in lung cancer: treatment and novel strategies. *J Clin Oncol.* (2022) 40:598–610. doi: 10.1200/JCO.21.01845

7. Ma W, Gilligan B, Yuan J, Li T. Current status and perspectives in translational biomarker research for PD-1/PD-L1 immune checkpoint blockade therapy. *J Hematol Oncol.* (2016) 9:47. doi: 10.1186/s13045-016-0277-y

8. Topalian S, Taube J, Pardoll D. Neoadjuvant checkpoint blockade for cancer immunotherapy. *Sci (New York N.Y.).* (2020) 367:6477. doi: 10.1126/science.aax0182

9. Rolfo C, Russo A. In search of lost biomarker for immunotherapy in small-cell lung cancer. *Clin Cancer Res.* (2023) 30:652-4. doi: 10.1158/1078-0432.CCR-23-3087

10. Somasundaram A, Burns T. The next generation of immunotherapy: keeping lung cancer in check. *J Hematol Oncol.* (2017) 10:87. doi: 10.1186/s13045-017-0456-5

11. Wu T, Madireddi S, De Almeida P, Banchereau R, Chen Y, Chitre A, et al. Peripheral T cell expansion predicts tumour infiltration and clinical response. *Nature.* (2020) 579:274–8. doi: 10.1038/s41586-020-2056-8

12. Jiang R, Cai X, Yang Z, Yan Y, Zou X, Guo L, et al. Elevated peripheral blood lymphocyte-to-monocyte ratio predicts a favorable prognosis in the patients with metastatic nasopharyngeal carcinoma. *Chin J Cancer.* (2015) 34:237–46. doi: 10.1186/s40880-015-0025-7

13. Pernot S, Terme M, Radosevic-Robin N, Castan F, Badoual C, Marcheteau E, et al. Infiltrating and peripheral immune cell analysis in advanced gastric cancer according to the Lauren classification and its prognostic significance. *Gastric Cancer*. (2020) 23:73–81. doi: 10.1007/s10120-019-00983-3

14. Kamphorst A, Pillai R, Yang S, Nasti T, Akondy R, Wieland A, et al. Proliferation of PD-1+ CD8 T cells in peripheral blood after PD-1-targeted therapy in lung cancer patients. *Proc Natl Acad Sci United States America*. (2017) 114:4993–8. doi: 10.1073/pnas.1705327114

15. Xu X, Wang D, Chen W, Li N, Suwinski R, Rossi A, et al. A nomogram model based on peripheral blood lymphocyte subsets to assess the prognosis of non-small cell lung cancer patients treated with immune checkpoint inhibitors. *Trans Lung Cancer Res*. (2021) 10:4511–25. doi: 10.21037/tlcr

16. Lahiri A, Maji A, Potdar P, Singh N, Parikh P, Bisht B, et al. Lung cancer immunotherapy: progress, pitfalls, and promises. *Mol Cancer*. (2023) 22:40. doi: 10.1186/s12943-023-01740-y

17. West H, Mccleod M, Hussein M, Morabito A, Rittmeyer A, Conter H, et al. Atezolizumab in combination with carboplatin plus nab-paclitaxel chemotherapy compared with chemotherapy alone as first-line treatment for metastatic non-squamous non-small-cell lung cancer (IMpower130): a multicentre, randomised, open-label, phase 3 trial. *Lancet Oncol*. (2019) 20:924–37. doi: 10.1016/S1470-2045(19)30167-6

18. Limagne E, Nuttin L, Thibaudin M, Jacquin E, Aucagne R, Bon M, et al. MEK inhibition overcomes chemoimmunotherapy resistance by inducing CXCL10 in cancer cells. *Cancer Cell*. (2022) 40:136–152.e12. doi: 10.1016/j.ccell.2021.12.009

19. Chen G, Li X, Li R, Wu K, Lei Z, Dai R, et al. Chemotherapy-induced neoantigen nanovaccines enhance checkpoint blockade cancer immunotherapy. *ACS nano*. (2023) 17:18818–31. doi: 10.1021/acsnano.3c03274

20. Hodge J, Garnett C, Farsaci B, Palena C, Tsang K, Ferrone S, et al. Chemotherapy-induced immunogenic modulation of tumor cells enhances killing by cytotoxic T lymphocytes and is distinct from immunogenic cell death. *Int J Cancer*. (2013) 133:624–36. doi: 10.1002/ijc.28070

21. Lehrich B, Zhang J, Monga S, Dhanasekaran R. Battle of the Biopsies: Role of tissue and liquid biopsy in hepatocellular carcinoma. *J hepatology*. (2023) 80:515-30. doi: 10.1016/j.jhep.2023.11.030

22. Luo H, Wei W, Ye Z, Zheng J, Xu R. Liquid biopsy of methylation biomarkers in cell-free DNA. *Trends Mol Med*. (2021) 27:482–500. doi: 10.1016/j.molmed.2020.12.011

23. Luoma A, Suo S, Wang Y, Gunasti L, Porter C, Nabilsi N, et al. Tissue-resident memory and circulating T cells are early responders to pre-surgical cancer immunotherapy. *Cell*. (2022) 185:2918–2935.e29. doi: 10.1016/j.cell.2022.06.018

24. Spitzer M, Carmi Y, Reticker-Flynn N, Kwek S, Madhireddy D, Martins M, et al. Systemic immunity is required for effective cancer immunotherapy. *Cell*. (2017) 168:487–502.e15. doi: 10.1016/j.cell.2016.12.022

25. Hiam-Galvez K, Allen B, Spitzer M. Systemic immunity in cancer. *Nat Rev Cancer*. (2021) 21:345–59. doi: 10.1038/s41568-021-00347-z

26. Ma T, Wen T, Cheng X, Wang Y, Wei P, Yang B, et al. Pathological complete response to neoadjuvant chemoimmunotherapy correlates with peripheral blood immune cell subsets and metastatic status of mediastinal lymph nodes (N2 lymph nodes) in non-small cell lung cancer. *Lung Cancer (Amsterdam Netherlands)*. (2022) 172:43–52. doi: 10.1016/j.lungcan.2022.08.002

27. Speiser D, Chijioke O, Schaeuble K, Münz C. CD4 T cells in cancer. *Nat Cancer*. (2023) 4:317–29. doi: 10.1038/s43018-023-00521-2

28. Bruni D, Angell H, Galon J. The immune contexture and Immunoscore in cancer prognosis and therapeutic efficacy. *Nat Rev Cancer*. (2020) 20:662–80. doi: 10.1038/s41568-020-0285-7

29. Denkert C, Von Minckwitz G, Darb-Esfahani S, Lederer B, Heppner B, Weber K, et al. Tumour-infiltrating lymphocytes and prognosis in different subtypes of breast cancer: a pooled analysis of 3771 patients treated with neoadjuvant therapy. *Lancet Oncol*. (2018) 19:40–50. doi: 10.1016/S1470-2045(17)30904-X

30. Kagamu H, Kitano S, Yamaguchi O, Yoshimura K, Horimoto K, Kitazawa M, et al. CD4 T-cell immunity in the peripheral blood correlates with response to anti-PD-1 therapy. *Cancer Immunol Res*. (2020) 8:334–44. doi: 10.1158/2326-6066.CIR-19-0574

31. Templeton A, Mcnamara M, Šeruga B, Vera-Badillo F, Aneja P, Ocaña A, et al. Prognostic role of neutrophil-to-lymphocyte ratio in solid tumors: a systematic review and meta-analysis. *J Natl Cancer Institute*. (2014) 106:dju124. doi: 10.1093/jnci/dju124

32. Tivey A, Church M, Rothwell D, Dive C, Cook N. Circulating tumour DNA - looking beyond the blood. *Nat Rev Clin Oncol*. (2022) 19:600–12. doi: 10.1038/s41571-022-00660-y

33. Donaldson J, Park B. Circulating tumor DNA: measurement and clinical utility. *Annu Rev Med*. (2018) 69:223–34. doi: 10.1146/annurev-med-041316-085721

34. Miggelbrink A, Jackson J, Lorrey S, Srinivasan E, Waibl-Polania J, Wilkinson D, et al. CD4 T-cell exhaustion: does it exist and what are its roles in cancer? *Clin Cancer Res*. (2021) 27:5742–52. doi: 10.1158/1078-0432.CCR-21-0206

35. Chen Y, Li P, Pan N, Gao R, Wen Z, Zhang T, et al. Tumor-released autophagosomes induces CD4 T cell-mediated immunosuppression via a TLR2-IL-6 cascade. *J immunotherapy Cancer*. (2019) 7:178. doi: 10.1186/s40425-019-0646-5

36. Kagamu H, Yamasaki S, Kitano S, Yamaguchi O, Mouri A, Shiono A, et al. Single-cell analysis reveals a CD4+ T-cell cluster that correlates with PD-1 blockade efficacy. *Cancer Res*. (2022) 82:4641–53. doi: 10.1158/0008-5472.CAN-22-0112

frontiers | Frontiers in Immunology

TYPE Original Research
PUBLISHED 11 April 2024
DOI 10.3389/fimmu.2024.1364728

OPEN ACCESS

EDITED BY
Paulo Rodrigues-Santos,
University of Coimbra, Portugal

REVIEWED BY
Dongdong Huang,
The First Affiliated Hospital of Wenzhou Medical University, China
Jianchun Yu,
Peking Union Medical College Hospital (CAMS), China

*CORRESPONDENCE
Cheng Du
dc1115010@sina.com
Liang Zhang
juwimingz@126.com
Jian Ming
mjjgc7878@163.com

†These authors have contributed equally to this work

RECEIVED 02 January 2024
ACCEPTED 01 April 2024
PUBLISHED 11 April 2024

CITATION
Ji H, Liu B, Jin P, Li Y, Cui L, Jin S, Wu J, Shan Y, Zhang Z, Ming J, Zhang L and Du C (2024) Creatinine-to-cystatin C ratio and body composition predict response to PD-1 inhibitors-based combination treatment in metastatic gastric cancer. *Front. Immunol.* 15:1364728. doi: 10.3389/fimmu.2024.1364728

Creatinine-to-cystatin C ratio and body composition predict response to PD-1 inhibitors-based combination treatment in metastatic gastric cancer

Hongjuan Ji[1†], Bona Liu[1†], Peng Jin[2†], Yingchun Li[3], Lili Cui[1], Shanxiu Jin[4], Jingran Wu[4], Yongqi Shan[5], Zhenyong Zhang[6], Jian Ming[3*], Liang Zhang[7*] and Cheng Du[1*]

[1]Department of Oncology, General Hospital of Northern Theater Command, Shenyang, China, [2]Department of Oncology, The Second Affiliated Hospital of Shandong First Medical University, Taian, China, [3]Department of Pathology, General Hospital of Northern Theater Command, Shenyang, China, [4]Department of Oncology, General Hospital of Northern Theater Command, Dalian Medical University, Shenyang, China, [5]Department of General Surgery, General Hospital of Northern Theater Command, Shenyang, China, [6]Department Oncology, Shengjing Hospital of China Medical University, Shenyang, China, [7]Department of Gastrointestinal Surgery, Xuzhou Central Hospital, Xuzhou Clinical School of Xuzhou Medical College, Xuzhou, China

Background: Creatinine-to-cystatin C ratio (CCR) and body composition (BC) parameters have emerged as significant prognostic factors in cancer patients. However, the potential effects of CCR in gastric cancer (GC) remains to be elucidated. This multi-center retrospective study explored the predictive and prognostic value of CCR and BC-parameters in patients with metastatic GC receiving PD-1 inhibitors-based combination therapy.

Methods: One hundred and thirteen GC patients undergoing PD-1 inhibitors-based combination therapy were enrolled at three academic medical centers from January 2021 to July 2023. A deep-learning platform based on U-Net was developed to automatically segment skeletal muscle index (SMI), subcutaneous adipose tissue index (SATI) and visceral adipose tissue index (VATI). Patients were divided into two groups based on the median of CCR or the upper tertile of BC-parameters. Logistic and Cox regression analysis were used to determine the effect of CCR and BC-parameters in predicting response rates and survival rates.

Results: The CCR was positively correlated with SMI (r=0.43; P<0.001), but not with SATI or VATI (P>0.05). Multivariable logistic analysis identified that both low CCR (OR=0.423, P=0.066 for ORR; OR=0.026, P=0.005 for DCR) and low SATI (OR=0.270, P=0.020 for ORR; OR=0.149, P=0.056 for DCR) were independently associated with worse objective response rate (ORR) and disease control rate (DCR). Patients with low CCR or low SATI had significantly lower 8-month progression-free survival (PFS) rate and 16-month overall survival (OS) rate than those with high CCR (PFS rate, 37.6% vs. 55.1%, P=0.011; OS rate, 19.4% vs. 44.9%, P=0.002) or those with high SATI (PFS rate, 37.2% vs. 53.8%, P=0.035; OS rate, 8.0% vs. 36.0%, P<0.001). Multivariate Cox analysis showed that low CCR (HR=2.395, 95% CI: 1.234-4.648, P=0.010 for PFS rate; HR=2.528, 95% CI: 1.317-4.854, P=0.005 for OS rate) and low SATI (HR=2.188, 95% CI: 1.050-4.560,

P=0.037 for PFS rate; HR=2.818, 95% CI: 1.381-5.752, P=0.004 for OS rate) were both independent prognostic factors of poor 8-month PFS rate and 16-month OS rate. A nomogram based on CCR and BC-parameters showed a good performance in predicting the 12- and 16-month OS, with a concordance index of 0.756 (95% CI, 0.722-0.789).

Conclusions: Low pre-treatment CCR and SATI were independently associated with lower response rates and worse survival in patients with metastatic GC receiving PD-1 inhibitors-based combination therapy.

KEYWORDS

creatinine-to-cystatin C ratio, body composition, subcutaneous adipose tissue index, sarcopenia, programmed cell death 1, gastric cancer

1 Introduction

Gastric cancer (GC) is among the most common cancer which lead to cancer-related mortality (1). A significant portion of patients receives a diagnosis at an advanced and inoperable stage. The introduction of immune checkpoint inhibitors (ICIs) has substantially improved the survival rates of patients with metastatic GC. Nevertheless, the response to PD-1 monotherapy is limited to a small subset of patients, potentially due to the heterogeneous nature of GC. Even with combinatorial therapy, the objective response rate remains constrained at 50-60% (2, 3). Therefore, it is crucial to identify novel factors influencing or predicting the efficacy and prognosis of PD-1 inhibitors in GC patients.

Serum creatinine and Cystatin C serve as biochemical markers for estimating the glomerular filtration rate (eGFR) and renal function in clinical practice. Creatinine, primarily originating from muscle metabolism, exhibits lower blood levels in cancer patients with reduced muscle mass, particularly in those with sarcopenia or cachexia (4). Cystatin C, a low molecular weight protein, is uniformly secreted by all nucleated cells with consistent productivity, unaffected by muscular metabolic processes (5). Leveraging the characteristics of creatinine and Cystatin C, the creatinine-to-cystatin C ratio (CCR) was initially proposed by Kashani et al. as a simplified method for diagnosing sarcopenia in patients (6). Since then, CCR has been extensively studied and established as a biomarker for the prognosis in patients with critically illness (7, 8), hypertension (9), type 2 diabetes (10, 11) and cancer (12–17). Recently, a retrospective study reported that low CCR was an independent biomarker of poor prognosis in non-small cell lung cancer (NSCLC) patients treated with PD-1 monotherapy (18). However, the potential role of CCR in predicting the treatment efficacy of ICIs combination therapy and prognosis in GC patients remains to be investigated.

The most important parameters of body composition (BC) are skeletal muscle index (SMI), subcutaneous adipose tissue index (SATI) and visceral adipose tissue index (VATI). These indices have undergone extensive study in past decades to elucidate their prognostic values in various cancer types (19–21). Sarcopenia, defined as a decline in both muscle mass and function, has long been established as a prognostic risk factor in cancer patients treated with ICIs (22, 23). In contrast to sarcopenia, studies evaluating the prognostic value of subcutaneous or visceral adipose tissue in cancer patients are still controversial (24), with the prognostic value reported as protective, detrimental or no effect. It may be due to the differences in disease contexts or treatment regimens. Notably, the potential impact of subcutaneous or visceral adipose tissue on treatment efficacy and prognosis in patients with metastatic GC receiving PD-1 inhibitors-based combination therapy remains unknown.

In this study, we aimed to explore whether the CCR and BC-parameters are associated with efficacy and prognosis in patients with metastatic GC receiving PD-1 inhibitors-based combination therapy.

2 Materials and method

2.1 Patient selection

In this study, we retrospectively enrolled 113 metastatic GC patients treated with PD-1 inhibitors-based combination therapy at three academic medical centers from January 2021 to July 2023. Inclusion criteria consisted of (a) age ≥ 18 years, (b) pathologically confirmed GC, (c) treated with at least one dose of PD-1 based combinatorial regimen. The exclusion criteria were as follows: (a) receiving PD-1 monotherapy or PD-L1 therapy, (b) high microsatellite instability (MSI-H) phenotype, (c) renal function impairment (eGFR<60ml/min/1.73m^2).

2.2 Clinical data collection

The following clinical variables, including age, gender, ECOG Performance Status (PS), height, weight, number of previous

therapies, presence or absence of ascites, degree of differentiation, number of organs with metastases, PD-L1 status, treatment regimen, creatinine (mg/dL), cystatin C (mg/L), platelet absolute ($P\times10^9$/L), neutrophil absolute ($N\times10^9$/L), and lymphocyte absolute ($L\times10^9$/L) were extracted from electronic medical records. PD-L1 positive was defined as a combined positive score (CPS) of ≥1 or a tumor proportion score (TPS) of ≥1%. All biochemical and routine blood parameters were measured in accredited laboratories. The relevant indicators were calculated as: CCR=creatinine/cystatin C×100; SII=P×N/L. CCR and SII were considered binary variables and dichotomized based on the median values.

2.3 Assessment of CT-based BC-parameters

We developed a deep-learning model based on U-Net to automatically segment CT images of SAT, VAT, and skeletal muscle at the third lumbar vertebra (L3) level. The model is available at https://body-compositions-assessment-tool.streamlit.app/. The performance of the model is summarized in Supplementary Materials (Supplementary Table 1; Supplementary Figure 1). According to the criteria commonly referenced in Asian cancer patients, sarcopenia was defined as SMI ≤40.8 cm^2/m^2 in men and ≤34.9 cm^2/m^2 in women (25). Additionally, we conducted calculations using X-tile analysis to determine the cut-off points of body composition parameters. The upper tertile of all indicators could clearly stratify the survival outcome. Therefore, based on both the reproducibility of the study and previous reports (26), we chose the upper tertile to classify the SATI, VATI and SMI.

2.4 Follow-up

The primary endpoints were 8-month PFS rate and 16-month OS rate, and the secondary endpoints were ORR and DCR. The assessment of treatment response was conducted according to the RECIST V.1.1 criteria (27). Objective response rate (ORR) and disease control rate (DCR) were defined as the proportion of patients who achieved a complete (CR) or partial response (PR) and CR, PR or stable disease (SD), respectively. Progression-free survival (PFS) rate at 8 months was calculated from PD-1 treatment initiation to death or progression disease (PD) with maximal follow-up of 8 months. Overall survival (OS) rate at 16 months was calculated from PD-1 treatment initiation to death or last follow-up with maximal follow-up of 16 months.

2.5 Statistical analysis

Statistical analysis was performed using SPSS 26.0. All continuous variables were reported as median and interquartile range (IQR), and categorical variables were reported as frequency and percentage. Multiple imputation (MI) was used to account for missing data on PD-L1 status and differentiation grade. Spearman correlation coefficient was performed to determine the association between CCR and BC-parameters. Univariable and multivariable logistic regression analysis were used to explore the factors influencing efficacy. The efficacy of predicting treatment response was compared by drawing receiver operating characteristic (ROC) curves, and the area under the ROC curves (AUCs) was compared using the Delong test. The variance inflation factor (VIF) method was used to select covariates with a maximum threshold of 5 to control for multicollinearity. Cox regression models were established to identify independent factors associated with PFS/OS. Kaplan-Meier analysis and log-rank test were utilized to compare the survival rates between groups. A prognostic nomogram was established to predict 12- and 16-month OS. The discriminant ability and predictive accuracy were evaluated by the Concordance index (C-index) and decision curve analysis (DCA). All tests were two-sided, and p values <0.05 were considered statistically significant.

3 Results

3.1 Baseline characteristics of patients

A total of 113 patients were included in the study. The median age was 63 years (IQR: 57-69) and 96 (85.0%) of the patients were male. Overall, 99 (87.6%) patients exhibited good performance status (ECOG PS 0-1) and 47 (41.6%) had a low degree of differentiation. 89 (78.8%) patients received PD-1 combined with chemotherapy and 94 (83.2%) patients were treated for the first line. Some missing data were observed in our study cohort. To enhance statistical power and decrease bias due to missing data, we used multiple-imputation to deal with missing data on PD-L1 status and differentiation grade. We also performed sensitivity analyses using a complete-case analysis for comparison. The results were still statistically significant. (Supplementary Table 2). Other detailed clinicopathological characteristics of the patients were depicted in Table 1. Representative images for U-Net-based segmentation were shown in Figure 1.

3.2 Association between CCR and BC-parameters

The CCR was positively correlated with SMA (r=0.49; P<0.001) and SMI (r=0.43; P<0.001), but not with SATI (r=-0.04; P>0.05) or VATI (r=0.15; P>0.05). No significant association between SII and BC-parameters was observed (Figure 2).

3.3 Assessment of treatment response

As shown in Table 2, low CCR and low SATI were significantly associated with worse ORR. Low CCR, low SATI, low SMI, sarcopenia, two or more lines of therapy and presence of ascites

10.3389/fimmu.2024.1364728

TABLE 1 Patient characteristics.

Variables	No. of patients (n=113)
Age, median (IQR), years	63.0 (57.0-69.0)
Sex, n (%)	
Male	96 (85.0)
Female	17 (15.0)
BMI, n (%)	
<18.5	18 (15.9)
18.5-23.9	65 (57.5)
>23.9	30 (26.5)
ECOG PS, n (%)	
0	22 (19.5)
1	77 (68.1)
≥ 2	14 (12.4)
No. of previous therapies, n (%)	
0	94 (83.2)
1	14 (12.4)
2 or more	5 (4.4)
No. of metastatic organs, n (%)	
1	52 (46.0)
2	52 (46.0)
3 or more	9 (8.0)
Ascites, n (%)	
Present	61 (54.0)
Absent	52 (46.0)
PD-L1 status, n (%)	
Positive	38 (33.6)
Negative	33 (29.2)
Unknown	42 (37.2)
Differentiation grade, n (%)	
Low	47 (41.6)
Other	25 (22.1)
Unknown	41 (36.3)
Treatments, n (%)	
Anti-PD-1+ Chemotherapy	89 (78.8)
Anti-PD-1+ Targeted therapy	15 (13.3)
Anti-PD-1+ Chemotherapy+ Targeted therapy	9 (8.0)
CCR, median (IQR)	71.48 (62.80-80.38)
SII, median (IQR)	596.08 (373.41-1073.32)
Body composition parameters, median (IQR)	
SATI	31.44 (17.59-42.28)
VATI	24.37 (11.95-35.08)
SMI	34.45 (27.30-40.34)

BMI, body mass index; ECOG PS, Eastern Cooperative Oncology Group performance status; PD-L1, programmed cell death-ligand 1; PD-1, programmed cell death 1; CCR, creatinine-to-cystatin C ratio; SII, systemic immune-inflammation index; SATI, subcutaneous adipose tissue index; VATI, visceral adipose tissue index; SMI, skeletal muscle index.

were highly linked to worse DCR. The results of multivariable logistic regression analysis showed that low SATI (OR=0.270, 95% CI: 0.090-0.814, P=0.020) was an independent risk factor for ORR, while low CCR (OR=0.423, 95% CI: 0.169-1.059, P=0.066) tend to be independently associated with ORR. Low CCR (OR=0.026, 95% CI: 0.002-0.335, P=0.005), two or more lines of therapy (OR=0.015, 95% CI: 0.001-0.190, P=0.001) and presence of ascites (OR=0.023, 95% CI: 0.002-0.299, P=0.004) were independent risk factors for DCR, while low SATI (OR=0.149, 95% CI: 0.021-1.051, P=0.056) tended to be significant (Table 3). Furthermore, ROC curves were calculated to compare the performance of different variables in predicting treatment response. The AUCs of the CCR, SMI and SATI were 0.616 (95% CI: 0.497-0.735), 0.570 (95% CI: 0.439-0.702) and 0.594 (95% CI: 0.473-0.715) for ORR and 0.787 (95% CI: 0.694-0.881), 0.773 (95% CI: 0.666-0.880) and 0.606 (95% CI: 0.460-0.752) for DCR, respectively (Figure 3). The AUC of CCR (0.787) was significantly higher than that of SATI (0.606) (Delong test: P=0.043) in predicting DCR. The differences between AUCs of other groups were not statistically significant in predicting of ORR or DCR. The predictive accuracy of the CCR, SMI and SATI for ORR/DCR were shown in Table 4. Therefore, it is believed that the CCR seems to be superior to other indexes in predicting treatment efficacy.

3.4 Progression-free survival

Univariate Cox regression analysis showed that low CCR, low SATI, low VATI, sarcopenia, high ECOG PS, two or more lines of therapy and presence of ascites were significantly associated with poor 8-month PFS rate. On multivariate analysis, low CCR (HR=2.395, 95% CI: 1.234-4.648, P=0.010), low SATI (HR=2.188, 95% CI: 1.050-4.560, P=0.037), two or more lines of therapy (HR=4.513, 95% CI: 2.073-9.826, P<0.001) and high ECOG PS (≥2) (HR=2.365, 95% CI: 1.089-5.138, P=0.030) remained independent prognostic factors for inferior 8-month PFS rate (Table 5). The Kaplan-Meier analysis highlighted those patients with low CCR had a significantly decreased 8-month PFS rate compared to those with high CCR (37.6% vs. 55.1%, P=0.011). Similar results were observed in patients with low SATI and low VATI compared to those with high SATI (37.2% vs. 53.8%, P=0.035) and high VATI (30.5% vs. 56.8%, P=0.014), respectively (Figure 4).

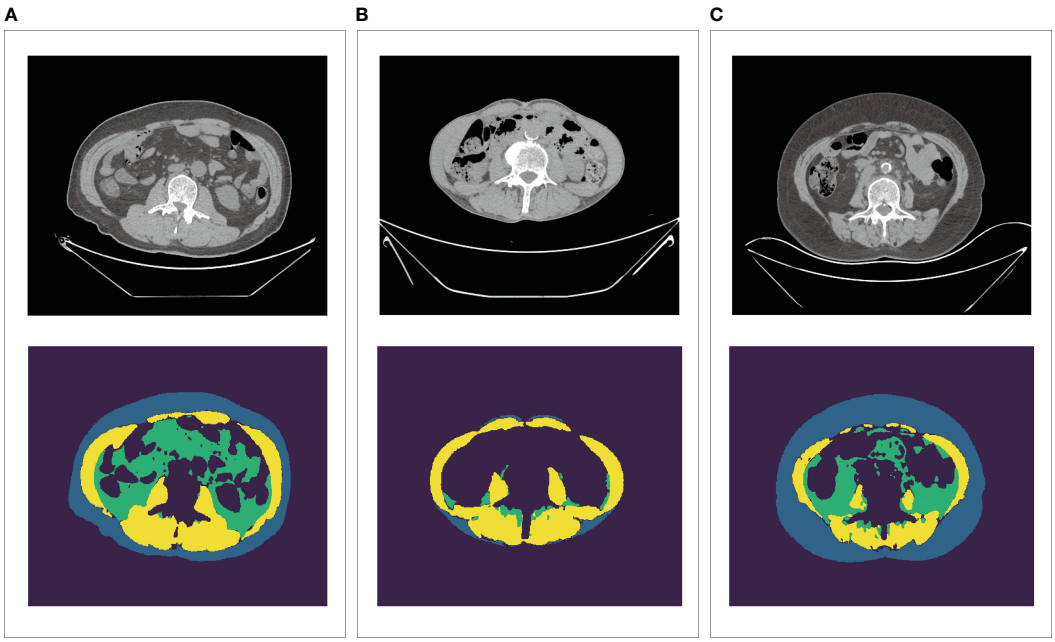

FIGURE 1
U-Net-based segmentation of body composition using CT images. Yellow=SMA, Blue=SATA, Green=VATA. **(A)** Representative of patients with high SMA and TATA. **(B)** Representative of patients with high SMA and low TATA. **(C)** Representative of patients with low SMA and high TATA. SMA, skeletal muscle area; SATA, subcutaneous adipose tissue area; VATA, visceral adipose tissue area, TATA, total adipose tissue area.

3.5 Overall survival

Univariate Cox regression analysis showed that low CCR, low SATI, low VATI, low SMI, sarcopenia, high ECOG PS, two or more lines of therapy and presence of ascites were significantly associated with poor 16-month OS rate. On multivariate analysis, low CCR (HR=2.528, 95% CI: 1.317-4.854, P=0.005), low SATI (HR=2.818, 95% CI: 1.381-5.752, P=0.004), two or more lines of therapy (HR=3.008, 95% CI: 1.417-6.387, P=0.004) and high ECOG PS (≥2) (HR=3.231, 95% CI: 1.512-6.905, P=0.002) remained independent prognostic factors for inferior 16-month OS rate (Table 6). When adjusting for CCR, SMI or sarcopenia alone,

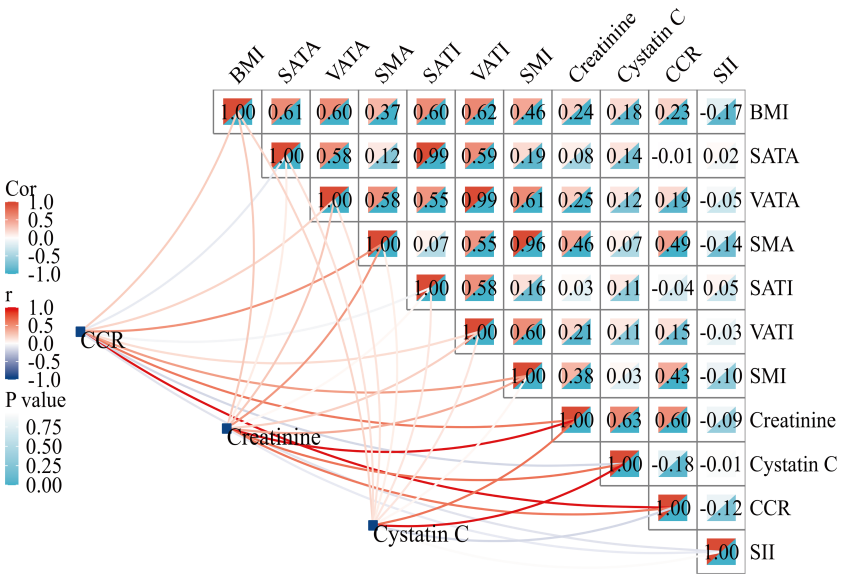

FIGURE 2
Correlation matrix between CCR and body composition parameters. BMI, body mass index; SATA, subcutaneous adipose tissue area; VATA, visceral adipose tissue area; SMA, skeletal muscle area; SATI, subcutaneous adipose tissue index; VATI, visceral adipose tissue index; SMI, skeletal muscle index; CCR, creatinine-to-cystatin C ratio; SII, systemic immune-inflammation index.

TABLE 2 Univariable logistic regression analysis for ORR and DCR.

Variables	Objective response rate			Disease control rate		
	OR	95%CI	P	OR	95%CI	P
Age	1.014	0.978 to 1.052	0.454	1.018	0.976 to 1.062	0.408
Sex						
Male/female	0.970	0.322 to 2.919	0.956	2.182	0.661 to 7.205	0.201
ECOG PS						
≥2/0-1	0.471	0.121 to 1.833	0.278	0.486	0.133 to 1.778	0.276
No. of previous therapies						
≥1/0	0.552	0.182 to 1.677	0.294	0.122	0.040 to 0.372	**<0.001**
No. of metastatic organs						
≥2/1	1.179	0.525 to 2.643	0.690	0.607	0.220 to 1.676	0.336
Ascites						
Present/absent	0.463	0.205 to 1.048	0.065	0.135	0.037 to 0.497	**0.003**
PD-L1 status						
Positive/negative	1.435	0.528 to 3.901	0.479	1.115	0.290 to 4.293	0.874
Differentiation grade						
Low/other	0.400	0.144 to 1.109	0.078	1.094	0.315 to 3.799	0.888
CCR						
≤71.48/>71.48	0.347	0.151 to 0.798	**0.013**	0.077	0.017 to 0.354	**0.001**
SII						
≤596.08/>596.08	0.821	0.368 to 1.829	0.629	1.692	0.627 to 4.568	0.299
SATI						
≤22.90/>22.90	0.269	0.091 to 0.798	**0.018**	0.346	0.123 to 0.977	**0.045**
VATI						
≤15.33/>15.33	0.560	0.215 to 1.459	0.235	0.371	0.132 to 1.042	0.060
SMI						
≤30.77/>30.77	0.952	0.378 to 2.401	0.918	0.261	0.091 to 0.746	**0.012**
CT-determined sarcopenia						
Yes/no	0.639	0.244 to 1.672	0.362	0.118	0.015 to 0.941	**0.044**

Bold values indicate statistical significance at the $p < 0.05$ level.
ECOG PS, Eastern Cooperative Oncology Group performance status; PD-L1, programmed cell death-ligand 1; CCR, creatinine-to-cystatin C ratio; SII, systemic immune-inflammation index; SATI, subcutaneous adipose tissue index; VATI, visceral adipose tissue index; SMI, skeletal muscle index.

both CCR and SMI, but not sarcopenia were independent prognostic factors (Supplementary Table 3). The Kaplan-Meier analysis highlighted those patients with low CCR had a significantly decreased 16-month OS rate compared to those with high CCR (19.4% vs. 44.9%, P=0.002). Similar results were observed in patients with low SATI, low VATI and low SMI compared to those with high SATI (8.0% vs. 36.0%, P<0.001), high VATI (12.7% vs. 36.6%, P=0.009) and high SMI (18.7% vs. 33.5%, P=0.029), respectively (Figure 5).

3.6 Construction of the nomogram

To evaluate the prognosis of GC comprehensively, we established a nomogram including ECOG PS, number of previous therapies, presence of ascites, CCR, SATI and VATI (Figure 6). Nomogram C-index was 0.756 (95% CI, 0.722-0.789), indicating an outstanding performance. In addition, DCA curves suggested that the combined model had a more significant predictive accuracy than the single model (Figure 7).

10.3389/fimmu.2024.1364728

TABLE 3 Multivariable logistic regression analysis for ORR and DCR.

Variables	Objective response rate			Disease control rate		
	OR	95%CI	P	OR	95%CI	P
No. of previous therapies						
≥1/0	–			0.015	0.001 to 0.190	**0.001**
Ascites						
Present/absent	–			0.023	0.002 to 0.299	**0.004**
CCR						
≤71.48/>71.48	0.423	0.169 to 1.059	0.066	0.026	0.002 to 0.335	**0.005**
SATI						
≤22.90/>22.90	0.270	0.090 to 0.814	**0.020**	0.149	0.021 to 1.051	0.056
SMI						
≤30.77/>30.77	–			0.356	0.045 to 2.824	0.328
CT-determined sarcopenia						
Yes/no	–			0.535	0.029 to 9.954	0.675

Bold values indicate statistical significance at the $p < 0.05$ level.
CCR, creatinine-to-cystatin C ratio; SATI, subcutaneous adipose tissue index; SMI, skeletal muscle index.

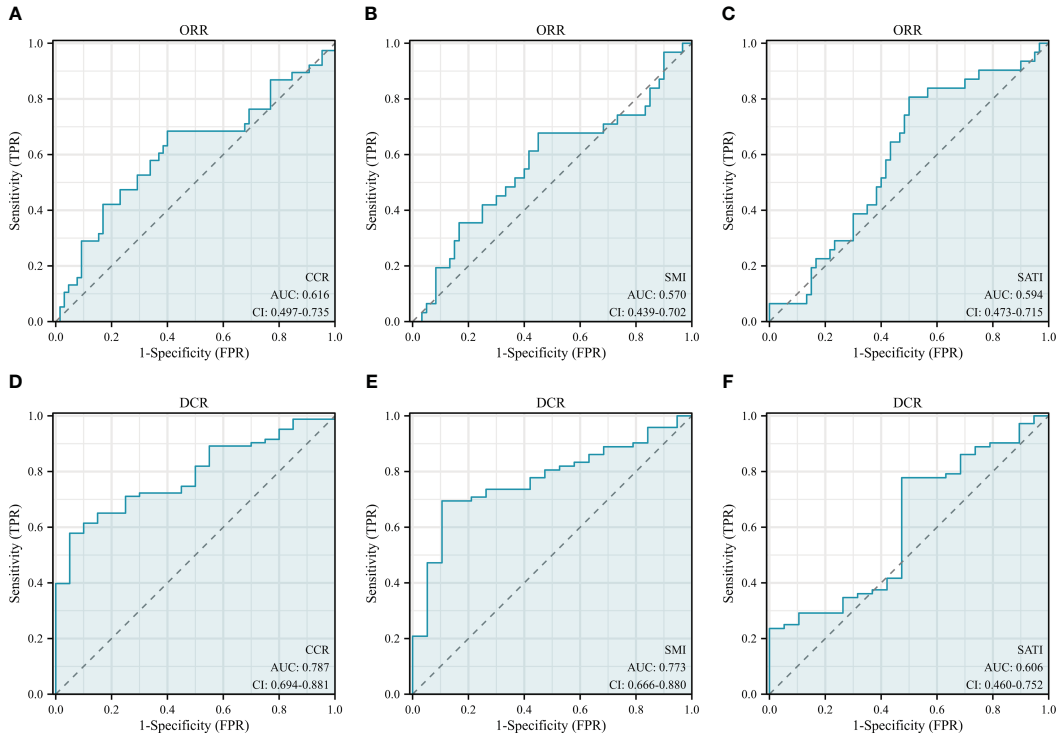

FIGURE 3
ROC curves of the **(A, D)** CCR, **(B, E)** SMI and **(C, F)** SATI for predicting treatment response. CCR, creatinine-to-cystatin C ratio; SMI, skeletal muscle index; SATI, subcutaneous adipose tissue index; ORR, objective response rate; DCR, disease control rate.

TABLE 4 Predictive accuracy of CCR, SMI and SATI for ORR/DCR.

	Objective response rate			Disease control rate		
	CCR	SMI	SATI	CCR	SMI	SATI
Sensitivity, %	68.4	67.7	80.6	57.8	69.4	77.8
Specificity, %	60.0	55.0	50.0	95.0	89.5	52.6
Accuracy, %	63.1	59.3	60.4	65.0	73.6	72.5
Positive predictive value, %	50.0	43.8	45.5	98.0	96.2	86.2
Negative predictive value, %	76.5	76.7	83.3	35.2	43.6	38.5

CCR, creatinine-to-cystatin C ratio; SMI, skeletal muscle index; SATI, subcutaneous adipose tissue index.

TABLE 5 Univariable and Multivariable Cox regression for 8-month PFS rate.

Variables	Univariable			Multivariable		
	HR	95%CI	P	HR	95%CI	P
Age	0.988	0.961 to 1.016	0.412			
Sex						
Male/female	0.806	0.392 to 1.658	0.559			
ECOG PS						
≥2/0-1	3.361	1.771 to 6.380	**<0.001**	2.365	1.089 to 5.138	**0.030**
No. of previous therapies						
≥1/0	2.849	1.555 to 5.218	**0.001**	4.513	2.073 to 9.826	**<0.001**
No. of metastatic organs						
≥2/1	1.233	0.706 to 2.155	0.461			
Ascites						
Present/absent	1.826	1.027 to 3.244	**0.040**	1.699	0.894 to 3.230	0.106
PD-L1 status						
Positive/negative	0.999	0.475 to 2.103	0.998			
Differentiation grade						
Low/other	1.008	0.489 to 2.080	0.982			
CCR						
≤71.48/>71.48	2.058	1.166 to 3.632	**0.013**	2.395	1.234 to 4.648	**0.010**
SII						
≤596.08/>596.08	0.668	0.382 to 1.167	0.156			
SATI						
≤22.90/>22.90	1.882	1.034 to 3.423	**0.038**	2.188	1.050 to 4.560	**0.037**
VATI						
≤15.33/>15.33	2.085	1.145 to 3.795	**0.016**	1.145	0.533 to 2.457	0.729
SMI						
≤30.77/>30.77	1.610	0.882 to 2.940	0.121			
CT-determined sarcopenia						
Yes/no	2.617	1.105 to 6.197	**0.029**	1.070	0.388 to 2.946	0.896

Bold values indicate statistical significance at the $p < 0.05$ level.
ECOG PS, Eastern Cooperative Oncology Group performance status; PD-L1, programmed death-ligand; CCR, creatinine-to-cystatin C ratio; SII, systemic immune-inflammation index; SATI, subcutaneous adipose tissue index; VATI, visceral adipose tissue index; SMI, skeletal muscle index.

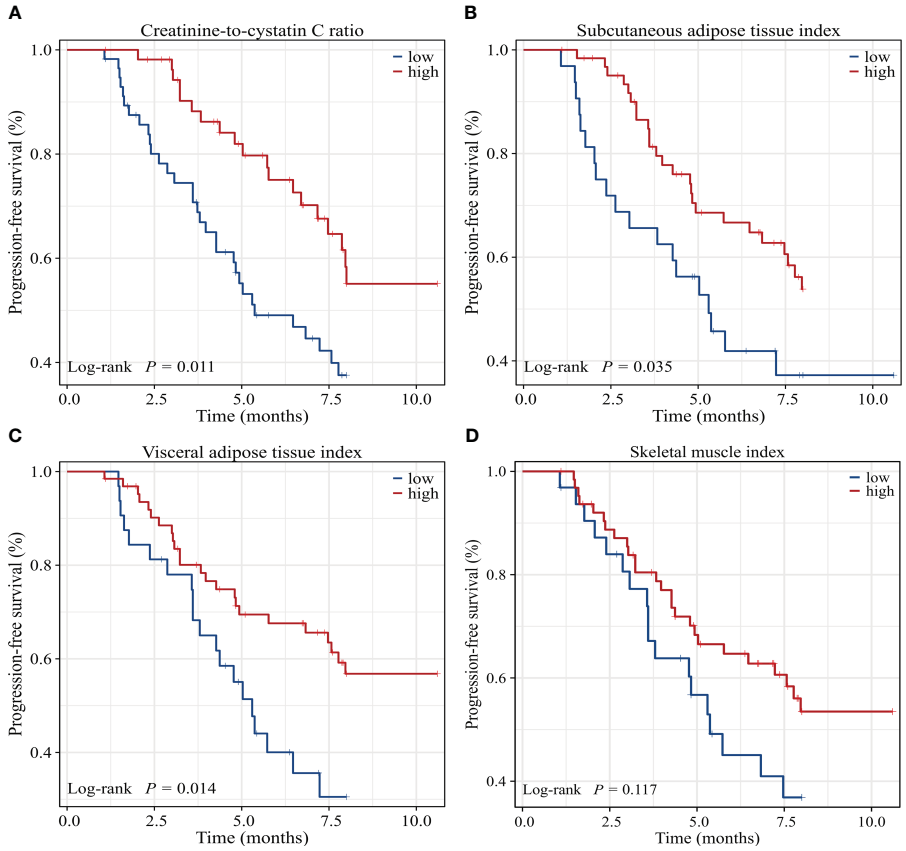

FIGURE 4
Kaplan-Meier survival curves of 8-month progression-free survival rate for GC patients dichotomized with **(A)** CCR, **(B)** SATI, **(C)** VATI and **(D)** SMI. CCR, creatinine-to-cystatin C ratio; SATI, subcutaneous adipose tissue index; VATI, visceral adipose tissue index; SMI, skeletal muscle index.

TABLE 6 Univariable and Multivariable Cox regression for 16-month OS rate.

Variables	Univariable			Multivariable		
	HR	95%CI	P	HR	95%CI	P
Age	0.985	0.961 to 1.009	0.217			
Sex						
Male/female	0.704	0.380 to 1.304	0.264			
ECOG PS						
≥2/0-1	3.282	1.724 to 6.248	**<0.001**	3.231	1.512 to 6.905	**0.002**
No. of previous therapies						
≥1/0	1.942	1.046 to 3.607	**0.036**	3.008	1.417 to 6.387	**0.004**
No. of metastatic organs						
≥2/1	0.865	0.512 to 1.464	0.589			
Ascites						
Present/absent	1.911	1.142 to 3.198	**0.014**	1.533	0.836 to 2.809	0.167
PD-L1 status						
Positive/negative	0.679	0.334 to 1.378	0.284			

(Continued)

TABLE 6 Continued

Variables	Univariable			Multivariable		
	HR	95%CI	P	HR	95%CI	P
Differentiation grade						
Low/other	1.560	0.756 to 3.219	0.229			
CCR						
≤71.48/>71.48	2.375	1.363 to 4.136	**0.002**	2.528	1.317 to 4.854	**0.005**
SII						
≤596.08/>596.08	0.666	0.397 to 1.118	0.124			
SATI						
≤22.90/>22.90	2.765	1.537 to 4.976	**0.001**	2.818	1.381 to 5.752	**0.004**
VATI						
≤15.33/>15.33	2.041	1.178 to 3.536	**0.011**	1.177	0.596 to 2.322	0.639
SMI						
≤30.77/>30.77	1.825	1.055 to 3.157	**0.031**	1.395	0.657 to 1.964	0.387
CT-determined sarcopenia						
Yes/no	2.158	1.107 to 4.206	**0.024**	0.915	0.382 to 2.192	0.843

Bold values indicate statistical significance at the $p < 0.05$ level.
ECOG PS, Eastern Cooperative Oncology Group performance status; PD-L1, programmed death-ligand 1; CCR, creatinine-to-cystatin C ratio; SII, systemic immune-inflammation index; SATI, subcutaneous adipose tissue index; VATI, visceral adipose tissue index; SMI, skeletal muscle index.

4 Discussion

Our retrospective multi-institutional analysis revealed significant predictive and prognostic value in pre-treatment CCR and SATI for patients with GC undergoing PD-1-based combination therapy. In brief, patients with lower CCR and SATI exhibited inferior response rates and lower survival rates. Furthermore, we successfully developed and validated a nomogram based on CCR and BC-parameters to predict survival in GC patients.

Recent evidence suggests that CCR serves as a promising indicator for predicting the prognosis of various cancers (28, 29). Zheng et al. demonstrated the utility of CCR as a prognostic factor for post-esophagectomy complications and long-term survival in esophageal cancer patients (14). Ding and colleagues independently found that CCR predicts recurrence-free survival in gastrointestinal stromal tumor patients (15). A retrospective study involving 3,060 patients showed a strong association between CCR at diagnosis and both 6- and 12-month survival (30). Despite the growing interest in CCR analysis in cancer patients, limited research has been conducted in the burgeoning field of cancer immunotherapy. A recent study highlighted the significant prognostic value of pre-treatment CCR in NSCLC patients undergoing PD-1 inhibitor monotherapy (18). In line with the previous studies, our findings indicated that a lower CCR was independently associated with lower survival rates. The novelty of our findings was that we demonstrated a potential link between CCR and ORR/DCR in patients with GC receiving PD-1 based combination therapy.

There are several possible mechanisms, which remain to be proved, to explain the effect of CCR on the efficacy and prognosis in GC patients. Firstly, CCR partially reflects muscle mass or SMI, which is a well-known risk factor for the efficacy and prognosis of GC patients treated with immunotherapy (31, 32). In addition, CCR may also be a marker of systemic inflammation. Previous studies reported that serum creatinine levels were low in patients with high white blood cell counts (33), while the levels of cystatin C were elevated in chronic inflammatory conditions (34). Consequently, low CCR may be associated with increased inflammation burden, which was reported to be poor prognostic factor in cancer patients (35). Finally, some researchers reported that cystatin C might be involved in cancer progression by antagonizing the suppressive functions of transforming growth factor β (TGF-β) (36). Therefore, CCR may be a promising predictive and prognostic biomarker in GC patients treated with ICIs.

Several studies have explored the impact of sarcopenia on outcomes in various cancers (37). A recent meta-analysis of 2501 patients from 26 trials concluded that sarcopenia predicts response rates and survival outcomes in solid cancers treated with ICIs (38). Kim et al. indicated that sarcopenia to be a standalone prognostic marker for PFS but not for OS in microsatellite-stable GC patients receiving immune monotherapy (31). Our results suggested that sarcopenia was not a significant predictor for survival rates on multivariate analysis. These inconsistencies might stem from variations in cut-off values of sarcopenia or differences in treatment regimen across studies.

VAT and SAT reflect both the nutritional and inflammatory status of cancer patients. Subcutaneous and visceral adiposity have different structures and functions and play different roles in immune and metabolic regulation. VAT secretes pro-

10.3389/fimmu.2024.1364728

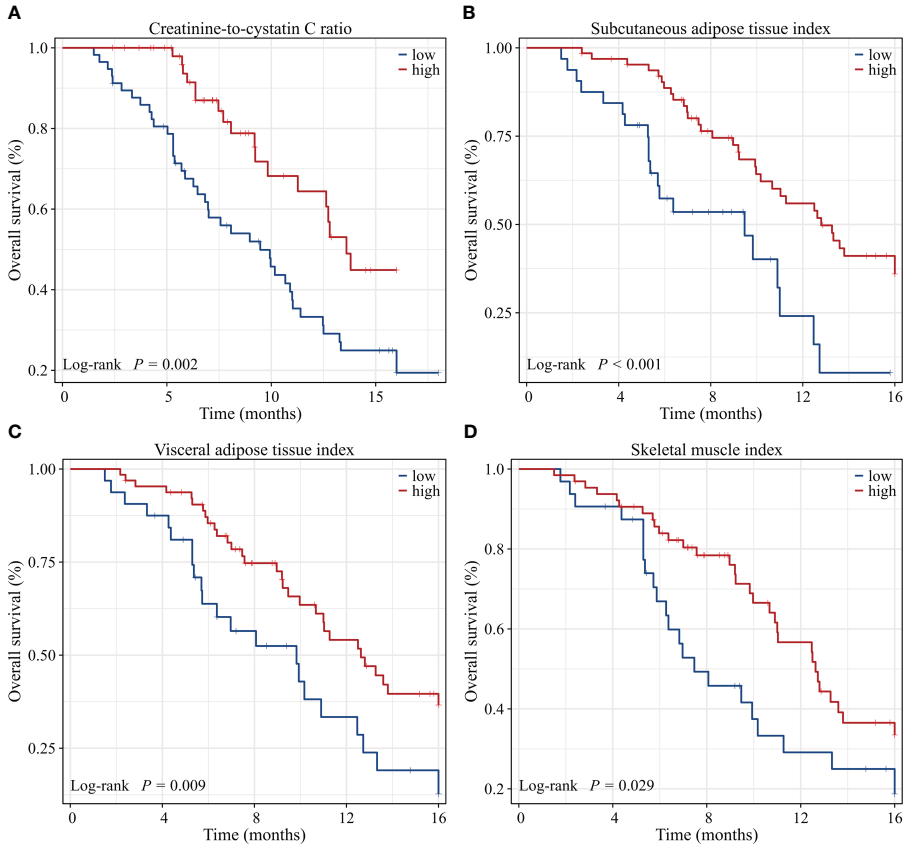

FIGURE 5
Kaplan-Meier survival curves of 16-month overall survival rate for GC patients dichotomized with **(A)** CCR, **(B)** SATI, **(C)** VATI and **(D)** SMI. CCR, creatinine-to-cystatin C ratio; SATI, subcutaneous adipose tissue index; VATI, visceral adipose tissue index; SMI, skeletal muscle index.

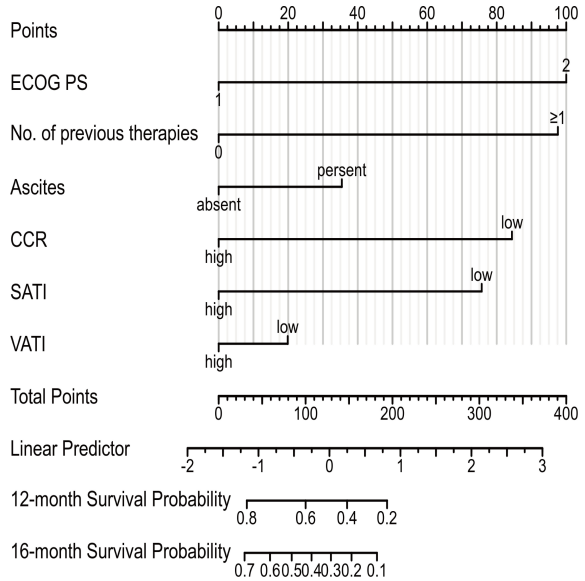

FIGURE 6
Prognostic nomogram to estimate their probability of survival at 12- and 16-month in patients with GC. ECOG PS, Eastern Cooperative Oncology Group performance status; CCR, creatinine-to-cystatin C ratio; SATI, subcutaneous adipose tissue index; VATI, visceral adipose tissue index.

inflammatory factors that contribute to systemic inflammation and metabolic disturbances (39). On the contrary, the leptin secreted by SAT can increase insulin sensitivity and lipid metabolism and exert beneficial effects on metabolism and anti-inflammatory (40). Several studies focusing on cancer patients have suggested a relationship between VAT or SAT and survival, although sometimes results are conflicting (41–44). He et al. reported that SATI but not VATI was significantly associated with OS in GC patients undergoing dual PD-1 and HER2 blockade (45). Our results demonstrated that low SATI was associated with lower response rates and survival rates, which aligned partially with their findings. Martini et al. found that high VATI was highly linked to improved PFS and showed a trend toward longer OS in urothelial carcinoma patients treated with ICIs (42). In contrast, Ke and colleagues argued that low VATI was linked to preferable prognosis in invasive bladder cancer patients receiving immunotherapy (46). Moreover, several studies demonstrated that high VATI was linked to increased incidence rates of post-operative complications in GC patients (47–49). Our study suggested that low VATI acted as a risk factor in univariate analysis, while it failed to serve an independent negative prognostic factor for survival in multivariate analysis in GC patients receiving PD-1 inhibitors-based combination therapy. The inconsistent effects of VATI on cancer treatment efficacy and survival may be explained by the differences in disease context,

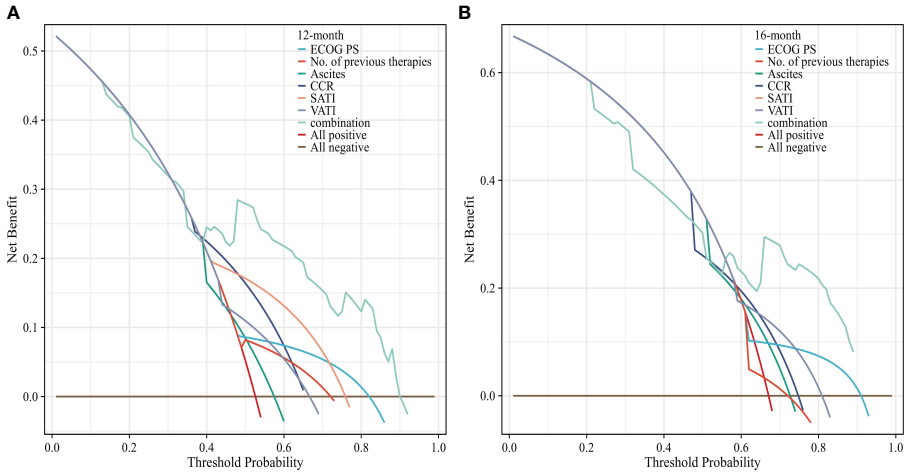

FIGURE 7
Decision curves analysis of the nomogram for **(A)** 12 and **(B)** 16 months OS. The x-axis represents the threshold probability, and the y-axis represents the net benefit. ECOG PS, Eastern Cooperative Oncology Group performance status; CCR, creatinine-to-cystatin C ratio; SATI, subcutaneous adipose tissue index; VATI, visceral adipose tissue index.

treatment regimen and patient characteristics (BMI, sex, age, et al.) (50). Next, we will continue to collect enough samples and stratify patients by their BMI and sex to further investigate the protective effect of subcutaneous and visceral adiposity in patients of different baseline characteristics.

To the best of our knowledge, this is the first study to investigate the effects of the CCR, SII and BC-parameters on response rates and survival outcomes in GC patients receiving PD-1 based combination therapy. However, our investigation has certain limitations. Firstly, it is a retrospective study with a small sample size and different treatment regimens of PD-1. Secondly, missing PD-L1 status data might affect the power of the statistical analysis, although no PD-L1 variation was observed in high or low CCR and SATI patients. Lastly, our study did not analyze ICIs-linked adverse events (AEs) due to the predominance of low to moderate-grade AEs. Consequently, larger prospective cohort studies are necessary to validate the findings presented in this retrospective analysis.

In conclusion, our study demonstrates that CCR and SATI are independent predictive and prognostic factors in patients with metastatic GC receiving PD-1 inhibitors-based combination therapy. The nomogram based on CCR and BC-parameters may assist in identifying potential patients who would benefit from PD-1 inhibitors. Therefore, further large-sample and prospective studies are necessary to validate our conclusions.

Data availability statement

The raw data supporting the conclusions of this article will be made available by the authors, without undue reservation.

Ethics statement

The studies involving humans were approved by General Hospital of Northern Theater Command Ethics Review Center. The studies were conducted in accordance with the local legislation and institutional requirements. The human samples used in this study were acquired from a by- product of routine care or industry. Written informed consent for participation was not required from the participants or the participants' legal guardians/ next of kin in accordance with the national legislation and institutional requirements.

Author contributions

HJ: Data curation, Formal analysis, Writing – original draft, Conceptualization, Investigation, Methodology. BL: Methodology, Writing – original draft, Investigation, Project administration. PJ: Validation, Writing – original draft, Resources, Visualization. YL: Visualization, Writing – original draft, Software. LC: Data curation, Writing – original draft, Validation. SJ: Data curation, Writing – original draft, Visualization. JW: Data curation, Writing – original draft, Software. YS: Supervision, Writing – original draft, Funding acquisition, Project administration. ZZ: Project administration, Writing – original draft, Resources. JM: Conceptualization, Writing – review & editing, Funding acquisition, Investigation, Methodology. LZ: Software, Writing – review & editing, Funding acquisition, Supervision. CD: Conceptualization, Funding acquisition, Writing – review & editing, Investigation, Methodology, Supervision.

Funding

The author(s) declare financial support was received for the research, authorship, and/or publication of this article. This research was supported by Liaoning Province Nature Science Foundation (2023JH2/101700101), Shenyang Municipal Medical Engineering Cross Research Foundation of china (22-321-32-09), Shenyang Municipal Natural Science Foundation (22-321-33-32),

and Pengcheng Talent-Medical Young Reserve Talent Training Program (XWRCHT20220002).

Acknowledgments

Despite the retrospective nature of this study, the authors still thank our patients for their commitment to treatment and our care.

Conflict of interest

The authors declare that the research was conducted in the absence of any commercial or financial relationships that could be construed as a potential conflict of interest.

Publisher's note

Supplementary material

The Supplementary Material for this article can be found online at: https://www.frontiersin.org/articles/10.3389/fimmu.2024.1364728/full#supplementary-material

References

1. Smyth EC, Nilsson M, Grabsch HI, van Grieken NC, Lordick F. Gastric cancer. *Lancet*. (2020) 396:635–48. doi: 10.1016/S0140-6736(20)31288-5

2. Shitara K, Van Cutsem E, Bang YJ, Fuchs C, Wyrwicz L, Lee KW, et al. Efficacy and safety of pembrolizumab or pembrolizumab plus chemotherapy vs chemotherapy alone for patients with first-line, advanced gastric cancer: the KEYNOTE-062 phase 3 randomized clinical trial. *JAMA Oncol*. (2020) 6:1571–80. doi: 10.1001/jamaoncol.2020.3370

3. Janjigian YY, Shitara K, Moehler M, Garrido M, Salman P, Shen L, et al. First-line nivolumab plus chemotherapy versus chemotherapy alone for advanced gastric, gastro-oesophageal junction, and oesophageal adenocarcinoma (CheckMate 649): a randomised, open-label, phase 3 trial. *Lancet*. (2021) 398:27–40. doi: 10.1016/S0140-6736(21)00797-2

4. Baxmann AC, Ahmed MS, Marques NC, Menon VB, Pereira AB, Kirsztajn GM, et al. Influence of muscle mass and physical activity on serum and urinary creatinine and serum cystatin C. *Clin J Am Soc Nephrol*. (2008) 3:348–54. doi: 10.2215/CJN.02870707

5. Onopiuk A, Tokarzewicz A, Gorodkiewicz E. Cystatin C: a kidney function biomarker. *Adv Clin Chem*. (2015) 68:57–69. doi: 10.1016/bs.acc.2014.11.007

6. Kashani KB, Frazee EN, Kukralova L, Sarvottam K, Herasevich V, Young PM, et al. Evaluating muscle mass by using markers of kidney function: development of the sarcopenia index. *Crit Care Med*. (2017) 45:e23–9. doi: 10.1097/CCM.0000000000002013

7. Jung CY, Joo YS, Kim HW, Han SH, Yoo TH, Kang SW, et al. Creatinine-cystatin C ratio and mortality in patients receiving intensive care and continuous kidney replacement therapy: A retrospective cohort study. *Am J Kidney Dis*. (2021) 77:509–516.e1. doi: 10.1053/j.ajkd.2020.08.014

8. Barreto EF, Poyant JO, Coville HH, Dierkhising RA, Kennedy CC, Gajic O, et al. Validation of the sarcopenia index to assess muscle mass in the critically ill: A novel application of kidney function markers. *Clin Nutr*. (2019) 38:1362–7. doi: 10.1016/j.clnu.2018.05.031

9. Liao L, Shi S, Ding B, Zhang R, Tu J, Zhao Y, et al. The relationship between serum creatinine/cystatin C ratio and mortality in hypertensive patients. *Nutr Metab Cardiovasc Dis*. (2023) 34:369–76. doi: 10.1016/j.numecd.2023.09.004

10. Osaka T, Hamaguchi M, Hashimoto Y, Ushigome E, Tanaka M, Yamazaki M, et al. Decreased the creatinine to cystatin C ratio is a surrogate marker of sarcopenia in patients with type 2 diabetes. *Diabetes Res Clin Pract*. (2018) 139:52–8. doi: 10.1016/j.diabres.2018.02.025

11. Wei W, Li S, Liu J, Liu Y, Chen K, Chen S, et al. Prognostic value of creatinine-to-cystatin c ratio in patients with type 2 diabetes mellitus: a cohort study. *Diabetol Metab Syndr*. (2022) 14:176. doi: 10.1186/s13098-022-00958-y

12. Harimoto N, Araki K, Yamanaka T, Hagiwara K, Ishii N, Tsukagoshi M, et al. The ratio of creatinine and cystatin C estimated glomerular filtration rates as a surrogate marker in patients with hepatocellular carcinoma undergoing hepatic resection. *J Hepatobiliary Pancreat Sci*. (2022) 29:964–73. doi: 10.1002/jhbp.1164

13. Tang T, Xie L, Hu S, Tan L, Lei X, Luo X, et al. Serum creatinine and cystatin C-based diagnostic indices for sarcopenia in advanced non-small cell lung cancer. *J Cachexia Sarcopenia Muscle*. (2022) 13:1800–10. doi: 10.1002/jcsm.12977

14. Zheng C, Wang E, Li JS, Xie K, Luo C, Ge QY, et al. Serum creatinine/cystatin C ratio as a screening tool for sarcopenia and prognostic indicator for patients with esophageal cancer. *BMC Geriatr*. (2022) 22:207. doi: 10.1186/s12877-022-02925-8

15. Ding P, Guo H, Sun C, Chen S, Yang P, Tian Y, et al. Serum creatinine/cystatin C ratio is a systemic marker of sarcopenia in patients with gastrointestinal stromal tumours. *Front Nutr*. (2022) 9:963265. doi: 10.3389/fnut.2022.963265

16. Gao S, Xie H, Wei L, Liu M, Liang Y, Wang Q, et al. Serum creatinine/cystatin C ratio as a prognostic indicator for patients with colorectal cancer. *Front Oncol*. (2023) 13:1155520. doi: 10.3389/fonc.2023.1155520

17. Tsukagoshi M, Watanabe A, Araki K, Ishii N, Hagiwara K, Hoshino K, et al. Usefulness of serum creatinine and cystatin C ratio as a screening tool for predicting prognosis in patients with pancreatic cancer. *Ann Gastroenterol Surg*. (2023) 7:784–92. doi: 10.1002/ags3.12671

18. Ashton E, Arrondeau J, Jouinot A, Boudou-Rouquette P, Hirsch L, Huillard O, et al. Impact of sarcopenia indexes on survival and severe immune acute toxicity in metastatic non-small cell lung cancer patients treated with PD-1 immune checkpoint inhibitors. *Clin Nutr*. (2023) 42:944–53. doi: 10.1016/j.clnu.2023.03.023

19. Bundred J, Kamarajah SK, Roberts KJ. Body composition assessment and sarcopenia in patients with pancreatic cancer: a systematic review and meta-analysis. *HPB (Oxford)*. (2019) 21:1603–12. doi: 10.1016/j.hpb.2019.05.018

20. Vrieling A, Kampman E, Knijnenburg NC, Mulders PF, Sedelaar JPM, Baracos VE, et al. Body composition in relation to clinical outcomes in renal cell cancer: A systematic review and meta-analysis. *Eur Urol Focus*. (2018) 4:420–34. doi: 10.1016/j.euf.2016.11.009

21. Kamarajah SK, Bundred J, Tan BHL. Body composition assessment and sarcopenia in patients with gastric cancer: a systematic review and meta-analysis. *Gastric Cancer*. (2019) 22:10–22. doi: 10.1007/s10120-018-0882-2

22. Martin L, Birdsell L, Macdonald N, Reiman T, Clandinin MT, McCargar LJ, et al. Cancer cachexia in the age of obesity: skeletal muscle depletion is a powerful prognostic factor, independent of body mass index. *J Clin Oncol*. (2013) 31:1539–47. doi: 10.1200/JCO.2012.45.2722

23. Cruz-Jentoft AJ, Bahat G, Bauer J, Boirie Y, Bruyere O, Cederholm T, et al. Sarcopenia: revised European consensus on definition and diagnosis. *Age Ageing*. (2019) 48:16–31. doi: 10.1093/ageing/afy169

24. Xiao J, Mazurak VC, Olobatuyi TA, Caan BJ, Prado CM. Visceral adiposity and cancer survival: a review of imaging studies. *Eur J Cancer Care (Engl)*. (2018) 27:e12611. doi: 10.1111/ecc.12611

25. Zhuang CL, Huang DD, Pang WY, Zhou CJ, Wang SL, Lou N, et al. Sarcopenia is an independent predictor of severe postoperative complications and long-term survival after radical gastrectomy for gastric cancer: analysis from a large-scale cohort. *Med (Baltimore)*. (2016) 95:e3164. doi: 10.1097/MD.0000000000003164

26. Crombe A, Kind M, Toulmonde M, Italiano A, Cousin S. Impact of CT-based body composition parameters at baseline, their early changes and response in metastatic cancer patients treated with immune checkpoint inhibitors. *Eur J Radiol*. (2020) 133:109340. doi: 10.1016/j.ejrad.2020.109340

27. Eisenhauer EA, Therasse P, Bogaerts J, Schwartz LH, Sargent D, Ford R, et al. New response evaluation criteria in solid tumours: revised RECIST guideline (version 1.1). *Eur J Cancer*. (2009) 45:228–47. doi: 10.1016/j.ejca.2008.10.026

28. Fu X, Tian Z, Wen S, Sun H, Thapa S, Xiong H, et al. A new index based on serum creatinine and cystatin C is useful for assessing sarcopenia in patients with advanced cancer. *Nutrition*. (2021) 82:111032. doi: 10.1016/j.nut.2020.111032

29. Sun J, Yang H, Cai W, Zheng J, Shen N, Yang X, et al. Serum creatinine/cystatin C ratio as a surrogate marker for sarcopenia in patients with gastric cancer. *BMC Gastroenterol*. (2022) 22:26. doi: 10.1186/s12876-022-02093-4

30. Jung CY, Kim HW, Han SH, Yoo TH, Kang SW, Park JT. Creatinine-cystatin C ratio and mortality in cancer patients: a retrospective cohort study. *J Cachexia Sarcopenia Muscle*. (2022) 13:2064–72. doi: 10.1002/jcsm.13006

31. Kim YY, Lee J, Jeong WK, Kim ST, Kim JH, Hong JY, et al. Prognostic significance of sarcopenia in microsatellite-stable gastric cancer patients treated with programmed death-1 inhibitors. *Gastric Cancer*. (2021) 24:457–66. doi: 10.1007/s10120-020-01124-x

32. Ulmann G, Kai J, Durand JP, Neveux N, Jouinot A, De Bandt JP, et al. Creatinine-to-cystatin C ratio and bioelectrical impedance analysis for the assessement of low lean body mass in cancer patients: Comparison to L3-computed tomography scan. *Nutrition*. (2021) 81:110895. doi: 10.1016/j.nut.2020.110895

33. Reddan DN, Klassen PS, Szczech LA, Coladonato JA, O'Shea S, Owen WF Jr., et al. White blood cells as a novel mortality predictor in haemodialysis patients. *Nephrol Dial Transplant*. (2003) 18:1167–73. doi: 10.1093/ndt/gfg066

34. Keller CR, Odden MC, Fried LF, Newman AB, Angleman S, Green CA, et al. Kidney function and markers of inflammation in elderly persons without chronic kidney disease: the health, aging, and body composition study. *Kidney Int*. (2007) 71:239–44. doi: 10.1038/sj.ki.5002042

35. Grivennikov SI, Greten FR, Karin M. Immunity, inflammation, and cancer. *Cell*. (2010) 140:883–99. doi: 10.1016/j.cell.2010.01.025

36. Zi M, Xu Y. Involvement of cystatin C in immunity and apoptosis. *Immunol Lett*. (2018) 196:80–90. doi: 10.1016/j.imlet.2018.01.006

37. Shachar SS, Williams GR, Muss HB, Nishijima TF. Prognostic value of sarcopenia in adults with solid tumours: A meta-analysis and systematic review. *Eur J Cancer*. (2016) 57:58–67. doi: 10.1016/j.ejca.2015.12.030

38. Takenaka Y, Oya R, Takemoto N, Inohara H. Predictive impact of sarcopenia in solid cancers treated with immune checkpoint inhibitors: a meta-analysis. *J Cachexia Sarcopenia Muscle*. (2021) 12:1122–35. doi: 10.1002/jcsm.12755

39. Deng T, Lyon CJ, Bergin S, Caligiuri MA, Hsueh WA. Obesity, inflammation, and cancer. *Annu Rev Pathol*. (2016) 11:421–49. doi: 10.1146/annurev-pathol-012615-044359

40. Ebadi M, Baracos VE, Bathe OF, Robinson LE, Mazurak VC. Loss of visceral adipose tissue precedes subcutaneous adipose tissue and associates with n-6 fatty acid content. *Clin Nutr*. (2016) 35:1347–53. doi: 10.1016/j.clnu.2016.02.014

41. Young AC, Quach HT, Song H, Davis EJ, Moslehi JJ, Ye F, et al. Impact of body composition on outcomes from anti-PD1 +/- anti-CTLA-4 treatment in melanoma. *J Immunother Cancer*. (2020) 8:e000821. doi: 10.1136/jitc-2020-000821

42. Martini DJ, Shabto JM, Goyal S, Liu Y, Olsen TA, Evans ST, et al. Body composition as an independent predictive and prognostic biomarker in advanced urothelial carcinoma patients treated with immune checkpoint inhibitors. *Oncologist*. (2021) 26:1017–25. doi: 10.1002/onco.13922

43. Khan A, Welman CJ, Abed A, O'Hanlon S, Redfern A, Azim S, et al. Association of computed tomography measures of muscle and adipose tissue and progressive changes throughout treatment with clinical endpoints in patients with advanced lung cancer treated with immune checkpoint inhibitors. *Cancers (Basel)*. (2023) 15:1382. doi: 10.3390/cancers15051382

44. Esposito A, Marra A, Bagnardi V, Frassoni S, Morganti S, Viale G, et al. Body mass index, adiposity and tumour infiltrating lymphocytes as prognostic biomarkers in patients treated with immunotherapy: A multi-parametric analysis. *Eur J Cancer*. (2021) 145:197–209. doi: 10.1016/j.ejca.2020.12.028

45. He M, Chen ZF, Zhang L, Gao X, Chong X, Li HS, et al. Associations of subcutaneous fat area and Systemic Immune-inflammation Index with survival in patients with advanced gastric cancer receiving dual PD-1 and HER2 blockade. *J Immunother Cancer*. (2023) 11:e007054. doi: 10.1136/jitc-2023-007054

46. Ke ZB, Chen H, Chen JY, Cai H, Lin YZ, Sun XL, et al. Preoperative abdominal fat distribution and systemic immune inflammation were associated with response to intravesical Bacillus Calmette-Guerin immunotherapy in patients with non-muscle invasive bladder cancer. *Clin Nutr*. (2021) 40:5792–801. doi: 10.1016/j.clnu.2021.10.019

47. Taniguchi Y, Kurokawa Y, Takahashi T, Saito T, Yamashita K, Tanaka K, et al. Impacts of preoperative psoas muscle mass and visceral fat area on postoperative short- and long-term outcomes in patients with gastric cancer. *World J Surg*. (2021) 45:815–21. doi: 10.1007/s00268-020-05857-9

48. Yang SJ, Li HR, Zhang WH, Liu K, Zhang DY, Sun LF, et al. Visceral fat area (VFA) superior to BMI for predicting postoperative complications after radical gastrectomy: a prospective cohort study. *J Gastrointest Surg*. (2020) 24:1298–306. doi: 10.1007/s11605-019-04259-0

49. Matsui R, Inaki N, Tsuji T. Impact of visceral adipose tissue on compliance of adjuvant chemotherapy and relapse-free survival after gastrectomy for gastric cancer: A propensity score matching analysis. *Clin Nutr*. (2021) 40:2745–53. doi: 10.1016/j.clnu.2021.04.019

50. Grossberg AJ, Chamchod S, Fuller CD, Mohamed AS, Heukelom J, Eichelberger H, et al. Association of body composition with survival and locoregional control of radiotherapy-treated head and neck squamous cell carcinoma. *JAMA Oncol*. (2016) 2:782–9. doi: 10.1001/jamaoncol.2015.6339

frontiers | Frontiers in Immunology

TYPE Systematic Review
PUBLISHED 24 May 2024
DOI 10.3389/fimmu.2024.1403771

OPEN ACCESS

EDITED BY
Raquel Tarazona,
University of Extremadura, Spain

REVIEWED BY
Luis De La Cruz-Merino,
Virgen Macarena University Hospital, Spain
Nikoleta Bizymi,
University of Crete, Greece
Katherine Bline,
Nationwide Children's Hospital, United States

*CORRESPONDENCE
Steffen Seyfried
steffen.seyfried@umm.de

†These authors share first authorship

‡These authors share last authorship

RECEIVED 19 March 2024
ACCEPTED 09 May 2024
PUBLISHED 24 May 2024

CITATION
Möller M, Orth V, Umansky V, Hetjens S, Braun V, Reißfelder C, Hardt J and Seyfried S (2024) Myeloid-derived suppressor cells in peripheral blood as predictive biomarkers in patients with solid tumors undergoing immune checkpoint therapy: systematic review and meta-analysis.
Front. Immunol. 15:1403771.
doi: 10.3389/fimmu.2024.1403771

Myeloid-derived suppressor cells in peripheral blood as predictive biomarkers in patients with solid tumors undergoing immune checkpoint therapy: systematic review and meta-analysis

Maximilian Möller[1†], Vanessa Orth[1†], Viktor Umansky[2,3,4], Svetlana Hetjens[5], Volker Braun[6], Christoph Reißfelder[1,4], Julia Hardt[1‡] and Steffen Seyfried[1*‡]

[1]Department of Surgery, Medical Faculty Mannheim, University Medical Center Mannheim, Heidelberg University, Mannheim, Germany, [2]Department of Dermatology, Venereology and Allergology, University Medical Center Mannheim, Heidelberg University, Mannheim, Germany, [3]Skin Cancer Unit, German Cancer Research Center (DKFZ), Heidelberg, Germany, [4]German Cancer Research Center (DKFZ)-Hector Cancer Institute, University Medical Centre Mannheim, Mannheim, Germany, [5]Department of Biometry and Statistics, Medical Faculty Mannheim, University Medical Center Mannheim, Heidelberg University, Mannheim, Germany, [6]Department of Library and Information Sciences, Medical Faculty Mannheim, Heidelberg University, Mannheim, Germany

Background: Immunotherapeutic approaches, including immune checkpoint inhibitor (ICI) therapy, are increasingly recognized for their potential. Despite notable successes, patient responses to these treatments vary significantly. The absence of reliable predictive and prognostic biomarkers hampers the ability to foresee outcomes. This meta-analysis aims to evaluate the predictive significance of circulating myeloid-derived suppressor cells (MDSC) in patients with solid tumors undergoing ICI therapy, focusing on progression-free survival (PFS) and overall survival (OS).

Methods: A comprehensive literature search was performed across PubMed and EMBASE from January 2007 to November 2023, utilizing keywords related to MDSC and ICI. We extracted hazard ratios (HRs) and 95% confidence intervals (CIs) directly from the publications or calculated them based on the reported data. A hazard ratio greater than 1 indicated a beneficial effect of low MDSC levels. We assessed heterogeneity and effect size through subgroup analyses.

Results: Our search yielded 4,023 articles, of which 17 studies involving 1,035 patients were included. The analysis revealed that patients with lower levels of circulating MDSC experienced significantly improved OS (HR=2.13 [95% CI 1.51–2.99]) and PFS (HR=1.87 [95% CI 1.29–2.72]) in response to ICI therapy. Notably, heterogeneity across these outcomes was primarily attributed to differences in polymorphonuclear MDSC (PMN-MDSC) subpopulations and varying cutoff methodologies used in the studies. The monocytic MDSC (M-MDSC) subpopulation emerged as a consistent and significant prognostic marker across various subgroup analyses, including ethnicity, tumor type, ICI target, sample size, and cutoff methodology.

10.3389/fimmu.2024.1403771

Conclusions: Our findings suggest that standardized assessment of MDSC, particularly M-MDSC, should be integral to ICI therapy strategies. These cells hold the promise of identifying patients at risk of poor response to ICI therapy, enabling tailored treatment approaches. Further research focusing on the standardization of markers and validation of cutoff methods is crucial for integrating MDSC into clinical practice.

Systematic Review Registration: https://www.crd.york.ac.uk/prospero/display_record.php?ID=CRD42023420095, identifier CRD42023420095.

KEYWORDS

immune checkpoint inhibitors, immunotherapy, myeloid-derived suppressor cells, MDSC, neoplasms, solid malignancies, prognosis, biomarkers

1 Introduction

Despite modern therapies, cancer is still one of the most common causes of death in industrialized countries. For example, in 2019, solid tumors such as tracheobronchial lung cancer, prostate and colon cancer were among the leading causes of death worldwide from cancer in men while it was breast, colon cancer and tracheobronchial lungs in women (1). The approval of immune checkpoint inhibitor (ICI) treatments, by the Food and Drug Administration in 2011provides alternative therapies to the standard chemotherapy regimens, particularly for the treatment of solid tumor malignancies It has been shown that T cells become anergic in cancer patients due to the interaction of programmed death -1 (PD-1) or cytotoxic-T-lymphocyte-associated protein-4 (CTLA-4) upregulated on activated T cells with their ligands PD-L1 and CD80 or CD86 respectively. Blocking this interaction could result in regaining anti-tumor T cell functions (2, 3).

With the introduction of Ipilimumab in the treatment of malignant melanoma, the median overall survival was increased from 6.4 months to 10 months compared to the control group (4). The survival curve in a cohort of patients with non-resectable malignant melanoma treated with ipilimumab reached a plateau between 20–26% after three years, indicating a long-term response (5). Another breakthrough was found in the treatment of non-small-cell lung carcinoma. Here, recent studies have shown that immunotherapy combined with chemotherapy already shows a survival advantage in the first line therapy compared to the single chemotherapy (median overall survival after 12 months: 69.2% in the combination group and 49.4% in the chemotherapy group) (6).

Despite these advancements, a subset of patients either fails to respond initially or loses responsiveness over time to such therapies. The search for explanations has increasingly focused on immunosuppressive mechanisms, including the role of myeloid-derived suppressor cells (MDSC). Studies have indicated an inverse relationship between the prognosis of solid tumor patients and the presence of immunosuppressive cell types such as MDSC and regulatory T-cells (Treg) within the tumor microenvironment (TME) and peripheral blood (7–9).

MDSCs represent a heterogeneous population of myeloid cells known for their immunosuppressive activities. They originate from immature myeloid cells that fail to differentiate under chronic inflammatory conditions, such as cancer (10, 11). In addition, normal mature myeloid cells could be converted into MDSC in cancer patients (12, 13). MDSCs are categorized into two subpopulations based on their phenotypic characteristics: monocytic MDSCs (M-MDSCs) and polymorphonuclear MDSCs (PMN-MDSCs). M-MDSCs are identified by the expression of surface markers $CD11b^{+}CD14^{+}HLA\text{-}DR^{low/-}CD15^{-}$, with CD33 also serving as an alternative marker to CD11b. This subgroup is morphologically comparable to monocytes. On the other hand, PMN-MDSCs, which express $CD11b^{+}CD14^{-}CD15^{+}$(CD66 as an alternative to CD15) markers, are morphologically akin to neutrophils (10, 11).

The discovery of Lectin-type oxidized LDL receptor 1 (LOX-1) as a specific ligand has refined the identification and separation of these cell types, facilitating a more accurate characterization and understanding of their roles within the tumor microenvironment (TME) and systemic circulation (14). A standardized gating strategy to identify M-MDSCs, based on common morphological criteria such as $CD14^{+}$ and HLA-DR expression, has been established recently, noting that functional examination of the immunosuppressive properties of MDSCs is the safest way to

Abbreviations: ICI, immune checkpoint inhibitor therapy; PD-1, programmed death -1; PD-L1, programmed death - Ligand 1; CTLA-4, cytotoxic-T-lymphocyte-associated protein-4, Treg, regulatory T-cells; TME, tumor microenvironment; PRISMA-P, Preferred Reporting Items for Systematic Reviews and Meta-Analysis Protocols 2020; QUIPS, Quality in Prognostic Studies; OS, overall survival; PFS, progression free survival; HR, Hazard ratio; 95% CI, 95% Confidence interval ; [lower limit of 95% CI, upper limit of 95% CI]; USA, United states of America; NSCLC, non-small cell lung cancer; NR, not reported; PBMC, Peripheral blood mononuclear cells; MDSC, myeloid-derived suppressor cells; M-MDSC, monocytic MDSC; PMN-MDSC, polymorphonuclear.

identify them (10). This advancement in methodology has been crucial for consistent and reproducible analysis of MDSC populations across various studies.

The suppressive mechanisms of MDSC include inhibiting T cells and other components of immune systems to facilitate tumor growth and survival (11). One of the major mechanisms of MDSC-mediated immunosuppression is linked to the upregulation of programmed cell death ligand 1 (PD-L1) interacting with its receptor PD-1 expressed on tumor-infiltrating T cells (10, 15),

They are also capable to inhibit anti-tumor T cell functions via production of nitric oxide (NO) and reactive oxygen species (ROS) as well as by upregulation of arginase 1 and Indolamin-2,3-Dioxygenase (11, 16–19).

They also interact synergistically with regulatory T cells (Tregs), promoting their expansion within the TME via the CD40 receptor (20). This interaction highlights the complex network of immunosuppressive pathways that contribute to tumor growth and survival.

Given these extensive immunosuppressive capabilities, MDSC subpopulations represent potential biomarkers for predicting patient outcomes, including responses to immunotherapies (11, 21–23). Furthermore, the recruitment of MDSCs from the bone marrow to the TME, driven by various cytokines (24) suggests that an early increase in circulating MDSC levels could serve as a negative prognostic indicator.

Despite existing research demonstrating a correlation between high levels of MDSCs in peripheral blood and adverse outcomes in solid tumors (9), the specific impact of MDSCs on the efficacy of immune checkpoint inhibitor (ICI) therapy remains underexplored. To date, no systematic review or meta-analysis has separately assessed the predictive value of circulating MDSCs on the response to ICI therapy in patients with solid tumors. This gap in the literature underscores the need for a comprehensive analysis that can elucidate the influence of circulating MDSC populations on overall survival and therapeutic response, thereby informing clinical decision-making and potentially guiding the development of more effective treatment strategies. The goal of this meta-analysis is to address this need by examining the relationship between MDSC levels in peripheral blood and patient outcomes in the context of ICI therapy.

2 Methods

This study was conceived as a meta-analysis to investigate whether elevated levels MDSCs and their subpopulations in peripheral blood serve as predictive markers for the response to immune checkpoint inhibitor (ICI) therapy or survival outcomes in patients with solid tumors. The PICO scheme for our research question was defined as:

- Population. Patients with solid tumors treated with ICI
- Intervention: measurement of MDSC in patients' peripheral blood by flow cytometry
- Comparison: high concentrations of MDSC compared to low concentrations of MDSC
- Outcome: Progression-free survival and overall survival

The study protocol was prospectively registered with PROSPERO (registration number CRD42023420095), adhering to the Preferred Reporting Items for Systematic Reviews and Meta-Analysis Protocols 2020 (PRISMA-P) guidelines, which underpin both the protocol and the manuscript structure (see Supplementary Table 2 for details).

2.1 Search strategy

The literature search was conducted in the PubMed and EMBASE databases from January 2007 to November 2023, utilizing the PubMed and EMBASE databases. A detailed search strategy was developed in collaboration with a medical librarian, incorporating terms and synonyms related to immune checkpoint inhibitors and "myeloid-derived suppressor cells" [MeSH], utilizing both OR and AND Boolean operators for term combination. Additionally, Google Scholar was employed to identify grey literature, and the reference lists of relevant articles were reviewed to uncover further studies.

2.2 Inclusion criteria

Inclusion criteria mandated that studies: (1) were prospective or retrospective cohort studies, clinical trials, or randomized controlled trials; (2) included patients diagnosed with solid neoplasms; (3) involved treatment with an immune checkpoint inhibitor; (4) measured MDSC levels in peripheral blood at a minimum of two time points, one of which must be prior to therapy initiation; (5) used cutoff values for MDSC levels to stratify patients; and (6) performed a correlation analysis with survival or other outcome parameters, including either (7) hazard ratios with 95% confidence intervals or provided sufficient data for their calculation.

2.3 Exclusion criteria

Excluded were studies that: (1) were reviews, case reports, animal studies, or *in vitro* studies; (2) did not measure MDSC levels using flow cytometry or measured them peritumorally or directly within tumor tissues; (3) targeted MDSCs directly as a therapeutic intervention; (4) provided insufficient data for hazard ratio calculations.

The eligible studies were screened in full text by two authors (MM, VO) with discrepancies resolved via a third author (SS).

2.4 Data extraction

The data were collected by both authors independently in a data matrix that included the first author, year of publication, country of origin, number of patients and age (median and/or range) of the

study population, tumor type and stage, type of therapy (immune checkpoint inhibitor with target) MDSC subpopulation, MDSC markers, cutoff values, and method of cutoff value determination, observed endpoints. We extracted hazard ratios with 95% confidence intervals for the endpoints overall survival (OS), progression free survival (PFS), disease free survival (DFS). If these were not specified, we calculated the hazard ratios according to method of Tierney (25) by estimating the necessary data from the Kaplan Meier curves. Alternatively, we extracted the HR from other sources if the data were already calculated there.

2.5 Risk of bias assessment

Using the QUIPS tool, one author (MM) assessed the risk of bias of the included studies. A second author (VO) independently reviewed the assessment. Disagreements were resolved by a third author (SS). The tool contains six categories of bias due to study participation, study attrition, prognostic factor measurement, outcome measurement, adjustment for other prognostic factors and bias due to statistical analysis and reporting. In each category, the authors could choose between low, moderate and high risk of bias (26).

2.6 Statistical analysis

For the statistical analysis, we used RevMan 5.4 (Review Manager Version 5.4. The Cochrane Collaboration, 2020) and Comprehensive Meta-Analysis software Version 4 (Biostat, Englewood, NJ 2022). We weighted them according to the generic inverse variance method. A hazard ratio >1 defined a preference for a low MDSC level at baseline. To detect heterogeneity, we used a χ^2 test and the I^2 value, which were considered significant if the χ^2 test assumed a value of $P<0.1$ or $I^2>50\%$ (27). Subgroup and sensitivity analyses further explored heterogeneity, while publication bias was assessed visually with a funnel plot and quantitatively via the Egger test. The Duval and Tweedie's trim-and-fill method was applied in cases of detected asymmetry, with a significance threshold set at $P<0.05$ (28). If the heterogeneity was significant, we used the random-effects model; otherwise, we used the fixed-effects model.

3 Results

3.1 Study characteristics

In our comprehensive search across three databases (PubMed, EMBASE, Google Scholar), we initially identified 4,023 articles. Upon removal of 1,197 duplicates, 2,731 articles remained for consideration. The initial screening of titles and abstracts facilitated the exclusion of 2,650 articles deemed not relevant to our research objectives. Further detailed examination of the full texts led to the exclusion of additional articles for various reasons: 12 articles were excluded due to lack of stratification of MDSC levels into high or low categories; 5 articles were omitted because they failed to collect baseline data; 7 articles were excluded for not incorporating immune checkpoint inhibitor (ICI) therapy; 5 articles were disregarded due to insufficient data for calculating Hazard ratios; 3 articles were eliminated because they did not measure MDSC in peripheral blood; and 32 articles were excluded for other reasons or because they did not align with the study's focus. Ultimately, 17 studies (29–45) were selected for inclusion in our meta-analysis, as illustrated in the PRISMA flow diagram (Figure 1).

These 17 studies collectively encompassed 1,035 patients, with the majority being melanoma cases (10 studies involving 720 patients). The next most significant group was patients with non-small cell lung cancer (NSCLC), represented by 207 patients across 3 studies. Other cancer types included in the analysis were prostate cancer (2 studies with 45 patients) and urothelial carcinoma (1 study with 30 patients), along with a study that pooled data from patients with various solid tumors (33 patients across 11 entities). Regarding ICI specificity, 8 studies targeted PD-1/PD-L1 exclusively, involving 428 patients; 5 studies focused solely on CTLA-4, including 359 patients; and 4 studies, comprising 248 patients, pooled effect measurements for patients treated with either PD-1/PD-L1 or CTLA-4 antibodies.

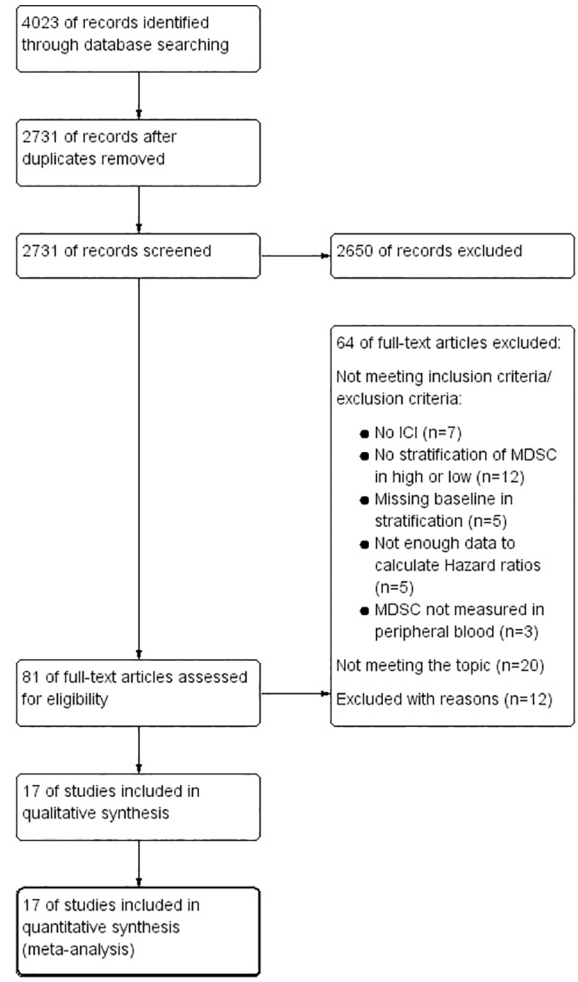

FIGURE 1
PRISMA Flow Chart, illustrating the study selection process.

A more detailed breakdown of these studies is provided in Table 1. Out of the included studies, 15 reported data on OS, and 9 included PFS data. The analysis of MDSC subtypes revealed that 2 studies examined total MDSC levels, 2 focused exclusively on PMN-MDSC, and 7 investigated monocytic MDSC (M-MDSC). Additionally, 6 studies presented data relevant to both PMN-MDSC and M-MDSC subgroups, offering a comprehensive overview of the impact of these immune cells on patient outcomes in the context of ICI therapy.

3.2 Progression-free survival

A high baseline MDSC value indicated a poorer response to ICI, according to PFS. The HR was 1.87 [95%CI 1.29–2.72] with an I^2 of 79%. Here, however, only the M-MDSC achieved a significant result (HR= 2.03 [95% CI 1.42–2.90]) with a moderate heterogeneity I^2 = 34% %. The other three populations were not significant (PMN MDSC HR=1.68 [95% CI 0.94–3.01] I^2 = 78%); total MDSC HR=2.21 (95%CI [0.68–7.16] I^2 = 48%). Due to the overall high heterogeneity, the HRs were also calculated here using a random effects model (Figure 2).

3.3 Overall survival

OS was lower with a high MDSC baseline value. This resulted in an HR=2.13 [95% CI 1.51–2.99] for OS after pooling the studies. The heterogeneity amounted to I^2 = 82%. However, only the M-MDSC reached a significant level. We calculated an HR=2.45 [95% CI 1.89–3.18] I^2 = 23%) for the M-MDSC. For the PMN-MDSC population, the HR was 1.47 [95%CI 0.90–2.42]. This resulted in I^2 = 68%. Overall, the heterogeneity was relatively high, which is why the HR was calculated using the random effects model (Figure 3).

3.4 Subgroup analysis

To delve deeper into the heterogeneity observed within our meta-analysis, we conducted detailed subgroup analyses focusing on variables such as geographic region, patient cohort size, type of cancer, stage of cancer, method and value used for cutoff determination, and the specific immune checkpoint target (PD-1/PD-L1 versus CTLA-4). Stratification for the number of patients and cutoff values was based on the median values within each respective group. The comprehensive findings of these subgroup analyses are presented in Supplementary Table 1. A reduction in heterogeneity was observed when studies utilized consistent methods for determining cutoff values, highlighting this as a significant factor in our analysis. The type of cancer entity did not impact heterogeneity. Predominantly, PMN-MDSC emerged as a primary source of heterogeneity, both in our primary and subgroup analyses.

In instances where a high degree of pooled heterogeneity was noted, it was often accompanied by significant heterogeneity within the PMN-MDSC subgroup, as detailed in the Supplementary Material. A visual inspection of the Forest plot readily identified the study by Passaro et al. as a potential primary contributor to this observed heterogeneity. Further analysis confirmed that the inclusion of Passaro et al. markedly influenced the heterogeneity levels: for the PMN-MDSC subgroup analyzing PFS, heterogeneity dramatically decreased from I^2=78% to 0% upon excluding this study, resulting in an adjusted HR of 2.18 (95% confidence interval [CI]: 1.46–3.26) and a revised pooled HR of 2.10 (95% CI: 1.68–2.62) with an I^2 of 0%. A similar pattern emerged within the overall survival subgroup; the exclusion of Passaro et al. halved the heterogeneity from I^2=68% to 39%, with an HR of 1.73 (95% CI: 1.04–2.88), leading to a pooled HR of 2.26 (95% CI: 1.81–2.83) and an I^2 of 27%.

This significant reduction in heterogeneity, particularly in the PFS PMN-MDSC population, from I^2=78% to a null value (I^2=0%) following the removal of Passaro et al., underscores the substantial impact this study had on the heterogeneity levels. Similarly, in the OS analysis, the heterogeneity within the PMN-MDSC subgroup was notably reduced by half (from I^2=68% to 39%), with the pooled HR adjusting to 2.26 (95% CI: 1.81–2.83) and an I^2 of 27%. These findings highlight the critical influence of specific studies on the heterogeneity of meta-analytic outcomes and underscore the importance of scrutinizing individual study contributions to the OS.

In addition, we explored the role of MDSCs as prognostic markers across various subgroups:

As shown in Table 2, MDSCs consistently demonstrated robust prognostic value for OS across all subgroups, except for non-small cell lung cancer (NSCLC), where the HR was 1.85 [95% CI 0.88–3.90]. For PFS, MDSCs showed strong predictive value, particularly in patients with advanced (stage IV) cancer, with an HR of 2.66 [95% CI 1.84–3.86]. Notably, MDSCs maintained low heterogeneity and high predictive value when the median cutoff method was employed.

In our detailed analysis (see Supplementary Table 1 for details), M-MDSC were identified as robust predictive markers for both OS and PFS in nearly all examined subgroups. In NSCLC specifically, M-MDSCs were predictive and prognostic for both outcome measures (OS: HR=2.55 [95% CI 1.36–4.78], PFS: HR=2.07 [95% CI 1.26–3.39]). Additionally, M-MDSCs showed strong predictive value for PFS across different cutoff determination methods (Cutoff method median: HR=1.96 [95% CI 1.40–2.72]; pooled different cutoff methods: HR=2.06 [95% CI 1.22–3.49]). Conversely, PMN-MDSCs were significant prognostic markers only in subgroups utilizing the median as the cutoff method, underscoring their potential as predictive markers in specific contexts (OS: HR=1.74 [95% CI 1.11–2.75]; PFS: HR= 2.29 [95% CI 1.39–3.77]).

3.5 Risk of bias

Our assessment of the risk of bias across various categories yielded heterogeneous outcomes, as detailed in Figures 4A, B. A notable observation was that the employment of non-standardized markers significantly elevated the risk of bias within the prognostic marker category. Specifically, the study attrition and confounder categories were identified as areas with a particularly high risk of

TABLE 1 Main characteristics of the 17 studies qualified to be included in this meta-analysis.

Author, year	Country	Cancer type	Stage	Immunotherapeutic agent (1=PD-1, 2=CTLA4, 3 PDL-1)	Sample size	Age$_a$	MDSC type	MDSC marker	Cutoff method	Cutoff value	Outcome	Data availability
Gaißler 2023 (31);	Germany	Melanoma	IV	(1)Pembrolizumab, (1) Nivolumab single or + (2) Ipilimumab	141	64	M-MDSC	M-MDSC: Lin- CD11b +/CD14+/CD33 +/HLA Drlow	other ‡	18,1% (%total mononuclear leucocytes)	PFS, OS	extracted paper
Tomela, 2023 (29);	Poland	Melanoma	III-IV	(1)Nivolumab, (1)Pembrolizumab	46	63 (32–92)	total MDSC M-MDSC PMN-MDSC	MDSC: CD11b+/HLA-DR −/low/CD33+, M-MDSC: CD14 +/CD33high/CD11b+/HLA-DR−/low and PMN-MDSC: CD66b +/CD33dim/CD11b+/HLA-DR−/low	Median	7.1%(total), 3% (PMN-MDSC), 4.1% (M-MDSC) (% alive PBMC)	PFS	calculated
Petrova, 2023 (30);	Germany	Melanoma	III-IV	(1)Pembrolizumab, (1)Nivolumab single or + (3)Ipilimumab	29	64 (41–84),	M-MDSC, PMN-MDSC	M-MDSC: HLA-DRlow/ −CD33highCD14+ PMN-MDSC: HLA-DRlow/ −CD33dimCD66b+Lin−;	Median	0.54% (PMN-MDSC) 0.73% (M-MDSC) (%alive PBMC)	PFS, OS	Extracted paper◆
Girardi, 2022 (32);	USA	Urothelian carcinoma	IV	(1)Nivolumab+Cabozantinib	30	64.5 (47–80)	M-MDSC PMN-MDSC	M-MDSC: CD14+ CD11b+ HLA−DRlow/− CD15−. PMN-MDSC: CD14− CD11b + CD15+;	Median	NR	PFS, OS	calculated
Bronte, 2022 (33);	Italy	NSCLC	III-IV	(1)Pembrolizumab, (1)Nivolumab (3)Atezolizumab, Combination	22	70.1 (64.8–75.0)	M-MDSC	M-MDSC: CD14 + HLA-DR − /lowCD11b + CD33 +	Median	1.9% (%CD45+)	PFS, OS	extracted paper
Araujo, 2021 (35);	Denmark	Solid tumor	mixed	mixed (1,2,3)	33	60 (36 -75)	M-MDSC	M-MDSC: CD14+ CD3- CD19- HLA-DR low, CD56-	Median	NR (% alive PBMC)	PFS, OS	extracted paper
Krebs, 2021 (34);	Germany	Melanoma	III-IV	(2)Ipilimumab (1,2)Ipilimumab/Nivolumab (1)Pembrolizumab, (1)Nivolumab	45	70 (27–86)	PMN-MDSC	PMN-MDSC: CD15+CD33+;	Median	0.5% (% alive PBMC)	OS	Calculated
de Coaña, 2020 (37);	Sweden	Melanoma	IV	(1)Nivolumab, (1)Pembrolizumab	36	68.5 (37–83)	M-MDSC PMN-MDSC	M-MDSC: CD14+HLA-DRlow/-; PMN-MDSC: NR	cutoff finder software	0.09% (PMN-MDSC), 10.70% (M-MDSC), (% alive PBMC)	OS,	extracted paper
Koh, 2020 (39);	Korea	NSCLC	I-IV	(1)Nivolumab, (1)Pembrolizumab	132	62 (34–88)	M-MDSC PMN-MDSC	PMN-MDSC: Lin− CD15+ CD14− CD11b+ HLA-DR −/low;	Median	NR	PFS, OS	extracted paper

(Continued)

10.3389/fimmu.2024.1403771

TABLE 1 Continued

Author, year	Country	Cancer type	Stage	Immunotherapeutic agent (1=PD-1, 2=CTLA4, 3 PDL-1)	Sample size	Age$_a$	MDSC type	MDSC marker	Cutoff method	Cutoff value	Outcome	Data availability
								M-MDSC: Lin– CD15–CD14+ HLA-DR–/low				
Passaro et al., 2020 (38);	Italy	NSCLC	III-IV	(1)Nivolumab	53	64 (56–70)	PMN-MDSC	PMN-MDSC: SSClow Lin–/HLA-DR–/lowCD33+/CD13+/CD11b+/CD15+/CD14–	other	6 cell/µL	PFS, OS	extracted paper
Karzai, 2018 (40),	USA	Prostate Cancer	IV	(1)durvalumab + olaparib	17	66 (45–79)	MDSC	MDSC: CD3+–CD19–CD56–HLA-DR– CD11b+CD33+	Median	1.26% (% total viable cells)	PFS	calculated
de Coaña, 2017 (36);	Sweden	Melanoma	IV	(2)Ipilimumab	43	(23–80)	M-MDSC, PMN-MDSC	PMN-MDSC: Lin-CD14-CD11b+ CD33+ CD15+ HLA-DRlo/neg; M-MDSC: CD14+ HLA-DRlo/neg	cutoff finder software	2.3%(PMN-MDSC); 18.6% (M-MDSC), (% alive PBMC)	OS	extracted paper
Sade-Feldman, 2016 (42);	Israel	Melanoma	IV	(2)Ipilimumab	56	60.7	MDSC	MDSC: CD33+CD11b+HLA-DR-	Data distribution	55.5% (as the CD33+CD11b+ (%) of gated HLA-DR – cells)	OS	calculated
Weber, 2016 (41);	USA	Melanoma	III-IV	(1)Nivolumab	92	60	M-MDSC	M-MDSC: Lin-CD11b+/CD14+/HLA Drlow	Median	12.6% (% alive PBMC)	OS	calculated
Martens, 2016 (43);	Europe (multicentral)	Melanoma	IV	(2)Ipilimumab	209 (MDSC measured n=164)	58	M-MDSC	MDSC: Lin–CD14+HLA-DR+–/niedrig	Other	5.1% (NR)	OS	extracted paper
Santegoets, 2014 (44);	Netherlands	Prostate Cancer	IV	(2) Ipilimumab + GVAX	28	NR	M-MDSC	M-MDSC: Lin- CD14+ HLA-DR-/low,	Cox regression	0.3% (NR)	OS	extracted paper
Kitano, 2014 (45);	USA	Melanoma	III-IV	(2)Ipilimumab	68	62 (34–83)	M–MDSC	M-MDSC: Lin- CD14+CD11b+ HLA-DRlow/-	Log-Rank-Statistic	14.9% (%HLA-DR low/– in Lin-CD14+CD11b+)	OS	extracted paper

United states of America (USA); non-small cell lung cancer (NSCLC); GVAX vaccine; myeloid-derived suppressor cells (MDSC); monocytic MDSC (M-MDSC); polymorphonuclear (PMN-MDSC); Peripheral blood mononuclear cells (PBMC); Programmed Cell Death Protein 1 (PD-1), Programmed cell death ligand-1 (PD-L1), cytotoxic T-lymphocyte-associated Protein 4 (CTLA-4), not reported (NR).

10.3389/fimmu.2024.1403771

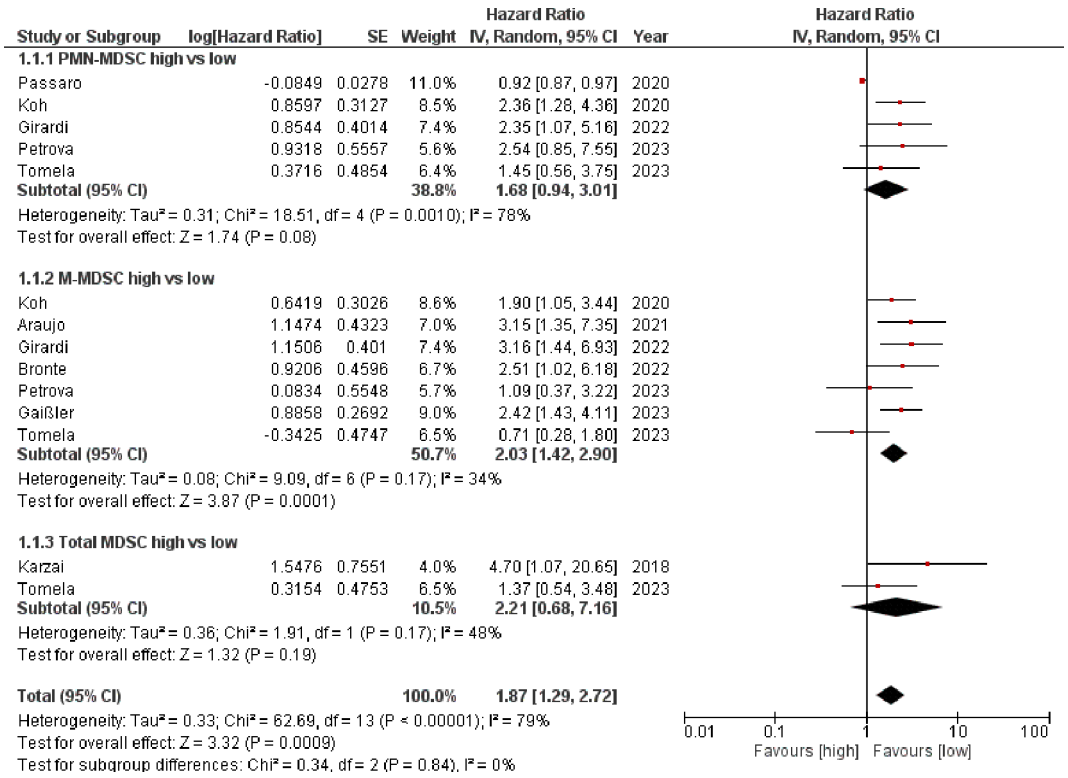

FIGURE 2
Forest plot illustrating the impact of myeloid-derived suppressor cell levels on progression-free survival in patients receiving immune checkpoint inhibitor therapy.

bias. This heightened risk was primarily attributed to inadequate descriptions of potential confounding variables or insufficient information regarding participants not included in the analysis. In the category of statistical analysis and reporting, a high risk of bias was frequently encountered; 8 out of 17 studies did not directly report hazard ratios, necessitating their estimation through the method proposed by Tierney et al. (25) or extracted from alternative sources. Specifically, hazard ratios were estimated for 6 studies using the Tierney et al. methodology, while for one study, hazard ratios were obtained from other published sources. Additionally, one study provided hazard ratios upon our direct request, highlighting the challenges and variability in data reporting practices across studies included in our meta-analysis.

3.6 Sensitivity analysis

To validate the reliability of our findings, we conducted a sensitivity analysis by excluding studies identified with a high risk of bias in any category. This stringent approach aimed to mitigate potential biases impacting our conclusions. Despite these exclusions, the pooled hazard ratios for both PFS and OS remained statistically significant, with PFS showing a hazard ratio of 2.59 [95% CI 1.73–3.87] and OS demonstrating a hazard ratio of 1.93 [95% CI 1.30–2.87]. However, heterogeneity remained in OS across all groups. This analysis was limited by the fact that PMN-MDSC or total MDSC could not be considered for PFS due to the lack of studies with low risk of bias here. The sensitivity analysis continues to show significant results, especially for the M-MDSC in OS: 2.23 [95% CI 1.49–3.35]. However, we observed persistent heterogeneity in OS across all evaluated groups, indicating variability that could not be fully accounted for by excluding studies with high bias risk.

A limitation of our sensitivity analysis emerged when considering the specific subtypes of MDSCs, particularly PMN-MDSC and total MDSC, for PFS outcomes. The absence of studies with a low risk of bias for these subgroups precluded their evaluation, underscoring a gap in the available literature. Despite these constraints, the sensitivity analysis underscored the significance of M-MDSC in predicting OS, with a hazard ratio of 2.23 [95% CI 1.49–3.35], reinforcing the potential prognostic value of this MDSC subtype in the context of immune checkpoint inhibitor therapy.

3.7 Publication bias

The analysis of OS and PFS data revealed asymmetry in the funnel plots, indicative of potential publication bias or other small-study effects (Figures 5A, B). This observation was further substantiated by the results of the Egger test, which demonstrated statistical significance with P<0.001 for PFS and P< 0.001 for OS, suggesting the presence of bias in the reported. In alignment with our predefined protocol, we employed the trim-and-fill method as a

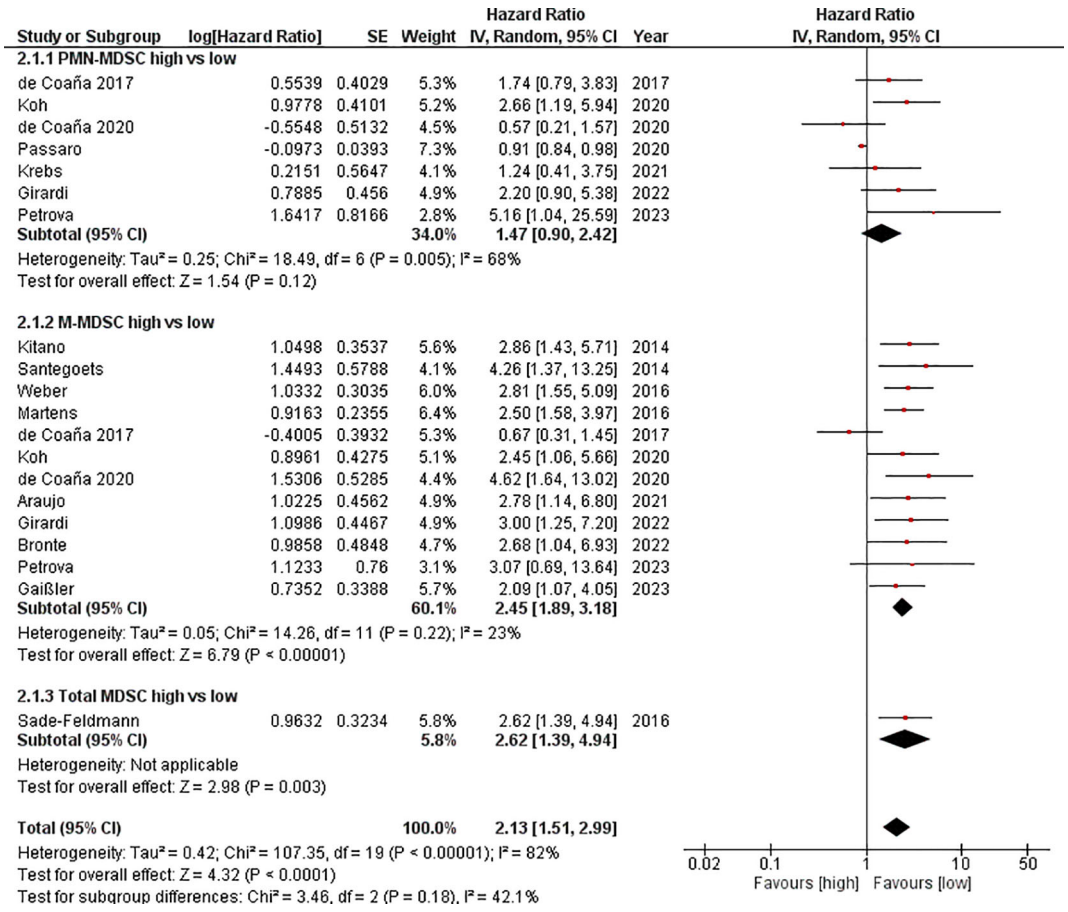

FIGURE 3
Forest plot illustrating the impact of myeloid-derived suppressor cell levels on overall survival in patients receiving immune checkpoint inhibitor therapy.

corrective measure to address this asymmetry, aiming to estimate the effect of potentially unpublished studies on our meta-analysis outcomes. The application of this method led to adjusted hazard ratios (HR) of 1.72 (95%CI 1.23, 2.41) for the PFS and 1.89 (95%CI 1.39, 2.58) for the OS. These revised estimates further underscore the robustness and statistical significance of our findings, reinforcing the predictive value of MDSC levels on the outcomes of patients undergoing immune checkpoint inhibitor therapy, even after accounting for potential publication bias.

4 Discussion

In our systematic review, we included 17 studies from which we were able to extract data for a meta-analysis. We included data from patients with melanoma (29–31, 34, 36, 37, 41–43, 45), NSCLC (33, 38, 39) prostate cancer (40, 44) and urothelial carcinoma (32). One study pooled data from solid tumors encompassing patients with 11 tumor entities (35).

Our findings indicate that MDSCs can predict both survival and response to ICIs, according to our endpoints of OS and PFS. Particularly, M-MDSCs are shown to be both a predictive and a prognostic marker. Analysis of the sub-cell populations revealed that M-MDSCs are significantly inversely correlated with OS and PFS. Although PMN-MDSCs did not reach statistical significance in our analysis, a trend was observed for both OS and PFS, suggesting the entire MDSC population as significant.

This meta-analysis aligns with previous meta-analyses that investigated MDSCs as predictive and prognostic markers in patients predominantly undergoing chemotherapy (9, 46).

The study of Koh et al. highlighted that M-MDSCs have even better predictive power of response and survival in NSCLC patients than PD-L1 expression on tumor cells (39), suggesting that MDSCs could enhance the predictive accuracy for OS and response rate across various tumor entities. Thus, the currently established markers such as PDL (in NSCLC) or LDH (in melanoma) could be supported by MDSC to predict a better correlation for OS and response rate in other tumor entities, as it has already been shown that patients (NSCLC) with a low PDL status also benefit from ICI (47).

The significance of our findings is underscored by Krebs et al. (34), who identified a subgroup of clinical non-responders to ICI, with an immune profile akin to responders, thus exhibiting prolonged OS. Similarly, Tomela et al. (29), found an inverse correlation between PMN-MDSC levels and PFS in the responder group.

10.3389/fimmu.2024.1403771

TABLE 2 Subgroup analysis of myeloid-derived suppressor cell and progression free survival or overall survival.

Subgroup	No Studies	No Patients	Random/ Fixed Model	PFS: pooled HR [95%CI]	I^2=	P Value	Random/ Fixed Model	OS: pooled HR [95%CI]	I^2=	P-Value
Melanoma	10	720	Fixed	1.66 [1.18, 2.33]	24%	0.003	Random	2.03 [1.46, 2.83]	51%	< 0.001
NSCLC	3	207	Random	1.68 [0.90, 3.13]	84%	0.10	Random	1.85 [0.88, 3.90]	82%	0.11
Cancer stage IV	8	515	Fixed	2.66 [1.84, 3.86]	0%	<0.001	Random	2.01 [1.39, 2.92]	56%	< 0.001
PD-1/PDL-1	8	428	Random	1.75 [1.15, 2.67]	77%	0.009	Random	2.04 [1.20, 3.48]	84%	0.009
CTLA-4	5	359		N/A	N/A	N/A	Random	2.09 [1.34, 3.27]	58%	0.001
Study population >median (n=45)	9	797	Random	1.48 [0.95, 2.30]	79%	0.09	Random	2.08 [1.28, 3.39]	88%	0.003
Study population <Median (n=44)	8	283	Fixed	2.56 [1.80, 3.65]	0%	<0.001	Random	2.14 [1.38, 3.32]	53%	< 0.001
Cutoff method: Median	9	446	Fixed	2.04 [1.60, 2.60]	5%	<0.001	Fixed	2.60 [1.96, 3.46]	0%	< 0.001
Cutoff method: other •	8	589	Random	1.44 [0.56, 3.71]	92%	0.45	Random	1.79 [1.13, 2.85]	86%	0.01
Western countries	16	903	Random	1.83 [1.21, 2.77]	78%	0.004	Random	2.08 [1.45, 2.99]	83%	< 0.001

Overall survival (OS); progression free survival (PFS); Hazard ratio (HR); 95% Confidence interval (95% CI); [lower limit of 95% CI, upper limit of 95% CI];•including Data distribution, Log-Rank statistic, Cox regression; not applicable (N/A).

Further research with a standardized gating strategy is crucial for establishing validated cut-off limits for MDSCs, thus facilitating their application in clinical practice as a dynamic prognostic marker. This could help identify patients who might benefit from ICI therapy or those at high risk of non-response, potentially making MDSCs a therapeutic target. The feasibility of this approach has been demonstrated by Tobin et al. (48). and the consideration of a cut-off value defined by healthy subjects as practiced by Kitano et al. (45) is also suggested.

Our analysis encountered significant heterogeneity, particularly notable within the PMN-MDSC subgroup. This variability arose partly from the diverse methods used across studies to define cut-off values, typically applying these thresholds as percentages of living peripheral blood mononuclear cells (PBMCs). Such methodological disparities were a key factor contributing to the observed heterogeneity.

Moreover, the landscape of immunotherapy, particularly with the introduction of ipilimumab in 2011, has undergone significant evolution. This breakthrough marked the beginning of an era characterized by the development and approval of various immune checkpoint inhibitors (ICIs), each with distinct indications. The evolving use of ICIs, including their combination therapies and earlier application in treatment protocols, has led to diverse study designs and populations. These changes reflect the dynamic nature of cancer treatment protocols and have inevitably influenced the heterogeneity observed in our meta-analysis.

This heterogeneity underscores the complexity of drawing generalized conclusions from the available data and highlights the need for standardized approaches in future research. This heterogeneity was addressed using a random effects model, as noted in the protocol, aiming to minimize its impact.

Lower MDSC correlated with a better prognosis, but it has not yet been possible to find a uniform cut-off value to use and implement the cell population as a clinically marker.

Subgroup analyses revealed significant effects for PFS and OS for both M-MDSC and PMN-MDSC populations when studies utilized consistent methods for determining cutoffs, with low heterogeneity. Notably, heterogeneity was attributed not only to tumor entities but also to inherent characteristics within each entity, though limited to NSCLC and melanoma due to the number of studies. Variations in the methodologies used to categorize PMN-MDSC, particularly in terms of gating strategies and the markers employed, have contributed to the observed heterogeneity in our analysis. An illustrative example is the approach taken by Passaro et al. (38), which stood out by utilizing absolute cell counts instead of percentage values for defining PMN-MDSC levels. This deviation underscores the broader issue of inconsistency in measurement techniques across studies, which adds to the challenge of synthesizing data and drawing uniform conclusions.

Despite the significant heterogeneity introduced by such methodological differences, our rigorous assessment process

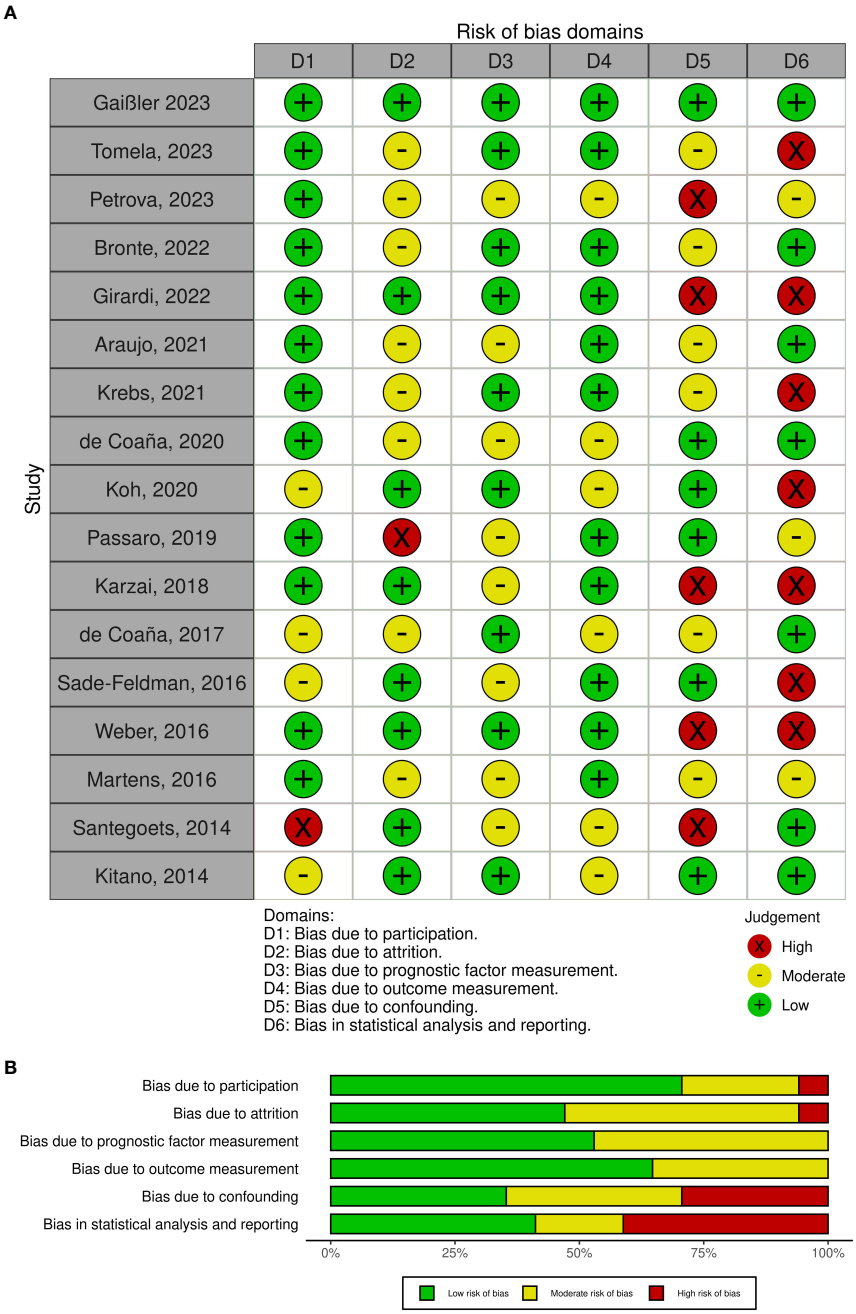

FIGURE 4
(A) Risk of bias summary plot. **(B)** Risk of bias assessment using the QUIPS tool.

confirmed that the study by Passaro et al. satisfied all predefined inclusion criteria. Therefore, in adherence to our commitment to a comprehensive and inclusive review, we retained the study by Passaro et al. within our meta-analysis. This decision reflects our endeavor to capture a wide spectrum of data and insights, even when faced with high heterogeneity, to ensure the robustness and breadth of our analysis.

In recent years, there has been a growing consensus regarding the identification of similar subpopulations of MDSCs using specific markers (10). This emerging agreement highlights the need for standardized markers to distinguish MDSC subpopulations clearly, especially to avoid confusion with neutrophils. A uniform marker, such as Lox-1, could serve this purpose effectively by providing a clear distinction. Additionally, the adoption of a myeloid score, which incorporates multiple validated markers as proposed by Huber et al., could offer a more nuanced understanding of MDSCs' role within the immune system (49). Furthermore, considering the complex interplay within the immune system, an alternative approach involves using an index that not only assesses the immunosuppressive impact of myeloid cells but also includes cytotoxic cells. This comprehensive index, as utilized by Araujo et al. (35), offers a more holistic view of the immune landscape. Such

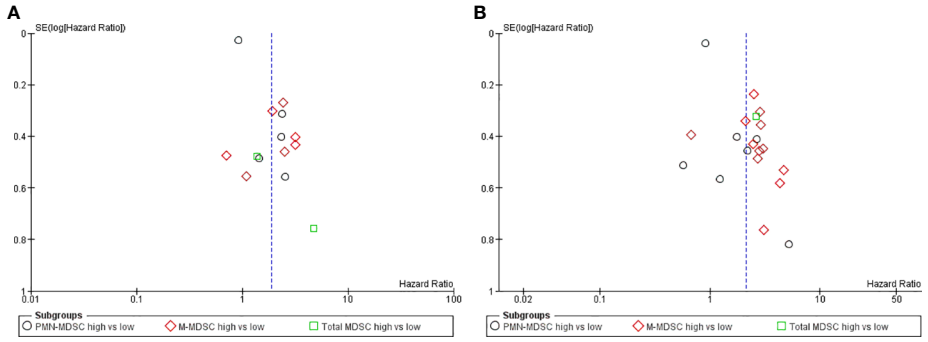

FIGURE 5
(A) Funnel plot progression free survival: Assessing the publication bias, the hazard ratio was plotted on the X-axis and the standard error corresponding to the logarithm of hazard ratio on the Y-axis. **(B)** Funnel plot overall survival: Assessing the publication bias, the hazard ratio was plotted on the X-axis and the standard error corresponding to the logarithm of hazard ratio on the Y-axis.

an index has the potential not only to enhance our understanding of the immune system's dynamics but also to serve as a valuable prognostic tool throughout the course of a disease. This multi-faceted approach acknowledges the intricate nature of immune responses and the importance of a comprehensive evaluation for both research and clinical applications (35). Here, the PMN-MDSC group is not significant, so they are not as immunosuppressive as initially expected and possibly the M-MDSC population takes on this characteristic. The two subgroups of MDSCs differ not only in terms of their phenotype, but also in terms of their mechanism of action: while PMN-MDSC are mainly antigen-specific, M-MDSC can be both antigen-specific and antigen-nonspecific (11). These differences may be the reason why PMN-MDSCs did not reach significance in this analysis: some studies have shown a stronger immunosuppressive capacity of M-MDSCs compared to PMN-MDSCs on T cells (16, 50, 51). This could explain the difference in significance in general, as T-cells are the main effectors in ICI. Bronte et al. (46) also note that M-MDSCs have been shown to have a continuous immunosuppressive effect on neoantigen-specific T cells (46, 52). Neoantigen load was negatively correlated with outcome in NSCLC patients (46, 53), suggesting that neoantigen inhibition is more relevant specifically in this tumor subgroup, which can only be addressed by M-MDSCs. This could be the reason for the altered behavior of PMN-MDSCs especially in this patient population. In addition, it should also be noted that the number of studies on PMN-MDSCs in this meta-analysis was relatively small and that the elimination of the study by Passaro et al. (38) as part of a sensitivity analysis increased the prognostic and predictive relevance of PMN-MDSCs.

Studies like Gaißler et al. highlight the prognostic significance of M-MDSC dynamics, showing that patients with initially high MDSC levels but subsequent reductions can achieve similar OS to those with consistently low levels (31). This is corroborated by findings from de Coaña (2017) et al.; after three weeks of therapy patients with lower M-MDSC had a better OS (HR= 2.89 (1.59–6.99) P= 0.002), nevertheless the baseline was not significant (36). The study conducted by Tarhini et al. (54) presents findings that align with a key observation: a significant reduction in the levels of total MDSCs is associated with improved PFS. This indicates that patients who experience a larger decrease in MDSC levels tend to have a longer period without disease progression, underscoring the potential role of MDSCs as dynamic biomarkers for treatment outcomes in cancer therapy.

The limitations of our study include several critical aspects that affect the interpretation and reliability of our results. Firstly, the variability of markers in our meta-analysis posed a significant challenge. Since 2016, there has been a convergence towards the use of standardized markers and gating strategies for MDSCs and their subpopulations, as recommended by Bronte et al. (10). Future research should adhere to these standardized markers to reduce variability. Secondly, our meta-analysis showed a high degree of heterogeneity, possible due to the use of different markers, study designs, and populations. We used a random effects model to address this issue. Furthermore, the assessment of risk of bias added complexity. The observed heterogeneous results necessitated a sensitivity analysis to assess the robustness of our results, particularly with regard to discrepancies in hazard ratio reporting. Seven of the 17 studies did not report hazard ratios with 95% confidence intervals. For one study we were able to obtain this by contacting the author, whereas for the remaining six studies we had to estimate it from Kaplan-Meier curves or other sources. This led to some uncertainty, which we considered in our risk of bias analysis. In addition, our analysis raised concerns about publication bias. Visual inspection of the funnel plot for OS and PFS indicated possible publication bias, which was confirmed by the Egger test. We estimated the impact of unpublished studies using Duval and Tweedie's trim-and-fill method.

In conclusion, the role of MDSCs, especially M-MDSCs, has been increasingly recognized and validated in the context of cancer immunotherapy. These cells have emerged as significant prognostic markers for predicting the response to immune checkpoint inhibitors. Their utility extends beyond mere prognostication; MDSCs offer a window into identifying patients who may not initially respond to therapy based on their baseline myeloid cell profiles. Such insights are invaluable for tailoring treatment approaches, potentially guiding the escalation of therapy to overcome resistance mechanisms.

Furthermore, MDSCs present a dynamic aspect of the tumor microenvironment that could be monitored over the course of treatment. By observing changes in MDSC levels, clinicians can gain insights into treatment efficacy in real-time, allowing for adjustments to therapy that could enhance outcomes. The potential of MDSCs extends to their viability as therapeutic targets themselves, suggesting that manipulating their levels or function could directly improve the efficacy of ICIs.

Despite the promising horizon that MDSCs represent in the realm of cancer therapy, several challenges remain. A critical barrier to the clinical integration of MDSCs as a biomarker is the lack of standardization in identifying and quantifying these cells. The field would greatly benefit from consensus on the markers used to define MDSC subpopulations and uniform cutoff methods to categorize their levels accurately. Addressing these challenges through future research is essential to harnessing the full potential of MDSCs in improving patient outcomes. By establishing standardized methodologies and integrating MDSC assessments into clinical practice, we can move closer to a future where cancer therapy is more personalized, predictive, and potent.

Data availability statement

The original contributions presented in the study are included in the article/Supplementary Material. Further inquiries can be directed to the corresponding author.

Author contributions

MM: Writing – original draft. VO: Writing – original draft. VU: Writing – review & editing. SH: Writing – review & editing. VB: Writing – review & editing. CR: Writing – review & editing. JH: Writing – original draft. SS: Writing – original draft.

Funding

The author(s) declare that no financial support was received for the research, authorship, and/or publication of this article.

Conflict of interest

The authors declare that the research was conducted in the absence of any commercial or financial relationships that could be construed as a potential conflict of interest.

Publisher's note

Supplementary material

The Supplementary Material for this article can be found online at: https://www.frontiersin.org/articles/10.3389/fimmu.2024.1403771/full#supplementary-material

References

1. Global Burden of Disease Cancer C, Kocarnik JM, Compton K, Dean FE, Fu W, Gaw BL, et al. Cancer incidence, mortality, years of life lost, years lived with disability, and disability-adjusted life years for 29 cancer groups from 2010 to 2019: A systematic analysis for the global burden of disease study 2019. *JAMA Oncol.* (2022) 8:420–44. doi: 10.1001/jamaoncol.2021.6987

2. Leach DR, Krummel MF, Allison JP. Enhancement of antitumor immunity by CTLA-4 blockade. *Science.* (1996) 271:1734–6. doi: 10.1126/science.271.5256.1734

3. Topalian SL, Drake CG, Pardoll DM. Targeting the PD-1/B7-H1(PD-L1) pathway to activate anti-tumor immunity. *Curr Opin Immunol.* (2012) 24:207–12. doi: 10.1016/j.coi.2011.12.009

4. Hodi FS, O'Day SJ, McDermott DF, Weber RW, Sosman JA, Haanen JB, et al. Improved survival with ipilimumab in patients with metastatic melanoma. *N Engl J Med.* (2010) 363:711–23. doi: 10.1056/NEJMoa1003466

5. SChadendorf D, Hodi FS, Robert C, Weber JS, Margolin K, Hamid O, et al. Pooled analysis of long-term survival data from phase II and phase III trials of ipilimumab in unresectable or metastatic melanoma. *J Clin Oncol.* (2015) 33:1889–94. doi: 10.1200/JCO.2014.56.2736

6. Gandhi L, Rodriguez-Abreu D, Gadgeel S, Esteban E, Felip E, De Angelis F, et al. Pembrolizumab plus chemotherapy in metastatic non-small-cell lung cancer. *N Engl J Med.* (2018) 378:2078–92. doi: 10.1056/NEJMoa1801005

7. Chevolet I, Speeckaert R, Schreuer M, Neyns B, Krysko O, Bachert C, et al. Clinical significance of plasmacytoid dendritic cells and myeloid-derived suppressor cells in melanoma. *J Transl Med.* (2015) 13:9. doi: 10.1186/s12967-014-0376-x

8. Shang B, Liu Y, Jiang SJ, Liu Y. Prognostic value of tumor-infiltrating FoxP3+ regulatory T cells in cancers: a systematic review and meta-analysis. *Sci Rep.* (2015) 5:15179. doi: 10.1038/srep15179

9. Wang PF, Song SY, Wang TJ, Ji WJ, Li SW, Liu N, et al. Prognostic role of pretreatment circulating MDSCs in patients with solid Malignancies: A meta-analysis of 40 studies. *Oncoimmunology.* (2018) 7:e1494113. doi: 10.1080/2162402X.2018.1494113

10. Bronte V, Brandau S, Chen SH, Colombo MP, Frey AB, Greten TF, et al. Recommendations for myeloid-derived suppressor cell nomenclature and characterization standards. *Nat Commun.* (2016) 7:12150. doi: 10.1038/ncomms12150

11. Gabrilovich DI. Myeloid-derived suppressor cells. *Cancer Immunol Res.* (2017) 5:3–8. doi: 10.1158/2326-6066.CIR-16-0297

12. Valenti R, Huber V, Iero M, Filipazzi P, Parmiani G, Rivoltini L. Tumor-released microvesicles as vehicles of immunosuppression. *Cancer Res.* (2007) 67:2912–5. doi: 10.1158/0008-5472.CAN-07-0520

13. Fleming V, Hu X, Weller C, Weber R, Groth C, Riester Z, et al. Melanoma extracellular vesicles generate immunosuppressive myeloid cells by upregulating PD-L1 via TLR4 signaling. *Cancer Res.* (2019) 79:4715–28. doi: 10.1158/0008-5472.CAN-19-0053

14. Condamine T, Dominguez GA, Youn JI, Kossenkov AV, Mony S, Alicea-Torres K, et al. Lectin-type oxidized LDL receptor-1 distinguishes population of human polymorphonuclear myeloid-derived suppressor cells in cancer patients. *Sci Immunol.* (2016) 1:aaf8943. doi: 10.1126/sciimmunol.aaf8943

15. Noman MZ, Desantis G, Janji B, Hasmim M, Karray S, Dessen P, et al. PD-L1 is a novel direct target of HIF-1alpha, and its blockade under hypoxia enhanced MDSC-mediated T cell activation. *J Exp Med.* (2014) 211:781–90. doi: 10.1084/jem.20131916

16. Movahedi K, Guilliams M, Van den Bossche J, Van den Bergh R, Gysemans C, Beschin A, et al. Identification of discrete tumor-induced myeloid-derived suppressor cell subpopulations with distinct T cell-suppressive activity. *Blood.* (2008) 111:4233–44. doi: 10.1182/blood-2007-07-099226

17. Gabrilovich DI, Ostrand-Rosenberg S, Bronte V. Coordinated regulation of myeloid cells by tumours. *Nat Rev Immunol*. (2012) 12:253–68. doi: 10.1038/nri3175

18. Nagaraj S, Gupta K, Pisarev V, Kinarsky L, Sherman S, Kang L, et al. Altered recognition of antigen is a mechanism of CD8+ T cell tolerance in cancer. *Nat Med*. (2007) 13:828–35. doi: 10.1038/nm1609

19. Youn JI, Nagaraj S, Collazo M, Gabrilovich DI. Subsets of myeloid-derived suppressor cells in tumor-bearing mice. *J Immunol*. (2008) 181:5791–802. doi: 10.4049/jimmunol.181.8.5791

20. Pan PY, Ma G, Weber KJ, Ozao-Choy J, Wang G, Yin B, et al. Immune stimulatory receptor CD40 is required for T-cell suppression and T regulatory cell activation mediated by myeloid-derived suppressor cells in cancer. *Cancer Res*. (2010) 70:99–108. doi: 10.1158/0008-5472.CAN-09-1882

21. Lasser SA, Ozbay Kurt FG, Arkhypov I, Utikal J, Umansky V. Myeloid-derived suppressor cells in cancer and cancer therapy. *Nat Rev Clin Oncol*. (2024) 21:147–64. doi: 10.1038/s41571-023-00846-y

22. De Sanctis F, Solito S, Ugel S, Molon B, Bronte V, Marigo I. MDSCs in cancer: Conceiving new prognostic and therapeutic targets. *Biochim Biophys Acta*. (2016) 1865:35–48. doi: 10.1016/j.bbcan.2015.08.001

23. Ozbay Kurt FG, Lasser S, Arkhypov I, Utikal J, Umansky V. Enhancing immunotherapy response in melanoma: myeloid-derived suppressor cells as a therapeutic target. *J Clin Invest*. (2023) 133. doi: 10.1172/JCI170762

24. Kumar V, Patel S, Tcyganov E, Gabrilovich DI. The nature of myeloid-derived suppressor cells in the tumor microenvironment. *Trends Immunol*. (2016) 37:208–20. doi: 10.1016/j.it.2016.01.004

25. Tierney JF, Stewart LA, Ghersi D, Burdett S, Sydes MR. Practical methods for incorporating summary time-to-event data into meta-analysis. *Trials*. (2007) 8:16. doi: 10.1186/1745-6215-8-16

26. Hayden JA, van der Windt DA, Cartwright JL, Cote P, Bombardier C. Assessing bias in studies of prognostic factors. *Ann Intern Med*. (2013) 158:280–6. doi: 10.7326/0003-4819-158-4-201302190-00009

27. Deeks JJ, Higgins JP, Altman DG. Chapter 10.10 heterogeneity. In: Higgins JP, Thomas J, Chandler J, Cumpston M, Li T, Page MJ, Welch VA, editors. *Cochrane Handbook for Systematic Reviews of Interventions Version 6.2 (updated February 2021). Cochrane, 2021*. London (GB): The Cochrane Collaboration (2021). Available at: http://training.cochrane.org/handbook.

28. McGuinness LA, Higgins JPT. Risk-of-bias VISualization (robvis): An R package and Shiny web app for visualizing risk-of-bias assessments. *Res Synth Methods*. (2021) 12:55–61. doi: 10.1002/jrsm.1411

29. Tomela K, Pietrzak B, Galus Ł, Mackiewicz J, Schmidt M, Mackiewicz AA, et al. Myeloid-derived suppressor cells (MDSC) in melanoma patients treated with anti-PD-1 immunotherapy. *Cells*. (2023) 12:789. doi: 10.3390/cells12050789

30. Petrova V, Groth C, Bitsch R, Arkhypov I, Simon SCS, Hetjens S, et al. Immunosuppressive capacity of circulating MDSC predicts response to immune checkpoint inhibitors in melanoma patients. *Front Immunol*. (2023) 14:1065767. doi: 10.3389/fimmu.2023.1065767

31. Gaißler A, Bochem J, Spreuer J, Ottmann S, Martens A, Amaral T, et al. Early decrease of blood myeloid-derived suppressor cells during checkpoint inhibition is a favorable biomarker in metastatic melanoma. *J Immunother Cancer*. (2023) 11:e006802. doi: 10.1136/jitc-2023-006802

32. Girardi DM, Niglio SA, Mortazavi A, Nadal R, Lara P, Pal SK, et al. Cabozantinib plus nivolumab phase I expansion study in patients with metastatic urothelial carcinoma refractory to immune checkpoint inhibitor therapy. *Clin Cancer Res*. (2022) 28:1353–62. doi: 10.1158/1078-0432.CCR-21-3726

33. Bronte G, Petracci E, De Matteis S, Canale M, Zampiva I, Priano I, et al. High levels of circulating monocytic myeloid-derived suppressive-like cells are associated with the primary resistance to immune checkpoint inhibitors in advanced non-small cell lung cancer: an exploratory analysis. *Front Immunol*. (2022) 13:866561. doi: 10.3389/fimmu.2022.866561

34. Krebs FK, Trzeciak ER, Zimmer S, Özistanbullu D, Mitzel-Rink H, Meissner M, et al. Immune signature as predictive marker for response to checkpoint inhibitor immunotherapy and overall survival in melanoma. *Cancer Med*. (2021) 10:1562–75. doi: 10.1002/cam4.3710

35. Araujo B, Hansen M, Spanggaard I, Rohrberg K, Reker Hadrup S, Lassen U, et al. Immune cell profiling of peripheral blood as signature for response during checkpoint inhibition across cancer types. *Front Oncol*. (2021) 11:558248. doi: 10.3389/fonc.2021.558248

36. de Coaña YP, Wolodarski M, Poschke I, Yoshimoto Y, Yang Y, Nyström M, et al. Ipilimumab treatment decreases monocytic MDSCs and increases CD8 effector memory T cells in long-term survivors with advanced melanoma. *Oncotarget*. (2017) 8:21539–53. doi: 10.18632/oncotarget.v8i13

37. Pico de Coaña Y, Wolodarski M, van der Haar Àvila I, Nakajima T, Rentouli S, Lundqvist A, et al. PD-1 checkpoint blockade in advanced melanoma patients: NK cells, monocytic subsets and host PD-L1 expression as predictive biomarker candidates. *Oncoimmunology*. (2020) 9:1786888. doi: 10.1080/2162402X.2020.1786888

38. Passaro A, Mancuso P, Gandini S, Spitaleri G, Labanca V, Guerini-Rocco E, et al. Gr-MDSC-linked asset as a potential immune biomarker in pretreated NSCLC receiving nivolumab as second-line therapy. *Clin Transl Oncol*. (2020) 22:603–11. doi: 10.1007/s12094-019-02166-z

39. Koh J, Kim Y, Lee KY, Hur JY, Kim MS, Kim B, et al. MDSC subtypes and CD39 expression on CD8(+) T cells predict the efficacy of anti-PD-1 immunotherapy in patients with advanced NSCLC. *Eur J Immunol*. (2020) 50:1810–9. doi: 10.1002/eji.202048534

40. Karzai F, VanderWeele D, Madan RA, Owens H, Cordes LM, Hankin A, et al. Activity of durvalumab plus olaparib in metastatic castration-resistant prostate cancer in men with and without DNA damage repair mutations. *J Immunother Cancer*. (2018) 6:141. doi: 10.1186/s40425-018-0463-2

41. Weber J, Gibney G, KudChadkar R, Yu B, Cheng P, Martinez AJ, et al. Phase I/II study of metastatic melanoma patients treated with nivolumab who had progressed after ipilimumab. *Cancer Immunol Res*. (2016) 4:345–53. doi: 10.1158/2326-6066.CIR-15-0193

42. Sade-Feldman M, Kanterman J, Klieger Y, Ish-Shalom E, Olga M, Saragovi A, et al. Clinical significance of circulating CD33+CD11b+HLA-DR- myeloid cells in patients with stage IV melanoma treated with ipilimumab. *Clin Cancer Res*. (2016) 22:5661–72. doi: 10.1158/1078-0432.CCR-15-3104

43. Martens A, Wistuba-Hamprecht K, Geukes Foppen M, Yuan J, Postow MA, Wong P, et al. Baseline peripheral blood biomarkers associated with clinical outcome of advanced melanoma patients treated with ipilimumab. *Clin Cancer Res*. (2016) 22:2908–18. doi: 10.1158/1078-0432.CCR-15-2412

44. Santegoets SJ, Stam AG, Lougheed SM, Gall H, Jooss K, Sacks N, et al. Myeloid derived suppressor and dendritic cell subsets are related to clinical outcome in prostate cancer patients treated with prostate GVAX and ipilimumab. *J Immunother Cancer*. (2014) 2:31. doi: 10.1186/s40425-014-0031-3

45. Kitano S, Postow MA, Ziegler CG, Kuk D, Panageas KS, Cortez C, et al. Computational algorithm-driven evaluation of monocytic myeloid-derived suppressor cell frequency for prediction of clinical outcomes. *Cancer Immunol Res*. (2014) 2:812–21. doi: 10.1158/2326-6066.CIR-14-0013

46. Bronte G, Calabro L, Olivieri F, Procopio AD, Crino L. The prognostic effects of circulating myeloid-derived suppressor cells in non-small cell lung cancer: systematic review and meta-analysis. *Clin Exp Med*. (2023) 23:1551–61. doi: 10.1007/s10238-022-00946-6

47. Doroshow DB, Sanmamed MF, Hastings K, Politi K, Rimm DL, Chen L, et al. Immunotherapy in non-small cell lung cancer: facts and hopes. *Clin Cancer Res*. (2019) 25:4592–602. doi: 10.1158/1078-0432.CCR-18-1538

48. Tobin RP, Cogswell DT, Cates VM, Davis DM, Borgers JSW, Van Gulick RJ, et al. Targeting MDSC differentiation using ATRA: A phase I/II clinical trial combining pembrolizumab and all-trans retinoic acid for metastatic melanoma. *Clin Cancer Res*. (2023) 29:1209–19. doi: 10.1158/1078-0432.CCR-22-2495

49. Huber V, Di Guardo L, Lalli L, Giardiello D, Cova A, Squarcina P, et al. Back to simplicity: a four-marker blood cell score to quantify prognostically relevant myeloid cells in melanoma patients. *J Immunother Cancer*. (2021) 9:e001167. doi: 10.1136/jitc-2020-001167

50. Wang SH, Lu QY, Guo YH, Song YY, Liu PJ, Wang YC. The blockage of Notch signalling promoted the generation of polymorphonuclear myeloid-derived suppressor cells with lower immunosuppression. *Eur J Cancer*. (2016) 68:90–105. doi: 10.1016/j.ejca.2016.08.019

51. Dolcetti L, Peranzoni E, Ugel S, Marigo I, Fernandez Gomez A, Mesa C, et al. Hierarchy of immunosuppressive strength among myeloid-derived suppressor cell subsets is determined by GM-CSF. *Eur J Immunol*. (2010) 40:22–35. doi: 10.1002/eji.200939903

52. Haverkamp JM, Smith AM, Weinlich R, Dillon CP, Qualls JE, Neale G, et al. Myeloid-derived suppressor activity is mediated by monocytic lineages maintained by continuous inhibition of extrinsic and intrinsic death pathways. *Immunity*. (2014) 41:947–59. doi: 10.1016/j.immuni.2014.10.020

53. Gong L, He R, Xu Y, Luo T, Jin K, Yuan W, et al. Neoantigen load as a prognostic and predictive marker for stage II/III non-small cell lung cancer in Chinese patients. *Thorac Cancer*. (2021) 12:2170–81. doi: 10.1111/1759-7714.14046

54. Tarhini AA, Edington H, Butterfield LH, Lin Y, Shuai Y, Tawbi H, et al. Immune monitoring of the circulation and the tumor microenvironment in patients with regionally advanced melanoma receiving neoadjuvant ipilimumab. *PloS One*. (2014) 9:e87705. doi: 10.1371/journal.pone.0087705

frontiers | Frontiers in Immunology

TYPE Original Research
PUBLISHED 11 July 2024
DOI 10.3389/fimmu.2024.1401097

OPEN ACCESS

EDITED BY
Paulo Rodrigues-Santos,
University of Coimbra, Portugal

REVIEWED BY
Lingeng Lu,
Yale University, United States
Kar Muthumani,
GeneOne Life Science, Inc.,
Republic of Korea

*CORRESPONDENCE
Margarita Zvirble
margarita.zvirble@gmail.com

†These authors share senior authorship

RECEIVED 14 March 2024
ACCEPTED 19 June 2024
PUBLISHED 11 July 2024

CITATION
Zvirble M, Survila Z, Bosas P, Dobrovolskiene N, Mlynska A, Zaleskis G, Jursenaite J, Characiejus D and Pasukoniene V (2024) Prognostic significance of soluble PD-L1 in prostate cancer. *Front. Immunol.* 15:1401097. doi: 10.3389/fimmu.2024.1401097

Prognostic significance of soluble PD-L1 in prostate cancer

Margarita Zvirble[1,2*], Zilvinas Survila[2], Paulius Bosas[3,4], Neringa Dobrovolskiene[1], Agata Mlynska[1,5], Gintaras Zaleskis[4], Jurgita Jursenaite[4], Dainius Characiejus[4,6†] and Vita Pasukoniene[1†]

[1]Laboratory of Immunology, National Cancer Institute, Vilnius, Lithuania, [2]Institute of Biosciences, Life Sciences Center, Vilnius University, Vilnius, Lithuania, [3]Department of Oncourology, National Cancer Institute, Vilnius, Lithuania, [4]Department of Immunology and Bioelectrochemistry, State Research Institute Centre for Innovative Medicine, Vilnius, Lithuania, [5]Department of Chemistry and Bioengineering, Vilnius Gediminas Technical University, Vilnius, Lithuania, [6]Department of Pathology and Forensic Medicine, Institute of Biomedical Sciences, Faculty of Medicine, Vilnius University, Vilnius, Lithuania

Purpose: The aim of this study was to assess the role of sPD-L1 and sPD-1 as potential biomarkers in prostate cancer (PCa). The association of the values of these soluble proteins were correlated to the clinical data: stage of disease, Gleason score, biochemical recurrence etc. For a comprehensive study, the relationship between sPD-L1 and sPD-1 and circulating immune cells was further investigated.

Methods: A total of 88 patients with pT2 and pT3 PCa diagnosis and 41 heathy men were enrolled. Soluble sPD-L1 and sPD-1 levels were measured in plasma by ELISA method. Immunophenotyping was performed by flow cytometry analysis.

Results: Our study's findings demonstrate that PCa patients had higher levels of circulating sPD-L1 and sPD-1 comparing to healthy controls ($p < 0.001$). We found a statistically significant ($p < 0.05$) relationship between improved progression free survival and lower initial sPD-L1 values. Furthermore, patients with a lower sPD-1/sPD-L1 ratio were associated with a higher probability of disease progression ($p < 0.05$). Additionally, a significant ($p < 0.05$) association was discovered between higher Gleason scores and elevated preoperative sPD-L1 levels and between sPD-1 and advanced stage of disease ($p < 0.05$). A strong correlation ($p < 0.05$), between immunosuppressive CD4+CD25+FoxP3+ regulatory T cells and baseline sPD-L1 was observed in patients with unfavorable postoperative course of the disease, supporting the idea that these elements influence each other in cancer progression. In addition to the postoperative drop in circulating PD-L1, the inverse relationship ($p < 0.05$), between the percentage of M-MDSC and sPD-L1 in patients with BCR suggests that M-MDSC is not a source of sPD-L1 in PCa patients.

Conclusion: Our findings suggest the potential of sPD-L1 as a promising prognostic marker in prostate cancer.

KEYWORDS

prostate cancer, soluble PD-L1 and PD-1, biomarkers, prognosis prediction, immune cells

1 Introduction

Prostate cancer (PCa) is still the second most prevalent type of cancer among men worldwide (1). Prostate specific antigen (PSA) is a widely used marker of diagnosis and prognosis in PCa, however there is evidence that changes in its levels are not related to survival outcomes (2) and PSA is often used mainly because of the lack of useful predictive markers (3).

Recently, soluble checkpoints PD-L1 and PD-1 (sPD-L1 and sPD-1), whose precursors are membrane bound PD-L1 and PD-1, have been the subject of intense research for their prognostic and predictive value in various cancers (4, 5). The dynamic alterations of membranous PD-L1 in the circulatory system, including sPD-L1 and other forms of PD-L1, are attributed to liquid biopsy technique (6).

Numerous cancer types have been found to have elevated sPD-L1 protein levels (7). A growing body of evidence revealed that patients with solid tumors and higher levels of soluble PD-L1 in their peripheral blood, have a significantly worse outcomes; this suggests that high levels of sPD-L1 could be a biomarker for poor prognosis (8, 9). In the meantime, patients with a variety of malignancies have higher levels of sPD-1 in their blood and pretherapeutic increase is associated to higher risk of cancer developing, the progression of the disease and a worse result, on the other hand, a stable or elevated sPD-1 levels following cancer treatment have been linked to better outcomes (5, 10, 11).

The origin of sPD-L1 remains unknown, as it could potentially originate from different sources, such as tumor cells (12, 13) and surrounding immune cells (7, 14) in particular, myeloid derived suppressive cells (MDSC) may serve as a natural source of sPD-L1 (15). Meanwhile human macrophages have been shown to express sPD-1 (16), other potential source of circulating sPD-1 is natural killer (NK) cells (17).

PCa is generally considered as an immunologically cold tumor with low PD-L1 expression, poor infiltration of immune T cells and with predominant immunosuppressive tumor microenvironment (TME) (18–23). T-regulatory cells (Tregs) and MDSC are prevailing immunosuppressive cells found within the TME (24) as well as in peripheral blood (25) of PCa. Insights into the interaction between cancer and the immune system may provide additional aspects of tumor development.

Despite the success of immunotherapy in other solid tumors, PCa treatment has shown limited response, particularly to single-agent checkpoint inhibition (20, 26). Radical prostatectomy (RP) and radiotherapy are the two most effective treatments for PCa that is primarily localized (27). The potential of sPD-L1 and sPD-1 as biomarkers for predicting treatment efficacy is suggested by changes in their levels following specific treatments, such as surgery, radiotherapy, and immunotherapy (5, 11). Even though PCa does not exhibit prominent PD-L1 expression, some scientific studies declares that sPD-L1, rather than membranous PD-L1, effectively predicts prognosis in other tumors (28).

Considering PCa as an immunologically cold tumor, the role of soluble PD-L1 and PD-1, and especially their association with peripheral blood immune cells, has not yet been thoroughly investigated in PCa tumors. The aim of this study was to evaluate the relationship between soluble PD-L1 and PD-1 molecules in the plasma of prostate cancer patients and their correlation with the clinical course of the disease. Additionally, we aimed to explore the association between soluble PD-L1 and PD-1 receptors and the immune status of patients. By unraveling these connections, our goal is to identify potential biomarkers that can inform the clinical progression of prostate cancer and shed light on the immune responses, paving the way for more targeted and personalized therapeutic interventions.

Abbreviations: PCa, Prostate cancer; PSA, Prostate specific antigen; sPD-1, soluble s-PD-1; sPD-L1, soluble PD-L1; TME, tumor microenvironment; MDSC, myeloid derived suppressive cells; NK, natural killer cells; Tregs, T-regulatory cells; RP, Radical prostatectomy; ADT, androgen deprivation therapy; BCR, Biochemical recurrence; PFS, progression free survival; ROC, receiver operating characteristic; mCRPC, Metastatic castration resistant prostate cancer; GC, Gastric cancer; HCC, Hepatocellular carcinoma; ccRCC, Clear cell renal cell carcinoma; OC, ovarian cancer; NSCLC, Non-small cell lung cancer; BC, breast cancer; OS, Overall survival; mCRC, metastatic colorectal cancer; AML, Acute myeloid leukemia; M-MDSC, monocytic myeloid derived suppressive cells, G-MDSC, granulocytic myeloid derived suppressive cells.

2 Materials and methods

2.1 Patients and healthy subjects

The study was approved by the Regional Review Board (Vilnius, Lithuania, 158200–17-928–442). All research methods were carried out in accordance with the relevant Lithuanian national guidelines and regulations. Written information about the study was provided to each study participant and written consent was obtained to participate in the study.

The inclusion criteria for patients were as follows (1) pT2 and pT3 PCa diagnosis. Exclusion criteria were as follows (1) history of other malignancies diagnosis or treatment; (2) androgen deprivation therapy (ADT), radiation therapy or chemotherapy prior to surgery and three months after surgery; (3) inflammatory conditions, immunosuppressive interventions, or autoimmune disease presence; (4) perioperative blood transfusions; (5) preoperative or postoperative white blood cell count exceeding 10,000 μL−1 (up to three months post-surgery); (6) abnormal levels of liver enzymes, glomerular filtration rate, C-reactive protein, or bilirubin, as previously described in preceding study involving the same cohort of patients (29).

All patients were followed up through clinic visits for 30 months following radical prostate excision. The starting point for follow-up was postoperative day 1. Endpoint events were as follows (1) biochemical recurrence (BCR); (2) failure of postoperative PSA to decrease to target < 0.2 ng/ml value; (3) the need of additional radiotherapy. Progression free survival (PFS) was defined as all above mentioned events.

Circulating preoperative and postoperative sPD-L1 and sPD-1 levels in PCa patients were compared with clinical-pathological data: Gleason score, biochemical recurrence (BCR), changes of prostate cancer antigen (PSA), need of radiation therapy, prostate cancer stage (pT2 and pT3), and associated to dynamic of alterations of immune cells (CD3+, CD4+, CD8+, CD19+, CD4+CD25+FoxP3+, CD3-CD16+CD56+, MDSC, CD8+CD69+), before surgery and three

months following radical prostatectomy (RP). The concentrations of soluble PD-L1 and PD-1, were also compared between healthy individuals and patients with prostate cancer.

The inclusion criteria for healthy controls were as follows: (1) similarity in age to the patient group (range: 47–76 years). Exclusion criteria were as follows (1) history of malignancy diagnosis or treatment; (2) inflammatory conditions, immunosuppressive interventions, or autoimmune disease presence; (3) use of immunosuppressive drugs: prednisolone, cyclosporine, etc.

2.2 Blood sampling

Soluble levels of sPD-L1 and sPD-1 were assessed in the peripheral blood of all participants in this study. The evaluation was carried out for patients at two time points: 0–1 day before surgery and approximately three months (82–107 days) after radical prostatectomy. Healthy subjects underwent a single assessment. Additionally, specific immune cell populations were examined in patients prior to surgery and at the three-month postoperative mark. Blood samples were collected from all participants by venipuncture into BD Vacutainer® tubes containing EDTA anticoagulant (BD Biosciences, San Jose, CA, USA). The tubes were gently shaken prior to the phenotypic staining procedure and subsequent flow cytometry analysis. Plasma for ELISA analysis was acquired through centrifugation, at 2500× g for 10 minutes and samples were stored at − 80°C until analysis of sPD-L1 and sPD-1 was performed. sPD-L1 and sPD-1 evaluation from cases and controls were processed simultaneously.

2.3 Analysis of soluble PD-L1 and PD-1

A commercially available human PD-L1 ELISA kit (Invitrogen, Thermo Fisher Scientific, Bender MedSystems GmbH Campus Vienna Biocenter, Vienna, Austria) was used to measure sPD-L1 protein concentrations in plasma. Similarly, a PD-1 human kit (Invitrogen, Thermo Fisher Scientific, Bender MedSystems GmbH Campus Vienna Biocenter, Vienna, Austria) was used to measure sPD-1 protein levels. The preparation of standards, samples, and all assay steps were conducted in accordance with the manufacturer's instructions. Each sample was analyzed in duplicate, and the optical density was assessed at 450 nm using a BioTek Elx800 TM plate reader (BIO-Tek Instruments, Inc. PO Box 998, Highland Park Winooski, Vermont, USA).

2.4 Analysis of immune cells

Whole blood samples, were used for flow cytometry analysis and processed in accordance with the manufacturer's guidelines. 100 µL of blood were added to each of the four flow cytometry tubes per patient and cell staining was conducted using the following antibodies. Tube 1: anti-CD25-PE/anti-CD4-FITC/anti-CD3-APC/anti-FoxP3-BV421™ (BioLegend, San Diego, CA, USA); tube 2: anti-CD8a-FITC/anti-CD69-APC/anti-CD3-BV510™ (BioLegend, San Diego, CA, USA); tube 3: anti-HLA-DR-PE/anti-CD14-FITC/anti-CD11b-BV421™/anti-CD33-APC (BioLegend, San Diego, CA, USA); tube 4: anti-CD56-PE/anti-CD16-APC/anti-CD3-FITC/anti-CD19-BV421™/anti-CD45-PerCP (BioLegend, San Diego, CA, USA). T regulatory cells were defined as $CD4^+$ $CD25^+$ $FoxP3^+$, NK cells as $CD3^-$ $CD16^+$ $CD56^+$, and total MDSCs as $CD45^+$ $CD3^-$ $CD19^-$ $CD56^-$ $CD16^-$ $HLA\text{-}DR^-$ $CD33^+$ $CD11b^+$. Cells were incubated with fluorescently labeled antibodies targeting cell surface markers, for 15 minutes in the darkness, to allow antibody binding. Subsequently, red blood cells were lysed for 15 minutes in the darkness using BD FACS Lysing solution (BD Biosciences, San Jose, CA, USA). Cells were washed twice to remove excess antibodies and lysing reagents in BD-Cell-Wash solution (BD Biosciences, San Jose, CA, USA) and then fixed in BD-Cell-Fix solution (BD Biosciences, San Jose, CA, USA). Immune components were analyzed by BD LSR II System flow cytometer (BD Biosciences, San Jose, CA, USA). Subset analysis was performed using BD FACSDivaTM Software (BD Biosciences, San Jose, CA, USA) with acquisition of a total of 20,000 events (29).

2.5 Statistics

The Shapiro-Wilks test was used to assess the normality of the data. Following that, Mann-Whitney U test with two-tailed hypothesis was employed to compare sPD-L1 and sPD-1 levels among patients and control group. Subsequently, Kruskal Wallis test was used to evaluate sPD-L1/sPD-1 levels between different patient's groups. The relationship between continuous and categorical data variables was examined using a Spearman correlation test. Survival probabilities were estimated using the Kaplan-Meier method, and group comparisons were made using the log-rank test. The Cox proportional hazards model was used to estimate the hazard ratios for progression-free survival associated with sPD-1, sPD-L1, Gleason score, pathological stage, and PSA levels. A univariate Cox regression analysis was conducted, and variables with a p-value of less than 0.1 in the univariate survival analysis were incorporated into the multivariate analysis. The threshold between high and low sPD-L1 and sPD-1 concentrations was determined by logistic regression, followed by calculation of the Youden index to establish the cutoff values. All analyses were carried out in Python version 3.11.4 (Python Software Foundation), with statistical significance set at $p < 0.05$.

3 Results

3.1 Characteristics of PCa population

A total of 88 patients with the pT2 and pT3 PCa diagnosis were included in our analysis. The median age of the patient group was 62.6 years, preoperative PSA levels ranged between 2.15 and 67.7 ng/ml and Gleason score was between 6 and 8 (grade group 1 to 4 respectively, according to ISUP). For 75 patients preoperative and postoperative sPD-L1 and sPD-1 pairs were determined to evaluate

10.3389/fimmu.2024.1401097

the dynamic of changes of soluble checkpoints after surgical treatment. Patient characteristics are summarized in Table 1.

3.2 Characteristics of control group

Eligible subjects (n = 41) were selected based on PSA level (<3 ng/ml), the subjects were at an average of 64.6 year (median 66), interquartile range (IQR) = 7. The control group was managed, and control samples were collected in collaboration with the biomedical research laboratory Rezus.lt. Characteristics of healthy subjects are summarized in Table 2.

3.3 sPD-L1 and sPD-1 in PCa patients and healthy subjects

Plasma sPD-L1 levels were significantly higher comparing to healthy control group (median 0.11 pg/ml) both in preoperative (median 2.51 pg/ml) and postoperative (median 1.94 pg/ml) groups of PCa patients ($p < 0.001$). sPD-1 concentrations at baseline (median 29.44 pg/ml) and after surgical treatment (median 33.89 pg/ml) were significantly higher comparing to healthy control group (median 17.18) $p < (0.001)$. sPD-L1 exhibits a statistically insignificant postoperative decline, whereas sPD-1 demonstrates a statistically significant postoperative increase ($p < 0.05$). sPD-L1 and sPD-1 values in the patients and in the controls are shown in Figure 1.

The sPD-1/sPD-L1 ratio exhibited statistically significant differences between both preoperative and postoperative patient groups compared to the control group. Postoperatively, we observed a notable rise in the sPD-1/sPD-L1 ratio, increasing from a median of 10.9 to 17.2 ($p < 0.05$). Remarkably, the control group had the highest median among all three groups at 116.7 (Figure 2).

TABLE 1 Characteristics of PCa patients.

Patient Characteristics	
No of patients (%)	88 (100%)
Age (years)	
<61	32 (36.4%)
61–65	26 (29.5%)
>65	30 (34.1%)
Preoperative PSA (ng/mL)	8.97 (2.15 – 67.7)
pT stage	
pT2	64 (72.2%)
pT3	24 (27.3%)
Gleason Grade	
Grade 1 [3 + 3]	24 (27.3%)
Grade 2 [3 + 4]	53 (60.2%)
Grade 3 [4 + 3]	10 (11.4%)
Grade 4 [4 + 4]	1 (1.1%)
Lymph node involvement	5 (5.7%)

TABLE 2 Characteristics of healthy subjects.

Control Characteristics	
No of individuals (%)	**41 (100%)**
Age (years)	
<61	**9 (22%)**
61–65	**11 (26.8%)**
>65	**21 (51.2%)**
PSA (ng/mL)	**1.19 (0 – 2.96)**

3.4 The association of sPD-L1 and sPD-1 with clinicopathological findings of PCa

Statistically significant association between baseline sPD-L1 and Gleason score was observed. Patients with grade group 3 has a significantly higher levels (median 23.5 pg/ml) of circulating PD-L1 comparing to grade group 1 (median 2.5 pg/ml) and grade group 2 (median 2.2 pg/ml) ($p < 0.05$), (Figure 3A). The grade group 4 was not analyzed because the number of subjects in that group was too small to obtain a reliable result. A statistically significant ($p < 0.05$) association between baseline sPD-1 concentration and advanced PCa stage was obtained (Figure 3B).

3.5 Prognostic and predictive value of sPD-L1 and sPD-1 in PCa

For progression free survival analysis, threshold of 7.66 pg/ml (specificity 85%, sensitivity 56%, AUC = 0.73) was established for preoperative plasma concentrations of sPD-L1, using receiver operating characteristic (ROC) curves (Figure 4B). PFS was compared between the low (< 7.66 pg/ml) and high (≥ 7.66 pg/ml) sPD-L1 groups by Kaplan-Meier analysis and log rank tests. Kaplan–Meier analysis revealed that postoperative PFS tended to be shorter in the high sPD-L1 group (n = 21) than in the low sPD-L1 group (n = 64) ($p < 0.05$) (Figure 4A). The difference in PFS survival between the groups was notable at 2 years post-surgery, with rates of 82% in the < 7.66 pg/mL group and 61% in the ≥ 7.66 pg/ml group. ROC analysis was conducted to assess the efficacy of sPD-1 as a classifier for PFS. However, sPD-1 was determined to be an ineffective classifier for PFS (AUC = 0.47). Subsequently, evaluation of PFS between the low (< 18.22 pg/ml) and high (≥ 18.22 pg/ml) sPD-1 groups was performed using Kaplan-Meier analysis and log-rank tests. Kaplan–Meier analysis showed that the low sPD-1 group (n = 15) as well as high sPD-1 group (n = 66) had no statistical significance for PFS estimation in PCa patients (Data not shown).

The potential of prognostic biomarkers for predicting PFS in PCa patients was investigated using Cox proportional hazard analysis. While the high sPD-L1 concentrations group exhibited significance in the univariate analysis, it failed to maintain

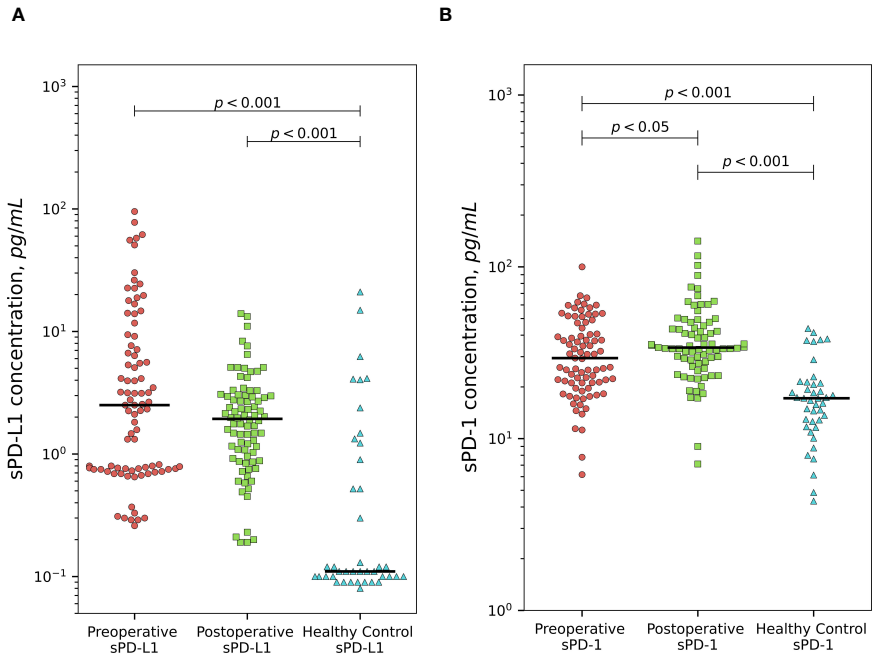

FIGURE 1
Comparison of sPD-L1 and sPD-1 levels between prostate cancer patients and healthy subjects. PCa patients demonstrates significantly higher preoperative and postoperative plasma sPD-L1 levels comparing to healthy individuals ($p < 0.001$). sPD-L1 results in statistically unsignificant postoperative decline. **(A)** Presurgical and postsurgical plasma sPD-1 levels in PCa patients are significantly higher than in healthy controls ($p < 0.001$). sPD-1 demonstrates statistically significant postoperative increase ($p < 0.05$) **(B)**.

significance in the multivariate model, suggesting it may not act as an independent predictor. Conversely, sPD-1 concentrations (both continuous and categorized) did not show significant associations with survival outcomes in univariate analysis, suggesting their reliability as predictors of PFS in this context may be limited. The results of the Cox proportional hazard analysis are summarized in Tables 3, 4.

3.6 The sPD-1/sPD-L1 ratio for PFS prediction

Based on the ROC curve analysis, a preoperative sPD-1/sPD-L1 ratio of 2.3 was identified (specificity 90%, sensitivity 56%, AUC = 0.66) (Figure 4D). Patients with a lower sPD-1/sPD-L1 ratio were associated with a higher probability of disease progression ($p < 0.05$). One year PFS was 75% in the group with < 2.3 sPD-1/sPD-L1 ratio, contrasting with 84% in the > 2.3 ratio group. Probabilities of PFS differed even more between groups at 2 years after surgery. At 2 years postoperatively, the < 2.3 sPD-1/sPD-L1 ratio group had a 45% probability of PFS, while the > 2.3 ratio group had an 81% probability (Figure 4C). In Cox analysis, categorizing the preoperative sPD-1/sPD-L1 ratio into high and low ratio groups yielded comparable results to single sPD-L1 (Tables 3, 4). However, in univariate analysis, similar to continuous sPD-L1, the continuous sPD-1/sPD-L1 ratio was not found to be significant. Furthermore, the postoperative ratio of sPD-1/sPD-L1 showed no prognostic significance in Cox regression and performed poorly as a classifier for PFS in ROC analysis.

3.7 The changes of sPD-L1 and sPD-1 after radical prostatectomy in PCa

There was no significant difference between preoperative values of sPD-L1 and after radical prostatectomy in the whole patient's group of PCa ($p = 0.12$). Scatterplot analysis revealed that the overall mean of sPD-L1 in the patient group decreased after surgery. According to detailed analysis, - individuals whose estimated initial sPD-L1 level was high (> 7.66 pg/ml) showed a statistically significant postoperative decrease ($p < 0.001$) and whose presurgical sPD-L1 level was low (< 7.66 pg/ml) showed a statistically significant postoperative increase ($p < 0.05$) (Figure 5A).

Tumor excision resulted in a noticeable sPD-1 increase ($p < 0.05$). According to scatterplot analysis post-operative concentrations of sPD-1 in PCa patients changed in variable way, however, the overall group mean concentrations after radical tumor removal were increased (Figure 5B).

3.8 The interplay between sPD-L1 and sPD-1 and circulating immune cells in PCa

There was no significant interplay between soluble PD-L1 and PD-1 and immune subsets CD3+, CD4+, CD8+, CD19+, CD3-CD16+CD56+, CD8+CD69+.

A high positive correlation ($r = 0.73$) ($p < 0.05$) between immunosuppressive CD4+CD25+FoxP3+ regulatory T cells and presurgical sPD-L1 was established in the patients with occurred BCR (Figure 6A). Among patients who have experienced BCR, was

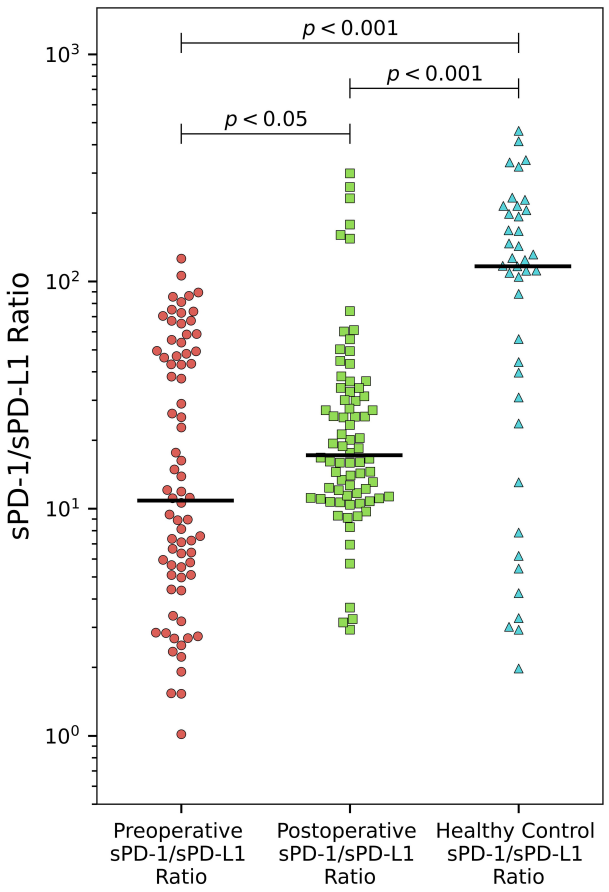

FIGURE 2
Alteration of sPD-/sPD-L1 ratio in PCa. The sPD-1/sPD-L1 ratio demonstrates significant increase after surgery ($p < 0.05$). Both preoperative and postoperative patient groups differ significantly compared to healthy controls ($p < 0.001$).

found a strong inverse correlation ($r = -0.72$) ($p < 0.05$) between preoperative sPD-L1 and percentage of M-MDSC (Figure 6B). In patients with favorable postoperative course of disease no correlations were found between sPD-L1 and Tregs ($r = -0.02$) ($p = 0.86$) and percentage of M-MDSC ($r = -0.21$) ($p < 0.10$) (Data not shown).

4 Discussion

4.1 Soluble PD-L1 and PD-1 in prostate cancer and healthy subjects

In present study, we performed a comprehensive analysis of circulating sPD-L1 and sPD-1 levels in a cohort comprising both PCa patients and healthy individuals. Prior to our investigation, -circulating sPD-L1 and sPD-1 levels have never been studied in PCa of the European male population. Levels of sPD-L1 and sPD-1 and their prognostic value in PCa were analyzed only in two trials – in African and in USA men populations (30, 31). Both studies showed elevated concentrations of these molecules in patients with metastatic castration-resistant prostate cancer (mCRPC) compared to healthy controls. Notably, these studies focused on a more aggressive form of prostate cancer compared to our research. Additionally, ADT was administered during the examination in the African male population and no surgical treatment was utilized in either study. Furthermore, it is recognized that prostate cancer affects African men nearly twice as frequently as European men (30), due to various genetic mutations (32).

Our investigation revealed elevated levels of soluble PD-L1 and PD-1 in the plasma of PCa patients, both before and after surgical treatment, compared to healthy controls (Figures 1A, B). sPD-L1 is found in healthy humans and significantly increases in the blood of

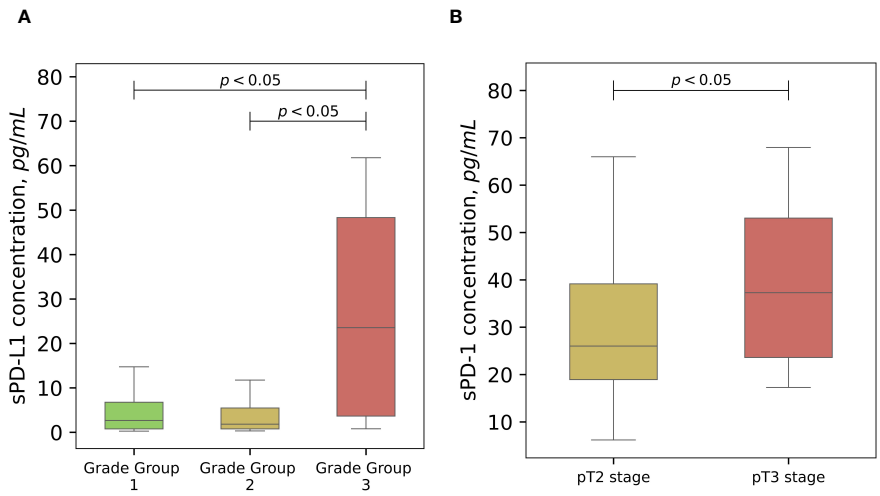

FIGURE 3
The associations of soluble PD-L1 and PD-1 with cancer progression. Variations of sPD-L1 concentration in the peripheral blood of PCa patients differs significantly ($p < 0,05$) according to Gleason grade groups, grade 3 group shows significant association with highly elevated levels of sPD-L1 **(A)**. Pretreatment sPD-1 levels demonstrate higher values in clinicopathological staging of PCa ($p < 0.05$) **(B)**.

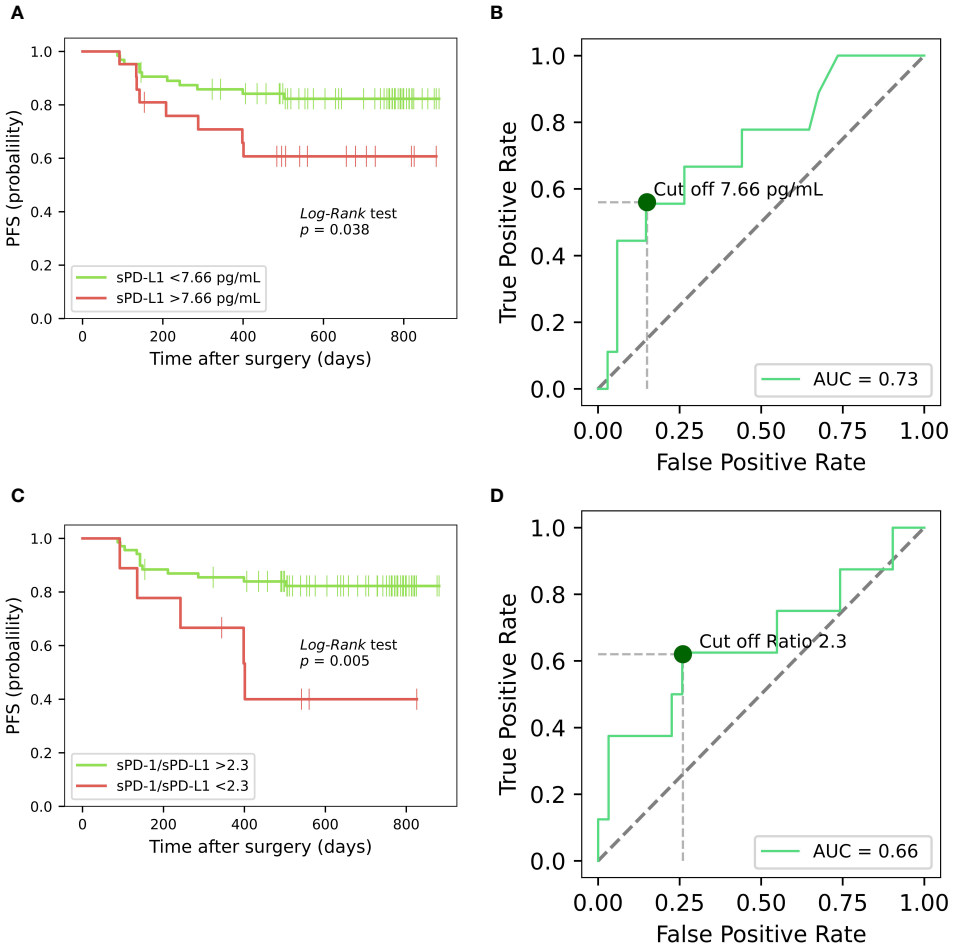

FIGURE 4
Kaplan-Meier analysis on the progression-free survival of prostate cancer patients, based on sPD-L1 and sPD-1/sPD-L1 ratio. Kaplan-Meier curves illustrates the progression-free survival of PCa patients based on high and low presurgical concentrations of sPD-L1, revealing that low pretreatment sPD-L1 levels are associated with prolonged PFS ($p < 0.05$) **(A)**. ROC curve for preoperative plasma concentrations of sPD-L1 for PFS prediction in PCa **(B)**. Kaplan-Meier analysis based on sPD-1/sPD-L1 ratio reveals that patients exhibiting a lower sPD-1/sPD-L1 ratio were correlated with an elevated probability of disease progression ($p < 0.05$) **(C)**. ROC curve of sPD-1/sPD-L1 ratio as classifier PFS in PCa **(D)**.

aged healthy individuals (33), the 51–70 years old people have the highest level of sPD-L1 (13). Our control group, meticulously selected, based on medical history and drug usage, closely mirrors the study population's age profile and the peak of sPD-L1 concentration in healthy individuals. This makes it an ideal reference for comparing sPD-L1 levels between PCa patients and healthy men. Elevated concentrations of circulating sPD-L1 were found in many cancers compared to controls, - in two separate studies of gastric cancer (GC) (34, 35) in hepatocellular carcinoma (HCC) (36) lung adenocarcinoma (37) clear cell renal cell carcinoma (ccRCC) (12), in different types of carcinomas (38), ovarian cancer (OC) (39), glioma (40, 41).

sPD-1 levels tend to be higher in various cancers compared to those in healthy subjects as well. Elevated levels were found in different subtypes of lymphoma (42), lung adenocarcinoma (37) and glioma (41).

We observed no significant correlation between PSA levels and sPD-L1 or sPD-1 in our patient's group. Furthermore, when stratifying patients based on median sPD-L1 and sPD-1 levels or utilizing logistic regression to define sPD-L1 groups, no significant differences in PSA levels were detected. These findings suggest that sPD-1 and sPD-L1 may hold promise as complementary biomarkers for prostate cancer screening, potentially enhancing the accuracy of screening alongside PSA testing.

4.2 The implications of sPD-L1 in prostate cancer

To assess the tumor-dependent relationship of sPD-L1 and sPD-1, we compared the preoperative and postoperative dynamics in prostate cancer patients. Our results showed no statistically significant decrease in sPD-L1 levels following tumor excision across the entire patient's cohort. Therefore, the individualized response to radical tumor removal demonstrates different directions of sPD-L1 changes in high and low groups of sPD-L1. Remarkably, patients with initially high sPD-L1 levels exhibited a statistically significant decrease postoperatively, whereas those with

10.3389/fimmu.2024.1401097

TABLE 3 The results of Cox proportional hazard, univariate analysis.

	Progression-free survival	
	Hazard Ratio (95% CI)	*P-value*
Gleason Grade Group		
Grade Group 1	Ref.	
Grade Group 2	6.95 (0.9–53)	0.061
Grade Group 3	31.43 (3.9–252)	0.001
PSA, ng/mL	1.04 (1.01–1.07)	0.005
pT stage		
pT2	Ref.	
pT3	11.2 (4.4–28.5)	$p<0.001$
sPD-1		
<18.22 pg/ml	Ref.	
>18.22 pg/mL	1.23 (0.4–4.3)	0.74
sPD-L1		
<7.66 pg/mL	Ref.	
>7.66 pg/mL	2.5 (1.02–6.3)	0.045
sPD-1, pg/mL	1.001 (0.98–1.03)	0.93
sPD-L1, pg/mL	1.015 (1–1.03)	0.08
sPD-1/sPD-L1 ratio		
<2.3	Ref	
>2.3	0.25 (0.09–0.72)	0.01
sPD-1/sPD-L1, ratio	1.0 (0.98–1.01)	0.58

low preoperative sPD-L1 levels demonstrated a statistically significant postsurgical increase (Figure 5A).

Surgical tumor removal has been associated with decreased levels of sPD-L1 in various cancers. In glioma patients, postoperative sPD-L1 levels were significantly lower than preoperative levels (41). Non-small cell lung cancer (NSCLC) patients undergoing radical surgery exhibited a significant increase in sPD-L1 one month post-surgery, followed by a slight decrease at three months (14), suggesting a poor link to tumor removal. While we lack serial data for postoperative changes in PCa patients, comparing with NSCLC studies, suggests that three months may be sufficient to assess the tumor and sPD-L1 dependence. These findings lead us to hypothesize that elevated baseline sPD-L1 levels may relate to tumor secretion. Additionally, sources other than tumor cells, might contribute to the relatively modest sPD-L1 levels observed in peripheral blood in PCa. Furthermore, Kaplan–Meier analysis based on high and low baseline sPD-L1 levels, showed contrasting predictions for PFS. This supports the notion that sPD-L1 in prostate cancer originates not only from tumor cells but also from other cellular sources (Figure 4A).

Low PD-L1 expression in the TME of prostate cancer can complicate the association with sPD-L1. However, PD-L1 expression by tumor cells in prostate cancer correlates with tumor stage, Gleason score, lymph node or distant metastases, surgical margin positivity and other. PD-L1 positivity rates vary in primary prostate cancers and different metastatic sites within the same patient (43), highlighting high heterogeneity of PCa tumor (44). Despite high membranous PD-L1 expression, some studies found no significant correlation between sPD-L1 and tissue PD-L1 (34).

To the best of our knowledge the values of soluble PD-L1 and PD-1 were not further investigated in association with PFS in PCa. Given the cold immune subtype of prostate tumor, Kaplan Meier analysis in our study revealed shortened PFS correlation with high baseline sPD-L1 values in PCa, as in many other tumors characterized by non-immunologically cold TME such as HCC (45), gastric cancer (46, 47), breast cancer (BC) (48) glioma (41) and several NSCLC studies (14, 49, 50).

The Cox proportional hazard test for PFS, initially identified sPD-L1 as a significant factor in the univariate analysis. However, upon conducting multivariate Cox analysis, sPD-L1 lost its significance. This suggests that sPD-L1 does not contribute additional prognostic value beyond established clinical factors such as Gleason score, PSA level, and disease stage in PCa. These results imply that while sPD-L1 may have shown promise in isolation, it does not offer incremental prognostic insight beyond conventional clinical parameters routinely used in PCa prognosis. The significance found in the univariate Cox model, but not in the multivariate Cox model, may also be attributed to the relatively small sample size of the group with disease progression (n = 23). Baseline sPD-L1 was good marker of tumor recurrence in BC (48) and of PFS in metastatic ccRCC patients, treated with sunitinib (51). A previous mentioned studies on soluble immune checkpoints in African and American populations did not explore their association with PFS.

The correlation between circulating sPD-L1 and overall survival (OS) has been observed across various cancers. Patients with high preoperative serum sPD-L1 levels showed significantly lower OS compared to those with low levels in gastric cancer (34, 46) and metastatic pancreatic cancer (52). Huang's meta-analysis (53) and another multicancer study by Scirocci (9), both found that elevated sPD-L1 levels were associated with worse survival outcomes. Pretreatment sPD-L1 levels were prognostic indicators for OS in patients with biliary tract cancer undergoing palliative chemotherapy (54). No deaths occurred during the follow-up period in our investigation.

Based on our investigation, disease progression correlates with elevated levels of circulating sPD-L1. Significantly elevated sPD-L1 levels were associated with higher Gleason scores, particularly with 4 + 3. This association was also observed among African men, as reported by Katangole (30), although their study showed a higher percentage (43.86%) of advanced PCa cases with Gleason scores of 8–10, whereas in our study, only one person had a Gleason score of 8. The predominant Gleason scores in our group were 6–7 (Table 1). The correlation between higher grade (group 3) and sPD-L1 suggests that sPD-L1 may contribute to the aggressiveness of the disease in our study's PCa patients. Consistent with our findings, the association of sPD-L1 with disease advancement parameters has been identified in various other tumors: in aggressive bladder cancer (55), advanced (ccRCC) (12), and gastric cancer (35). Baseline sPD-L1 has proven to be a reliable tumor marker in metastatic breast cancer (48) and has been linked

10.3389/fimmu.2024.1401097

TABLE 4 The results of Cox proportional hazard, multivariate analysis.

Variable	Model 1 sPD-L1 pg/mL (continuous)		Model 2 sPD-L1 (categorical)		Model 3 sPD-1/sPD-L1 ratio (categorical)	
	Hazard Ratio (95% CI)	*P-value*	Hazard Ratio (95% CI)	*P-value*	Hazard Ratio (95% CI)	*P-value*
Gleason Grade Group						
Grade Group 1	Ref.		Ref.		Ref.	
Grade Group 2	15.6 (0.9–266)	0.06	15.9 (0.9–273)	0.06	73.3 (0.5–9800)	0.08
Grade Group 3	71.3 (3.7–1376)	0.005	56.9 (3.2–1018)	0.006	131.75 (1–16790)	0.049
PSA, ng/mL	1.05 (1.004–1.11)	0.03	1.06 (1.05–1.11)	0.03	1.09 (1.0–1.19)	0.053
pT stage						
pT2	Ref.		Ref.		Ref.	
pT3	5.7 (1.9–17.4)	0.002	5.3 (1.7–16.7)	0.004	5.7 (1.9–17.8)	0.002
sPD-L1, pg/mL	1.0 (0.96–1.02)	0.5	–	–	–	
sPD-L1						
<7.66 pg/mL	–		Ref.		–	
>7.66 pg/mL	–		0.96 (0.3–3.2)	0.95	–	
sPD-1/sPD-L1 ratio						
<2.3	–		–		Ref	
>2.3	–		–		0.51 (0.11–2.3)	0.39

to rapid metastatic progression in metastatic ccRCC (51), as well as to the size of metastases in colorectal cancer (56). Elevated initial sPD-L1 levels have been associated with poorer prognosis in ccRCC (57), soft tissue sarcomas (28), pancreatic adenocarcinoma (58), lung cancer (49, 59), hepatocellular carcinoma (36), and lower-grade glioma (40). Moreover, high pretreatment sPD-L1 levels have been linked to low disease control rates in various advanced solid tumors, including melanoma, NSCLC and other (60). As in our study, higher sPD-L1 score values are linked with increased tumor invasiveness, potentially aiding in the identification of high-risk

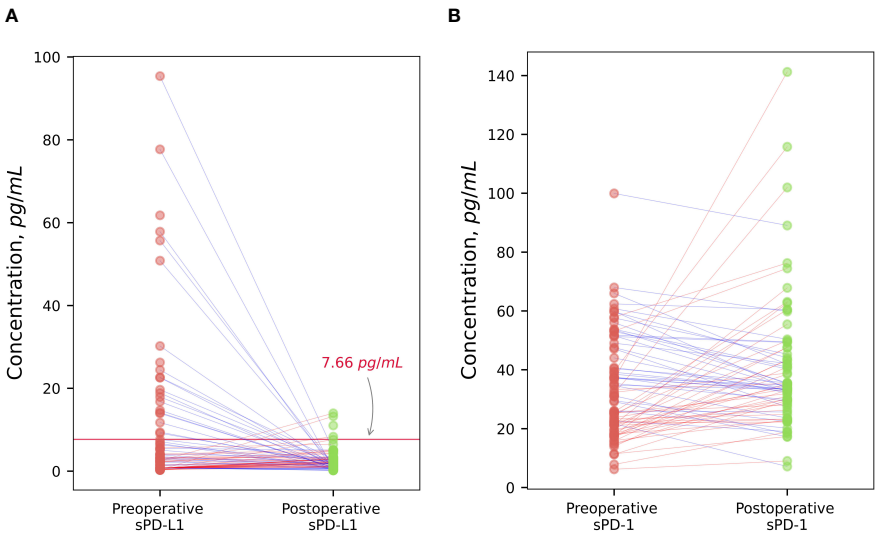

FIGURE 5
The dynamic of changes of sPD-L1 and sPD-1 after surgical treatment. Radical prostatectomy in individualized scatterplot analysis demonstrated statistically significant decrease ($p < 0.001$) of high baseline sPD-L1 level (> 7.66 pg/ml), and statistically significant increase ($p < 0.05$) of low preoperative sPD-L1 levels (< 7,66 pg/ml), whereas the postoperative variation of sPD-L1 in the whole group of patients varied and was insignificant **(A)**. Individualized sPD-1 response to surgical tumor removal showed statistically significant increase ($p < 0.05$) **(B)**.

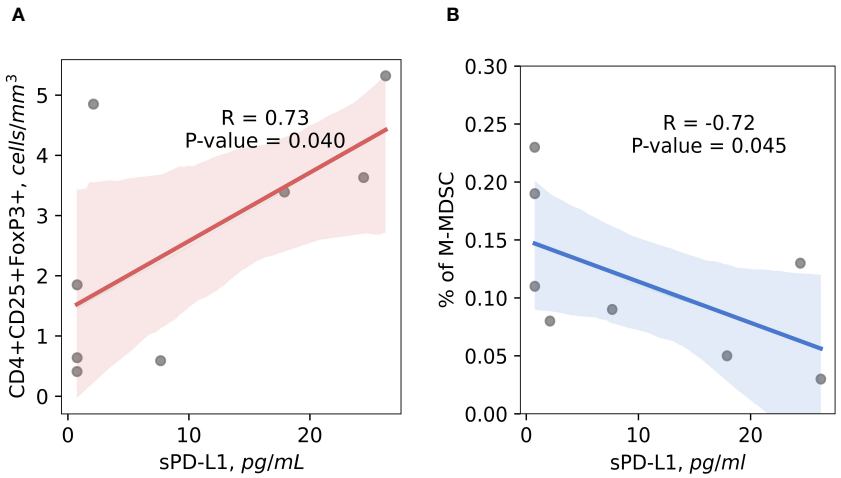

FIGURE 6
The correlation between preoperative circulating immunosuppressive cells and sPD-L1. Preoperative CD4+CD25+FoxP3+ Tregs cells positively correlates with sPD-L1 in patients with occurred BCR, suggesting the contribution for cancer progression (R = 0.73) ($p < 0.05$) **(A)**. Baseline percentage of M-MDSC cells and sPD-L1 shows significant inverse correlation in the peripheral blood of prostate cancer patients with BCR occurred, indicating that monocytic MDSC are not associated with sPD-L1 production in complicated disease (r = -0.72) ($p < 0.05$) **(B)**.

patients who could benefit from prostate biopsy. This approach could help reduce the number of unnecessary biopsies in PCa.

4.3 The impact of sPD-1 in prostate cancer progression

We observed a significant increase in sPD1 levels following tumor excision. Elevated sPD-1 levels following cancer treatment, including surgery, are believed to be associated with favorable outcomes (5). Postreatment sPD-1 levels varies across different cancers: notably increased post immunotherapy vaccine application in mCRPC cases (31) and after anti-PD-1 antibody therapy in solid tumors (61). However, glioma patients had lower postoperative sPD-1 levels compared to preoperative levels (41). Higher post-ICI monotherapy sPD-1 levels were linked to longer overall survival in NSCLC patients (49) and advanced EGFR-mutated NSCLC patients treated with erlotinib (62). Despite the significant elevation of sPD-1 levels following radical prostatectomy, suggesting potential better outcomes, our investigation found no correlation between prognosis and higher postoperative circulating sPD-1 levels. Hypothetically, the postoperative increase in soluble PD-1 levels could be attributed to various factors and mechanisms. Studies suggest sPD-1's potential to counteract the immunosuppressive effects of PD-1/PD-L1, restoring T-cell function and enhancing antitumor immunity (11, 63). On the other hand, sPD-L1 has been shown to suppress peripheral T lymphocytes (5, 12). The decrease in sPD-L1 post-surgery aligns with the natural T lymphocyte recovery seen with radical tumor resection (64). Overall, tumor excision removes the immune system's suppressive burden, potentially leading to immune restoration and an increase in sPD-1 levels.

We discovered a statistically significant association between baseline sPD-1 concentration and advanced cancer stage, suggesting a potential correlation between sPD-1 levels and poorer prognosis in PCa. The higher concentration of sPD-1 in pT3 lesions could be useful for doctors to more accurately determine the stage of the cancer. In metastatic ccRCC higher concentrations of sPD-1 tended to correlate with advanced cancer stage as well (51). For patients with metastatic colorectal cancer (mCRC), soluble PD-1, similar to soluble PD-L1, was linked to clinically worse levels of various peripheral blood parameters and metastatic tumor burden (56) and predicted systemic inflammation in pancreatic cancer (65). Although our data reflects finding between pretreatment sPD-1 levels and tumor progression in other cancers, the precise mechanism of the role of sPD-1 remains unclear. We hypothesize that as cancer progresses, there might be an increase in soluble PD-1 as part of the complex interplay between the tumor and the immune system. The tumor microenvironment can release factors that promote the shedding of PD-1 from cell surfaces, resulting in elevated soluble PD-1 levels, particularly since the exact source of sPD-1 is still unknown. Additionally, tumor-associated inflammation can trigger an immune response, leading to higher soluble PD-1 levels as part of immune regulation. Some studies have confirmed the association of sPD-1 with systemic inflammation in the context of cancer progression (65). Further studies are needed to determine the exact mechanism that underlies the connection between malignancy and sPD-1 (11).

Our findings regarding initial sPD-1 levels and PFS did not show statistical significance and according to results of Cox analysis, sPD-1 may not be a reliable predictor of PFS. Contrary, in other cancer studies it has been demonstrated that untreated cancer patients with elevated sPD-1 will have unfavorable survival outcomes (5, 11). High sPD-1 concentrations predict reduced PFS duration in glioma (41) NSCLC (50) mCRC (56) and pancreatic adenocarcinoma (58). Poor survival in diffuse large B cell lymphoma was indicated by a correlation between high initial sPD-1 levels and the PD1+ T cells infiltrating the tumor (66). In contrast a high level of sPD-1 correlated with prolonged PFS in HCC (45). In metastatic ccRCC

patients receiving sunitinib (51) treatment and patients treated with nivolumab and ipilimumab in melanoma, sPD-1 levels were significant predictive markers of PFS (67).

4.4 The sPD-1/sPD-L1 ratio for PCa prognosis prediction

PD-1 and sPD-L1 may exert opposing functions potentially creating either an active (11, 63) or immunosuppressive (5, 12, 38, 68) environment depending on their respective concentrations. In our study, the sPD-1/sPD-L1 ratio was significantly different before surgery and after surgery compared with the control group, which exhibited highest values (Figure 2). We found a statistically significant association between initial sPD-1/sPD-L1 ratio and PFS. Patients exhibiting a lower sPD-1/sPD-L1 ratio were associated with a shorter PFS ($p < 0.05$). Similar results were observed for patient survival by sPD-1/PD-L1 ratio in melanoma treated with immune checkpoint blockade (69), as well as in the context of low sPD-1 and high sPD-L1 combination for PD-1 antibody monotherapy across various cancers (70). In our study, we observed a significant increase in the sPD-1/sPD-L1 ratio after surgery in the entire prostate cancer (PCa) population. This supports preoperative findings indicating a correlation between a higher baseline sPD-1/sPD-L1 ratio and improved prognosis. The postoperative rise in the sPD-1/sPD-L1 ratio suggests a favorable prognosis, particularly considering the highest ratio observed in healthy subjects. In the melanoma study, patients undergoing immunotherapy exhibited around a 30% decrease in mortality risk at a specific time point among those with elevated ratios of sPD-1/sPD-L1 (69). However, in our study, the sPD-1/sPD-L1 ratio demonstrated significance in Cox univariate analysis for PFS but lost its significance in the multivariate analysis, suggesting that it does not offer additional prognostic value beyond established clinical factors in PCa prognosis. Moreover, while the preoperative ratio could distinguish patients more likely to experience disease progression, we did not observe any discernible pattern in the change (increase or decrease) of the sPD-1/sPD-L1 ratio and prognosis.

4.5 The relationship between sPD-L1 and immunosuppressive cells

There are multiple ways in which cancer cells can suppress the immune system's ability to fight tumors. These include increasing the levels of immune checkpoint proteins and enhancing the immunosuppressive effects of regulatory T cells and MDSCs infiltrating the TME (71). To analyze how the interactions of sPD-L1 and sPD-1 with circulating immune cells affect tumor progression, we further explored the relationships between sPD-L1, sPD-1, and circulating immune cells in both favorable and unfavorable disease outcomes. Preoperative levels of immunosuppressive cells such as Tregs and MDSC, showed notable correlations with baseline sPD-L1 levels in postoperative BCR patients. Conversely, no correlations were observed between sPD-L1 and immune cell populations in patients with a favorable disease course. No notable correlations were found between sPD-L1 and sPD-1 levels and immune cell populations like CD3+, CD4+, CD8+, and NK cells, which typically exhibits antitumor effects in whole PCa patients population.

Soluble PD-L1 and PD-1 were found to impact clinically worse laboratory parameters in mCRC, as indicated by Dank (56). Additionally, Castello (72) discovered an association between metabolic tumor burden and sPD-L1 levels in NSCLC, while Kruger (65) revealed a link between sPD-L1 and sPD-1 with systemic inflammation in pancreatic cancer. These findings suggest a systemic effect of these soluble molecules on unfavorable prognosis and cancer progression. However, further studies investigating the effects of soluble PD-L1 and PD-1 on disease progression beyond intrinsic clinical findings are still limited.

Based on the possible systemic effect of soluble PD-L1 and PD-1, our analysis revealed a positive correlation between sPD-L1 and immunosuppressive circulating CD4+CD25+FOXP3+ T regulatory cells in PCa patients with an unfavorable course of disease, suggesting potential role of this interaction in disease progression and upregulated immunosuppressive activity. Several cancer studies support PD-L1's involvement in T regulatory cell proliferation and immunosuppression. PD-L1 regulates induced Treg cells development and functionality (73), later these cells have been shown to be induced and sustained by PD-L1 in glioblastoma (74). Acute myeloid leukemia (AML) expressing PD-L1, may enhances Treg cells expansion, which, in turn, stimulates AML cell growth via production of specific interleukins (75). Additionally, sPD-L1 was found to induce B regulatory cell differentiation and regulate Treg induction through CD19+ B cells (76). Recent data from Liang (38) suggests circulating sPD-L1 beyond the TME promotes cancer growth. Our findings, along with these studies, suggest sPD-L1 enhances the immunosuppressive effects of T regulatory cells, potentially driving the progression of cancer.

MDSCs, known to contribute to sPD-L1 production, in addition to tumor cells (77). However, it remains unclear whether monocytic (M-MDSC) or granulocytic (G-MDSC) subtypes predominantly produce sPD-L1 (60). Studies in tumor-bearing mice have shown higher percentages of PD-L1+ G-MDSCs and M-MDSCs compared to tumor-free mice, with M-MDSCs exhibiting the highest proportion of PD-L1 expression (78). Oh's study suggests that sPD-L1 originates primarily from G-MDSCs (60). In a mouse colon cancer model, the tumor microenvironment had the highest concentration of PD-L1+ MDSCs compared to peripheral blood and secondary lymphoid organs (78). Conversely, ovarian cancer showed a strong link between PD-L1+ M-MDSCs and sPD-L1 in the bloodstream, suggesting sPD-L1 as a potential marker for monitoring PD-L1+ myeloid cells in untreated OC without invasive procedures (39). Our study found an inverse correlation between baseline sPD-L1 levels and M-MDSC percentage in patients with BCR, suggesting M-MDSCs are not a major source of sPD-L1 in PCa with unfavorable course. Additionally, patients with high baseline sPD-L1 levels were associated with shorter PFS, (including BCR) and showed significant postoperative decreases, indicating a link between high sPD-L1 and tumor. This supports our hypothesis that high sPD-L1 levels may be linked to tumor secretion. We aimed to link the

immune cells we studied with sPD-L1, anticipating that they might serve as an additional source of sPD-L1; however, we did not find any such associations.

5 Conclusion

New cancer biomarkers may be provided by the implementation of the easily, into clinical practice, introducible sPD-L1 and sPD-1, as these have demonstrated significance in tumor prognosis and possible systemic effect for cancer proliferation. In our study, sPD-L1 and sPD-1 levels were higher in PCa patients compared to healthy individuals. High initial sPD-L1 concentrations correlated with poorer PFS, as well as a low sPD-1/sPD-L1 ratio and has emerged as a valuable prognostic marker for PCa. Additionally, a strong link between sPD-L1 and CD4+CD25+Foxp3+ regulatory T cells in BCR cases was observed, indicating sPD-L1's systemic impact on tumor progression. We found an inverse relationship between M-MDSC percentage and sPD-L1 in BCR patients. This, along with high sPD-L1 levels associating with shortened PFS and postoperative decrease, suggests M-MDSC might not be the source of sPD-L1 in PCa patients. Our findings suggest sPD-L1 elevation relates to tumor progression and initial concentration of sPD-L1 is appropriate to predict the course of disease. Although sPD-L1 may be linked with other PCa diagnostic tools utilized in clinical settings, its convenient accessibility facilitates the implementation of more thorough screening protocols. Future directions, - more detailed studies of the interactions of PD-L1 and sPD-1 with immune cells in other tumors and the association of exposure with adverse prognosis in larger cohorts are needed, as well as detailed studies of the associations with other parameters supporting their systemic effect for tumor progression and origin. In conclusion, - the results of this study suggest that pretreatment plasma sPD-L1 concentrations can be used for prognosis prediction and could be helpful in biopsy decisions in prostate cancer.

6 Limitations of the study

There were some limitations in the current study. First, this is a single-center study, with relatively small study cohort. Second, the profile of immune cells has not been studied widely enough.

Data availability statement

The raw data supporting the conclusions of this article will be made available by the authors, without undue reservation.

Ethics statement

The studies involving humans were approved by Vilnius Regional Ethics Committee on Biomedical Research, (Vilnius, Lithuania). The studies were conducted in accordance with the local legislation and institutional requirements. The participants provided their written informed consent to participate in this study.

Author contributions

MZ: Data curation, Investigation, Resources, Validation, Visualization, Writing – original draft. ZS: Data curation, Formal analysis, Investigation, Validation, Visualization, Writing – review & editing. PB: Data curation, Investigation, Validation, Writing – review & editing. ND: Data curation, Investigation, Writing – review & editing. AM: Data curation, Investigation, Writing – review & editing. GZ: Conceptualization, Writing – review & editing. JJ: Project administration, Writing – review & editing. DC: Funding acquisition, Resources, Supervision, Validation, Visualization, Writing – review & editing. VP: Project administration, Supervision, Validation, Visualization, Writing – review & editing, Conceptualization.

Funding

The author(s) declare financial support was received for the research, authorship, and/or publication of this article. This research was funded by a grant (No. S-MIP-22–4) from the Research Council of Lithuania and in part supported by Research Council of Lithuania as a grant for MZ PhD studies.

Conflict of interest

The authors declare that the research was conducted in the absence of any commercial or financial relationships that could be construed as a potential conflict of interest.

Publisher's note

References

1. Bergengren O, Pekala KR, Matsoukas K, Fainberg J, Mungovan SF, Bratt O, et al. Update on prostate cancer epidemiology and risk factors-A systematic review. *Eur Urol.* (2023) 84:191–206. doi: 10.1016/j.eururo.2023.04.021

2. Tian S, Lei Z, Gong Z, Sun Z, Xu D, Piao M. Clinical implication of prognostic and predictive biomarkers for castration-resistant prostate cancer: a systematic review. *Cancer Cell Int.* (2020) 20:409. doi: 10.1186/s12935-020-01508-0

3. Strasner A, Karin M. Immune infiltration and prostate cancer. *Front Oncol*. (2015) 5:128. doi: 10.3389/fonc.2015.00128

4. Khairil Anwar NA, Mohd Nazri MN, Murtadha AH, Mohd Adzemi ER, Balakrishnan V, Mustaffa KMF, et al. Prognostic prospect of soluble programmed cell death ligand-1 in cancer management. *Acta Biochim Biophys Sin (Shanghai)*. (2021) 53:961–78. doi: 10.1093/abbs/gmab077

5. Khan M, Zhao Z, Arooj S, Fu Y, Liao G. Soluble PD-1: predictive, prognostic, and therapeutic value for cancer immunotherapy. *Front Immunol*. (2020) 11:587460. doi: 10.3389/fimmu.2020.587460

6. Zhao X, Bao Y, Meng B, Xu Z, Li S, Wang X, et al. From rough to precise: PD-L1 evaluation for predicting the efficacy of PD-1/PD-L1 blockades. *Front Immunol*. (2022) 13:920021. doi: 10.3389/fimmu.2022.920021

7. Bailly C, Thuru X, Quesnel B. Soluble programmed death ligand-1 (sPD-L1): A pool of circulating proteins implicated in health and diseases. *Cancers (Basel)*. (2021) 13:3034. doi: 10.3390/cancers13123034

8. Wei W, Xu B, Wang Y, Wu C, Jiang J, Wu C. Prognostic significance of circulating soluble programmed death ligand-1 in patients with solid tumors: A meta-analysis. *Med (Baltimore)*. (2018) 97:e9617. doi: 10.1097/MD.0000000000009617

9. Scirocchi F, Strigari L, Di Filippo A, Napoletano C, Pace A, Rahimi H, et al. Soluble PD-L1 as a prognostic factor for immunotherapy treatment in solid tumors: systematic review and meta-analysis. *Int J Mol Sci*. (2022) 23:14496. doi: 10.3390/ijms232214496

10. Zhu X, Lang J. Soluble PD-1 and PD-L1: predictive and prognostic significance in cancer. *Oncotarget*. (2017) 8:97671–82. doi: 10.18632/oncotarget.v8i57

11. Niu M, Liu Y, Yi M, Jiao D, Wu K. Biological characteristics and clinical significance of soluble PD-1/PD-L1 and exosomal PD-L1 in cancer. *Front Immunol*. (2022) 13:827921. doi: 10.3389/fimmu.2022.827921

12. Frigola X, Inman BA, Lohse CM, Krco CJ, Cheville JC, Thompson RH, et al. Identification of a soluble form of B7-H1 that retains immunosuppressive activity and is associated with aggressive renal cell carcinoma. *Clin Cancer Res*. (2011) 17:1915–23. doi: 10.1158/1078-0432.CCR-10-0250

13. Chen Y, Wang Q, Shi B, Xu P, Hu Z, Bai L, et al. Development of a sandwich ELISA for evaluating soluble PD-L1 (CD274) in human sera of different ages as well as supernatants of PD-L1+ cell lines. *Cytokine*. (2011) 56:231–8. doi: 10.1016/j.cyto.2011.06.004

14. Teramoto K, Igarashi T, Kataoka Y, Ishida M, Hanaoka J, Sumimoto H, et al. Prognostic impact of soluble PD-L1 derived from tumor-associated macrophages in non-small-cell lung cancer. *Cancer Immunol Immunother*. (2023) 72:3755–64. doi: 10.1007/s00262-023-03527-y

15. Frigola X, Inman BA, Krco CJ, Liu X, Harrington SM, Bulur PA, et al. Soluble B7-H1: differences in production between dendritic cells and T cells. *Immunol Lett*. (2012) 142:78–82. doi: 10.1016/j.imlet.2011.11.001

16. Antonsen KW, Hviid CVB, Hagensen MK, Sørensen BS, Møller HJ. Soluble PD-1 (sPD-1) is expressed in human macrophages. *Cell Immunol*. (2021) 369:104435. doi: 10.1016/j.cellimm.2021.104435

17. Mariotti FR, Ingegnere T, Landolina N, Vacca P, Munari E, Moretta L. Analysis of the mechanisms regulating soluble PD-1 production and function in human NK cells. *Front Immunol*. (2023) 14:1229341. doi: 10.3389/fimmu.2023.1229341

18. Bou-Dargham MJ, Sha L, Sang QA, Zhang J. Immune landscape of human prostate cancer: immune evasion mechanisms and biomarkers for personalized immunotherapy. *BMC Cancer*. (2020) 20:572. doi: 10.1186/s12885-020-07058-y

19. Zhang Y, Campbell BK, Stylli SS, Corcoran NM, Hovens CM. The prostate cancer immune microenvironment, biomarkers and therapeutic intervention. *Uro 2*. (2022) 2:74–92. doi: 10.3390/uro2020010

20. Wang I, Song L, Wang BY, Rezazadeh Kalebasty A, Uchio E, Zi X. Prostate cancer immunotherapy: a review of recent advancements with novel treatment methods and efficacy. *Am J Clin Exp Urol*. (2022) 10:210–33.

21. Maselli FM, Giuliani F, Laface C, Perrone M, Melaccio A, De Santis P, et al. Immunotherapy in prostate cancer: state of art and new therapeutic perspectives. *Curr Oncol*. (2023) 30:5769–94. doi: 10.3390/curroncol30060432

22. Palano MT, Gallazzi M, Cucchiara M, Dehò F, Capogrosso P, Bruno A, et al. The tumor innate immune microenvironment in prostate cancer: an overview of soluble factors and cellular effectors. *Explor Target Antitumor Ther*. (2022) 3:694–718. doi: 10.37349/etat.2022.00108

23. Messex JK, Liou GY. Impact of immune cells in the tumor microenvironment of prostate cancer metastasis. *Life (Basel)*. (2023) 13:333. doi: 10.3390/life13020333

24. Kgatle MM, Boshomane TMG, Lawal IO, Mokoala KMG, Mokgoro NP, Lourens N, et al. Immune checkpoints, inhibitors and radionuclides in prostate cancer: promising combinatorial therapy approach. *Int J Mol Sci*. (2021) 22:4109. doi: 10.3390/ijms22084109

25. Idorn M, Køllgaard T, Kongsted P, Sengeløv L, Thor Straten P. Correlation between frequencies of blood monocytic myeloid-derived suppressor cells, regulatory T cells and negative prognostic markers in patients with castration-resistant metastatic prostate cancer. *Cancer Immunol Immunother*. (2014) 63:1177–87. doi: 10.1007/s00262-014-1591-2

26. Bilusic M, Madan RA, Gulley JL. Immunotherapy of prostate cancer: facts and hopes. *Clin Cancer Res*. (2017) 23:6764–70. doi: 10.1158/1078-0432.CCR-17-0019

27. Wallis CJD, Glaser A, Hu JC, Huland H, Lawrentschuk N, Moon D, et al. Survival and complications following surgery and radiation for localized prostate cancer: an international collaborative review. *Eur Urol*. (2018) 73:11–20. doi: 10.1016/j.eururo.2017.05.055

28. Asanuma K, Nakamura T, Hayashi A, Okamoto T, Iino T, Asanuma Y, et al. Soluble programmed death-ligand 1 rather than PD-L1 on tumor cells effectively predicts metastasis and prognosis in soft tissue sarcomas. *Sci Rep*. (2020) 10:9077. doi: 10.1038/s41598-020-65895-0

29. Bosas P, Zaleskis G, Dabkevičiene D, Dobrovolskiene N, Mlynska A, Tikuišis R. Immunophenotype rearrangement in response to tumor excision may be related to the risk of biochemical recurrence in prostate cancer patients. *J Clin Med*. (2021) 10:3709. doi: 10.3390/jcm10163709

30. Katongole P, Sande OJ, Reynolds SJ, Joloba M, Kajumbula H, Kalungi S, et al. Soluble programmed death-ligand 1 (sPD-L1) is elevated in aggressive prostate cancer disease among African men. *Oncol Ther*. (2022) 10:185–93. doi: 10.1007/s40487-022-00184-6

31. Bilusic M, McMahon S, Madan RA, Karzai F, Tsai YT, Donahue RN, et al. Phase I study of a multitargeted recombinant Ad5 PSA/MUC-1/brachyury-based immunotherapy vaccine in patients with metastatic castration-resistant prostate cancer (mCRPC). *J Immunother Cancer*. (2021) 9:e002374. doi: 10.1136/jitc-2021-002374

32. Kheirandish P, Chinegwundoh F. Ethnic differences in prostate cancer. *Br J Cancer*. (2011) 105:481–5. doi: 10.1038/bjc.2011.273

33. Wu Y, Chen W, Xu ZP, Gu W. PD-L1 distribution and perspective for cancer immunotherapy-blockade, knockdown, or inhibition. *Front Immunol*. (2019) 10:2022. doi: 10.3389/fimmu.2019.02022

34. Shigemori T, Toiyama Y, Okugawa Y, Yamamoto A, Yin C, Narumi A, et al. Soluble PD-L1 expression in circulation as a predictive marker for recurrence and prognosis in gastric cancer: direct comparison of the clinical burden between tissue and serum PD-L1 expression. *Ann Surg Oncol*. (2019) 26:876–83. doi: 10.1245/s10434-018-07112-x

35. Zheng Z, Bu Z, Liu X, Zhang L, Li Z, Wu A, et al. Level of circulating PD-L1 expression in patients with advanced gastric cancer and its clinical implications. *Chin J Cancer Res*. (2014) 26:104–11. doi: 10.3978/j.issn.1000-9604.2014.02.08

36. Finkelmeier F, Canli Ö, Tal A, Pleli T, Trojan J, Schmidt M, et al. High levels of the soluble programmed death-ligand (sPD-L1) identify hepatocellular carcinoma patients with a poor prognosis. *Eur J Cancer*. (2016) 59:152–9. doi: 10.1016/j.ejca.2016.03.002

37. Wu Y, Guo H, Yue J, Xu P. Serum sPD1 and sPDL1 as Biomarkers for Evaluating the Immune State of Lung Adenocarcinoma Patients. *J Immunol Res*. (2022) 2022:9101912. doi: 10.1155/2022/9101912

38. Liang Z, Chen W, Guo Y, Ren Y, Tian Y, Cai W, et al. Soluble monomeric human programmed cell death-ligand 1 inhibits the functions of activated T cells. *Front Immunol*. (2023) 14:1133883. doi: 10.3389/fimmu.2023.1133883

39. Okła K, Rajtak A, Czerwonka A, Bobiński M, Wawruszak A, Tarkowski R, et al. Accumulation of blood-circulating PD-L1-expressing M-MDSCs and monocytes/macrophages in pretreatment ovarian cancer patients is associated with soluble PD-L1. *J Transl Med*. (2020) 18:258. doi: 10.1186/s12967-020-02389-7

40. Mair MJ, Pajenda S, Ilhan-Mutlu A, Steindl A, Kiesel B, Widhalm G, et al. Soluble PD-L1 is associated with local and systemic inflammation markers in primary and secondary brain tumours. *ESMO Open*. (2020) 5:e000863. doi: 10.1136/esmoopen-2020-000863

41. Liu S, Zhu Y, Zhang C, Liu J, Lv H, Zhang G, et al. Soluble programmed death-1 (sPD-1) and programmed death ligand 1 (sPD-L1) as potential biomarkers for the diagnosis and prognosis of glioma patients. *J Med Biochem*. (2020) 39:444–51. doi: 10.5937/jomb0-24692

42. Mortensen JB, Monrad I, Enemark MB, Ludvigsen M, Kamper P, Bjerre M, et al. Soluble programmed cell death protein 1 (sPD-1) and the soluble programmed cell death ligands 1 and 2 (sPD-L1 and sPD-L2) in lymphoid Malignancies. *Eur J Haematol*. (2021) 107:81–91. doi: 10.1111/ejh.13621

43. Palicelli A, Bonacini M, Croci S, Magi-Galluzzi C, Cañete-Portillo S, Chaux A. What do we have to know about PD-L1 expression in prostate cancer? A systematic literature review. Part 2: clinic-pathologic correlations. *Cells*. (2021) 10:3. doi: 10.3390/cells10113165

44. Ge R, Wang Z, Cheng L. Tumor microenvironment heterogeneity an important mediator of prostate cancer progression and therapeutic resistance. *NPJ Precis Onc*. (2022) 6:31. doi: 10.1038/s41698-022-00272-w

45. Chang B, Huang T, Wei H, Shen L, Zhu D, He W, et al. The correlation and prognostic value of serum levels of soluble programmed death protein 1 (sPD-1) and soluble programmed death-ligand 1 (sPD-L1) in patients with hepatocellular carcinoma. *Cancer Immunol Immunother*. (2019) 68:353–63. doi: 10.1007/s00262-018-2271-4

46. Park W, Bang JH, Nam AR, Jin MH, Seo H, Kim JM, et al. Prognostic value of serum soluble programmed death-ligand 1 and dynamics during chemotherapy in advanced gastric cancer patients. *Cancer Res Treat*. (2021) 53:199–206. doi: 10.4143/crt.2020.497

47. Shin K, Kim J, Park SJ, Lee MA, Park JM, Choi MG, et al. Prognostic value of soluble PD-L1 and exosomal PD-L1 in advanced gastric cancer patients receiving systemic chemotherapy. *Sci Rep*. (2023) 13:6952. doi: 10.1038/s41598-023-33128-9

48. Han B, Dong L, Zhou J, Yang Y, Guo J, Xuan Q. The clinical implication of soluble PD-L1 (sPD-L1) in patients with breast cancer and its biological function in regulating the function of T lymphocyte. *Cancer Immunol Immunother*. (2021) 70:2893–909. doi: 10.1007/s00262-021-02898-4

49. Himuro H, Nakahara Y, Igarashi Y, Kouro T, Higashijima N, Matsuo N, et al. Clinical roles of soluble PD-1 and PD-L1 in plasma of NSCLC patients treated with immune checkpoint inhibitors. *Cancer Immunol Immunother*. (2023) 72:2829–40. doi: 10.1007/s00262-023-03464-w

50. Tiako Meyo M, Jouinot A, Giroux-Leprieur E, Fabre E, Wislez M, Alifano M, et al. Predictive value of soluble PD-1, PD-L1, VEGFA, CD40 ligand and CD44 for nivolumab therapy in advanced non-small cell lung cancer: A case-control study. *Cancers (Basel)*. (2020) 12:473. doi: 10.3390/cancers12020473

51. Montemagno C, Hagege A, Borchiellini D, Thamphya B, Rastoin O, Ambrosetti D, et al. Soluble forms of PD-L1 and PD-1 as prognostic and predictive markers of sunitinib efficacy in patients with metastatic clear cell renal cell carcinoma. *Oncoimmunology*. (2020) 9:1846901. doi: 10.1080/2162402X.2020.1846901

52. Park H, Bang JH, Nam AR, Eun Park J, Hua Jin M, Bang YJ, et al. Prognostic implications of soluble programmed death-ligand 1 and its dynamics during chemotherapy in unresectable pancreatic cancer. *Sci Rep*. (2019) 9:11131. doi: 10.1038/s41598-019-47330-1

53. Huang P, Hu W, Zhu Y, Wu Y, Lin H. The prognostic value of circulating soluble programmed death ligand-1 in cancers: A meta-analysis. *Front Oncol*. (2021) 10:626932. doi: 10.3389/fonc.2020.626932

54. Ha H, Bang JH, Nam AR, Park JE, Jin MH, Bang YJ, et al. Dynamics of soluble programmed death-ligand 1 (sPDL1) during chemotherapy and its prognostic implications in cancer patients: biomarker development in immuno-oncology. *Cancer Res Treat*. (2019) 51:832–40. doi: 10.4143/crt.2018.311

55. Vikerfors A, Davidsson S, Frey J, Jerlström T, Carlsson J. Soluble PD-L1 in serum and urine in urinary bladder cancer patients. *Cancers (Basel)*. (2021) 13:5841. doi: 10.3390/cancers13225841

56. Dank M, Mühl D, Herold M, Hornyák L, Szasz AM, Herold Z. Does elevated pre-treatment plasma PD-L1 level indicate an increased tumor burden and worse prognosis in metastatic colorectal cancer? *J Clin Med*. (2022) 11:4815. doi: 10.3390/jcm11164815

57. Larrinaga G, Solano-Iturri JD, Errarte P, Unda M, Loizaga-Iriarte A, Pérez-Fernández A, et al. Soluble PD-L1 is an independent prognostic factor in clear cell renal cell carcinoma. *Cancers (Basel)*. (2021) 13:667. doi: 10.3390/cancers13040667

58. Bian B, Fanale D, Dusetti N, Roque J, Pastor S, Chretien AS, et al. Prognostic significance of circulating PD-1, PD-L1, pan-BTN3As, BTN3A1 and BTLA in patients with pancreatic adenocarcinoma. *Oncoimmunology*. (2019) 8:e1561120. doi: 10.1080/2162402X.2018.1561120

59. Abu Hejleh T, Furqan M, Ballas Z, Clamon G. The clinical significance of soluble PD-1 and PD-L1 in lung cancer. *Crit Rev Oncol Hematol*. (2019) 143:148–52. doi: 10.1016/j.critrevonc.2019.08.009

60. Oh SY, Kim S, Keam B, Kim TM, Kim DW, Heo DS. Soluble PD-L1 is a predictive and prognostic biomarker in advanced cancer patients who receive immune checkpoint blockade treatment. *Sci Rep*. (2021) 11:19712. doi: 10.1038/s41598-021-99311-y

61. Ohkuma R, Ieguchi K, Watanabe M, Takayanagi D, Goshima T, Onoue R, et al. Increased plasma soluble PD-1 concentration correlates with disease progression in patients with cancer treated with anti-PD-1 antibodies. *Biomedicines*. (2021) 9:1929. doi: 10.3390/biomedicines9121929

62. Sorensen SF, Demuth C, Weber B, Sorensen BS, Meldgaard P. Increase in soluble PD-1 is associated with prolonged survival in patients with advanced EGFR-mutated non-small cell lung cancer treated with erlotinib. *Lung Cancer*. (2016) 100:77–84. doi: 10.1016/j.lungcan.2016.08.001

63. Shin SP, Seo HH, Shin JH, Park HB, Lim DP. Eom HS Adenovirus expressing both thymidine kinase and soluble PD1 enhances antitumor immunity by strengthening CD8 T-cell response. *Mol Ther*. (2013) 21:688–95. doi: 10.1038/mt.2012.252

64. Brown MD, van der Most R, Vivian JB, Lake RA, Larma I, Robinson BW. Loss of antigen cross-presentation after complete tumor resection is associated with the generation of protective tumor-specific CD8(+) T-cell immunity. *Oncoimmunology*. (2012) 1:1084–94. doi: 10.4161/onci.20924

65. Kruger S, Legenstein ML, Rösgen V, Haas M, Modest DP, Westphalen CB, et al. Serum levels of soluble programmed death protein 1 (sPD-1) and soluble programmed death ligand 1 (sPD-L1) in advanced pancreatic cancer. *Oncoimmunology*. (2017) 6:e1310358. doi: 10.1080/2162402X.2017.1310358

66. Vajavaara H, Mortensen JB, Leivonen SK, Hansen IM, Ludvigsen M, Holte H, et al. Soluble PD-1 but not PD-L1 levels predict poor outcome in patients with high-risk diffuse large B-cell lymphoma. *Cancers (Basel)*. (2021) 13:398. doi: 10.3390/cancers13030398

67. Pedersen JG, Sokac M, Sørensen BS, Luczak AA, Aggerholm-Pedersen N, Birkbak NJ, et al. Increased soluble PD-1 predicts response to nivolumab plus ipilimumab in melanoma. *Cancers (Basel)*. (2022) 14:3342. doi: 10.3390/cancers14143342

68. Liang Z, Tian Y, Cai W, Weng Z, Li Y, Zhang H. High-affinity human PD-L1 variants attenuate the suppression of T cell activation. *Oncotarget*. (2017) 8:88360–75. doi: 10.18632/oncotarget.v8i51

69. Lu L, Risch E, Halaban R, Zhen P, Bacchiocchi A, Risch HA. Dynamic changes of circulating soluble PD-1/PD-L1 and its association with patient survival in immune checkpoint blockade-treated melanoma. *Int Immunopharmacol*. (2023) 118:110092. doi: 10.1016/j.intimp.2023.110092

70. Kurosaki T, Chamoto K, Suzuki S, Kanemura H, Mitani S, Tanaka K. The combination of soluble forms of PD-1 and PD-L1 as a predictive marker of PD-1 blockade in patients with advanced cancers: a multicenter retrospective study. *Front Immunol*. (2023) 14:1325462. doi: 10.3389/fimmu.2023.1325462

71. Lin D, Wang X, Choi SYC, Ci X, Dong X, Wang Y. Immune phenotypes of prostate cancer cells: Evidence of epithelial immune cell-like transition? *Asian J Urol*. (2016) 3:195–202. doi: 10.1016/j.ajur.2016.08.002

72. Castello A, Rossi S, Toschi L, Mansi L, Lopci E. Soluble PD-L1 in NSCLC patients treated with checkpoint inhibitors and its correlation with metabolic parameters. *Cancers (Basel)*. (2020) 12:1373. doi: 10.3390/cancers12061373

73. Francisco LM, Salinas VH, Brown KE, Vanguri VK, Freeman GJ, Kuchroo VK, et al. PD-L1 regulates the development, maintenance, and function of induced regulatory T cells. *J Exp Med*. (2009) 206:3015–29. doi: 10.1084/jem.20090847

74. DiDomenico J, Lamano JB, Oyon D, Li Y, Veliceasa D, Kaur G, et al. The immune checkpoint protein PD-L1 induces and maintains regulatory T cells in glioblastoma. *Oncoimmunology*. (2018) 7:e1448329. doi: 10.1080/2162402X.2018.1448329

75. Dong Y, Han Y, Huang Y, Jiang S, Huang Z, Chen R, et al. PD-L1 is expressed and promotes the expansion of regulatory T cells in acute myeloid leukemia. *Front Immunol*. (2020) 11:1710. doi: 10.3389/fimmu.2020.01710

76. Li X, Du H, Zhan S, Liu W, Wang Z, Lan J, et al. The interaction between the soluble programmed death ligand-1 (sPD-L1) and PD-1+ regulator B cells mediates immunosuppression in triple-negative breast cancer. *Front Immunol*. (2022) 13:830606. doi: 10.3389/fimmu.2022.830606

77. Bocanegra A, Blanco E, Fernandez-Hinojal G, Arasanz H, Chocarro L, Zuazo M, et al. PD-L1 in systemic immunity: unraveling its contribution to PD-1/PD-L1 blockade immunotherapy. *Int J Mol Sci*. (2020) 21:5918. doi: 10.3390/ijms21165918

78. Lu C, Redd PS, Lee JR, Savage N, Liu K. The expression profiles and regulation of PD-L1 in tumor-induced myeloid-derived suppressor cells. *Oncoimmunology*. (2016) 5:e1247135. doi: 10.1080/2162402X.2016.1247135

frontiers | Frontiers in Immunology

TYPE Original Research
PUBLISHED 15 August 2024
DOI 10.3389/fimmu.2024.1424393

OPEN ACCESS

EDITED BY
Raquel Tarazona,
University of Extremadura, Spain

REVIEWED BY
Katarina Mirjacic Martinovic,
Institute of Oncology and Radiology of Serbia, Serbia
Danay Saavedra,
Center of Molecular Immunology, Cuba

*CORRESPONDENCE
Yongsheng Zhang
zhangys1985@jlu.edu.cn
Jing Huang
huangj@jlu.edu.cn

RECEIVED 28 April 2024
ACCEPTED 30 July 2024
PUBLISHED 15 August 2024

CITATION
Wang Y, Sun C, Liu M, Xu P, Li Y, Zhang Y and Huang J (2024) Dysregulated gene expression of SUMO machinery components induces the resistance to anti-PD-1 immunotherapy in lung cancer by upregulating the death of peripheral blood lymphocytes.
Front. Immunol. 15:1424393.
doi: 10.3389/fimmu.2024.1424393

Dysregulated gene expression of SUMO machinery components induces the resistance to anti-PD-1 immunotherapy in lung cancer by upregulating the death of peripheral blood lymphocytes

Ying Wang[1], Chao Sun[2], Mengmeng Liu[1], Panyang Xu[1], Yanyan Li[1], Yongsheng Zhang[3]* and Jing Huang[1]*

[1]Department of Laboratory Medicine, The First Hospital of Jilin University, Changchun, China, [2]Cancer Center, The First Hospital of Jilin University, Changchun, China, [3]Prenatal Diagnosis Center, Reproductive Medicine Center, The First Hospital of Jilin University, Changchun, China

Background: The majority of patients with lung cancer exhibit drug resistance after anti-PD-1 immunotherapy, leading to shortened patient survival time. Previous studies have suggested an association between epigenetic abnormalities such as methylation and clinical response to anti-PD-1 immunotherapy, while the role of SUMOylation in resistance to anti-PD-1 antibody immunotherapy is still unclear.

Methods: Here, the mRNA expression of 15 SUMO machinery components in PBMC from lung cancer patients receiving anti-PD-1 immunotherapy were analyzed using real-time PCR. Base on the percentage change in mRNA levels, the relationship between the expression of SUMO machinery components and outcomes of anti-PD-1 immunotherapy, and the influencing factors of SUMOylation were evaluated. PBMC was treated with different concentrations of 2-D08 (a specific inhibitor of SUMOylation) *in vitro*, and analyzed the activation and the death rates of lymphocyte subsets by flow cytometry analysis.

Results: A predictive method, base on the gene expression of three SUMO machinery components (*SUMO1*, *SUMO3* and *UBE2I*), were developed to distinguish non-responders to PD-1 inhibitors. Furthermore, the number of lymphocytes in peripheral blood significantly reduced in the dysregulated SUMOylation groups (the percentage change >100 or -50 ~ -100 groups). *In vitro* studies confirmed that lightly low SUMOylation level improved the activation status of T and NK lymphocytes, but extremely low SUMOylation level lead to the increased death rates of lymphocytes.

Conclusion: Our findings implied that dysregulated gene expression of SUMO machinery components could induce the resistance of anti-PD-1 immunotherapy in lung cancer by upregulating the death of peripheral blood lymphocytes. These data might provide effective circulating biomarkers for predicting the efficacy of anti-PD-1 immunotherapy, and uncovered a novel regulatory mechanism of resistance to anti-PD-1 immunotherapy.

KEYWORDS

PD-1, resistance, Sumoylation, lymphocyte, peripheral blood

Introduction

Lung cancer is one of the malignant diseases with high incidence and mortality (1, 2). Since most patients with advanced lung cancer lose the opportunity for surgical resection, they often require anti-tumor immunotherapy, such as anti-programmed cell death-1 (PD-1) immunotherapy (3). However, the majority of patients remained unresponsive or worsening of disease after PD-1 blockade, which is known as the resistance to anti-PD-1 immunotherapy (4). Research indicates that resistance is a common cause of shortened survival and increased mortality in patients with anti-PD-1 immunotherapy (5). Therefore, it is important to comprehend mechanisms of the resistance to anti-PD-1 immunotherapy and identify patients who may potentially benefit from therapeutic schedule.

Numerous studies on anti-PD-1 immunotherapy have shown that epigenetic aberrations may lead to the resistance to PD-1 inhibition, thereby leading to poor prognosis (6, 7). Small ubiquitin-like modification (SUMOylation) is an epigenetic modification gaining most of the research interest recently (8). During SUMOylation, small ubiquitin-like modifiers (SUMO) are covalently attached to target proteins via an enzymatic cascade that requires the sequential action of SUMO activating enzyme, SUMO conjugating enzyme and SUMO ligases (9, 10). Similar to other epigenetic modifications, the covalent conjugation of SUMO to protein substrates is a reversible modification and cleaved by SUMO specific proteases (SENPs), i.e., deSUMOylation (11). Cumulative studies have indicated that SUMOylation regulates a number of biological processes, including carcinogenesis, cell cycle progression, apoptosis and immune responses (12). To date, five categories of SUMO machinery components had been identified, including SUMO isoforms (SUMO1~4), SUMO activating enzyme (SAE1 and UBA2), SUMO conjugating enzyme (Ubc9, encoded by *UBE2I*), SUMO ligases (PIAS1, etc) and SUMO specific proteases (SENP1, 2, 3, 5, 6, 7) (9, 10). Owing to the critical roles of SUMO machinery components in maintaining the steady-state level between SUMOylated and deSUMOylated in substrate proteins, it is conceivable that altered expression of these components can lead to various diseases, particularly cancer (13). For example, in glioblastoma (GBM), SUMO machinery components are upregulated, such as SUMO activating enzyme (SAE1), SUMO conjugating enzyme (Ubc9) and SUMO specific protease (SENP1), promoting tumor progression (14). Similarly, upregulated SUMO conjugating enzyme (Ubc9) promoted transcription factor Slug SUMOylation play a crucial role in hypoxia-induced lung cancer progression (15). Recently, epigenetic drugs have been shown to reduce the resistance of certain cancer patients to PD-1 inhibitors (16). For example, inhibitors of histone deacetylase or inhibitors of DNA Methyltransferase effectively overcome the resistance to anti-PD-1 immunotherapy in breast cancer and melanoma (17, 18). However, the role of SUMOylation in the resistance to anti-PD-1 immunotherapy is still unclear.

In anti-PD-1 immunotherapy, treatment with the PD-1 blockade interrupted the inhibitory effect mediated by PD-1/PD-L1 axis and restored activity of lymphocytes, which are the main effector cells with an anti-tumor function (19). Recent studies have found that, during anti-PD-1 immunotherapy, only a small fraction of tumor-infiltrating lymphocytes can specifically recognize and attack cancer cells to achieve therapeutic effects (20, 21). When they are exhausted, the continuous recruitment of a large number of peripheral blood lymphocytes into tumors for supplementing tumor infiltrating lymphocytes may be important for subsequent anti-PD-1 treatment responsiveness (22, 23). At present, the number of peripheral blood lymphocytes has been adopted as a clinical prediction tool for the therapeutic efficacy of anti-PD-1 immunotherapy (24, 25). Therefore, analyzing the factors that cause changes in peripheral blood lymphocyte count during anti-PD-1 immunotherapy may help to understand the mechanism of the resistance to anti-PD-1 immunotherapy and improve treatment efficacy.

In this study, we focused attention on the mRNA expression of 15 SUMO machinery components, including four SUMO genes (*SUMO1~4*), two SUMO activating enzyme genes (*SAE1* and *UBA2*), a SUMO conjugating enzyme gene (*UBE2I*), two SUMO ligase genes (*PIAS1* and *PIAS2*) and six SUMO specific protease genes (*SENP 1,2,3,5,6,7*), in peripheral blood mononuclear cells (PBMC). By analyzing these genes of 105 patients with lung cancer during anti-PD-1 immunotherapy, we developed a predictive method, based on the *SUMO1*, *SUMO3* and *UBE2I*, to distinguish non-responders with a progressive disease. Further analysis showed that dysregulated gene expression of SUMO machinery components was associated with decreased peripheral lymphocyte

counts during the resistance process of anti-PD-1 immunotherapy in lung cancer. The *in vitro* experiments validated that dysregulated SUMOylation were one reason for inducing increased lymphocyte death. Together, these results indicated that dysregulated gene expression of SUMO machinery components may be a potential underlying cause of developing resistance to anti-PD-1 immunotherapy, and effective circulating biomarkers for predicting the efficacy of this treatment.

Materials and methods

Study design

Patients were enrolled from conventional treatments at the First Hospital of Jilin University, Changchun, China, from January 2023 to December 2023. For inclusion criteria: patients were diagnosed with late-stage lung cancer (stage III/IV, including local, regional and distant recurrence). The treatment regimens were determined by clinicians based on the patient's condition. All enrolled patients received PD-1 mAb intravenously once every 3 weeks until disease progression or unacceptable toxicity. Based on Response Evaluation Criteria in Solid Tumors (RECIST) V.1.1 criteria, these patients were divided into a responder (R) group and a non-responder (NR) group. Responders were defined as a patient who achieved complete response (CR), partial response (PR) or stable disease (SD) after anti-PD-1 immunotherapy for more than 24 weeks. Non-responders were defined as a patient who had progressive disease (PD) after anti-PD-1 immunotherapy for less than 24 weeks. Patients with other malignancies or comorbidities (e.g., heart failure, severe diabetes mellitus) were excluded. The study was approved by the Human Ethics Committee of the First Hospital of Jilin University (23K155-001). All participants had signed informed consent forms before collecting samples.

Real-time PCR

PBMC were isolated from lung cancer patients who received anti-PD-1 immunotherapy for 9 weeks by using Ficoll-Hypaque (Sigma Aldrich, USA) density gradient centrifugation. The 9th week is in line with the recommended time node for the first response assessment of tumor according to the guidelines and consensus (26–28). Total RNA was extracted from PBMC using MolPure Cell RNA Kit (YEASEN Biotech Co., Ltd, China) following the manufacturer's instructions. cDNA synthesis was carried out by using Hifair III 1st Strand cDNA Synthesis SuperMix for qPCR (YEASEN Biotech Co., Ltd, China). The mRNA expression of 15 SUMO machinery components were analyzed by real-time PCR using the SYBR Green PCR Master Mix (YEASEN Biotech Co., Ltd, China). Considering the comparability of data, we combined the mRNA expression levels of PBMC from 10 untreated patients with lung cancer as the baseline value and defined it as 1. The relative mRNA expression levels of 15 SUMO machinery components in PBMC were calculated using the $2^{-\Delta\Delta CT}$ method. GAPDH served as an internal control. The sequences of real-time PCR primers were shown as Supplementary Table 1.

Prediction model

We calculated the percentage changes in relative mRNA level of 15 SUMO machinery components in PBMC from 105 lung cancer patients as the following formula: [(express value-baseline value)/baseline value]×100%. The utilization of the percentage change formula for data normalization had been implemented in multiple studies searching for biomarkers of cancer immunotherapy efficacy (29–31). We developed a risk score base on different percentage changes in SUMO machinery components, which could be used to identify the high risk patients for developing NR. The risk score of patient was defined as 2, if the percentage change in mRNA level of SUMO machinery components in PBMC was greater than 100 times or less than -50~-100 times. The risk score of patient was defined as 1, if the percentage change in mRNA level of SUMO machinery components in PBMC was less than 100 times and greater than -50. Receiver operating characteristic (ROC) curves were used to assess diagnostic accuracy of changes in SUMO machinery components in predicting the probability of NR.

PBMC under treatment with the SUMOylation inhibitor

To investigate the effect of SUMOylation inhibition on lymphocytes in peripheral blood, we chose 2-D08 (YEASEN Biotech Co., Ltd, China) to treat PBMC. 2-D08 is a specific inhibitor of SUMOylation that blocks the transfer of SUMO protein from the SUMO-Conjugating Enzyme (Ubc9) thioester conjugate to substrates. In the *in vitro* culture system, PBMCs isolated from 27 lung cancer patients treated with PD-1 antibody were cultured in RPMI1640 medium containing 10% fetal bovine serum (FBS; Thermo fisher scientific, USA). Along with the concentration of 2-D08 gradually increased, we observed the dose effect of SUMOylation inhibition on lymphocytes. After 24 hours of adding 2-D08, PBMCs were harvested and analyzed by flow cytometry.

Flow cytometry analysis

Samples were tested by 10-colour/three laser flow cytometer (FACSCantoTM, BD Bioscience, USA) and analyzed by BD FACSDiva™ software (BD Bioscience, USA). The following fluorescently-conjugated antibodies were used for cell phenotypic analysis: CD45- PerCP (BD Bioscience, USA; Cat#652803), CD3-FITC (BD Bioscience, USA; Cat#349201), CD4-APC-Cy7 (BD Bioscience, USA; Cat#557871), CD8-PE-Cy7 (BD Bioscience, USA; Cat#557746), CD19-APC (BD Bioscience, USA; Cat#652804), CD56- BV510 (BD Bioscience, USA; Cat#563041), CD69-Alexa Fluor 700 (BD Bioscience, USA; Cat#560739). The death of lymphocytes was measured by staining with Annexin V-PE antibody (BD Bioscience, USA; Cat#559763). All antibodies for flow cytometry in this study were purchased from BD Biosciences. The gating strategy for cell subsets were shown in corresponding figures.

Statistical analysis

Differences among normally distributed variables were analyzed using a Student's t-test. For variables that were not normally distributed, a Mann-Whitney U test or Kruskal-Wallis ANOVA test was used. Statistical significance was shown as: * $P< 0.05$, ** $P< 0.01$. *** $P< 0.001$. Statistical analyses were performed using Prism 10.0 (GraphPad Prism, RRID: SCR_002798) and SPSS 27.0 statistical software package (SPSS, RRID: SCR_002865).

Results

The relationship between dysregulated gene expression of SUMO machinery components in PBMC and the prevalence rates of NR

To search for potential regulatory points that may influence clinical response to anti-PD-1 immunotherapy, we explored the relative mRNA expression of 15 SUMO machinery components in PBMC from 105 lung cancer patients (53 responders and 52 non-responders) for 9 weeks after anti-PD-1 immunotherapy (Figures 1A–C; Supplementary Figures 1, 2). We found that the average expression levels of each gene in PBMC was not significantly different between R group and NR group. However, compared with the R group, the dots in the scatter plot of gene expression in the NR group appeared to be more scattered. Subsequently, based on analysis of variance, the discretization of relative mRNA expression of 15 SUMO machinery components between the R and NR groups was investigated. As expected, except for *SUMO4*, *SAE1*, *PIAS1* and *SENP5*, the discretization of the other 11 genes in the NR group was significantly higher than that in the R group (all p values < 0.05).

In order to accurately evaluate the relationship between the mRNA expression of SUMO machinery components and outcomes of anti-PD-1 immunotherapy, we used the formula [(express value-baseline value)/baseline value] ×100% to calculate the relative percentage change in SUMO machinery component mRNA levels after implementation of anti PD-1 immunotherapy. The baseline value is the average mRNA expression level of corresponding SUMO machinery component in PBMCs of 10 untreated lung cancer patients. By calculating, we obtained the percentage change in relative mRNA levels and used it as an indicator of the severity of SUMOylation dysfunction (32–34). Based on the distribution of percentage change data, we roughly divided it into five groups, which are >100, 50~100, 0~50, 0~-50, -50~-100. Then the prevalence rates of NR based on specific percentage changes in relative mRNA levels were analyzed. The results showed that the prevalence rates of NR had significant differences among diverse

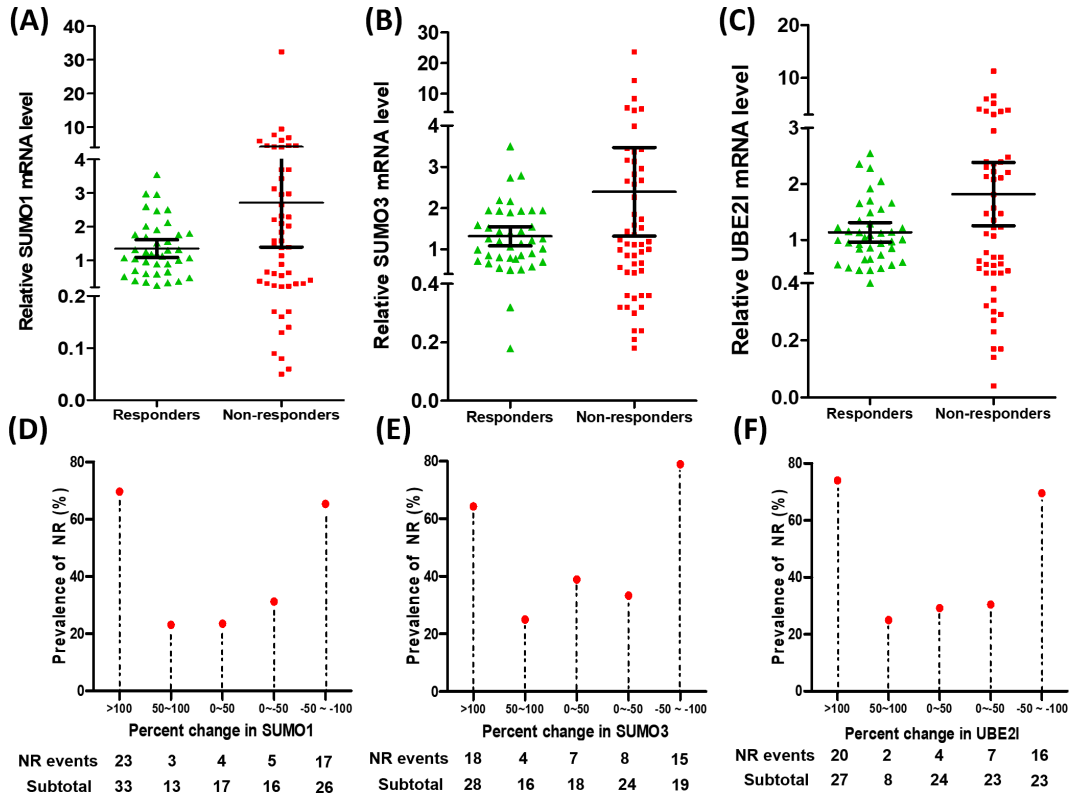

FIGURE 1
Dysregulated gene expression of SUMO machinery components in PBMC was associated with the prevalence rates of NR. **(A–C)** The relative mRNA expression of *SUMO1* **(A)**, *SUMO3* **(B)** and *UBE2I* **(C)** in PBMC from responders (n=53) and non-responders (n=52). Data were expressed as mean ± 95%CI. **(D–F)** The percentage change in the relative mRNA expression of three SUMO machinery components (*SUMO1*, *SUMO3* and *UBE2I*) was associated with the prevalence rates of NR.

percentage change groups of *SUMO1* (Figure 1D, p=0.001), *SUMO3* (Figure 1E, p=0.003) and *UBE2I* (Figure 1F, p<0.001). Notably, the prevalence rates of NR significantly increased in the highest percentage change group (>100) and the lowest percentage change group (-50~-100), compared with other three groups. On the contrary, the percentage change of other 12 genes had no significant correlation with the prevalence rates of NR (Supplementary Figures 1, 2). These results indicate that the dysregulation of *SUMO1*, *SUMO3*, and *UBE2I* expression in PBMC was positively correlated with the occurrence of NR and played an important role in the resistance process of anti PD-1 immunotherapy.

The predictive value of the mRNA levels of *SUMO1*, *SUMO3* and *UBE2I* in PBMC for clinical response to anti-PD-1 immunotherapy

To evaluate the predictive ability of *SUMO1*, *SUMO3* and *UBE2I* for clinical response to anti-PD-1 therapy, we developed a risk score based on different percentage changes in mRNA level of three genes. The patients were grouped into the high-risk group and scored as 2, if the percentage change in mRNA level of three genes in PBMC was greater than 100 times or less than -50~-100 times. The patient was grouped into the low-risk group and scored as 1, if the percentage change in mRNA level of three genes in PBMC was less than 100 times and greater than -50. ROC curves was used to assess diagnostic accuracy of the percentage change in three genes to predict the probability of NR (Figure 2). *SUMO1* predicted the probability of NR with a sensitivity of 75.0% and specificity of 67.9% (cut-off value: 1.5; area under the curve [AUC]: 0.715; 95% confidence interval [CI]: 0.614 to 0.815; P <0.001). The AUC for *SUMO3* to predict NR was 0.704 (cut-off value: 1.5; 95% CI: 0.603 to 0.805; P < 0.001), and the sensitivity and specificity were 63.5% and 77.4%, respectively. ROC analysis revealed that *UBE2I* (cut-off value: 1.5; AUC: 0.733; 95% CI 0.635-0.831; P < 0.001; sensitivity: 69.2%; specificity: 77.4%) had best predictive power for the probability of NR among three genes. Moreover, the analysis of combined three genes (cut-off value, AUC, sensitivity and specificity of 5.5, 0.791, 57.7% and 96.2%, respectively) yielded a higher diagnostic accuracy than that of single gene in NR diagnosis. These results suggested that the percentage change in mRNA level of 3 SUMO machinery components (*SUMO1*, *SUMO3* and *UBE2I*), either alone or in combination, could to some extent predict clinical response to anti-PD-1 immunotherapy.

The influencing factors of dysregulated SUMO machinery components in peripheral blood of lung cancer patients

Due to the best predictive ability of *UBE2I* for NR among SUMO machinery components, we attempted to identify the influencing factors of SUMOylation based on the percentage change in mRNA level of *UBE2I*. The enrolled 105 patients were divided into five groups for evaluation of sociodemographic, clinical, and peripheral leukocyte characteristics. As shown in Table 1, the results showed that the percentage change in mRNA level of *UBE2I* was not associated with age, sex, histology, disease stage and treatment. By analyzing peripheral leukocyte characteristics, we found that the number of leukocytes (white blood cells, WBC) (Figure 3A), neutrophils (NEU) (Figure 3B) and monocytes (MON) (Figure 3C) had no significant differences among five groups. However, as shown in Figure 3D, the number of lymphocytes (LYM) were significantly reduced in the highest percentage change group (>100) and the lowest percentage change group (-50~-100). Subsequently, we analyzed the data of lymphocyte subsets from 90 patients who underwent peripheral lymphocyte subset analysis. The results showed that there was no significant differences in the proportion of various lymphocyte subsets among five groups (Figures 3E–H). Furthermore, based on the percentage change in mRNA level of *SUMO1* (Supplementary Figure 3) and *SUMO3* (Supplementary Figure 4), the characteristics of peripheral leukocytes were similar with *UBE2I*. Our data indicated that SUMOylation related non-response to anti-

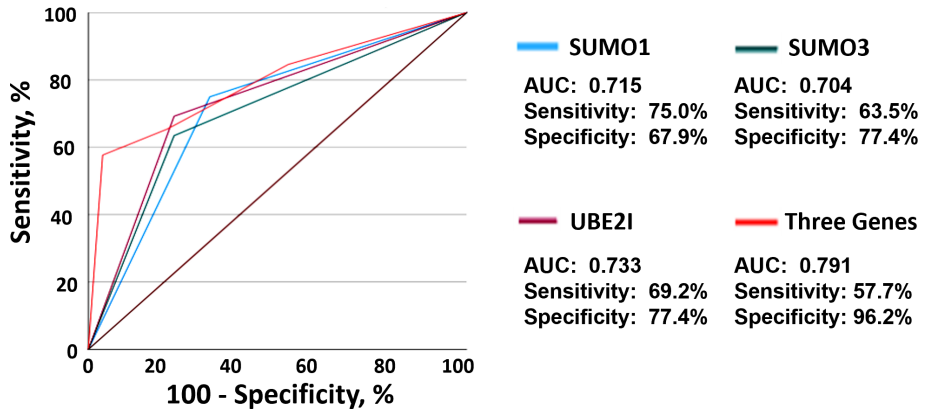

FIGURE 2
The mRNA levels of three SUMO machinery components predicted clinical response to anti-PD-1 immunotherapy. ROC analysis based on *SUMO1* (blue), *SUMO3* (green), *UBE2I* (purple) and combined three genes (red) for the diagnosis of non-responders was shown.

10.3389/fimmu.2024.1424393

TABLE 1 Baseline characteristics and *UBE2I* expression.

Patient characteristics	The percentage change of *UBE2I*					*P Value*
	>100 n=27	50~100 n=8	0 ~ 50 n=24	0~ -50 n=23	-50 ~ -100 n=23	
Age, years						*0.102*
Median	60.19	66.25	62.92	62.61	64.52	
Range	51~77	48~72	44~79	50~80	43~83	
Sex, No. (%)						*0.552*
Male	23 (85.19)	6 (75.00)	17 (70.83)	15 (65.22)	18 (78.26)	
Female	4 (14.81)	2 (25.00)	7 (29.17)	8 (34.78)	5 (21.74)	
Histology, No. (%)						*0.776*
Adenocarcinoma	8 (29.63)	3 (37.50)	10 (41.67)	11 (47.82)	10 (43.48)	
Squamous cell carcinoma	13 (48.16)	3 (37.50)	11 (45.83)	6 (26.09)	10 (43.48)	
Small cell carcinoma	6 (22.21)	2 (25.00)	3 (12.50)	6 (26.09)	3 (13.04)	
Disease stage, No. (%)						*0.784*
c-stage III	11 (40.74)	2 (25.00)	7 (29.17)	10 (43.48)	8 (34.78)	
c-stage IV	16 (59.26)	6 (75.00)	17 (70.83)	13 (56.52)	15 (65.22)	
Treatment, No. (%)						*0.346*
Anti–PD-1	9 (33.33)	1 (12.50)	7 (29.17)	3 (13.04)	8 (34.78)	
Chemotherapy+ anti-PD-1	18 (66.67)	7 (87.50)	17 (70.83)	20 (86.96)	15 (65.22)	

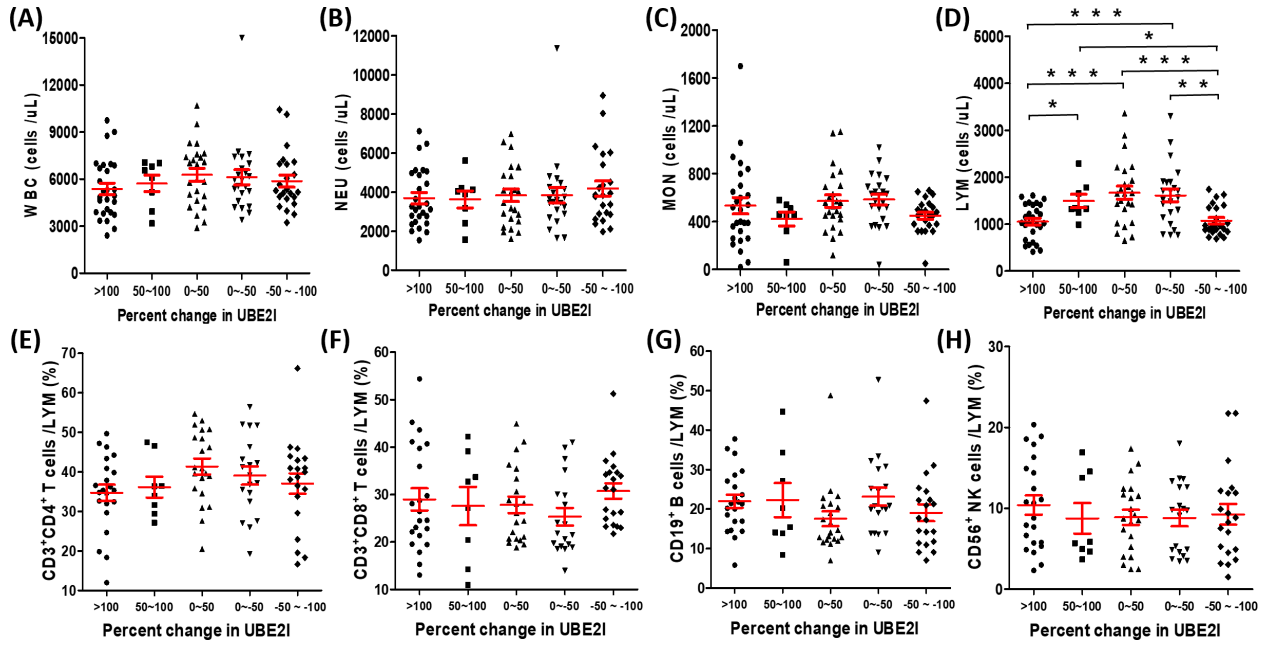

FIGURE 3
Association between the percentage change in *UBE2I* mRNA level and different white blood cell populations in peripheral blood of lung cancer patients. **(A–D)** The absolute counts of white blood cell (WBC), neutrophils (NEU), monocytes (MON) and lymphocytes (LYM) were compared among different groups base on the percentage change of *UBE2I*. **(E–H)** The percentages of lymphocyte subsets were compared among different groups base on the percentage change of *UBE2I*. Student's paired t-test, * $P < 0.05$, ** $P < 0.01$, *** $P < 0.001$.

PD-1 immunotherapy might be associated with decreased peripheral lymphocyte count.

The regulatory effect of SUMOylation inhibition on lymphocyte activity and death

To investigate the effect of SUMOylation on lymphocytes in peripheral blood, we treated PBMC of 27 lung cancer patients receiving PD-1 treatment with different concentrations of 2-D08 (a specific inhibitor of SUMOylation) *in vitro*, and analyzed the activation status ($CD69^+$) and the death rates (Annexin V^+) of different lymphocyte subsets by flow cytometry analysis. The gating strategy was presented in Figure 4A. We found that the percentages of $CD45^+CD3^+CD4^+CD69^+$T cells (Figure 4B), $CD45^+CD3^+CD8^+CD69^+$T cells (Figure 4C) and $CD45^+CD3^-CD56^+CD69^+$NK cells (Figure 4D) were significantly up-regulated in a 2-D08 dose-dependent manner, but the gradually increasing concentrations of 2-D08 had no effect on the percentages of $CD45^+CD3^-CD19^+CD69^+$B cells (Figure 4E). Similarly, 2-D08 increased the percentage of $CD45^+CD3^+CD4^+$Annexin V^+T cells (Figure 4B), $CD45^+CD3^+CD8^+$Annexin V^+T cells (Figure 4C), and $CD45^+CD3^-CD19^+$Annexin V^+B cells (Figure 4E) in a dose-dependent manner at concentrations greater than 10μM. However, it was worth noting that 2-D08 reduced the percentage of these cells at 5μM concentrations (Figures 4B, C, E). Besides, $CD45^+CD3^-CD56^+$NK cells also displayed an increased percentage of Annexin V^+ cells at higher concentrations of 2-D08 (≥20μM) (Figure 4D). These results suggested that although inhibition of SUMOylation levels could improve the activation status of T and NK lymphocytes, extreme decline in SUMOylation levels would lead to the increased death rates of lymphocytes.

Discussion

In this study, we found that the dysregulated mRNA expression (extremely high or low level) of three SUMO machinery components (*SUMO1*, *SUMO3* and *UBE2I*) in PBMC was related to the resistance to anti-PD-1 immunotherapy. The mRNA expression of SUMO genes (either *SUMO1* or *SUMO3*) plus the only SUMO E2 conjugating enzyme gene (*UBE2I*) was necessary for SUMOylation, and the abnormal change of their expression had a significant impact on SUMOylation level in PBMC (35). Therefore, we speculated that dysregulated SUMOylation (extremely high or low level) in PBMC may promote the occurrence of resistance to anti-PD-1 immunotherapy in lung cancer. It had been shown that up-regulation of certain SUMO machinery components correlated with the resistance in lung cancer (36). For example, *UBA2* was highly expressed in lung cancer and it knockdown increased the sensitivity of cancer cell to etoposide and cisplatin (37). *SENP1* had been reported to overexpressed in patients with lung cancer, and had a negative correlation with treatment response and could potentially predict chemosensitivity (38, 39). In spite of this, up-regulation of certain SUMO machinery components associated with favorable treatment response in some cases such as *UBE2I* 10920CG genotype enhances sensitivity to irinotecan chemotherapy in lung cancer through upregulation of *SUMO1* in tumor cells (40). These findings suggested that SUMOylation might play a complex and crucial role in the resistance of lung cancer. However, previous researchers mainly focused on the SUMOylation level during the development of resistance in tumor cells, rather than lymphocytes, which is the main effector cell in anti-PD-1 immunotherapy (41, 42). The main subpopulation of PBMC analyzed in this study is lymphocyte (43, 44). It was reported that the homeostasis and function of lymphocytes could be used to predict the response to anti-PD-1 immunotherapy in lung cancer (25). Although the steady-state level of SUMOylation played an essential role in the homeostasis and function of lymphocytes, the relationship between dysregulated SUMOylation in lymphocytes and the resistance to anti-PD-1 immunotherapy in lung cancer was still unclear (45–48).

By analyzing the immunotherapy cohort of lung cancer, we found that dysregulated gene expression of SUMO machinery components were associated with decreased peripheral blood lymphocytes counts. It was reported that the dynamically monitoring with peripheral blood lymphocytes count had great value in assessing treatment efficacy and predicting prognosis of anti-PD-1 immunotherapy (25, 49, 50). Interestingly, some researchers had found that decreased peripheral lymphocyte counts before treatment was not associated with poorer survival in patients, but persistence of decreased peripheral lymphocyte counts after 12 weeks of immunotherapy might be a poor prognostic marker of patient survival (51). However, the reason for a decreased of peripheral blood lymphocytes during therapy is unclear. Our findings evidenced that dysregulated SUMOylation is an inducing factor of decreased peripheral blood lymphocytes during anti-PD-1 immunotherapy. In *in vitro* experiments, we found that lightly low SUMOylation level (PBMC was treated with less than 5 μM 2-D08) was associated with the decreased death rates of lymphocyte, but extremely low SUMOylation level (PBMC was treated with greater than 10μM 2-D08) was associated with the increased death rates of lymphocyte. The results indicated that the steady-state level of SUMOylation might be promoting effective therapeutic response of anti-PD-1 immunotherapy by maintaining peripheral blood lymphocyte number, but dysregulated SUMOylation might be detrimental to treatment by promoting peripheral blood lymphocyte death. According to the reports, accumulation of SUMOylated STAT5 and SUMOylated Daxx resulted in growth suppression of lymphocyte (52, 53). Furthermore, in a mouse model of pancreatic ductal adenocarcinoma (PDAC), the SUMOylation inhibitor treated mice demonstrated a decrease in absolute numbers of peripheral lymphocytes. Although the SUMOylation inhibitor efficiently limited tumor growth by inhibiting cancer cell cycle progression and activating interferon signaling in lymphocytes, mouse were only well tolerated during short term treatment (54). We speculate that a strong decrease of peripheral blood lymphocyte induced by the SUMOylation inhibitor may be the main reason for the interruption of later experiments. Remarkably, the number of total lymphocyte was significantly reduced in the highest/lowest percentage change group, but there was no significant difference in the proportion of various lymphocyte subsets among five

10.3389/fimmu.2024.1424393

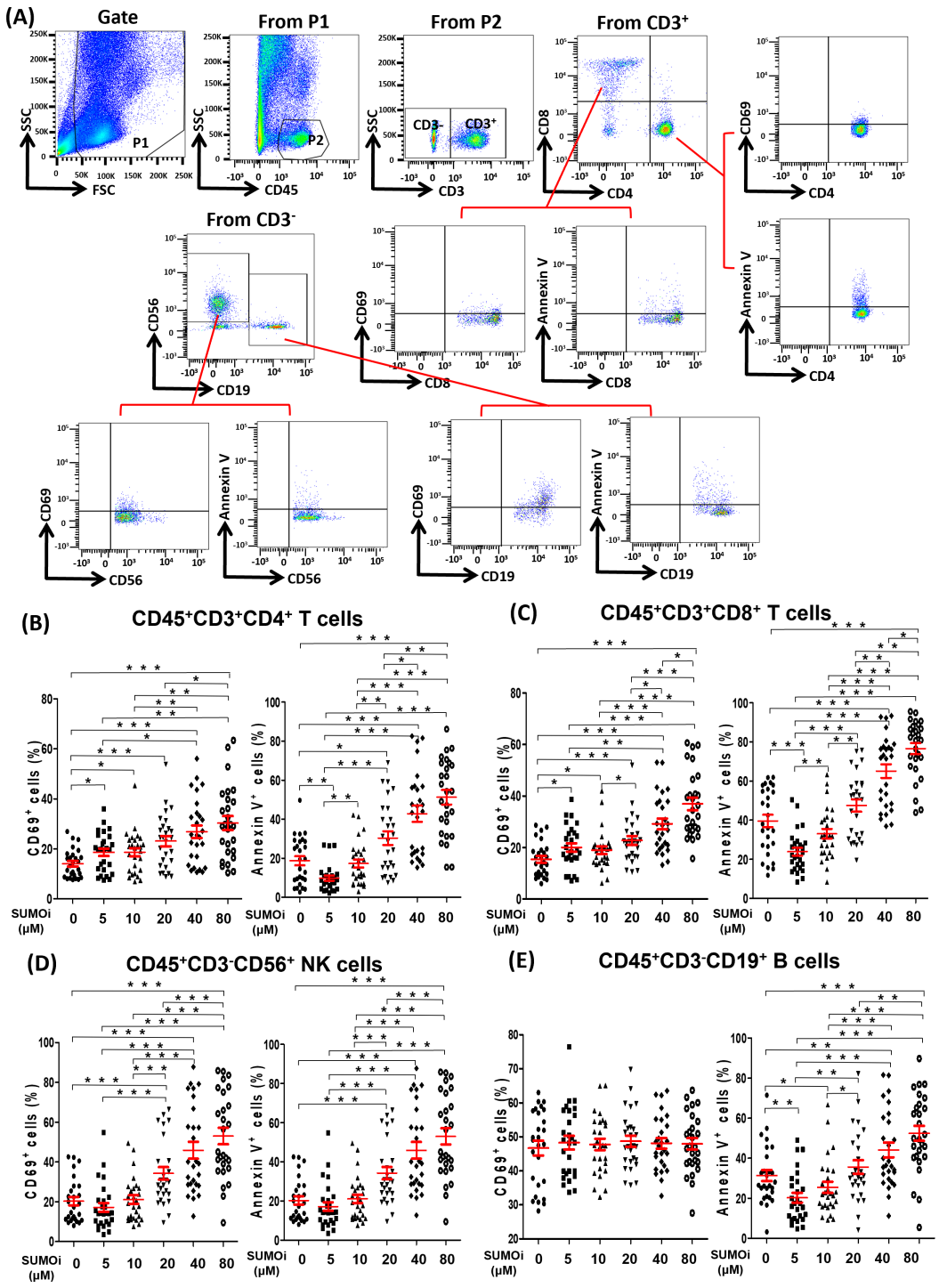

FIGURE 4
The relationship between the SUMOylation inhibition and the phenotype of lymphocyte. **(A)** Flow-cytometry dot plots showed the strategy for gating peripheral blood lymphocyte cells with $CD69^+$ and Annexin V^+ phenotype. **(B-E)** The expression of CD69 and Annexin V were analyzed on $CD45^+CD3^+CD4^+$ T cells **(B)**, $CD45^+CD3^+CD8^+$ T cells **(C)**, $CD45^+CD3^-CD56^+$ NK cells **(D)** and $CD45^+CD3^-CD19^+$ B cells **(E)**. Student's paired t-test, * $P < 0.05$, ** $P < 0.01$, *** $P < 0.001$.

percentage change groups. This seemed to be related to the similar decreased degree of different lymphocyte subsets induced by dysregulated SUMOylation. In *in vitro* experiments, we found that SUMOylation inhibitors induced death of different lymphocyte subsets in a dose-dependent manner. Similarly, researchers found that both T and B cell development exhibited severe defects in SUMO specific protease 1 gene knockout mice (52). The above evidence suggested that dysregulated SUMOylation might lead to decrease the number of various lymphocyte subsets in a similar degree. This will result in a decrease in the number of total

lymphocytes, but the proportions of various lymphocyte subsets remain unchanged.

Base on the mRNA expression of three SUMO machinery components (*SUMO1*, *SUMO3* and *UBE2I*), we displayed a predictive method to distinguish the resistance to anti-PD-1 immunotherapy. Among these three genes, *UBE2I* had the best predictive ability (AUC = 0.733) for the resistance to anti-PD-1 immunotherapy. It may be that *UBE2I*, the only SUMO conjugating enzyme gene found so far, plays a crucial role in the rate of the SUMOylation cycle (55, 56). ROC curve analysis revealed that the combined expression of *SUMO1*/*SUMO3*/*UBE2I* showed moderate prediction performance for therapeutic responses (AUC = 0.791). Recently, many biomarkers, such as single-cell RNA sequencing or non-targeted metabolomics from tumor samples, and immune infiltration in the tumor microenvironment, had been shown to be potentially useful to predict therapeutic response in lung cancer patients treated with anti-PD-1 immunotherapy (57, 58). However, local analysis of tumor tissue might be severely limited by the amount of available samples, especially since tissue would be consumed by routine molecular analyses (59). Our predictive model, either a single gene or a combination of three genes, can serve as an easily accessible circulating biomarker to evaluate anti-PD-1 treatment response, which could help clinicians to intuitively analyze initial treatment expectation.

In conclusion, our research developed a predictive method, based on the gene expression of three SUMO machinery components (*SUMO1*, *SUMO3* and *UBE2I*), to distinguish the resistance to anti-PD-1 immunotherapy. Furthermore, our findings implied that the decreased peripheral blood lymphocytes induced by dysregulated SUMOylation might be an inducing factor for the resistance to anti-PD-1 immunotherapy in lung cancer. These data might provide effective circulating biomarkers for predicting the efficacy of anti-PD-1 immunotherapy, and uncovered a novel regulatory mechanism of resistance to anti-PD-1 immunotherapy.

Data availability statement

The raw data supporting the conclusions of this article will be made available by the authors, without undue reservation.

Ethics statement

The studies involving humans were approved by The Human Ethics Committee of the First Hospital of Jilin University. The studies were conducted in accordance with the local legislation and institutional requirements. The participants provided their written informed consent to participate in this study.

Author contributions

YW: Conceptualization, Formal analysis, Funding acquisition, Investigation, Methodology, Writing – original draft. CS: Data curation, Formal analysis, Resources, Writing – review & editing. ML: Methodology, Resources, Visualization, Writing – review & editing. PX: Data curation, Validation, Writing – review & editing. YL: Project administration, Supervision, Writing – review & editing. YZ: Conceptualization, Funding acquisition, Writing – review & editing. JH: Supervision, Writing – review & editing.

Funding

The author(s) declare financial support was received for the research, authorship, and/or publication of this article. This work was supported by The Science and Technology Innovation Platform of Jilin Province (YDZJ202202CXJD050), The 12th Youth Found of The First Hospital of Jilin University (JDYY11202134) and The Training Program for Excellent Young Teacher of Jilin University (419080500583).

Acknowledgments

We would like to thank all participants involved in this study.

Conflict of interest

The authors declare that the research was conducted in the absence of any commercial or financial relationships that could be construed as a potential conflict of interest.

Publisher's note

Supplementary material

The Supplementary Material for this article can be found online at: https://www.frontiersin.org/articles/10.3389/fimmu.2024.1424393/full#supplementary-material

References

1. Chen P, Liu Y, Wen Y, Zhou C. Non-small cell lung cancer in China. *Cancer Commun (Lond)*. (2022) 42:937–70. doi: 10.1002/cac2.12359

2. Lahiri A, Maji A, Potdar PD, Singh N, Parikh P, Bisht B, et al. Lung cancer immunotherapy: progress, pitfalls, and promises. *Mol Cancer*. (2023) 22:40. doi: 10.1186/s12943-023-01740-y

3. Yin J, Wu Y, Yang X, Gan L, Xue J. Checkpoint inhibitor pneumonitis induced by anti-PD-1/PD-L1 therapy in non-small-cell lung cancer: occurrence and mechanism. *Front Immunol*. (2022) 13:830631. doi: 10.3389/fimmu.2022.830631

4. Marei HE, Hasan A, Pozzoli G, Cenciarelli C. Cancer immunotherapy with immune checkpoint inhibitors (ICIs): potential, mechanisms of resistance, and strategies for reinvigorating T cell responsiveness when resistance is acquired. *Cancer Cell Int*. (2023) 23:64. doi: 10.1186/s12935-023-02902-0

5. Bai X, Kim M, Kasumova G, Si L, Tang B, Cui C, et al. Radiological dynamics and SITC-defined resistance types of advanced melanoma during anti-PD-1 monotherapy: an independent single-blind observational study on an international cohort. *J Immunother Cancer*. (2021) 9:e002092. doi: 10.1136/jitc-2020-002092

6. Liu Z, Li X, Gao Y, Liu J, Feng Y, Liu Y, et al. Epigenetic reprogramming of Runx3 reinforces $CD8^+$ T-cell function and improves the clinical response to immunotherapy. *Mol Cancer*. (2023) 22:84. doi: 10.1186/s12943-023-01768-0

7. Dai M, Liu M, Yang H, Küçük C, You H. New insights into epigenetic regulation of resistance to PD-1/PD-L1 blockade cancer immunotherapy: mechanisms and therapeutic opportunities. *Exp Hematol Oncol*. (2022) 11:101. doi: 10.1186/s40164-022-00356-0

8. Chen Y. A new immuno-oncology target - SUMOylation. *Trends Cancer*. (2023) 9:606–8. doi: 10.1016/j.trecan.2023.04.010

9. Gu Y, Fang Y, Wu X, Xu T, Hu T, Xu Y, et al. The emerging roles of SUMOylation in the tumor microenvironment and therapeutic implications. *Exp Hematol Oncol*. (2023) 12:58. doi: 10.1186/s40164-023-00420-3

10. Chang HM, Yeh E. SUMO: from bench to bedside. *Physiol Rev*. (2020) 100:1599–619. doi: 10.1152/physrev.00025.2019

11. Tokarz P, Woźniak K. SENP proteases as potential targets for cancer therapy. *Cancers (Basel)*. (2021) 13:2059. doi: 10.3390/cancers13092059

12. ST K, Joshi G, Arya P, Mahajan V, Chaturvedi A, Mishra RK. SUMO and SUMOylation pathway at the forefront of host immune response. *Front Cell Dev Biol*. (2021) 9:681057. doi: 10.3389/fcell.2021.681057

13. Du L, Liu W, Rosen ST. Targeting SUMOylation in cancer. *Curr Opin Oncol*. (2021) 33:520–5. doi: 10.1097/CCO.0000000000000765

14. Kunadis E, Lakiotaki E, Korkolopoulou P, Piperi C. Targeting post-translational histone modifying enzymes in glioblastoma. *Pharmacol Ther*. (2021) 220:107721. doi: 10.1016/j.pharmthera.2020.107721

15. Hung PF, Hong TM, Chang CC, Hung CL, Hsu YL, Chang YL, et al. Hypoxia-induced Slug SUMOylation enhances lung cancer metastasis. *J Exp Clin Cancer Res*. (2019) 38:5. doi: 10.1186/s13046-018-0996-8

16. Gracia-Hernandez M, Munoz Z, Villagra A. Enhancing therapeutic approaches for melanoma patients targeting epigenetic modifiers. *Cancers (Basel)*. (2021) 13:6180. doi: 10.3390/cancers13246180

17. Ma S, Zhao Y, Lee WC, Ong LT, Lee PL, Jiang Z, et al. Hypoxia induces HIF1α-dependent epigenetic vulnerability in triple negative breast cancer to confer immune effector dysfunction and resistance to anti-PD-1 immunotherapy. *Nat Commun*. (2022) 13:4118. doi: 10.1038/s41467-022-31764-9

18. Amaro A, Reggiani F, Fenoglio D, Gangemi R, Tosi A, Parodi A, et al. Guadecitabine increases response to combined anti-CTLA-4 and anti-PD-1 treatment in mouse melanoma in *vivo* by controlling T-cells, myeloid derived suppressor and NK cells. *J Exp Clin Cancer Res*. (2023) 42:67. doi: 10.1186/s13046-023-02628-x

19. Borst J, Busselaar J, Bosma D, Ossendorp F. Mechanism of action of PD-1 receptor/ligand targeted cancer immunotherapy. *Eur J Immunol*. (2021) 51:1911–20. doi: 10.1002/eji.202048994

20. Sun C, Nagaoka K, Kobayashi Y, Maejima K, Nakagawa H, Nakajima J, et al. Immunotherapies targeting neoantigens are effective in PD-1 blockade-resistant tumors. *Int J Cancer*. (2023) 152:1463–75. doi: 10.1002/ijc.34382

21. Simoni Y, Becht E, Fehlings M, Loh CY, Koo SL, Teng KWW, et al. Bystander CD8(+) T cells are abundant and phenotypically distinct in human tumor infiltrates. *Nature*. (2018) 557:575–9. doi: 10.1038/s41586-018-0130-2

22. Luoma AM, Suo S, Wang Y, Gunasti L, Porter CBM, Nabilsi N, et al. Tissue-resident memory and circulating T cells are early responders to pre-surgical cancer immunotherapy. *Cell*. (2022) 185:2918–35.e29. doi: 10.1016/j.cell.2022.06.018

23. Liu B, Hu X, Feng K, Gao R, Xue Z, Zhang S, et al. Temporal single-cell tracing reveals clonal revival and expansion of precursor exhausted T cells during anti-PD-1 therapy in lung cancer. *Nat Cancer*. (2022) 3:108–21. doi: 10.1038/s43018-021-00292-8

24. Du X, Wen S, Shi R, Xia J, Wang R, Zhang Y, et al. Peripheral blood lymphocytes differentiation patterns in responses/outcomes to immune checkpoint blockade therapies in non-small cell lung cancer: a retrospective study. *BMC Cancer*. (2023) 23:83. doi: 10.1186/s12885-023-10502-4

25. Kamphorst AO, Pillai RN, Yang S, Nasti TH, Akondy RS, Wieland A, et al. Proliferation of PD-1^+ CD8 T cells in peripheral blood after PD-1-targeted therapy in lung cancer patients. *Proc Natl Acad Sci U.S.A*. (2017) 114:4993–8. doi: 10.1073/pnas.1705327114

26. Brahmer JR, Govindan R, Anders RA, Antonia SJ, Sagorsky S, Davies MJ, et al. The Society for Immunotherapy of Cancer consensus statement on immunotherapy for the treatment of non-small cell lung cancer (NSCLC). *J Immunother Cancer*. (2018) 6:75. doi: 10.1186/s40425-018-0382-2

27. Wolchok JD, Hoos A, O'Day S, Weber JS, Hamid O, Lebbé C, et al. Guidelines for the evaluation of immune therapy activity in solid tumors: immune-related response criteria. *Clin Cancer Res*. (2009) 15:7412–20. doi: 10.1158/1078-0432.CCR-09-1624

28. Seymour L, Bogaerts J, Perrone A, Ford R, Schwartz LH, Mandrekar S, et al. iRECIST: guidelines for response criteria for use in trials testing immunotherapeutics. *Lancet Oncol*. (2017) 18:e143–52. doi: 10.1016/S1470-2045(17)30074-8

29. Fowler NH, Davis RE, Rawal S, Nastoupil L, Hagemeister FB, McLaughlin P, et al. Safety, activity, and immune effects of lenalidomide and rituximab in untreated indolent lymphoma. *Lancet Oncol*. (2014) 15:1311–8. doi: 10.1016/S1470-2045(14)70455-3

30. Boland JL, Zhou Q, Iasonos AE, O'Cearbhaill RE, Konner J, Callahan M, et al. Utility of serum CA-125 monitoring in patients with ovarian cancer undergoing immune checkpoint inhibitor therapy. *Gynecol Oncol*. (2020) 158:303–8. doi: 10.1016/j.ygyno.2020.04.710

31. Lin YJ, Kang YM, Wu YH, Chen YW, Hu YW. Lymphocytopenia and survival after whole-brain radiotherapy in patients with small-cell lung cancer. *Thorac Cancer*. (2023) 14:1268–75. doi: 10.1111/1759-7714.14868

32. Yood RA, Ottery FD, Irish W, Wolfson M. Effect of pegloticase on renal function in patients with chronic kidney disease: a *post hoc* subgroup analysis of 2 randomized, placebo-controlled, phase 3 clinical trials. *BMC Res Notes*. (2014) 7:54. doi: 10.1186/1756-0500-7-54

33. Middleton PG, Mall MA, Dřevínek P, Lands LC, McKone EF, Polineni D, et al. Elexacaftor-tezacaftor-ivacaftor for cystic fibrosis with a single phe508del allele. *N Engl J Med*. (2019) 381:1809–19. doi: 10.1056/NEJMoa1908639

34. Banerji A, Bernstein JA, Johnston DT, Lumry WR, Magerl M, Maurer M, et al. Long-term prevention of hereditary angioedema attacks with lanadelumab: The HELP OLE Study. *Allergy*. (2022) 77:979–90. doi: 10.1111/all.15011

35. Wu W, Huang C. SUMOylation and DeSUMOylation: Prospective therapeutic targets in cancer. *Life Sci*. (2023) 332:122085. doi: 10.1016/j.lfs.2023.122085

36. Yu L, Lin N, Ye Y, Zhuang H, Zou S, Song Y, et al. The prognosis, chemotherapy and immunotherapy efficacy of the SUMOylation pathway signature and the role of UBA2 in lung adenocarcinoma. *Aging (Albany NY)*. (2024) 16:4378–95. doi: 10.18632/aging.205594

37. Liu X, Xu Y, Pang Z, Guo F, Qin Q, Yin T, et al. Knockdown of SUMO-activating enzyme subunit 2 (SAE2) suppresses cancer Malignancy and enhances chemotherapy sensitivity in small cell lung cancer. *J Hematol Oncol*. (2015) 8:67. doi: 10.1186/s13045-015-0164-y

38. Liu K, Zhang J, Wang H. Small ubiquitin-like modifier/sentrin-specific peptidase 1 associates with chemotherapy and is a risk factor for poor prognosis of non-small cell lung cancer. *J Clin Lab Anal*. (2018) 32:e22611. doi: 10.1002/jcla.22611

39. Mu J, Zuo Y, Yang W, Chen Z, Liu Z, Tu J, et al. Over-expression of small ubiquitin-like modifier proteases 1 predicts chemo-sensitivity and poor survival in non-small cell lung cancer. *Chin Med J (Engl)*. (2014) 127:4060–5. doi: 10.3760/cma.j.issn.0366-6999.20141013

40. Han JY, Lee GK, Yoo SY, Yoon SJ, Cho EY, Kim HT, et al. Association of SUMO1 and UBC9 genotypes with tumor response in non-small-cell lung cancer treated with irinotecan-based chemotherapy. *Pharmacogenomics J*. (2010) 10:86–93. doi: 10.1038/tpj.2009.46

41. Yuan H, Lu Y, Chan YT, Zhang C, Wang N, Feng Y. The role of protein SUMOylation in human hepatocellular carcinoma: A potential target of new drug discovery and development. *Cancers (Basel)*. (2021) 13:5700. doi: 10.3390/cancers13225700

42. Zhao Q, Ma Y, Li Z, Zhang K, Zheng M, Zhang S. The function of SUMOylation and its role in the development of cancer cells under stress conditions: A systematic review. *Stem Cells Int*. (2020) 2020:8835714. doi: 10.1155/2020/8835714

43. Borsci G, Barbieri S, Guardamagna I, Lonati L, Ottolenghi A, Ivaldi GB, et al. Immunophenotyping reveals no significant perturbation to PBMC subsets when co-cultured with colorectal adenocarcinoma caco-2 cells exposed to X-rays. *Front Immunol*. (2020) 11:1077. doi: 10.3389/fimmu.2020.01077

44. Wei SC, Levine JH, Cogdill AP, Zhao Y, Anang NAS, Andrews MC, et al. Distinct cellular mechanisms underlie anti-CTLA-4 and anti-PD-1 checkpoint blockade. *Cell*. (2017) 170:1120–33.e17. doi: 10.1016/j.cell.2017.07.024

45. Sun F, Wang FX, Zhu H, Yue TT, Yang CL, Luo JH, et al. SUMOylation of PDPK1 Is required to maintain glycolysis-dependent CD4 T-cell homeostasis. *Cell Death Dis*. (2022) 13:181. doi: 10.1038/s41419-022-04622-1

46. Huang CH, Yang TT, Lin KI. Mechanisms and functions of SUMOylation in health and disease: a review focusing on immune cells. *J BioMed Sci*. (2024) 31:16. doi: 10.1186/s12929-024-01003-y

47. Ding X, Wang A, Ma X, Demarque M, Jin W, Xin H, et al. Protein SUMOylation is required for regulatory T cell expansion and function. *Cell Rep*. (2016) 16:1055–66. doi: 10.1016/j.celrep.2016.06.056

48. Garaude J, Farrás R, Bossis G, Charni S, Piechaczyk M, Hipskind RA, et al. SUMOylation regulates the transcriptional activity of JunB in T lymphocytes. *J Immunol*. (2008) 180:5983–90. doi: 10.4049/jimmunol.180.9.5983

49. Kagamu H, Kitano S, Yamaguchi O, Yoshimura K, Horimoto K, Kitazawa M, et al. CD4(+) T-cell immunity in the peripheral blood correlates with response to anti-PD-1 therapy. *Cancer Immunol Res*. (2020) 8:334–44. doi: 10.1158/2326-6066.CIR-19-0574

50. Lao J, Xu H, Liang Z, Luo C, Shu L, Xie Y, et al. Peripheral changes in T cells predict efficacy of anti-PD-1 immunotherapy in non-small cell lung cancer. *Immunobiology*. (2023) 228:152391. doi: 10.1016/j.imbio.2023.152391

51. Chen Y, Wen S, Xia J, Du X, Wu Y, Pan B, et al. Association of dynamic changes in peripheral blood indexes with response to PD-1 inhibitor-based combination therapy and survival among patients with advanced non-small cell lung cancer. *Front Immunol*. (2021) 12:672271. doi: 10.3389/fimmu.2021.672271

52. Muromoto R, Ishida M, Sugiyama K, Sekine Y, Oritani K, Shimoda K, et al. Sumoylation of Daxx regulates IFN-induced growth suppression of B lymphocytes and the hormone receptor-mediated transactivation. *J Immunol*. (2006) 177:1160–70. doi: 10.4049/jimmunol.177.2.1160

53. Van Nguyen T, Angkasekwinai P, Dou H, Lin FM, Lu LS, Cheng J, et al. SUMO-specific protease 1 is critical for early lymphoid development through regulation of STAT5 activation. *Mol Cell*. (2012) 45:210–21. doi: 10.1016/j.molcel.2011.12.026

54. Kumar S, Schoonderwoerd M, Kroonen JS, de Graaf IJ, Sluijter M, Ruano D, et al. Targeting pancreatic cancer by TAK-981: a SUMOylation inhibitor that activates the immune system and blocks cancer cell cycle progression in a preclinical model. *Gut*. (2022) 71:2266–83. doi: 10.1136/gutjnl-2021-324834

55. Huang J, Tan X, Liu Y, Jiang K, Luo J. Knockdown of UBE2I inhibits tumorigenesis and enhances chemosensitivity of cholangiocarcinoma via modulating p27kip1 nuclear export. *Mol Carcinog*. (2023) 62:700–15. doi: 10.1002/mc.23518

56. Han ZJ, Feng YH, Gu BH, Li YM, Chen H. The post-translational modification, SUMOylation, and cancer (Review). *Int J Oncol*. (2018) 52:1081–94. doi: 10.3892/ijo.2018.4280

57. Hu J, Zhang L, Xia H, Yan Y, Zhu X, Sun F, et al. Tumor microenvironment remodeling after neoadjuvant immunotherapy in non-small cell lung cancer revealed by single-cell RNA sequencing. *Genome Med*. (2023) 15:14. doi: 10.1186/s13073-023-01164-9

58. Ricciuti B, Lamberti G, Puchala SR, Mahadevan NR, Lin JR, Alessi JV, et al. Genomic and immunophenotypic landscape of acquired resistance to PD-(L)1 blockade in non-small-cell lung cancer. *J Clin Oncol*. (2024) 42:1311–21. doi: 10.1200/JCO.23.00580

59. Russano M, Napolitano A, Ribelli G, Iuliani M, Simonetti S, Citarella F, et al. Liquid biopsy and tumor heterogeneity in metastatic solid tumors: the potentiality of blood samples. *J Exp Clin Cancer Res*. (2020) 39:95. doi: 10.1186/s13046-020-01601-2

frontiers | Frontiers in Oncology

TYPE Original Research
PUBLISHED 19 August 2024
DOI 10.3389/fonc.2024.1380195

OPEN ACCESS

EDITED BY
Paulo Rodrigues-Santos,
University of Coimbra, Portugal

REVIEWED BY
Calin Cainap,
University of Medicine and Pharmacy Iuliu Hatieganu, Romania
Fernando Mendes,
Polytechnical Institute of Coimbra, Portugal
Nelson López Sejas,
University of Extremadura, Spain
Diogo Teófilo De Castro Soares Regateiro,
Francisco Gentil Portuguese Oncology Institute of Coimbra, Portugal

*CORRESPONDENCE
Wei Zhang
zwmary84512@163.com

†These authors have contributed equally to this work and share first authorship

RECEIVED 01 February 2024
ACCEPTED 25 July 2024
PUBLISHED 19 August 2024

CITATION
Jia H, Liang L, Chen X, Zha W, Diao W and Zhang W (2024) Predictive value of peri-chemotherapy hematological parameters for febrile neutropenia in patients with cancer. *Front. Oncol.* 14:1380195. doi: 10.3389/fonc.2024.1380195

Predictive value of peri-chemotherapy hematological parameters for febrile neutropenia in patients with cancer

Hongyuan Jia[1†], Long Liang[1†], Xue Chen[2], Wenzhong Zha[3], Wei Diao[4] and Wei Zhang[4*]

[1]Department of Radiation Oncology, Sichuan Clinical Research Center for Cancer, Sichuan Cancer Hospital and Institute, Sichuan Cancer Center, Affiliated Cancer Hospital of University of Electronic Science and Technology of China, Chengdu, China, [2]Cancer Center, Sichuan Taikang Hospital, Chengdu, Sichuan, China, [3]Department of Biomedical Informatics. Sichuan Cancer Hospital and Institute, Sichuan Cancer Center, School of Medicine, University of Electronic Science and Technology of China, Chengdu, China, [4]Department of Nuclear Medicine, Sichuan Clinical Research Center for Cancer, Sichuan Cancer Hospital and Institute, Sichuan Cancer Center, Affiliated Cancer Hospital of University of Electronic Science and Technology of China, Chengdu, China

Objective: The aim of this study was to compare hematological parameters pre- and early post-chemotherapy, and evaluate their values for predicting febrile neutropenia (FN).

Methods: Patients diagnosed with malignant solid tumors receiving chemotherapy were included. Blood cell counts peri-chemotherapy and clinical information were retrieved from the hospital information system. We used the least absolute shrinkage and selection operator (LASSO) method for variable selection and fitted selected variables to a logistic model. We assessed the performance of the prediction model by the area under the ROC curve.

Results: The study population consisted of 4,130 patients with common solid tumors receiving a three-week chemotherapy regimen in Sichuan Cancer Hospital from February 2019 to March 2022. In the FN group, change percentage of neutrophil count decreased less (–0.02, CI: –0.88 to 3.48 vs. –0.04, CI: –0.83 to 2.24). Among hematological parameters, lower post-chemotherapy lymphocyte count (OR 0.942, CI: 0.934–0.949), change percentage of platelet (OR 0.965, CI: 0.955–0.975) and higher change percentage of post-chemotherapy neutrophil count (OR 1.015, CI: 1.011–1.018), and pre-chemotherapy NLR (OR 1.002, CI: 1.002–1.002) predicted an increased risk of FN. These factors improved the predicting model based on clinical factors alone. The AUC of the combination model was 0.8275.

Conclusion: Peri-chemotherapy hematological markers improve the prediction of FN.

KEYWORDS

febrile neutropenia, chemotherapy, hematological parameters, prediction, nomogram

1 Introduction

Chemotherapy-induced febrile neutropenia (FN) is one of the most concerning sequelae in patients with cancer undergoing chemotherapy (1). It often leads to serious infections and causes dose reduction and delays that may impair survival outcomes (2). Current guidelines recommend prophylactic granulocyte colony-stimulating factor (G-CSF) based on the estimated FN risk (3). They are mainly based on a chemotherapy regimen, considering specific individual patient characteristics. However, until now, there is no widely accepted mechanism to quantify patient-specific risk.

Several models that focused on certain predictors have been proposed. These factors include tumor type, number of chemotherapy cycles, and chemotherapy regimen (4). Individual patient characteristics, such as age and comorbidities, are also associated with FN risk (5). Lyman's model is a widely used risk model published in 2011 with an area under the receiver operating characteristics curve (AUC) of 0.81. Its risk factors included patient-specific variables such as age, receipt of prior chemotherapy, cancer type, white blood cell count, and liver and renal function parameters before chemotherapy (6). In a recent external validation study, the Lyman model demonstrated moderate predicting value with an AUC of 0.7475. It also included too many variables, which limits an easy use in clinical practice.

Blood cell counts are essential and economic tests during chemotherapy. They are needed before chemotherapy to determine whether chemotherapy is feasible. Blood cell counts before chemotherapy such as white blood cell count, absolute neutrophil count, and lymphocyte count have been shown of certain value in predicting FN (7, 8). Blood cell counts are also commonly performed within a few days of chemotherapy in clinical practice, while severe neutropenia usually occurs 7 to 10 days after chemotherapy. Except for hematological parameters sampled before chemotherapy, these parameters early after chemotherapy may function better to predict FN risk. Moreover, hematological parameter-derived indexes such as systemic inflammatory index (SII), neutrophil–lymphocyte ratio (NLR), and platelet–lymphocyte ratio (PLR) were related to host immune status. They are widely used in predicting the prognosis of cancer as well as some non-malignant diseases (9–11). However, it has not been fully elucidated whether blood cell counts before and early after chemotherapy and their derived indicators can increase the predictive value in addition to patient-specific variables.

In the current study, we compared pre- and early post-chemotherapy hematological parameters between non-FN and FN groups. We selected key factors for predicting FN from all variables by the least absolute shrinkage and selection operator (LASSO) method. We then establish three models based on hematological or clinical features alone or a combination of both and compare their performances. This study is of the largest data to date to compare pre- and early post-chemotherapy hematological parameters and analyze their predictive value for FN. We aimed to compare hematological parameters pre- and early post-chemotherapy, and evaluate their values for predicting FN.

2 Materials and methods

2.1 Study population

We retrospectively searched the hospital information system (HIS) for chemotherapy data between January 2019 and November 2022 at Sichuan Cancer Hospital. The center is a key center for cancer care in southwest China with 1,500 beds that provides services for over 100,000 patients per year. Inclusion criteria were patients with solid tumors receiving a three-week intravenous chemotherapy regimen, having blood cell counts 1 day before chemotherapy and early after chemotherapy (within 1 to 4 days), and at least three routine blood tests within 3 weeks after chemotherapy. Excluding criteria were incomplete or missing data on the hematological markers or clinical characteristics necessary for analysis. Chemotherapy regimens and dosage were chosen by treating medicines according to guidelines and individual patient conditions. The protocol was approved by the institutional review board and conducted in accordance with the Declaration of Helsinki and adhered to Good Clinical Practice guidelines. The requirement for written informed consent was waived by the institutional review board.

2.2 Study variables and outcome

Patients' clinical features were automatically extracted using structured query language (SQL) from HIS, including tumor type, stage, age, sex, height, weight, concurrent radiation, prior surgery, comorbidities, cycles, and regimen of chemotherapy. We also searched the blood test database based on the list of patients and matched the treatment delivery date and blood test date. SII, NLR, and PLR were calculated. The changing rate (cr) and changing percentage (cp) were defined as the difference between pre- and post-chemotherapy values divided by the time interval or the pre-chemotherapy value; for example, the changing rate and change percentage of lymphocyte are defined as $crL = (postL - preL)/time\ interval$ and $cpL = (postL - preL)/preL$. FN was defined as current or anticipated absolute neutrophil count less than 500/mm^3 with a temperature of ≥101°F (38.3°C) or ≥100.4°F (≥38.0°C) sustained ≥1 h according to the definition of the Infectious Diseases Society of America.

2.3 Features selection and modeling

The data were divided into a training set and a validation set in a 7:3 ratio. Multicategory variables, such as cancer type and chemotherapy regimen, were encoded using one hot encoder. We used the LASSO method to select key factors and fitted them to logistic regression models based on clinical or hematological features, or a combination of both. Performances of the predicting models were evaluated by receiver operating characteristic curve (ROC) on the testing datasets. To help physicians to easily determine the risk of the disease developing after chemotherapy, a nomogram was developed using risk factors selected from the final multivariable regression model.

2.4 Statistics

Comparisons for continuous variables were performed using the Mann–Whitney test, and for categorical variables, the chi-squared test or Fisher's exact test was used. The level of significance was set at $p < 0.05$. All statistical analyses were carried out using the R software version 3.4.3 (https://www.R-project.org/). For LASSO regression, R package glmnet (version 2.0–16) was used (12).

3 Results

3.1 Patient characteristics

Of the 5,440 patients who met the inclusion criteria, 1,310 were excluded from analysis for the following reasons: insufficient number of blood tests, incomplete information, and not following the 3-week intravenous chemotherapy regimen. The final dataset included 4,130 patients of 6,595 chemotherapy cycles. Among these, FN occurred in 623 (9.45%) of all cycles. The median cycle of chemotherapy was 2 (1–8). The median age was 54.00 (36.00–71.00) years or older. Among these 6,595 chemotherapy cycles, patients in 3,460 cycles (52.46%) were women. Cervical cancer (24.7%) was the most common diagnosis, followed by colorectal cancer (22.1%). The characteristics of the patients prior to each chemotherapy cycle are summarized in Table 1. The patients who had FN were typically women ($p < 0.001$), lower weight ($p < 0.001$), with concurrent radiation ($p < 0.0010$), and receiving specific chemotherapy drug such as docetaxel ($p < 0.001$).

3.2 Comparison of hematological parameters

Median values for neutrophils, lymphocytes, platelets, hemoglobin, and their change rate and change percentage before and early after chemotherapy are presented in Table 2; Figure 1. SII, NLR, PLR, and their change rate were also calculated. Compared with the non-FN group, the FN group had lower early post-chemotherapy lymphocyte, platelet, and hemoglobin counts (0.46, CI: 0.13–1.58 vs. 0.74, CI: 0.18–1.88, 131.00, CI: 64.00–248.00 vs. 154.00, CI: 78.00–298.00, 112.00, CI: 86.00–137.00 vs. 116.00, CI: 88.00–143.00, respectively), while post-chemotherapy neutrophils were higher (4.48, CI: 1.23–14.89 vs. 4.05, CI: 2.02–13.30, respectively). Lymphocytes (−0.44, CI: −0.79 to 0.25 vs. −0.32, CI: −0.73 to 0.39) and platelets (−0.24, CI: −1.01 to 0.20 vs. −0.18, CI: −0.79 to 0.24) had deeper decreasing amplitude in the FN group; in addition, their decreasing rates were faster (−0.08, CI: −0.28 to 0.04 vs. −0.06, CI: −0.29 to 0.10 and −7.33, CI: −25.65 to 6.64 vs. −0.06, CI:−0.29 to 0.10). The FN group had higher SII, NLR, and PLR before and early after chemotherapy, and the increasing rate of these indicators after chemotherapy was also higher.

3.3 Features selection and modeling

The optimal λ value of 0.0015289 was selected for the LASSO model by using 10-fold cross-validation (Figure 2). Using the LASSO method, 12 variables out of 28 hematological parameters were selected, including prePLT and preN. A total of 25 variables out of 37 clinical factors were selected, including Docetaxel and relative dose intensity (RDI). The selected hematological or clinical indicators are further fitted for a logistic regression model either alone or in combination. The combined model had the best prediction performance with an AUC of 0.8275, compared with 0.7412 and 0.7883, of models based on hematological or clinical parameters alone, respectively (Figure 3). Risk factors included in the combined model were postL; cpN; cpPLT; preNLR; age; sex; cycle of chemotherapy; specific drugs such as paclitaxel, docetaxel, carboplatin, nedaplatin, and etoposide; cancer of esophagus; and RDI. The odds ratios of the combined model are shown in Table 3. Among hematological parameters, lower postL (OR 0.942, CI: 0.934–0.949) and cpPLT (OR 0.965, CI: 0.955–0.975) and higher cpN (OR 1.015, CI: 1.011–1.018) and preNLR (OR 1.002, CI: 1.002–1.002) predicted an increased risk of FN. With a cutoff value of 0.125, the sensitivity and specificity were 0.800 and 0.736, respectively. The precision and accuracy of the model were 0.800 and 0.741, respectively. For the convenience of clinical utility, we constructed a nomogram based on the combination model (Figure 4A). Calibration curve indicated that the nomogram functions well (Figure 4B).

4 Discussion

Multiple previous studies have tried to predict FN using demographic, disease, and treatment characteristics. Clinical features such as older age, advanced disease, and early cycles of chemotherapy have all been reported to be associated with increased risk of severe neutropenia. However, it is unclear whether blood cell counts and their derivatives in the pre- and early post-chemotherapy period could further increase the predictive power for FN. In this study, we systematically compared them and found that platelets and lymphocytes decrease more in the FN group, while inflammatory index SII, NLR, and PLR increase more in FN group. Interestingly, a decreasing rate of neutrophil count was higher in the FN group. We then used the LASSO method to select key factors from a series of clinical and hematological factors. We further fitted three regression models based on selected hematological and clinical factors either alone or in combination. Compared with the prediction model based on clinical factors, the model combining clinical factors and hematological indicators has better predictive performance. In order to facilitate clinical application, we finally developed a nomogram for easy clinical utility.

The main tumor types in this study were cervical cancer and colorectal cancer, with breast cancer accounting for a smaller

TABLE 1 Patient characteristics.

Variable	Category	Non-FN	FN	All	*p*-value
Age	–	54.00, CI:36.00-71.00	55.00, CI:39.00-71.00	54.00, CI:36.00-71.00	0.0316
BMI	–	22.31, CI:17.90-28.08	22.03, CI:17.89-27.36	22.31, CI:17.90-28.04	0.0054
BSA	–	1.59, CI:1.37-1.85	1.55, CI:1.34-1.78	1.58, CI:1.37-1.85	0.0000
Cycle of CH	–	2.00, CI:1.00-8.00	2.00, CI:1.00-6.00	2.00, CI:1.00-8.00	0.0000
Height	–	160.00, CI:150.00-173.00	158.00, CI:149.70-170.00	160.00, CI:150.00-173.00	0.0000
Weight	–	58.00, CI:45.00-75.00	56.00, CI:43.00-70.00	58.00, CI:45.00-75.00	0.0000
Cancer type	Breast	78(1.31%)	25(4.01%)	103(1.56%)	0.0000
	Cervix	1409(23.59%)	222(35.63%)	1631(24.73%)	
	Colorectum	1296(21.70%)	22(3.53%)	1318(19.98%)	
	Endometrium	182(3.05%)	38(6.10%)	220(3.34%)	
	Esophagus	525(8.79%)	92(14.77%)	617(9.36%)	
	Head and Neck	384(6.43%)	45(7.22%)	429(6.50%)	
	Liver	280(4.69%)	5(0.80%)	285(4.32%)	
	Lung	792(13.26%)	67(10.75%)	859(13.03%)	
	NPC	613(10.26%)	70(11.24%)	683(10.36%)	
	Ovum	243(4.07%)	27(4.33%)	270(4.09%)	
	Stomach	170(2.85%)	10(1.61%)	180(2.73%)	
Diabetes	No	5773(96.67%)	610(97.91%)	6383(96.79%)	0.0794
	Yes	199(3.33%)	13(2.09%)	212(3.21%)	
Hypertension	No	5620(94.11%)	596(95.67%)	6216(94.25%)	0.1059
	Yes	352(5.89%)	27(4.33%)	379(5.75%)	
Metastasis	No	5511(92.28%)	578(92.78%)	6089(92.33%)	0.0001
	Yes	461(7.72%)	45(7.22%)	506(7.67%)	
Radiation	No	3855(64.55%)	349(56.02%)	4204(63.75%)	0.0000
	Yes	2117(35.45%)	274(43.98%)	2391(36.25%)	
Sex	Female	3056(51.17%)	404(64.85%)	3460(52.46%)	0.0000
	Male	2916(48.83%)	219(35.15%)	3135(47.54%)	
Prior surgery	No	3908(65.44%)	442(70.95%)	4350(65.96%)	0.0073
	Yes	2064(34.56%)	181(29.05%)	2245(34.04%)	
Regime	Carboplatin	1180(11.36%)	165(14.60%)	1345(11.67%)	0.0000
	Cisplatin	2014(19.38%)	242(21.42%)	2256(19.58%)	
	Docetaxel	684(6.58%)	251(22.21%)	935(8.12%)	
	Etoposide	176(1.69%)	19(1.68%)	195(1.69%)	
	Fluorouracil	1495(14.39%)	39(3.45%)	1534(13.31%)	
	Ifosfamide	21(0.20%)	2(0.18%)	23(0.20%)	
	Irinotecan	348(3.35%)	15(1.33%)	363(3.15%)	
	Lobaplatin	281(2.70%)	45(3.98%)	326(2.83%)	
	Nedaplatin	521(5.01%)	68(6.02%)	589(5.11%)	
	Oxaliplatin	1350(12.99%)	28(2.48%)	1378(11.96%)	

(Continued)

TABLE 1 Continued

Variable	Category	Non-FN	FN	All	*p*-value
	Paclitaxel	2062(19.84%)	248(21.95%)	2310(20.05%)	
	Pemetrexed	259(2.49%)	8(0.71%)	267(2.32%)	
RDI	–	0.914(CI:0.6397-1.046)	0.948(CI:0.569-1.051)	0.9185(CI:6265-1.0471)	0.0035

BMI, body mass index; BSA, body surface area; CH, chemotherapy; CI, confidence interval; NPC, nasopharyngeal carcinoma; RDI, relative drug intensity; -, not applicable.

TABLE 2 Comparison of hematological parameters between non-FN and FN groups.

Variable	Non-FN	FN	Unit	*p*-value
cpHGB	−0.03, CI: −0.16 to 0.11	−0.05, CI: −0.19 to 0.10	–	0.0001
cpL	−0.32, CI: −0.73 to 0.39	−0.44, CI: −0.79 to 0.25	–	0.0000
cpN	−0.04, CI: −0.83 to 2.24	−0.02, CI: −0.88 to 3.48	–	0.3737
cpNLR	0.36, CI: −0.74 to 5.60	0.74, CI: −0.79 to 8.60	–	0.0000
cpPLR	0.26, CI: −0.41 to 2.28	0.43, CI: −0.41 to 2.69	–	0.0000
cpPLT	−0.18, CI: −0.79 to 0.24	−0.24, CI: −1.01 to 0.20	–	0.0000
cpSII	0.14, CI: −0.77 to 4.88	0.32, CI: −0.85 to 6.63	–	0.0005
crHGB	−0.86, CI: −5.40 to 2.75	−1.20, CI: −5.97 to 2.43	g/L*d	0.0002
crL	−0.06, CI: −0.29 to 0.10	−0.08, CI: −0.28 to 0.04	10^9/L*d	0.0001
crN	−0.03, CI: −3.17 to 2.23	−0.02, CI: −3.88 to 2.82	10^9/L*d	0.2462
crNLR	0.25, CI: −3.87 to 6.02	0.57, CI: −5.52 to 11.76	–	0.0000
crPLR	8.47, CI: −25.11 to 120.10	15.76, CI: −27.90 to 149.16	–	0.0000
crPLT	−6.00, CI: −26.33 to 10.81	−7.33, CI: −25.65 to 6.64	10^9/L*d	0.0003
crSII	16.15, CI: −669.94 to 1,062.95	42.17, CI: −823.06 to 1,528.80	10^9/L*d	0.0001
postHGB	116.00, CI: 88.00 to 143.00	112.00, CI: 86.00 to 137.00	g/L	0.0000
postL	0.74, CI: 0.18 to 1.88	0.46, CI: 0.13 to 1.58	10^9/L	0.0000
postN	4.05, CI: 2.02 to 13.30	4.48, CI: 1.23 to 14.89	10^9/L	0.0018
postNLR	5.88, CI: 1.69 to 34.92	9.96, CI: 1.86 to 52.48	–	0.0000
postPLR	211.60, CI: 73.08 to 921.57	272.00, CI: 85.08 to 1,041.25	–	0.0000
postPLT	154.00, CI: 78.00 to 298.00	131.00, CI: 64.00 to 248.00	10^9/L	0.0000
postSII	926.92, CI: 221.34 to 6,083.53	1,235.56, CI: 211.06 to 7,687.20	10^9/L	0.0000
preHGB	120.00, CI: 92.00 to 148.00	118.00, CI: 92.10 to 142.90	g/L	0.0001
preL	1.13, CI: 0.34 to 2.23	0.93, CI: 0.29 to 2.08	10^9/L	0.0000
preN	4.39, CI: 2.06 to 17.67	4.40, CI: 2.00 to 20.44	10^9/L	0.3489
preNLR	4.08, CI: 1.30 to 29.64	5.03, CI: 1.42 to 38.72	–	0.0000
prePLR	166.19, CI: 67.17 to 555.00	179.61, CI: 68.06 to 582.63	–	0.0107
prePLT	179.00, CI: 92.00 to 347.00	166.00, CI: 85.00 to 294.00	10^9/L	0.0000
preSII	783.18, CI: 204.36 to 5,165.35	860.85, CI: 211.48 to 5,837.99	10^9/L	0.0193

Cp, change percentage; Cr, change rate; L, lymphocyte; N, neutrophil; PLT, platelet; HGB, hemoglobin; SII, systemic immune inflammatory index; NLR, neutrophil–lymphocyte ratio; PLR, platelet–lymphocyte ratio; -, dimensionless.

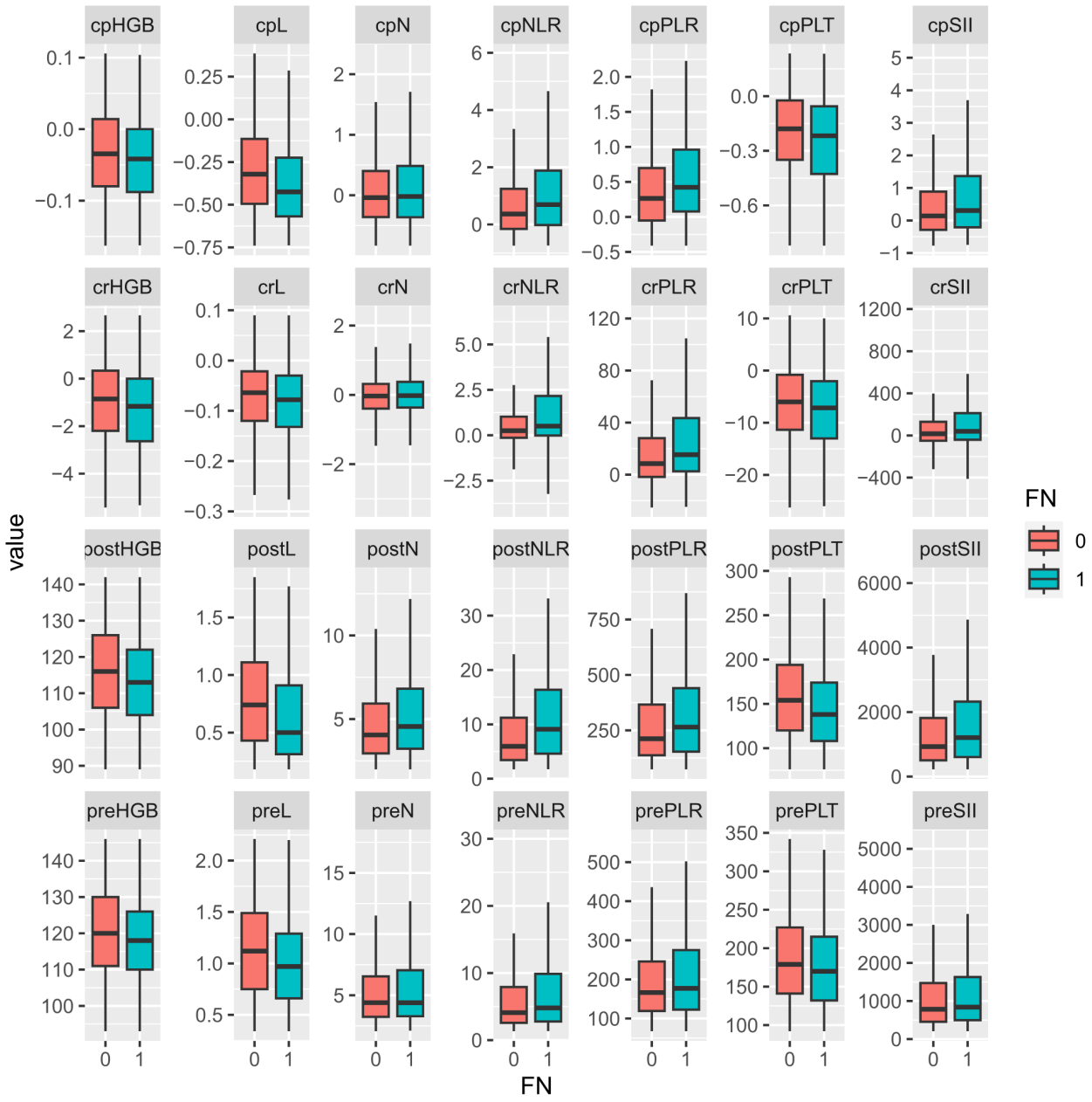

FIGURE 1
Comparison of hematological parameters and their changes between non-FN and FN groups. "0" for the non-FN group and "1" for the FN group. Prefix; cp, change percentage; cr, change rate; post, post-chemotherapy; pre, pre-chemotherapy. HGB, hemoglobulin; L, lymphocyte; N, neutrophil; NLR, neutrophil-to-lymphocyte ratio; PLR, platelet-to-lymphocyte ratio; PLT, platelet; SII, systemic immune inflammation index.

proportion. In previous studies, breast cancer usually occupies a larger proportion. Correspondingly, the proportion of patients receiving radiotherapy and with non-metastatic disease was relatively large in this study. We established a predictive model for FN in this new group for the first time.

In the non-FN and FN groups, as expected, cell counts of neutrophils, lymphocytes, platelets, and hemoglobulin levels decreased after chemotherapy. However, it is worth noting that in the FN group, the neutrophil count decreased less early after chemotherapy instead (−0.02, CI: −0.88 to 3.48 vs. −0.04, CI: −0.83 to 2.24). SII, NLR, and PLR, the indicators reflecting inflammation, all increased after chemotherapy, especially in the FN group. This is similar to the results of Cho et al. In their study, neutrophil counts were 3.329 ± 2.278 and 3.067 ± 1.343 5 days after chemotherapy in the FN and non-FN groups, respectively (p = 0.052), while there was no difference in the number of neutrophils between the two groups before chemotherapy (3.725 ± 1.550 vs. 3.815 ± 1.420, p = 0.383) (13). Therefore, we speculate that the lower decrease in neutrophil count after chemotherapy in the FN group is a manifestation of the potential inflammatory response superimposed on the direct neutrophil killing effect of chemotherapy drugs. Furthermore, elevated inflammatory

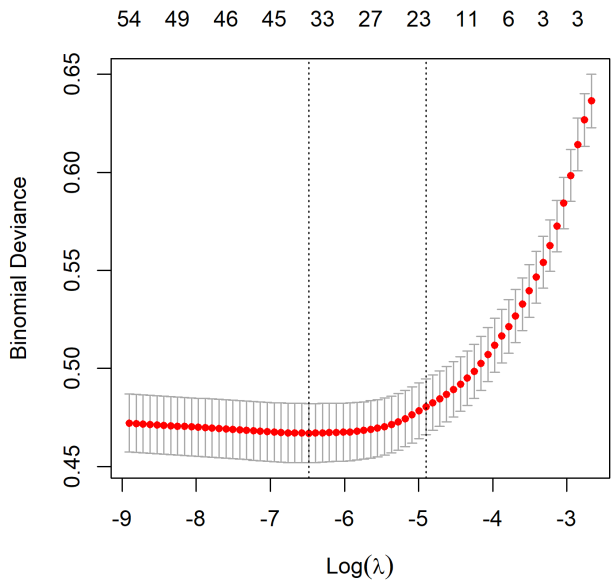

FIGURE 2
Feature selection by LASSO. A λ value of 0.0015289 was chosen, corresponding to the dotted line on the left.

markers may be caused by tumor necrosis. There may be a correlation between tumor sensitivity to drugs and bone marrow sensitivity to drugs. After the death of neutrophils mobilized into peripheral blood, they are not replenished by bone marrow regeneration (14). Thus, it is unstable and associates with more severe neutropenia.

The LASSO method can select key factors from a large number of variables. In one study, the prediction results of the LASSO

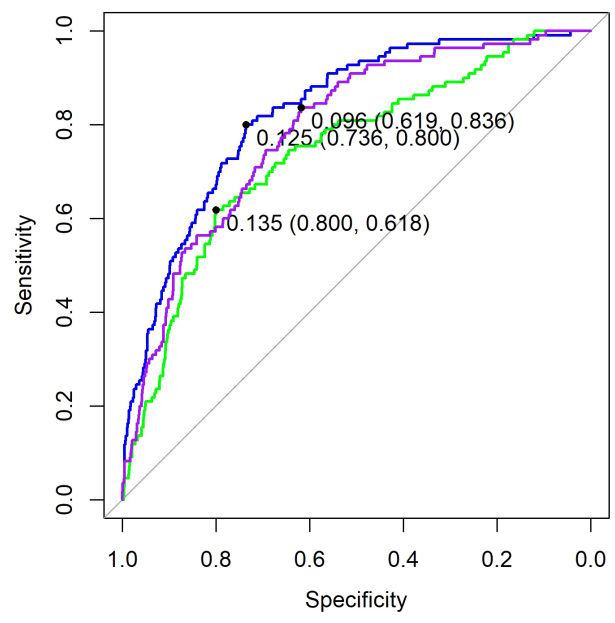

FIGURE 3
ROC of three models. Purple, the model based on clinical factors alone. Green, the model based on hematological factors alone. Blue, the model based on the combination of both.

TABLE 3 OR of risk factor for models based on the combination of clinical and hematological parameters.

Risk factor	OR	*p*-value
postL	0.941, CI: 0.934–0.949	0.0000
cpN	1.015, CI: 1.012–1.018	0.0000
cpPLT	0.965, CI: 0.955–0.975	0.0006
preNLR	1.002, CI: 1.002–1.002	0.0000
Age	1.001, CI: 1.001–1.002	0.0002
Cycle of CH	0.995, CI: 0.993–0.996	0.0020
Paclitaxel	1.054, CI: 1.042–1.065	0.0000
Carboplatin	0.969, CI: 0.953–0.984	0.0454
Docetaxel	1.230, CI: 1.214–1.246	0.0000
Nedaplatin	0.950, CI: 0.933–0.968	0.0052
Etoposide	1.081, CI: 1.056–1.107	0.0008
Esophagus	1.038, CI: 1.023–1.052	0.0085
Sex	0.968, CI: 0.96–0.977	0.0003
RDI	1.124, CI: 1.089–1.16	0.0002

CI, confidence interval.

model exceeded those of the traditional Lyman model (15). In this study, because there are too many independent variables, it is not suitable to perform logistic regression directly. Therefore, we first use the LASSO method to screen all variables, and then build a logistic regression model. The variables finally included in the model are cpN, cpPLT, preNLR, age, sex, cycle of chemotherapy, paclitaxel, docetaxel, carboplatin, nedaplatin, etoposide, esophagus, and RDI. We found that decreased cell counts of lymphocyte after chemotherapy predicted an increased risk of FN. Our results are consistent with some previous studies. Early lymphocyte count has the value of predicting FN, and the predictive significance on day 5 is greater than that on day 1 (16). The predictive value of PLT was proposed in a small retrospective analysis of patients with prostate cancer and NSCLC (17, 18). Our research further confirmed it with a much larger population. Previous studies also showed that lymphocyte count and immature platelet fraction level could predict recovery in patients who had developed severe neutropenia (19, 20). This indicated that changes in platelets and lymphocytes are more sensitive than changes in neutrophils during FN. Similarly, during the process of neutrophil decline, these two indicators can also help determine its severity. In the Jenkins study, pre-chemotherapy absolute neutrophil count and lymphocyte count predicted the risk of FN (7). However, in our study, when analyzed together with post-chemotherapy indicators and their change, except for pre-chemotherapy NLR, other pre-chemotherapy indicators did not have independent predictive effects.

Several clinical factors have been shown to affect the development of neutropenia in previous studies. Our study also found similar clinical predictors. These factors include age, sex, specific cancer type, and chemotherapy agents. Among various chemotherapy drugs, we found that docetaxel-containing

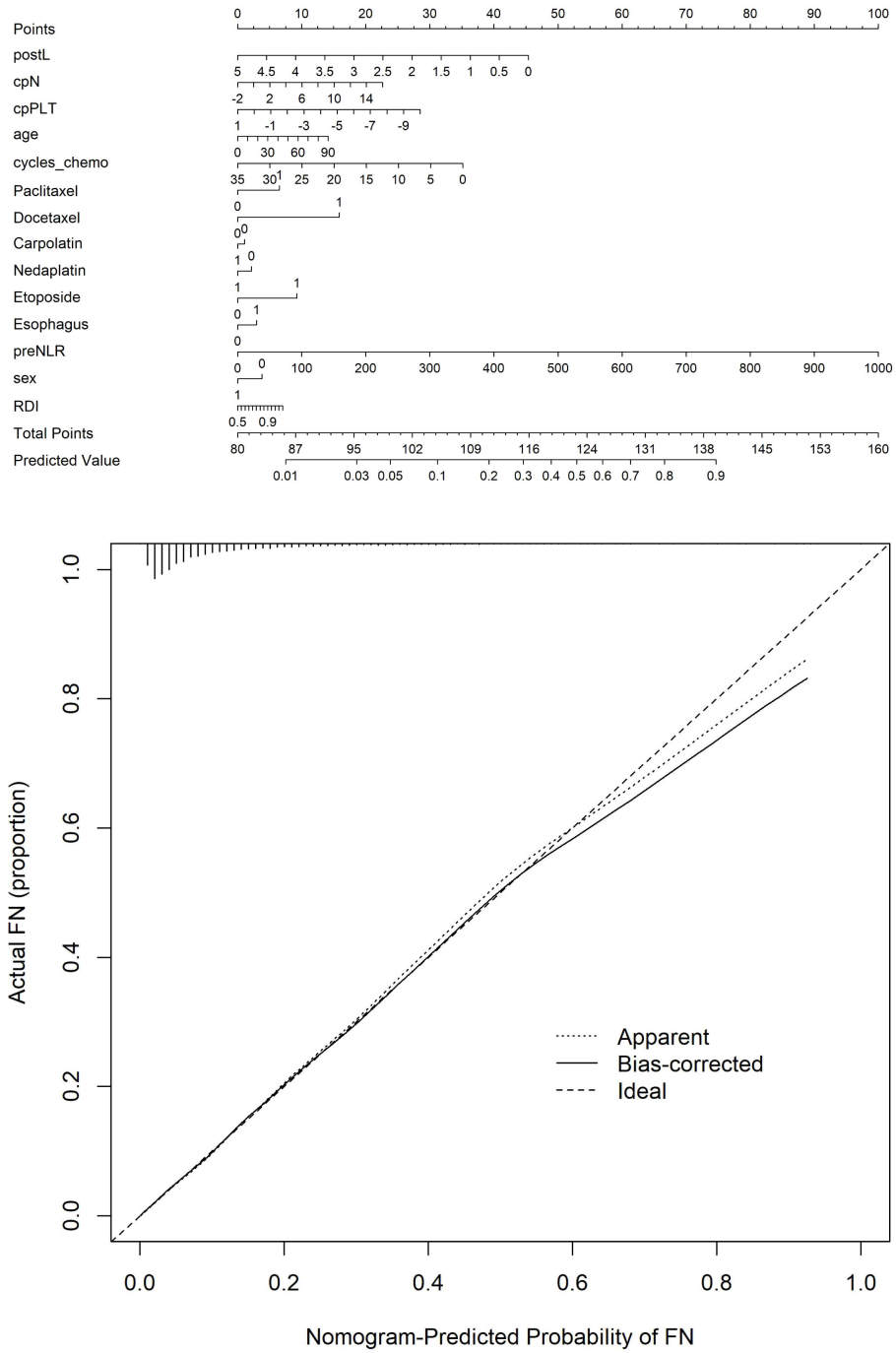

FIGURE 4
(A) Nomogram for predicting FN. **(B)** Calibration curve of the nomogram.

chemotherapy regimens were significantly associated with an increased risk of FN. Previous studies indicate that concurrent radiation and previous surgery are risk factors for FN, while they failed to be of significance in the current model. There may be confouding effect regarding radiation dose, volume, location of target, and time to previous surgery. Thus, these results should be explained carefully and needed further studies.

The advantage of our model is the incorporation of early hematological indicators, which increased the AUC to 0.8275. The AUC value of our model is higher than that from historical data. Previous studies have reported the predictive value of some single hematological indicators, and many of them have a small sample size. Our study was the first comprehensive research on multiple hematological indicators before and after chemotherapy.

This study has certain limitations. First, the inherent susceptibility of patients to FN is related to their genetic profile, which should be included in analysis. Second, this study is a single-center retrospective study and may have bias. In the future, it is necessary to incorporate more predictive factors and to conduct multicenter prospective studies to further optimize the predictive model for FN after chemotherapy.

5 Conclusions

In summary, our research demonstrated that early post-chemotherapy hematological markers can improve the prediction of FN. The combined model can help in the early identification of patients with high FN risk, thereby accordingly adopting preventive measures.

Data availability statement

The raw data supporting the conclusions of this article will be made available by the authors, without undue reservation.

Ethics statement

The studies were approved by the institutional review board of Sichuan Cancer Hospital. The studies were conducted in accordance with the local legislation and institutional requirements. Written informed consent for participation in this study was waived by the review board.

Author contributions

HJ: Conceptualization, Writing – original draft, Writing – review & editing. LL: Data curation, Formal analysis, Writing – original draft, Writing – review & editing. XC: Data curation, Investigation, Methodology, Writing – review & editing. WzZ: Data curation, Methodology, Resources, Software, Writing – review & editing. WD: Methodology, Software, Writing – review & editing. WZ: Supervision, Validation, Visualization, Writing – original draft, Writing – review & editing.

Funding

The author(s) declare financial support was received for the research, authorship, and/or publication of this article. This study was supported by the Science and Technology Department of Sichuan Province (Grant No. 2023NSFSC1719), the Sichuan Cancer Hospital Outstanding Youth Funding (Grant No. YB2021031 and YB2023014).

Acknowledgments

We thank Dr. Linling Zhang for her statistical advice.

Conflict of interest

The authors declare that the research was conducted in the absence of any commercial or financial relationships that could be construed as a potential conflict of interest.

Publisher's note

References

1. Pizzo PA. Management of patients with fever and neutropenia through the arc of time: A narrative review. *Ann Internal Med.* (2019) 170:389–97. doi: 10.7326/M18-3192

2. Blayney DW, Schwartzberg L. Chemotherapy-induced neutropenia and emerging agents for prevention and treatment: A review. *Cancer Treat Rev.* (2022) 109:102427. doi: 10.1016/j.ctrv.2022.102427

3. Smith TJ, Bohlke K, Lyman GH, Carson KR, Crawford J, Cross SJ, et al. Recommendations for the use of WBC growth factors: American society of clinical oncology clinical practice guideline update. *J Clin Oncol.* (2015) 33:3199–212. doi: 10.1200/JCO.2015.62.3488

4. Weycker D, Li X, Edelsberg J, Barron R, Kartashov A, Xu H, et al. Risk and consequences of chemotherapy-induced febrile neutropenia in patients with metastatic solid tumors. *J Oncol practice.* (2015) 11:47–54. doi: 10.1200/JOP.2014.001492

5. Li X, Luthra R, Morrow PK, Fisher MD, Reiner M, Barron RL, et al. Comorbidities among patients with cancer who do and do not develop febrile neutropenia during the first chemotherapy cycle. *J Oncol Pharm Practice.* (2016) 22:679–89. doi: 10.1177/1078155215603229

6. Lyman GH, Kuderer NM, Crawford J, Wolff DA, Culakova E, Poniewierski MS, et al. Predicting individual risk of neutropenic complications in patients receiving cancer chemotherapy. *Cancer.* (2011) 117:1917–27. doi: 10.1002/cncr.25691

7. Jenkins P, Scaife J, Freeman S. Validation of a predictive model that identifies patients at high risk of developing febrile neutropaenia following chemotherapy for breast cancer. *Ann Oncol.* (2012) 23:1766–71. doi: 10.1093/annonc/mdr493

8. Lyman GH, Abella E, Pettengell R. Risk factors for febrile neutropenia among patients with cancer receiving chemotherapy: A systematic review. *Crit Rev oncology/hematology.* (2014) 90:190–9. doi: 10.1016/j.critrevonc.2013.12.006

9. Xue J, Ma D, Jiang J, Liu Y. Diagnostic and prognostic value of immune/inflammation biomarkers for venous thromboembolism: Is it reliable for clinical practice? *J Inflammation Res.* (2021) 14:5059. doi: 10.2147/JIR.S327014

10. Almășan O, Leucuța D-C, Hedeșiu M. Blood cell count inflammatory markers as prognostic indicators of periodontitis: A systematic review and meta-analysis. *J Personalized Med.* (2022) 12:992. doi: 10.3390/jpm12060992

11. Banna GL, Friedlaender A, Tagliamento M, Mollica V, Cortellini A, Rebuzzi SE, et al. Biological rationale for peripheral blood cell–derived inflammatory indices and related prognostic scores in patients with advanced non-small-cell lung cancer. *Curr Oncol Rep.* (2022) 24:1851–62. doi: 10.1007/s11912-022-01335-8

12. Friedman J, Hastie T, Tibshirani R. Regularization paths for generalized linear models via coordinate descent. *J Stat Software*. (2010) 33:1. doi: 10.18637/jss.v033.i01

13. Cho B-J, Kim KM, Bilegsaikhan S-E, Suh YJ. Machine learning improves the prediction of febrile neutropenia in korean inpatients undergoing chemotherapy for breast cancer. *Sci Rep*. (2020) 10:14803. doi: 10.1038/s41598-020-71927-6

14. Koenderman L, Tesselaar K, Vrisekoop N. Human neutrophil kinetics: A call to revisit old evidence. *Trends Immunol*. (2022) 43(11):868–76. doi: 10.1016/j.it.2022.09.008

15. Venäläinen MS, Heervä E, Hirvonen O, Saraei S, Suomi T, Mikkola T, et al. Improved risk prediction of chemotherapy-induced neutropenia—model development and validation with real-world data. *Cancer Med*. (2022) 11:654–63. doi: 10.1002/cam4.4465

16. Ray-Coquard I, Borg C, Bachelot T, Sebban C, Philip I, Clapisson G, et al. Baseline and early lymphopenia predict for the risk of febrile neutropenia after chemotherapy. *Br J Cancer*. (2003) 88:181–6. doi: 10.1038/sj.bjc.6600724

17. Kataoka R, Hata T, Hosomi K, Hirata A, Goto E, Nishihara M, et al. Platelet count and dose, but not comorbidities, predict severe neutropenia in cabazitaxel-treated prostate cancer patients: A retrospective observational study. *Int J Clin Pharmacol Ther*. (2023) 61(9):386–93. doi: 10.5414/CP204393

18. Uchida M, Yamaguchi Y, Hosomi S, Ikesue H, Mori Y, Maegawa N, et al. Risk factors for febrile neutropenia induced by docetaxel chemotherapy in patients with non-small cell lung cancer. *Biol Pharm Bulletin*. (2020) 43:1235–40. doi: 10.1248/bpb.b20-00266

19. Zheng B, Huang Z, Huang Y, Hong L, Li J, Wu J. Predictive value of monocytes and lymphocytes for short-term neutrophil changes in chemotherapy-induced severe neutropenia in solid tumors. *Supportive Care Cancer*. (2020) 28:1289–94. doi: 10.1007/s00520-019-04946-3

20. Salvador C, Meryk A, Hetzer B, Bargehr C, Kropshofer G, Meister B, et al. Immature platelet fraction predicts early marrow recovery in febrile neutropenia. *Sci Rep*. (2023) 13(1):3371. doi: 10.21203/rs.3.rs-1661219/v1

frontiers | Frontiers in Immunology

TYPE Original Research
PUBLISHED 21 August 2024
DOI 10.3389/fimmu.2024.1421036

OPEN ACCESS

EDITED BY
Paulo Rodrigues-Santos,
University of Coimbra, Portugal

REVIEWED BY
Mauro Di Ianni,
University of Studies G. d'Annunzio Chieti and Pescara, Italy
Olga Janouskova,
Jan Evangelista Purkyně University in Ústí nad Labem, Czechia

*CORRESPONDENCE
Allyson Guimarães Costa
allyson.gui.costa@gmail.com

†These authors share senior authorship

RECEIVED 21 April 2024
ACCEPTED 25 July 2024
PUBLISHED 21 August 2024

CITATION
Magalhães-Gama F, Malheiros Araújo Silvestrini M, Neves JCF, Araújo ND, Alves-Hanna FS, Kerr MWA, Carvalho MPSS, Tarragô AM, Soares Pontes G, Martins-Filho OA, Malheiro A, Teixeira-Carvalho A and Costa AG (2024) Exploring cell-derived extracellular vesicles in peripheral blood and bone marrow of B-cell acute lymphoblastic leukemia pediatric patients: proof-of-concept study. *Front. Immunol.* 15:1421036. doi: 10.3389/fimmu.2024.1421036

Exploring cell-derived extracellular vesicles in peripheral blood and bone marrow of B-cell acute lymphoblastic leukemia pediatric patients: proof-of-concept study

Fábio Magalhães-Gama[1,2,3,4], Marina Malheiros Araújo Silvestrini[3,4], Juliana Costa Ferreira Neves[2,5], Nilberto Dias Araújo[1,2,6], Fabíola Silva Alves-Hanna[1,2], Marlon Wendell Athaydes Kerr[2,6], Maria Perpétuo Socorro Sampaio Carvalho[2,6], Andréa Monteiro Tarragô[2,6], Gemilson Soares Pontes[1,6,7], Olindo Assis Martins-Filho[3,4,6], Adriana Malheiro[1,2,6], Andréa Teixeira-Carvalho[3,4,6†] and Allyson Guimarães Costa[1,2,6*†]

[1]Programa de Pós-graduação em Imunologia Básica e Aplicada, Instituto de Ciências Biológicas, Universidade Federal do Amazonas (UFAM), Manaus, Brazil, [2]Diretoria de Ensino e Pesquisa, Fundação Hospitalar de Hematologia e Hemoterapia do Amazonas (HEMOAM), Manaus, Brazil, [3]Programa de Pós-graduação em Ciências da Saúde, Instituto René Rachou - Fundação Oswaldo Cruz (FIOCRUZ) Minas, Belo Horizonte, Brazil, [4]Grupo Integrado de Pesquisas em Biomarcadores, Belo Horizonte, Brazil, [5]Programa de Pós-graduação em Medicina Tropical, Universidade do Estado do Amazonas (UEA), Manaus, Brazil, [6]Programa de Pós-graduação em Ciências Aplicadas à Hematologia, UEA, Manaus, Brazil, [7]Laboratório de Virologia e Imunologia, Instituto Nacional de Pesquisas da Amazônia (INPA), Manaus, Brazil

Extracellular vesicles (EVs) are heterogeneous, phospholipid membrane enclosed particles that are secreted by healthy and cancerous cells. EVs are present in diverse biological fluids and have been associated with the severity of diseases, which indicates their potential as biomarkers for diagnosis, prognosis and as therapeutic targets. This study investigated the phenotypic characteristics of EVs derived from peripheral blood (PB) and bone marrow (BM) in pediatric patients with B-cell acute lymphoblastic leukemia (B-ALL) during different treatment stages. PB and BM plasma were collected from 20 B-ALL patients at three time points during induction therapy, referred to as: diagnosis baseline (D0), day 15 of induction therapy (D15) and the end of the induction therapy (D35). In addition, PB samples were collected from 10 healthy children at a single

Abbreviations: ADAM17, A Disintegrin and Metalloproteinase 17; AUC, area under the curve; ATG3, Autophagy Related Protein 3; B-ALL, B cell acute lymphoblastic leukemia; BM, bone marrow; CD, cluster of differentiation; D0, diagnosis baseline; D15, day 15 of the induction therapy; D35, end of the induction therapy; EVs, extracellular vesicles; IQR, interquartile range; ISEV, International Society for Extracellular Vesicles; LR, likelihood ratio; mAB, monoclonal antibody; NTA, nanoparticle tracking analysis; PB, peripheral blood; ROC, receiver operating characteristic; RT, room temperature; SEM, scanning electron microscopy; Se, sensitivity; Sp, specificity; TEM, transmission electron microscopy.

time point. The EVs were measured using CytoFLEX S flow cytometer. Calibration beads were employed to ensure accurate size analysis. The following, fluorescent-labeled specific cellular markers were used to label the EVs: Annexin V (phosphatidylserine), CD235a (erythrocyte), CD41a (platelet), CD51 (endothelial cell), CD45 (leukocyte), CD66b (neutrophil), CD14 (monocyte), CD3 (T lymphocyte), CD19, CD34 and CD10 (B lymphoblast/leukemic blast). Our results demonstrate that B-ALL patients had a marked production of EV-CD51/61$^+$, EV-CD10$^+$, EV-CD19$^+$ and EV-CD10$^+$CD19$^+$ (double-positive) with a decrease in EV-CD41a$^+$ on D0. However, the kinetics and signature of production during induction therapy revealed a clear decline in EV-CD10$^+$ and EV-CD19$^+$, with an increase of EV-CD41a$^+$ on D35. Furthermore, B-ALL patients showed a complex biological network, exhibiting distinct profiles on D0 and D35. Interestingly, fold change and ROC curve analysis demonstrated that EV-CD10$^+$CD19$^+$ were associated with B-ALL patients, exhibited excellent clinical performance and standing out as a potential diagnostic biomarker. In conclusion, our data indicate that EVs represent a promising field of investigation in B-ALL, offering the possibility of identifying potential biomarkers and therapeutic targets.

KEYWORDS

childhood leukemia, leukemic microenvironment, extracellular vesicles, nano-flow cytometry, biomarkers

Introduction

B-cell acute lymphoblastic leukemia (B-ALL) is characterized by an abnormal proliferation of B lymphoblasts/leukemic cells in the bone marrow (BM), which are released into the bloodstream and extramedullary tissues, and is the most common childhood cancer in the world (1, 2). The immunological mechanisms involved in triggering or maintaining B-ALL in patients are still being investigated. Similar to other cancers, B-ALL is characterized by a complex interplay between the immune system and leukemic cells throughout progression of the disease (3). In this context, it is important to highlight that the leukemic microenvironment comprises a diverse cellular landscape. This includes leukemic cells, hematopoietic stem cells, immune cells and bone marrow stromal cells. Together, they form a singular network of intrinsic interactions that can be explored by leukemic cells to contribute to the progression of cancer (4–6).

Historically, these interactions have been shown to be modulated by several immunological mediators, including cytokines, chemokines and growth factors (7–9). In a similar way to what occurs in these molecules, recent advances in cancer biology have revealed that heterogeneous cell membrane-derived vesicles, termed extracellular vesicles (EVs), which include exosomes and microvesicles, are released in large quantities by cancer cells, acting as key mediators of cellular communication, through bioactive charges transfer, as proteins, lipids and nucleic acids (10, 11). In addition, some studies have shown that cancer cell-derived EVs are capable of transporting oncogenic factors. These factors can then be transported and internalized by surrounding cells, leading to alterations in the gene expression of recipient cells. This process can significantly impact the progression of the disease (12–14).

Although studies in ALL are scarce compared to solid tumors, EVs have been shown to play an important role in bidirectional communication between leukemic cells and bone marrow stromal cells. Leukemic EVs targeting hematopoietic stem cells and progenitors have been shown to affect the quiescence and maintenance of the hematopoietic compartment (15). On the other hand, EVs derived from endothelial cells and mesenchymal cells sustain the activities and offer a role in protecting leukemic blasts (16, 17). In the context of tumor immunity, it was also demonstrated that EVs derived from leukemic blasts inhibit the biological function of natural killer cells and effector T cells by increasing the expression of Foxp3 and the signaling of regulatory cytokines, including TGF-β and IL-10 (18, 19). Collectively, these features highlight the potential of EVs as promising biomarkers in B-ALL, since EV levels can not only predict therapeutic responses but are also easily detectable in blood via minimally invasive methods (20).

Therefore, the aim of the present investigation was to analyze the immunophenotypic profile of cell-derived EVs in the PB and BM aspirates of newly diagnosed B-ALL patients undergoing remission induction therapy. By investigating these EVs, we hope to provide insight into the use of EVs as potential biomarkers in childhood leukemia.

10.3389/fimmu.2024.1421036

Materials and methods

Ethics statement

This study was submitted to and approved by the Ethics Committee at Fundação Hospitalar de Hematologia e Hemoterapia do Amazonas (HEMOAM), under protocol registration number #739.563. Prior to the inclusion of all the patients and controls in the study, all the respective parents or legal guardians read and signed the informed assent form. The study was carried out in accordance with the principles of the Helsinki Declaration and Resolution 466/2012 of the Brazilian National Health Council, which relates to research involving human participants.

Patients and control subjects

The study population consisted of 20 patients under the age of 15 who had been recently diagnosed with B-ALL at Fundação HEMOAM, the reference center for diagnosis and treatment of hematological diseases in the state of Amazonas, Brazil. The diagnosis was performed according to the classification criteria and guidelines of the World Health Organization (21). The B-ALL patients were subdivided into two subgroups (B-ALL peripheral blood [PB] and B-ALL bone marrow [BM]), according to the biological material used to measure the EVs. The B-ALL PB group consisted of 10 patients (7 males and 3 females), with a median age of 3 years; IQR = 2-9. The BM group consisted of 10 patients (8 males and 2 females), with a median age of 5 years; IQR = 3-6. Additionally, 10 children without leukemia (5 males and 5 females) with a median age of 9 years, IQR = 6-13, were included as a control group. For this, only PB samples were collected to provide a reference value in the analyses, since BM aspiration is a very invasive procedure. The children recruited in this study had not experienced any infections for at least four weeks prior to the collection of samples and did not present immunological alterations in the leukocyte series. The demographic and clinical data, together with the hematological patterns of the studied population are summarized in Tables 1, 2, respectively.

Treatment regimen

All the B-ALL patients underwent remission induction therapy (according to the protocol and guidelines found in the Brazilian Group for Treatment of Childhood Leukemia, version 2009), which is an intensive stage of chemotherapy of fundamental importance for the prognosis of patients, and whose objective is to achieve disease remission, with less than 5% lymphoblasts in five weeks. The treatment regimen includes the drugs prednisone, dexamethasone, vincristine, daunorubicin, L-asparaginase and MADIT (intrathecal methotrexate, cytarabine and dexamethasone) (22).

TABLE 1 Demographic and clinical characteristics of the study population.

Variables	CG PB (n=10)	B-ALL PB (n=10)	B-ALL BM (n=10)
Age, median (IQR)	9 (6-13)	3 (2-9)	5 (3-6)
Sex, Male/Female	5M/5F	7M/3F	8M/2F
Age group, n (%)			
1 to <5	1 (10%)	7 (70%)	4 (40%)
5 to <10	4 (40%)	1 (10%)	5 (50%)
10 to <15	5 (50%)	2 (20%)	1 (10%)
Immunophenotyping			
Common B-ALL ($CD10^+$)	–	10 (100%)	10 (100%)
CNS infiltration			
Absent	–	10 (100%)	10 (100%)
Present	–	0 (0%)	0 (0%)
Cytogenetics			
Good prognosis	–	10 (100%)	10 (100%)
Poor prognosis	–	0 (0%)	0 (0%)
Risk stratification at D0			
Low Risk	–	7 (24%)	6 (27%)
High Risk	–	3 (24%)	4 (55%)
Risk re-stratification at D15			
True low risk	–	0 (0%)	1 (10%)
Low intermediate risk	–	6 (60%)	5 (50%)
High risk rapid responder	–	3 (30%)	4 (40%)
High risk slow responder	–	1 (10%)	0 (0%)
MRD at D15			
Negative	–	1 (10%)	1 (10%)
Positive	–	9 (90%)	9 (90%)
Myelogram at D35 [n (%)]			
M1	–	100 (100%)	100 (100%)
M2	–	0 (0%)	0 (0%)
M3	–	0 (0%)	0 (0%)

CG, control group; B-ALL, B-cell acute lymphoblastic leukemia; PB, peripheral blood; BM, bone marrow; IQR, interquartile range; CNS, central nervous system; MRD, measurable residual disease; D0, diagnosis baseline; D15, day 15 of induction therapy; D35, end of the induction therapy; M1, <5% lymphoblasts; M2, 5-25% lymphoblasts; M3, >25% lymphoblasts.

Biological sample collection

The PB and BM samples of the B-ALL patients were obtained by venipuncture and iliac crest aspiration, respectively, at three consecutive time points, referred to as: D0 (diagnosis baseline), D15 (day 15 of induction therapy) and D35 (end of the induction therapy). In addition, PB samples from controls were obtained (single time point) via venipuncture. After collection, the biological samples

TABLE 2 Hematological characteristics of the study population.

Characteristics	CG PB (n = 10)	B-ALL PB (n = 10)	B-ALL BM (n = 10)	*p-value*
Total leukocytes (x10^3/uL), median (IQR)	7,540 (6,788-8,178)	9,135 (4,593-12,195)	56,735 (41,865-76,825)	**0.0014**^{b}
Lymphoblasts ABS [%], median (IQR)	–	7,239 [62%] (995- 8,278)	47,964 [82%] (28,483-64,920)	**0.0048**^{b}
Neutrophils (x10^3/uL), median (IQR)	3.24 (2.89-3.55)	0.43 (0.18-0.98)	0.30 (0.21-0.64)	**<0.0001**^{a}
Lymphocytes (x10^3/uL), median (IQR)	3.18 (2.50-3.73)	3.10 (2.25- 4.29)	3.19 (3.13-4.61)	0.7031
Monocytes (x10^3/uL), median (IQR)	0.40 (0.29-0.54)	0.11 (0.00-0.21)	0.13 (0.05-0.27)	**0.0005**^{a}
Hemoglobin (g/dL), median (IQR)	13.4 (12.3-13.7)	8.3 (3.7-9.7)	7.1 (4.6-8.1)	**0.0010**^{a}
Platelets (x10^3/uL), median (IQR)	325 (302-434)	54 (28-101)	53 (24-89)	**<0.0001**^{a}

CG, control group; BM, bone marrow; PB, peripheral blood; IQR, interquartile range. Reference values: Leukocytes: 5.2 - 12.4 x10^3/µL; Neutrophils: 1.9 - 8 x10^3/µL; Lymphocytes: 0.9 - 5.2 x10^3/µL; Monocytes: 0.16 - 1 x10^3/µL; Hemoglobin: 12 - 18 g/dL; Platelets: 130 - 140 x10^3/µL. Significant differences of $p<0.05$ are represented in bold with the following superscript letters: "a" and "b", which refer to comparisons of the B-ALL PB group with the CG and B-ALL BM group, respectively.

were transferred to EDTA vacuum tubes (BD Vacutainer® EDTA K2) and submitted to centrifugation at 600 *x*g, for 10 minutes at room temperature (RT). Subsequently, the supernatants or platelet-poor plasma were collected and immediately stored at -80°C until processing for EV measurement.

Sample preparation and extracellular vesicle measurement via flow cytometry

Initially, the samples were thawed at 37 °C and then centrifuged at 1,500 *x*g for 5 minutes to obtain platelet-free plasma. The latter was diluted in a citrate buffer solution containing heparin (1 µg/mL) and centrifuged at 1,500 *x*g for 90 minutes at RT. The EV-rich sediment was resuspended in commercially available Annexin V buffer (25 mM $CaCl_2$ solution in 140 mM NaCl and 10 mM HEPES, pH 7.4; BD Bioscience, San Diego, CA, USA) to obtain the EV suspension. Aliquots of 100 µL of EV suspension were transferred to a plate containing 2 µL of distinct monoclonal antibodies (mAB) to evaluate the immunophenotypes of the study panel. Of importance, prior to staining, mABs were centrifuged at 1,500 x g for 30 minutes to remove fluorescent particles. The panel was composed of specific markers of B cell lineage and maturation stage, which are used for the diagnosis and monitoring of B-ALL. Markers of cellular populations/elements (erythrocytes, platelets and leukocytes) were also used, which are frequently used as parameters for classifying therapeutic response. Thus, the study panel was composed of CD235a (erythrocyte), CD41a (platelets), CD51 (endothelial cell), CD45 (leukocytes), CD66b (neutrophils), CD14 (monocytes), CD3 (T lymphocytes), CD19 (B lymphocyte/B lymphoblast) and CD34 and CD10 (B lymphoblast/leukemic blast); and 2.5 µL of Annexin V-FITC, which binds to phosphatidylserine residues expressed on the surface of EVs. Internal autofluorescence control was included in each trial run, in which an aliquot of EV suspension was incubated in the absence of mAB and Annexin V-FITC (all purchased from BD Bioscience, San Diego, CA, USA). Additionally, aliquots of mAB and Annexin V-FITC, incubated in the absence of EVs, were also used as internal controls. After incubation for 30 minutes in the dark at RT, 300 µL of Annexin V buffer was added to the wells of each plate and then transferred to FACS tubes. The samples were acquired in a flow cytometer (CytoFLEX S, Beckman Coulter, Brea, CA, USA) with volume control aspirated per minute. The CytoFLEX S has a volumetric sample injection system that allows counting of absolute particles. The sample flow rate was 30 µL/min, and the sample acquisition occurred during 2 minutes per sample. Calibration beads (Megamix-Plus FSC and SSC, Biocytex, Marseille, France) with standard sizes of 100, 160, 200, 240, 300, 500, 900 nm were used to identify different EV size ranges, defined as: small EVs (sEVs): 100-200 nm; medium EVs (mEVs): 201-500 nm; and large EVs (lEVs): 501-900 nm. The steps of the protocol are summarized in Figure 1. Different gating strategies were used to analyze the phenotypic characteristics and size of the EVs, according Megamix beads, as illustrated in Supplementary Figures 1, 2.

Conventional statistical analysis

The comparative analysis between the B-ALL patients and controls was carried out using Student's t test or the Mann-Whitney test. Comparisons among the timepoints of induction therapy (D0, D15 and D35) and EV size ranges (sEVs, mEVs and lEVs) were performed using one-way ANOVA followed by the Tukey or Friedman tests followed by Dunn's test; along with the paired t test or Wilcoxon matched-pairs signed-ranks test. In all cases, the Shapiro-Wilk test was used to verify the normality of the data and significance was considered when p was <0.05. The GraphPad Prism software v8.0.2 (San Diego, CA, USA) was used for statistical analysis.

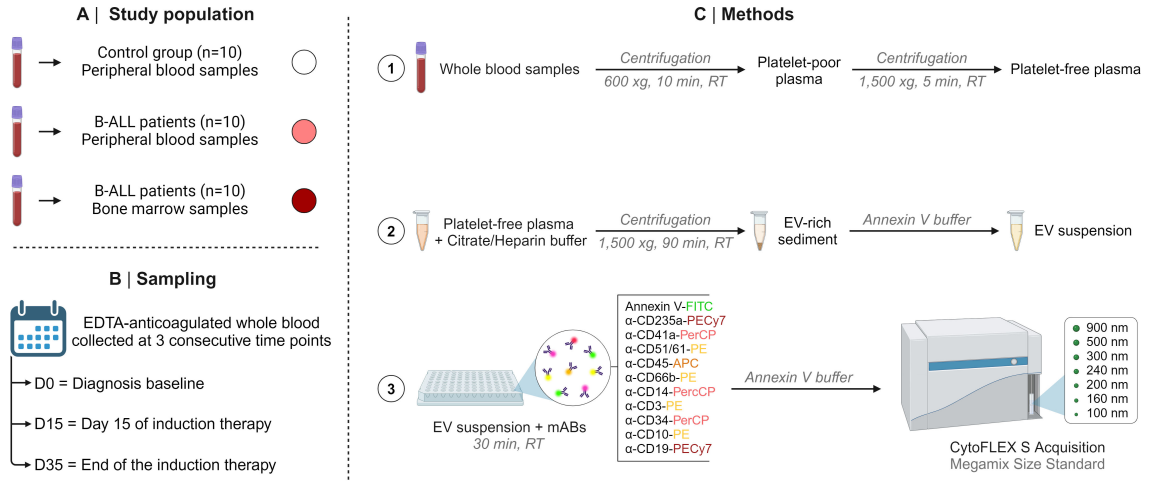

FIGURE 1
Compendium of study. The study population **(A)**, sampling **(B)**, and methods **(C)**, including the steps of the protocol are summarized in this figure.

Overall signatures of extracellular vesicles

The signature analysis was carried out according to Kerr et al. (2021) (23), by converting the original results of each variable expressed as a continuous variable in categorical data. For this purpose, the global median values obtained for the whole data universe from all participants (B-ALL patients on different days of induction therapy and the controls) as the cut-off to classify the patients with low (below the cut-off) or high (above the cut-off) production of EVs. The following cut-offs were used: (EV-CD235a$^+$ = 27,917; EV-CD41a$^+$ = 658; EV-CD51/61$^+$ = 4,839; EV-CD45$^+$ = 296; CD66b$^+$ = 797; EV-CD14$^+$ = 200; EV-CD3$^+$ = 445; EV-CD34$^+$ = 299; EV-CD10$^+$ = 3,289; and EV-CD19$^+$ = 7,617) expressed as an absolute number of EVs/mm^3 of plasma. The overall signatures were assembled in radar charts using the 50th percentile as a threshold to identify the proportion of subjects with EV populations above the global median cut-off.

Biological networks of extracellular vesicles

Analysis of correlation networks was performed to evaluate the multiple associations among the EV populations in the B-ALL patients and the controls. The association between the EV levels was determined by using the Spearman correlation coefficient in GraphPad Prism, v8.0.2 (GraphPad Software, San Diego, CA, USA), and statistical significance was considered only if p was <0.05. After performing the correlation analysis between EV populations, a database was created using Microsoft Excel® program. Then, the significant correlations were compiled using the open source Cytoscape software, v3.9.1 (National Institute of General Medical Sciences, Bethesda, MD, USA). The biological networks were constructed using circular layouts in which each EV population is represented by a globular node, in which the larger the nodule size, the greater the number of correlations established. The correlation indices (r) were used to categorize the correlation strength as negative (r <0), moderate (0.36≥ r ≤0.68), or strong (r >0.68), which were represented by connecting edges, as proposed by Taylor (1990) (24). Cytoscape software and Microsoft PowerPoint program were used for the graphics.

Fold change and performance analysis of extracellular vesicles

The magnitude of change in the EV levels in the B-ALL patients was calculated as the proportion ratio between the serum levels observed for each B-ALL patient at the diagnosis baseline (D0) divided by the median values reported for the control group. The magnitude of changes in the EV levels in the PB were determined considering decreased (≤ 1x) and increased (≥ 1x) levels in relation to the median values observed in the control group. Bubble charts were generated using Microsoft Excel®. Receiver operating characteristic (ROC) curve analysis (25) was carried out to assess the performance of EVs as biomarkers for B-ALL in the study population. ROC curve data were used to define cut-off points for the EVs evaluated. Performance indices of sensitivity (Se), specificity (Sp) and likelihood ratio (LR) were calculated at a specific cut-off and the area under the curve (AUC) and p-value were considered as indicators of global accuracy. The MedCalc v7.3.0 (Ostend, West Flemish, BE) and GraphPad Prism software v8.0.2 (San Diego, CA, USA) were used for statistical analysis and construction of the ROC curves.

Results

Characterization of the profiles of the extracellular vesicles at diagnosis baseline

The characterization of the EV profile at diagnosis (D0) demonstrated that the B-ALL PB group had a decrease in platelet-derived EVs (EV-CD41a$^+$) and an increase in endothelial cell-derived EVs (EV-CD51/61$^+$) and B lymphoblasts/lymphocytes with CD10 and CD19 phenotype (EV-CD10$^+$ and EV-CD19$^+$) when compared to

10.3389/fimmu.2024.1421036

control group. Additionally, an increase in the levels of EV-CD51/61$^+$ and EV-CD19$^+$ was observed when compared to the B-ALL BM group. Nevertheless, a thorough analysis revealed a trend towards increased levels of leukocyte-derived EVs (EV-CD45$^+$), neutrophils (EV-CD66b$^+$), monocytes (EV-CD14$^+$) and B lymphoblast with the CD34 phenotype (EV-CD34$^+$) in the B-ALL BM group (Figure 2).

Kinetics of extracellular vesicles during induction therapy

The analysis of EV kinetics of in PB and BM was performed on the samples from D0, D15 and D35 to assess the EV levels on diagnosis, at the beginning and at the end of induction therapy (Figure 3). The results demonstrated a decrease in EV-CD235a$^+$, EV-CD51/61$^+$, EV-CD45$^+$ and EV-CD66b$^+$ in the PB group on D15. Moreover, there was a noticeable decline in EV-CD10$^+$ and EV-CD19$^+$ on D15 and D35. This trend was similarly observed in the B-ALL BM group, wherein EV-CD10$^+$ decreased at D15 and D35. However, EV-CD19$^+$ exhibited a distinct pattern, decreasing on D15 and increasing on D35. Furthermore, both the B-ALL PB and B-ALL BM groups showed an increase in EV-CD41a$^+$ on D35. In addition, a specific an increase in EV-CD14$^+$ and EV-CD45$^+$ was observed in the B-ALL PB and B-ALL BM groups, respectively.

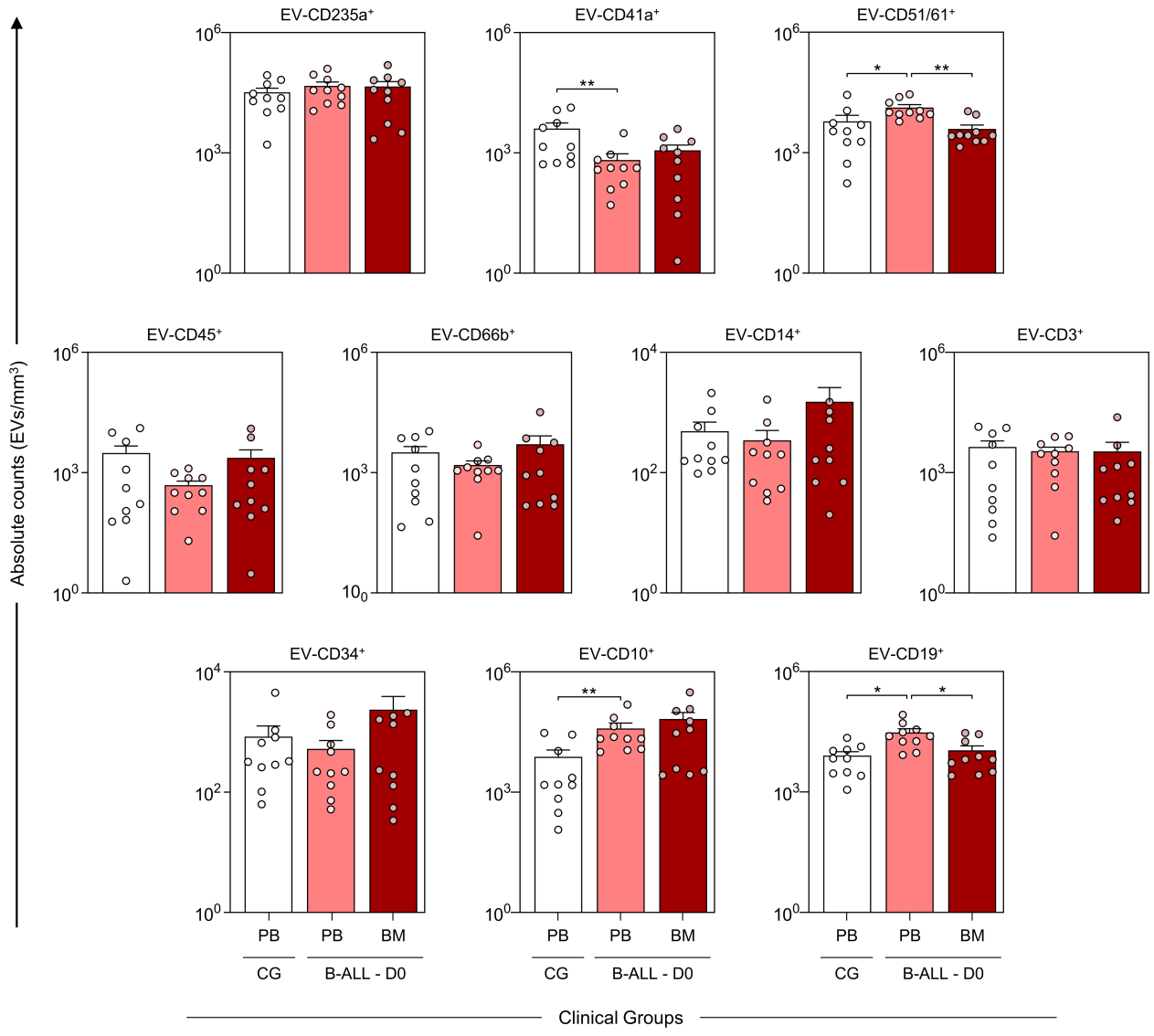

FIGURE 2
Characterization of the profile of the extracellular vesicles at diagnosis baseline. The EV populations were measured at the time of diagnosis in the B-ALL PB ( ) and B-ALL BM ( ) groups and in the control group (CG) ( ). The count and immunophenotypic characterization of EVs was performed using flow cytometry, as described in the Materials and Methods section. The results are presented using bar and symbol charts, reported in log10 scale, showing the mean with standard error of the absolute number of EVs/mm^3 of plasma. Statistical analyses were performed using Student's t test or the Mann-Whitney test and significant differences are highlighted by asterisks for p<0.01 (**) or p<0.05 (*).

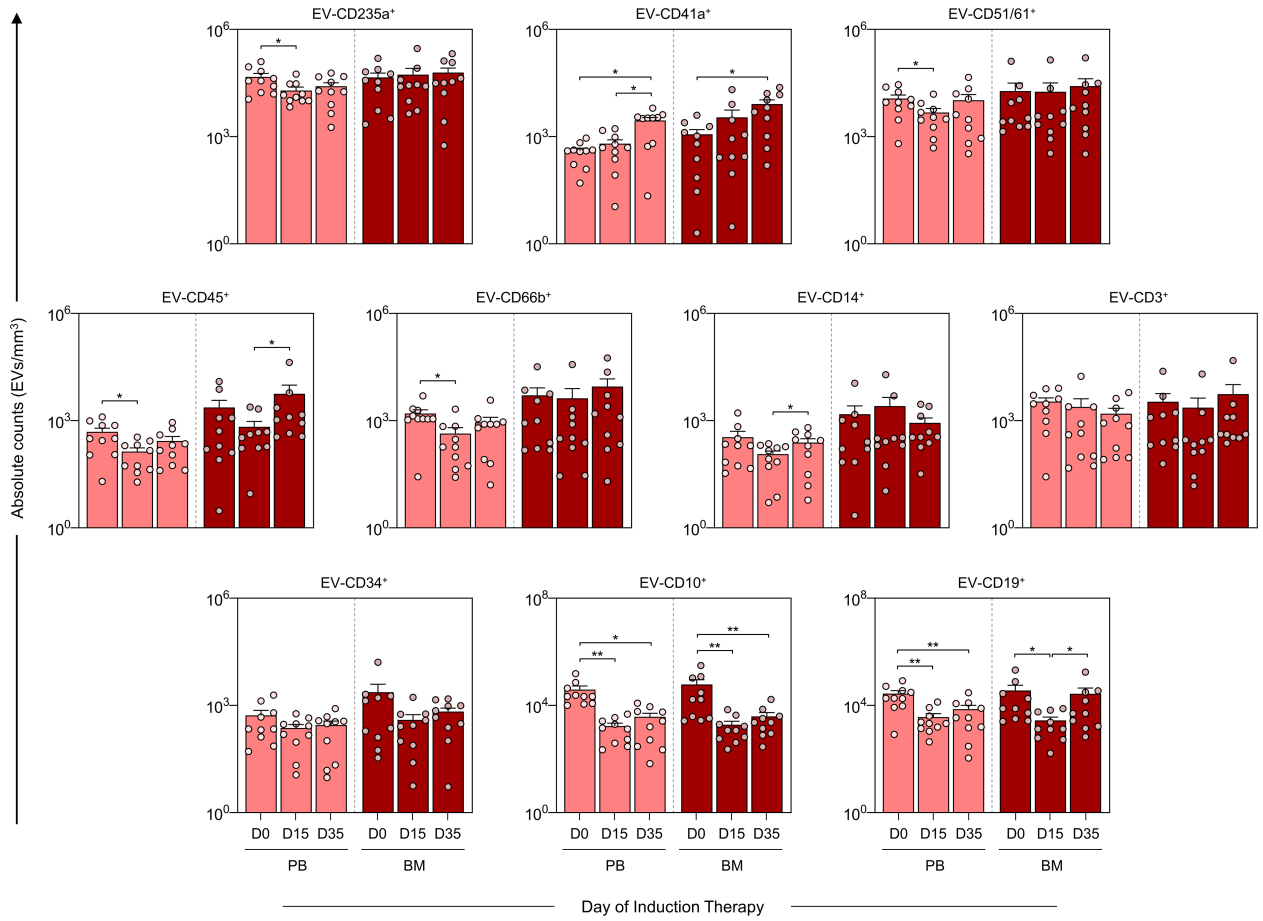

FIGURE 3
Kinetics of extracellular vesicles during induction therapy. The EV populations were measured on D0, D15, and D35 in the B-ALL PB ( ) and B-ALL BM ( ) groups to assess the behavior of these EVs during remission induction therapy. The count and immunophenotypic characterization of the EVs was performed using flow cytometry, as described in the Materials and Methods section. The results are presented using bar and symbol charts, reported in log10 scale, showing the mean with standard error of the absolute number of EVs/mm^3 of plasma. Statistical analyses were performed using a paired t test or Wilcoxon matched-pairs signed-rank test for comparisons between D0, D15 and D35 and significant differences are highlighted by asterisks for p<0.01 (**) or p<0.05 (*).

Kinetics of extracellular vesicles according to size range

To better understand the size distribution of the EV populations evaluated, we used calibration beads with specific sizes (100, 160, 200, 240, 300, 500, 900 nm). Based on this calibration, we classified the EVs into three size ranges: small EVs (sEV: 100-200 nm), medium EVs (mEV: 201-500 nm) and large EVs (lEV: 501-900 nm) (Figure 4). On diagnosis baseline and throughout induction therapy (D0, D15 and D35) in the B-ALL PB group, there was a consistent predominance of EV-CD235a$^+$ and EV-CD51/61$^+$ in the sEV and mEV size ranges. In contrast, the EV-CD45$^+$, EV-CD14$^+$, EV-CD34$^+$ populations showed a predominance of lEV during the treatment. The EV-CD41a$^+$ population showed an increase in sEV on D0 compared to control group, followed by an increase in mEV on both D15 and D35, compared to lEV. In addition, EV-CD10$^+$ and EV-CD19$^+$ exhibited a predominance of sEV, followed by mEV on D0 (Figure 4A). In the B-ALL BM group, EV-CD235a$^+$ predominated in both sEV and mEV ranges, while EV-CD14$^+$ and EV-CD34$^+$ exhibited a predominance of lEV. On D0, the EV-CD10$^+$ and CD19$^+$ populations showed an increase in sEV compared to lEV (Figure 4B).

Signature of extracellular vesicles during induction therapy

To further refine the characterization of the EV profile in the B-ALL patients (Figure 5), we calculated the median for each EV population across all the patients. This median value was then used as a cut-off to categorize patients as low or high producers of specific EVs. Our findings demonstrated that on D0, compared to the control group, the B-ALL PB group displayed a greater production of most EV populations, except for EV-CD41a$^+$ and EV-CD34$^+$. On D15, there was a significant decrease in the production of all EV populations. By D35, only EV-CD3$^+$ was observed and EV-CD14$^+$ remained elevated. In contrast, the B-ALL BM group exhibited a different pattern. On D0, high production was observed for EV-CD235a$^+$, EV-CD66b$^+$, EV-CD10$^+$ and EV-CD19$^+$. By D15, only

10.3389/fimmu.2024.1421036

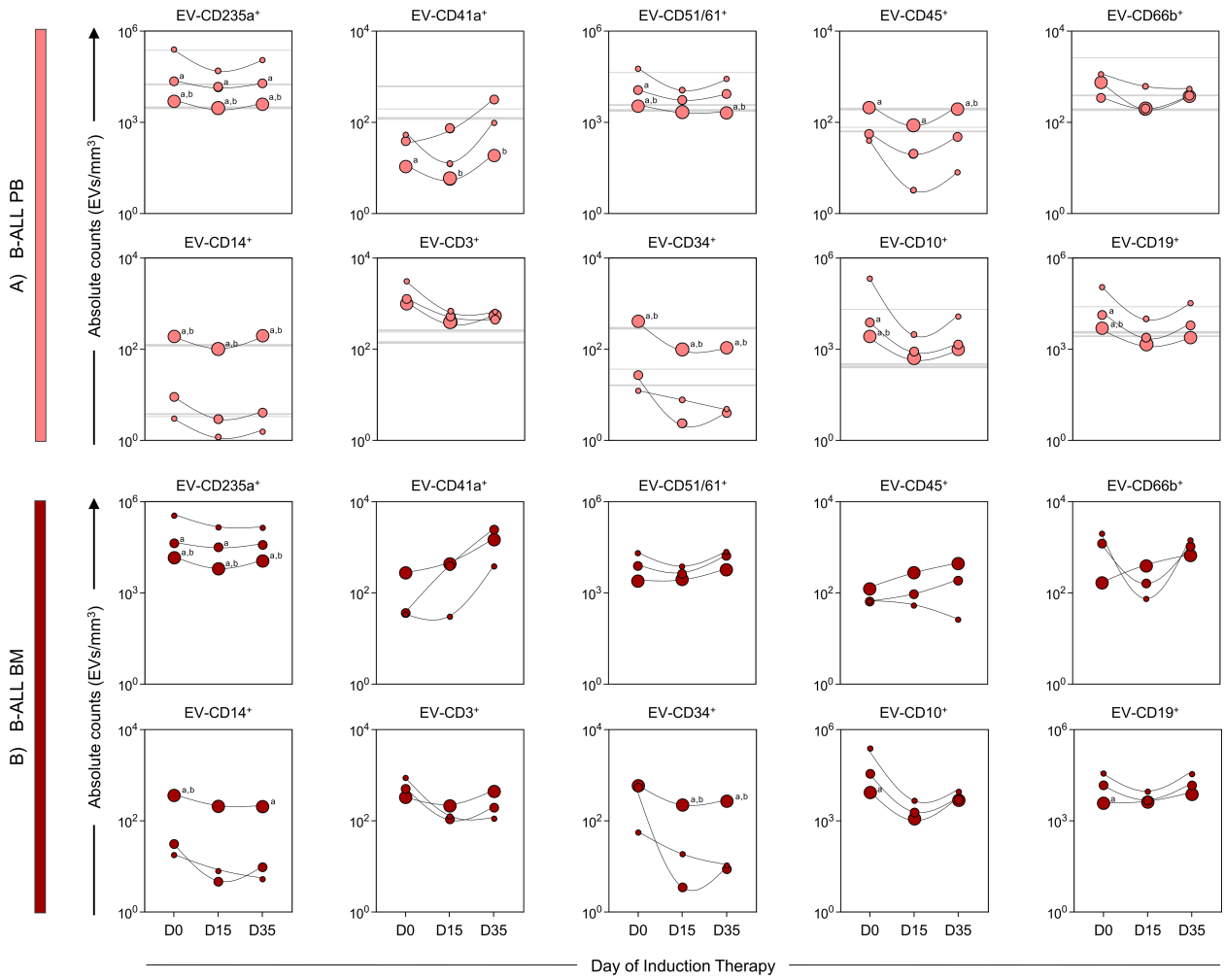

FIGURE 4
Kinetics of extracellular vesicles according to size range. The EV populations were analyzed in **(A)** B-ALL PB (●) and **(B)** B-ALL BM (●) groups according to their size, based on Megamix beads size range, being divided into small EVs = 100-200 nm (sEVs), medium EVs = 201-500 nm (mEVs) and large EVs = 501-900 nm (lEVs), represented by the symbols: "●", "●" and "●", respectively. For the control group, sEVs, mEVs, and lEVs were represented by gray background lines: "—", "—" and "—", respectively. The count, size and immunophenotypic characterization of the EVs was performed using flow cytometry, as described in the Materials and Methods section. The results are presented using symbol charts, reported in log10 scale, showing the median of the absolute number of EVs/mm^3 of plasma. Statistical analyses were performed using a paired t test or Wilcoxon matched-pairs signed-rank test for comparisons between sEVs, mEVs, and lEVs and significant differences are represented by the letters: "a" and "b", which refer to the comparisons with sEVs and mEVs, respectively.

EV-CD45$^+$ and EV-CD14$^+$ showed an increase. Nonetheless, on D35, there was an increase in the production of most EV populations, except EV-CD3$^+$, EV-CD10$^+$ and EV-CD19$^+$.

Biological network of extracellular vesicles during induction therapy

The construction of integrative biological networks was performed to assess the complex interactions between EV populations during induction therapy (Figure 6). The results demonstrated that the B-ALL PB group exhibited a network with a restricted number of interactions on D0. On D15, a minor decrease in the number of neighborhood connections was observed. Despite this, on D35, there was a substantial increase in the number of interactions between EV populations, resulting in a network with a profile that was more similar to the control group. Similarly, the B-ALL BM group's network displayed a restricted number of interactions on D0 when compared to the control group. This number increased slightly on D15, followed by a significant increase in interactions between EV populations on D35.

Fold change and performance of extracellular vesicles CD10$^+$and CD19$^+$ as diagnostic biomarkers of B-ALL

To identify potential diagnostic biomarkers, we performed a translational analysis that focused on EV-CD10$^+$ and EV-CD19$^+$ levels measured in the PB of the B-ALL patients at D0. Our findings

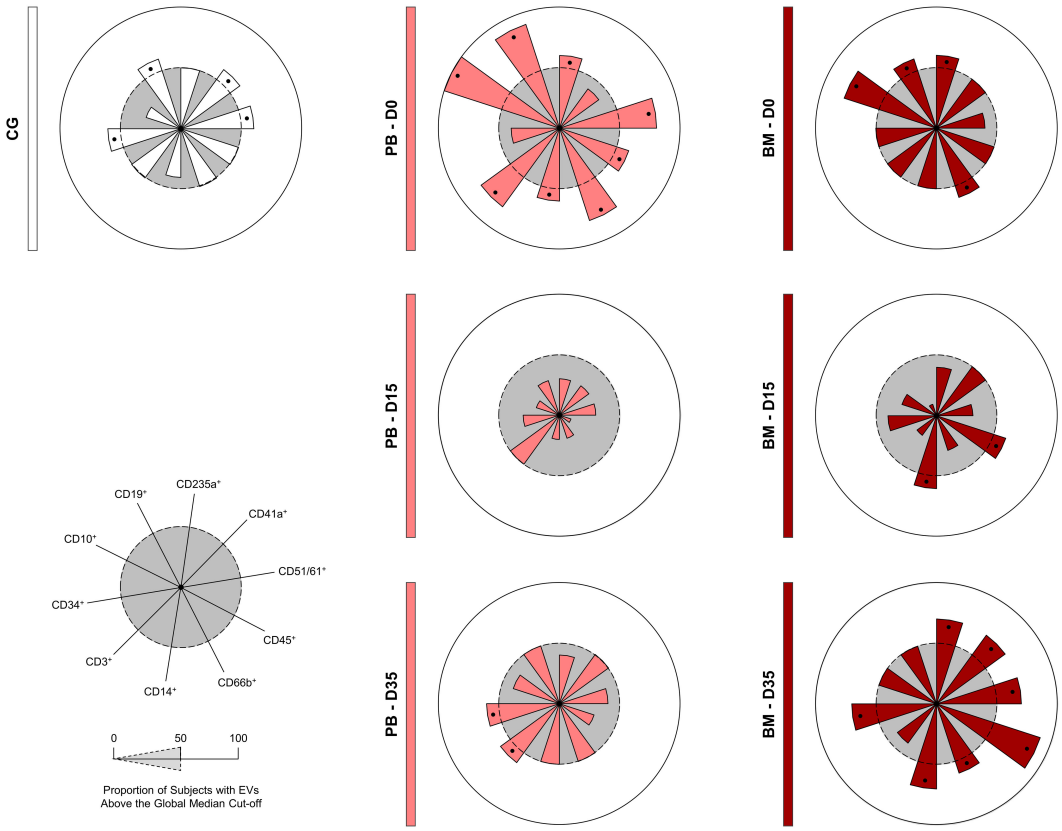

FIGURE 5
Signature of extracellular vesicles during induction therapy. The overall signature of EV populations in the B-ALL patients was assembled on D0, D15 and D35. Data, originally expressed as absolute number of EVs/mm^3 of plasma, were converted into categorical data using the global median values, which were used as a cut-off point to classify the study population as being a low or high producer of the EVs evaluated. The overall signatures were assembled in radar charts using the 50th percentile as the threshold (central circle/gray zone) to identify EV populations with increased levels in a higher proportion of patients. Cellular markers: CD235a (erythrocyte), CD41a (platelet), CD51 (endothelial cell), CD45 (leukocyte), CD66b (neutrophil), CD14 (monocyte), CD3 (T lymphocyte), CD34 and CD10 (B lymphoblast/Leukemic blast) and CD19 (B lymphocyte/B lymphoblast).

revealed significant changes in EV levels in the B-ALL patients when compared to the control group at D0. EV-CD10$^+$ levels showed the most dramatic increase (over 5-fold), followed by EV-CD19$^+$ (over 3.5-fold) and EV-CD51/61 (over 2-fold). In addition, EV-CD41a exhibited a significant decrease (below 1.5-fold) (Figures 7A, B). To assess the diagnostic potential of these EV levels in the B-ALL patients, we performed ROC curve analysis. This analysis calculates the area under the curve (AUC), a measure of overall accuracy, along with sensitivity (Se), specificity (Sp) and likelihood ratio (LR) to evaluate how well an EV level discriminates B-ALL from the control group. Data analysis demonstrated that EV-CD10$^+$ showed high performance (Se = 100.0% and Sp = 70.0%) and good global accuracy (AUC = 0.860 and p = 0.0065) to discriminate the B-ALL PB group from the control group. However, EV-CD19$^+$ levels exhibit a moderate performance (Se=75.0% and Sp=87.5%) and global accuracy (AUC = 0.844 and p = 0.0209) (Figure 7C). Additionally, EV-CD41a and EV-CD51/61 also presented moderate/high performance (Se = 66.7% and Sp = 100.0%/Se = 100.0% and Sp = 75.0%, respectively) and global accuracy (AUC = 0.852 and p = 0.0118/AUC = 0.812 and p = 0.0357, respectively) (Supplementary Figure 3).

Profile, Kinetic, fold change and performance of extracellular vesicles CD10$^+$CD19$^+$ as diagnostic biomarkers of B-ALL

Aiming of investigating whether CD10$^+$ and CD19$^+$ markers were present simultaneously in EVs, we carried out a strategy to evaluate EV-CD10$^+$CD19$^+$ (double-positive) in our study population. Compilation of data relating to the EVs profile; kinetics during induction therapy; fold change analysis; and performance of EV-CD10$^+$CD19$^+$ as biomarkers, are represented in Figure 8. The results demonstrated that B-ALL patients showed a significant increase in serum levels of EV-CD10$^+$CD19$^+$ compared to GC (Figure 8A). During induction therapy, a decline in D15 was observed in both the B-ALL PB and the B-ALL BM groups (Figure 8B). Regarding the fold change analysis, it was observed that B-ALL PB showed a pronounced increase in EV-CD10$^+$CD10$^+$ levels (more than 5 times) (Figures 8C, D). In parallel, the ROC curve analysis on D0 revealed excellent performance (Se = 100.0% and Sp = 87.5%) and global accuracy (AUC = 0.984 and p = 0.0011) to discriminate the B-ALL PB patients from the CG (Figure 8E).

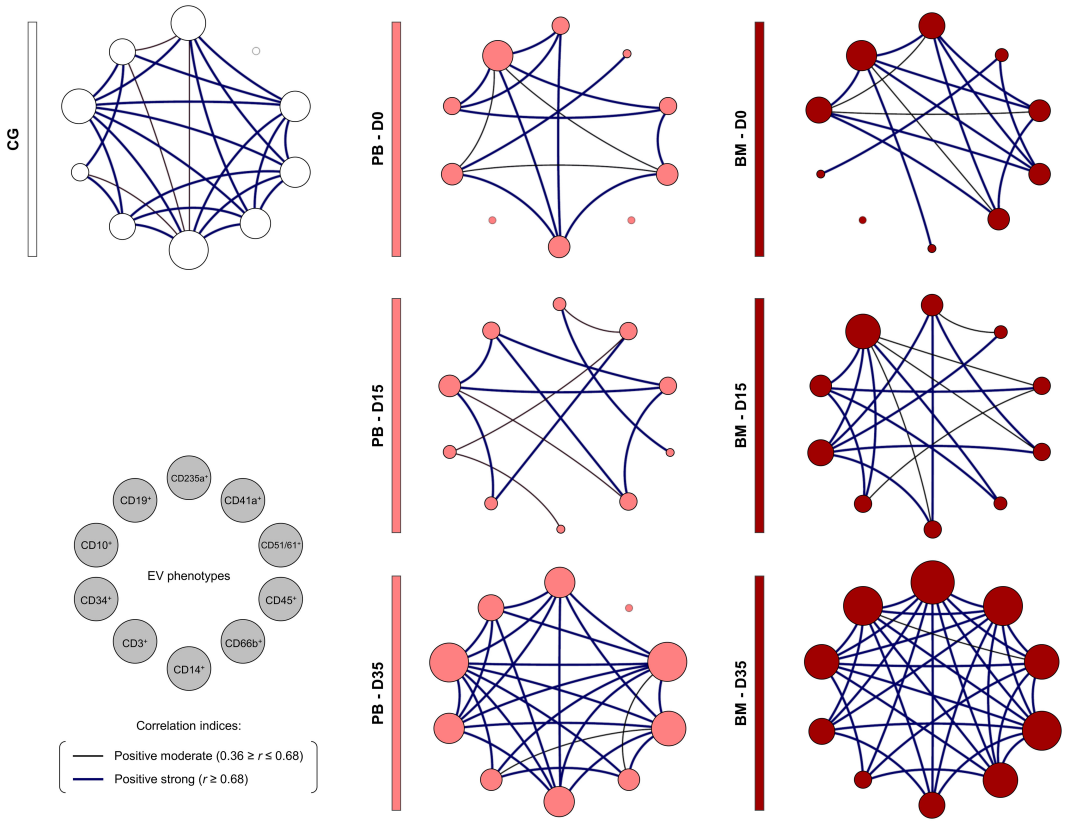

FIGURE 6
Biological network of extracellular vesicles during induction therapy. Integrative networks were assembled to identify the complex interactions among EV populations during induction therapy. Colored nodes are used to identify the EVs in the B-ALL PB (●) and B-ALL BM (●) groups and in the control group (CG) (○), where the larger the node, the greater the number of interactions established. Correlation analysis was employed to construct integrative networks according to significant "r" scores at $p<0.05$ using the Spearman correlation test. Connecting edges illustrate the positive correlations between pairs of attributes, according to the strength of correlation as described in the Materials and Methods section. Different colored and thickness are used to represent moderate correlations (black fine edges) and strong correlations (dark blue solid edges). Cellular markers: CD235a (erythrocyte), CD41a (platelet), CD51 (endothelial cell), CD45 (leukocyte), CD66b (neutrophil), CD14 (monocyte), CD3 (T lymphocyte), CD34 and CD10 (B lymphoblast/Leukemic blast) and CD19 (B lymphocyte/B lymphoblast).

Discussion

Growing evidence shows that the bone marrow (BM) microenvironment plays a crucial role in the survival of leukemic blasts and that communication between these cancer cells and surrounding cells can be mediated by various soluble immune molecules such as cytokines, chemokines and growth factors (5, 8, 9). Much like what occurs in other signaling molecules, recent advances in cancer biology have revealed that EVs are released in large quantities by cancer cells. These EVs act as key mediators in cell communication, carrying bioactive loads capable of reprogramming stromal and immune cells, thereby creating a favorable microenvironment for leukemic survival and progression (11). In this study, we analyzed the profile of leukemic blast-derived EVs (EV-CD34$^+$/CD10$^+$/CD19$^+$) in the peripheral blood (PB) and BM plasma of pediatric patients with B-ALL (B-ALL PB and B-ALL BM, respectively), at diagnosis baseline (D0) and during induction therapy (D15 and D35). Of interest, we also analyzed the levels of erythrocyte-derived EVs (EV-CD235a$^+$), platelets (EV-CD41a$^+$) and endothelial cells (EV-CD51/61$^+$), as well as leukocyte-derived EVs (EV-CD45$^+$), neutrophils (EV-CD66b$^+$), monocytes (EV-CD14$^+$), T lymphocytes (EV-CD3$^+$) and B lymphocytes (EV-CD19$^+$).

EVs contained in blood mainly originate from platelets and erythrocytes and account for about 50% of the total vesicles in healthy subjects (26). In our data, we detected a decrease in EV-CD41a$^+$ levels in the B-ALL PB group compared to the control group (Figure 2), which reflects the intense thrombocytopenia observed in the blood count on D0 (Table 2). However, on D35, there was an increase in EV-CD41a$^+$, indicating recovery of thrombopoiesis with increased platelet production (Figure 3). In the context of solid tumors, platelets are reported to play a role in the mechanisms by which cancer cells can accelerate their growth rate and evade the immune system (27–29). However, studies investigating the role of platelets in hematological malignancies are scarce (30–32). From a therapeutic point of view, it is considered that platelet count can be used as a parameter for prognostic assessment of ALL patients during and after induction therapy (33, 34). These questions highlight the need for in-depth investigations into the interactions of EV-CD41a$^+$ with leukemic blasts, as well as its use as a biomarker related to thrombopoiesis or recovery of normal hematopoiesis.

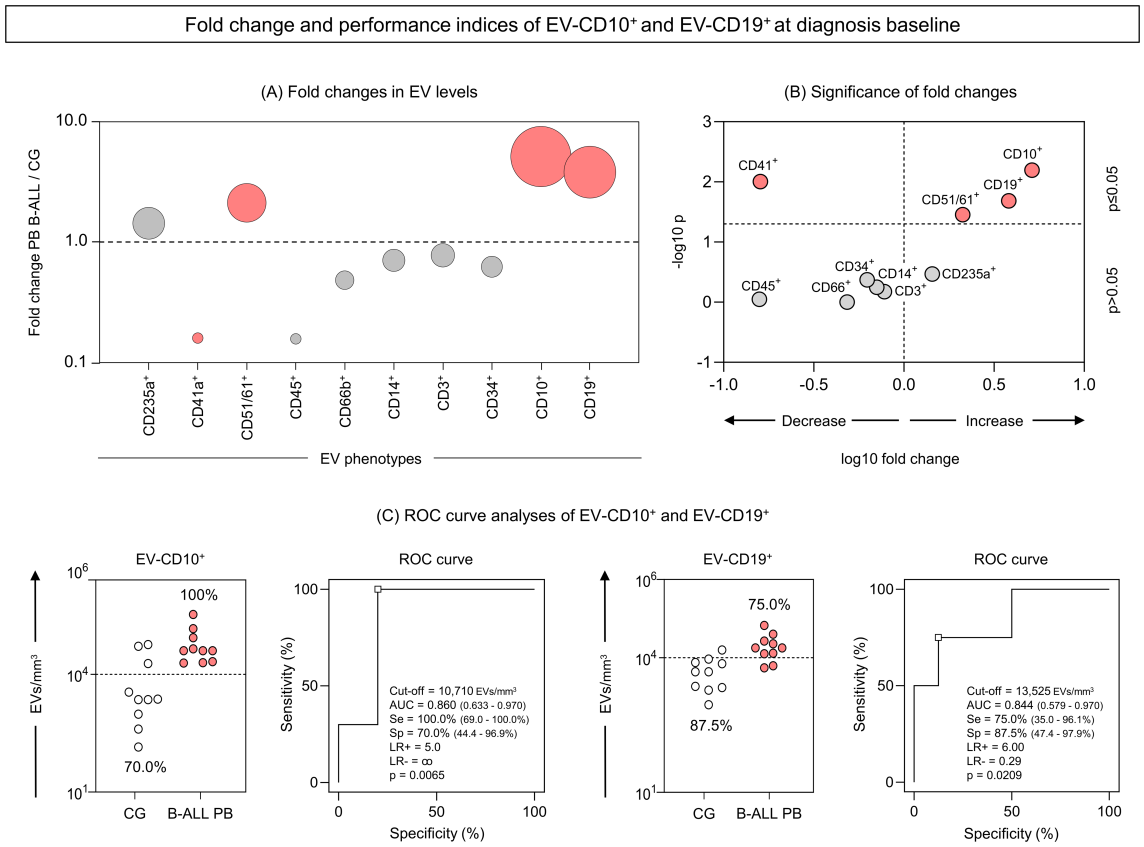

FIGURE 7
Fold change and performance of the extracellular vesicles CD10$^+$ and CD19$^+$ as diagnostic biomarkers of B-ALL. The fold changes **(A)** and significance of fold changes **(B)** were performed in the peripheral blood of the B-ALL patients at the diagnosis baseline as described in the Materials and Methods section. Receiver operating characteristic (ROC) curve analysis was carried out to assess the performance of EV-CD10$^+$ and EV-CD19$^+$ levels as diagnostic biomarkers for B-ALL **(C)**. ROC curves were assembled to define the cut-off points and calculate the following performance indices: sensitivity (Se), specificity (Sp), likelihood ratio (LR), the best cut-off point, as well as the area under the curve (AUC) and p-value as indicators of global accuracy, as described in the Materials and Methods section.

The fraction of EVs derived from endothelial cells (EV-ECs) is relatively low in physiological conditions but is highly increased in pathologies characterized by endothelial dysfunction, such as thrombotic thrombocytopenic purpura, diabetes or hypertension (35). When the release of EVs derives from activated ECs, their action has been frequently associated with inflammatory processes and procoagulant states (36, 37). Our results identified high levels of EV-CD51/61$^+$ on D0 in the B-ALL PB group when compared to the control group (Figure 2). These findings are important as they indicate greater activation of the endothelium in leukemia, which may be associated with an increased risk of thrombosis. Importantly, venous thromboembolism is described as a serious and relatively common condition in pediatric ALL patients (38, 39), and reported incidences vary from 1.1% to 36.7% (40, 41). Mechanisms underlying the increased risk are not completely understood, but studies have shown that besides treatment components, the malignancy itself can contribute to a prothrombotic state (42, 43). In this scenario, EV-ECs emerge as a potential contributor to these events since they are one of the EV populations with the most pronounced coagulation activity. This is a feature that is due to the high expression of active tissue factor, which is the main initiator of the coagulation cascade reactions (44, 45).

Not less important, pro-angiogenic effects of EV-ECs were also reported and considered to be a potential mechanism that leads to neovascularization (46, 47). One recent study demonstrated that the secretion of EC-derived EVs containing angiopoietin like 2 (ANGPTL2) played important roles in the development of murine B-ALL, sustaining leukemogenic activities of leukemic blasts (16). Collectively, these data indicate that EV-ECs actively participate in inflammation, coagulation and angiogenesis. This functional repertoire introduces the possibility of using EV-ECs as biomarkers and therapeutic targets in cancer; however, the field remains very obscure and requires further investigations, especially in the context of acute leukemias.

Regarding markers associated with leukemic blasts, our B-ALL patients showed an increase in EV-CD10$^+$ and EV-CD19$^+$ (Figure 2). CD19 is a signal amplifying coreceptor expressed throughout B-cell development, though not in the mature plasma cell stage; it is, however, the single best clinical marker for B-cell identity (48). Instead, CD10, also known as common acute lymphoblastic leukemia antigen (CALLA), is a type II cell surface integral membrane protein of the M13 family, which is specifically

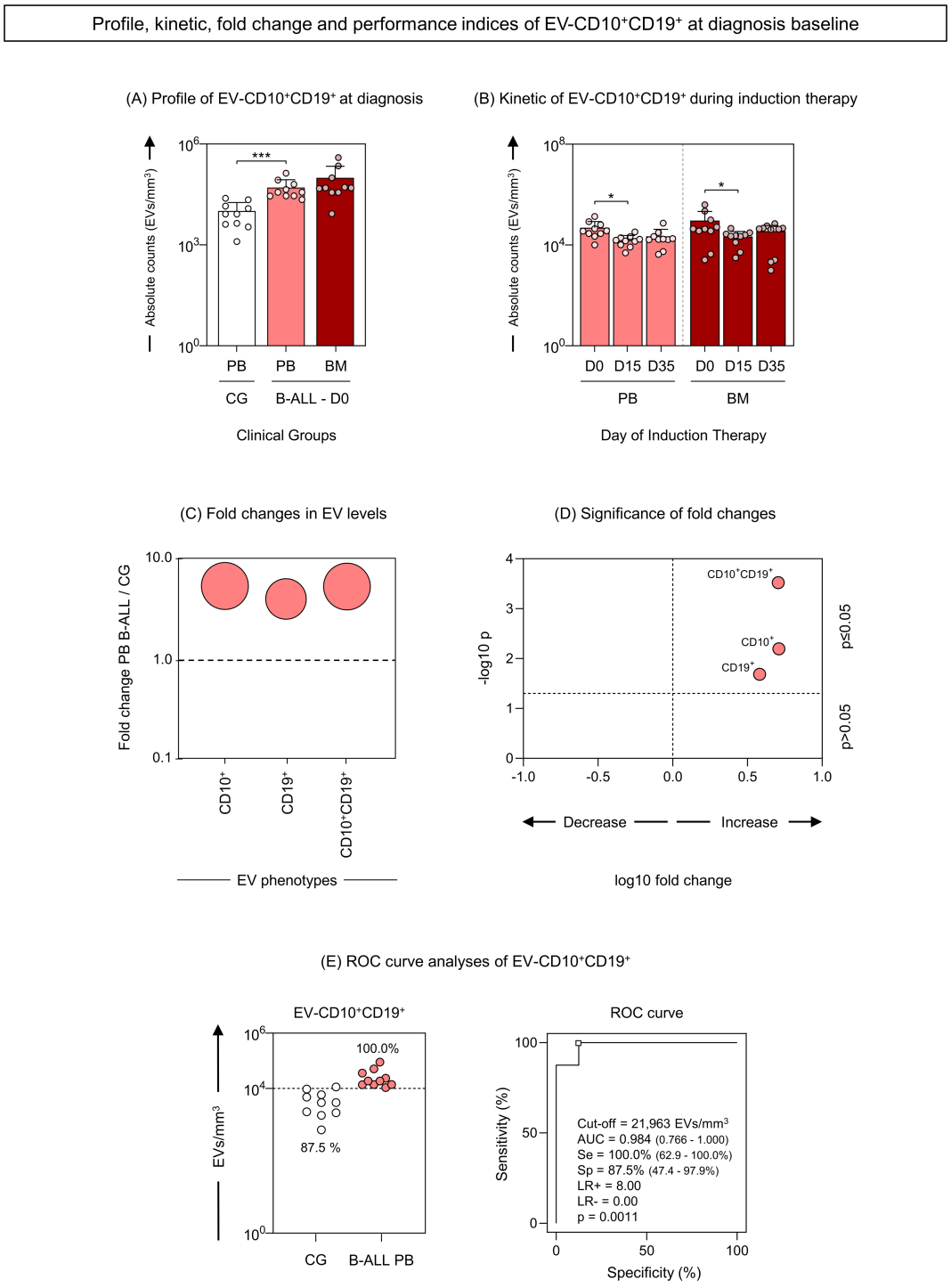

FIGURE 8
Profile, kinetic, fold change and performance of extracellular vesicles CD10$^+$CD19$^+$ as diagnostic biomarkers of B-ALL. The EV-CD10$^+$CD19$^+$ (double-positive) populations were analyzed at the diagnosis baseline **(A)** and during induction therapy **(B)** in the B-ALL PB ( ) and B-ALL BM ( ) groups and in the control group (CG) ( ). The count and immunophenotypic characterization of EV-CD10$^+$CD19$^+$ was performed using flow cytometry. The results are presented using bar and symbol charts, reported in log10 scale, showing the mean with standard error of the absolute number of EVs/mm^3 of plasma. Statistical analyses were performed using the Mann-Whitney test or Wilcoxon matched-pairs signed-rank test and significant differences are highlighted by asterisks for $p<0.001$ (***) or $p<0.05$ (*). The fold changes **(C)** and significance of fold changes **(D)** were performed in the peripheral blood of the B-ALL patients at the diagnosis baseline. Receiver operating characteristic (ROC) curve analysis **(E)** was carried out to assess the performance of EV-CD10$^+$CD19$^+$ plasma levels as diagnostic biomarkers for B-ALL. ROC curves were assembled to define the cut-off points and calculate the following performance indices: sensitivity (Se), specificity (Sp), likelihood ratio (LR), the best cut-off point, as well as the area under the curve (AUC) and p-value as indicators of global accuracy.

expressed in the early stages of the lymphoid progenitor, thus aiding in the identification of stages in B lymphocyte development (49). CD10 is widely used to distinguish most cases of ALL from other hematologic malignancies, and is commonly used in diagnosis via flow cytometry and monitoring of hematologic malignancies of B cell origin, in the categorization of the mature and blastic stage, and also for detection of measurable residual disease (50, 51). Originally identified in leukemic blasts, CD10 was later detected in cells from the prostate, kidney, intestine and endometrium (52, 53). The presence of CD10 in other cells suggests a varied role that is not specifically restricted to hematologic malignancies. Biologically, its main function is to metabolize polypeptides through peptide cleavage between hydrophobic residues, leading to the inactivation of a variety of physiologically active neuropeptides (54).

In the context of cancer, CD10 activity and its high expression has been correlated with a poor prognosis and decreased survival in a variety of malignancies, through mechanisms that include therapeutic drug and radiation resistance, increased tumor grade and a more aggressive phenotype (invasion and metastasis) (54–60). In the ontogeny of B lymphocytes, CD10, present in pre-B lymphocytes, is transiently expressed during different stages of maturation and disappears in mature B lymphocytes. In this sense, by evaluating the kinetics during induction therapy, it was possible to observe a clear decline in the EV-CD10$^+$ levels in B-ALL PB and B-ALL BM on D35. In parallel, a decline in EV-CD19$^+$ was observed in B-ALL PB; while, in B-ALL BM, a distinct behavior was observed, with a decrease on D15 followed by an increase on D35 (Figure 3). In a similar way, the EV signature during induction therapy demonstrated that, on D0, a greater proportion of B-ALL patients exhibited high production of EV-CD10$^+$ and EV-CD19$^+$, in contrast to on D35 (Figure 5). Collectively, these findings may be indicative of the elimination or meaningful decrease of leukemic blasts on D35, with subsequent production of mature B lymphocytes and EV-CD19$^+$ (mature B lymphocyte-derived EVs) in the medullary compartment.

The signature analysis also demonstrated important changes in the other EV populations during induction therapy. Where on D0, B-ALL PB presented a higher proportion of high-producers of EVs, followed by a decline on D15 and D35, on the other hand, B-ALL BM presented a lower proportion of high-producers of EVs on D0, followed by an increase on D15 and D35 (Figure 5). Interestingly, the analysis of the integrative network of EVs also exhibited notable changes during treatment, but with a distinct behavior. On D0, B-ALL PB patients exhibited a network of EVs that was characterized by a limited number of interactions. However, on D35, a network more like that of the control group was observed. This network was characterized by an increase of connections among EV populations, with emphasis on EVs derived from leukocytes (CD45$^+$, CD66$^+$, CD14$^+$ and CD3$^+$). In parallel, B-ALL BM presented a profile similar to that of B-ALL PB, but with a greater number of interactions, which can be explained by the greater complexity of the medullary microenvironment (Figure 6). Similar behavior was observed in a previous study, where on D35, the B-ALL patients exhibited a network of cytokines characterized by an increase of multiple connections. This was composed of greater interactions among the mediators of the different response profiles, suggesting the recovery of pro-inflammatory response (61).

The most critical issue to be highlighted and evaluated in our data is whether the EVs originate specifically from leukemic blasts or from another cellular source, albeit on a smaller scale. This is of great importance because, if the former is true, then EV-CD10$^+$ and EV-CD19$^+$ can be qualified as very promising biomarkers of diagnosis and therapeutic response in ALL. Aiming to answer this question, the double-positivity of EVs for the CD10$^+$ and CD19$^+$ markers was evaluated. Incredibly, our results demonstrate that, just like EV-CD10$^+$ and EV-CD19$^+$, the double positive EVs (EV-CD10$^+$CD19$^+$) were elevated in B-ALL PB patients at diagnosis, with a 5-fold magnitude of change in relation to the CG (Figures 8A–D). However, the ROC curve analysis revealed an even better clinical performance (AUC = 0.984) in discriminating B-ALL patients from CG (Figure 8E), compared to isolated EV-CD10$^+$ (AUC = 0.860) and EV-CD19$^+$ (AUC = 0,844) (Figure 7), highlighting the potential of these vesicles as biomarkers.

Although these results appear promising, they still require further investigation. Such investigations involve a richer analysis of the protein cargo of EVs, as well as their impact on the leukemic microenvironment. Although scarce, studies in B-ALL have demonstrated that EVs derived from leukemic blasts are enriched in tetraspanins (CD9, CD61 and CD81), adhesion molecules (CD29 and CD1446), in addition to lineage-specific markers (CD10, CD19 and CD22) (17, 62). Furthermore, proteomic analyze revealed that A Disintegrin and Metalloproteinase 17 (ADAM17) and Autophagy Related Protein 3 (ATG3) molecules were highly expressed in EVs derived from plasma of B-ALL patients, being found enriched in the Notch and autophagy pathways, respectively. In addition, ROC curve analyzes revealed that ADAM17 and ATG3 showed high clinical performance (AUC = 0.989 and AUC = 0.956, respectively), reinforcing that EVs enriched by the proteins may represent valuable biomarkers in B-ALL (63).

Noteworthy, this study has limitations: i) Since it is a segment study, in many cases, the sample volume was insufficient to perform EV assays. This ended up leading to a reduction in the study population, which compromised the analysis of association with the clinical prognosis; ii) Another limitation was the non-application of other methods for evaluation of EVs, as nanoparticle tracking analysis (NTA), and transmission electron microscopy (TEM) or scanning electron Microscopy (SEM), which would provide more accurate data on the size range and diversity of EVs; iii) Finally, given the absence of an ultracentrifuge, the isolation protocol applied was not that recommended by the International Society for Extracellular Vesicles (ISEV) guidelines (64), which could result in a lower yield in the purification of EVs and imply the co-isolation of potential contaminants.

However, it is important to highlight that this is a proof-of-concept study. Additional studies will be carried out to fill the gaps and correct the limitations left by this study. In this sense, from a larger study population, we will seek to carry out a richer characterization, from a phenotypic and protein cargo point of view, aiming to explore the impact of EVs on the clinical prognosis of patients with B-ALL undergoing chemotherapy and remission.

Conclusion

Our data demonstrated that: (i) The B-ALL patients exhibited a decrease in EV-CD41a$^+$ on D0 that is followed by a progressive increase on D15 and D35, indicating recovery of thrombopoiesis; (ii) The B-ALL patients showed a marked production of EV-CD51/61$^+$, indicating greater activation of ECs; (iii) In our cohort, CD10 and CD19 were the most expressed markers in the leukemic blasts; (iv) EV-CD10$^+$ and EV-CD19$^+$ showed predominance in the Megamix beads size range of 100-200 nm, configuring them as "small vesicles"; (v) The B-ALL patients exhibited dynamic EV kinetics and signatures during induction therapy, exhibiting distinct profiles on D0 and D35; (vi) The B-ALL patients showed a marked increase in the number of connections on D35, displaying a biological network that was more similar to that of the control group; (vii) EV-CD10$^+$CD19$^+$ (double-positives) were also increased and exhibited excellent clinical performance and general accuracy for discriminating the B-ALL patients from the CG, and are possibly associated with unfavorable outcomes.

Finally, our data indicate that EVs represent a potential field of investigation in ALL. Future studies should explore the cargos carried by EVs-CD10$^+$CD19$^+$, how it affects the leukemic microenvironment and, ultimately, its potential as a combined diagnostic and prognostic biomarker for B-ALL. If successful, leukemic EVs could become a valuable liquid biopsy tool, allowing the real-time monitoring of malignancy progression.

Data availability statement

The original contributions presented in the study are included in the article/Supplementary Material. Further inquiries can be directed to the corresponding author.

Ethics statement

This study was submitted to and approved by the Ethics Committee at Fundação Hospitalar de Hematologia e Hemoterapia do Amazonas (HEMOAM), under protocol registration number #739.563. The studies were conducted in accordance with the local legislation and institutional requirements. Written informed consent for participation in this study was provided by the participants' legal guardians/next of kin.

Author contributions

FM-G: Conceptualization, Formal analysis, Investigation, Methodology, Writing – original draft, Writing – review & editing. MM: Investigation, Methodology, Writing – original draft. JN: Formal analysis, Writing – original draft, Investigation, Methodology. NA: Formal analysis, Investigation, Methodology, Writing – original draft. FA-H: Formal analysis, Investigation, Methodology, Writing – original draft, Supervision. MK: Investigation, Methodology, Writing – original draft, Validation. MC: Investigation, Methodology, Supervision, Writing – original draft. AT: Investigation, Methodology, Project administration, Writing – original draft. GS: Conceptualization, Formal analysis, Funding acquisition, Writing – review & editing, Data curation. OM-F: Conceptualization, Data curation, Formal analysis, Writing – review & editing, Funding acquisition, Writing – original draft. AM: Formal analysis, Funding acquisition, Methodology, Supervision, Writing – original draft. AT-C: Conceptualization, Data curation, Formal analysis, Funding acquisition, Writing – original draft, Writing – review & editing. AC: Conceptualization, Formal analysis, Funding acquisition, Supervision, Writing – original draft, Writing – review & editing.

Funding

The author(s) declare financial support was received for the research, authorship, and/or publication of this article. Financial support was provided in the form of grants from Fundação de Amparo à Pesquisa do Estado do Amazonas (FAPEAM) (Pró-Estado Program - #002/2008, #007/2018, #005/2019 and POSGRAD Program #002/2023 and #002/2024), Conselho Nacional de Desenvolvimento Científico e Tecnológico (CNPq) and Coordenação de Aperfeiçoamento de Pessoal de Nível Superior (CAPES) (PROCAD-Amazônia 2018 Program - #88881.200581/2018-01 and PDPG-CONSOLIDACAO-3-4 Program #88887.707248/2022-00). FM-G, MM, JN, NA, MK, and FA-H have fellowships from FAPEAM, CAPES and CNPq (Masters and PhD student fellowships). OM-F is a level 1 research fellow from CNPq and a research fellow from the program supported by the Universidade do Estado do Amazonas (PROVISIT No. 005/2023-PROPESP/UEA). AT-C and AC are a level 2 research fellow from CNPq. The funders made no contribution to the study's design, data collection and analysis, decision to publish or preparation of the manuscript.

Acknowledgments

The authors thank the Diretoria de Ensino e Pesquisa at Fundação HEMOAM and Programa de Desenvolvimento Tecnológico em Insumos para Saúde da FIOCRUZ (PDTIS-FIOCRUZ) for the use of their facilities. We are also grateful to the patients and controls who participated in the study, as well as their parents or legal guardians for allowing participation. Finally, we thank the Grupo Integrado de Pesquisas em Biomarcadores of the Instituto René Rachou, Fundação Oswaldo Cruz (FIOCRUZ-Minas), for the excellent technical assistance and support with the trials.

Conflict of interest

The authors declare that the research was conducted in the absence of any commercial or financial relationships that could be construed as a potential conflict of interest.

Publisher's note

Supplementary material

The Supplementary Material for this article can be found online at: https://www.frontiersin.org/articles/10.3389/fimmu.2024.1421036/full#supplementary-material

SUPPLEMENTARY FIGURE 1
Analysis of strategies for the phenotypic characterization of EVs using flow cytometry.

SUPPLEMENTARY FIGURE 2
Analysis of strategies for the phenotypic characterization of EVs using flow cytometry according to size range.

SUPPLEMENTARY FIGURE 3
Fold change and performance of the extracellular vesicles CD41a$^+$ and CD51/61$^+$ as diagnostic biomarkers of B-ALL. The fold changes **(A)** and significance of fold changes **(B)** were performed in the peripheral blood of the B-ALL patients at the diagnosis baseline as described in the Materials and Methods section. Receiver operating characteristic (ROC) curve analysis was carried out to assess the performance of EV-CD41a$^+$ and EV-CD51/61$^+$ levels as diagnostic biomarkers for B-ALL **(C)**. ROC curves were assembled to define the cut-off points and calculate the following performance indices: sensitivity (Se), specificity (Sp), likelihood ratio (LR), the best cut-off point, as well as the area under the curve (AUC) and p-value as indicators of global accuracy, as described in the Materials and Methods section.

References

1. Carroll WL, Bhojwani D, Min DJ, Raetz E, Relling M, Davies S, et al. Pediatric acute lymphoblastic leukemia. *Hematol Am Soc Hematol Educ Progr*. (2003) 2003:102–31. doi: 10.1182/asheducation-2003.1.102

2. Terwilliger T, Abdul-Hay M. Acute lymphoblastic leukemia: a comprehensive review and 2017 update. *Blood Cancer J*. (2017) 7:e577. doi: 10.1038/bcj.2017.53

3. Vinay DS, Ryan EP, Pawelec G, Talib WH, Stagg J, Elkord E, et al. Immune evasion in cancer: Mechanistic basis and therapeutic strategies. *Semin Cancer Biol*. (2015) 35:S185–98. doi: 10.1016/j.semcancer.2015.03.004

4. Emon B, Bauer J, Jain Y, Jung B, Saif T. Biophysics of tumor microenvironment and cancer metastasis - A mini review. *Comput Struct Biotechnol J*. (2018) 16:279–87. doi: 10.1016/j.csbj.2018.07.003

5. Chiarini F, Lonetti A, Evangelisti C, Buontempo F, Orsini E, Evangelisti C, et al. Advances in understanding the acute lymphoblastic leukemia bone marrow microenvironment: From biology to therapeutic targeting. *Biochim Biophys Acta - Mol Cell Res*. (2016) 1863:449–63. doi: 10.1016/j.bbamcr.2015.08.015

6. Tabe Y, Konopleva M. Advances in understanding the leukaemia microenvironment. *Br J Haematol*. (2014) 164:767–78. doi: 10.1111/bjh.12725

7. Burkholder B, Huang RY, Burgess R, Luo S, Jones VS, Zhang W, et al. Tumor-induced perturbations of cytokines and immune cell networks. *Biochim Biophys Acta - Rev Cancer*. (2014) 1845:182–201. doi: 10.1016/j.bbcan.2014.01.004

8. Sheu BC. Cytokine regulation networks in the cancer microenvironment. *Front Biosci*. (2008) 13):6255. doi: 10.2741/3152

9. Nagarsheth N, Wicha MS, Zou W. Chemokines in the cancer microenvironment and their relevance in cancer immunotherapy. *Nat Rev Immunol*. (2017) 17:559–72. doi: 10.1038/nri.2017.49

10. Meldolesi J. Exosomes and ectosomes in intercellular communication. *Curr Biol*. (2018) 28:R435–44. doi: 10.1016/j.cub.2018.01.059

11. Pando A, Reagan JL, Quesenberry P, Fast LD. Extracellular vesicles in leukemia. *Leuk Res*. (2018) 64:52–60. doi: 10.1016/j.leukres.2017.11.011

12. Martins VR, Dias MS, Hainaut P. Tumor-cell-derived microvesicles as carriers of molecular information in cancer. *Curr Opin Oncol*. (2013) 25:66–75. doi: 10.1097/CCO.0b013e32835b7c81

13. Skog J, Würdinger T, van Rijn S, Meijer DH, Gainche L, Curry WT, et al. Glioblastoma microvesicles transport RNA and proteins that promote tumour growth and provide diagnostic biomarkers. *Nat Cell Biol*. (2008) 10:1470–6. doi: 10.1038/ncb1800

14. Lee Y, Andaloussi S EL, Wood MJA. Exosomes and microvesicles: extracellular vesicles for genetic information transfer and gene therapy. *Hum Mol Genet*. (2012) 21: R125–34. doi: 10.1093/hmg/dds317

15. Georgievski A, Michel A, Thomas C, Mlamla Z, Pais de Barros JP, Lemaire-Ewing S, et al. Acute lymphoblastic leukemia-derived extracellular vesicles affect quiescence of hematopoietic stem and progenitor cells. *Cell Death Dis*. (2022) 13:337. doi: 10.1038/s41419-022-04761-5

16. Huang D, Yuan Y, Cao L, Zhang D, Jiang Y, Zhang Y, et al. Endothelial-derived small extracellular vesicles support B-cell acute lymphoblastic leukemia development. *Cell Oncol*. (2023) 47:129–40. doi: 10.1007/s13402-023-00855-0

17. Amirpour M, Kuhestani-Dehaghi B, Kheyrandish S, Hajipirloo LK, Khaffafpour Z, Keshavarz F, et al. The impact of exosomes derived from B-cell acute lymphoblastic leukemia as a growth factor on bone marrow mesenchymal stromal cells. *Mol Biol Rep*. (2024) 51:749. doi: 10.1007/s11033-024-09674-4

18. Yu H, Huang T, Wang D, Chen L, Lan X, Liu X, et al. Acute lymphoblastic leukemia-derived exosome inhibits cytotoxicity of natural killer cells by TGF-β signaling pathway. *3 Biotech*. (2021) 11:313. doi: 10.1007/s13205-021-02817-5

19. Gholipour E, Kahroba H, Soltani N, Samadi P, Sarvarian P, Vakili-Samiani S, et al. Paediatric pre-B acute lymphoblastic leukaemia-derived exosomes regulate immune function in human T cells. *J Cell Mol Med*. (2022) 26:4566–76. doi: 10.1111/jcmm.17482

20. Srivastava A, Rathore S, Munshi A, Ramesh R. Extracellular vesicles in oncology: from immune suppression to immunotherapy. *AAPS J*. (2021) 23:30. doi: 10.1208/s12248-021-00554-4

21. World Health Organization (WHO). *World health organization classification of tumours of haematopoietic and lymphoid tissues*. (2016).

22. Sociedade Brasileira de Oncologia Pediátrica. *Protocolo brasileiro de tratamento da leucemia linfóide aguda na infância GBTLI LLA-2009*. (2011).

23. Kerr MWA, Magalhães-Gama F, Ibiapina HNS, Hanna FSA, Xabregas LA, Alves EB, et al. Bone marrow soluble immunological mediators as clinical prognosis biomarkers in B-cell acute lymphoblastic leukemia patients undergoing induction therapy. *Front Oncol*. (2021) 11:3631. doi: 10.3389/fonc.2021.696032

24. Taylor R. Interpretation of the correlation coefficient: A basic review. *J Diagn Med Sonogr*. (1990) 6:35–9. doi: 10.1177/875647939000600106

25. Swets JA. Measuring the accuracy of diagnostic systems. *Sci (80-)*. (1988) 240:1285–93. doi: 10.1126/science.3287615

26. Arraud N, Linares R, Tan S, Gounou C, Pasquet J-M, Mornet S, et al. Extracellular vesicles from blood plasma: determination of their morphology, size, phenotype and concentration. *J Thromb Haemost*. (2014) 12:614–27. doi: 10.1111/jth.12554

27. Goubran HA, Stakiw J, Radosevic M, Burnouf T. Platelets effects on tumor growth. *Semin Oncol*. (2014) 41:359–69. doi: 10.1053/j.seminoncol.2014.04.006

28. Catani MV, Savini I, Tullio V, Gasperi V. The "Janus face" of platelets in cancer. *Int J Mol Sci*. (2020) 21:788. doi: 10.3390/ijms21030788

29. Schmied L, Höglund P, Meinke S. Platelet-mediated protection of cancer cells from immune surveillance – possible implications for cancer immunotherapy. *Front Immunol*. (2021) 12:640578/full. doi: 10.3389/fimmu.2021.640578/full

30. Zhang L, Liu J, Qin X, Liu W. Platelet–acute leukemia interactions. *Clin Chim Acta*. (2022) 536:29–38. doi: 10.1016/j.cca.2022.09.015

31. Yan M, Jurasz P. The role of platelets in the tumor microenvironment: From solid tumors to leukemia. *Biochim Biophys Acta - Mol Cell Res*. (2016) 1863:392–400. doi: 10.1016/j.bbamcr.2015.07.008

32. Li Y, Wang S, Xiao H, Lu F, Zhang B, Zhou T. Evaluation and validation of the prognostic value of platelet indices in patients with leukemia. *Clin Exp Med*. (2023) 23:1835–44. doi: 10.1007/s10238-022-00985-z

33. Lee JW, Cho B. Prognostic factors and treatment of pediatric acute lymphoblastic leukemia. *Korean J Pediatr*. (2017) 60:129. doi: 10.3345/kjp.2017.60.5.129

34. Dai Q, Shi R, Zhang G, Yang H, Wang Y, Ye L, et al. Combined use of peripheral blood blast count and platelet count during and after induction therapy to predict prognosis in children with acute lymphoblastic leukemia. *Med (Baltimore)*. (2021) 100: e25548. doi: 10.1097/MD.0000000000025548

35. Desideri E, Ciccarone F, Ciriolo MR, Fratantonio D. Extracellular vesicles in endothelial cells: from mediators of cell-to-cell communication to cargo delivery tools. *Free Radic Biol Med*. (2021) 172:508–20. doi: 10.1016/j.freeradbiomed.2021.06.030

36. Brodsky SV, Malinowski K, Golightly M, Jesty J, Goligorsky MS. Plasminogen activator inhibitor-1 promotes formation of endothelial microparticles with procoagulant potential. *Circulation*. (2002) 106:2372–8. doi: 10.1161/01.CIR.0000033972.90653.AF

37. Abid Hussein MN, Böing AN, Biró É, Hoek FJ, Vogel GMT, Meuleman DG, et al. Phospholipid composition of *in vitro* endothelial microparticles and their *in vivo* thrombogenic properties. *Thromb Res*. (2008) 121:865–71. doi: 10.1016/j.thromres.2007.08.005

38. Schmiegelow K, Attarbaschi A, Barzilai S, Escherich G, Frandsen TL, Halsey C, et al. Consensus definitions of 14 severe acute toxic effects for childhood lymphoblastic leukaemia treatment: a Delphi consensus. *Lancet Oncol*. (2016) 17:e231–9. doi: 10.1016/S1470-2045(16)30035-3

39. Klaassen ILM, Lauw MN, Fiocco M, van der Sluis IM, Pieters R, Middeldorp S, et al. Venous thromboembolism in a large cohort of children with acute lymphoblastic leukemia: Risk factors and effect on prognosis. *Res Pract Thromb Haemost*. (2019) 3:234–41. doi: 10.1002/rth2.12182

40. Caruso V, Iacoviello L, Di Castelnuovo A, Storti S, Mariani G, de Gaetano G, et al. Thrombotic complications in childhood acute lymphoblastic leukemia: a meta-analysis of 17 prospective studies comprising 1752 pediatric patients. *Blood*. (2006) 108:2216–22. doi: 10.1182/blood-2006-04-015511

41. Athale UH, Chan AK. Thrombosis in children with acute lymphoblastic leukemia. *Thromb Res*. (2003) 111:125–31. doi: 10.1016/j.thromres.2003.10.013

42. Appel IM, Hop WCJ, van Kessel-Bakvis C, Stigter R, Pieters R. L-Asparaginase and the effect of age on coagulation and fibrinolysis in childhood acute lymphoblastic leukemia. *Thromb Haemost*. (2008) 100:330–7.

43. Nowak-Göttl U, Kenet G, Mitchell LG. Thrombosis in childhood acute lymphoblastic leukaemia: epidemiology, aetiology, diagnosis, prevention and treatment. *Best Pract Res Clin Haematol*. (2009) 22:103–14. doi: 10.1016/j.beha.2009.01.003

44. Antonova OA, Yakushkin VV, Mazurov AV. Coagulation activity of membrane microparticles. *Biochem (Moscow) Suppl Ser A Membr Cell Biol*. (2019) 13:169–86. doi: 10.1134/S1990747819030036

45. Tripisciano C, Weiss R, Eichhorn T, Spittler A, Heuser T, Fischer MB, et al. Different potential of extracellular vesicles to support thrombin generation: contributions of phosphatidylserine, tissue factor, and cellular origin. *Sci Rep*. (2017) 7:6522. doi: 10.1038/s41598-017-03262-2

46. Deregibus MC, Cantaluppi V, Calogero R, Lo Iacono M, Tetta C, Biancone L, et al. Endothelial progenitor cell–derived microvesicles activate an angiogenic program in endothelial cells by a horizontal transfer of mRNA. *Blood*. (2007) 110:2440–8. doi: 10.1182/blood-2007-03-078709

47. Lacroix R, Sabatier F, Mialhe A, Basire A, Pannell R, Borghi H, et al. Activation of plasminogen into plasmin at the surface of endothelial microparticles: a mechanism that modulates angiogenic properties of endothelial progenitor cells *in vitro*. *Blood*. (2007) 110:2432–9. doi: 10.1182/blood-2007-02-069997

48. Mei HE, Wirries I, Frölich D, Brisslert M, Giesecke C, Grün JR, et al. A unique population of IgG-expressing plasma cells lacking CD19 is enriched in human bone marrow. *Blood*. (2015) 125:1739–48. doi: 10.1182/blood-2014-02-555169

49. Vale AM, Schroeder HW. Clinical consequences of defects in B-cell development. *J Allergy Clin Immunol*. (2010) 125:778–87. doi: 10.1016/j.jaci.2010.02.018

50. Borowitz MJ, Devidas M, Hunger SP, Bowman WP, Carroll AJ, Carroll WL, et al. Clinical significance of minimal residual disease in childhood acute lymphoblastic leukemia and its relationship to other prognostic factors: a Children's Oncology Group study. *Blood*. (2008) 111:5477–85. doi: 10.1182/blood-2008-01-132837

51. Cherian S, Hedley BD, Keeney M. Common flow cytometry pitfalls in diagnostic hematopathology. *Cytom Part B Clin Cytom*. (2019) 96:449–63. doi: 10.1002/cyto.b.21854

52. Greaves MF, Brown G, Rapson NT, Lister TA. Antisera to acute lymphoblastic leukemia cells. *Clin Immunol Immunopathol*. (1975) 4:67–84. doi: 10.1016/0090-1229(75)90041-0

53. Ritz J, Pesando JM, Notis-McConarty J, Lazarus H, Schlossman SF. A monoclonal antibody to human acute lymphoblastic leukaemia antigen. *Nature*. (1980) 283:583–5. doi: 10.1038/283583a0

54. Shipp MA, Tarr GE, Chen CY, Switzer SN, Hersh LB, Stein H, et al. CD10/neutral endopeptidase 24.11 hydrolyzes bombesin-like peptides and regulates the growth of small cell carcinomas of the lung. *Proc Natl Acad Sci*. (1991) 88:10662–6. doi: 10.1073/pnas.88.23.10662

55. Fukusumi T, Ishii H, Konno M, Yasui T, Nakahara S, Takenaka Y, et al. CD10 as a novel marker of therapeutic resistance and cancer stem cells in head and neck squamous cell carcinoma. *Br J Cancer*. (2014) 111:506–14. doi: 10.1038/bjc.2014.289

56. Jang TJ, Park JB, Lee JI. The expression of CD10 and CD15 is progressively increased during colorectal cancer development. *Korean J Pathol*. (2013) 47:340. doi: 10.4132/KoreanJPathol.2013.47.4.340

57. Jana S, Jha B, Patel C, Jana D, Agarwal A. CD10-A new prognostic stromal marker in breast carcinoma, its utility, limitations and role in breast cancer pathogenesis. *Indian J Pathol Microbiol*. (2014) 57:530. doi: 10.4103/0377-4929.142639

58. Sasaki T, Kuniyasu H, Luo Y, Fujiwara R, Kitayoshi M, Tanabe E, et al. Serum CD10 is associated with liver metastasis in colorectal cancer. *J Surg Res*. (2014) 192:390–4. doi: 10.1016/j.jss.2014.05.071

59. Dall'Era MA, True LD, Siegel AF, Porter MP, Sherertz TM, Liu AY. Differential expression of CD10 in prostate cancer and its clinical implication. *BMC Urol*. (2007) 7:3. doi: 10.1186/1471-2490-7-3

60. Tse GMK. Stromal CD10 expression in mammary fibroadenomas and phyllodes tumours. *J Clin Pathol*. (2005) 58:185–9. doi: 10.1136/jcp.2004.020917

61. Magalhães-Gama F, Kerr MWA, de Araújo ND, Ibiapina HNS, Neves JCF, Hanna FSA, et al. Imbalance of chemokines and cytokines in the bone marrow microenvironment of children with B-cell acute lymphoblastic leukemia. *J Oncol*. (2021) 2021:1–9. doi: 10.1155/2021/5530650

62. Miljkovic-Licina M, Arraud N, Zahra AD, Ropraz P, Matthes T. Quantification and phenotypic characterization of extracellular vesicles from patients with acute myeloid and B-cell lymphoblastic leukemia. *Cancers (Basel)*. (2021) 14:56. doi: 10.3390/cancers14010056

63. Zhu S, Xing C, Li R, Cheng Z, Deng M, Luo Y, et al. Proteomic profiling of plasma exosomes from patients with B-cell acute lymphoblastic leukemia. *Sci Rep*. (2022) 12:11975. doi: 10.1038/s41598-022-16282-4

64. Welsh JA, Goberdhan DCI, O'Driscoll L, Buzas EI, Blenkiron C, Bussolati B, et al. Minimal information for studies of extracellular vesicles (MISEV2023): From basic to advanced approaches. *J Extracell Vesicles*. (2024) 13. doi: 10.1002/jev2.12404

frontiers | Frontiers in Immunology

TYPE Original Research
PUBLISHED 23 September 2024
DOI 10.3389/fimmu.2024.1415804

OPEN ACCESS

EDITED BY
Paulo Rodrigues-Santos,
University of Coimbra, Portugal

REVIEWED BY
Michael G. White,
University of Texas MD Anderson Cancer Center, United States
Alex Giakoustidis,
Aristotle University of Thessaloniki, Greece

*CORRESPONDENCE
Manuel Macias-Gonzalez
mmacias.manuel@gmail.com
Hatim Boughanem
h.b.boughanem@gmail.com

†These authors have contributed equally to this work and share first authorship

‡These authors have contributed equally to this work and share senior authorship

RECEIVED 11 April 2024
ACCEPTED 30 August 2024
PUBLISHED 23 September 2024

CITATION
Garcia-Flores LA, Dawid De Vera MT, Pilo J, Rego A, Gomez-Casado G, Arranz-Salas I, Hierro Martín I, Alcaide J, Torres E, Ortega-Gomez A, Boughanem H and Macias-Gonzalez M (2024) Increased neutrophil counts are associated with poor overall survival in patients with colorectal cancer: a five-year retrospective analysis.
Front. Immunol. 15:1415804.
doi: 10.3389/fimmu.2024.1415804

Increased neutrophil counts are associated with poor overall survival in patients with colorectal cancer: a five-year retrospective analysis

Libia Alejandra Garcia-Flores[1,2†], María Teresa Dawid De Vera[3†], Jesus Pilo[1,2], Alejandro Rego[1,2], Gema Gomez-Casado[1,2], Isabel Arranz-Salas[3], Isabel Hierro Martín[3], Julia Alcaide[4], Esperanza Torres[5], Almudena Ortega-Gomez[1,2,6], Hatim Boughanem[1,2,6,7,8*‡] and Manuel Macias-Gonzalez[1,2,6*‡]

[1]Department of Endocrinology and Nutrition, Virgen de la Victoria University Hospital, Málaga, Spain, [2]Institute of Biomedical Research in Malaga (IBIMA)-Bionand Platform, University of Malaga, Málaga, Spain, [3]Unidad de Gestión Clínica Intercentros (UGCI) de Anatomía Patológica, Instituto de Investigación Biomédica de Málaga (IBIMA), Hospital Universitario Virgen de la Victoria, Universidad de Málaga, Málaga, Spain, [4]Medical Oncology Service, Hospital Regional Universitario de Málaga, Biomedical Research Institute of Malaga (IBIMA), Málaga, Spain, [5]Unidad de Gestión Clínica Intercentros (UGCI) de Oncología Médica, Instituto de Investigación Biomédica de Málaga (IBIMA), Hospital Universitario Virgen de la Victoria, Málaga, Spain, [6]Centro de Investigación Biomédica en Red (CIBER) Fisiopatologia Obesidad y Nutricion (CIBEROBN), Instituto de Salud Carlos III, Madrid, Spain, [7]Lipids and Atherosclerosis Unit, Department of Internal Medicine, Hospital Universitario Reina Sofia, Cordoba, Spain, [8]Maimonides Institute for Biomedical Research in Cordoba (IMIBIC), Cordoba, Spain

Background: Colorectal cancer (CRC) continues to be a major health concern in today's world. Despite conflictive findings, evidence supports systemic inflammation's impact on CRC patients' survival rates. Therefore, this study aims to assess the prognostic role of the innate immune system in patients with CRC.

Method: A total of 449 patients were included, with a 5-year follow-up period, and absolute neutrophil counts and their related ratios were measured.

Results: The non-survival group had increased levels of white blood cells, neutrophils (both $p<0.001$), and monocytes ($p=0.038$), compared to the survival group, along with other neutrophil-related ratios. We observed increased mortality risk in patients in the highest tertile of white blood cells [HR=1.85 (1.09-3.13), $p<0.05$], neutrophils [HR=1.78 (95% CI: 1.07-2.96), $p<0.05$], and monocytes [HR=2.11 (95% CI: 1.22-3.63)], compared to the lowest tertile, after adjusting for all clinicopathological variables. Random forest analysis identified neutrophils as the most crucial variable in predicting survival rates, having an AUC of 0.712, considering all clinicopathological variables. A positive relationship between neutrophil counts and metastasis was observed when neutrophil counts are considered continuous ($\beta=0.92$ (0.41), $p<0.05$) and tumor size (width) when neutrophils were considered as logistic variable (T1 vs T3) [OR=1.42, (95% CI: 1.05-1.98), $p<0.05$].

Conclusion: This study offers comprehensive insights into the immune factors that impact the prognosis of CRC, emphasizing the need for personalized prognostic tools.

KEYWORDS

colorectal cancer, neutrophils, overall survival, prognosis, inflammation

Introduction

Colorectal cancer (CRC), accounts for 10% of all cancer diagnoses and is the third most commonly diagnosed, as well as the second leading cause of cancer-related deaths worldwide (1). While enhanced screening has improved survival rates, the five-year survival rate for advanced CRC remains approximately 20%, largely dependent on the tumor stage (2). The health impact of CRC is largely attributed to systemic inflammation, a key factor in its development and progression (3, 4). Inflammatory tumors in CRC are linked to lower survival rates after relapse, highlighting the significance of understanding the role of inflammation role in CRC (5). Recent research has turned to circulating inflammatory markers, particularly neutrophils, as indicators for cancer prognosis and progression (6, 7). Specifically, neutrophils have been strongly associated with various cancer outcomes (8). For instance, a systematic review and meta-analysis encompassing 71 publications and 32,788 patients confirmed that an NLR (neutrophil-to-lymphocyte ratio) was associated with poor patient outcomes, including overall survival (Hazard Ratio (HR) = 1.84, 95% CI: 1.68 – 2.03) and surrogate endpoints, such as disease recurrence and progression-free survival (HR = 1.72, 95% CI: 1.51 – 1.95) (9). Other immune biomarkers, such as interleukin 8 (IL8) and LMR (lymphocyte-to-monocyte ratio) have also been identified as significant prognostic factors (10), suggesting the utility of immune system biomarkers in predicting the prognosis of CRC. Despite these findings, the complete potential of these markers in CRC prognosis is not fully comprehended, and the dual role of neutrophils in CRC complicates their prognostic value (11). Therefore, it is crucial to understand their potential role in predicting CRC survival, to establish preventive and follow-up strategies.

In this study, we hypothesized that inflammatory and immune system biomarkers could be potential indicators for predicting the outcome in CRC patients. This retrospective study aims to examine the relevance of specific routine inflammatory and immune system biomarkers in predicting the survival of patients with CRC and to explore clinicopathological variables that could impact these biomarkers. In addition, our objective was also to develop comprehensive predictive models for overall survival in CRC patients, which could improve patient management and healthcare outcomes by enhancing predictive accuracy.

Materials and methods

Study design and patients included in the study

This study included 623 patients diagnosed with CRC at Virgen de la Victoria University Hospital, Málaga, Spain, between January 1999 to May 2017. Patients included in the study were diagnosed with CRC through colonoscopy and biopsy, with comprehensive medical records and pathological examinations available. Biopsy samples were classified histologically according to the World Health Organization's criteria (12). After selecting patients diagnosed with CRC, the majority underwent tumor resection surgery. Surgical procedures included hemicolectomy, lower anterior resection, and total meso-colorectal excision, often involving ileostomy. Specifically, among patients with stage I and II cancer, 97.5% underwent tumor resection, with only 2.5% not undergoing surgery. For stage III, 96.0% had their tumors removed, while 4.0% did not. However, patients in stage IV included various procedures such as hemicolectomy, metastasectomy, and sigmoidectomy. All patients selected for inclusion had not received any adjuvant treatment prior to surgery (Figure 1). Post-surgery, patients were monitored for a minimum of five years, with follow-up visits every three months in the first two years and every six months thereafter, including physical exams, biochemical assays, and colonoscopies. The study complied with the Declaration of Helsinki and was approved by the ethics committee (PEIBA: 0582-N-23) of University Hospital "Virgen de la Victoria", Málaga, Spain, following relevant guidelines and regulations.

Samples included in the study

The study involved collecting blood samples from all participants. After an overnight fast, venous blood samples were obtained from the median cubital vein. These samples were collected within 24 hours before surgery to ensure they reflected the preoperative immune status of the patients. In some cases, blood samples were taken up to a month before surgery due to medical reasons for delaying the operation. Serum samples were obtained through centrifugation of blood samples at 4,000 r.p.m. for 15 minutes at 4°C.

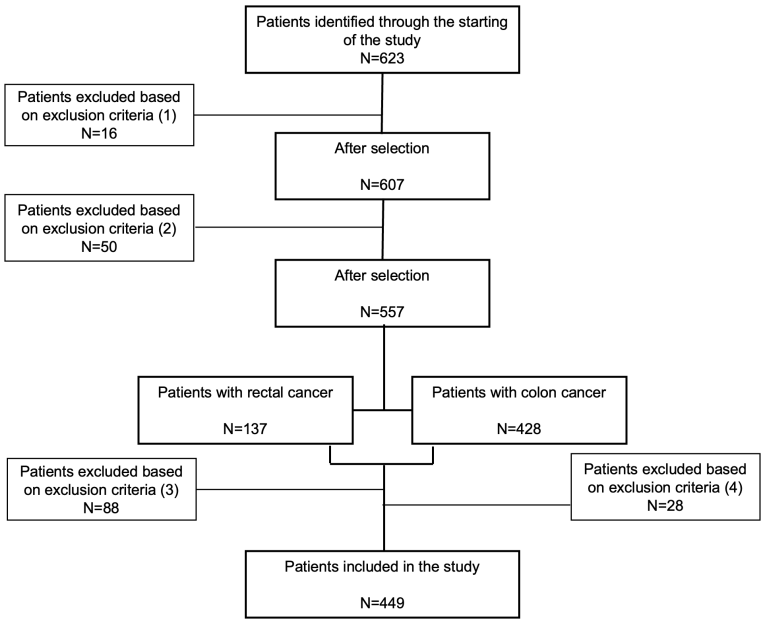

FIGURE 1
Flow diagram of patient selection for inclusion in our study. A total of 623 participants were initially identified as potential candidates. Exclusions were made for the following reasons: (1) sixteen participants from 1997 to 2011 were excluded due to incomplete histopathologic diagnostic records; (2) fifty patients were excluded due to missing clinicopathological data; (3) eighty-eight rectal cancer patients and (4) twenty-eight colon cancer patients were excluded because they had received neoadjuvant treatment (radiotherapy, chemotherapy, or both) before surgery, or their vital status was unconfirmed. Ultimately, 449 patients were included in the final analysis.

Serum levels of fasting glucose, total cholesterol, triglycerides, high-density lipoprotein (HDL), and Low-density lipoprotein (LDL) cholesterol (calculated using the Friedewald equation) were assessed with a Dimension Autoanalyzer (Dade Behring Inc., Deerfield, IL, USA). Fasting insulin levels were measured through radioimmunoassay (BioSource International Inc. (Camarillo, CA, USA)), and insulin resistance was calculated using the homeostasis model assessment (HOMA-IR) formula: HOMA-IR = fasting insulin (IU/mL) × fasting glucose (mmol/L)/22.5. Flow cytometry analyzed various blood components including basophils, eosinophils, lymphocytes, monocytes, neutrophils, and platelets, and several ratios (Supplementary Table 1) were computed to evaluate systemic inflammation.

Statistical analysis

This study utilized descriptive statistics to analyze demographic and clinical data, presenting continuous variables with mean and standard deviation (SD), and categorical data as frequencies and percentages. The Mann-Whitney and Chi-squared tests compared categorical data. Survival data were analyzed using Kaplan-Meier curves and Cox regression. Linear and logistic regressions examined the relationship between neutrophil counts and cancer outcomes, calculating odds ratios. To identify the most significant predictors of mortality, a random forest analysis was performed using mean decrease in accuracy (MDA). Finally, the prognostic performance of the model was evaluated by determining the Area Under the Curve (AUC) in the receiver operating characteristic (ROC) analysis. Statistical analyses were conducted using SPSS 26.0 (Chicago, IL, USA) and R v3.5.1(R Foundation for Statistical Computing, Vienna, Austria), with a significance threshold of $p<0.05$.

Results

Baseline clinicopathological variables of the patients included in the study

The study included 449 patients with CRC (Figure 1). Patients were categorized based on their survival status following a 5-year follow-up period. Among them, 262 patients with CRC were recorded as survivors, while 196 patients did not survive. Table 1 summarizes the characteristics and clinicopathological features of the patients included in the study. We found that the non-survival group was significantly older than the survival group ($p<0.001$). When comparing tumor stages (TNM classification) between survival and non-survival groups significant differences were observed. A majority of non-survival group patients were in advanced stages of the disease (28.1% in stage III and 46.4% in stage IV). In contrast, only 5% of the survival group patients were in stage IV, with a higher proportion in the earlier stages (I and II) ($p<0.001$). Moreover, a higher percentage of patients in the non-survival group (34.1%) had high-grade histology compared to the survival group (19.9%) ($p=0.005$). In addition, metastasis was present in 51.2% of the non-survival group, compared to just 9.46% in the survival group ($p<0.001$). Disease recurrence also showed a marked disparity, occurring in 30.5% of the non-survival group versus 9.19% of the survival group ($p<0.001$).

10.3389/fimmu.2024.1415804

TABLE 1 Baseline characteristic of patients with colorectal cancer divided by survival and non-survival patients, including biochemical and clinicopathological variables.

Variables	Survival	Non-survival	*p* value
	N=262	*N=196*	
Age, years	67.1 (11.9)	71.8 (11.4)	<0.001***
Sex, (Males vs Females):			0.098
Males,	138 (54.5%)	123 (62.8%)	
Females,	115 (45.5%)	73 (37.2%)	
Weight, kg	73.9 (12.9)	72.2 (14.5)	0.256
Body-mass index, kg/m²	27.6 (4.39)	27.5 (6.47)	0.855
Fasting glucose plasma, mg/dL	110 (38.5)	119 (58.8)	0.055
HbA1c, %	15.7 (27.9)	6.61 (1.45)	0.356
Total cholesterol, mg/dL	178 (45.9)	169 (47.9)	0.309
Triglycerides, mg/dL	133 (76.1)	134 (58.7)	0.955
HDL cholesterol, mg/dL	46.4 (12.9)	41.1 (16.0)	0.304
LDL cholesterol, mg/dL	107 (45.8)	105 (45.7)	0.867
Type 2 Diabetes Mellitus, %:			1.000
No	187 (73.9%)	144 (73.5%)	
Yes	66 (26.1%)	52 (26.5%)	
Alcohol consumption, %:			0.300
No	142 (68.9%)	114 (74.5%)	
Yes	64 (31.1%)	39 (25.5%)	
Smoking, %:			0.499
No	198 (85.0%)	136 (81.9%)	
Yes	35 (15.0%)	30 (18.1%)	
Familial history of colorectal cancer			0.096
No	126 (49.8%)	114 (58.2%)	
Yes	127 (50.2%)	82 (41.8%)	
Tumor site:			0.235
Rectum	32 (12.6%)	17 (8.67%)	
Colon	221 (87.4%)	179 (91.3%)	
Tumor grade histology:			0.060
G1	93 (42.5%)	44 (30.8%)	
G2	101 (46.1%)	71 (49.7%)	
G3	21 (9.59%)	23 (16.1%)	
Tumor stage, TNM			<0.001***
I	8 (4.42%)	4 (2.61%)	
II	83 (45.9%)	35 (22.9%)	
III	81 (44.8%)	43 (28.1%)	
IV	9 (4.97%)	71 (46.4%)	
Histology grade			0.005**
Low grade	164 (80.0%)	89 (65.9%)	
High grade	41 (20.0%)	46 (34.1%)	
Tumor size width, cm	4.54 (1.78)	4.47 (2.01)	0.807
Tumor size large, cm	3.53 (1.66)	3.30 (1.66)	0.387
Metastasis:			<0.001***
No	201 (90.5%)	81 (48.8%)	
Yes	21 (9.46%)	85 (51.2%)	
Chemotherapy:			0.698
No	139 (55.2%)	102 (52.8%)	
Yes	113 (44.8%)	91 (47.2%)	
Radiotherapy:			0.277
No	217 (94.3%)	140 (90.9%)	
Yes	13 (5.65%)	14 (9.09%)	
Disease recurrence:			<0.001***
No	165 (90.7%)	73 (69.5%)	
Yes	17 (9.34%)	32 (30.5%)	
KRAS mutation:			0.062
No	22 (64.7%)	32 (43.2%)	
Yes	12 (35.3%)	42 (56.8%)	

Data are represented as mean (SD) or n (%). Groups were divided according to survival outcomes after 5-years of follow-up. Asterisk indicates significant difference between groups according to the Mann Whitney test and Chi squared test was used for variables expressed as percentage (***p<0.001, **p<0.01). Histologic Type groups: G1.-Polypoid, pedunculated, Exophytic, Ulcerated or Ulcerated-central, Coliform and Vegetative, G2.-Necrotic, Ulcerated, and Ulcerated-necrotic, G3.-Mucinous, and G4.-Stenotic and Stenotic-ulcerated. Histologic Type Groups and TNM stage categories were based on the protocol for examination of resection specimens from patients with primary Carcinoma of the colon and rectum by the College of American Pathologists version 4.2.0.0, 2021. Tumor site includes colon: right-sided and left-sided colon, as well as transversal colon. HbA1c, Hemoglobin glycosylated; HDL, high density lipoprotein; KRAS, Kirsten Rat Sarcoma Viral Oncogene Homolog; LDL, low density lipoprotein.

Baseline circulating leukocytes of the patients included in the study

To assess the impact of systemic inflammation on overall survival, we analyzed leukocyte counts and inflammatory variables in our study cohort. We observed that the non-survival group had higher levels of white blood cell (p<0.001), neutrophil (p<0.001), monocyte (p=0.035), and platelet (p=0.003) counts compared to the survival group (Table 2). Additionally, we observed lower levels of circulating albumin in the non-survival group compared to the survival group (p=0.007). Moreover, various ratios derived from circulating immune cells demonstrated higher values in the non-survival group than in the survival group, including NER (p<0.017), NLR (p<0.001), NPR (p=0.039), NWR (p=0.006), PLR (p=0.001), and LMR (p=0.001) (Table 2).

Association between inflammatory variables and the risk of mortality

To evaluate the correlation between inflammatory variables and the risk of mortality, a logistic regression analysis was performed.

TABLE 2 Baseline inflammatory and immune profile of patients with colorectal cancer divided by survival and non-survival patients.

Variables	Survival	Non-survival	*p* value
	N=252	*N=193*	
White blood cells, 10^3/μL	7.29 (2.44)	8.69 (3.59)	<0.001***
Neutrophils, 10^3/μL	4.85 (2.17)	6.13 (3.38)	<0.001***
Monocytes, 10^3/μL	0.55 (0.50)	0.63 (0.32)	0.038*
Lymphocytes, 10^3/μL	1.68 (0.54)	1.64 (0.63)	0.502
Platelets, 10^3/μL	282 (108)	314 (118)	0.003**
NER,	32.4 (21.7)	38.8 (28.7)	0.011*
NLR,	3.22 (2.02)	4.48 (3.69)	<0.001***
NMR,	10.7 (9.88)	10.5 (5.18)	0.726
NPR,	0.02 (0.01)	0.02 (0.01)	0.021*
NWR,	0.65 (0.09)	0.68 (0.11)	0.004**
NBR,	99.9 (67.0)	134 (156)	0.006**
PLR,	184 (92.0)	221 (123)	<0.001***
LMR,	3.89 (3.23)	3.11 (1.79)	0.001**
hsCRP, mg/dL	53.9 (68.1)	73.1 (91.0)	0.213
Albumin, mg/dL	3.43 (0.56)	3.12 (0.56)	0.007**

Data are represented as mean (SD) or n (%). Groups were divided according to survival outcomes after 5-years of follow-up. Asterisk indicates significant difference between groups according to the Mann Whitney test and Chi squared test was used for variables expressed as percentage (***p<0.001, **p<0.01, *p<0.05). hsCRP, High-sensitive C reactive protein; NBR, Neutrophil-to-basophil Ratio; NER, Neutrophil-to-eosinophil Ratio; NERR, Neutrophil-to-erythrocyte Ratio; NHR, Neutrophil-to-HDL Ratio; NMR, Neutrophil-to-monocyte ratio; NLR, Neutrophil-to-lymphocyte ratio; NPR, Neutrophil-to- platelet ratio; LDL, light density lipoprotein.

Patients were stratified into tertiles based on baseline absolute neutrophil counts and other ratios. Tertile 1 (T1) comprised patients with the lowest neutrophil counts, Tertile 2 (T2) included those with intermediate counts, and Tertile 3 (T3) consisted of patients with the highest counts. Following adjustments for BMI, sex, age, chemotherapy, radiotherapy, cancer stage (I+II vs. III+IV), tumor site (colon vs. rectum), and histological grade (low vs. high grade), we observed that patients in T3 of white blood cells [HR=1.85 (1.09-3.13), p<0.05], NPR [HR=2.14 (95% CI: 1.21-3.47), p<0.01], NLR [HR=2.05 (95% CI: 1.21-3.47), p<0.01], neutrophils [HR=1.78 (95% CI: 1.07-2.96), p<0.05], and monocytes [HR=2.11 (95% CI: 1.22-3.63), p<0.01] had an increased risk of mortality when compared to those in T1 (Figure 2A). To determine the significant variables for predicting mortality within our population, we performed a random forest analysis. Monocytes, neutrophils, and white blood cells emerged as the most crucial factors in predicting mortality (Figure 2B).

Immune system variables and overall survival rate

To assess the value of these variables as predictive tools for overall survival in our population, Kaplan-Meier curves derived from Cox regression were generated. We observed that patients within T3 of neutrophils had poorer survival, with a median of 42.5 months, compared to both T2 and T1 (both with p<0.001) (Figure 3A). Additionally, to evaluate the prognostic value of neutrophils, ROC curves were constructed. When analyzing neutrophils alone, the AUC was 0.611. Incorporating clinicopathological variables increased the AUC to 0.702. However, considering all variables together further improved the AUC to 0.712 (Figure 3B). Similar patterns were observed for monocytes and white blood cells. Patients within T3 of monocytes and white blood cells had poorer survival, compared to both T2 and T1 (both with p<0.001) (Supplementary Figures 1A, C). Additionally, to evaluate the prognostic value of monocytes and white blood cells, the AUC was 0.616 and 0.611, respectively. Incorporating clinicopathological variables increased the AUC to 0.714 and 0.710, respectively (Supplementary Figures 1B, D).

Finally, we conducted an analysis to identify factors influencing neutrophil counts, utilizing both linear and logistic regressions. After adjusting by age, sex, BMI, familial history of cancer, smoking, alcohol consumption and the presence of type 2 diabetes mellitus, the results showed that there is a positive relationship between neutrophil counts and the occurrence of metastasis when neutrophil counts are considered continuous (β=0.92 (0.41), p<0.05) and tumor size (width) when neutrophils were considered as logistic variable (T1 vs T3) [OR=1.42, (95% CI: 1.05-1.98), p<0.05] (Table 3).

Discussion

In this retrospective study, we examined the survival outcomes of patients with CRC over five years. The study focused on assessing

10.3389/fimmu.2024.1415804

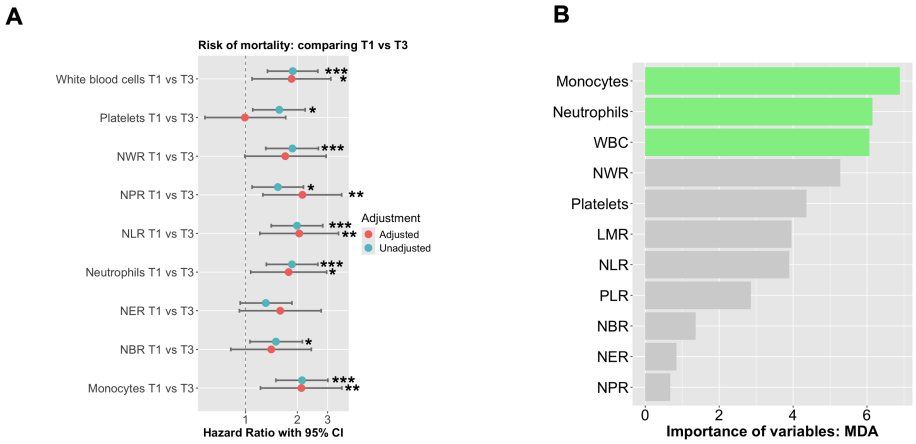

FIGURE 2
The probability of mortality according to absolute neutrophil counts was analyzed using Cox proportional hazards regression. **(A)** The analysis was performed using Cox regression curves with tertiles of absolute neutrophil counts at baseline, both unadjusted and adjusted for BMI, sex, age, chemo- and radiotherapy, cancer stage (I+II vs III+IV), tumor site (colon vs rectum) + Histological grade (low vs high grade). T1 represents low neutrophil levels, T2 represents intermediate levels, and T3 represents high neutrophil levels. **(B)** Random forest of all significant variables included in our study to predict mortality. The symbols *, **, and *** indicate statistical significance, where * represents $p < 0.05$, ** represents $p < 0.01$, and *** represents $p < 0.001$.

inflammatory and immune system biomarkers as prognostic indicators among both survivors and non-survivors. Our findings suggest that several biomarkers associated with neutrophils and their related ratios are effective predictors of overall survival in CRC patients. Particularly, neutrophils and monocytes emerged as the most significant predictors in the random forest model. Utilizing tertiles based on neutrophil counts, we observed that highest tertile of neutrophils at baseline showed notably poorer overall survival rates compared to the middle and the lowest tertiles. This observation yielded an AUC of 0.712, after incorporating all relevant clinicopathological variables, suggesting the potential of neutrophils and other variables as valuable prognostic indicators for predicting overall survival in patients with CRC. This study also highlights the potential role of neutrophils in cancer progression and disease relapse, warranting further research to clarify these observations.

Several biomarkers have been identified as potential indicators for diagnosis, prognosis, and treatment response in CRC (13). Specifically, there is an emerging predictive biomarker for cancer prognosis, which includes immune-related biomarkers for managing patients with CRC (13, 14). Laboratory markers of systemic inflammatory response have been extensively studied as prognostic and predictive tools in CRC (15). Neutrophils and related markers, such as NLR, have been widely proposed as diagnostic and prognostic biomarkers in several studies (16–18), as well as for overall survival in CRC (16, 19, 20). In our study, Cox

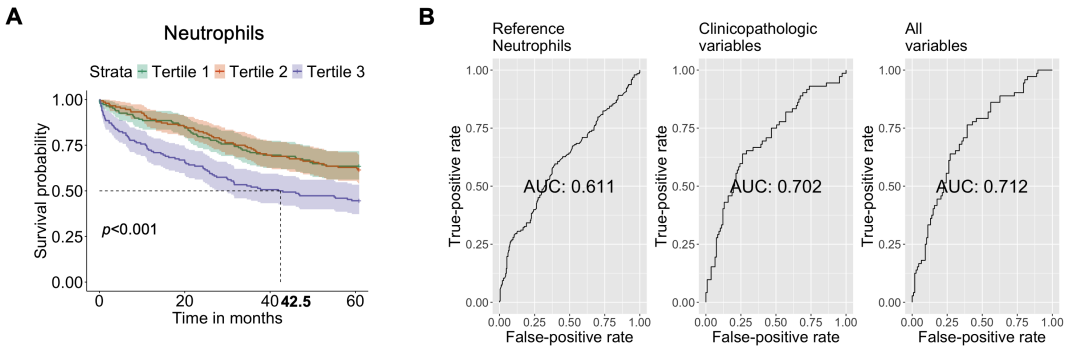

FIGURE 3
Prognostic Value of Hematological Parameters and Clinical-pathologic Variables in Predicting Mortality in CRC. **(A)** Cox regression analysis by comparing T1 and T2 vs T3, to predict the risk of mortality using neutrophil-related ratios. **(B)** Three Receiver Operating Characteristic (ROC) curves with corresponding Areas Under the Curve (AUC).

10.3389/fimmu.2024.1415804

TABLE 3 Logistic and linear regression analysis to predict those clinicopathological variables that are associated with neutrophil counts.

Variables	Variables	Neutrophils (continuous)	Neutrophils (T1 vs T3)
		β (SD)	OR (95% CI)
Tumor site (colon vs rectum)	Unadjusted	0.39 (0.45)	1.28 (0.58 – 2.88)
	Adjusted	0.40 (0.60)	1.89 (0.06 – 22.11)
Tumor stage (I+II vs III+IV)	Unadjusted	0.53 (0.33)	1.18 (0.69 – 2.01)
	Adjusted	0.59 (0.41)	1.39 (0.89 – 2.84)
Tumor size, width (cm)	Unadjusted	0.27 (0.11)*	1.44 (1.18 – 1.83)***
	Adjusted	0.13 (0.14)	1.42 (1.05 – 1.98)*
Tumor size, large (cm)	Unadjusted	0.33 (0.13)*	1.51 (1.18 – 2.02)**
	Adjusted	0.11 (0.17)	1.33 (0.99 – 1.88)
Metastasis (No vs Yes)	Unadjusted	1.19 (0.32)***	1.92 (1.12 – 3.31)*
	Adjusted	0.92 (0.41)*	1.97 (0.96 – 4.08)
Chemotherapy (No vs Yes)	Unadjusted	0.45 (0.27)	0.99 (0.63 – 1.58)
	Adjusted	0.74 (0.37)	1.13 (0.57 – 2.25)
Radiotherapy (No vs Yes)	Unadjusted	0.59 (0.58)	1.33 (0.53 – 3.41)
	Adjusted	0.43 (0.74)	0.78 (0.21 – 2.69)
Chemotherapy + Radiotherapy (No vs Yes)	Unadjusted	0.53 (0.26)*	1.04 (0.66 – 1.64)
	Adjusted	0.72 (0.37)	1.10 (0.56 – 2.19)
Histology grade (Low vs high grade)	Unadjusted	-0.21 (0.36)	1.01 (0.55 – 1.83)
	Adjusted	-0.41 (0.44)	0.78 (0.36 – 1.66)
Recurrence (Yes vs no)	Unadjusted	-0.21 (0.36)	0.63 (0.26 – 1.47)
	Adjusted	-0.39 (0.44)	0.55 (0.14 – 1.76)

Linear regression analysis using neutrophil counts as continuous variable and by comparing the highest vs the lowest tertiles of neutrophils as categoric variables. Adjusted model was adjusted for age, gender, BMI, familial history, smoking history, alcohol consumption and the presence of type 2 diabetes mellitus. Asterisk indicates significant difference between groups (***p<0.001, **p<0.01, *p<0.05).

logistic regression analysis revealed that increased NLR values were associated with poorer survival rates in CRC patients, even after adjusting for all relevant clinicopathological variables. This indicates the potential of NLR as a biomarker in CRC. Furthermore, other immune cell parameters, such as neutrophil and monocyte counts, as well as other ratios, showed reliable predictive utility, suggesting the involvement of the immune system in cancer progression and survival outcomes. However, in our study, a random forest analysis proposed neutrophils and monocytes as the most important predictor of overall survival, which supports previous findings, highlighting a mechanistic role in CRC.

When comparing neutrophil tertiles, the highest tertile displayed lower overall survival rates compared to the middle and lowest tertile, with a median survival of approximately 42.5 months and an AUC of 0.712. Accordingly, Mercier et al., 2018 reported that an increased platelet-neutrophil-to-lymphocyte ratio was linked to poor overall survival, with a median survival of 9.6 months in metastatic CRC patients (8). Yang et al. (2021) also conducted a study indicating that a high NLR correlated with poor progression-free survival, with a median of 6.1 months (21). These findings collectively suggest that neutrophil counts and related ratios serve as reliable predictors for CRC prognosis. Nonetheless, additional studies are necessary to comprehend their mechanistic role in CRC.

Tumor-associated neutrophils showed both pro- and anti-cancer effects, playing a dual role in both direct and indirect manners in the initiation and advancement of tumors (11). Tumors can stimulate increased production of neutrophils in the bone marrow and attract them to the tumor site (22). Once there, neutrophils are often polarized toward phenotypes that promote tumor growth and metastasis (23). Our linear and logistic regression analysis revealed a strong association between neutrophil levels and metastasis and tumor size, which aligns with previous research (24, 25). Studies have consistently highlighted the multifaceted role of neutrophils in various stages of the metastatic process, including creating a premetastatic niche and facilitating tumor cell invasion, migration, intravasation, and extravasation (24). Conversely, some findings emphasize a protective aspect of neutrophils against metastasis by activating and recruiting T cells and other leukocytes to the metastatic site (26).

Our research also emphasizes the importance of monocytes as a key predictor of mortality. In the case of CRC, monocyte counts have been identified as an independent prognostic factor for predicting the outcome. Higher absolute monocyte counts were significantly linked to poorer overall survival and progression-free survival outcomes (27). Furthermore, a meta-analysis revealed that distant metastatic status and increased absolute monocyte count were linked to worse outcomes in CRC patients (28). Cancer significantly impacts immune system functionality, reflected in altered immune cell counts, which serve as potential indicators of patient prognosis. Neutrophils play a key role in recruiting monocytes to the site of the injury. As a result of this process being disrupted, patients with tumors often have higher levels of immature neutrophils and monocytes in the bloodstream. These cells not only multiply in number but also move to the tumor's environment, worsening local immune suppression (29).

We must acknowledge several limitations of our study. Its retrospective nature and single-center design may limit the generalizability of our findings. Nonetheless, our study offers valuable insights into the role of immune markers in CRC

prognosis within a large cohort. Nevertheless, the variability in our results over time may be due to the lack of detailed data on treatment regimens, demographic characteristics, lifestyle factors, disease awareness, and screening practices—all of which are known to significantly influence survival outcomes. Additionally, a significant limitation of our study is the absence of mismatch repair (MMR) status data for a portion of our cohort, as routine testing for MMR was not consistently included in diagnostic protocols until 2014. This missing data may have influenced our ability to fully assess the relationship between MMR status and immune responses. Furthermore, we prioritized overall survival over progression-free survival (PFS) and recurrence data in our analysis due to the inconsistent availability of PFS and recurrence data across the patient cohort. Out of the patients in the study, only 133 (29.0%) were confirmed as positive for recurrence or progression, while 56 patients (12.2%) had negative outcomes, and 269 patients (58.7%) had indeterminate results. As overall survival was the most consistently documented outcome, it was the most suitable measure for our study. We acknowledge the limitation regarding the small number of stage IV patients in our study. This limited sample size does not allow us to perform a robust descriptive analysis of neutrophil counts as predictive values specifically for this subgroup. However, we acknowledge that this focus may limit our ability to thoroughly investigate the relationships between the biomarkers studied and cancer-specific outcomes such as PFS and recurrence. As a result, some nuances in the association between these biomarkers and disease progression may not be fully captured in our analysis. Therefore, we suggest that future studies explore the impact of these variables on CRC survival through prospective, larger, multicentric cohorts, as this will be crucial in validating and expanding upon our findings.

Conclusion

In conclusion, our research suggests that higher neutrophil counts in patients with CRC can serve as potential risk factors for mortality and reliable prognostic indicators over a 5-year follow-up period. Our analysis identified neutrophils as the most significant predictors of overall survival. Additionally, our study brings attention to certain clinicopathological variables, such as metastasis and tumor size that can influence neutrophil counts, implying their role in these processes. These findings provide a foundation for creating personalized and effective prognostic tools in CRC management. Further research has the potential to improve our understanding of the prognostic role of neutrophils in CRC and could offer valuable insights into the mechanistic aspects of the development process of CRC.

Data availability statement

The raw data supporting the conclusions of this article will be made available by the authors, without undue reservation. Any private information will be removed to follow data privacy laws.

Ethics statement

The study complied with the Declaration of Helsinki and was approved by the ethics committee (PEIBA: 0582-N-23) of University Hospital "Virgen de la Victoria", Málaga, Spain, following relevant guidelines and regulations. The studies were conducted in accordance with the local legislation and institutional requirements. Written informed consent for participation in this study was provided by the participants' legal guardians/next of kin.

Author contributions

LG-F: Writing – original draft, Methodology, Investigation, Formal analysis, Conceptualization. MD: Writing – original draft, Validation, Project administration, Methodology, Investigation, Formal analysis, Data curation. JP: Writing – review & editing, Methodology, Investigation. AR: Writing – original draft, Methodology, Investigation. GG-C: Writing – review & editing, Methodology, Investigation. IA-S: Writing – review & editing, Methodology, Investigation. IH: Writing – review & editing, Methodology, Investigation. JA: Writing – review & editing, Investigation, Conceptualization. ET: Writing – review & editing, Investigation, Conceptualization. AO-G: Writing – review & editing, Investigation, Conceptualization. HB: Writing – review & editing, Writing – original draft, Visualization, Software, Methodology, Investigation, Formal analysis. MG: Writing – review & editing, Validation, Supervision, Resources, Project administration, Investigation, Funding acquisition.

Funding

The author(s) declare financial support was received for the research, authorship, and/or publication of this article. This study was supported by the "Centro de Investigacion Biomédica en Red Fisiopatología de la Obesidad y Nutricion", which is an initiative of the "Instituto de Salud Carlos III" (ISCIII) of Spain, financed by the European Regional Development Fund under "A way to make Europe"/"Investing in your future" (CB06/03), a grant from ISCIII (PI18/01399). This work was supported by the Carlos III Health Institute (PI21/00633), co-funded by the European Union, from Programa Operativo FEDER 2014-2020 of the Consejería de Economía y Conocimiento de la Junta de Andalucía. and a grant from the Consejeria Universidad, Investigacion e Innovacion Junta de Andalucia (PY20-01270). HB was supported by a predoctoral fellowship ("Plan Propio IBIMA 2020 A.1 Contratos predoctoral", Ref.: predoc20_002 and by a "Sara Borrell" postdoctoral contract (CD22/00053) from the Instituto de Salud Carlos III-Madrid (Spain), "Financiado por la Unión Europea-NextGenerationEU" and the plan Recuperación, Transformación y Resiliencia. GG-C was supported by a predoctoral contract (FI23/00104). LG-F was supported by a "Sara Borrell" postdoctoral contract (CD21/000131) from the Instituto de Salud Carlos III—Madrid (Spain). AO-G was supported by a "Miguel

Servet" postdoctoral contract (CP020/0060). MG was the recipient of the Nicolas Monardes Programme from the "Servicio Andaluz de Salud, Junta de Andalucia", Spain (RC-0001-2018 and C-0029-2014).

Conflict of interest

The authors declare that the research was conducted in the absence of any commercial or financial relationships that could be construed as a potential conflict of interest.

Publisher's note

Supplementary material

The Supplementary Material for this article can be found online at: https://www.frontiersin.org/articles/10.3389/fimmu.2024.1415804/full#supplementary-material

SUPPLEMENTARY FIGURE 1
Prognostic Value of Hematological Parameters and Clinicopathological Variables in Predicting Mortality in CRC. Cox regression analysis comparing Tertiles 1 (T1) and 2 (T2) versus Tertile 3 (T3) for **(A)** monocytes and **(C)** white blood cells. Receiver Operating Characteristic (ROC) curves demonstrate the predictive performance of **(B)** monocytes and **(D)** white blood cells, with corresponding Areas Under the Curve (AUC).

References

1. Sung H, Ferlay J, Siegel RL, Laversanne M, Soerjomataram I, Jemal A, et al. Global cancer statistics 2020: GLOBOCAN estimates of incidence and mortality worldwide for 36 cancers in 185 countries. *CA Cancer J Clin*. (2021) 71:209–49. doi: 10.3322/caac.21660

2. Brierley J, O'Sullivan B, Asamura H, Byrd D, Huang SH, Lee A, et al. Global Consultation on Cancer Staging: promoting consistent understanding and use. *Nat Rev Clin Oncol*. (2019) 16:763–71. doi: 10.1038/s41571-019-0253-x

3. Balkwill F, Mantovani A. Inflammation and cancer: back to virchow? *Lancet*. (2001) 357:539–45. doi: 10.1016/S0140-6736(00)04046-0

4. Yamamoto T, Kawada K, Obama K. Inflammation-related biomarkers for the prediction of prognosis in colorectal cancer patients. *Int J Mol Sci*. (2021) 22:8002. doi: 10.3390/ijms22158002

5. Guinney J, Dienstmann R, Wang X, De Reyniès A, Schlicker A, Soneson C, et al. The consensus molecular subtypes of colorectal cancer. *Nat Med*. (2015) 21:1350–6. doi: 10.1038/nm.3967

6. You JF, Hsu YJ, Chern YJ, Cheng CC, Jong BK, Liao CK, et al. Preoperative cancer inflammation prognostic index as a superior predictor of short- and long-term outcomes in patients with stage I–III colorectal cancer after curative surgery. *Cancers (Basel)*. (2022) 14(24):6232. doi: 10.3390/cancers14246232

7. Tuomisto AE, Mäkinen MJ, Väyrynen JP. Systemic inflammation in colorectal cancer: Underlying factors, effects, and prognostic significance. *World J Gastroenterol*. (2019) 25:4383–404. doi: 10.3748/wjg.v25.i31.4383

8. Mercier J, Voutsadakis IA. The platelets-neutrophils to lymphocytes ratio: A new prognostic marker in metastatic colorectal cancer. *J Gastrointest Oncol*. (2018) 9:478–86. doi: 10.21037/jgo.2018.03.13

9. Naszai M, Kurjan A, Maughan TS. The prognostic utility of pre-treatment neutrophil-to-lymphocyte-ratio (NLR) in colorectal cancer: A systematic review and meta-analysis. *Cancer Med*. (2021) 10:5983–97. doi: 10.1002/cam4.4143

10. Park JW, Chang HJ, Yeo HY, Han N, Kim BC, Kong SY, et al. The relationships between systemic cytokine profiles and inflammatory markers in colorectal cancer and the prognostic significance of these parameters. *Br J Cancer*. (2020) 123:610–8. doi: 10.1038/s41416-020-0924-5

11. Zheng W, Wu J, Peng Y, Sun J, Cheng P, Huang Q. Tumor-associated neutrophils in colorectal cancer development, progression and immunotherapy. *Cancers (Basel)*. (2022) 14(19):4755. doi: 10.3390/cancers14194755

12. Bosman FT, Carneiro F, Hruban RH, Theise ND. *WHO Classification of Tumours of the Digestive System: WHO Classification of Tumours, Volume 3* (2010). IARC Press. Available online at: https://books.google.co.id/books?id=yo1TZp23Y8oC (Accessed November 12, 2023).

13. Ogunwobi OO, Mahmood F, Akingboye A. Biomarkers in colorectal cancer: Current research and future prospects. *Int J Mol Sci*. (2020) 21:1–20. doi: 10.3390/ijms21155311

14. Koulis C, Yap R, Engel R, Jardé T, Wilkins S, Solon G, et al. Personalized medicine—Current and emerging predictive and prognostic biomarkers in colorectal cancer. *Cancers (Basel)*. (2020) 12(4):812. doi: 10.3390/cancers12040812

15. McMillan DC. Systemic inflammation, nutritional status and survival in patients with cancer. *Curr Opin Clin Nutr Metab Care*. (2009) 12:223–6. doi: 10.1097/MCO.0b013e32832a7902

16. Zhang J, Zhang HY, Li J, Shao XY, Zhang CX. The elevated NLR, PLR and PLT may predict the prognosis of patients with colorectal cancer: a systematic review and meta-analysis. *Oncotarget*. (2017) 8:68837–46. doi: 10.18632/oncotarget.18575

17. Dimitriou N, Felekouras E, Karavokyros I, Alexandrou A, Pikoulis E, Griniatsos J. Neutrophils to lymphocytes ratio as a useful prognosticator for stage II colorectal cancer patients. *BMC Cancer*. (2018) 18(1):1202. doi: 10.1186/s12885-018-5042-x

18. Park Y, Lee K, Lee J, Oh S. Prediction of oncologic outcome using systemic neutrophil-to-lymphocyte ratio in stage II and III colon cancer. *Ann Oncol*. (2019) 30:iv5. doi: 10.1093/annonc/mdz155.017

19. Pedrazzani C, Mantovani G, Fernandes E, Bagante F, Luca Salvagno G, Surci N, et al. Assessment of neutrophil-to-lymphocyte ratio, platelet-to-lymphocyte ratio and platelet count as predictors of long-term outcome after R0 resection for colorectal cancer. *Sci Rep*. (2017) 7(1):1494. doi: 10.1038/s41598-017-01652-0

20. Mizuno R, Kawada K, Itatani Y, Ogawa R, Kiyasu Y, Sakai Y. The role of tumor-associated neutrophils in colorectal cancer. *Int J Mol Sci*. (2019) 20(3):529. doi: 10.3390/ijms20030529

21. Yang Z, Li Y, Zhang K, Deng X, Yang S, Wang Z. Dynamics of neutrophil-to-lymphocyte ratio predict outcomes of metastatic colorectal carcinoma patients treated by FOLFOX. *J Gastrointest Oncol*. (2021) 12:2846. doi: 10.21037/JGO-21-716

22. Furze RC, Rankin SM. Neutrophil mobilization and clearance in the bone marrow. *Immunology*. (2008) 125:281–8. doi: 10.1111/j.1365-2567.2008.02950.x

23. Fridlender ZG, Sun J, Kim S, Kapoor V, Cheng G, Ling L, et al. Polarization of tumor-associated neutrophil phenotype by TGF-β: "N1" versus "N2" TAN. *Cancer Cell*. (2009) 16:183–94. doi: 10.1016/j.ccr.2009.06.017

24. Xiong S, Dong L, Cheng L. Neutrophils in cancer carcinogenesis and metastasis. *J Hematol Oncol*. (2021) 14:1–17. doi: 10.1186/s13045-021-01187-y

25. Li Y, Xu T, Wang X, Jia X, Ren M, Wang X. The prognostic utility of preoperative neutrophil-to-lymphocyte ratio (NLR) in patients with colorectal liver metastasis: a systematic review and meta-analysis. *Cancer Cell Int*. (2023) 23:1–14. doi: 10.1186/s12935-023-02876-z

26. Granot Z, Henke E, Comen EA, King TA, Norton L, Benezra R. Tumor entrained neutrophils inhibit seeding in the premetastatic lung. *Cancer Cell*. (2011) 20:300–14. doi: 10.1016/j.ccr.2011.08.012

27. Li Z, Xu Z, Huang Y, Zhao R, Cui Y, Zhou Y, et al. The predictive value and the correlation of peripheral absolute monocyte count, tumor-associated macrophage and microvessel density in patients with colon cancer. *Med*. (2018) 97(21):e10759. doi: 10.1097/MD.0000000000010759

28. Wen S, Chen N, Hu Y, Huang L, Peng J, Yang M, et al. Elevated peripheral absolute monocyte count related to clinicopathological features and poor prognosis in solid tumors: Systematic review, meta-analysis, and meta-regression. *Cancer Med*. (2021) 10:1690–714. doi: 10.1002/cam4.3773

29. Hiam-Galvez KJ, Allen BM, Spitzer MH. Systemic immunity in cancer. *Nat Rev Cancer*. (2021) 21:345–59. doi: 10.1038/s41568-021-00347-z

frontiers | Frontiers in Immunology

TYPE Original Research
PUBLISHED 21 October 2024
DOI 10.3389/fimmu.2024.1391840

OPEN ACCESS

EDITED BY
Giovanna Schiavoni,
National Institute of Health (ISS), Italy

REVIEWED BY
Sean J. Judge,
Memorial Sloan Kettering Cancer Center, United States
Jun Liu,
Dongguan Hospital of Guangzhou University of Chinese Medicine, China

*CORRESPONDENCE
Paulo Rodrigues-Santos
paulo.santos@fmed.uc.pt

RECEIVED 26 February 2024
ACCEPTED 30 September 2024
PUBLISHED 21 October 2024

CITATION
Almeida JS, Sousa LM, Couceiro P, Andrade TF, Alves V, Martinho A, Rodrigues J, Fonseca R, Freitas-Tavares P, Santos-Rosa M, Casanova JM and Rodrigues-Santos P (2024) Peripheral immune profiling of soft tissue sarcoma: perspectives for disease monitoring. *Front. Immunol.* 15:1391840. doi: 10.3389/fimmu.2024.1391840

Peripheral immune profiling of soft tissue sarcoma: perspectives for disease monitoring

Jani Sofia Almeida[1,2,3,4,5,6], Luana Madalena Sousa[1,5,6], Patrícia Couceiro[1,3,4,5,6], Tânia Fortes Andrade[1], Vera Alves[2,3,4,5,6], António Martinho[7], Joana Rodrigues[6,8], Ruben Fonseca[6,8], Paulo Freitas-Tavares[6,8], Manuel Santos-Rosa[2,3,4,5,6], José Manuel Casanova[3,4,5,6,8] and Paulo Rodrigues-Santos[1,2,3,4,5,6]*

[1]Center for Neurosciences and Cell Biology (CNC), Laboratory of Immunology and Oncology, University of Coimbra, Coimbra, Portugal, [2]Faculty of Medicine (FMUC), Institute of Immunology, University of Coimbra, Coimbra, Portugal, [3]Center for Investigation in Environment, Genetics and Oncobiology (CIMAGO), University of Coimbra, Coimbra, Portugal, [4]Coimbra Institute for Clinical and Biomedical Research (iCBR), University of Coimbra, Coimbra, Portugal, [5]Center for Innovation in Biomedicine and Biotechnology (CIBB), University of Coimbra, Coimbra, Portugal, [6]Clinical and Academic Centre of Coimbra (CACC), Coimbra, Portugal, [7]Portuguese Institute for Blood and Transplantation (IPST), Blood and Transplantation Center of Coimbra, Coimbra, Portugal, [8]Tumor Unit of the Locomotor Apparatus, University Clinic of Orthopedics, Orthopedics Oncology Service, Coimbra Hospital and Universitary Centre (CHUC), Coimbra, Portugal

Studying the tumor microenvironment and surrounding lymph nodes is the main focus of current immunological research on soft tissue sarcomas (STS). However, due to the restricted opportunity to examine tumor samples, alternative approaches are required to evaluate immune responses in non-surgical patients. Therefore, the purpose of this study was to evaluate the peripheral immune profile of STS patients, characterize patients accordingly and explore the impact of peripheral immunotypes on patient survival. Blood samples were collected from 55 STS patients and age-matched healthy donors (HD) controls. Deep immunophenotyping and gene expression analysis of whole blood was analyzed using multiparametric flow cytometry and real-time RT-qPCR, respectively. Using xMAP technology, proteomic analysis was also carried out on plasma samples. Unsupervised clustering analysis was used to classify patients based on their immune profiles to further analyze the impact of peripheral immunotypes on patient survival. Significant differences were found between STS patients and HD controls. It was found a contraction of B cells and CD4 T cells compartment, along with decreased expression levels of ICOSLG and CD40LG; a major contribution of suppressor factors, as increased frequency of M-MDSC and memory Tregs, increased expression levels of ARG1, and increased plasma levels of IL-10, soluble VISTA and soluble TIMD-4; and a compromised cytotoxic potential associated with NK and CD8 T cells, namely decreased frequency of $CD56^{dim}$ NK cells, and decreased levels of PRF1, GZMB, and KLRK1. In addition, the patients were classified into three peripheral immunotype groups: "immune-high," "immune-intermediate," and "immune-low." Furthermore, it was found a correlation between these immunotypes and patient survival. Patients classified as "immune-high" exhibited higher levels of

immune-related factors linked to cytotoxic/effector activity and longer survival times, whereas patients classified as "immune-low" displayed higher levels of immune factors associated with immunosuppression and shorter survival times. In conclusion, it can be suggested that STS patients have a compromised systemic immunity, and the correlation between immunotypes and survival emphasizes the importance of studying peripheral blood samples in STS. Assessing the peripheral immune response holds promise as a useful method for monitoring and forecasting outcomes in STS.

KEYWORDS

soft tissue sarcoma, immunophenotyping, gene expression profiling, cytokines, chemokines, growth factors, immune checkpoints

1 Introduction

Soft tissue sarcomas (STS) represent a broad class of rare and highly heterogeneous mesenchymal tumors. The estimated incidence is 1.5–3.0 times per 100,000 individuals annually, and the World Health Organization (WHO) documented over 100 histopathological subtypes in 2020 (1–3). The main concerns in STS, given the 20% 5-year survival rate for advanced cancer, is the rate of recurrence and metastatic disease, which presents a treatment challenge (3–5). Consequently, it is essential to regularly monitor STS patients in order to forecast the course of the disease. To follow up with STS patients, clinical practice currently uses imaging methods and evaluates general cancer biomarkers (6, 7). But since there aren't any particular biomarkers for STS used in clinical care, there's an opportunity to look into and find cellular and molecular factors that can be used to aid doctors in clinical management.

Research on immune-related parameters as possible indicators of cancer development has increased dramatically as a result of immunotherapy's advancements (8–10). This push for improved prognostic, diagnostic, and monitoring approaches in cancer has reignited interest in immunologic markers within STS. Inspired by William B. Coley's early 20th-century work on immunotherapy in sarcomas (11), there is a growing recognition of the immune system's critical role in STS. While STS has traditionally been viewed as "cold" tumors with limited immune response (12–14), emerging evidence challenges this perception. Recent studies have highlighted the variability in tumor mutational burden, the presence of an occasionally "hot" tumor microenvironment, and observed responses to immunotherapy, underscoring the complex and nuanced role of immunity in STS (15, 16).

The immune contexture in STS tumors is marked by specific features, including tumor-associated macrophages (TAM), dysfunctional tumor-infiltrating lymphocytes (TIL), reduced CD8 T cell and NK cell activity, increased Treg cells, limited B cell infiltration, and impaired dendritic cell (DC) function (17–20). Moreover, gene expression analysis of tumor samples in STS shown that a 20-gene signature related to cytotoxic immune response further strengthened the prognostic potential of the 67-gene Complexity Index in SARComas (CINSARC) transcriptomic signature, that is a promising predictor of metastatic disease in STS (21–23). Additionally, blood plasma cytokine analysis in STS has shown correlations with clinical parameters (24, 25), suggesting that plasma proteins could be valuable for patient stratification and monitoring. Recent studies also highlight the importance of tumor immunotypes, such as Sarcoma Immune Classes (SIC A-E), in predicting patient outcomes and potential responses to immunotherapy (18, 26, 27). Although understanding the tumor's local immune status is crucial, challenges related to scheduling and sample availability can limit the effectiveness of monitoring systems that depend on tumor samples. Therefore, it is essential to explore alternative collection methods, such as analyzing peripheral blood samples.

Systemic immunity plays a critical role in cancer control, with changes in peripheral immune compositions both impacting and reflecting tumor responses (28). Alterations in circulating immune cells have been associated with prognosis across various cancer types, indicating their potential as survival markers (29–32). Although research on STS is limited, existing studies have shown that circulating immune cells, immune-related gene expression, and plasma cytokine levels hold promise for patient stratification (8, 23, 24, 33). These insights emphasize the need for comprehensive assessments of both cellular and molecular parameters in peripheral blood, which could help identify distinct immunotypes and provide a more nuanced understanding of a patient's immune status. Consequently, investigating circulating biomarkers as predictors of disease outcomes in STS represents a valuable and promising area of research.

Hence, this study hypothesizes that peripheral immune profiles can function as biomarkers for distinguishing disease status and monitoring treatment responses in patients with STS. The research aims to evaluate the systemic immune compartment of STS patients, and assess the impact of histological classification, treatment response, and therapy. By analyzing immune cells, immune-related genes (IRG), and immune-related soluble factors

(IRSF), the study seeks to identify distinct peripheral immunotypes associated with those variables. Additionally, the study explores the correlation of immunotype classification with survival outcome. It is anticipated that compromised systemic immunity in STS patients will be reflected in distinct immune profiles, which may vary in their impact on survival. The focus on systemic immune-related biomarkers represents a significant shift, introducing non-invasive, real-time monitoring methods that could transform the clinical approach to STS.

2 Materials and methods

2.1 STS patients and healthy donor controls

From November 2018 to February 2023, peripheral blood samples and clinical data were collected at the Tumor Unit of the Locomotor Apparatus, University Clinic of Orthopedics, Orthopedics Oncology Service, Coimbra Hospital and Universitary Centre, which is a European Reference Center for Adult STS Treatment. The inclusion criteria for patients were confirmed STS diagnostic, not including gastrointestinal tumor type (GIST), and age greater than 18 years. Patients with confirmed viral or bacterial infections were excluded from the study. A total of 55 STS patients' peripheral blood samples and age-matched healthy donors (HD) controls were examined. For research involving human subjects, the World Medical Association's Helsinki Declaration is adhered to in this work. All participants gave their informed consent after receiving thorough information regarding the goal of the study. The Coimbra Hospital and Universitary Center, Portugal, and the University of Coimbra's Faculty of Medicine Ethics Committee provided ethical permission for this study, with references CE-018/2021 and CHUC-021-19, respectively. The study's patient population's clinical and demographic information was outlined in Table 1 and in more detail in Supplementary File S1.

The patient cohort reflects the heterogeneous population encountered in real-world settings for STS. Therefore, patients were categorized by histological types, including leiomyosarcoma (LMS), liposarcoma (LS), undifferentiated sarcoma (US), synovial sarcoma (SS), and a miscellaneous "Other" group for histotypes with three or fewer patients. To analyze treatment impact and patient response, they were further divided into groups: those recommended for primary tumor surgery (DX), those with stable disease (SD), and those with disease progression (PD), with classifications made by the clinical team. Additionally, patients were sorted by their therapy regimen at the time of sample collection, resulting in four distinct groups: those receiving anthracycline-based therapy (ANTHRA), those on trabectedin-based therapy following anthracycline treatment (ANTHRA + TRAB), those on first-line trabectedin treatment (TRAB), and those following various other treatments ("OTHER"). Other factors such as gender, anatomical site, and presence of metastatic disease were also evaluated, but since no significant differences were found, these data are not included here (data not shown).

TABLE 1 Demographic and clinical characteristics of STS patients enrolled in the study.

Characteristic, unit	N (%) or mean (SD)
Samples	55 (100%)
Age, years	54 ± 15
Sex (% of females)	29 (52.7%)
Disease status	
Non-metastatic	20 (36.4%)
Primary	16 (29.1%)
Recurrence	4 (7.3%)
Metastatic	35 (63.6%)
Primary	25 (45.1%)
Recurrence	10 (18.2%)
Primary anatomical localization	
Extremity	22 (40.0%)
Upper limb	20 (36.4%)
Lower limb	2 (6.4%)
Trunk (not retroperitoneal)	16 (29.1%)
Thorax	5 (9.1%)
Pelvis	4 (7.3%)
Trunk, unspecified	3 (5.5%)
Heart	1 (1.8%)
Liver	1 (1.8%)
Jejunum	1 (1.8%)
Adrenal gland	1 (1.8%)
Retroperitoneal	7 (12.7%)
Gynecological region	9 (16.4%)
Uterus	8 (14.5%)
Spermatic cord	1 (1.8%)
Head and neck	1 (1.8%)
Lineage of cell differentiation	
Leiomyosarcoma	18 (32.7%)
Liposarcoma	9 (16.4%)
Undifferentiated sarcoma	9 (16.4%)
Synovial sarcoma	8 (14.5%)
Other	11 (20%)
Malignant peripheral nerve sheath tumor	3 (5.5%)
Haemangiosarcoma	2 (3.6%)
Clear cell sarcoma	2 (3.6%)
Alveolar soft part sarcoma	1 (1.8%)

(Continued)

TABLE 1 Continued

Characteristic, unit	N (%) or mean (SD)
Lineage of cell differentiation	
Rhabdomyosarcoma	1 (1.8%)
Embryonal sarcoma	1 (1.8%)
Endometrial stromal sarcoma	1 (1.8%)
Treatment and response	
Surgery (diagnostic/recurrence)	8 (14.5%)
Stable disease (chemotherapy)	26 (47.3%)
Progression disease (chemotherapy)	21 (38.2%)
Therapy	
Anthracycline-based therapy	9 (16.4%)
Anthracycline-based therapy followed by trabectedin-based therapy	19 (34.5%)
Trabectedin-based therapy	8 (14.5%)
Other	11 (20%)
Not applicable	8 (14.5%)
Survival	
Alive with disease	31 (56.4%)
Dead of disease	20 (36.4%)
Dead of other causes	4 (7.3%)
Time after collection (TAC estimated, months)	15 ± 12 months
Time after diagnosis (TAD estimated, months)	42 ± 34 months

2.2 Peripheral immunophenotyping

For immunophenotyping, peripheral blood samples collected from 55 STS patients and 45 HD controls were analyzed. First, with the use of the hematological counter DxH500 (Beckman Coulter, Pasadena, CA, USA), the absolute frequency (AF) of total leucocytes (LEU) and the AF and relative frequency (RF) of the major LEU populations, such as lymphocytes (LY), monocytes (MO), and granulocytes (GR), were determined.

Then, peripheral blood samples were stained and prepared for flow cytometry analysis using an 8-color flow cytometer, BD FACSCanto II (BD Biosciences, San Jose, CA, USA), with BD FACSDiva software (BD Biosciences, San Jose, CA, USA). Initially, 100 µL of peripheral blood or up to $1x10^6$ LEU were incubated with fluorochrome-conjugated monoclonal antibodies (mAbs) for 15 minutes in the dark at room temperature. Following staining, red blood cells were lysed using 2 mL of BD Lysing Solution (BD Biosciences, San Jose, CA, USA) for 10 minutes under the same conditions. The samples were then centrifuged at 450 × *g* for 5 minutes; the supernatant was discarded, and the pellet was resuspended in 2 mL of 1x phosphate buffer saline (PBS) for washing. After a second centrifugation at 450 × *g* for 5 minutes, the supernatant was discarded, and the cells were resuspended in 1x PBS for acquisition.

The antibody panel employed, as previously described in the literature (34, 35), included 6 different combinations of fluorochrome-conjugated mAbs, enabling the identification of 83 immune cell populations. These included various lymphocyte subpopulations, dendritic cells (DC), and myeloid-derived suppressor cells (MDSC), along with key receptors related to cell maturation, activation, and suppression. The antibodies were titrated to determine the optimal concentration for up to $1x10^6$ LEU in 100 µL, with detailed antibody specifications provided in Supplementary File S2. Data analysis was performed using FlowJo v.10.7 software (BD Biosciences, Ashland, OR, USA), and the gating strategy is outlined in Supplementary File S3.

2.3 Whole blood immune-related gene expression profiling

Approximately 9 mL of whole blood from 55 STS patients and 45 HD controls was drawn into PAXgene Blood RNA Tubes® (PreAnalytiX, Hombrechtikon, Switzerland), which stabilize and preserve RNA. After collection, the tubes were gently inverted to mix with the stabilization reagent and stored at room temperature for at least 2 hours. They were then frozen at -80°C until RNA extraction. RNA extraction was performed using the PAXgene Blood RNA Kit® (PreAnalytiX, Hombrechtikon, Switzerland). The RNA PAXgene tubes were centrifuged at 3 000 × *g* for 10 minutes to pellet cellular components. The pellet was resuspended in RNase-free water, vortexed, and centrifuged again. The cell lysate was incubated with buffers and proteinase K at 55°C for 10 minutes, then homogenized using the PAXgene Shredder spin column. After adding absolute ethanol, the lysate was transferred to PAXgene RNA spin columns, where RNA was bound, washed, and treated with DNase I to remove DNA. RNA was eluted twice with 40 µL of elution buffer, heat-denatured at 65°C, and stored at -20°C overnight. RNA quality was assessed using a Nanodrop 2000 spectrophotometer (Thermo Fisher Scientific, Waltham, MA, USA), with acceptable ratios of 1.8-2.0 for 260/280 nm and 260/230 nm.

cDNA synthesis was carried out using the iScript™ Reverse Transcription Supermix (BIO-RAD, Hercules, CA, USA). RNA samples (32 µL) were mixed with 8 µL of iScript RT supermix and incubated at 25°C for 5 minutes, 46°C for 20 minutes, and then heated at 95°C for 1 minute to inactivate the reverse transcriptase. The cDNA was stored at -20°C. The concentration and quality of cDNA were also assessed using the Nanodrop 2000 spectrophotometer. For gene expression analysis, real-time RT-qPCR was performed using two 96-well plates to accommodate the 120 samples. The iTaq™ Universal SYBR® Green Supermix (BIO-RAD, Hercules, CA, USA) was used for PCR reactions. Gene-specific primers were obtained from Primer Bank or custom-synthesized and reconstituted. The PCR conditions included an initial denaturation at 95°C for 2 minutes, followed by 50 cycles of denaturation at 95°C for 10 seconds, annealing/extension at 60°C for 30 seconds, and a melt curve analysis from 65 to 97°C.

Calibrated normalized relative quantification (CNRQ) of gene expression was determined using qBase+ v3.2 software (Biogazelle, Gent, Belgium). In total, 99 IRG were measured, and reference genes were selected based on the methodology described by Vandesompele and colleagues (36). The primers used, along with their specifications, were detailed in Supplementary File S4.

2.4 Plasmatic immune-related multiplex analyte profiling

Multiplex analyte profiling (xMAP®) was conducted on plasma samples from 20 STS patients and 20 HD controls. IRSF were analyzed using four pre-configured panels of target analytes, including one panel for general immune monitoring (Human Immune Monitoring 65-plex ProcartaPlex Panel) and three panels dedicated to immune checkpoint molecules (Human Immuno-Oncology Checkpoint 14-Plex ProcartaPlex Panel 1, Panel 2, and the 10-Plex ProcartaPlex Panel 3). The analysis was performed in accordance with the manufacturer's instructions, and the Luminex xMAP® (100/200™ system) was used to quantify the soluble proteins present in plasma samples. The data obtained from the analysis was processed using the ProcartaPlex™ Analysis App (https://apps.thermofisher.com/apps/procartaplex). Analytes with concentrations below or above the limit of detection were excluded from the analysis, resulting in a total of 81 analytes being included in the final analysis. Details of the target analytes in each immunoassay kit are provided in Supplementary File S5.

2.5 Bioinformatic tools

Principal component analysis (PCA) and unsupervised clustering analysis were conducted using the ClustVis software, accessed online at https://biit.cs.ut.ee/clustvis (37). All analyses, from data normalization to final outcomes, were performed entirely within this online tool. Initially, the data were normalized using the ln (x + 1) transformation to ensure proper distribution. PCA prediction ellipses were applied to differentiate between patient groups annotated for histological classification, treatment/response, and therapy, with unit variance scaling used for rows. Principal components (PC) were calculated using single value decomposition (SVD) with imputation. The prediction ellipses indicate the 0.95 probability range for new observations within the same group. Unsupervised clustering analysis was performed to categorize patients based on selected immune-related factors. For this analysis, rows were centered, and unit variance scaling was applied to ensure consistency in data distribution. Missing values were estimated using imputation methods. The clustering of rows was conducted using Euclidean distance as the metric, paired with Ward linkage to optimize the clustering hierarchy. Similarly, columns were clustered using a correlation distance metric combined with Ward linkage to assess the relationships between the immune factors.

The identified IRG and IRSF in each cluster for rows were further submitted to normal gene set analysis using the online software STRING version 11.5 (https://string-db.org) to construct protein-protein interaction (PPI) networks (38). The PPI network enrichment was measured, and the gene ontology (GO) pathway enrichment analysis was assessed (count in network, strength, and FDR).

2.6 Statistical analysis

For comparison of multiple variables, it was used the GraphPad Prism version 9.0.2 for macOS (GraphPad Software, San Diego, CA, USA). Data normalization was performed with arcsinh transformation for flow cytometry data and log10 transformation for RT-qPCR and xMAP® data. Non-normally distributed variables between two groups (STS patients vs. HD control) were analyzed using multiple Mann-Whitney U tests, with false discovery rate (FDR) control and Bonferroni-Dunn correction applied. For more than two groups (e.g., histological classification, treatment/response, therapy), two-way ANOVA with FDR control followed by Bonferroni's post-test was employed. Significance levels were set at $p < 0.05$, $q = 0.05$, and $\alpha = 0.05$. Original values for median and inter-quartile range (IQR) were used for graphical and descriptive data.

Spearman's correlation coefficient, calculated using GraphPad Prism version 9.0.2 for macOS (GraphPad Software, San Diego, CA, USA), was used to assess correlations between immune-related factors (immune cells, IRG, or IRSF), with significance set at $p < 0.05$.

Time-to-event survival analyses were conducted using IBM SPSS Statistics for Mac OS 26.0 (IBM Corp, Armonk, NY, USA). Cox regression and/or log-rank tests were used to evaluate the impact of studied parameters on patient survival. The variable time was defined as the time after collection (TAC), from the collection date until death or the study's end. In some cases, time after diagnosis (TAD) was tested. Given the rarity of these tumors, using TAC instead of TAD allowed us to include more patients and gather sufficient data. To address variability in collection dates and potential bias, our analysis systematically integrated collection times into the study design. Patients who died from other causes (4 patients) were excluded. For individual variables, Cox regression analysis with hazard ratios and log-rank tests using dichotomous variables based on median values were performed. For multiple variables, standardization and multicollinearity assessments were conducted, followed by multivariate Cox analysis using Enter or Stepwise Forward Conditional methods. The proportional hazards assumption was checked using interaction terms with the log of time. Kaplan-Meier curves and log-rank tests were used to analyze the impact of peripheral immunotypes on patient survival, with multivariate Cox analysis performed as previously described.

3 Results

In this study an extensive analysis of immune-related factors was conducted in peripheral blood samples from 55 STS patients and age-matched HD controls. Immunophenotyping of peripheral blood was conducted by flow cytometry to assess the frequency of

83 immune cell populations, including major and minor myeloid and lymphoid cell populations, along with receptors involved in maturation, activation, and suppression. Gene expression analysis using real-time RT-qPCR was employed to evaluate the relative quantity of 99 IRG associated with immune response, as suppression, activation, and cytotoxicity. Similarly, 81 IRSF were quantified in plasma samples collected from 20 STS patients and 20 HD controls by xMAP® technology using standard commercial panels.

Moreover, STS patients were studied according to histological classification, treatment/response, and therapy regimen to discuss how these clinical parameters may influence the alterations observed in STS patients comparatively with HD controls. For IRSF, due to the low sample size, statistical analysis according to histological classification and therapy were excluded, and for treatment and response evaluation, only SD and PD patients were included.

Each set of analysis of immune cells, IRG and IRSF, was performed on the same sample collected from each STS patient, allowing the construction of peripheral immune profiles based on the combined data. Afterwards, unsupervised clustering analysis was performed to identify similar immune profiles within patients and classify patients according to their immunotype. The immunotype classification was inspected for its impact on patient survival in order to explore the potential of peripheral blood samples as a tool for STS monitoring.

3.1 Contraction of B cell and CD4 T cell compartments in STS patients

The immunophenotyping was performed on peripheral blood samples collected from STS patients and HD controls. Using the automated hematological counter, the leucocyte absolute frequency and the GR, MO, and LY absolute and relative frequencies were assessed. It was observed a significant decrease in LY absolute and relative frequency (0.9 cells/<L, IQR: 0.6–1.4, N = 49; 16.6% of LEU, IQR: 8.4–27.6, N = 49; respectively) when compared with HD controls (2.1 cells/<L, IQR: 1.7–2.5, N = 45, adjusted p (adj p) < 0.000001; 32.9% of LEU, IQR: 24.5–39.6, N = 45, adj p = 0.000002) (Supplementary Files S6A, B). Alongside, it was observed an increase in the relative frequency of GR in STS patients (74.3% of LEU, IQR: 57.8–82.5, N = 49) compared with HD controls (61.1% of LEU, IQR: 52.9–67.6, N = 45, adj p = 0.011569) (Supplementary file S6B). No significant alterations were observed for both absolute and relative frequencies of MO (Supplementary Files S6A, B). Using flow cytometry, the relative frequency of DC and MDSC was assessed, and the absolute frequency of both was estimated based on the LEU absolute count. Yet no significant alterations were observed (Supplementary Files S6A, B). Similarly, no differences were observed when analyzing the groups of patients according to the clinical parameters (data not shown).

It was also considered the frequency of LY subpopulations. The comparative analysis between STS patients and HD controls revealed that STS patients have significantly lower B cell absolute and relative frequency (0.02 cells/<L, IQR: 0.01–0.11, N = 49; 2.5% of LY, IQR: 0.5–9.8, N = 55; respectively) when compared with HD controls (0.19 cells/<L, IQR: 0.16–0.27, N = 45, adj p < 0.000001; 10.5% of total LY, IQR: 7.8–12.4, N = 45, adj p = 0.002370) (Figures 1A, B). The absolute frequency of T cells (0.69 cells/<L, IQR: 0.39–1.06, N = 49) and NK cells (0.08 cells/<L, IQR: 0.05–0.16, N = 49) was also significantly decreased in STS patients when compared with HD controls (1.38 cells/<L, IQR: 1.13–1.34, N = 45, adj p = 0.000004; 0.26 cells/<L, IQR: 0.16–0.4, N = 45, adj p < 0.000001; respectively), whereas no significant differences were observed for relative frequencies (Supplementary Files S7A, B). No significant differences were observed for the absolute or relative frequency of NKT-like cells (Supplementary Files S7A, B).

Considering the clinical parameters, significant differences were observed in the relative frequency of B cells. According to histological classification, LS patients exhibited a significantly higher frequency of B cells (8.5% of LY, IQR: 2.5–20.1, N = 9) when compared with LMS (2.1% of LY, IQR: 0.8–7.8, N = 18, adj p = 0.0351) and SS patients (0.7% of LY, IQR: 0.2–3.4, N = 8, adj p = 0.0011) (Figure 1C). Regarding treatment and response, a significant lower relative frequency of B cells was observed in SD (1.1% of LY, IQR: 0.4–5.1, N = 26, adj p < 0.0001) and PD (2.3% of LY, IQR: 1.1–10.9, N = 21, adj p = 0.0035) patients compared with DX patients (13.5% of LY, IQR: 10.3–18.4, N = 8) (Figure 1C). Lastly, when analyzing the therapy regimen, it was observed that there were significantly lower levels of B cells in ANTHRA patients (0.14% of LY, IQR: 0.09–0.74, N = 9) than in the TRAB (6.1% of LY, IQR: 2.6–12.1, N = 8, adj p = 0.0004) or OTHER (6.7% of LY, IQR: 0.5–12.3, N = 11, adj p = 0.0007) group of patients (Figure 1C).

In whole blood gene expression analysis, lower expression levels of CD27, CD40LG, and ICOSLG (0.586 CNRQ, IQR: 0.208–1.843, N = 55; 0.600 CNRQ, IQR: 0.364–1.651, N = 55; 0.400 CNRQ, IQR: 0.209–2.952, N = 49; respectively) were observed in STS patients comparatively with HD controls (3.059 CNRQ, IQR: 1.497–4.649, N = 45, adj p < 0.000001; 1.899 CNRQ, IQR: 1.018–2.608, N = 45, adj p = 0.004186; 3.060 CNRQ, IQR: 1.776–4.430, N = 45, adj p = 0.00001; respectively) (Figure 1D). Considering the clinical parameters evaluated, no significant differences were observed (data not shown), yet PD patients exhibit a tendency for a decrease in the plasma levels of ICOS-L (561.9 pg/mL, IQR: 258.6–808.8, N = 20) compared with SD patients (1470.3 pg/mL, IQR: 1211.6–1813.1, N = 6, FDR = 0.008359; adj p = 0.000103) (Figure 1E).

Moreover, besides no alterations in the relative frequency of T cells (Supplementary File S7B), it was observed a significant reduction in the absolute and relative frequency of CD4 T cells (0.32 cells/<L, IQR: 0.17–0.57, N = 49; 46.3% of T cells, IQR: 36.2–60.6, N = 55; respectively) in STS patients comparatively with HD controls (0.9 cells/<L, IQR: 0.68–1.03, N = 45, adj p < 0.000001; 59.8% of T cells, IQR: 55.3–67.8, N = 45, p = 0.000963; respectively) (Figures 1F, G; Supplementary File S8). The gene expression analysis revealed decreased expression levels of CD28 and IL2RA in STS patients (0.770 CNRQ, IQR: 0.331–2.681, N = 55; 0.583 CNRQ, IQR: 0.277–1.709, N = 54) comparatively with HD controls (3.059 CNRQ, IQR: 1.497–4.639, N = 45, adj p = 0.000116; 2.429, IQR: 1.638–3.510, N = 45, adj p = 0.000011; respectively) (Figure 1H).

Furthermore, the correlation analysis of B cells and CD4 T cells with the IRG CD27, CD40LG, and ICOSLG in STS patients showed

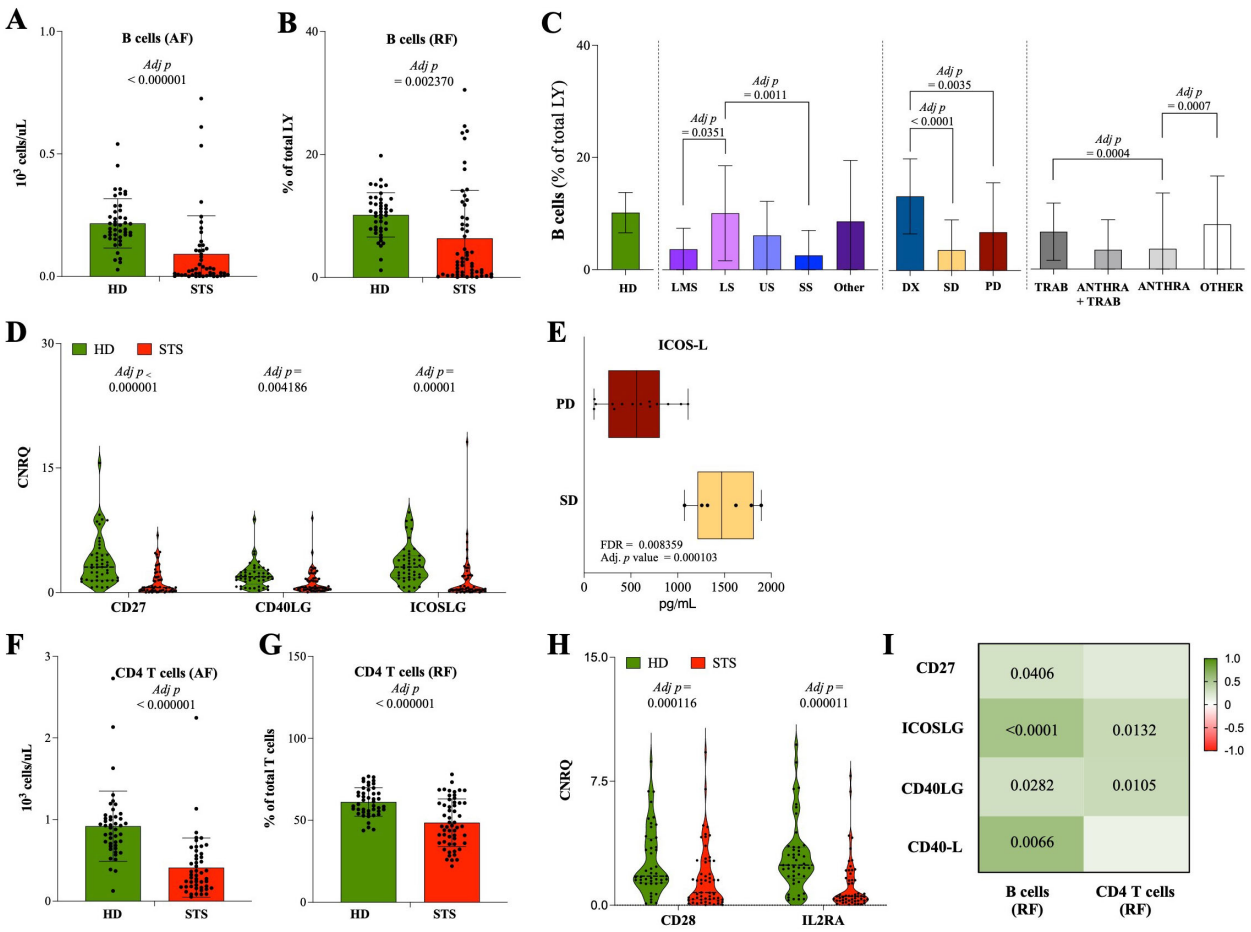

FIGURE 1
Contraction of B cell and CD4 T cell compartments in STS patients. Multiparametric flow cytometry and real-time RT-qPCR were used to analyze immune cells and IRG in peripheral whole blood samples, and xMAP technology was used to analyze IRSF in plasma samples. **(A)** Absolute frequency of B cells observed in STS patients and HD controls. **(B)** Relative frequency of B cells observed in STS patients and HD controls. **(C)** Relative frequency of B cells according to histological classification, treatment/response, and therapy. **(D)** Relative quantification of the IRG CD27, ICOSLG, and CD40LG observed in STS patients and HD controls. **(E)** Relative quantification of the IRSF ICOS-L according to treatment/response. **(F)** Absolute frequency of CD4 T cells observed in STS patients and HD controls. **(G)** Relative frequency of CD4 T cells observed in STS patients and HD controls. **(H)** Relative quantification of the IRG CD28 and IL2RA observed in STS patients and HD controls. **(I)** Correlation analysis of B cells and CD4 T cells with the IRG CD27, ICOSLG, and CD40LG, and with the IRSF CD40-L. Original values were used for data representation using Tukey method, while transformed values of immune cells (arcsin transformed), IRG (log10 transformed), and IRSF (log10 transformed) were used for statistical analysis. In A, B, D-H, it was conducted multiple Mann-Whitney U tests controlling for FDR, followed by Bonferroni-Dunn method to obtain the adjusted *p*-values. In C, it was conducted 2-way ANOVA controlling for FDR (q = 0.05), followed by Bonferroni's post-test for multiple comparisons between groups. In I, Spearman's correlation analysis was performed, and the coefficient matrix was plotted, with significant *p*-values represented. The color scale represents the direction of association, green means positive correlation and red means negative correlation. Statistical significance was set at $p < 0.05$, q = 0.05 and a = 0.05. Legend: HD, healthy donors; STS, soft tissue sarcoma; LMS, leiomyosarcoma; LS, liposarcoma; US, undifferentiated sarcoma; SS, synovial sarcoma; DX, patients indicated for surgery; SD, stable disease; PD, progression disease; TRAB, trabectedin-base chemotherapy; ANTHRA, anthracycline-based therapy; ANTHRA + TRAB, trabectedin-based therapy after anthracycline-based therapy; AF, absolute frequency; RF, relative frequency; IRG, immune-related genes; IRSF, immune-related soluble factors; CNRQ, calibrated normalized relative quantity; FDR, false discovery rate; Adj p, adjusted p-value.

a significant positive correlation between the relative frequency of B cells and the gene expression levels of the IRG CD27 (Spearman r = 0.277, $p = 0.0406$), ICOSLG (Spearman r = 0.541, $p < 0.0001$), and CD40LG (Spearman r = 0.296, $p = 0.0282$), and the plasma levels of CD40-L (Spearman r = 0.586, $p = 0.0066$). Similarly, the relative frequency of CD4 T cells was found to be positively correlated with the gene expression levels of ICOSLG (Spearman r = 0.352, $p = 0.0132$) and CD40LG (Spearman r = 0.342, $p = 0.0105$), with statistical value (Figure 1I).

3.2 The major impact of immunosuppression (MDSC and Treg) in STS patients

In this cohort of STS patients, a significant expansion of circulating monocytic-MDSC (M-MDSC) was observed (79.7% of MDSC, IQR: 58.5–88.6, N = 54) when compared with the HD controls (54.3% of MDSC, IQR: 35.1–72.3, N = 35, adj $p = 0.00652$) (Figure 2A). The gene expression levels of the IRG ARG1 were also found to be significantly

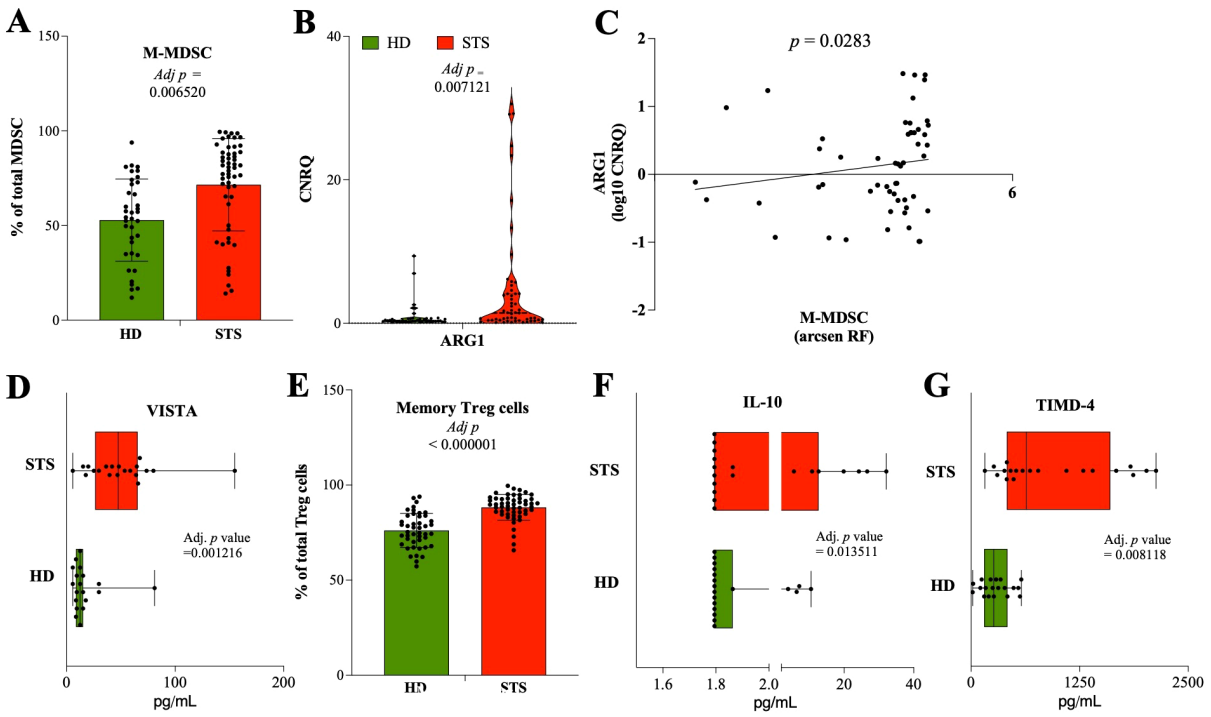

FIGURE 2
Major impact of immunosuppression (MDSC and Treg) in STS patients. Multiparametric flow cytometry and real-time RT-qPCR were used to analyze immune cells and IRG in peripheral whole blood samples, and xMAP technology was used to analyze IRSF in plasma samples. **(A)** Relative frequency of M-MDSC cells observed in STS patients and HD controls. **(B)** Relative quantification of the IRG ARG1 observed in STS patients and HD controls. **(C)** Correlation analysis of M-MDSC with the IRG ARG1. **(D)** Relative quantification of the IRSF TIMD-4 observed in STS patients and HD controls. **(E)** Relative frequency of Treg cells observed in STS patients and HD controls. **(F)** Relative quantification of the IRSF IL-10 observed in STS patients and HD controls. **(G)** Relative quantification of the IRG TIMD-4 observed in STS patients and HD controls. Original values were used for data representation using Tukey method, while transformed values of immune cells (arcsin transformed), IRG (log10 transformed), and IRSF (log10 transformed) were used for statistical analysis. In **(A, B, D-G)**, it was conducted multiple Mann-Whitney U tests controlling for FDR, followed by Bonferroni-Dunn method to obtain the adjusted *p*-values. In **(C)**, Spearman's correlation analysis was performed. Statistical significance was set at $p < 0.05$, $q = 0.05$ and $\alpha = 0.05$. HD, healthy donors; STS, soft tissue sarcoma; MDSC, myeloid-derived suppressor cells; M-MDSC, monocytic-MDSC; Treg, regulatory T cells; IRG, immune-related genes; IRSF, immune-related soluble factors; CNRQ, calibrated normalized relative quantity; FDR, false discovery rate; Adj p, adjusted p-value.

increased in STS patients' peripheral whole blood (1.419, IQR: 0.420–4.124, N = 55), compared with HD controls (0.335 CNRQ, IQR: 0.256–0.658, N = 43, adj p = 007121) (Figure 2B). Moreover, the relative frequency of circulating M-MDSC and the gene expression levels of ARG1 were to be found positively correlated in STS patients, with a statistical value (Spearman r = 0.2985, p = 0.0283) (Figure 2C). Using xMAP technology, the quantification of soluble VISTA in plasma samples was found to be superior in STS patients (47.6 pg/mL, IQR: 26.3–65.5, N = 20) than in HD controls (12.5 pg/mL, IQR: 8.6–15.2, N = 19, adj p = 0.001216) (Figure 2D).

The maturation state of CD4 T cells was evaluated, and it was observed that there was a decreased relative frequency of *naïve* CD4 T cells (9.4% of CD4 T cells, IQR: 5.2–21.8, N = 55) in STS patients than in HD controls (34.3% of CD4 T cells, IQR: 17.1–43, N = 45, adj $p < 0.000001$) (Supplementary File S9A). The relative frequency of Th1, Th2, Th17, and Treg cells was also evaluated. Significantly lower frequencies of Th2 cells (42.2% of CD4 T cells, IQR: 25.9–52.6, N = 55) and increased frequencies of Th17 cells (13.2% of CD4 T cells, IQR: 10.1–19, N = 55) were observed in STS patients when compared with HD controls (53.1% of CD4 T cells, IQR: 46.4–63.6, N = 45, adj p = 001292; 7.2% of CD4 T cells; IQR: 6.1–11.6, N = 45, adj p = 000194; respectively), while no differences were observed for Th1 nor Treg cells (Supplementary File S9B). On the other hand, the frequency of memory Treg cells was found increased in the peripheral blood of STS patients (89.7% of Treg cells, IQR: 85.3–92.8, N = 53) compared with HD controls (75.3% of Treg cells, IQR: 69.5–83.7, N = 75.3, adj $p < 0.000001$) (Figure 2E). The analysis of plasma samples also revealed a higher significant quantification of IL-10 in STS patients (1.8 pg/mL, IQR: 1.8–12.7, N = 19) than in HD controls (1.8 pg/mL, IQR: 1.8–1.9, N = 19, adj p = 0.013511) (Figure 2F). Moreover, the analysis of the IRSF revealed increased levels of TIMD-4 in plasma samples from STS patients (635.9 pg/mL, IQR: 411.1–1603.8, N = 20) compared with HD controls (261.5 pg/mL, IQR: 150.5–418.9, N = 19, adj p = 0.008118) (Figure 2G).

3.3 Compromised cytotoxic potential associated with CD56^{dim} NK cells and CD8 T cells in STS patients

The analysis of the peripheral blood and plasma samples showed a significant increase in the relative frequency of CD8 T

10.3389/fimmu.2024.1391840

cells (45.7% of T cells, IQR: 32.4–57.1, N = 55) in STS patients when compared with HD controls (32.9% of T cells, IQR: 26–37.8, N = 45, adj p = 0.001186) (Figure 3A), while no differences were observed for absolute frequency (Supplementary File S8A). Similarly, no alterations were observed for CD8 T cell subpopulations according to maturation states (Supplementary File S9C). Moreover, the relative frequency of CD56^{dim} NK cells was found to be significantly lower in STS patients (88.5% of NK cells, IQR: 77.7–94.3, N = 55) than in HD controls (97% of NK cells, IQR: 95.6–98.4, N = 45, adj p < 0.000001) (Figure 3B). The analysis according to treatment/response revealed significant increased levels of CD56^{bright} NK cells in PD patients (13.7% of NK cells, IQR: 9.1–29.2, N = 21) in comparison with DX patients (4.4% of NK cells, IQR: 2.6–10.2, N = 8, p = 0.0078) (Figure 3C). Gene expression analysis of whole blood samples showed that STS patients had significantly decreased levels of the IRG PRF1 (0.484, IQR: 0.185–2.049, N = 55), GZMB (0.515 CNRQ, IQR: 0.351–1.457, N = 55), and KLRK1 (0.545 CNRQ, IQR: 0.318–2.047, N = 55) comparatively to HD controls (2.365 CNRQ, IQR: 1.675–3.772, N = 45, adj p = 0.000188; 1.705, IQR: 1.312–2.453, N = 45, adj p = 0.000525; 2.098 CNRQ, IQR: 1.580–3.354, N = 45, adj p = 0.000965; respectively) (Figure 3D). It was also shown that ANTHRA patients

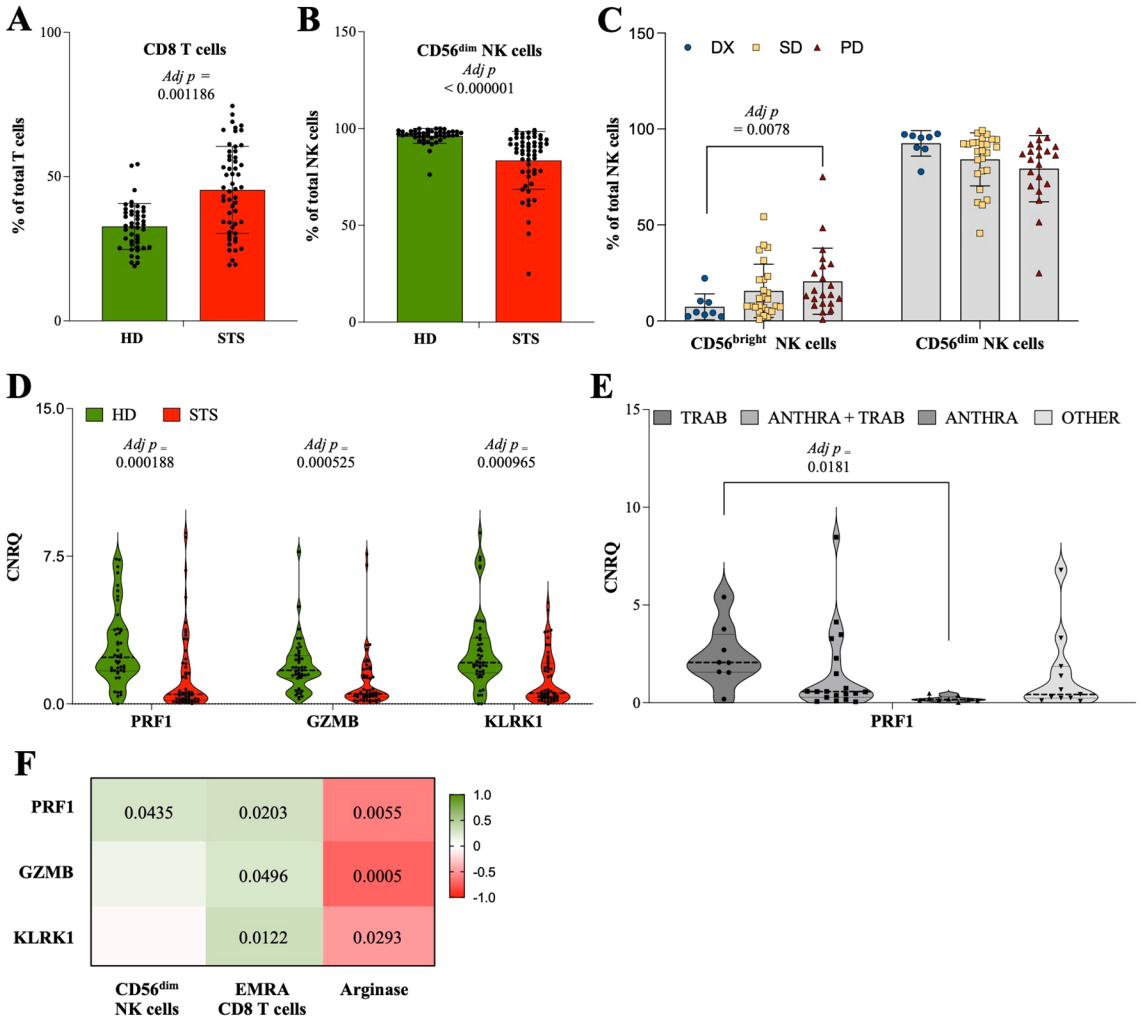

FIGURE 3
Compromised cytotoxic potential associated with CD56^{dim} NK cells and CD8 T cells in STS patients. Multiparametric flow cytometry and real-time RT-qPCR were used to analyze immune cells and IRG in peripheral whole blood samples. **(A)** Relative frequency of CD8 T cells observed in STS patients and HD controls. **(B)** Relative frequency of CD56^{dim} NK cells observed in STS patients and HD controls. **(C)** Relative frequency of CD56^{dim} NK cells according to treatment/response. **(D)** Relative quantification of the IRG PRF1, GZMB, and KLRK1 observed in STS patients and HD controls. **(E)** Relative quantification of the IRG PRF1 according to therapy. **(F)** Correlation analysis of CD56^{dim} NK cells, EMRA CD8 T cells, and the IRSF arginase with the IRG PRF1, GZMB, and KLRK1. Original values were used for data representation using Tukey method, while transformed values of immune cells (arcsin transformed) and IRG (log10 transformed) were used for statistical analysis. In **(A, B, D)** it was conducted multiple Mann-Whitney U tests controlling for FDR, followed by Bonferroni-Dunn method to obtain the adjusted p-values. In **(C, E)**, it was conducted 2-way ANOVA controlling for FDR (q = 0.05), followed by Bonferroni's post-test for multiple comparisons between groups. In F, Spearman's correlation analysis was performed, and the coefficient matrix was plotted, with significant p-values represented. The color scale represents the direction of association, green means positive correlation and red means negative correlation. Statistical significance was set at p < 0.05, q = 0.05 and α = 0.05. HD, healthy donors; STS, soft tissue sarcoma; DX, patients indicated for surgery; SD, stable disease; PD, progression disease; TRAB, trabectedin-base chemotherapy; ANTHRA, anthracycline-based therapy; ANTHRA + TRAB, trabectedin-based therapy after anthracycline-based therapy; IRG, immune-related genes; CNRQ, calibrated normalized relative quantity; FDR, false discovery rate; Adj p, adjusted p-value.

exhibited lower levels of PRF1 (0.168 CNRQ, IQR: 0.111–0.306, N = 9), which were significantly decreased comparatively with TRAB patients (2.060 CNRQ, IQR: 1.560–3.500, N = 8, adj p = 0.0181) (Figure 3E). Additionally, through the correlation analysis of CD8 T cells and CD56^{dim} NK cells with the gene expression levels of PRF1, GZMB, and KLRK1 in STS patients, it was observed a significant positive correlation of CD56^{dim} NK cells with PRF1 (Spearman r = 0.273, p = 0.0435) and EMRA CD8 T cells with PRF1 (Spearman r = 0.312, p = 0.0203), GZMB (Spearman r = 0.266, p = 0.0496), and KLRD1 (Spearman r = 0.336, p = 0.0122) (Figure 3F). Contrarily, the plasma level of Arginase in STS patients (699.6 pg/mL, IQR: 91.5–3417, N = 20) was found to be negatively correlated, with statistical value, with PRF1 (Spearman r = -0.597, p = 0.0055), GZMB (Spearman r = -0.708, p = 0.0005), and KLRK1 (Spearman r = -0.487, p = 0.0293) (Figure 3F).

3.4 Immunotype classification and impact on patient survival

Furthermore, it was aimed at integrating the data obtained from flow cytometry, real-time RT-qPCR, and xMAP analysis to construct peripheral immune profiles and explore their value for monitoring STS patients. To achieve that, and considering the large number of variables, immune cells, IRG, and IRSF, first it was investigated the potential impact of each variable on patient survival, defined as time-to-death event counting from the time of the sample collection to the event of death or the end of the study (May 2023), denominated as time after collection (TAC). Through Cox regression and log-rank tests with an appreciation of KM curves, it was identified immune-related factors significantly correlated with patient survival. The calculated hazard ratio associated with the Cox regression analysis indicated the level of risk or protection associated with each variable. Detailed statistics are depicted in Figure 4. Within the immune cell populations analyzed, increased levels of GR (AF), polymorphonuclear-MDSC (PMN-MDSC), Th2, and *naïve* CD8 T cells were indicated as risk factors, whereas increased levels of MO, DC, LY, T cells, EM CD4 T, and Th1 cells were indicated as protection factors (Figure 4). Among IRG, heightened levels of ARG1 were linked to increased risk, while increased levels of GZMB, CD69, CD3D, NCR2, KLRD1, CCL2, CCL4, CD96, TIGIT, and CD40LG were associated with protection (Figure 4). In the analysis of IRSF, factors such as IL-2, IL-5, IL-10, IL-17A, IFN-γ, MMP1, bNGF, TLSP, VISTA, TIMD-4, PVR, and CTLA-4 were indicated as risk factors, while an increased level of soluble ICOS-L was associated with protection in STS patients (Figure 4).

It was also performed a multivariable Cox proportional hazards regression analysis to assess the impact of immune-related variables on patient survival, adjusting for commonly known prognostic factors such as tumor site (extremity, trunk non-RPS, RPS, gynecologic, head & neck), tumor grade (low grade, high grade, metastatic primary, metastatic recurrent), age at diagnosis, and age at collection time. Due to high multicollinearity and the sample size relative to the number of variables, a Stepwise Method with Forward selection (Likelihood Ratio) was employed. Data was standardized, and the proportional hazards assumption was checked using interaction terms with the log of time. The results indicated that gene expression of CD40LG (p = 0.001), and the combination of CD40LG and the relative frequency of PMN-MDSC (p = 0.022), are significant predictors of patient survival (Supplementary File S10). The proportional hazards assumption was validated for both CD40LG and PMN-MDSC predictors (p > 0.05).

Next, a database containing individual parameters associated with either risk or protection (comprising 35 immune-related variables) for each of the 55 STS patients included in the study was constructed and then uploaded into the ClustVis web platform (http://biit.cs.ut.ee/clustvis/) for data visualization. The data was processed using PCA prediction ellipses and heatmaps (37). For data normalization and to reduce skewness, the original values were transformed (ln (x + 1)), and row centering and unit variance scaling were applied to enhance comparability across different immune-related factors. Additionally, imputation methods were employed to handle missing values, ensuring accurate estimations. Unit variance scaling was applied to rows and SVD with imputation was used to calculate PC.

First, histological classification, treatment/response, and therapy were considered for creating PCA prediction ellipses (Figure 5A). The degree of a similarity or dissimilarity between the groups might be deduced by looking at the placement and overlap of the ellipses. The X and Y axes are represented by PC1 and PC2, which explain 26.3% and 10.7% of the total variation, respectively. The overlap observed in the prediction ellipses indicated an independence of peripheral immunotypes from histological classification, treatment/response, and therapy. Following this, unsupervised clustering analysis was conducted, resulting in the generation of a heatmap featuring 55 columns (representing patients) and 35 rows (representing immune factors) (Figure 5B, left). The clustering of columns (patients) utilized the correlation distance metric and Ward linkage, while the clustering of rows (immune-related factors) employed Euclidean distance and Ward linkage. The analysis revealed three major patient clusters, denoted as P1, P2, and P3, which comprised 17/55, 14/55, and 24/55 of the patients, respectively. Moreover, two clusters were identified for the rows, representing the immune-related factors: an upper cluster (C1) containing 17/35 factors and a lower cluster (C2) containing 18/35 factors.

Then, the immune-related variables that distinguish between patient groups were examined. In C1, the immune populations GR (#), PMN-MDSC (%), *Naïve* CD8 T cells (%), and Th2 cells (%) were clustered together with the IRG ARG1, and the IRSF sVISTA, sCTLA-4, IL-5, bNFG, sIL10, sTLSP, L-2, IL-17A, IFN-g, sMMP-1, sPVR, and sTIMD-4. In C2, the immune populations MO%, DC%, LY%, T cells %, EM CD4 T cells%, and Th1 cells% were clustered together with the IRG CD3D, CCL4, GZMB, CD96, NCR2, TIGIT, CD40LG, KLRC2, CD69, and CCL2, and the IRSF sICOS-L. Using STRING version 11.5 (https://string-db.org), a bioinformatic analysis compared the set of genes and proteins within each C1 and C2 cluster with the whole proteome to identify associated biological pathways (38). For each cluster, a table with factor names and normalized means against the HD controls was uploaded, and a PPI network analysis was constructed (Figure 5B, right). The PPI

10.3389/fimmu.2024.1391840

	Cox regression	Log Rank (Mantel-Cox)	TAC Estimation (mean, SE, n)	
	Sig.	*Sig.*	*Low*	*High*
Immune cells				
GR (AF)	0.001	0.012	40 ± 4 (24)	17 ± 3 (21)
PMN-MDSC (RF)	0.001	0.047	33 ± 5 (26)	23 ± 5 (25)
Naïve CD8 T (RF)	0.002	0.013	40 ± 4 (25)	19 ± 4 (26)
Th2 (RF)	0.017	0.023	42 ± 4 (24)	21 ± 4 (27)
MO (RF)	0.013	0.187	20 ± 3 (24)	37 ± 4 (21)
DC (RF)	0.034	0.040	20 ± 4 (27)	37 ± 4 (24)
LY (RF)	0.007	0.009	17 ± 3 (23)	42 ± 4 (22)
T cells (RF)	0.009	0.027	24 ± 5 (26)	31 ± 5 (25)
EM CD4 T (RF)	0.001	0.005	21 ± 4 (26)	36 ± 5 (25)
Th1 (RF)	0.028	0.027	17 ± 2 (27)	38 ± 4 (24)
Immune-related genes				
ARG1	0.043	0.354	33 ± 4 (26)	23 ± 5 (25)
CD3D	0.001	0.284	26 ± 4 (27)	31 ± 5 (24)
CD69	0.006	0.004	20 ± 4 (24)	35 ± 7 (24)
NCR2	0.035	0.043	17 ± 3 (26)	37 ± 5 (24)
KLRC2	0.020	0.362	20 ± 3 (27)	34 ± 4 (23)
KLRD1	0.003	0.000	18 ± 4 (27)	40 ± 6 (23)
GZMB	0.020	0.240	25 ± 5 (27)	31 ± 5 (24)
CCL2	0.004	0.006	22 ± 4 (26)	24 ± 2 (25)
CCL4	0.014	0.006	22 ± 4 (28)	36 ± 5 (23)
CD96	0.021	0.180	23 ± 4 (27)	35 ± 5 (23)
TIGIT	0.006	0.079	24 ± 5 (25)	33 ± 5 (25)
CD40LG	0.037	0.158	25 ± 4 (27)	32 ± 5 (24)
Immune-related soluble factors				
IL-2	0.012	0.057	26 ± 6 (8)	7 ± 6 (8)
IL-5	0.044	0.043	24 ± 7 (9)	7 ± 4 (7)
IL-10	0.023	0.015	27 ± 7 (8)	6 ± 4 (8)
IL-17A	0.007	0.019	27 ± 7 (8)	6 ± 4 (8)
IFN-γ	0.018	0.015	27 ± 7 (8)	6 ± 4 (8)
NGF-β	0.022	0.034	25 ± 7 (8)	8 ± 4 (8)
MMP1	0.008	0.002	25 ± 6 (10)	1 ± 0 (6)
TSLP	0.017	0.015	27 ± 7 (8)	6 ± 4 (8)
CTLA-4	0.009	0.037	25 ± 7 (8)	8 ± 4 (9)
PVR	0.002	0.007	28 ± 6 (8)	5 ± 3 (9)
TIMD-4	0.004	0.001	27 ± 6 (9)	4 ± 2 (8)
VISTA	0.014	0.009	28 ± 8 (7)	7 ± 3 (10)
ICOS-L	0.001	0.001	4 ± 2 (9)	30 ± 6 (8)

Legend: Sig – significance; SE – standard error; n – number of samples

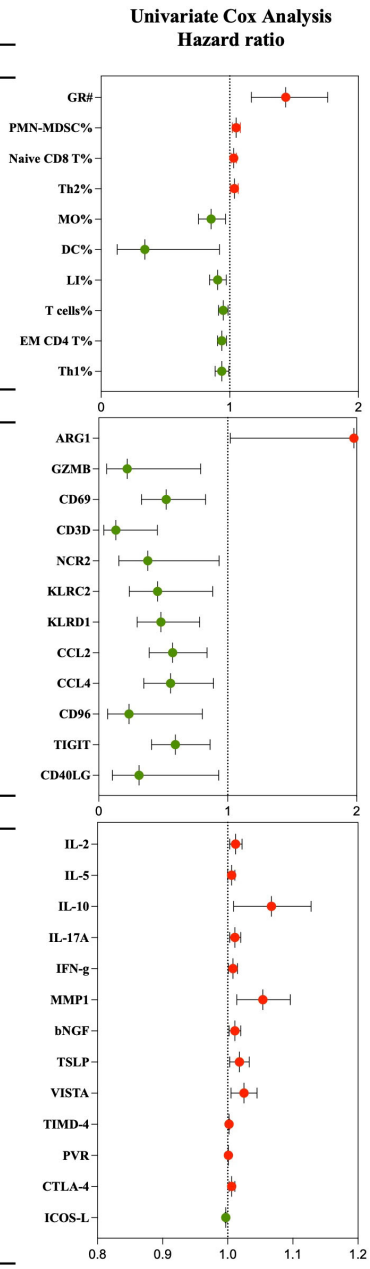

FIGURE 4
Immune-related factors individually associated with patient survival. Multiparametric flow cytometry and real-time RT-qPCR were used to analyze immune cells and IRG in peripheral whole blood samples, and xMAP technology was used to analyze IRSF in plasma samples. Univariate Cox analysis, log-rank test, and graphical representation of the survival-associated hazard ratio. Red and green dots represent factors associated with risk and protection, respectively. Statistical significance was set at $p < 0.05$. GR, granulocytes; AF, absolute frequency; RF, frequency; MO, monocytes; DC, dendritic cells; MDSC, myeloid-derived suppressor cells; PMN-MDSC, polymorphonuclear-MDSC; LY, lymphocytes; DN, double negative; EM, effector memory; Th, T helper.; IRG, immune-related genes; IRSF, immune-related soluble factors.

network enrichment value was < $1x10^{-16}$ for both sets of genes (C1 and C2). A functional enrichment analysis of the GO pathway was performed for each gene or protein set, and the top five significant pathways with higher strength were considered. For C1, the top five GO biological processes identified were: positive regulation of plasma cell differentiation, positive regulation of interleukin-23 production, positive regulation of MHC class II biosynthetic process, negative regulation of interleukin-17 production, and positive regulation of regulatory T cell differentiation (Figure 5B, right, top). For C2, the top five GO biological processes identified were: regulation of NK cell chemotaxis, eosinophil chemotaxis, positive regulation of endothelial cell apoptotic process, negative regulation of NK cell-mediated immunity, and stimulatory C-type lectin receptor signaling pathway (Figure 5B, right, bottom).

Moreover, individual correlations between each immune cell population and IRG and IRSF were investigated. A multivariate

10.3389/fimmu.2024.1391840

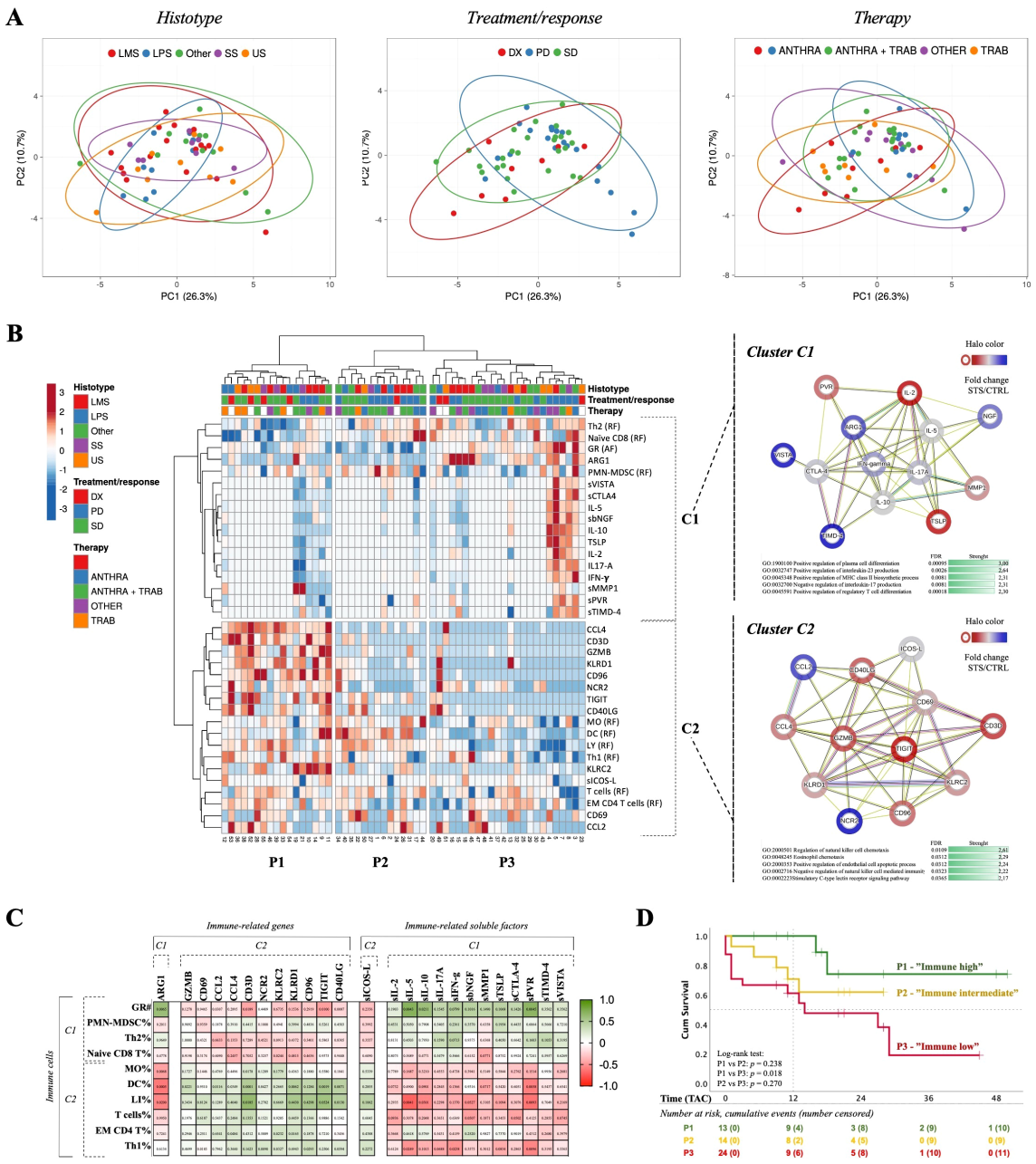

FIGURE 5
Immunotype classification and impact on patient survival. Multiparametric flow cytometry and real-time RT-qPCR were used to analyze immune cells and IRG in peripheral whole blood samples, and xMAP technology was used to analyze IRSF in plasma samples. **(A)** PCA according to histological classification, treatment/response, and therapy. Unit variance scaling was applied to rows and SVD with imputation was used to calculate principal components. Prediction ellipses are such that with a 0.95 probability, a new observation from the same group will fall inside the ellipse. **(B)** Unsupervised clustering analysis of the selected immune cells, IRG and IRSF, and PPI network of IRG and IRSF identified in both C1 and C2 clusters. Heatmap to visualize clustering of multivariate data for 55 STS patients. ClustVis was accessed online (https://biit.cs.ut.ee/clustvis) and patients were plotted by columns while the selected parameters were plotted by rows. Three clusters of patients (P1, P2 and P3) and two clusters of immune-related factors (C1 and C2) were identified. PPI and cluster analysis of the immune-related factors present in each cluster of the heatmap constructed for the 55 STS patients, using the online software STRING (version 11.5). C1 cluster, 13 nodes and 45 edges. The PPI network enrichment was found to be statistically significant ($p < 1.0e^{-16}$). C2 cluster, 12 nodes and 45 edges. The PPI network enrichment was found to be statistically significant ($p < 1.0e^{-16}$). **(C)** Spearman's correlation analysis of immune cells clustered in C1 and C2 with IRG and IRSF. The coefficient matrix was plotted with the *p*-values represented. The color scale represents the direction of association, green means positive correlation and red means negative correlation. **(D)** Survival analysis based on peripheral immunotypes. Kaplan-Meier curves generated from a cohort of 55 STS patients, categorized into P1 ("immune high"), P2 ("immune intermediate"), and P3 ("immune low") immunotypes. Censored events were identified as a cross in the respective curves. The number of patients at risk are represented in the table below the graph. Statistical significance was set at $p < 0.05$. PCA, principal component analysis; PC, principal component; IRG, immune-related genes; IRSF, immune-related soluble factors; LMS, leiomyosarcoma; LS, liposarcoma; US, Undifferentiated sarcoma; SS, synovial sarcoma. ANTHRA, Anthracycline-based chemotherapy; TRAB, trabectedin-based therapy; Naïve, patients indicated for surgery; PPI, protein-protein interaction; IRG, immune-related genes.; IRSF, immune-related soluble factors; UC, upper cluster; LC, lower cluster; GO, gene ontology; FDR, false discovery rate; TAC, time after collection.

analysis was conducted, and a Spearman correlation matrix was plotted, depicting the degree of association between factors (Spearman's R for each pair) (Figure 5C). The colored scale in the matrix indicates the correlation direction, with green representing a positive correlation and red representing a negative correlation. Wells with values in the matrix represent significant *p*-values. Immune cells individually associated with risk (GR (#), PMN-MDSC (%), *naïve* CD8 T cells (%), Th2 (%)) exhibited a similar correlation pattern with IRG and IRSF. Conversely, immune cell populations associated with protection (MO%, DC%, LY%, T cells %, EM CD4 T cells, and Th1 cells%) demonstrated a similar pattern within each other, opposite to that observed for risk-associated populations.

Considering GO functional analysis, Spearman correlation analysis, and immunobiology knowledge, it was determined that the C1 cluster was enriched in inflammatory/immunosuppressive factors, while the C2 cluster was enriched in effector/cytotoxic factors. Therefore, the peripheral immune profiles P1, P2, and P3 were categorized as "immune high," "immune intermediate," and "immune low," respectively. P1 patients displayed reduced levels of C1 factors along with elevated levels of C2 factors, contrary to the observation for P3 patients. P2 patients exhibited intermediate expression levels of C1 and C2 factors, reflecting an intermediate profile.

The implication of peripheral immunotypes on patient clinical outcomes was then investigated. Similar to the survival analysis performed for individual factors, the TAC was set from the time of blood collection until death event occurrence or the end of the study. The resulting KM curves are shown in Figure 5D. The P1 "immune high," P2 "immune intermediate," and P3 "immune low" patients exhibited an estimated TAC of 41 months (N = 13), 20 months (N = 14), and 19 months (N = 24), respectively. The survival rate at 12 months for C1 "immune high" was 100%, whereas for C2 "immune intermediate" it was 70%, and for C1 "immune low" it was about 60%. The log-rank test was employed, and significant differences were observed for the survival curves of C1 "immune high" and C3 "immune low" patients (*p*-value = 0.018). The survival analysis of immunotypes using TAD was assessed, but no significant values were found (Supplementary File S11).

In line with the survival analysis of individual variables, the significance of peripheral immunotypes was assessed using a multivariate Cox regression model adjusted for tumor site, tumor grade, age at diagnosis, and age at collection time. The overall model, which incorporated all variables, significantly predicted patient survival when employing both the Enter ($p = 0.003$) and forward Stepwise ($p = 0.023$) methods (Figure 6A). Using the Enter method, the variable immunotypes ($p = 0.016$) retained its significance. Additionally, age at diagnosis ($p = 0.005$) and age at collection ($p = 0.004$) were also found to be significant (Figure 6B). Conversely, using the Stepwise method, the variable immunotypes was the only factor that remained significant ($p = 0.029$) (Figure 6B). The proportional hazards assumption was validated for immunotypes ($p > 0.05$).

4 Discussion

The current monitoring methods for patients with STS lack effectiveness, prompting the need for alternative approaches. While previous studies have linked patient survival to the immune environment within tumor sites, our comprehension of the overall systemic immune status of STS patients remains incomplete. Utilizing peripheral blood collection as a minimally invasive means, this study aimed to assess the immune status of STS patients, providing advantages over traditional tumor sampling methods. The study aimed to evaluate immune cells, IRG, and

A

Multivariate Cox Analysis – Omnibus Tests of Model Coefficients					
Enter Method			**Forward Stepwise Conditional (LR) Method**		
Overall (score)			*Overall (score)*		
Chi-square	df	Sig.	Chi-square	df	Sig.
17.873	5	0.003	5.192	1	0.023

B

Multivariate Cox Analysis – Variables in the equation															
	Enter Method					**Forward Stepwise Conditional (LR) Method**					**Univariate Cox Analysis**				
	B	*Sig.*	*Exp(B)*	*95.0% CI*		*B*	*Sig.*	*Exp(B)*	*95.0% CI*		*Sig.*	*Exp(B)*	*95.0% CI*	
Variables in the Equation				Lower	Upper				Lower	Upper			Lower	Upper
Age at Diagnostic	0.264	0.005	1.302	1.084	1.565						0.716	0.995	0.967	1.023
Age at Collection	-0.282	0.004	0.754	0.624	0.912						0.468	0.989	0.961	1.019
Tumor site	-0.372	0.076	0.689	0.457	1.040						0.916	0.978	0.653	1.467
Tumor Grade	1.471	0.054	4.355	0.975	19.449						0.042	4.550	1.054	19.641
Immunotypes	0.813	0.016	2.256	1.165	4.368	0.715	0.029	2.044	1.075	3.885	0.021	2.127	1.123	4.026

FIGURE 6
Multivariate Cox analysis of immunotypes adjusting for common prognostic factors. Multiparametric flow cytometry and real-time RT-qPCR were used to analyze immune cells and IRG in peripheral whole blood samples, and xMAP technology was used to analyze IRSF in plasma samples. Enter and stepwise method with forward selection (likelihood ratio) for immunotypes adjusting for tumor site (extremity, trunk non-RPS, RPS, gynecologic, head & neck), tumor grade (low grade (non-metastatic primary); high grade (non-metastatic primary recurrent; metastatic primary; metastatic recurrent), age at diagnosis, and age at collection time. **(A)** Overall model including all the variables. Enter and forward Stepwise Conditional (LR) method. **(B)** Variables in the equation for the Enter and forward Stepwise Conditional (LR) method, and univariate Cox analysis. Statistical significance was set at $p < 0.05$.

IRSF, identify peripheral immune profiles, and investigate their association with patient survival. Consequently, the findings suggested impaired systemic immunity in STS patients, with the analysis of peripheral immunotypes indicating an impact on patient survival.

4.1 Contraction of B cell and CD4 T cell compartments in STS patients

Analysis of major leukocyte populations revealed significant lymphopenia accompanied by an expansion of GR, predominantly neutrophils (NEU). These observations align with findings from previous studies in STS and cancer in general (24, 30, 39–41). For example, systemic inflammation indices like the neutrophil-to-lymphocyte ratio (NLR) have been proposed as prognostic factors in STS and cancer overall (42–46). A high NLR, indicative of NEU expansion and LY reduction, is commonly associated with a poorer prognosis. The decrease in LY counts may be attributed to various factors, including the tumor's peripheral effects (47–49) and chemotherapy-induced decline (50), which is noteworthy considering that most patients in our study were undergoing chemotherapy.

Besides the studies highlighting the significance of major leukocyte populations, there exists a gap in research investigating in-depth analyses of immune cell populations, IRG, or IRSF in the peripheral blood of STS patients. Therefore, our study uncovered compelling findings. The decrease in B cells and CD4 T cells, consistent with the observations by Kim et al. (51), along with the reduced gene expression levels of ICOSLG and CD40LG, which are positively associated with both B cells and CD4 T cells, suggests impaired activation of these cell types. B cells have been implicated in the context of STS within the tumor site, where higher infiltration and the presence of B cell-rich tertiary lymphoid structures (TLS) correlate with improved clinical outcomes (17, 18, 52). The peripheral reduction of B cells may hinder their migration to the tumor site, potentially weakening immune responses in the tumor microenvironment (TME). Decreased circulating levels of CD4 T cells have also been documented in other solid tumors (53, 54), suggesting a potential decrease in CD4 T cell infiltration, particularly Th1 cells crucial for effective immune responses. It's worth noting that reduced levels in both populations may be associated with chemotherapy (50). However, only B cells exhibited a significant reduction compared to patients not undergoing chemotherapy (DX patients), indicating that the decrease in CD4 T cells is not solely attributable to chemotherapy. Moreover, analysis based on chemotherapy regimens revealed that ANTHRA patients exhibited the lowest frequency of B cells, consistent with a study in breast cancer demonstrating the impact of anthracyclines on the B cell compartment (55). Interestingly, TRAB patients exhibited significantly higher levels of B cells, suggesting a potential advantage of trabectedin over anthracyclines.

In addition to the decrease in B cells and CD4 T cells, the gene expression levels of ICOSLG and CD40LG were also found to be reduced in these patients. Both ICOS/ICOS-L and CD40/CD40LG play critical roles in the communication between B cells and CD4 T cells, among other immune functions (56, 57). Furthermore, the downregulation of these pathways has been implicated in cancer (58, 59). For instance, in LS, there's evidence of a correlation between ICOS expression in tumors and improved clinical outcomes (60), which aligns with the tendency for decreased plasma levels of ICOS-L observed in our study's PD patients. Additionally, LS patients exhibited increased frequencies of B cells. Furthermore, other immune-related genes like CD27, associated with switch memory B cells, and CD28 and IL2RA, linked to T cells, were also found to be decreased in the peripheral blood of these patients. Therefore, beyond the decrease in frequencies, the observed reduction in B cells, CD4 T cells, and the mentioned IRG suggests impaired activation of circulating B and CD4 T cells in STS patients, potentially leading to diminished migration of effector cells to the TME.

4.2 The major impact of immunosuppression (MDSC and Treg) in STS patients

Furthermore, an increase in suppressor populations, notably M-MDSC and memory Treg cells, was observed, along with elevated gene expression levels of the IRG ARG1 and increased plasma levels of VISTA, TIMD-4, and IL-10. In studies involving sarcoma patients, elevated levels of M-MDSC have been linked to reduced treatment efficacy, tumor growth, and a poorer prognosis (51, 61). Additionally, increased gene expression levels of ARG1 were found to be positively correlated with the heightened frequency of M-MDSC in this study. M-MDSC are known to be robust producers of arginase-1, which can inhibit NK and T cell cytotoxicity by depleting arginine from the microenvironment (62–65). Moreover, in STS, both ARG1 and ARG2 gene expression have been identified in tumor samples, suggesting an immunosuppressive TME that may impede an effective immune response (66). Hence, beyond the TME, it can be hypothesized that the expansion of M-MDSC leads to the release of arginase-1 into the peripheral microenvironment, inhibiting the cytotoxic function of T and NK cells and thereby contributing to impaired systemic immunity.

Moreover, an increase in plasma levels of the immune checkpoint VISTA was observed. This molecule has been proposed as a significant factor for immunotherapy in STS, as its expression on tumor samples has been associated with tumor grade, tumor-infiltrating lymphocyte numbers, and PD-1 expression (67). Particularly in SS, the expression of VISTA by macrophages has been shown to inhibit the infiltration of T cells in *ex vivo* experiments (68). Additionally, VISTA may influence the differentiation of MDSC (69, 70). Therefore, considering the expansion of M-MDSC, increased levels of VISTA may potentially promote the differentiation and expansion of circulating M-MDSC.

Furthermore, an increase in memory Treg cells and IL-10 plasma levels was observed. In STS and other solid tumors, the presence of Treg cells in tumor samples has been associated with

worse outcomes (19, 71), suggesting a similar scenario in the periphery. Hence, the increased levels of memory Tregs, besides the reduced levels of CD4 T cells, may contribute to an immunosuppressive microenvironment. Studies have reported that M-MDSC may promote the expansion of Treg cells via the release of IL-10 into the environment (72–74), aligning with the observations for M-MDSC, memory Treg cells, and IL-10 in this study. Increased plasma levels of IL-10 have been documented in pediatric STS patients and are associated with advanced disease, poor response to chemotherapy, and unfavorable outcomes (75). IL-10 has been correlated with increased suppression of T cells in cancer patients and associated with worse survival (76, 77). Additionally, increased plasma levels of TIMD-4 were also observed in this study. TIMD-4, or TIM-4, is another immune checkpoint molecule involved in T cell regulation. In cancer, its expression in tumor samples has been correlated with worse patient outcomes due to decreased effector function of tumor-infiltrating CD8 T cells (78, 79). Although studies evaluating this molecule in STS are rare, a case report of LS showed expression of TIM-3 or TIM-4 in tumor samples, indicating a direct involvement in cancer progression (80). Considering the findings for M-MDSC, ARG1, soluble VISTA, Treg cells, IL-10, and soluble TIMD-4, it can be suggested that immunosuppression at the periphery has a significant impact, sustaining impaired systemic immunity, which may limit the anti-tumoral immune response at the tumor site.

4.3 Compromised cytotoxic potential associated with CD56^{dim} NK cells and CD8 T cells in STS patients

Furthermore, a decrease in CD56^{dim} NK cells and a reduction in the gene expression levels of cytotoxic-related factors PRF1, GZMB, and KLRK1 were observed. NK cells are professional killer cells crucial for tumor cell clearance, with their infiltration within tumors typically associated with better prognoses (81). NK cells can be categorized into two major subpopulations: CD56^{bright} NK cells, which are adept at secreting cytokines and chemokines, and CD56^{dim} NK cells, which exhibit greater cytotoxic activity (82). Therefore, the decreased frequency of CD56^{dim} NK cells may imply a diminished cytotoxic potential of circulating NK cells in STS patients. The observation of increased levels of CD56^{bright} NK cells and decreased levels of CD56^{dim} NK cells in PD patients further supports this assumption. Similarly, CD8 T cells are known for their cytotoxic activity. In this study, an expansion of circulating CD8 T cells was observed, suggesting an increased presence of these cells in the periphery. However, there was no observed increase in the effector CD8 T cell subpopulations EM and EMRA, indicating that despite the expansion of total CD8 T cells, there isn't a proportional increase in the cells with the capacity to clear tumor cells. Additionally, a decrease in the gene expression levels of important cytotoxic factors such as PRF1, GZMB, and KLRK1 was noted. PRF1 was found to be positively correlated with CD56^{dim} NK cells, while PRF1, GZMB, and KLRK1 were significantly correlated with EMRA CD8 T cells. PRF1 and GZMB encode pore-forming and cytotoxic granules, respectively, involved in the cytotoxic process of NK and T cells against tumor cells (83–86). Therefore, the decreased gene expression of both may indicate an ineffective cytotoxic capacity of circulating NK and T cells. Moreover, significantly higher levels of PRF1 were observed in TRAB patients compared to ANTHRA patients. Trabectedin has demonstrated immunomodulatory effects by inhibiting tumor-associated macrophages and inducing NK-mediated cytotoxicity in cancer, as multiple myeloma (87–89). This suggests that trabectedin may enhance NK and T cell function by mitigating the effects of the TME on the systemic immune response. This could also contribute to some of the advantages of trabectedin over anthracyclines in STS treatment.

Indeed, a previous study demonstrated that peripheral NK cells from STS patients are dysfunctional, as they are unable to lyse tumor cells *in vitro* (90). Lower frequencies of circulating CD8 T cells producing PRF1 were observed in gastric cancer compared to healthy individuals (91). Additionally, lower gene expression levels of KLRK1, which encodes the activatory receptor NKG2D expressed by both NK and T cells, were noted. This aligns with previous reports showing decreased expression of NKG2D by circulating NK cells and the association of NKG2D+ CD8 T cells with improved disease-free survival in STS patients (90). Moreover, *in vitro* studies have shown that NKG2D mediates NK cell cytotoxic activity against sarcoma cells (92). Interestingly, a negative correlation was observed between the gene expression levels of PRF1, GZMB, and KLRK1 and the plasma levels of arginase-1. Considering the role of arginase-1, possibly released by M-MDSC, in inhibiting the cytotoxic capacity of NK and T cells (3, 62–65), this finding further supports the proposed immunosuppressed systemic immunity sustained by the expansion of M-MDSC. This expansion leads to the inhibition of NK and T cell cytotoxicity via the release of arginase-1 and the depletion of arginine from the circulation. Taken together, these findings suggest a decreased cytotoxic capacity of NK and T cells in the peripheral blood of STS patients, likely influenced by pro-tumoral mediators in circulation.

4.4 Immunotype classification and impact on patient survival

Next, it was employed unsupervised clustering analysis using immune cells, IRG and IRSF, and three distinct peripheral immune profiles (P1, P2, and P3), based on immune-related factors (C1 and C2), were identified in this cohort of STS patients. The contribution of each immune-related factor delineate the differences in the immune profiles among patients, and the investigation into the factors comprising each cluster (C1 and C2) unveiled unique associations. Cluster C1 showed associations of GR, PMN-MDSC, Th2 cells, and *naïve* CD8 T cells, with IRG such as ARG1, and IRSF like soluble IL-10, VISTA, and TIMD-4, alongside other immune checkpoint molecules and inflammatory mediators. GO pathway analysis suggested a potential association with immune suppression, particularly with Treg cells. In contrast, cluster C2 displayed associations between MO, DC, LY, T cells, EM CD4 T cells, and Th1 cells with IRG like GZMB and CD40LG, as well as the soluble factor ICOS-L, among others, correlated with cytotoxicity. GO

pathway enrichment indicated a correlation with cytotoxicity, particularly associated with NK cells. These findings highlight distinct immune profiles in STS patients, providing insights into potential mechanisms underlying immune responses and suggesting avenues for patient classification and immune monitoring.

Although circulating Treg cells did not show a correlation with patient survival in this study, the observed expansion of memory Tregs may be associated with these findings, contributing to heightened immunosuppression of systemic immunity in STS, aligning with studies in STS showing that Treg cell infiltration in tumors reflects an increased risk of local recurrence (19). Additionally, the correlation patterns between GR and IRSF underscore the importance of GR in sustaining an inflammatory microenvironment in STS, aligning with findings from other studies in the field (43, 44, 93). On the other hand, both NK cells and CD8 T cells are renowned for their potent anti-tumor activity and have been extensively investigated for their ability to eliminate tumor cells (94, 95). In the context of STS, the presence of infiltrating NK cells and CD8 T cells has been linked to increased survival (96, 97). While the involvement of the ICOS-L pathway in T cells has been previously explored, it is crucial to highlight the protective nature of Th1 cells and DC, both of which exhibit a significant positive correlation with ICOS-L in this study. This correlation suggests that, despite limited studies in the context of STS, the heightened activation of Th1 cells by DC through the ICOS-L pathway might also play a crucial role in disease management and control.

Therefore, based on the immune factors in clusters C1 and C2, patients were categorized into "immune high," "immune intermediate," and "immune low" immunotypes. "Immune high" patients (P1) showed elevated cytotoxic-associated factors and lower inflammatory or immunosuppression-related factors, while "immune low" patients (P3) exhibited the opposite pattern. P2 patients fell into the "immune intermediate" category. Analysis of survival rates revealed that "immune high" patients had a significantly better survival outcome compared to "immune low" patients, with a 12-month survival rate of 100% versus 60%, respectively. "Immune intermediate" patients showed survival rates in-between the other two groups. This highlights the potential of peripheral immunotypes as biomarkers for predicting outcomes in STS.

Patients classified as "immune high" exhibited elevated levels of effector memory (EM) CD4 T cells, along with increased expression of CD40LG and ICOS-L. These markers suggest that B cells and CD4 T cells in these patients maintain robust functionality, which is crucial for effective immune responses. Additionally, these patients showed heightened levels of cytotoxic activity markers like GZMB, indicating a more vigorous and effective immune attack against tumor cells. In contrast, patients categorized as "immune low" displayed higher levels of suppressive factors commonly associated with Treg cells and MDSCs, such as the IRG ARG1 and plasma cytokine IL-10. The presence of these suppressive factors implies a compromised immune response, likely due to immune suppression mechanisms that inhibit effective anti-tumor activity. These observations highlight the critical role of immune mechanisms in influencing patient survival, with "immune high" subtypes benefiting from a more active and functional immune system, whereas "immune low" subtypes face challenges from immune suppression.

Recent years have seen a growing interest in incorporating diverse immune-related parameters to explore their predictive value in cancer survival and therapy response (98). In sarcoma patients, tumoral immunotypes have been proposed to optimize therapeutic strategies (27). For instance, in US, unsupervised clustering analysis of tumor samples identified three distinct immunological clusters also labeled as "immune high," "immune intermediate," and "immune low" (99). These clusters showed significant associations with overall survival in primary tumors. Moreover, comprehensive immune profiling has revealed LMS with an active and "hot" TME, highlighting the importance of immune competence for an effective anti-tumoral response (100). Beyond the analysis of tumor samples, peripheral immune profiles have also shown correlations with patient survival in various cancers (101–103), and in STS, gene expression profiles from TCGA databases have identified immune signatures linked to clinical outcomes (104). Additionally, in patients with US, an "immune-high" profile has been linked to a favorable response to ICI therapy (105).

The multivariate analysis identified CD40LG gene expression and PMN-MDSC frequency as significant predictors of patient survival. Although the overall model incorporating all variables did not significantly predict patient survival, the identification of these specific markers (CD40LG and PMN-MDSC) underscores their potential clinical relevance. Moreover, when discussing the advantages of utilizing peripheral phenotypes over individual-related parameters, it is important to emphasize the robustness of immunotypes in multivariate analyses. In this study, immunotypes retained their significance even after adjusting for common clinical and personal characteristics, demonstrating their ability to capture relevant information that might be overlooked when only individual variables are considered. Specifically, when using Cox regression models to evaluate individual immune cells, IRG, and IRSF, peripheral immunotypes provide a distinct advantage. They integrate a broader spectrum of immune-related data, thereby offering a more comprehensive and stable measure of immune status compared to isolated individual parameters.

Thus, the incorporation of immune profiles into prognostic models may improve patient outcomes, treatment regimens, and risk stratification. Immune profiling is pivotal for identifying patients with heightened immune cytotoxicity who may benefit from immunotherapeutic interventions to boost anti-tumor immune responses. Conversely, those with low immune activity and higher immunosuppression may need strategies to overcome immune evasion and restore function, enabling more precise patient management and tailored therapies based on their immunotype. While histological classification might have a reduced impact on observed patient immunotypes, recent studies underscore significant immune-related differences among STS histotypes (105–109), potentially correlating with varying sensitivity to immune responses and tumor aggressiveness. For instance, investigations into ICI therapy in STS patients reveal promising treatment responses in specific histotypes such as US and LMS. The independence of immunotypes from histological classification presents a significant advantage for monitoring STS

patients, allowing for patient-specific categorization within the disease's inherent heterogeneity. Yet, specific alterations in immune parameters were observed, suggesting that monitoring these changes could also complement histotype classification. Moreover, the prevalence of the "immune low" immunotype is higher in PD patients, aligning with lower survival rates. Despite the suggested impact of trabectedin in promoting improved systemic immunity, no discernible effect was noted for immunotype classification. This is crucial for therapeutic interventions, where shifts in immune-related factors might correlate directly with treatment responses.

In conclusion, this study revealed contraction and impairment of circulating B and CD4 T cells, expansion of suppressor cells such as M-MDSC and Treg, and increased levels of immune-related factors associated with inhibition, including ARG1, soluble VISTA, soluble TIMD-4, and IL-10. Moreover, compromised cytotoxic function was observed due to reductions in cytotoxic factors like PRF1 and GZMB, along with cytotoxic NK cells and activatory receptors such as KLRK1 (NKG2D), indicating compromised systemic immunity in STS patients. Unsupervised clustering analysis identified three distinct immunotypes, each characterized by varying levels of immunosuppression or activation and cytotoxicity-related factors. Patients (P1) with lower levels of immunosuppressor factors (C1) and higher levels of factors related to the activation and cytotoxicity of NK and T cells (C2) exhibited superior survival rates compared to patients (P3) with the opposite pattern. These findings suggest impaired immunity in STS patients with impact on patient survival, highlighting the potential of monitoring STS patients using peripheral blood samples to evaluate the immune status of a patient as an alternative to tumor sample evaluation. Additionally, classifying STS patients into more homogeneous groups may streamline clinical management.

This study provides valuable insights into the peripheral immune landscape in STS patients, but several limitations must be acknowledged. The small sample size limits the statistical power and the ability to accurately evaluate clinical parameters, emphasizing the need for larger cohorts. Additionally, the variability in diagnostic timing and non-standardized sample collection times introduce heterogeneity, making it challenging to isolate newly diagnosed patients and impacting the consistency of the data. The cross-sectional design further restricts the study by not capturing immune dynamics over time, which is crucial for understanding disease progression and treatment response. Without external validation of the immunotypes identified, the generalizability of these findings remains uncertain, suggesting a need for future studies to validate these results in larger, diverse cohorts.

Building on the current findings, future research should focus on longitudinal studies to monitor changes in the immune landscape over time and under different treatment regimens. This approach will provide deeper insights into the prognostic and predictive significance of immune profiling in STS. Additionally, there is a need for interventions aimed at modulating peripheral immune responses, which could potentially improve clinical outcomes. Future trials should aim to standardize and validate immunotype classification, ultimately integrating these insights into clinical practice to enhance the management of STS patients.

Data availability statement

The original contributions presented in the study are included in the article/Supplementary Materials. Further inquiries can be directed to the corresponding author.

Ethics statement

The studies involving humans were approved by The Coimbra Hospital and Universitary Center Ethics Committee and the University of Coimbra's Faculty of Medicine Ethics Committee. The studies were conducted in accordance with the local legislation and institutional requirements. The participants provided their written informed consent to participate in this study.

Author contributions

JSA: Writing – review & editing, Writing – original draft, Methodology, Investigation, Formal analysis, Data curation. LMS: Writing – review & editing, Investigation. PC: Writing – review & editing, Investigation. TFA: Writing – review & editing, Investigation. VA: Writing – review & editing, Investigation. AM: Writing – review & editing, Investigation. JR: Writing – review & editing, Investigation. RF: Writing – review & editing, Investigation. PF-T: Writing – review & editing, Investigation. MS-R: Writing – review & editing, Investigation. JMC: Writing – review & editing, Writing – original draft, Investigation. PR-S: Writing – review & editing, Writing – original draft, Visualization, Validation, Supervision, Resources, Project administration, Methodology, Investigation, Funding acquisition, Formal analysis, Data curation, Conceptualization.

Funding

The author(s) declare financial support was received for the research, authorship, and/or publication of this article. This work was supported by the European Regional Development Fund (ERDF), through the Centro 2020 Regional Operational Program and through the COMPETE 2020-Operational Programme for Competitiveness and Internationalisation and Portuguese national funds via FCT-Fundação para a Ciência e a Tecnologia, under the projects POCI-01-0145-FEDER-007440, UIDB/04539/2020 and UIDP/04539/2020. JSA was supported by the PhD Grant (SFRH/BD/148007/2019) from the Portuguese Science and Technology Foundation (FCT), through the European Social Fund from the European Union.

Conflict of interest

The authors declare that the research was conducted in the absence of any commercial or financial relationships that could be construed as a potential conflict of interest.

The author(s) declared that they were an editorial board member of Frontiers, at the time of submission. This had no impact on the peer review process and the final decision.

Publisher's note

All claims expressed in this article are solely those of the authors and do not necessarily represent those of their affiliated organizations, or those of the publisher, the editors and the reviewers. Any product that may be evaluated in this article, or claim that may be made by its manufacturer, is not guaranteed or endorsed by the publisher.

Supplementary material

The Supplementary Material for this article can be found online at: https://www.frontiersin.org/articles/10.3389/fimmu.2024.1391840/full#supplementary-material

References

1. WHO Classification of Tumours Editorial Board. Soft tissue and bone tumours. In: *WHO classification of tumours series, 5th ed*, vol. 3. International Agency for Research on Cancer, Lyon (France (2020). Available at: https://publications.Iarc.fr/588.

2. Bray F, Ferlay J, Laversanne M, Brewster DH, Gombe Mbalawa C, Kohler B, et al. Cancer Incidence in Five Continents: Inclusion criteria, highlights from Volume X and the global status of cancer registration. *Int J Cancer*. (2015) 137:2060–71. doi: 10.1002/ijc.29670

3. Stiller CA, Trama A, Serraino D, Rossi S, Navarro C, Chirlaque MD, et al. Descriptive epidemiology of sarcomas in Europe: report from the RARECARE project. *Eur J Cancer*. (2013) 49:684–95. doi: 10.1016/j.ejca.2012.09.011

4. Stiller CA, Botta L, Brewster DH, Ho VKY, Frezza AM, Whelan J, et al. Survival of adults with cancers of bone or soft tissue in Europe-Report from the EUROCARE-5 study. *Cancer Epidemiol*. (2018) 56:146–53. doi: 10.1016/j.canep.2018.08.010

5. American Cancer Society. Survival rates for Soft Tissue Sarcoma. Available online at: https://www.cancer.org/cancer/types/soft-tissue-sarcoma/detection-diagnosis-staging/survival-rates.html (Accessed November 7, 2023).

6. Gronchi A, Miah AB, Dei Tos AP, Abecassis N, Bajpai J, Bauer S, et al. Electronic address: clinicalguidelines@esmo.org. Soft tissue and visceral sarcomas: ESMO-EURACAN-GENTURIS Clinical Practice Guidelines for diagnosis, treatment and follow-up☆. *Ann Oncol*. (2021) 32:1348–65. doi: 10.1016/j.annonc.2021.07.006

7. von Mehren M, Kane JM, Agulnik M, Bui MM, Carr-Ascher J, Choy E, et al. Soft tissue sarcoma, version 2.2022, NCCN clinical practice guidelines in oncology. *J Natl Compr Canc Netw*. (2022) 20:815–33. doi: 10.6004/jnccn.2022.0035

8. Birdi HK, Jirovec A, Cortés-Kaplan S, Werier J, Nessim C, Diallo JS, et al. Immunotherapy for sarcomas: new frontiers and unveiled opportunities. *J Immunother Cancer*. (2021) 9:e001580. doi: 10.1136/jitc-2020-001580

9. Gnjatic S, Bronte V, Brunet LR, Butler MO, Disis ML, Galon J, et al. Identifying baseline immune-related biomarkers to predict clinical outcome of immunotherapy. *J Immunother Cancer*. (2017) 5:44. doi: 10.1186/s40425-017-0243-4

10. Dancsok AR, Setsu N, Gao D, Blay JY, Thomas D, Maki RG, et al. Expression of lymphocyte immunoregulatory biomarkers in bone and soft-tissue sarcomas. *Mod Pathol*. (2019) 32:1772–85. doi: 10.1038/s41379-019-0312-y

11. Coley WB. The Treatment of Inoperable Sarcoma by Bacterial Toxins (the Mixed Toxins of the Streptococcus erysipelas and the Bacillus prodigiosus). *Proc R Soc Med*. (1910) 3:1–48. doi: 10.1177/003591571000301601

12. Antonescu CR. The role of genetic testing in soft tissue sarcoma. *Histopathology*. (2006) 48:13–21. doi: 10.1111/j.1365-2559.2005.02285.x

13. Taylor BS, Barretina J, Maki RG, Antonescu CR, Singer S, Ladanyi M. Advances in sarcoma genomics and new therapeutic targets. *Nat Rev Cancer*. (2011) 11:541–57. doi: 10.1038/nrc3087

14. Banks LB, D'Angelo SP. The role of immunotherapy in the management of soft tissue sarcomas: current landscape and future outlook. *J Natl Compr Canc Netw*. (2022) 20:834–44. doi: 10.6004/jnccn.2022.7027

15. Nacev BA, Jones KB, Intlekofer AM, Yu JSE, Allis CD, Tap WD, et al. The epigenomics of sarcoma. *Nat Rev Cancer*. (2020) 20:608–23. doi: 10.1038/s41568-020-0288-4

16. Tazzari M, Bergamaschi L, De Vita A, Collini P, Barisella M, Bertolotti A, et al. Molecular determinants of soft tissue sarcoma immunity: targets for immune intervention. *Int J Mol Sci*. (2021) 22:7518. doi: 10.3390/ijms22147518

17. Fridman WH, Meylan M, Petitprez F, Sun CM, Italiano A, Sautès-Fridman C. B cells and tertiary lymphoid structures as determinants of tumour immune contexture and clinical outcome. *Nat Rev Clin Oncol*. (2022) 19:441–57. doi: 10.1038/s41571-022-00619-z

18. Petitprez F, de Reyniès A, Keung EZ, Chen TW, Sun CM, Calderaro J, et al. B cells are associated with survival and immunotherapy response in sarcoma. *Nature*. (2020) 577:556–60. doi: 10.1038/s41586-019-1906-8

19. Smolle MA, Herbsthofer L, Granegger B, Goda M, Brcic I, Bergovec M, et al. T-regulatory cells predict clinical outcome in soft tissue sarcoma patients: a clinico-pathological study. *Br J Cancer*. (2021) 125:717–24. doi: 10.1038/s41416-021-01456-0

20. Albarrán V, Villamayor ML, Pozas J, Chamorro J, Rosero DI, San Román M, et al. Current landscape of immunotherapy for advanced sarcoma. *Cancers (Basel)*. (2023) 15:2287. doi: 10.3390/cancers15082287

21. Le Guellec S, Lesluyes T, Sarot E, Valle C, Filleron T, Rochaix P, et al. Validation of the Complexity INdex in SARComas prognostic signature on formalin-fixed, paraffin-embedded, soft-tissue sarcomas. *Ann Oncol*. (2018) 29:1828–35. doi: 10.1093/annonc/mdy194

22. Chibon F, Lagarde P, Salas S, Pérot G, Brouste V, Tirode F, et al. Validated prediction of clinical outcome in sarcomas and multiple types of cancer on the basis of a gene expression signature related to genome complexity. *Nat Med*. (2010) 16:781–7. doi: 10.1038/nm.2174

23. Bertucci F, Niziers V, de Nonneville A, Finetti P, Mescam L, Mir O, et al. Immunologic constant of rejection signature is prognostic in soft-tissue sarcoma and refines the CINSARC signature. *J Immunother Cancer*. (2022) 10:e003687. doi: 10.1136/jitc-2021-003687

24. Ruka W, Rutkowski P, Kaminska J, Rysinska A, Steffen J. Alterations of routine blood tests in adult patients with soft tissue sarcomas: relationships to cytokine serum levels and prognostic significance. *Ann Oncol*. (2001) 12:1423–32. doi: 10.1023/a:1012527006566

25. Rutkowski P, Kamińska J, Kowalska M, Ruka W, Steffen J. Cytokine and cytokine receptor serum levels in adult bone sarcoma patients: correlations with local tumor extent and prognosis. *J Surg Oncol*. (2003) 84:151–9. doi: 10.1002/jso.10305

26. Petitprez F, Reyniès A, Chen TW-W, Sun C-M, Lacroix L, Adam J, et al. Immune classification of soft tissue sarcoma and its association with molecular characteristics, and clinical outcome. *Ann Oncol*. (2018) 29:vi35–vi36, 2018. doi: 10.1093/annonc/mdy319

27. Weng W, Yu L, Li Z, Tan C, Lv J, Lao IW, et al. The immune subtypes and landscape of sarcomas. *BMC Immunol*. (2022) 23:46. doi: 10.1186/s12865-022-00522-3

28. Allen BM, Hiam KJ, Burnett CE, Venida A, DeBarge R, Tenvooren I, et al. Systemic dysfunction and plasticity of the immune macroenvironment in cancer models. *Nat Med*. (2020) 26:1125–34. doi: 10.1038/s41591-020-0892-6

29. Qi L, Li B, Dong Y, Xu H, Chen L, Wang H, et al. Deconvolution of the gene expression profiles of valuable banked blood specimens for studying the prognostic values of altered peripheral immune cell proportions in cancer patients. *PloS One*. (2014) 9:e100934. doi: 10.1371/journal.pone.0100934

30. Ray-Coquard I, Cropet C, Van Glabbeke M, Sebban C, Le Cesne A, Judson I, et al. Lymphopenia as a prognostic factor for overall survival in advanced carcinomas, sarcomas, and lymphomas. *Cancer Res*. (2009) 69:5383–91. doi: 10.1158/0008-5472.CAN-08-3845

31. Hwang M, Canzoniero JV, Rosner S, Zhang G, White JR, Belcaid Z, et al. Peripheral blood immune cell dynamics reflect antitumor immune responses and predict clinical response to immunotherapy. *J Immunother Cancer*. (2022) 10:e004688. doi: 10.1136/jitc-2022-004688

32. Ferrucci PF, Ascierto PA, Pigozzo J, Del Vecchio M, Maio M, Antonini Cappellini GC, et al. Baseline neutrophils and derived neutrophil-to-lymphocyte ratio: prognostic relevance in metastatic melanoma patients receiving ipilimumab. *Ann Oncol*. (2016) 27:732–8. doi: 10.1093/annonc/mdw016

33. Cader FZ, Hu X, Goh WL, Wienand K, Ouyang J, Mandato E, et al. A peripheral immune signature of responsiveness to PD-1 blockade in patients with classical Hodgkin lymphoma. *Nat Med*. (2020) 26:1468–79. doi: 10.1038/s41591-020-1006-1

34. Maecker HT, McCoy JP, Nussenblatt R. Standardizing immunophenotyping for the human immunology project. *Nat Rev Immunol*. (2012) 12:191–200. doi: 10.1038/nri3158

35. Bronte V, Brandau S, Chen SH, Colombo MP, Frey AB, Greten TF, et al. Recommendations for myeloid-derived suppressor cell nomenclature and characterization standards. *Nat Commun*. (2016) 7:12150. doi: 10.1038/ncomms12150

36. Vandesompele J, De Preter K, Pattyn F, Poppe B, Van Roy N, De Paepe A, et al. Accurate normalization of real-time quantitative RT-PCR data by geometric averaging of multiple internal control genes. *Genome Biol*. (2002) 3:RESEARCH0034. doi: 10.1186/gb-2002-3-7-research0034

37. Metsalu T, Vilo J. ClustVis: a web tool for visualizing clustering of multivariate data using Principal Component Analysis and heatmap. *Nucleic Acids Res*. (2015) 43: W566–70. doi: 10.1093/nar/gkv468

38. Szklarczyk D, Gable AL, Lyon D, Junge A, Wyder S, Huerta-Cepas J, et al. STRING v11: protein- protein association networks with increased coverage, supporting functional discovery in genome-wide experimental datasets. *Nucleic Acids Res*. (2019) 47:D607–13. doi: 10.1093/nar/gky1131

39. Choi ES, Kim HS, Han I. Elevated preoperative systemic inflammatory markers predict poor outcome in localized soft tissue sarcoma. *Ann Surg Oncol*. (2014) 21:778–85. doi: 10.1245/s10434-013-3418-3

40. Brewster R, Purington N, Henry S, Wood D, Ganjoo K, Bui N. Evaluation of absolute lymphocyte count at diagnosis and mortality among patients with localized bone or soft tissue sarcoma. *JAMA Netw Open*. (2021) 4:e210845. doi: 10.1001/jamanetworkopen.2021.0845

41. Mihara A, Iwanaga R, Yukata K, Fujii K, Muramatsu K, Ihara K, et al. Neutrophil-, monocyte- and platelet-to-lymphocyte ratios, and absolute lymphocyte count for diagnosis of Malignant soft-tissue tumors. *Anticancer Res*. (2023) 43:3349–57. doi: 10.21873/anticanres.16511

42. Chan JY, Zhang Z, Chew W, Tan GF, Lim CL, Zhou L, et al. Biological significance and prognostic relevance of peripheral blood neutrophil-to-lymphocyte ratio in soft tissue sarcoma. *Sci Rep*. (2018) 8:11959. doi: 10.1038/s41598-018-30442-5

43. Strong EA, Park SH, Ethun CG, Chow B, King D, Bedi M, et al. High neutrophil-lymphocyte ratio is not independently associated with worse survival or recurrence in patients with extremity soft tissue sarcoma. *Surgery*. (2020) 168:760–7. doi: 10.1016/j.surg.2020.06.017

44. Griffiths TT, Arango MWF, Smith IM, Wade RG. The baseline neutrophil lymphocyte ratio predicts survival in soft-tissue sarcoma: A 17-year cohort study. *J Plast Reconstr Aesthet Surg*. (2022) 75:1372–9. doi: 10.1016/j.bjps.2021.11.063

45. Templeton AJ, McNamara MG, Šeruga B, Vera-Badillo FE, Aneja P, Ocaña A, et al. Prognostic role of neutrophil-to-lymphocyte ratio in solid tumors: a systematic review and meta-analysis. *J Natl Cancer Inst*. (2014) 106:dju124. doi: 10.1093/jnci/dju124

46. Cupp MA, Cariolou M, Tzoulaki I, Aune D, Evangelou E, Berlanga-Taylor AJ. Neutrophil to lymphocyte ratio and cancer prognosis: an umbrella review of systematic reviews and meta-analyses of observational studies. *BMC Med*. (2020) 18:360. doi: 10.1186/s12916-020-01817-1

47. Labani-Motlagh A, Ashja-Mahdavi M, Loskog A. The tumor microenvironment: A milieu hindering and obstructing antitumor immune responses. *Front Immunol*. (2020) 11:940. doi: 10.3389/fimmu.2020.00940

48. Seidel JA, Otsuka A, Kabashima K. Anti-PD-1 and anti-CTLA-4 therapies in cancer: mechanisms of action, efficacy, and limitations. *Front Oncol*. (2018) 8:86. doi: 10.3389/fonc.2018.00086

49. Waidhauser J, Nerlinger P, Sommer F, Wolf S, Eser S, Löhr P, et al. Circulating lymphocytes reflect the local immune response in patients with colorectal carcinoma. *Diagn (Basel)*. (2022) 12:1408. doi: 10.3390/diagnostics12061408

50. Wang W, Wang Y, Cao Z. Changes of proportions of circulating lymphocyte subsets in cancer patients after chemotherapy. *Transl Cancer Res*. (2021) 10:4169–79. doi: 10.21037/tcr-21-1688

51. Kim Y, Kobayashi E, Suehara Y, Ito A, Kubota D, Tanzawa Y, et al. Immunological status of peripheral blood is associated with prognosis in patients with bone and soft-tissue sarcoma. *Oncol Lett*. (2021) 21:212. doi: 10.3892/ol.2021.12473

52. Nyström H, Jönsson M, Nilbert M, Carneiro A. Immune-cell infiltration in high-grade soft tissue sarcomas; prognostic implications of tumor-associated macrophages and B-cells. *Acta Oncol*. (2023) 62:33–9. doi: 10.1080/0284186X.2023.2172688

53. Taipale K, Liikanen I, Juhila J, Karioja-Kallio A, Oksanen M, Turkki R, et al. T-cell subsets in peripheral blood and tumors of patients treated with oncolytic adenoviruses. *Mol Ther*. (2015) 23:964–73. doi: 10.1038/mt.2015.17

54. Munisamy S, Radhakrishnan AK, Ramdas P, Samuel PJ, Singh VA. Immune biomarkers in blood from sarcoma patients: A pilot study. *Curr Oncol*. (2022) 29:5585–603. doi: 10.3390/curroncol29080441

55. Wijayahadi N, Haron MR, Stanslas J, Yusuf Z. Changes in cellular immunity during chemotherapy for primary breast cancer with anthracycline regimens. *J Chemother*. (2007) 19:716–23. doi: 10.1179/joc.2007.19.6.716

56. Greenwald RJ, Freeman GJ, Sharpe AH. The B7 family revisited. *Annu Rev Immunol*. (2005) 23:515–48. doi: 10.1146/annurev.immunol.23.021704.115611

57. Miga A, Masters S, Gonzalez M, Noelle RJ. The role of CD40-CD154 interactions in the regulation of cell mediated immunity. *Immunol Invest*. (2000) 29:111–4. doi: 10.3109/08820130009062292

58. Ara A, Ahmed KA, Xiang J. Multiple effects of CD40-CD40L axis in immunity against infection and cancer. *Immunotargets Ther*. (2018) 7:55–61. doi: 10.2147/ITT.S163614

59. Zhang Y, Luo Y, Qin SL, Mu YF, Qi Y, Yu MH, et al. The clinical impact of ICOS signal in colorectal cancer patients. *Oncoimmunology*. (2016) 5:e1141857. doi: 10.1080/2162402X.2016.1141857

60. Schroeder BA, LaFranzo NA, LaFleur BJ, Gittelman RM, Vignali M, Zhang S, et al. CD4+ T cell and M2 macrophage infiltration predict dedifferentiated liposarcoma patient outcomes. *J Immunother Cancer*. (2021) 9:e002812. doi: 10.1136/jitc-2021-002812

61. García-Domínguez DJ, Sánchez-Margalet V, de la Cruz-Merino L, Hontecillas-Prieto L. Knowing the myeloid-derived suppressor cells: Another enemy of sarcomas patients. *Int Rev Cell Mol Biol*. (2023) 375:93–116. doi: 10.1016/bs.ircmb.2022.11.003

62. Hegde S, Leader AM, Merad M. MDSC: Markers, development, states, and unaddressed complexity. *Immunity*. (2021) 54:875–84. doi: 10.1016/j.immuni.2021.04.004

63. Yang Y, Li C, Liu T, Dai X, Bazhin AV. Myeloid-derived suppressor cells in tumors: from mechanisms to antigen specificity and microenvironmental regulation. *Front Immunol*. (2020) 11:1371. doi: 10.3389/fimmu.2020.01371

64. Li X, Zhong J, Deng X, Guo X, Lu Y, Lin J, et al. Targeting myeloid-derived suppressor cells to enhance the antitumor efficacy of immune checkpoint blockade therapy. *Front Immunol*. (2021) 12:754196. doi: 10.3389/fimmu.2021.754196

65. Gabrilovich DI, Ostrand-Rosenberg S, Bronte V. Coordinated regulation of myeloid cells by tumours. *Nat Rev Immunol*. (2012) 12:253–68. doi: 10.1038/nri3175

66. Yan X, Takahara M, Xie L, Gondo C, Setsu N, Oda Y, et al. Arginine metabolism in soft tissue sarcoma. *J Dermatol Sci*. (2011) 61(3):211–5. doi: 10.1016/j.jdermsci.2010.12.009

67. Albertsmeier M, Altendorf-Hofmann A, Lindner LH, Issels RD, Kampmann E, Dürr HR, et al. VISTA in soft tissue sarcomas: A perspective for immunotherapy? *Cancers (Basel)*. (2022) 14:1006. doi: 10.3390/cancers14041006

68. Luk SJ, Schoppmeyer R, Ijsselsteijn ME, Somarakis A, Acem I, Remst DFG, et al. VISTA expression on cancer-associated endothelium selectively prevents T-cell extravasation. *Cancer Immunol Res*. (2023) 11:1480–92. doi: 10.1158/2326-6066.CIR-22-0759

69. Xu W, Dong J, Zheng Y, Zhou J, Yuan Y, Ta HM, et al. Immune-checkpoint protein VISTA regulates antitumor immunity by controlling myeloid cell-mediated inflammation and immunosuppression. *Cancer Immunol Res*. (2019) 7:1497–510. doi: 10.1158/2326-6066.CIR-18-0489

70. Deng J, Li J, Sarde A, Lines JL, Lee YC, Qian DC, et al. Hypoxia-induced VISTA promotes the suppressive function of myeloid-derived suppressor cells in the tumor microenvironment. *Cancer Immunol Res*. (2019) 7:1079–90. doi: 10.1158/2326-6066.CIR-18-0507

71. Camarillo D, Leslie K, Unemori P, Koba Yashi A, McCune-Smith K, Maurer T. Regulatory T cells are present in Kaposi's sarcoma and increasingly frequent in advanced disease. *Infect Agents Cancer*. (2009) 4:P12. doi: 10.1186/1750-9378-4-S2-P12

72. Haist M, Stege H, Grabbe S, Bros M. The functional crosstalk between myeloid derived suppressor cells and regulatory T cells within the immunosuppressive tumor microenvironment. *Cancers (Basel)*. (2021) 13:210. doi: 10.3390/cancers13020210

73. Park MJ, Lee SH, Kim EK, Lee EJ, Baek JA, Park SH, et al. Interleukin-10 produced by myeloid-derived suppressor cells is critical for the induction of Tregs and attenuation of rheumatoid inflammation in mice. *Sci Rep*. (2018) 8:3753. doi: 10.1038/s41598-018-21856-2

74. Yaseen MM, Abuharfeil NM, Darmani H, Daoud A. Mechanisms of immune suppression by myeloid-derived suppressor cells: the role of interleukin-10 as a key immunoregulatory cytokine. *Open Biol*. (2020) 10:200111. doi: 10.1098/rsob.200111

75. Bien E, Krawczyk M, Izycka-Swieszewska E, Trzonkowski P, Kazanowska B, Adamkiewicz-Drozynska E, et al. Deregulated systemic IL-10/IL-12 balance in advanced and poor prognosis paediatric soft tissue sarcomas. *Biomarkers*. (2013) 18:204–15. doi: 10.3109/1354750X.2013.764351

76. Stanilov N, Miteva L, Deliysky T, Jovchev J, Stanilova S. Advanced colorectal cancer is associated with enhanced IL-23 and IL-10 serum levels. *Lab Med*. (2010) 3:159–63. doi: 10.1309/LM7T43AQZIUPIOWZ

77. Zhao S, Wu D, Wu P, Wang Z, Huang J. Serum IL-10 predicts worse outcome in cancer patients: A meta-analysis. *PloS One*. (2015) 10:e0139598. doi: 10.1371/journal.pone.0139598

78. Chow A, SChad S, Green MD, Hellmann MD, Allaj V, Ceglia N, et al. Tim-4$^+$ cavity-resident macrophages impair anti-tumor CD8$^+$ T cell immunity. *Cancer Cell*. (2021) 39:973–988.e9. doi: 10.1016/j.ccell.2021.05.006

79. Rodriguez PC, Ruffell B. Cavity macrophages stop anti-tumor T cells. *Cancer Cell*. (2021) 39:900–2. doi: 10.1016/j.ccell.2021.06.007

80. Li H, Zhou X, Ran Q, Wang L. Parapharyngeal liposarcoma: a case report. *Diagn Pathol*. (2013) 8:42. doi: 10.1186/1746-1596-8-42

81. Melaiu O, Lucarini V, Cifaldi L, Fruci D. Influence of the tumor microenvironment on NK cell function in solid tumors. *Front Immunol*. (2020) 10:3038. doi: 10.3389/fimmu.2019.03038

82. Cooper MA, Fehniger TA, Caligiuri MA. The biology of human natural killer-cell subsets. *Trends Immunol*. (2001) 22:633–40. doi: 10.1016/s1471-4906(01)02060-9

83. López-Botet M, Muntasell A, Vilches C. The CD94/NKG2C+ NK-cell subset on the edge of innate and adaptive immunity to human cytomegalovirus infection. *Semin Immunol*. (2014) 26:145–51. doi: 10.1016/j.smim.2014.03.002

84. Cerwenka A, Lanier LL. Natural killer cell memory in infection, inflammation and cancer. *Nat Rev Immunol*. (2016) 16:112–23. doi: 10.1038/nri.2015.9

85. Ni J, Miller M, Stojanovic A, Garbi N, Cerwenka A. Sustained effector function of IL-12/15/18-preactivated NK cells against established tumors. *J Exp Med*. (2012) 209:2351–65. doi: 10.1084/jem.20120944

86. Rufer N, Zippelius A, Batard P, Pittet MJ, Kurth I, Corthesy P, et al. Ex vivo characterization of human CD8+ T subsets with distinct replicative history and partial effector functions. *Blood*. (2003) 102:1779–87. doi: 10.1182/blood-2003-02-0420

87. Belgiovine C, Frapolli R, Liguori M, Digifico E, Colombo FS, Meroni M, et al. Inhibition of tumor-associated macrophages by trabectedin improves the antitumor adaptive immunity in response to anti-PD-1 therapy. *Eur J Immunol*. (2021) 51:2677–86. doi: 10.1002/eji.202149379

88. Povo-Retana A, Mojena M, Stremtan AB, Fernández-García VB, Gómez-Sáez A, Nuevo-Tapioles C, et al. Specific effects of trabectedin and lurbinectedin on human macrophage function and fate-novel insights. *Cancers (Basel)*. (2020) 12:3060. doi: 10.3390/cancers12103060

89. Cucè M, Gallo Cantafio ME, Siciliano MA, Riillo C, Caracciolo D, Scionti F, et al. Trabectedin triggers direct and NK-mediated cytotoxicity in multiple myeloma. *J Hematol Oncol*. (2019) 12:32. doi: 10.1186/s13045-019-0714-9

90. Bücklein V, Adunka T, Mendler AN, Issels R, Subklewe M, Schmollinger JC, et al. Progressive natural killer cell dysfunction associated with alterations in subset proportions and receptor expression in soft-tissue sarcoma patients. *Oncoimmunology*. (2016) 5:e1178421. doi: 10.1080/2162402X.2016.1178421

91. Chochi K, Ichikura T, Majima T, Kawabata T, Matsumoto A, Sugasawa H, et al. The increase of CD57+ T cells in the peripheral blood and their impaired immune functions in patients with advanced gastric cancer. *Oncol Rep*. (2003) 10:1443–8. doi: 10.3892/or.10.5.1443

92. Sayitoglu EC, Georgoudaki AM, Chrobok M, Ozkazanc D, Josey BJ, Arif M, et al. Boosting natural killer cell-mediated targeting of sarcoma through DNAM-1 and NKG2D. *Front Immunol*. (2020) 11:40. doi: 10.3389/fimmu.2020.00040

93. Szkandera J, Absenger G, Liegl-Atzwanger B, Pichler M, Stotz M, Samonigg H, et al. Elevated preoperative neutrophil/lymphocyte ratio is associated with poor prognosis in soft-tissue sarcoma patients. *Br J Cancer*. (2013) 108:1677–83. doi: 10.1038/bjc.2013.135

94. Raskov H, Orhan A, Christensen JP, Gögenur I. Cytotoxic $CD8^+$ T cells in cancer and cancer immunotherapy. *Br J Cancer*. (2021) 124:359–67. doi: 10.1038/s41416-020-01048-4

95. Wolf NK, Kissiov DU, Raulet DH. Roles of natural killer cells in immunity to cancer, and applications to immunotherapy. *Nat Rev Immunol*. (2023) 23:90–105. doi: 10.1038/s41577-022-00732-1

96. Cruz SM, Sholevar CJ, Judge SJ, Darrow MA, Iranpur KR, Farley LE, et al. Intratumoral $NKp46^+$ natural killer cells are spatially distanced from T and $MHC\text{-}I^+$ cells with prognostic implications in soft tissue sarcoma. *Front Immunol*. (2023) 14:1230534. doi: 10.3389/fimmu.2023.1230534

97. Judge SJ, Bloomstein JD, Sholevar CJ, Darrow MA, Stoffel KM, Vick LV, et al. Transcriptome analysis of tumor-infiltrating lymphocytes identifies NK cell gene signatures associated with lymphocyte infiltration and survival in soft tissue sarcomas. *Front Immunol*. (2022) 13:893177. doi: 10.3389/fimmu.2022.893177

98. Botticelli A, Pomati G, Cirillo A, Scagnoli S, Pisegna S, Chiavassa A, et al. The role of immune profile in predicting outcomes in cancer patients treated with immunotherapy. *Front Immunol*. (2022) 13:974087. doi: 10.3389/fimmu.2022.974087

99. Lazcano R, Barreto CM, Salazar R, Carapeto F, Traweek RS, Leung CH, et al. The immune landscape of undifferentiated pleomorphic sarcoma. *Front Oncol*. (2022) 12:1008484. doi: 10.3389/fonc.2022.1008484

100. Feng X, Tonon L, Li H, Darbo E, Pleasance E, Macagno N, et al. Comprehensive immune profiling unveils a subset of leiomyosarcoma with "Hot" Tumor immune microenvironment. *Cancers (Basel)*. (2023) 15:3705. doi: 10.3390/cancers15143705

101. Dutta AK, Alberge JB, Sklavenitis-Pistofidis R, Lightbody ED, Getz G, Ghobrial IM. Single-cell profiling of tumour evolution in multiple myeloma - opportunities for precision medicine. *Nat Rev Clin Oncol*. (2022) 19:223–36. doi: 10.1038/s41571-021-00593-y

102. Krijgsman D, de Vries NL, Skovbo A, Andersen MN, Swets M, Bastiaannet E, et al. Characterization of circulating T-, NK-, and NKT cell subsets in patients with colorectal cancer: the peripheral blood immune cell profile. *Cancer Immunol Immunother*. (2019) 68:1011–24. doi: 10.1007/s00262-019-02343-7

103. Shi J, Liu J, Tu X, Li B, Tong Z, Wang T, et al. Single-cell immune signature for detecting early-stage HCC and early assessing anti-PD-1 immunotherapy efficacy. *J Immunother Cancer*. (2022) 10:e003133. doi: 10.1136/jitc-2021-003133

104. Shen R, Liu B, Li X, Yu T, Xu K, Ma J. Development and validation of an immune gene-set based prognostic signature for soft tissue sarcoma. *BMC Cancer*. (2021) 21:144. doi: 10.1186/s12885-021-07852-2

105. Toulmonde M, Lucchesi C, Verbeke S, Crombe A, Adam J, Geneste D, et al. High throughput profiling of undifferentiated pleomorphic sarcomas identifies two main subgroups with distinct immune profile, clinical outcome and sensitivity to targeted therapies. *EBioMedicine*. (2020) 62:103131. doi: 10.1016/j.ebiom.2020.103131

106. Yarchoan M, Hopkins A, Jaffee EM. Tumor mutational burden and response rate to PD-1 inhibition. *N Engl J Med*. (2017) 377:2500–1. doi: 10.1056/NEJMc1713444

107. Pollack SM, He Q, Yearley JH, Emerson R, Vignali M, Zhang Y, et al. T-cell infiltration and clonality correlate with programmed cell death protein 1 and programmed death-ligand 1 expression in patients with soft tissue sarcomas. *Cancer*. (2017) 123:3291–304. doi: 10.1002/cncr.30726

108. Resag A, Toffanin G, Benešová I, Müller L, Potkrajcic V, Ozaniak A, et al. The immune contexture of liposarcoma and its clinical implications. *Cancers (Basel)*. (2022) 14:4578. doi: 10.3390/cancers14194578

109. Saerens M, Brusselaers N, Rottey S, Decruyenaere A, Creytens D, Lapeire L. Immune checkpoint inhibitors in treatment of soft-tissue sarcoma: A systematic review and meta-analysis. *Eur J Cancer*. (2021) 152:165–82. doi: 10.1016/j.ejca.2021.04.034

Frontiers in Immunology

Explores novel approaches and diagnoses to treat immune disorders.

The official journal of the International Union of Immunological Societies (IUIS) and the most cited in its field, leading the way for research across basic, translational and clinical immunology.

Discover the latest Research Topics

See more →

Frontiers

Avenue du Tribunal-Fédéral 34
1005 Lausanne, Switzerland
frontiersin.org

Contact us

+41 (0)21 510 17 00
frontiersin.org/about/contact